Clinical Platelet Lipidomics in Targeted and Untargeted Approach by Liquid Chromatography Coupled to Mass Spectrometry

Dissertation

der Mathematisch-Naturwissenschaftlichen Fakultät

der Eberhard Karls Universität Tübingen

zur Erlangung des Grades eines

Doktors der Naturwissenschaften

(Dr. rer. nat.)

vorgelegt von

Xiaoqing Fu

aus Jiangsu, China

Tübingen

2023

Gedruckt mit Genehmigung der Mathematisch-Naturwissenschaftlichen Fakultät der Eberhard Karls Universität Tübingen.

Tag der mündlichen Qualifikation:	02.08.2023
Dekan:	Prof. Dr. Thilo Stehle
1. Berichterstatter/-in:	Prof. Dr. Michael Lämmerhofer
2. Berichterstatter/-in:	Jun.-Prof. Dr. Matthias Gehringer

The research described in this thesis was conducted between October 1st 2019 and June 13th 2023 at the Institute of Pharmaceutical Sciences, Division Pharmaceutical (Bio-)Analysis, Eberhard Karls Universität Tübingen under the supervision of Prof. Dr. Michael Lämmerhofer.

Dedicated to my parents Jingang Fu and Yuhong Du,

and to my grandparents Zhongyun Fu and Yanmei Chu

Contents

I. Summary

Lipids are bioactive compounds playing various roles in energy storage, membrane function and signal transduction. A comprehensive lipid profiling in organs, cells or biological samples could provide new ideas to help find biomarkers or understand the mechanism of different pathways. Over the last decades, technological innovations and breakthroughs in analytical chemistry from the aspects of separation science including the highly efficient sub-2 μm particles for stationary phases and new chiral stationary phases for liquid chromatography (LC) and mass spectrometry (MS) including the high-resolution MS instruments with enhanced sensitivity and diversity on data acquisition modes bring us the opportunity for ongoing decryption of the lipidome and its pathways and networks.

The so-called lipidomics which is a subset of metabolomics attracts however increasing interests and attentions from researchers recently. Some attention has been put on platelet lipidome for several decades when the first comprehensive lipid analysis in platelet could be traced back to 1962. Platelets are small cellular components of blood with a primary role in hemostasis which in contrary are also responsible for a pathological condition called thrombosis that might results in cardiovascular disease (CVD) such as heart attack and stroke. During the hemostasis, lipids play important roles, especially the fatty acids and their derivatives such as oxylipins which are involved in platelets activation. Therefore, the analysis of platelets lipidomics is particularly interesting and the platelet lipidomic landscape might be considered as a powerful tool for diagnostic and prognostic biomarkers for CVD.

In this work, different analytical methods based on the LC-MS for lipidomics analysis including targeted and untargeted approaches were developed and optimized. **In the first project**, we reported an advanced monophasic extraction protocol with methanol/methyl tert-butyl-ether/isopropanol, MeOH/MTBE/IPA (1.3:1:1, v/v/v) as extraction solvents, bead homogenizer for cell disruption and MeOH/MTBE (1:1, v/v) as reconstitution solvent which provides optimal cellular and subcellular extraction efficiencies for both polar (e.g. acylcarnitines) and apolar lipids (e.g. triglycerides TGs). It is simplified (no phase separation), eco-friendly (reduced solvent consumption and no halogenated ones), fast (5 min for 24 samples in parallel), and can be easily adapted for cells, plasma, and tissue. Therefore, it has great potential for large-scale clinical lipidomics studies. **In the second project**, a fast and sensitive method for qualitative and quantitative analysis of each enantiomers of 3-Hydroxy fatty acids (3-OH-FAs) from C8-C18 by using a triple quadrupole instrument as a detector in a targeted, selected reaction monitoring (SRM) mode was reported. The validated method was applied to investigate

the alteration of 3-OH-FA enantiomers in platelets and plasma samples from coronary artery disease (CAD) patients with the findings that different predominance for R or S in dependence on carbon chain length can be observed, which might be associated with different functional enzymes of mitochondrial and peroxisomal β-oxidation. Finally, our study provides a new strategy for chiral separation and enantioselective analysis, showing great potential for targeted metabolomics in clinical biomarker discovery. **In the third project**, we reported a methodology for untargeted isomer-selective branched chain fatty acids (BCFAs) profiling covering distinct chain length (C5-C20) with different branching types (methyl Me or ethyl Et) and branching positions (2Me, 3Me, 4Me, 6Me, *anteiso* and *iso*-BCFAs) without precolumn derivatization with ultrahigh performance liquid chromatography coupled with electrospray ionization and tandem mass spectrometry (UHPLC-ESI-MS/MS) by quadrupole-time-of-flight (QTOF) instrument with sequential window acquisition of all theoretical fragment ion mass spectra (SWATH). The new method showed strong potential for BCFAs profiling in bacterial samples including different isomers *anteiso* and *iso*-BCFAs, which could be a useful tool for related subdisciplines in metabolomics. **The fourth and fifth projects** were related to the oxidized FAs oxylipins where in project 4 a microLC method was established with a capillary column coupled with quadrupole linear ion trap (QTrap) with SRM for MS/MS detection of 42 oxylipins with 13 internal standards for signal normalization. The method is sensitive with limit of quantification (LOQ) between 30 to 150 pg/mL and accurate, with good extarction recovery by solid phase extraction. The second analytical method for oxylipins from project 5 is the enantioselective separation of oxylipins based on the mordern Chiralpak IA-U LC column coupled with triple quadrupoles (QqQ) by SRM MS/MS detection. The new method showed peak resolution and great sensitivity and is applied for the oxylipins analysis in human platelets with the findings that in most of the case single enantiomers were detected in platelet samples because of the enzymatic oxidation while both enantiomers were deteted during autooxidation of polyunsaturated fatty acids (PUFAs).

The above described five projects are mainly the analytical method development based on the LC-MS for lipidomics. Further, three more projects on the application of analytical methods to the clinical platelets lipidomics study were conducted. **In the sixth project**, through the general lipids profiling by untargetd lipidomics approach and the targeted oxylipins method (method developed form the fourth and fifth projects) in platelets of CAD patients (n=230) treated in-vitro with a selective CXCR7 receptor agonist, untreated control, thrombin-activated platelets as well as CXCR7 agonist/thrombin activated platelets, it was found that platelet lipidome in

CXCR7 agonist treated groups showed significant alteration e.g downregulation of oxylipins and lysophosphatidylinositols upon thrombin activating. Our investigation proved that platelet ACKR3/CXCR7 favors antiplatelet lipids over an atherothrombotic lipidome and regulates thromboinflammation which may offer a novel therapeutic strategy in CAD. **In the seventh and eighth projects**, platelet lipidome in a CAD cohort (n = 139) in untargeted lipidomics approach was characterized. Lipids alteration was observed between acute coronary syndrome (ACS) and chronic coronary syndrome (CCS) patients especially the medium-chain phosphatidylcholine (MC-PC) that are upregulated in ACS, which may play a role in the pathophysiology of ACS. Similarly, significant lipid change was observed between CAD patient and those treated with statin (n=105) where TGs, cholesterol esters CEs, palmitic acid are upregulated and MC-PC and PUFA-PC levels are downregulated in platelets of CAD patients with statin treatment, providing the evidence for significant effects of statin on the platelet lipidome.

II. Zusammenfassung

Lipide sind bioaktive Verbindungen, die bei der Energiespeicherung, der Membranfunktion und der Signaltransduktion verschiedene Rollen spielen. Eine umfassende Erstellung von Lipidprofilen in Organen, Zellen oder biologischen Proben könnte neue Ideen liefern, um Biomarker zu finden oder die Mechanismen verschiedener Stoffwechselwege zu verstehen. In den letzten Jahrzehnten haben technologische Innovationen und Durchbrüche in der analytischen Chemie in Bezug auf die Trennwissenschaft, einschließlich der hocheffizienten Sub-2-µm-Partikel für stationäre Phasen und der chiralen stationären Phase für die Flüssigchromatographie (LC) und die Massenspektrometrie (MS), einschließlich der hochauflösenden MS-Instrumente mit verbesserter Empfindlichkeit und einer Vielzahl von Datenerfassungsmodi, uns die Möglichkeit zur fortlaufenden Entschlüsselung des Lipidoms und seiner Wege und Netzwerke gegeben.

Die so genannte Lipidomik, die eine Untergruppe der Metabolomik ist, stößt jedoch in letzter Zeit aufzunehmendes Interesse und Aufmerksamkeit bei den Forschern. Dem Lipidom der Blutplättchen wird seit mehreren Jahrzehnten Aufmerksamkeit geschenkt, wobei die erste umfassende Lipidanalyse der Blutplättchen auf das Jahr 1962 zurückgeführt werden kann. Thrombozyten sind kleine zelluläre Bestandteile des Blutes, die eine primäre Rolle bei der Blutstillung spielen und im Gegensatz dazu auch für die Entstehung von Thrombosen verantwortlich sind, die zu Herz-Kreislauf-Erkrankungen wie Herzinfarkt und Schlaganfall führen können. Während der Blutstillung spielen Lipide eine wichtige Rolle, insbesondere die Fettsäuren und ihre Derivate wie Oxylipine sind an der Aktivierung der Blutplättchen beteiligt. Daher ist die Analyse der Lipidomik der Blutplättchen besonders interessant, und die Lipidomik der Blutplättchen könnte als leistungsfähiges Instrument für diagnostische und prognostische Biomarker für koronare Herzkrankheit (KHK) angesehen werden.

In dieser Arbeit wurden verschiedene auf der LC-MS basierende Analysemethoden für die Lipidomik-Analyse entwickelt und optimiert, darunter gezielte und nicht gezielte Ansätze. **Im ersten Projekt** berichteten wir über ein fortschrittliches monophasisches Extraktionsprotokoll mit Methanol/Methyl-tert-butylether/Isopropanol, MeOH/MTBE/IPA (1,3:1:1, v/v/v) als Extraktionslösungsmittel, einem Perlenhomogenisator für den Zellaufschluss und MeOH/MTBE (1:1, v/v) als Rekonstitutionslösungsmittel, das optimale zelluläre und subzelluläre Extraktionseffizienzen sowohl für polare (z. B. Acylcarnitine) als auch apolare Lipide (z. B. Triglyceride TGs) bietet. Das Verfahren ist einfach (keine Phasentrennung), umweltfreundlich (geringerer Lösungsmittelverbrauch und keine halogenisierten Lösungsmittel), schnell (5

Minuten für 24 Proben parallel) und kann leicht für Zellen, Plasma und Gewebe angepasst werden. Daher hat es ein beachtliches Potenzial für groß angelegte klinische Lipidomics-Studien. **Im zweiten Projekt** wurde eine schnelle und empfindliche Methode zur qualitativen und quantitativen Analyse der einzelnen Enantiomere von 3-Hydroxyfettsäuren (3-OH-FAs) aus C8-C18 unter Verwendung eines Triple-Quadrupol-Instruments als Detektor in einem gezielten SRM-Modus (Selected Reaction Monitoring) vorgestellt. Die validierte Methode wurde angewandt, um die Veränderung von 3-OH-FA-Enantiomeren in Thrombozyten und Plasmaproben von KHK-Patienten zu untersuchen. Dabei wurde festgestellt, dass in Abhängigkeit von der Länge der Kohlenstoffkette eine unterschiedliche Dominanz von R oder S zu beobachten ist, was mit unterschiedlichen funktionellen Enzymen der mitochondrialen und peroxisomalen β-Oxidation in Verbindung gebracht werden könnte. Schließlich bietet unsere Studie eine neue Strategie für die chirale Trennung und enantioselektive Analyse, die ein großes Potenzial für die gezielte Metabolomik bei der Entdeckung klinischer Biomarker zeigt. **Im dritten Projekt** berichteten wir über eine Methodik zur ungezielten isomerselektiven Profilierung von verzweigtkettigen Fettsäuren (BCFAs), die verschiedene Kettenlängen (C5-C20) mit unterschiedlichen Verzweigungstypen (Methyl Me oder Ethyl Et) und Verzweigungspositionen (2Me, 3Me, 4Me, 6Me, *anteiso* und *iso*-BCFAs) ohne Vorsäulen-Derivatisierung mit Ultrahochleistungs-Flüssigkeitschromatographie, Elektrospray-Ionisierung und Tandem-Massenspektrometrie (UHPLC-ESI-MS/MS) durch Quadrupol-Flugzeitinstrument (QTOF) mit sequenzieller Fenstererfassung aller theoretischen Fragment-Ionen-Massenspektren (SWATH) abdeckt. Die neue Methode zeigte ein starkes Potenzial für die Erstellung von BCFA-Profilen in bakteriellen Proben, einschließlich verschiedener Isomere anteiso und iso-BCFAs, was ein nützliches Werkzeug für verwandte Subdisziplinen in der Metabolomik sein könnte. **Das vierte und fünfte Projekt** bezog sich auf die oxidierten FAs Oxylipine, von denen eine MikroLC-Methode mit einer Kapillarsäule, die mit Quadrupol-Linear-Ionenfalle (QTrap) gekoppelt ist, mit planmäßiger ausgewählter Reaktionsüberwachung (SRM) für die MS/MS-Erkennung von 42 Oxylipinen mit 13 internen Standards für die Signalnormalisierung. Die Methode ist empfindlich mit einer Quantifizierungsgrenze (LOQ) von 30 bis 150 pg/ml und präzise mit guter Extraktionswiederfindung durch Festphasenextraktion. Die zweite Analysemethode für Oxylipine aus Projekt 5 ist die enantioselektive Trennung von Oxylipinen auf der Grundlage der modernen Chiralpak-LC-Säule IA-U, die mit Dreifach-Quadrupolen (QqQ) gekoppelt ist, durch SRM MS/MS-Detektion. Die neue Methode zeigte Spitzenauflösung und hohe Empfindlichkeit und wird für die Analyse von Oxylipinen in menschlichen Blutplättchen angewandt. Dabei wurde festgestellt, dass in den meisten Fällen aufgrund der enzymatischen Oxidation

einzelne Enantiomere in Blutplättchenproben nachgewiesen wurden, während bei der Autooxidation von mehrfach ungesättigten Fettsäuren (PUFAs) beide Enantiomere nachgewiesen wurden.

Bei den oben beschriebenen fünf Projekten handelt es sich hauptsächlich um die Entwicklung von Analysemethoden auf der Grundlage der LC-MS für die Lipidomik. Darüber hinaus wurden drei weitere Projekte zur Anwendung von Analysemethoden für die klinische Thrombozyten-Lipidomik-Studie durchgeführt. **Im sechsten Projekt** wurde durch die allgemeine Erstellung von Lipidprofilen mittels eines ungezielten Lipidomics-Ansatzes und der gezielten Oxylipin-Methode (Methode entwickelt aus dem 4. und 5. Projekt) in Thrombozyten von KHK-Patienten (n=230), die in vitro mit einem selektiven CXCR7-Rezeptor-Agonisten behandelt wurden, sowie in unbehandelten Kontroll-, Thrombin-aktivierten und CXCR7-Agonisten/Thrombin-aktivierten Thrombozyten festgestellt, dass das Lipidom der Thrombozyten in den mit CXCR7-Agonisten behandelten Gruppen signifikante Veränderungen aufwies, z. B. eine Herabregulierung von Oxylipinen und Lysophosphatidylinositolen bei Thrombinaktivierung. Unsere Untersuchungen haben gezeigt, dass ACKR3/CXCR7 in den Thrombozyten antithrombozytäre Lipide gegenüber einem atherothrombotischen Lipidom begünstigt und die Thromboinflammation reguliert, was eine neue therapeutische Strategie bei KHK darstellen könnte. **Im siebten und achten Projekt** wurde das Lipidom der Thrombozyten in einer KHK-Kohorte (n = 139) mit einem nicht zielgerichteten Lipidom-Ansatz charakterisiert. Es wurden Lipidveränderungen zwischen Patienten mit akutem Koronarsyndrom (ACS) und Patienten mit chronischem Koronarsyndrom (CCS) festgestellt, insbesondere die mittelkettigen Phosphatidylcholine (MC-PC), die bei ACS hochreguliert sind, was eine Rolle in der Pathophysiologie von ACS spielen könnte. Ebenso wurden signifikante Lipidveränderungen zwischen KHK-Patienten und den mit Statin behandelten Patienten (n=105) beobachtet, wobei TGs, CEs und Palmitinsäure in den Blutplättchen von KHK-Patienten mit Statin-Behandlung hochreguliert und MC-PC und PUFA-PC herabreguliert wurden, was den Beweis für mildernde Effekte von Statin auf das Lipidom der Blutplättchen liefert.

III. List of publications

List of publications included in this thesis

Pubilication I

X. Fu, C. Calderón, T. Harm, M. Gawaz, M. Lämmerhofer, Advanced unified monophasic lipid extraction protocol with wide coverage on the polarity scale optimized for large-scale untargeted clinical lipidomics analysis of platelets, Analytica Chimica Acta, 1221 (2022) 340155.

https://doi.org/10.1016/j.aca.2022.340155

Pubilication II

X. Fu, Z. Xu, M. Gawaz, M. Lämmerhofer, UHPLC-MS/MS method for chiral separation of 3-hydroxy fatty acids on amylose-based chiral stationary phase and its application for the enantioselective analysis in plasma and platelets, Journal of Pharmaceutical and Biomedical Analysis, 223 (2023) 115151.

https://doi.org/10.1016/j.jpba.2022.115151

Pubilication III

X. Fu, N. Hafza, F. Götz, M. Lämmerhofer, Profiling of branched chain and straight chain saturated fatty acids by ultra-high performance liquid chromatography-mass spectrometry, Journal of Chromatography A, 1703 (2023) 464111.

https://doi.org/10.1016/j.chroma.2023.464111

Publication IV

M. Cebo, X. Fu, M. Gawaz, M. Chatterjee, M. Lämmerhofer, Micro-UHPLC-MS/MS method for analysis of oxylipins in plasma and platelets, Journal of Pharmaceutical and Biomedical Analysis, 189 (2020) 113426.

https://doi.org/10.1016/j.jpba.2020.113426

Publication V

M. Cebo, X. Fu, M. Gawaz, M. Chatterjee, M. Lämmerhofer, Enantioselective ultra-high performance liquid chromatography-tandem mass spectrometry method based on sub-2µm particle polysaccharide column for chiral separation of oxylipins and its application for the analysis of autoxidized fatty acids and platelet releasates, Journal of Chromatography A, 1624 (2020) 461206.

https://doi.org/10.1016/j.chroma.2020.461206

Publication VI

M. Cebo, K. Dittrich, X. Fu, M.C. Manke, F. Emschermann, J. Rheinlaender, H. von Eysmondt, N. Ferreirós, J. Sudman, A. Witte, Platelet ACKR3/CXCR7 favors antiplatelet lipids over an atherothrombotic lipidome and regulates thromboinflammation, Blood, 139 (2022) 1722-1742.

https://doi.org/10.1182/blood.2021013097

Publication VII

T. Harm, A. Bild, K. Dittrich, A. Goldschmied, J. Nestele, M. Chatterjee, X. Fu, K. Kolb, T. Castor, O. Borst, Acute coronary syndrome is associated with a substantial change in the platelet lipidome, Cardiovascular Research, 118 (2022) 1904-1916.

https://doi.org/10.1093/cvr/cvab238

Publication VIII

T. Harm, M. Frey, K. Dittrich, A. Goldschmied, A.-K. Rohlfing, X. Fu, A. Brun, T. Castor, D. Rath, K. Müller, Statin treatment is associated with alterations in the platelet lipidome, Thrombosis and Haemostasis, (2023).

https://doi.org/10.1055/s-0043-1764353

List of other publications during the research period

Pubilication IX

X. Fu, M. Cebo, T. Ikegami, M. Lämmerhofer, Separation of carbohydrate isomers and anomers on poly-N-(1H-tetrazole-5-yl)-methacrylamide-bonded stationary phase by hydrophilic interaction chromatography as well as determination of anomer interconversion energy barriers, Journal of Chromatography A, 1620 (2020) 460981.

https://doi.org/10.1016/j.chroma.2020.460981

Pubilication X

X. Fu, M. Cebo, T. Ikegami, M. Lämmerhofer, Retention characteristics of poly(N-(1H-tetrazole-5-yl)-methacrylamide)-bonded stationary phase in hydrophilic interaction chromatography, Journal of Chromatography A, 1609 (2020) 460500.

https://doi.org/10.1016/j.chroma.2019.460500

Publication XI

L. Davani, X. Fu, A. De Simone, P. Li, S. Montanari, M. Lämmerhofer, V. Andrisano, Aβ1-42 peptide toxicity on neuronal cells: A lipidomic study, Journal of Pharmaceutical and Biomedical Analysis, 219 (2022) 114876.

https://doi.org/10.1016/j.jpba.2022.114876

Publication XII

L. Huang, M. Matsuo, C. Calderón, S.-H. Fan, A.V. Ammanath, X. Fu, N. Li, A. Luqman, M. Ullrich, F. Herrmann, Molecular basis of rhodomyrtone resistance in Staphylococcus aureus, Mbio, 13 (2022) e03833-03821.

https://doi.org/10.1128/mbio.03833-21

Publication XIII

A. Fink, A.-K. Rohlfing, V. Dicenta, D. Schaale, M. Kremser, Z. Laspa, M. Sigle, X. Fu, A. Pelzer, M. Fischer, The Subtilisin-Like Protease Furin Regulates Hemin-Dependent Ectodomain Shedding of Glycoprotein VI, Thrombosis and Haemostasis, (2023).

https://doi.org/10.1055/s-0043-1768057

Publication XIV

A. Kengmo Tchoupa, A.M. Elsherbini, X. Fu, O. Ghaneme, L. Seibert, M.A. Boecker, M. Lebtig, J. Camus, S. Papadopoulos Lambidis, B. Schittek, Lipase-mediated detoxification of host-derived antimicrobial fatty acids by Staphylococcus aureus, bioRxiv, (2023) 2023.2005.2015.540481. preprint

https://doi.org/10.1101/2023.05.15.540481

Pubilication XV (ready for submission)

Kristina Dittrich#, Xiaoqing Fu#, Malgorzata Cebo, Marcel Lackner, Lena-Sophie Menig-Benzig, Benjamin Bouzabia, Johannes Rheinlaender, Hadra-sioux Banks-machado, Hendrik von Eysmondt, Matthias Schwab, Sandra Beer-Hammer, Elke Schaeffeler, Ute Hofmann, Mathias Haag, Dominik Rath, Tobias Geisler, Meinrad Gawaz, Tilman E. Schäffer, Michael Lämmerhofer, Madhumita Chatterjee. Platelet ACKR3/CXCR7 Enhances Anticoagulant Acylcarnitine Levels and Modulates Thrombotic Response to Lipids: relevance for Coronary Artery Disease. # shared first authorship.

IV. Author contributions of the publications listed in the thesis

Publication I

Advanced unified monophasic lipid extraction protocol with wide coverage on the polarity scale optimized for large-scale untargeted clinical lipidomics analysis of platelets

Xiaoqing Fu

General concept

Method development

Sample preparation and analysis

Data processing and interpretation

Main writing of the manuscript

Dr. Carlos Calderón

Sample preparation and analysis

Discussion of results and interpretation

Proofreading of the manuscript

Tobias Harm

Platelets collection and isolation

Proofreading of the manuscript

Prof. Dr. Meinrad Gawaz

Coordination and financing of the biological part of the project

Proofreading of the manuscript

Prof. Dr. Michael Lämmerhofer

Generation, initiation, coordination and financing of the project

Discussion of results and interpretation

Partial writing and editing of the manuscript

Proofreading and final approval of the manuscript

Corresponding author

Publication II

UHPLC-MS/MS method for chiral separation of 3-hydroxy fatty acids on amylose-based chiral stationary phase and its application for the enantioselective analysis in plasma and platelets

Xiaoqing Fu

General concept

Method development

Sample preparation and analysis

Data processing and interpretation

Main writing of the manuscript

Zhanjian Xu

Method development

Sample preparation and analysis

Data processing and results discussion

Partial writing of the manuscript

Prof. Dr. Meinrad Gawaz

Coordination and financing of the biological part of the project

Proofreading of the manuscript

Prof. Dr. Michael Lämmerhofer

Generation, initiation, coordination and financing of the project

Discussion of results and interpretation

Partial writing and editing of the manuscript

Proofreading and final approval of the manuscript

Corresponding author

Publication III

Profiling of branched chain and straight chain saturated fatty acids by ultra-high performance liquid chromatography-mass spectrometry

Xiaoqing Fu

General concept

Method development

Sample preparation and analysis

Data processing and interpretation

Main writing of the manuscript

Nourhane Hafza

Staphylococcus cell culture and collection

Partial writing of the manuscript

Prof. Dr. Friedrich Götz

Coordination and financing of the *Staphylococcus* part of the project

Proofreading of the manuscript

Prof. Dr. Michael Lämmerhofer

Generation, initiation, coordination and financing of the project

Discussion of results and interpretation

Partial writing and editing of the manuscript

Proofreading and final approval of the manuscript

Corresponding author

Publication IV

Micro-UHPLC-MS/MS method for analysis of oxylipins in plasma and platelets.

Małgorzata Cebo

General concept

Method development

Sample preparation and analysis

Data processing and interpretation

Main writing of the manuscript

Xiaoqing Fu

Sample preparation and analysis

LC-MS instruments maintenance

Proofreading of the manuscript

Prof. Dr. Meinrad Gawaz

Coordination and financing of the biological part of the project

Proofreading of the manuscript

Dr. Madhumita Chatterjee

Platelets collection, isolation and in-vitro treatment

Biological interpretation

Correction and editing of the manuscript

Prof. Dr. Michael Lämmerhofer

Generation, initiation, coordination and financing of the project

Discussion of results and interpretation

Partial writing and editing of the manuscript

Proofreading and final approval of the manuscript

Corresponding author

Publication V

Enantioselective ultra-high performance liquid chromatography-tandem mass spectrometry method based on sub-2µm particle polysaccharide column for chiral separation of oxylipins and its application for the analysis of autoxidized fatty acids and platelet releasates.

Małgorzata Cebo

General concept

Method development

Sample preparation and analysis

Data processing and interpretation

Main writing of the manuscript

Xiaoqing Fu

Sample preparation and analysis

LC-MS instruments maintenance

Proofreading of the manuscript

Prof. Dr. Meinrad Gawaz

Coordination and financing of the biological part of the project

Proofreading of the manuscript

Dr. Madhumita Chatterjee

Platelets collection, isolation and in-vitro treatment

Biological interpretation

Correction and editing of the manuscript

Prof. Dr. Michael Lämmerhofer

Generation, initiation, coordination and financing of the project

Discussion of results and interpretation

Partial writing and editing of the manuscript

Proofreading and final approval of the manuscript

Corresponding author

Publication VI

Platelet ACKR3/CXCR7 favors antiplatelet lipids over an atherothrombotic lipidome and regulates thromboinflammation

Malgorzata Cebo

Sample preparation and analysis for lipidomics part

Proofreading of the manuscript

Kristina Dittrich

Sample preparation and analysis for lipidomics part

Proofreading of the manuscript

Xiaoqing Fu

Sample preparation and analysis for lipidomics part

Proofreading of the manuscript

Mailin C. Manke performed intravital microscopy (IVM);

Frederic Emscher-mann performed thromboelastography and Legendplex analysis;

Johannes Rheinlaender and **Hendrik von Eysmondt** performed SICM;

Nerea Ferreirós analyzed cAMP levels;

Jessica Sudman analyzed the MI/RI model;

Alexander Witte analysed tail bleeding time;

Lisann Pelzl characterized HIT patients;

Dominik Rath analyzed clinical data;

Tilman E. Schäffer supervised SICM;

Oliver Borst (IVM), **Tobias Geisler** (CAD cohort), **Tamam Bakchoul** (HIT), and **Meinrad Gawaz** (MI/RI model) collaborated in the project;

Prof. Dr. Michael Lämmerhofer

Supervision of the lipidomics analysis

Discussion of results

Proofreading and editing of the manuscript

Dr. Madhumita Chatterjee

Project design, supervision, experimentation, data analysis, and manuscript writing

Corresponding author

Publication VII

Acute coronary syndrome is associated with a substantial change in the platelet lipidome

Tobias Harm: performing data acquisition, experiments, experimental/statistical analysis and interpretation, writing manuscript;

Alexander Bild: performing blood sampling, clinical data acquisition;

Kristina Dittrich: performing UHPLC-ESI-QTOF-MS/MS protocols, data acquisition and processing;

Andreas Goldschmied: performing blood sampling, clinical data acquisition;

Jeremy Nestele: performing blood sampling, clinical data acquisition;

Madhumita Chatterjee: revision and critical assessment of the manuscript;

Xiaoqing Fu: performing UHPLC-ESI-QTOF-MS/MS protocols, data acquisition and processing;

Kyra Kolb: performing in vitro platelet function analysis;

Tatsiana Castor: assessment of clinical data and manuscript revision;

Oliver Borst: assessment of clinical data and manuscript revision;

Tobias Geisler: assessment of clinical data and manuscript revision;

Dominik Rath: performing clinical data acquisition, statistical analysis and manuscript writing;

Prof. Dr. Michael Lämmerhofer

Supervision of UHPLC-ESI-QTOF-MS/MS measurements and critical manuscript revision;

Prof. Dr. Meinrad Gawaz

Conceptual design, data interpretation, writing and revising manuscript

Corresponding author

Publication VIII

Statin Treatment Is Associated with Alterations in the Platelet Lipidome

Note: Contributions of the authors and other co-authors were not included here (except Xiaoqing Fu, Michael Lämmerhofer and Meinrad Gawaz).

(Tobias Harm, Moritz Frey, Kristina Dittrich, Andreas Goldschmied, Anne-Katrin Rohlf-ing, Xiaoqing Fu, Adrian Brun, Tatsiana Castor, Dominik Rath, Karin Müller, Michael Lammer-hofer, Meinrad Gawaz)

Xiaoqing Fu

Lipidomics analysis

Confirmation of the side chain composition of mid-chain PC (MCPC)

Prof. Dr. Michael Lämmerhofer

Supervision of lipidomics analysis

Discussion of results and interpretation

Proofreading and editing of the manuscript

Prof. Dr. Meinrad Gawaz

Conceptual design, data interpretation, writing and revising manuscript

Corresponding author

V. List of oral presentation

ANAKON 2023, April 11-14, 2023, Vienna, Austria.

Advanced unified monophasic lipid extraction protocol with wide coverage on the polarity scale optimized for large-scale untargeted clinical lipidomics analysis of platelets.

Xiaoqing Fu, Michael Lämmerhofer

VI. List of poster presentation

Recent Developments in Pharmaceutical Analysis (RDPA 2021), September 5-8, 2021, Modena, Italy.

Evaluation of common lipid extraction methods and cell disruption methods for untargeted lipidomic study in platelets.

Xiaoqing Fu, Michael Lämmerhofer

50th International Symposium on High Performance Liquid Phase Separations and Related Techniques (HPLC 2022), June 18-23, 2022, San Diego, USA.

Enantioselective UHPLC-MS/MS method based on 1.6 μm particle polysaccharide column for chiral separation of 3-hydroxyfatty acids and its application for the analysis of platelet and plasma samples.

Xiaoqing Fu, Zhanjian Xu, Michael Lämmerhofer

17th International Symposium on Hyphenated Techniques in Chromatography and Separation Technology (HTC-17), January 26-28, 2022, Ghent, Belgium.

Advanced unified monophasic lipid extraction protocol optimized for large-scale untargeted clinical lipidomics analysis.

Xiaoqing Fu, Madhumita Chatterjee, Meinrad Gawaz, Michael Lämmerhofer

51th International Symposium on High Performance Liquid Phase Separations and Related Techniques (HPLC 2023), June 18-22, 2023, Düsseldorf, Germany.

Advanced unified monophasic lipid extraction protocol with wide coverage on the polarity scale optimized for large-scale untargeted clinical lipidomics analysis of platelets.

Xiaoqing Fu, Michael Lämmerhofer

4th International Symposium "Platelets" 2022, Würzburg, Germany, June 23-25

Platelet lipidomics profiling in a large-scale clinical cohort of CAD patients.

Kristina Dittrich, Xiaoqing Fu, Adrian Brun, Meinrad Gawaz, Tobias Geisler, Madhumita

Chatterjee, Michael Lämmerhofer

5th "Novel Concepts in Innate Immunity" (NCII) conference, Tübingen, Germany, May 31-june 02.

Xiaoqing Fu, Alba Bruns, Jan Zamal, Tamam Bakchoul, Michael Lämmerhofer, Madhumita Chatterjee

VII. Abbreviations

12-HHT	12-Hydroxyheptadecatrienoic acid
12-KHT	12-keto-heptadecatrienoic acid
3-OH-FAs	3-Hydroxy fatty acids
AA	Arachidonic acid
AAPS	American Association of Pharmaceutical Scientists
ACN	Acetonitrile
ACP	Acyl carrier protein
ACS	Acute coronary syndrome
ADC	Analog-to-digital
ADP	Adenosine diphosphate
AIF	All-ion fragmentation
ALA	Alpha-linolenic acid
APCI	Atmospheric pressure ionization
BCAAs	Branched chain amino acids
BCFA	Branched chain fatty acids
BHA	Butylated hydroxyanisole
BHT	Butylated hydroxytoluene
B-MIS	Best-matched internal standard
BMP	Bis(monoacylglycerol)phosphate
CAD	Coronary artery disease
CAR	Acylcarnitine
CCMN	Cross-contribution compensating multiple standard normalization
CCS	Collision cross section
CCS	Chronic coronary syndrome
CE	Cholesterol ester
CE	Collision energy
CEM	Continuous electron multiplier
$CHCl_3$	Chloroform
CID	Collision-induced dissociation
CL	Cardiolipins
CoA	Coenzyme A
COX	Cyclooxygenases
CV	Coefficient of variation
CVD	Cardiovascular diseases
CYP450	Cytochrome P450 monooxygenases
DB	Double bond
DC	Direct current
DCM	Dichloromethane
DDA	Data-dependent acquisition
DG	Diacylglycerol
DGLA	Dihomo-gamma linolenic acid
DGLA	Dihomo-γ-linolenic acid

DHA	Docosahexaenoic acid
DIA	Data-independent acquisition
DiHETrE	Dihydroxyeicosatrienoic acid
DiHODE	Dihydroxyoctadeca(di)enoic acid
DiHOME	Dihydroxyoctadeca(mono)enoic acid
DP	Declustering potential
DTS	Dense tubular system
EPA	Eicosapentaenoic acid
EpDPE	Epoxyedocosapentaenoic acid
EpETE	Epoxyeicosatetraenoic acid
EpODE	Epoxyoctadeca(di)enoic acid
EpOME	Epoxyoctadeca(mono)enoic acid
EpTrE	Eicosatrienoic acid
EQA	External quality assessment
ESI	Electrospray ionization
FA	Fatty acyls
FAME	Fatty acid methyl esters
FAO	Fatty acid oxidation
FAS	Fatty acid synthase
FATPs	Fatty acid transport protein
FDA	U.S. Food and Drug Administration
FT-ICR	Fourier transform ion cyclotron resonance
GC	Gas chromatography
GL	Glycerolipids
GlcA	Glucuronic acid
GlcNAc	N-acetylglucosamine
GP	Glycerophospholipids
GP	Glycoproteins
H_2O	Water
HDoHE	Hydroxydocosahexaenoic acid
HEPE	Hydroxyeicosapentaenoic acid
HETE	Hydroxyeicosatetraenoic acid
HETrEs	Hydroxyeicosatrienoic acid
Hex	Hexose
HILIC	Hydrophilic interaction liquid chromatography
HODE	Hydroxyoctadecadienoic acid
HpDoHE	Hydroperoxydocosahexaenoic acid
HpETE	Hydroperoxyeicosatetraenoic acid
HRMS	High resolution mass spectrometry
HSCCC	High-speed counter-current chromatography
IDA	Information dependent acquisition
IEC	International Electrotechnical Commission
IP_3	Inositol-1,4,5-trisphosphate
IPA	Isopropanol

IS	Internal standard
ISO	International standardization organization
IUPAC-IUBMB	International Union of Pure and Applied Chemistry
LA	Linoleic acid
LC	Liquid chromatography
LCAD	Long-chain acyl-coenzyme A dehydrogenase
LCFA	Long-chain fatty acids
LC-HRMS	Liquid chromatography coupled to high resolution mass spectrometry
LC-MS	Liquid chromatography coupled with mass spectrometry
LDL	Low density lipoprotein
LIPID MAPS	Lipid Metabolites and Pathways Strategy
LIT	Linear ion trap
LLE	Liquid-liquid extraction
LLOQ	Low limit of quantification
LMSD	LIPID MAPS Structure Database
LOD	Limit of detection
LOESS	Locally (weighted) estimated scatterplot smoothing
LOQ	Limit of quantification
LOX	Lipoxygenases
LPA	Lysophosphatidic acid
LPC	Lysophosphatidylcholine
LPE	Lysophosphoethanolamine
LSI	Lipidomics Standards Initiative
LTs	leukotrienes
MALDI	Matrix-assisted laser desorption ionization
MCAD	Medium-chain acyl-coenzyme A dehydrogenase
MCFA	Medium-chain fatty acids
MCHAD	Medium-chain-3-hydroxyacyl-coenzyme A (CoA) dehydrogenase
MCKAT	Medium-chain 3-ketoacyl-CoA thiolase
MCP	Microchannel plate
MC-PC	Medium-chain phosphatidylcholine
ME	Matrix effect
MeOH	Methanol
MMC	MeOH/MTBE/$CHCl_3$
MMIPA	MeOH/MTBE/IPA
MRM	Multiple reaction monitoring
MS	Mass spectrometry
MS/MS	Tandem mass spectrometry
MTBE	Methyl tert-butyl ether
MTP	Mitochondrial trifunctional protein
MUFA	Monounsaturated fatty acids
NADPH	Nicotinamide Adenine Dinucleotide Phosphate
NIST SRM 1950	National Institute of Standards and Technology Standard Reference Material 1950

NMR	Nuclear magnetic resonance
NOMIS	Normalization using optimal selection of multiple internal standards
NPLC	normal phase liquid chromatography
OxoETE	Oxo-eicosatetraenoic acid
oxPLs	Oxidized phospholipids
PA	Phosphatidic acid
PC	Phosphatidylcholine
PCA	Principal component analysis
PC-O	Ether-linked phosphatidylcholine (alkyl-linkage)
PC-P	Ether-linked phosphatidylcholine (alkenyl-linkage)
PDE	Prostaglandin E series
PE	Phosphoethanolamine
PE	Process efficiency
PGD	Prostaglandin D series
PGF1α	Prostaglandin F1α series
PGI	Prostaglandin I series
PIP_2	Phosphatidylinositol-4,5-bisphosphate
PK	Polyketides
PKC	Protein kinase C
PLA2	phospholipase A2 series
PLA_2	Phospholipase A2
PLCγ	Phospholipase Cγ
ppm	Parts per million
PR	Prenol lipids
PS	Phosphatidylserine
PT	Proficiency testing
PUFA	Polyunsaturated fatty acids
PUFA-PC	Polyunsaturated fatty acid phosphatidylcholine
QC	Quality control
QqQ	Triple quadrupoles
QTOF	Quadrupole-time-of-flight
QTrap	Quadrupole linear ion trap
RE	Extraction recovery
RF	Radio frequency
RF	Response factor
RPLC	Reversed phase liquid chromatography
RT	Retention time
RvD	Resolvins D series
RvE	Resolvins E series
S1P	Sphingosine-1-phosphate
SCAD	Short-chain acyl-coenzyme A dehydrogenase
SCFA	Short-chain fatty acids
SCHAD	Short-chain-3-hydroxyacyl-coenzyme A (CoA) dehydrogenase
SFA	Saturated fatty acids

SFC	Supercritical fluid chromatography
SL	Saccharolipids
SM	Sphingomyelin
SOPs	Standard operating procedures
SP	Sphingolipids
SPE	Solid-phase extraction
SRM	Selected reaction monitoring
ST	Sterol lipids
SVM	Support-vector-machine
SWATH	Sequential window acquisition of all theoretical fragment ion mass spectra
TDC	Time-to-digital
TG	Triacylglycerol
TOF	Time-of-flight
TP	Thromboxane receptor
TPP	Triphenylphosphonium
TPP	Three-phase partitioning
TriHOME	Trihydroxyoctadeca(mono)enoic acid
TXA	Thromboxane A series
TXB	Thromboxane B series
UHPLC	Ultrahigh performance liquid chromatography
ULOQ	Upper limit of quantification
VLCFA	Very long chain fatty acids
vWF	Von Willebrand factor

VIII. Introduction

1. Lipids

Lipids play an important role in energy storage, cell membrane structure and regulatory function, and cell signalling [1]. The historical origins of the term lipid can date back to hundred years ago while the word “Lipid” was first introduced in 1923 by a French pharmacologist and became the preferred term. General textbooks describe lipid as a fatty or waxy organic compound that is readily soluble in a nonpolar solvent but not in a polar solvent[2]. However, this simplified definition may mislead the understanding for lipid and underestimate the complexity and diversity of lipids. In order to harmonize and standardize the lipid classification, an international consortium Lipid Metabolites and Pathways Strategy (LIPID MAPS) was established by gathering experts in lipid research to unify the lipid definition, spearhead the lipid classification, standardize the methodologies for mass spectrometry analysis of lipids and provide the analysis tools for lipid research. According to the LIPID MAPS, lipids are defined as hydrophobic or amphipathic small molecules that may originate entirely or in part by carbanion-based condensations of thioesters (fatty acids, polyketides, etc. see Fig. 1A) and/or by carbocation-based condensations of isoprene units (prenols, sterols, etc. see Fig. 1A) [3], which is from the view of biochemists.

A

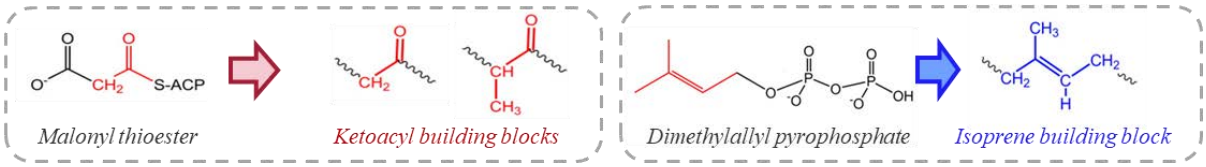

B

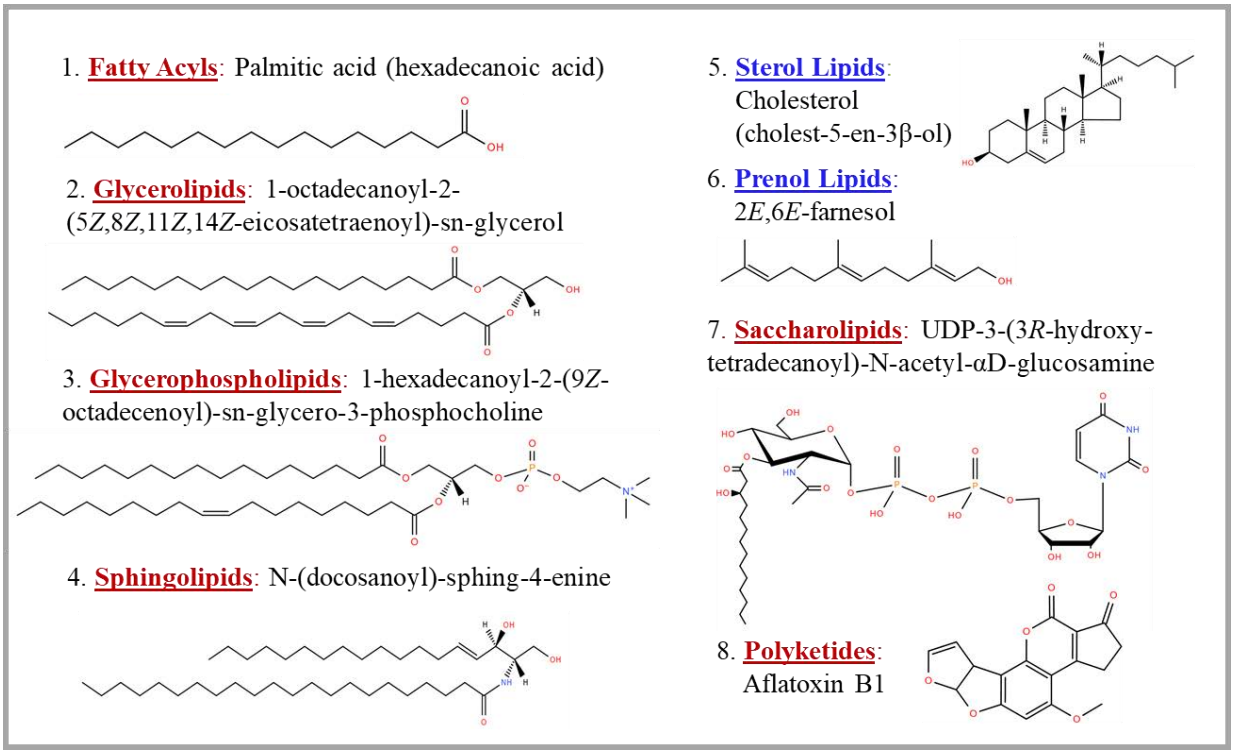

C

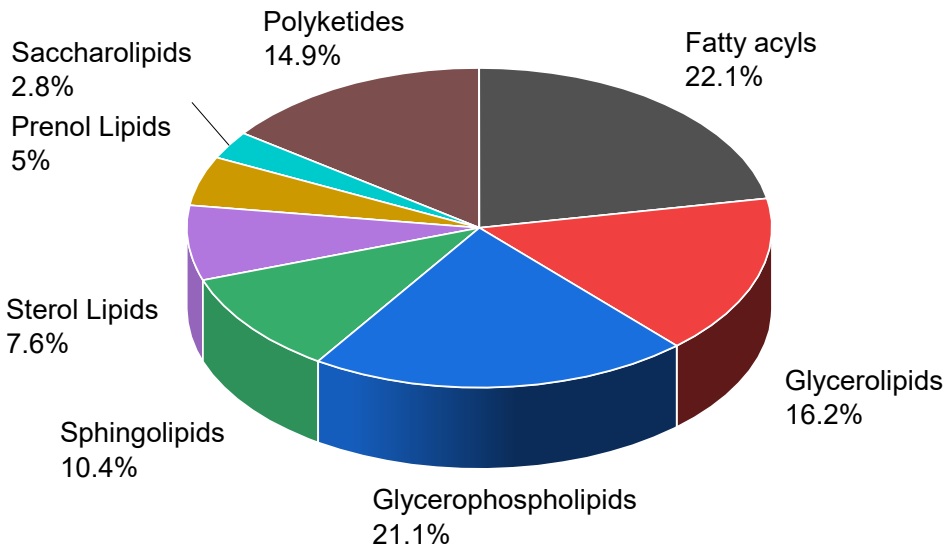

Figure 1 *A: Structure of ketoacyl and isoprene building blocks and examples for each unit. B: Eight main lipid categories according to LIPID MAPS with an example for each category. C: Distribution of Eight main lipid categories.*

1.1 Classification of lipids

The Lipid Classification System of LIPID MAPS is comprised of eight lipid categories[4-6], that is Fatty acyls (FA), Glycerolipids (GL), Glycerophospholipids (GP), Sphingolipids (SP), Sterol lipids (ST), Prenol lipids (PR), Saccharolipids (SL) and Polyketides (PK), each with its own subclassification hierarchy (Fig. 1). According to the LIPID MAPS® Structure Database (LMSD) [7], which is a relational database encompassing structures and annotations of biologically relevant lipids, 47949 (latest update in June 2023) unique lipid structures are included in the LMSD with Fatty acyls (FA, 22.05%), Glycerolipids (GL, 16.16%), Glycerophospholipids (GP, 21.06%), Sphingolipids (SP, 10.39%), Sterol Lipids (ST, 7.57%), Prenol Lipids (PR, 5.01%), Saccharolipids (SL, 2.33%) and Polyketides (PK, 14.95%), which comprises the world's largest lipid-only database [7] (Fig. 1B).

As a result of the diversity and complexity of the lipids that have been discovered over the last three decades, a systematic and unified naming scheme was required to simplify the lipid research and reporting for chemists, biologists, and biomedical researchers. The nomenclature proposal by LIPID MAPS [8, 9] follows the existing IUPAC-IUBMB (International Union of Pure and Applied Chemistry) rules [10] closely with the recently discovered lipid classes included.

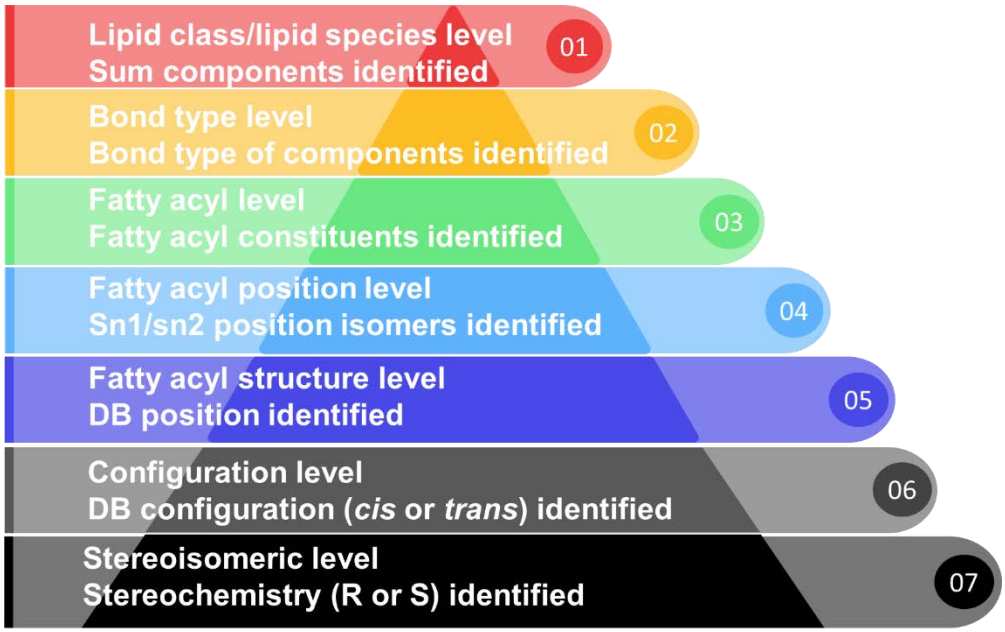

Figure 2 *Seven levels for lipid identification and the rules for each level.*

There are different levels for lipid nomenclature depending on the structural resolution (Fig. 2). The basic level (Level 1) with lipid category or class identification usually summarize only the structure specific lipid class abbreviation heads with the sum components based on their mass including carbon number and double bonds (DB) number. When structural ambiguities are present (e.g., bond type, hydroxyl groups, branched chains) and recognized, the level 2 structural resolution can be realized. Taking ether PC 34:3 as an example (Fig. 3), with low resolution MS instrument only the PC class can be confirmed according to the m/z (whether PC O-34:3 (m/z= 741.567) or PC 33:3 (m/z= 741.531) is unknown). If an ether bond can be recognized by high resolution MS instrument, the level 2 bond type level PC O-34:3 can be confirmed [8]. Since lipids from the same class or subclass contain various isomers including positional isomers (e.g. fatty acyl chains with opposite position in sn1 and sn2, different DB position, fig. 3a) and configurational isomers (e.g. geometric isomers with cis or trans, stereo-isomers with R or S enantiomers, Fig. 3a), further levels of annotation are required when the mentioned structures can be identified through advanced MS approaches for a standardized, practical and concise reporting of data. When fragments of fatty acyls are observed which means the fatty acyl chains are recognized, the structure should be indicated as PC O-16:1_18:2 (Fig. 3c, level 3). It is worth to mention that the underscore sign '_' between fatty acyl chains means that the sn1 or sn2 position of the fatty acyl chains are unknown, once the position of sn1 and sn2 of fatty acyl chains are identified, the structure can be further annotated as PC O-16:1/18:2 (Fig. 3c, level 4). Here the sn1 position of fatty acyl chain is written on the left of the slash sign "/" while sn2 position on the right side. What is more, it should be mentioned that there are two types of ether bond, one is simple ether bond without any neighbouring double bonds next to the oxygen atom (Letter O) and another one is the vinyl linkage with double bond directly next to the oxygen atom (Letter P) (see Fig. 3a and 3b). If the types of the linkage can be identified, then the structure can be further annotated as PC O- (belongs to subspecies 1-alkyl,2-acylglycerophosphocholines) or PC P- (belongs to subspecies 1-(1Z-alkenyl),2-acyl-glycerophosphocholines, well known as plasmalogens). Furthermore, when the DB position is identified, the structure can be summarized as PC O-16:1 (9)/18:2 (9,12) (Fig. 3c, level 5). Meanwhile, if the configurations of the DB cis or trans are known as well, a more detailed annotation can be used as PC O-16:1 (9Z)/18:2 (9Z,12Z) (Fig. 3c, level 6). Finally, level 7 defines the stereochemistry of the structure with chiral center, which is namely PC O-16:1 (9Z)/18:2 (9Z,12Z) [R]. This is the general rules for lipid nomenclature. Each lipid category (8 main categories in LIPID MAPS) has their own specific rules based on the structure, which

were summarized in Table. 1 [8] (Prenol Lipids (PR), Saccharolipids (SL) and Polyketides (PK) are excluded since they are not the main research category in this thesis).

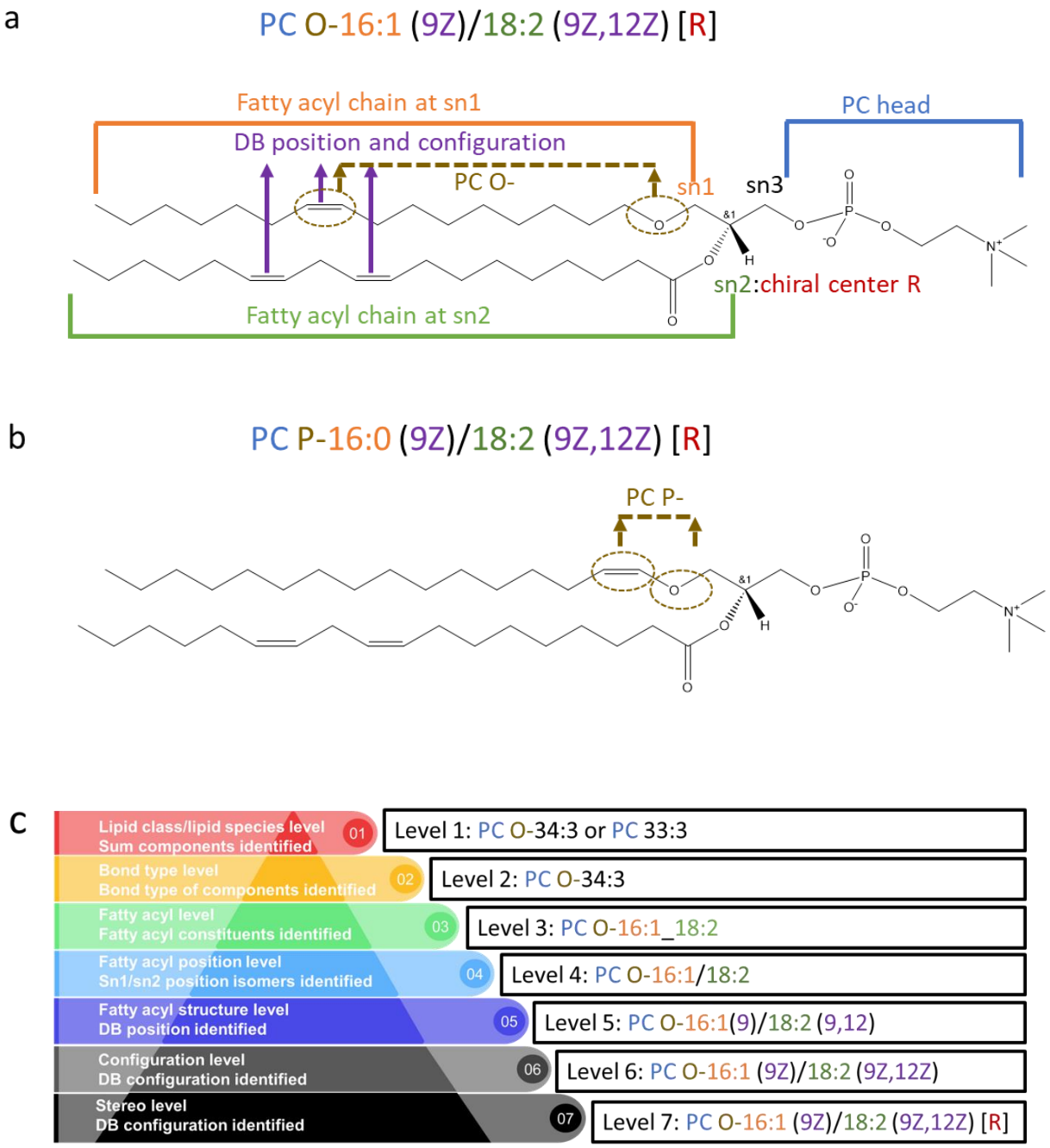

Figure 3 *A: Structure of 1-(9Z-hexadecenyl)-2-(9Z,12Z-octadecadienoyl)-sn-glycero-3-phosphocholine. B: Structure of another type of ether phosphatidylcholines with a different ether linkage (PC (P-18:0/20:4)) from A (PC (O-18:0/20:4)). C: Seven levels of lipid identification based on the example of analyte with m/z= 741.5 with subclass of phosphocholine.*

Table 1 *Rules for lipid nomenclature[8].*

FATTY ACYLS (FA)	**GLYCEROLIPIDS (GL)**	**GLYCEROPHOSPHOLIPIDS (GP)**	**SPHINGOLIPIDS (SP)**	**STEROLS (ST)**
Lipid class abbreviation number of C-atoms: number of double bonds	Lipid class abbreviation number of C-atoms: number of double bonds	Lipid class abbreviation number of C-atoms: number of double bonds	Lipid class abbreviation number of C-atoms: number of double bonds of the sphingoid base (left side of /) separated by a slash from the number of carbons: number of double bonds of the N-linked fatty acid (right side of /)	Lipid class abbreviation number of C-atoms: number of double bonds
Functional groups (OH for hydroxyl group, O for keto group and Me for methyl branch): 1. after the number of double bonds (DB) separated by an underscore: DB_OH 2. order of functional groups when more than one functional groups: Double bonds_OH_O_Me	Fatty acyl chains: Separator _: sn-position of the fatty acids is not known. Separator /: sn-position of fatty acids is proven. (order sn-1/ sn-2/ sn-3 for GL; sn-1/ sn-2 or sn-2/ sn-3 for GP); no FA linked 0:0	Fatty acyl chains: Separator _: sn-position of the fatty acids is not known. Separator /: sn-position of fatty acids is proven. (order sn-1/ sn-2/ sn-3 for GL; sn-1/ sn-2 or sn-2/ sn-3 for GP); no FA linked 0:0	Hydroxyl groups in sphingoid base: 1. the number of OH groups in sphingoid base is known (m for mono, d for di, t for tri and e for tetra), in front of the number of carbons of sphingoid base (Cer d18:1/18:0) 2. the position of OH is known: after the DB of sphingoid base (Cer d18:1 (1OH, 3OH)/18:0)	Functional groups: at least one hydroxyl group at position 3, after the number of double bonds separated by an underscore and followed by the number of groups if more than one (ST 24:1_OH3)
Double bond position: a number followed by geometry (Z for cis, E for trans) after DB	Bond types: in front of the sum of C-atoms O = proven O-alkyl-bond P = proven O-alk-1-enyl-bond More than one “non”-ester bond: d for di, t for tri and e for tetra	Bond types: in front of the sum of C-atoms O = proven O-alkyl-bond P = proven O-alk-1-enyl-bond More than one “non”-ester bond: d for di, t for tri and e for tetra	Other rules concerning the DB position and configurations are the same as for FA	Case of bile acids: shorthand notation is prefaced by A to indicate an acid (ST A24_OH)
(*R*) and (*S*) configurations are preferred for side-chain stereochemistry and are given in italics in parentheses	Other rules concerning the DB position and configurations are the same as for FA	For BMP and CL classes, the sn-position order: sn-2/ sn-3/ sn-2 ′/ sn-3 ′ and sn-1/ sn-2/ sn-1 ′/ sn-2 ′ (CL 18:1/18:2/18:2/18:2 sn-1/ sn-2/ sn-1 ′/ sn-2 ′)		Conjugating groups: 1. taurine (T) or glycine (G) conjugated to the carboxylic acid group of bile acids through an amide bond (ST A24_OH_T) 2.sulfuric acid (S) conjugated to a hydroxyl group through an ester bond (ST 27:1_OH_O_S) 3.glucuronic acid (GlcA), N-acetylglucosamine (GlcNAc) and hexose (Hex) sugars linked to a hydroxyl group through an acetal linkage (ST 27:1_OH2_S_GlcA)
		Other rules concerning the DB position and configurations are the same as for FA		

1.2 Fatty acid and its oxidation

Fatty acids (FAs) as a physiologically important class of molecules which belong to the main category fatty acyls play an important role in energy storage, membrane structure, and various signaling pathways [11]. As one of the most important bioactive molecules, they are often used as an entry point for the study of lipid metabolism. Fatty acids can be classified in different ways: (1) Carbon chain length (2) Saturation degrees (3) linear and branched. According to carbon chain length the FAs can be classified into short-chain fatty acids (SCFA, C≤5), medium-chain fatty acids (MCFA, C6-C12), long-chain fatty acids (LCFA, C13-C21) and very long chain fatty acids (VLCFA, C≥22)[12]. While based on the saturation degree, FAs can be divided into saturated fatty acids (SFA, no double bonds C=C), monounsaturated fatty acids (MUFA, single double bond C=C) and polyunsaturated fatty acids (PUFA, two or more than two double bonds C=C). When considering the linear or branched state, FAs can be further classified into straight chain fatty acids (SCFA) and branched chain fatty acids (BCFA) (Fig. 4).

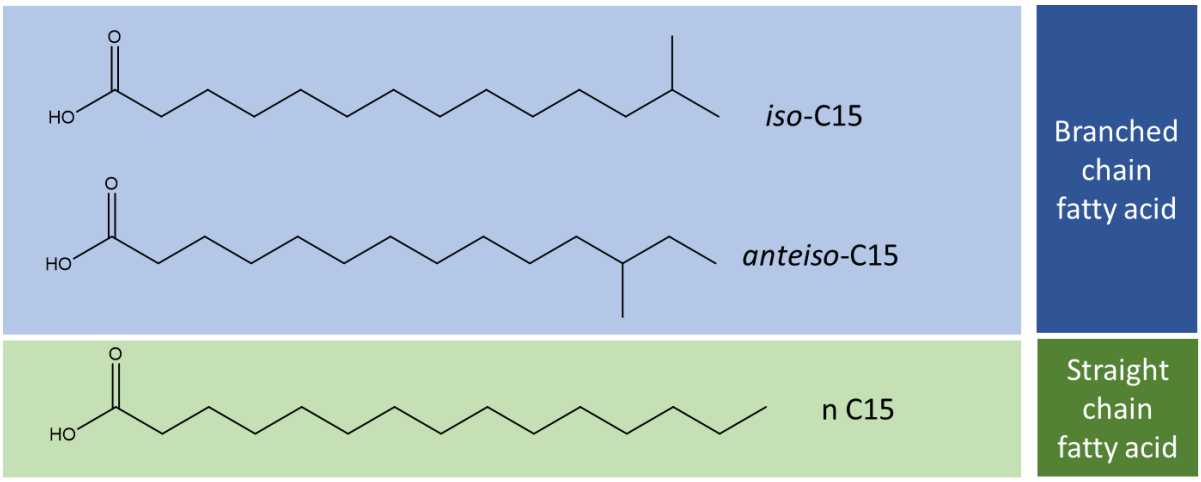

Figure 4 *Structure of branched chain fatty acids (including isomethyl and anteisomethyl branched chain) and straight chain fatty acid with total carbon chain length C=15.*

1.2.1 Branched chain and straight chain fatty acids

Both straight chain (SCFA) and branched chain fatty acids (BCFA) have their unique functions in nature. In mammalian cells, SCFA are the most common and abundant fatty acids, especially with carbon chain length from C14-C24. Among the SCFA, even chain fatty acids e.g. FA 16:0 (Palmitic acid), FA 18:0 (Stearic acid) and FA 20:0 (Arachidic acid) are normally the most abundant in human plasma or platelets while odd-chain fatty acids e.g. FA 15:0 (Pentadecylic acid) and FA 17:0 (Margaric acid) are mainly produced by some microorganisms [13, 14]. The

fatty acid biosynthesis (Fig. 5) can be simply described as (I) Transfer: the acetyl group is transferred to a pantothenate group of acyl carrier protein (ACP), a region of the large mammalian fatty acid synthase (FAS) protein. Then, another transfer from the pantothenate of the ACP to cysteine sulfhydral (–SH) group on FAS happens. (II) Elongation: the pantothenate–SH group accepts a malonyl group from malonyl-CoA and then releases the CO2 group to generate a 4-carbon β keto acid derivative. (III) Reduction: a reduction of acetoacetyl-Enz. by Nicotinamide Adenine Dinucleotide Phosphate (NADPH) to D-β-hydroxybutyryl-Enz. takes place. (IV) Dehydration: β-hydroxy acid derivative removes one molecule H_2O to form a tans-double bond. (V) Reduction: a reduction happens again by NADPH to form the saturated fatty acid [15, 16]. The cycle of transfer, elongation, reduction, dehydration, and reduction continues until palmitic acid (FA 16:0) is made.

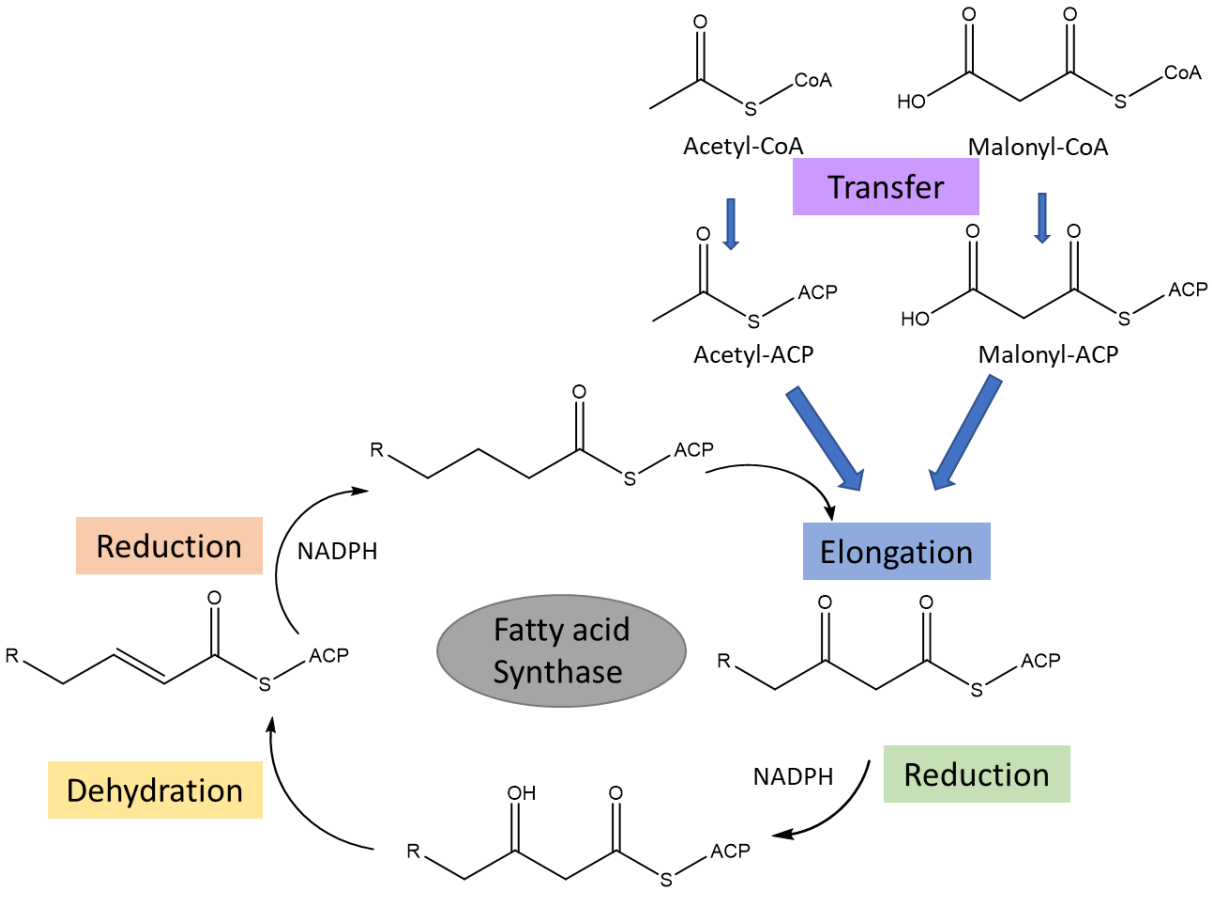

Figure 5 *Biological pathway of fatty acid synthesis starting from transfer, elongation, reduction, dehydration and reduction.*

Unlike SCFA, BCFA are most often found in bacteria. They are commonly saturated FAs substituted with one (mono-) or more (di-/poly-) methyl-branch(es) on the carbon chain with either an iso structure where the branch point is on the penultimate carbon atom (i.e., one from

the end) or an anteiso structure where the branch point is located on the antepenultimate carbon atom (i.e., two from the end) (Fig. 4). The monomethyl BCFAs are typically derived from branched chain amino acids (BCAAs) including valine, leucine, and isoleucine [17]. In the common biosynthetic pathways, the BCAAs are firstly transaminated to α-ketoacids and then decarboxylated and converted into branched short-chain carboxylic acid coenzyme A thioesters and finally the products are elongated by BCFA synthetase, with malonyl-CoA as the chain extender, to form the iso- and anteiso-BCFAs [18]. The iso BCFAs with even chain length (total carbon number) for example iso-14:0 and iso-16:0 are derived from valine while with odd chain length (iso-15:0, iso-17:0) from leucine. In contrast, anteiso BCFAs are derived from isoleucine. In addition to the most common iso or anteiso methyl-position, some other methyl-positions were also found in nature for example 10-methyl-hexadecanoic acid (FA 16:0;10Me), 11-methyl-octadecanoic acid (FA 18:0;11Me) in the sponge Verongia aerophoba [19] and also 2, 3, 4, 6-monomethyl-FAs from C7-C12 were the main BCFAs component in the preen gland of the fulmar [20]. The biosynthesis of these kind of BCFAs remain to a large extent unknown, but most probably the structures was produced by methylmalonyl-CoA instead of malonyl-CoA to insert the methyl group and for the elongation of the fatty acyl chain.

1.2.2 Oxidized fatty acids

The oxidation of fatty acids is one of the most important fatty acid metabolic pathways which belongs to catabolic processes that generate energy and results in the formation of different kinds of bioactive fatty acid derivatives. There are different fatty acid oxidation (FAO) pathways that occur in multiple regions of the cell, namely, the β-oxidation which happens either in mitochondria or in peroxisome, α-oxidation in peroxisome, and ω-oxidation occurring in the endoplasmic reticulum. Mitochondrial β-oxidation remains the predominant pathway for fatty acid degradation [21]. For substrates which cannot be oxidized by the mitochondrial FAO pathway, e.g. very long chain fatty acids or branched chain fatty acids, the other pathways will compensate [22].

The fatty acid derivatives 3-Hydroxy fatty acids (3-OH-FAs) are mainly formed in the hydration step during β-oxidation of saturated straight-chain fatty acids. With the aid of the fatty acid transport protein (FATPs), the long-chain fatty acids are able to enter the human cell membrane and are activated to acyl-CoA. As the next step, the acyl-CoA is transported through the mitochondrial membrane into the mitochondrial matrix with aid of carnitine shuttle and ready for fatty acid β-oxidation after back-convesion into acyl-CoAs. The complete fatty acid oxidation undergoes four repeated biochemical reactions: dehydrogenation, hydration, second

dehydrogenation, and thiolytic cleavage. From the perspective of acyl-CoA ester, it is firstly dehydrogenated by acyl-CoA dehydrogenase to produce trans-2-enoyl-CoA, resulting in the formation of a double bond in the saturated carbon chain. Then the enoyl-CoA hydratase catalyzes and hydrates the trans-2-enoyl-CoA into 3-L-hydroxyacyl-CoA, with the addition of a hydroxyl group on the β-carbon as the second step. In the third step, the formed 3-L-hydroxyacyl-CoA is catalyzed by the corresponding 3-L-hydroxyacyl-CoA dehydrogenase and yields 3-ketoacyl-CoA ester. Finally, a thiolytic cleavage takes place in the 3-ketoacyl-CoA, leading to a two-carbon shortened acyl-CoA ester and an acetyl-CoA. Each cycle releases an acetyl-CoA unit from the initial acyl-CoA ester, and such cycle will repeat until the fatty acid acyl-CoA ester is decomposed into several molecules of acetyl-CoA [22, 23] (Fig. 6). 3-OH-FAs are important in various biological systems, as metabolites of fatty acid oxidation, constituent of lipid A which is part of endotoxins of Gram-negative bacterial outer membranes [24], as side chains of lipopeptides and other natural products [25, 26]. What is more, they also have significant relevance as diagnostic biomarkers of several inherited metabolic diseases [27].

Another group of important fatty acid metabolites are oxylipins which is a family of oxygenated natural products that are formed from dioxygen-dependent oxidation of fatty acids pathways. Oxylipins are oxidized polyunsaturated fatty acids (PUFAs) formed either by participation of enzymes or non-enzymatic auto-oxidation [28, 29]. There are three main families of enzymes which are involved in the *in-vivo* production of oxylipins, that is COX enzymes (cyclooxygenases), LOX enzymes (lipoxygenases), and CYP450 (cytochrome P450 monooxygenases) [30]. Each family contains different forms of enzymes and distinct specificities, e.g. COX with 5-, 12- and 15-COX, LOX with LOX-1 and LOX-2 and CYP450 as a large family of enzyme with CYP2J and CYP2C. The most common PUFA substrates for these enzymes are linoleic acid (LA, FA 18:2), alpha-linolenic acid (ALA, FA 18:3), eicosapentaenoic acid (EPA, FA 20:5), docosahexaenoic acid (DHA, FA 22:6), dihomo-gamma linolenic acid (DGLA, FA 20:3) and arachidonic acid (AA, FA 20:4). The PUFAs derived oxylipins by different enzymes are summarized in Table. 2.

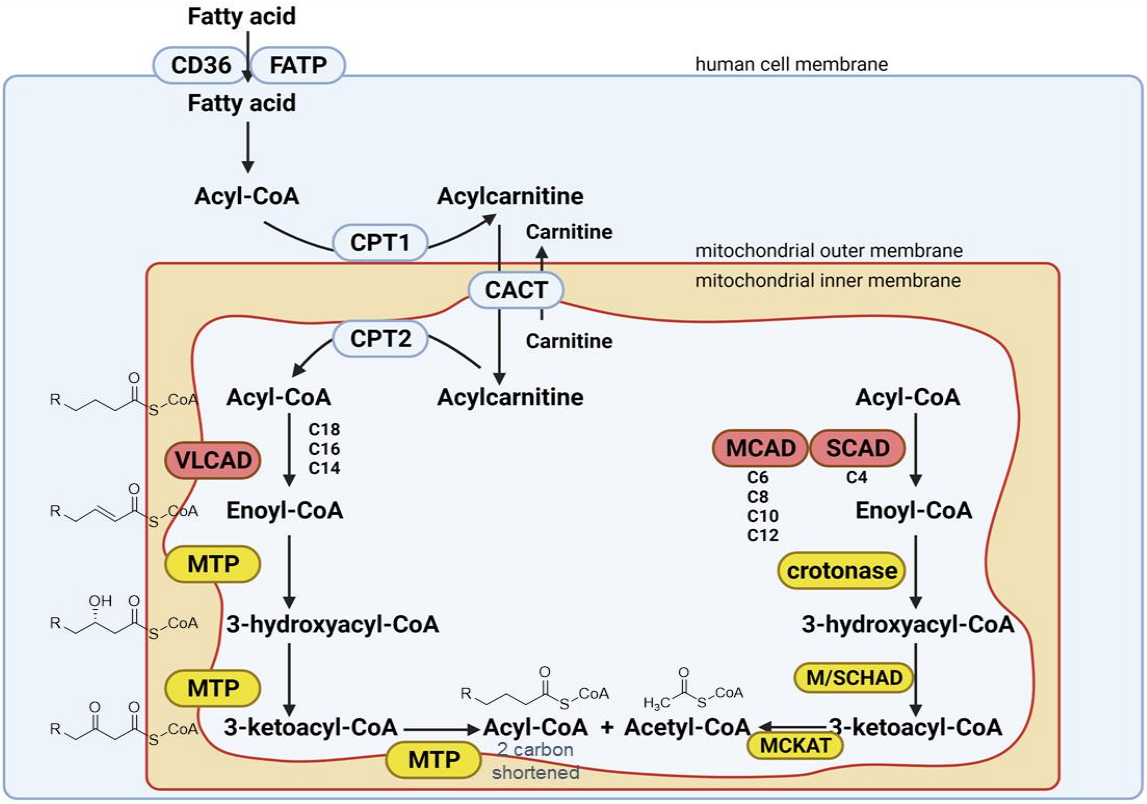

Figure 6 *Mitochondrial fatty acid β-oxidation in humans covering different carbon chain length (adapted with permission from [23]. Copyright © 2010 John Wiley & Sons, Ltd.). Recreated in BioRender.com.*

Most of the oxylipins are very sensitive and unstable. Typically, oxylipins are not stored in tissues but are formed on demand by liberation of PUFAs from membrane phospholipids with the aid of enzyme cytosolic phospholipase A2 (PLA2) [31]. Also, they exist in nature with a very low concentration, which makes the analysis of oxylipins challenging [32]. However, they are highly bioactive and play numerous biological roles [31]. Oxylipins typically act in an autocrine (a form of cell signaling in which a cell secretes a hormone or chemical messenger that binds to autocrine receptors on that same cell, leading to changes) in the cell or paracrine manner (a type of cellular communication in which a cell produces a signal to induce changes in nearby cells, altering the behavior of those cells) [33]. In general, oxylipins derived from omega-6 fatty acids are more pro-inflammatory while from omega-3 fatty acids more anti-inflammatory [34]. Recognizing the fact that the exact mechanisms of action or even their biological roles remain still unknown, the topic on the research of oxylipins remains attractive and challenging, but of high interests.

Table 2 *Polyunsaturated fatty acids (PUFAs) derived oxylipins by different enzymes.*

PUFAs	Enzymes	Products	Further products	
DGLA (FA 20:3)	**COX**	PGD1		
		PDE1		
		PGF1α		
		TXA1	TXB1	
	LOX	HETrEs		
AA (FA 20:4)	**COX**	PGD2		
		PGE2		
		PGI2	6-keto-PGF1α	
		PGF2α		
		TXA2	TXB2	
		12-HHT	12-KHT	
	LOX	HpETE	HETEs	OxoETEs
			Leukotrienes (series4)	Lipoxins (series4)
	CYP450	EpTrEs	DiHETrEs	
		HETEs		
EPA (FA 20:5)	**COX**	PGD3		
		PDE3		
		PGF3α		
		TXA3	TXB3	
	LOX	HpEpEs	HEPEs	
			RvEs	
			Leukotrienes (series5)	Lipoxins (series5)
	CYP450	HEPEs		
		EpETEs	DiHETEs	
DHA (FA 22:6)	**LOX**	HpDoHEs	HDoHEs	
			RvD, Maresins, Protectins	
	CYP450	EpDPEs	DiHDPEs	
		HDoHEs		
LA (FA 18:2)	**LOX**	HODEs	TriHOMEs	
	CYP450	EpOMEs	DiHOMEs	
ALA (FA 18:3)	**LOX**	HOTrEs		
	CYP450	EpODEs	DiHODEs	

2. Introduction to lipidomics

The concept “lipidome” was firstly introduced, before the analytical approach of “lipidomics” emerged, as the complete lipid profile within a cell, tissue, organism, or ecosystem [35]. Until 2003 the concept “lipidomics” was first defined by Han and Gross through a comprehensive mass spectrometric approach for the study of lipids from biological samples on a large scale [36]. Lipidomics which is a global approach for lipid analysis involved in the large-scale study of pathways and networks of cellular lipids in biological systems is one of the most recent research areas amongst omics and is the subset of metabolomics [37]. Although, it attracts lots of interests from biological and analytical scientists to apply this powerful tool for the study on cardiovascular disease, obesity, atherosclerosis, and cancer, among others. As a relatively recent research field, the analytical platform of lipidomics is highly reliable on the advanced technologies such as separation technology (e.g. liquid chromatography) [38, 39], mass spectrometry (MS) [40, 41] or nuclear magnetic resonance (NMR) spectroscopy [42, 43].

2.1 MS in lipidomics

Mass spectrometry (MS) is a technique dedicated for structural elucidation and quantification based on the mass to charge ratio (*m/z*) of individual analytes [44]. It is widely used in omics research due to the high selectivity and sensitivity. Nowadays, different MS based lipidomics approaches including shortgun lipidomics and LC-MS based lipidomics have become the gold-standard methods for lipidomics research. A mass spectrometer generally consists of three main parts: an ion source, a mass analyzer and a detector. Fundamental aspects of MS will be introduced in the following parts.

2.1.1 Ionization

The ionization takes place in the ion source where gas-phase ions can be generated in order to allow their subsequent separation in a mass analyzer and finally detection of the separated ions by various principles. Different types of ion sources were introduced based on the property of analytes including electrospray ionization (ESI) which is the softest ionization for polar and ionic substances, atmospheric pressure ionization (APCI) which is for mid polar to less polar compounds, matrix-assisted laser desorption ionization (MALDI) that is predominately used for macromolecule analysis and in imaging MS approaches and so on [45].

ESI is the one utilized for the experimental work in this dissertation. In ESI, a solution containing analyte is introduced towards the source through a narrow needle that is held at an electric potential of several kV. An electrostatic field was formed by the high potential where the solution coming out from the needle is polarized and forms a Taylor cone at the tip. Multiply

charged droplets are released from the cone supported by the application of a nebulizer gas (mostly N_2 or synthetic air) to create a spray as initial droplets (in µm). In the next step, the solvent is evaporated from the droplets caused by high temperature produced in heaters and by the heater gas. As a result, the charged droplets get smaller with increased surface charge density until they reach the Rayleigh limit and then the droplets explode into several smaller droplets with lower surface charge density which is called Coulombic explosion. These processes repeat until all the solvent is evaporated and single molecular ions are generated (Fig. 7).

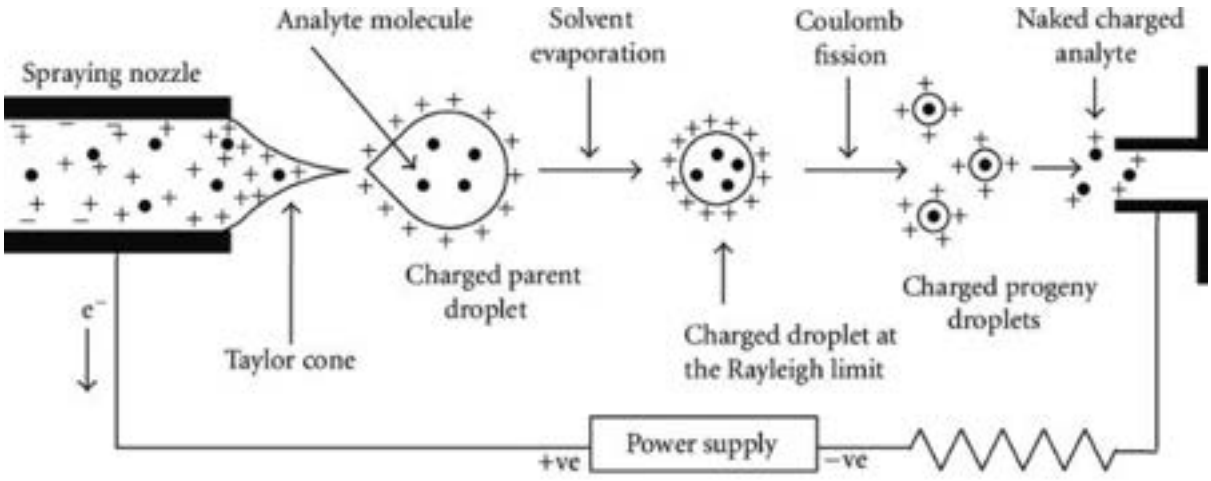

***Figure** 7 Scheme of the working principle of ESI[46].*

ESI usually yields [M+H] +, [M-H] - or adduct ions depending on the polarity, pH and modifier content in the solution (e.g. [M+NH4] +, [M+HCOO] -). It is widely used in lipidomics analysis because of the possibility of the ionization for almost all lipids from polar (acylcarnitine CAR, lysophosphatidylcholine LPC, lysophosphoethanolamine LPE and so on) to neutral lipids (cholesterol ester CE, triacylglycerol TG and so on) and even large molecules (e.g. Cardiolipins CL). However, the main limitation of ESI is the so-called matrix effect which is caused by the presence of co-eluting compounds in sample matrix during ionization of analyte resulting in ion enhancement or ion suppression.

2.1.2 Mass Analyzers

Mass analyzer is the next important compartment to separate the ions generated in the ion source based on their *m/z*. There are many types of mass analyzers based on different principles and construction, and therefore showing very different performance and can be applied for different research purposes. The most commonly employed mass analyzer by commercialized

instruments are quadrupole, ion trap, Fourier transform ion cyclotron resonance (FT-ICR), Orbitrap or time-of-flight (TOF) mass analyzers. There are several important analyzer characteristics: Mass resolving power, mass accuracy, mass range, acquisition speed and linear dynamic range [44, 47]. The mass resolving power describes the ability to distinguish two peaks with slight difference in *m/z*. The mass accuracy is the variance of measured *m/z* to the true *m/z*, which is usually reported as parts per million (ppm). The mass range is the range of *m/z* an analyzer could achieve, which is particular important for macromolecules. Acquisition speed refers to the time frame of the experiment and ultimately is used to determine the number of spectra per unit time that can be generated while the linear dynamic range is the range over which ion signal is linearly responded to analyte concentration. The characteristics of mentioned mass analyzers are summarized in Table 3. Each analyzer type has its strengths and weaknesses. To compensate, two or more mass analyzers for tandem mass spectrometry (MS/MS) is often equipped in Mass spectrometers, e.g. triple quadrupoles (QqQ) or QTraps (combined quadrupoles and linear ion traps) which are commonly utilized for targeted and quantitative lipid studies, whereas QTOF (combined quadrupoles and TOF) and Orbitraps combined with quadrupoles or linear ion traps are widely used in untargeted lipidomics analysis.

Table 3 *Performance characteristics of typically used mass analyser[44, 48, 49].*

Mass analyzer	Resolving power*	Mass accuracy (ppm)	Acquisition speed (Hz)	Identification	Quantification
Quadrupole	1,000	100-1000	10-20	+	+++
LIT	10,000	50-100	10-30	++	+
TOF	40,000	2-50	10-100	++	++
Orbitrap	150,000	1-5	10-40	+++	++
FT-ICR	1,000,000	0.1-1	0.5-2	+++	++

* at m/z 1,000

2.1.2.1 Quadrupole

Quadrupole mass analyzers consist of four parallel rods with two positive and other two negative polarity, which is used to selectively stabilize or destabilize the paths of ions passing through a superimposed radio frequency (RF) and direct current (DC) quadrupole field created between four parallel rods. Ions are forced into a helical trajectory in the center of the quadrupole, for which only ions with one particular *m/z* have a stable trajectory based on a specific RF/DC setting. In dependence on the different combinations of RF/DC, distinct ions can be transmitted (Fig. 8A). When setting the DC with zero which is so-called RF-only mode [50],

the quadrupole acts as an “open” quadrupole with wide m/z transmission windows and is employed as ion guides or collision cells instead of mass filters.

A magnetically enhanced quadrupole mass analyzer includes an additional magnetic field, either applied axially or transversely to enhance the resolution and/or sensitivity [51, 52]. A common commercialized instrument applying the enhanced quadrupole mass analyzer is the triple quadrupole mass spectrometer (QqQ) where three consecutive quadrupole stages are included: (1) the first acting as a mass filter to transmit a precursor ion with specific *m/z* value to the second quadrupole; (2) the second acting as a collision chamber, wherein the precursor ion can be degraded into fragments. (3) the third acting as a mass filter as well, to transmit a particular fragment ion to the detector.

2.1.2.2 Linear ion trap (LIT)

The linear ion trap works similarly as the quadrupole mass analyzer with ion trajectory by changing RF/DC ratio, but the ions are trapped and sequentially ejected. The trapping occurs primarily in the RF and DC fields, with two-dimensional RF delivered to LIT rods to trap ions and DC applied to the back-trapping element to reflect ions back to the central region axially (Fig. 8B). Trapped ion can be then excited by applying a supplemental oscillatory excitation voltage to the endcap electrodes so that the trapping voltage amplitude and/or excitation voltage frequency is varied to bring ions into a resonance condition in order of their *m/z* ratio [53, 54].

The typical application of a linear ion trap mass analyzer is the commercialized instrument QTrap mass spectrometer where in a QTrap device, the third quadrupole can be configured as a LIT to enhance the performance and flexibility compared to QqQ. This technology is unique and based on a triple quadrupole mass analyzer configuration, but with extra power to provide additional and unique MS and MS/MS scan such as Enhanced Product Ion scan and multiple reaction monitoring $(MRM)^3$ for quantitative analysis.

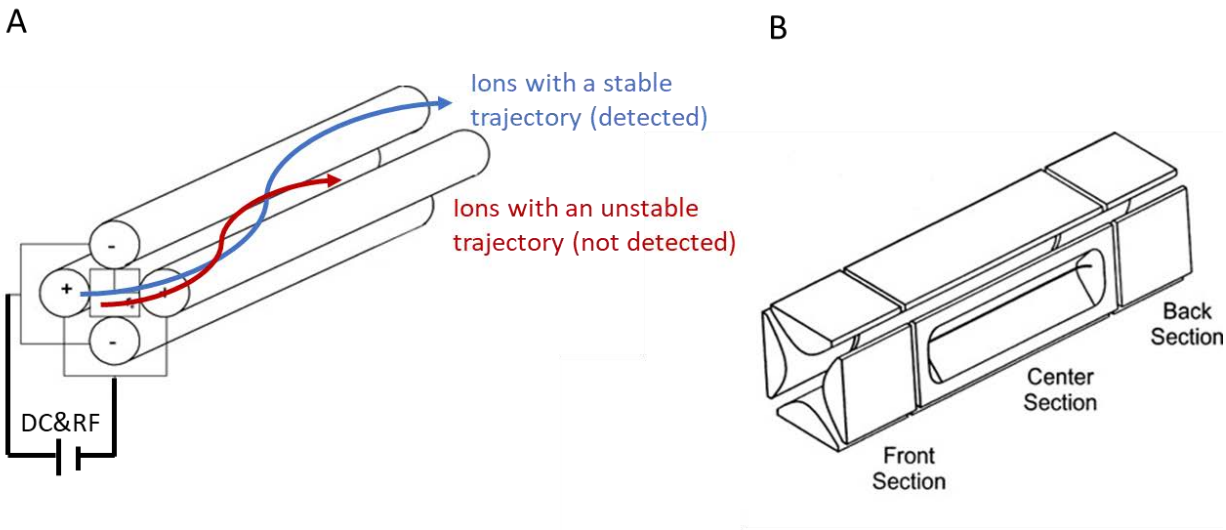

Figure 8 *Basic components of A: quadrupole equipped with four rods with applied DC and RF to charge the rods in opposite polarities and B: LIT with front, center and back section. Reproduced with permission from [55].Copyright © 2002, American Chemical Society.*

2.1.2.3 Time of flight (TOF)

The principle of TOF is based on the determination of ion flight times in a field-free region after acceleration by a potential (V) [56]. Different ions show distinct velocities (v) after uniform acceleration in a field (V) to reach a defined kinetic energy.

$$\frac{m}{z} = 2eV\left(\frac{t}{L}\right)^2$$

Where e is the charge of electron, V is the potential applied to ions, L is the length of drift tube, t is the time ions need to cross the drift tube (drift time). According to the equation, heavier ions with higher *m/z* travel slower than those with lower *m/z*.

In order to compensate the disparate velocities or nonuniform angles of the beam in a continuous ion beam with the same *m/z*, the equipment of TOF is particular important to regain the lost resolution (Fig. 9). Entering ions are gathered in a field-less region before they are accelerated by a short pulse to the drift tube. With the orthogonal ion acceleration, ions which have longer way to the detector, are actually closer to the pulse source and therefore are more strongly accelerated. On the way to the detector they join the ions with the same *m/z* that have less accelerating energy and therefore achieve the identical flight times. In addition, the ion

mirror could further compensate the different kinetic energies of ions with the same *m/z* by elongating flight path of ions with higher initial velocity until they are reflected to the detector.

In a QTOF instrument, three mass analyzers are employed: mass filtering quadrupole (Q1); a collision cell for analyte fragmentation (Q2) and the TOF for fragments filtering. Hybrid TOF instruments with quadrupoles (QTOF) could achieve high mass resolutions with the range of 10,000-50,000 and high acquisition speed which allows comprehensive analysis especially in untargeted assay lipidomics.

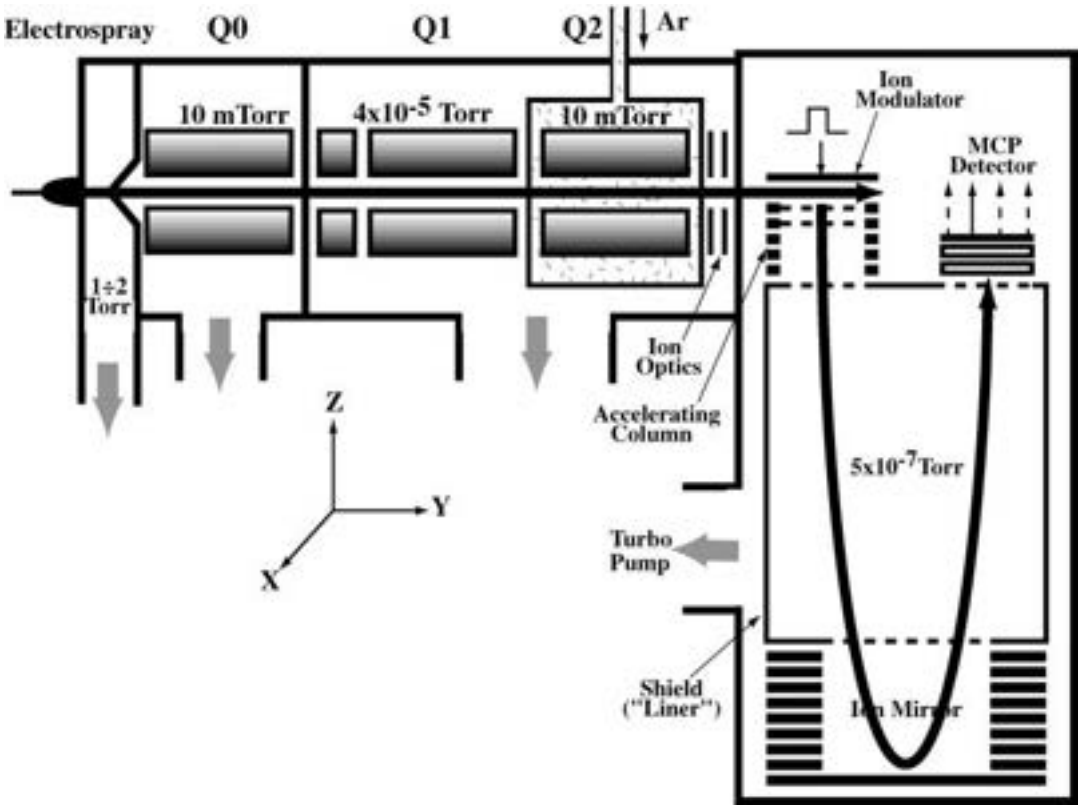

Figure 9 *Structure of a QTOF instrument (TripleTOF 5600) equipped with Q0 as ion guide, Q1 as mass filtering, Q2 as collision cell and TOF for the fragments filtering. Reproduced with permission from [57]. Copyright © 2001 John Wiley & Sons, Ltd.*

2.1.3 Detectors

Detectors as the last component in mass spectrometer play an important role as well since they are used to convert the ions into virtualized signals in forms of an electron current that can be measured. The most commonly used detector is the continuous electron multiplier (CEM) which has fast response and good sensitivity by signal amplification and enrichment to 10^6 times. During detection, accelerated ions strike the detector surface and release several secondary particles (negative mode: positive ions; positive mode: negative ions and electrons) [58].

The secondary particles further strike the detector surface and release electrons to continue the cascade until the signal reach 10^6 times.

The last step of ion detection is the digitalization of electron current signal into computer data by a converter with either analog-to-digital (ADC) with a wide linear dynamic range or time-to-digital (TDC) with a high time resolution.

In case of QQQ and QTrap instruments, CEM was employed with ADC as the converter while the Sciex QTOF instrument is equipped with microchannel plate (MCP) as CEM and TDC as converter owing to the high sensitivity [59].

2.1.4 Data acquisitions

In MS, different data acquisition approaches are applied for different purposes. Generally, data acquisition can be divided into targeted and untargeted approaches based on different MS instruments. Current exploratory methods for lipidomics mostly rely on separation using liquid or gas chromatography (LC or GC) coupled with mass spectrometers which enables to acquire high resolution and enormous data with in parallel lengthy processing and data acquisition. In lipidomics, targeted acquisition is used for analysis of pre-selective compounds for an absolute quantification and hypothesis driven while untargeted approach is acquired for a comprehensive lipid profiling in cells or biological fluid in order to generate hypothesis and for relative quantification.

2.1.4.1 Targeted approach

In modern research, identification and absolute quantification of biomarkers or important signalling molecules are becoming increasingly important for discovery, validation, and monitoring. In order to improve the sensitivity, to achieve high specificity, accuracy, and reproducibility, such data can be acquired using multiple reaction monitoring (MRM), also called selected reaction monitoring (SRM) following specific signals after fragmentation of targeted analytes. These assays are usually performed on low resolution MS instrument QqQ and QTrap. Taking QqQ as an example, the first quadrupole Q1 filters the targeted precursor ion within narrow mass ranges (~1 Da), then the selected precursor ion is subsequently fragmented at collision-induced dissociation (CID) in Q2 and finally Q3 again defines a narrow unit (0.7-1) *m/z* range to allow only a characteristic fragment to reach the detector (Fig. 10A). In this way, a higher sensitivity can be reached because of the effective noise filtration by Q1 and Q3. In this process, the targeted analysis is based on the monitoring of a specific precursor/product pair of the known compound, referred as 'transition' [60]. Integration of the chromatographic peaks for each transition provides possibility for targeted quantification of selected known analytes.

Normally, the number of transitions is dependent on how many targets are going to be analysed during one LC-MS run, however, the simultaneous analysis of multiple compounds is highly limited by the maximum cycle time of each MS cycle. The dwell time, which measures the time of one transition and is instrument dependent of all transitions sum up to the cycle time which is restricted in LC-MS analysis. If the cycle time is too long, there will be not sufficient data point for the chromatographic peaks that might be poorly defined and not suitable for quantitative analysis. In this case, the dwell time needs to be shorter (lower sensitivity) if a high number of compounds are simultaneously analysed. In order to overcome the sensitivity loss and increase the number of targets in one LC-MS run at the same time, scheduled MRM was developed where data are acquired at the panning detection time window around the retention time of each targets so that single MRM can be recorded with longer dwell time to increase the sensitivity [61].

2.1.4.2 Untargeted approach

Untargeted lipidomics is emerging as a powerful and attractive technology for discovery of biomarkers, generating hypothesis and studying the metabolic pathways. Liquid chromatography coupled to high resolution mass spectrometry (LC-HRMS) is currently the most prominent analytical platform for a comprehensive lipid profiling. In MS of untargeted approach, data acquisitions are mainly divided into data-dependent acquisition (DDA) and data-independent acquisition (DIA) [62, 63] which are performed on high resolution instruments QTOF and Orbitrap.

In DDA mode, the MS instrument performs firstly a MS full-scan followed by MS/MS analysis on a list of precursor ions selected from the full-scan spectrum. Usually the selection of the precursor is information dependent (e.g. intensity) with so-called information dependent acquisition (IDA). The advantage of DDA mode is that it is time efficient to facilitate an accelerated and autonomous data acquisition with high quality of spectra in MS2 level of triggered analytes for identification. However, a potential limitation of DDA mode is the loss of important metabolic features of MS2 spectra because of low MS abundance that will not be selected for MS2 product ion scan, which causes a fundamental problem for the detection and quantification of low abundant metabolites in DDA mode [64]. To address the limitation of DDA in acquiring MS2 spectra, DIA mode that can theoretically generate MS2 spectra for all precursor ions provides alternative way for untargeted lipidomics.

In DIA mode, after a MS full-scan through the precursor ion *m/z* with a wide range, an unbiased acquisition of MS2 spectra for the entire *m/z* range is followed up. There are three commonly

used DIA methods including all-ion fragmentation (AIF) (or MS^E first reported on QTOF instrument of Waters [65]), MS/MS^{ALL} [66] and sequential window acquisition of all theoretical fragment-ion spectra (SWATH) [67]. In AIF mode, two TOF scans, one with low collision energy (CE) for precursor ion detection and another with high CE for fragmentation of the entire mass range are carried out to obtain a highly complex MS2 spectra that needs to be deconvoluted. With the second approach MS/MS^{ALL}, fragmentations are obtained by discrete stepping of the unit mass extraction windows of Q1 to enable the fragmentation of precursors one by one instead of simultaneously. However, this procedure requires extremely long cycle time which is not compatible with LC-MS lipidomics. Instead of unit mass precursor isolation, the third approach SWATH allows to set Q1 transmission windows in variable width which could be able to overcome the extremely long cycle time. In SWATH, different width of Q1 isolation windows are conducted based on the MS distribution so that the defined windows can be acquired stepwise to obtain fragmentation of broad range of ions in reasonable cycle time with better selectivity (Fig. 10B). However, similarly as in AIF, the acquired MS2 spectra in defined mass range in SWATH are complex that need to be deconvoluted based on the retention time of different fragments (Fig. 10B). Some open source software e.g. MS-Dial [68] make the deconvolution easier and efficient to be realized. Ultimately, SWATH was proven to yield reliable and reproducible full comprehensive data of both MS and MS/MS level for qualitative and quantitative analysis of a global set of analytes [69], which is therefore nowadays the most preferred MS approach for untargeted lipidomics in our research group.

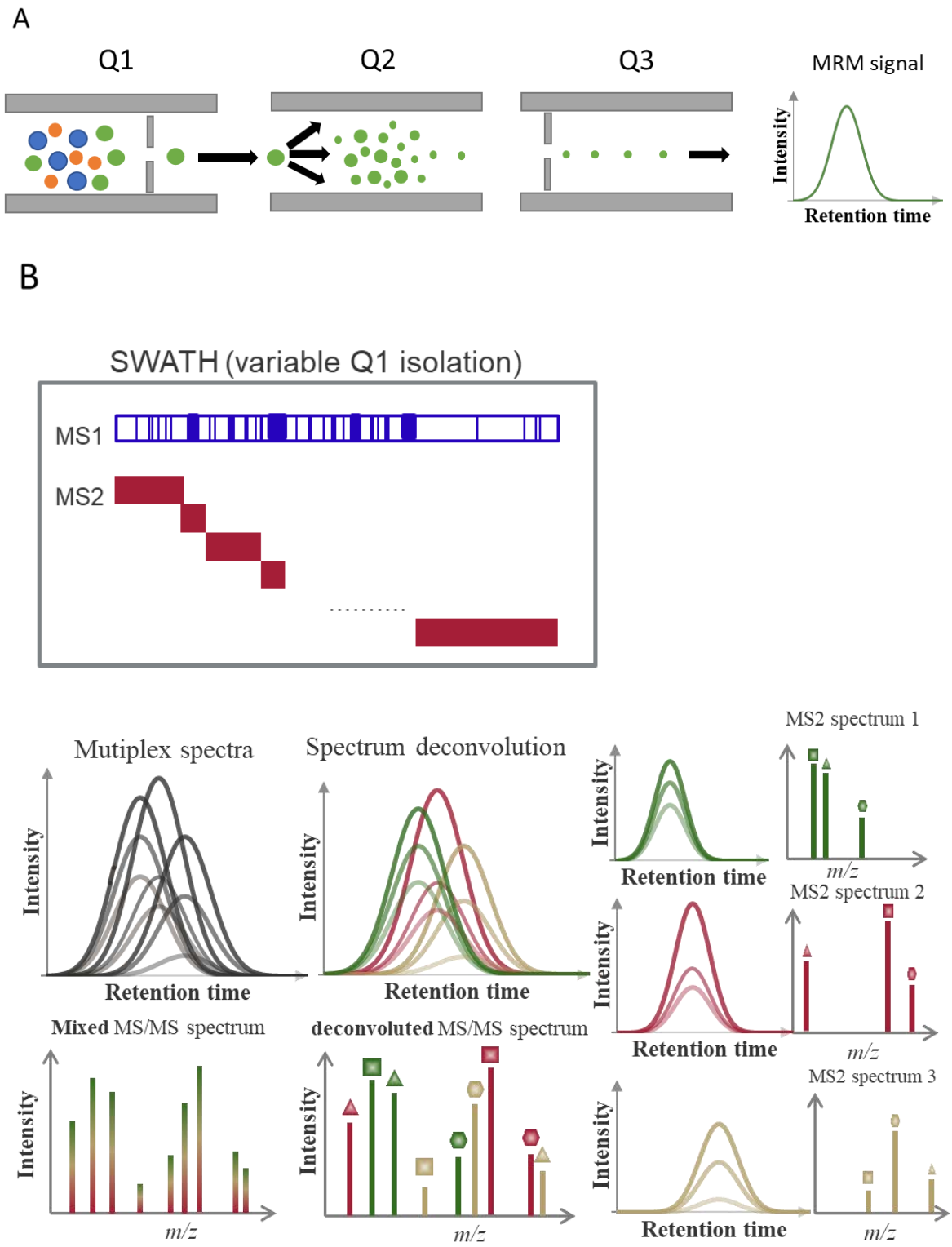

Figure 10 *A Illustration of targeted data acquisition approaches showing multiple reaction monitoring (MRM). B Illustration of untargeted data acquisition approaches with SWATH and the spectra deconvolution procedures based on SWATH.*

2.2 Separation technology in lipidomics

MS based lipidomics is usually coupled with prior chromatographic separation with high separation capacity which are important for reducing matrix effects, separating lipid isomers and enriching low-abundance lipid molecules [70]. Gas chromatography (GC), liquid chromatography (LC) and supercritical fluid chromatography (SFC) are among the most commonly used separation technologies. GC is the first separation technology that was coupled with MS for lipid analysis [71]. It is a powerful separation method with high separation efficiency with however the limitation to non-volatile lipids that need to be derivatized before detection. Thus, GC is the predominant method for fatty acid analysis after derivatization to fatty acid methyl esters (FAME), which are volatile [72]. While LC could provide good selectivity and sensitivity and is suitable for the separation of both volatile and non-volatile lipids, thus is the most universal chromatography method for lipid separation in both targeted and untargeted lipidomics.

In LC, there are mainly two approaches for lipid separation, that is lipid class separation and lipid species separation. Generally, normal-phase LC (NPLC) and hydrophilic interaction liquid chromatography (HILIC) separates lipid compounds based on their head groups; lipids from the same lipid class will co-elute in the NPLC and HILIC which is called lipid class separation. In contrast, reversed phase HPLC separates lipids according to the hydrophobicity of their FA chains which could provide lipid species separation, and their elution order is associated with the length and number of double bonds in the FA chain.

2.2.1 Lipid species separation

RPLC has been mostly widely used for the analysis of complex lipids in cells or biological fluid which provides good isobaric and isomeric selectivity for many lipids, making RPLC the most frequently used technique (over 70% among other LC techniques [73]) in LC-MS lipidomics research.

In RPLC, nonpolar stationary phase based on silica particles which are functionalized with hydrophobic ligands, e.g. C8, C18 and C30 are employed [74]. Commercially available RP columns Acquity UPLC BEH C18, Zorbax Eclipse XDB-C18, Acquity UPLC HSS T3, Acquity UPLC BEH C8, Kinetex C18, Acquity UPLC CSH C18 or Ascentis Express C8 columns are widely applied for lipidomics study[73]. With the improvement of the chromatographic separation, ultrahigh performance LC (UHPLC) system was introduced with high back pressure up to 1200 bar where columns with sub-2 μm particles could be operated in high flow rate with highly effective separation with increased peak capacity, resolution, analytical speed,

sensitivity and decreased matrix effects achieved [75]. Mobile phase used in RPLC are usually polar mixtures of water and water miscible organic solvent, e.g. weak mobile phase such as H_2O/MeOH (50:50), H_2O/ACN (40:60–60:40), H_2O/MeOH/ACN, H_2O/IPA (95:5) and strong mobile phase consisting of iso-propanol (IPA) such as IPA/ACN (95:5–70:30), IPA/MeOH/H_2O (50:30:20) [73]. What is more, mobile phase additives such as ammonium acetate, ammonium formate, acetic acid or formic acid are highly recommended during the LC run in order to improve the selectivity and sensitivity according to different analytes.

RPLC provides good lipid separation for most of the lipid classes except for phosphatidic acid PA, phosphatidylserine PS with broad peak shape and sphingosine-1-phosphate (S1P) which is not detectable in RP mode. In RPLC, the polar lipid classes acylcarnitine CAR, lysophosphatidylcholine LPC, lysophosphoethanolamine LPE and FA eluted firstly followed by lipid classes phosphatidylcholine PC, phosphoethanolamine PE, sphingomyelin SM, diacylglycerol DG and the non-polar lipid classes triacylglycerol TG, cholesterol ester CE elute in the end. Since RPLC separates the lipids according to the hydrophobicity of their FA chains, a separation of lipids with different carbon chain length and number of DB could be observed in each lipid class with a characteristic order where the RT is linearly correlated with *m/z* value (carbon chain length and DB) [76], which enables the RT prediction for unknown compounds. This phenomenon provides an orthogonal parameter for lipid annotation during data processing.

In RPLC based lipidomics, because of the lipid species separation instead of lipid class separation, the lack of coelution of internal standards (IS) with their respective analytes especially in untargeted lipidomics where one IS per class is included will affect the ionization efficiency, thus affecting the matrix effects correction, the performance of IS-based normalization and quantification strategies [77].

2.2.2 Lipid class separation

NPLC, HILIC and SFC are the three techniques commonly used for lipid class separation. Lipids with the same polar head elute at the same time including the IS per class, which shows great potential for quantification of lipids as individual classes and is an alternative approach to RPLC (around 30%) in lipidomics research [73].

All these three techniques utilize polar stationary phases, e.g. bare silica as the most common one with various silica modifications such as polyvinyl alcohol or dihydroxypropyl [78]. They are distinguished mainly by the different mobile phases. Highly non-polar solvents such as heptane, chloroform have to be used in NPLC. Unlike NPLC, the mobile phase in HILIC

usually contain a certain percentage of water (5–40%) to generate a stagnant enriched water layer on the surface of stationary phase for the analytes for partitioning. Water-miscible organic solvents such as isopropanol (IPA), acetonitrile (ACN) and methanol (MeOH) are frequently used with combination of H_2O, e.g. ACN/H_2O (95–90:5–10), ACN/MeOH/H_2O (55:35:10), ACN/IPA (80:20) [73]. In SFC, supercritical CO2 which has similar polarity as hexane is used as the mobile phase while methanol is often used as the mobile phase modifier [79]. Compared to NPLC, HILIC is more compatible with MS [80] with however relatively poor retention time repeatability, low peak capacities, low flexibility and high complexity especially for peak deconvolution during data processing. Because of the additional detection of some lipid classes such as PA, PS and S1P where RPLC could not provide good performance on these lipids, HILIC is frequently used as an alternative approach besides RPLC to provide additional information on such polar lipids.

3. Workflow in lipidomics

A general workflow for lipidomics consist of sample preparation (sampling and lipid extraction), LC-MS measurement and data processing (some detailed information was described in Fig. 11). Each step is of equal importance in order to acquire high throughput and reliable data for a reasonable elucidation of mechanisms in the biological pathways and find out the potential biomarkers.

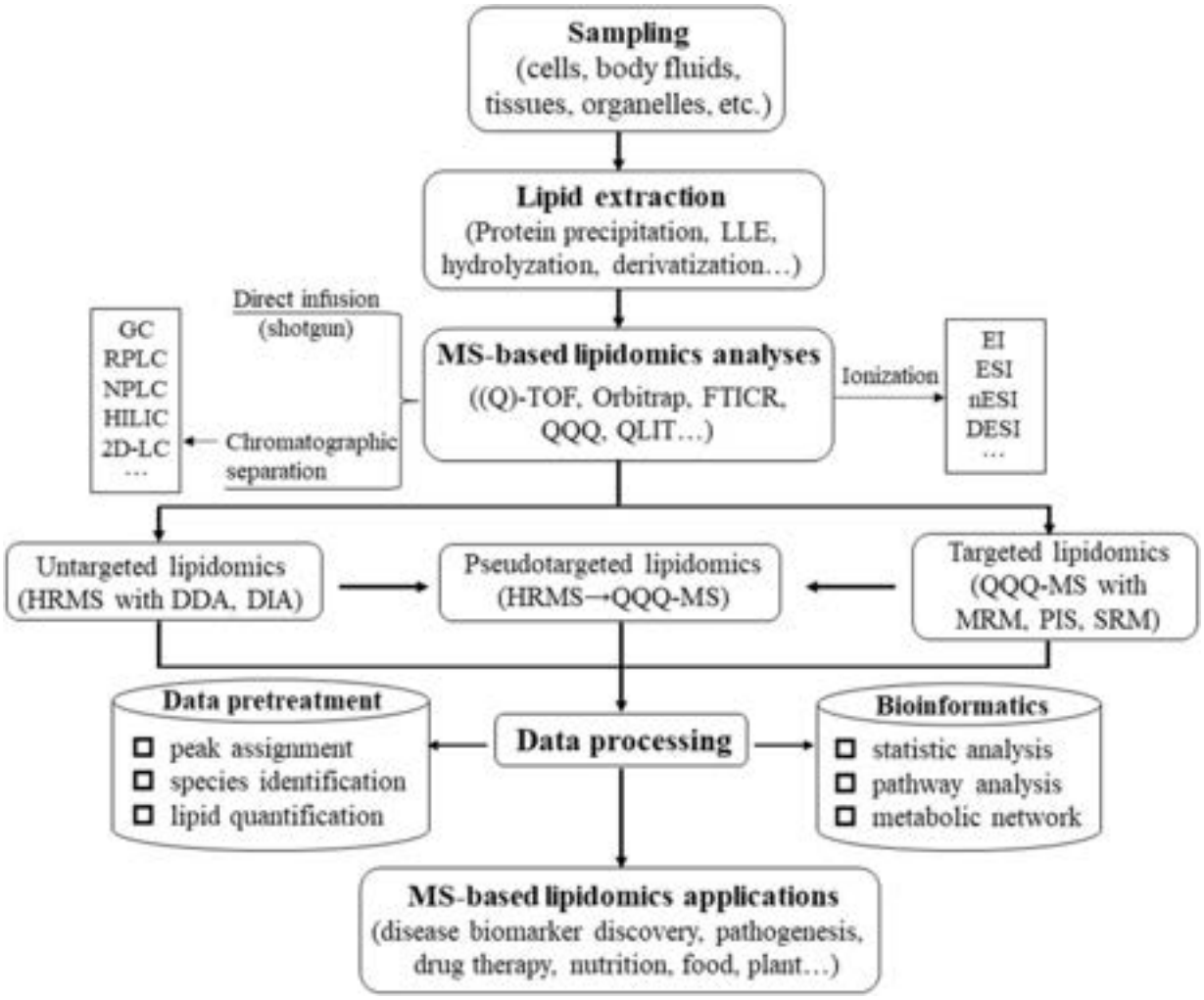

Figure 11 *A workflow of MS-based analytical strategies for untargeted and targeted lipidomics. Reproduced with permission from[81]. Copyright © 2020 Elsevier B.V.*

The most uncertainty that can be introduced to a lipidomic study is sample preparation since it is the pre-analytical period which can bring different systematic and manual variation. Before lipid extraction, an important step is the sample storage. Many lipids especially the oxylipins are very sensitive and unstable, a proper storage including light-absorbing containers, extremely low temperature (-80°C) and in some case the spiking of antioxidant such as butylated hydroxytoluene (BHT), butylated hydroxyanisole (BHA), or triphenylphosphonium (TPP) could help efficiently avoid further degradation of lipids such as oxidation, peroxidation and hydrolysis [82]. Many studies have investigated the effect of storage time on the results of various lipids species in different kinds of biological samples [83-86]. There is certain evidence for lipid concentration changes during storage (Fig. 12). What is more, for liquid-state samples such as plasma and urine, the freeze–thaw cycles cannot be avoided. In this case, a

recommended number of freeze-thaw cycles of less than 4 need to be followed in case of any significant lipidome changes during the freeze–thaw procedure [83]. In general, a long-term storage of samples is not recommended in order to avoid any possible pre-analytical biases due to degradation in the study sample sets.

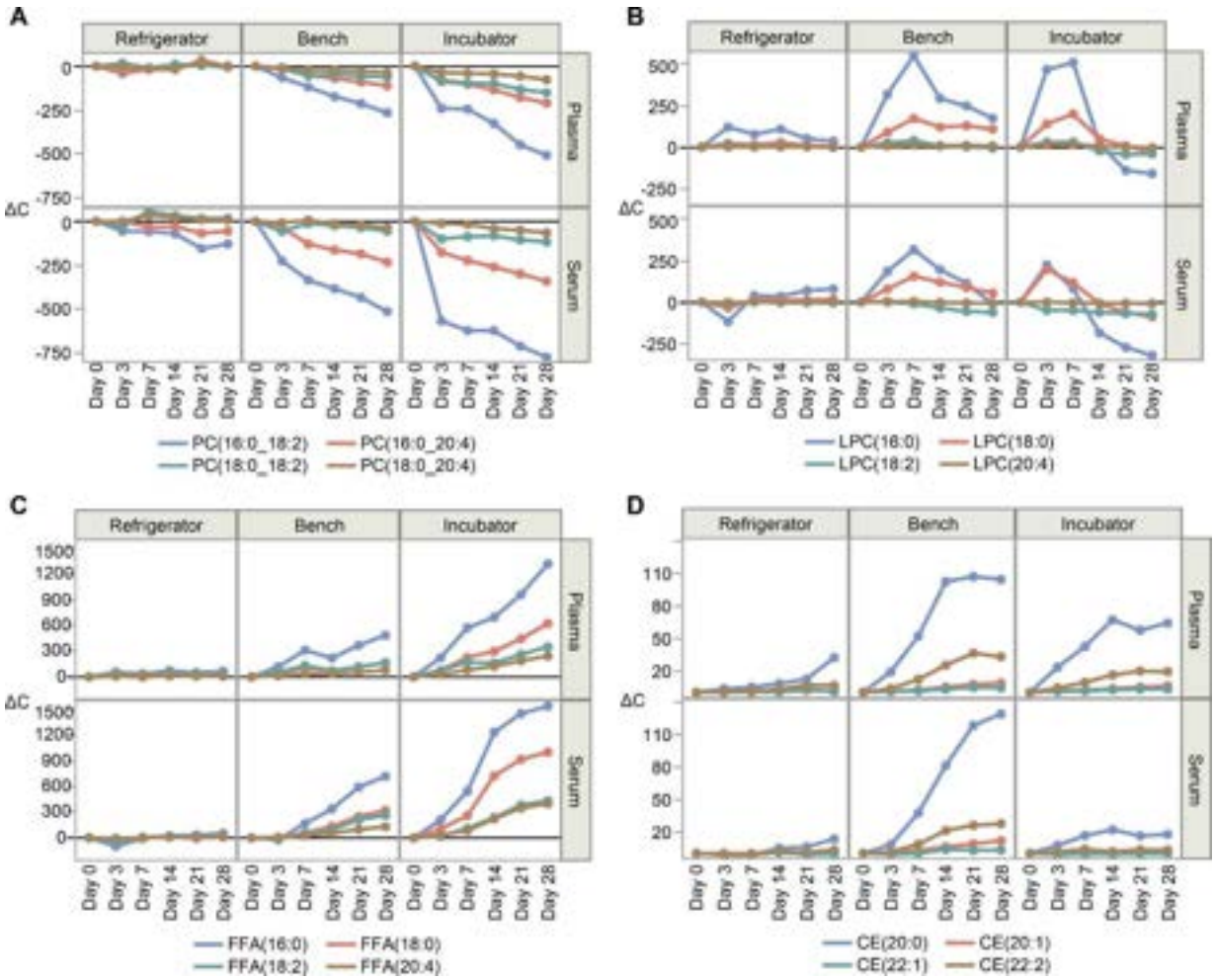

Figure 12 *Concentration changes (ΔC) of lipid class PC, LPC, FFA and CE in plasma and serum within 28 days' storage under different storage conditions[85].*

3.1.2 Lipid extraction

As the first step for lipidomic study, an efficient extraction of lipids from cells or other biological matrices was required. A suitable extraction solvent should be able to cover as many lipids as possible including both relatively polar lipids, neutral and non-polar lipids (the polarity of different lipid classes and extraction solvents is summarized in Fig. 13). Meanwhile, the extraction procedure should be adapted to reduce chemical interferences and matrix effects, exhibit high extraction recoveries with good precision for sensitive and robust accurate quantitative analysis.

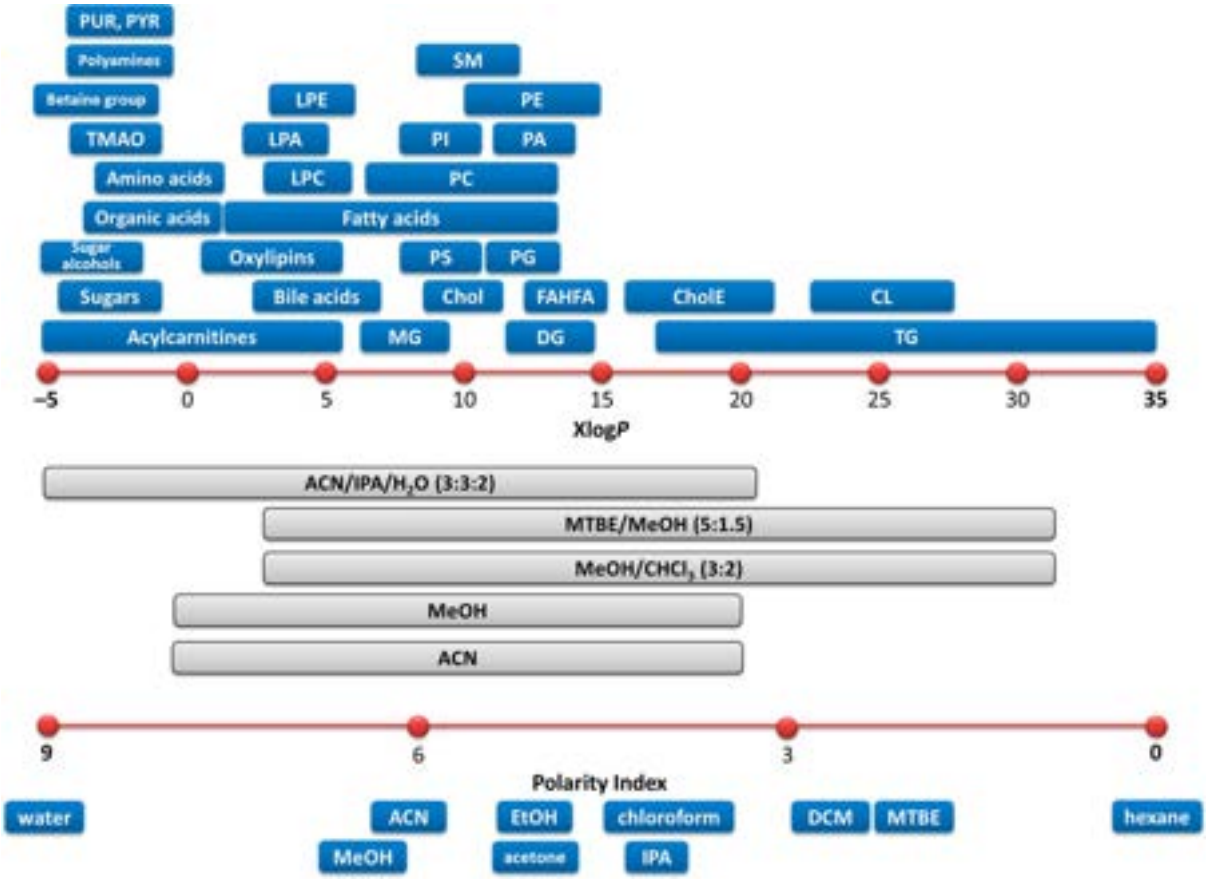

Figure 13 *Predicted octanol/water partition coefficient (X log P) range of common metabolites (including polar metabolites and lipids) in blood plasma and polarity index of solvents used for sample extraction. Legend: Cer, ceramides; Chol, cholesterol; CholE, cholesteryl esters; CL, cardiolipins; DG, diacylglycerols; FAHFA, fatty acid esters of hydroxyl fatty acids; LPA, lysophosphatidic acids; LPC, lysophosphatidylcholines; LPE, lysophosphatidylethanolamines; MG, monoacylglycerols; PA, phosphatidic acids; PC, phosphatidylcholines; PE, phosphatidylethanolamines; PG, phosphatidylglycerols; PI, phosphatidylinositols; PS, phosphatidylserines; PUR, purines; PYR, pyrimidines; SM, sphingomyelins; TG, triacylglycerols; TMAO, trimethylamine N-oxide. Reproduced with permission from [87]. Copyright © 2016, American Chemical Society.*

3.1.2.1 Liquid-liquid extraction (LLE)

The LLE protocols are without doubt the most commonly used protocols for lipidomic study especially under the untargeted approach. In general, the LLE includes mainly biphasic and monophasic extraction. Recently, triphasic extraction was also applied for lipidomic study by some groups with its benefits of triphasic partitioning which could cover different types of extracts [88, 89].

The most commonly used protocols for lipid extraction were introduced more than 70 years ago by Folch et al. [90] and Bligh and Dyer [91] with a biphasic liquid-liquid extraction system of chloroform/methanol/water, $CHCl_3$/MeOH/H_2O. These methods, in which lipids are collected in the lower $CHCl_3$-rich layer, have been frequently described as “gold standards” for

lipid extraction [39, 92, 93]. Some modifications have been made by researchers to substitute $CHCl_3$ by dichloromethane (DCM) as a less toxic alternative in some studies [39]. Nevertheless, the liquid-liquid extraction systems of $CHCl_3$/MeOH/H_2O are still the most classic lipid extraction methods. Hexane-isopropanol-water (Hexane-IPA-H_2O) was proposed in 1978 by Hara et al. [94] as a less toxic option. Later this method was modified by adding acetic acid to improve extraction efficiency for acidic lipids [95]. Recently, other biphasic extraction protocols such as MTBE/MeOH/H_2O and Butanol/MeOH/H_2O were introduced by Matyash et al. [96] and Löfgren et al. [97], respectively. The former has largely replaced the classical Folch and Bligh&Dyer protocols due to its advantage that the upper layer is the lipid-rich organic phase which can be easily collected without the risk of contamination of the sample with proteins from the interface between the two layers, a problem when lipids need to be retrieved from the lower chloroform-rich layer [97, 98].

Three-phase solvent systems were not as often used as biphasic systems. In triphasic system, the extraction solvents are usually partitioned into three layers: an organic phase at the top (specific for non-polar lipids), a salt-rich aqueous phase at the bottom (polar molecules such as carbohydrates) and a salt-lean aqueous phase in the middle (proteins). This protocol provides the possibility for full use of all fractions in three layers simultaneously for lipidomics, metabolomics and proteomics study. The so-called three-phase partitioning (TPP) only needs alcohols and inorganic salts, typically tert-butanol and ammonia sulfate to form a three-layers system [99]. Another possibility for the generation of triphasic systems is the mixtures of four kinds of solvents. This kind of triphasic system is built from a two-phase system normally composed of n-hexane, acetonitrile and water in combination with a fourth solvent such as methyl acetate, ethyl acetate, methyl tert-butyl-methyl-ether or dichloromethane to create the third phase [88]. It is proven to be efficient for high-speed counter-current chromatography (HSCCC) to separate multiple components with a wide range of hydrophobicity [89]. The possible triphasic solvents composed of n-hexane–methyl acetate–acetonitrile–water (4:4:3:4, v/v/v/v) [89], n-hexane-tert-butyl methyl ether-acetonitrile-water 2:3:3:2 (v/v/v/v) [88] and so on.

Both biphasic and triphasic extraction protocols have the disadvantages of risk for contamination of sample with proteins from other layers and the complex operation to separate the different fractions form different layers, which is not a good choice for large-scale lipidomic study. For this reason, many researchers have recently propagated simple monophasic lipid extraction protocols using protein precipitation methods based on organic solvents using either a single

or a combination of miscible ones [100-104]. In these methods, proteins are precipitated by denaturing organic solvent and then removed by centrifugation. The use of MMC (MeOH/MTBE/$CHCl_3$) [102], butanol and MeOH [105], isopropanol (IPA) with low percentage of H_2O [106, 107] and MMIPA (MeOH/MTBE/IPA) [108] as organic solvent mixtures have been described to exhibit good performance and wide coverage of diverse lipid classes. The monophasic extraction system is simple for operation and convenient for automation of lipid extraction in large-scale clinical lipidomic study, which is recommended in this thesis for the lipidomic study.

3.1.2.2 Solid-phase extraction (SPE)

Solid phase extraction is another feasible option for lipid extraction which is adapted for different lipid species. The principle is based on the different adsorption ability of lipids on the stationary phase, which leads to a stronger or weaker elution along with the elution solvents to realize the removal of impurities and pre-concentration of targeted compounds. There are different kinds of SPE cartridge including reversed phase with adsorbent of non-polar or weakly polar such as C8 or C18 [109-111] to extract medium to non-polar compounds, normal phase with adsorbent of polar bonded silica gel, alumina and silica-silver to extract polar compounds [112] or ion-exchange SPE cartridge [113] with adsorbent of charged ion exchange resin such as aliphatic quaternary propyl bonded silica gel and aliphatic sulfonic acid bonded silica gel to extract charged compounds. Additionally, HILIC mode [114] and mixed mode [115] SPE cartridges (rely on two or more retention mechanisms) are also widely used for specific lipid classes such as oxidized cardiolipins [114] and oxylipins [116]. The SPE process mainly consists of pre-conditioning, sample loading, cartridge washing and elution. During this process, the targeted compounds can interact with solid cartridge until the eluent solvent is added. With SPE procedure the complex sample matrices can be simplified in order to reduce the matrix effect and the ion suppression in mass spectrometry can be reduced. Moreover, the targeted compounds which are present at low levels can be purified and concentrated to improve the sensitivity and reach the limit of detection (LOD) or quantification (LOQ) [116]. SPE protocols are more typically used for targeted lipidomics with specific lipid species especially those with low concentration level in matrices such as oxylipins and steroid or eicosanoid species.

3.1.2.3 Homogenization

Besides the adequate extraction solvents, a suitable cell disruption method contributes to the improvement of lipid yields as it enhances the release of intracellular lipids from different subcompartments (e.g., tissue region, cell type, organelles). Cell disruption methods can be

theoretically classified into mechanical and non-mechanical methods [117]. Reported methods for the disruption of mammalian cells include Dounce and Potter–Elvehjem homogenization [118], grinding with glass beads [119], nitrogen cavitation [120] and sonication [121]. In addition, chemical [122] and biological methods with enzymatic lysis have been reported as well [123]. Nevertheless, in most cases, the effectiveness of a disruption method relies on the cell type. In the context of cellular lipidomics, the integration of cell disruption methods has been rarely systematically investigated. However, it is of great importance because cell disruption breaks the cells and improves the accessibility to the intracellular and subcellular components for increasing extraction efficiency especially for non-membrane structural lipids such as cardiolipins (CL) that are existing in mitochondria (examples of incomplete cell disruption were shown in Fig. 14). The disruption procedure may also help to overcome kinetic mass transfer limitations during extraction.

3.1.2.4 Other factors

The extraction solvent systems and the cell disruption method are critical for general lipids yield during extraction. Additionally, the extraction cycles and reconstitution solvents could also have an effect on the extraction recovery [124]. In common analytical sample preparation protocols using liquid extraction, exhaustive extraction of analytes is achieved by repeated extraction. As such a multi- or two-step extraction is hard to realize in a large-scale clinical sample batch and would be extremely tedious. Hence, an extraction protocol with efficient lipid recoveries with 1 cycle extraction is of importance to be capable to apply for large-scale lipidomic study. What is more, the reconstitution solvents can contribute to the final lipid recovery especially when lipid extracts are dried longer than actually required. A quantitative redissolution is of great importance for a robust workflow. The proper reconstitution solvents could not only increase the extraction recovery but also improve the peak shape during the LC-MS measurements. Ideally reconstitution solvents should have maximum solubility for all lipids without detrimental effects on chromatography i.e. broad peak shape or front-tailing and back-tailing of the analytes especially early eluted ones. Micro- or nano-LC systems in RP mode are particularly sensitive to reconstitution solvents with peak distortion effects since the injection volume is critical for the whole system volume and any improper reconstitution solvents can consequently result in premature elution, peak broadening and loss of sensitivity [115, 125]. Therefore, MeOH, IPA/MeOH (2:1; v/v), IPA/$CHCl_3$ (9:1; v/v), IPA/ACN/H_2O (2:2:1; v/v/v), IPA, $CHCl_3$/MeOH (1:1; v/v), MTBE/MeOH (1:1; v/v), MeOH/H_2O (2:3; v/v) and so on as common reconstitution solvents should be tested during the method development and

optimization especially in targeted lipidomics with specific lipid species as target compounds and the micro-LC and nano-LC assays, which is always ignored but of equal importance during sample preparation.

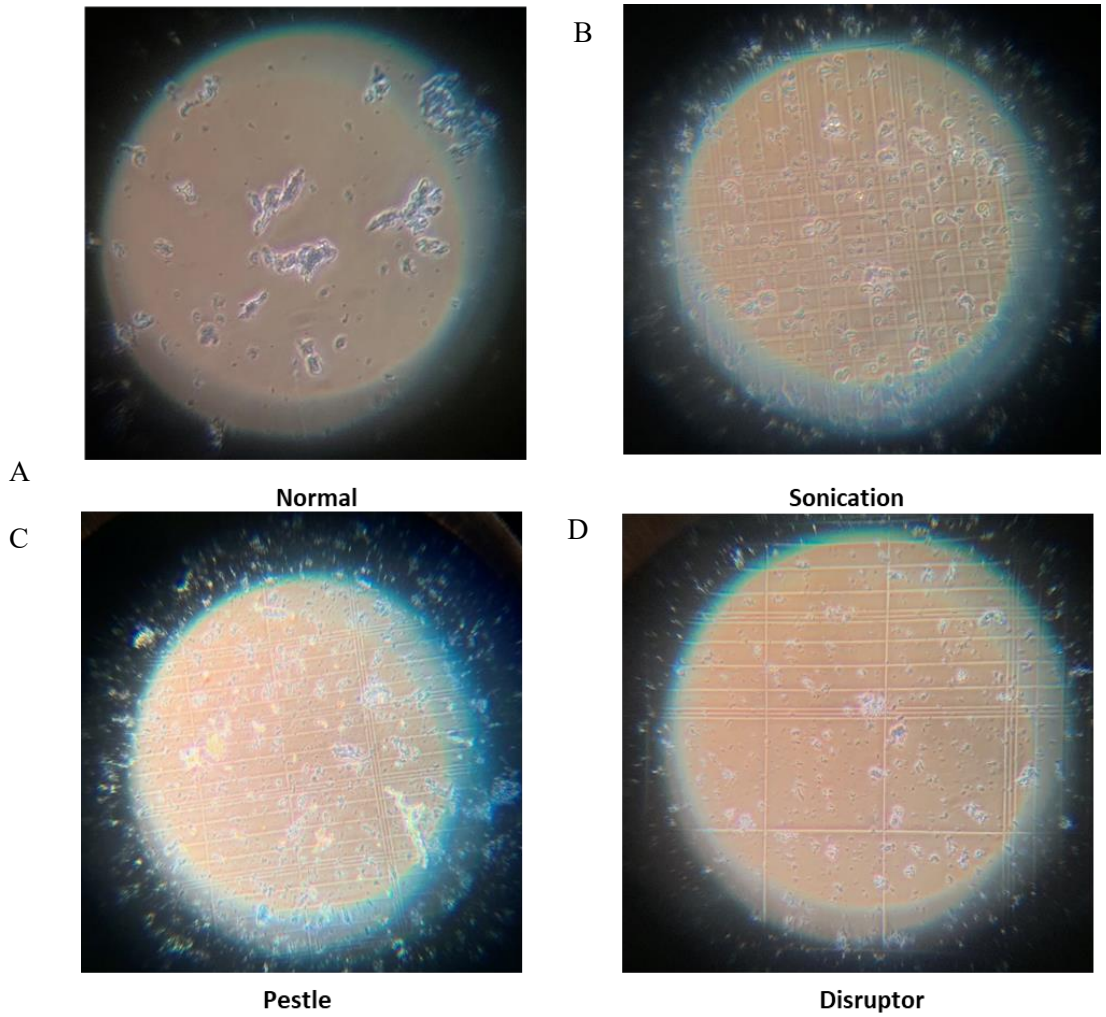

Figure 14 *State of platelets after cell disruption by different methods A: only vortexing; B: water-bath sonication; C: with pestle and D: with handheld ultrasonic cell disruptor under microscope. The cells are not completely disrupted because of the visible cell residues.*

3.2 Untargeted and targeted MS-based analysis

A comprehensive analysis of full lipidome in biological samples is challenging not only because of the requirements for a broad spectrum of analytical methodologies but also the diversity of lipid species in different matrices with broad concentration ranging from picomolar to micromolar and large chemical and structural diversity including different hydrocarbon backbone lengths, branching, unsaturation and functional groups in the same lipid class. In general, the main analytical platforms for lipidomics are (1) untargeted analysis which is an approach

for qualitative analysis and hypothesis-generating and (2) targeted analysis which is an approach for quantitative analysis and hypothesis-validation.

Untargeted analysis is able to simultaneously extract all detectable lipids in a sample in a non-selective way in order to produce as much as possible high throughput that covers different lipid species with a wide range of polarities and concentration levels. One of the preferred approach for untargeted lipidomics is data independent acquisition (DIA) such as SWATH (sequential window acquisition of all theoretical fragment-ion mass spectra) [126] [124] which allows to acquire complex full fragments of precursors based on Q1 transmission windows of variable width to improve selectivity (see section 2.1). In untargeted assay, the wide range of lipids and high throughput is with the cost of sensitivity. Since thousands of lipids with a wide range of polarities and concentration levels could be extracted and analysed in LC-MS method, the final injection concentration and injection volume should be counted into consideration. On the one hand, the dilution or concentration factors of different types of biological matrices and injection volume should be adjusted in order to cover the most important classes that are present at low concentration to gain efficient sensitivity in LC-MS measurements, on the other hand, the most abundant lipid classes should not be overloaded on LC-MS system with a saturation of the MS-detector. All these aspects should be considered during an untargeted lipidomics study. The advantage of untargeted lipidomics is clearly the possibility of simultaneous analysis of whole lipidome in biological samples with valuable information for hypothesis-generating while the disadvantage could be that untargeted lipidomics are only possible for relative quantification by signal intensities that are subsequently normalized by class specific internal standards (IS) which are mainly used for checking the lipids recovery and robustness of the analysis such as retention time, peak shape, mass accuracy rather than for quantification.

Targeted analysis is able to selectively extract a particular set of lipids which can avoid interferences of impurities, reduce matrix effect, improve extraction efficiency and sensitivity for targeted compounds in LC-MS method. The most common approaches are selected/multiple reaction monitoring (SRM/MRM) which is a mature, stable, and widely used powerful quantitative method in LC-MS based targeted analysis [115, 127]. In targeted assay, the reference standards of targeted compounds should be available or at least the theoretical rules for bond cleavage of the targeted compounds should be known in order to prepare necessary transition pairs including precursor Q1 and specific fragments Q3 for MRM measurements. Scheduled MRM transitions based on retention time enables to make the number of MRM transitions unlimited by the cycle time and extremely maximize the number of MRM transitions in each

measurement. The advantage of targeted lipidomics is the improved sensitivity for specific compounds that are low abundant in nature which may not be able to detect in untargeted ways. Moreover, absolute quantification with isotope labeled IS could be realized in targeted lipidomics. However, the improved sensitivity is typically sacrificed at the expense of a wider coverage, as a result, some valuable information can be missing. What is more, targeted lipidomic is only possible to characterize defined groups of lipids instead of unknowns which can be equally detected in untargeted lipidomics.

3.3 Data processing

Untargeted lipidomics produces a large amount of data. Appropriate data processing is critical for extracting useful information from such complex data matrix for biomarker discovery where thousands of lipids are measured in the biological matrices. Typical informatic frameworks include data (pre-) processing (peak integration, identification, and normalization), statistical analysis and metabolic pathways analysis for hypothesis generating where the pre-processing is the determinative step to guarantee the good data quality for further statistical analysis.

3.3.1 Tools for lipid identification and normalization

The correct identification of lipids is the fundamental step for an untargeted assay based on the LC-MS lipidomics. The lipid annotation and identification can be supported by MS-based databases or libraries e.g. LipidBlast [128], LMSD [7], METLIN [129] and so on to improve the confidence level. The MS method for untargeted lipidomics assay usually starts from a MS full scan with high resolution mass spectrometry (HRMS) to acquire the information of accurate mass and isotopic pattern of precursors in order to initiate the sum formula. Afterwards, fragments were obtained with data independent acquisition (DIA) strategy including all-ion fragmentation (AIF) or MS^E [130, 131] and MS^{all} [66] approaches or Sequential Windowed Acquisition of All Theoretical Fragment Ion Mass Spectra (SWATH) [132] by Quadrupole Time-of-Flight (QTOF) to acquire mixed MS/MS spectra that need to be deconvoluted. The main limitation of all ion fragmentation is the highly complex MS/MS spectra without connection to the precursor ions while the SWATH windows could to some extent link the MS/MS spectra to the desired precursor range which makes the deconvolution easier. MS/MS spectral annotation is indispensable for (i) differentiating between coeluting isobaric lipids at the lipid class annotation level (e.g., PE 38:4), (ii) obtaining structural information for fatty acyl chains (e.g., PE 18:0_20:4), and (iii) differentiating between coeluting regio-isomers (e.g., PE 18:0/20:4, PC 20:4/18:0) [133]. The deconvolution which is able to purify composite spectra by assigning

fragments to their precursors is usually supported by software such as MS-DIAL [134, 135], OpenMS [136] and LipidMatch [137] which are "all-in-one" software to process data and generate peak tables. MS/MS spectral matching to the library which were either created by experimentally obtained reference spectra or the computer-generated fragment patterns (so-called in silico MS/MS libraries) is the first step for identification of lipids, however, some isomeric or enantiomeric compounds share the similar or identical MS/MS spectra where only from the MS part it is not possible to differentiate the highly similar compounds. In this case, the separation technology such as liquid chromatography and ion mobility could to the largest extent support the identification with the orthogonal information like retention time or collision cross section (CCS) [87] to further enhance the confidence level of identification. Particularly when the reversed-phase liquid chromatography (RPLC) is applied for which the retention time follows certain rules depending on the physicochemical properties correlated with *m/z* value, i.e. number of double bonds and number of carbon length based on the same lipid class, the lipid elution patterns could support the identification and find out the miss-annotations [138] (Fig. 15). Therefore, the orthogonal information not only MS/MS spectra but also retention time or CCS value are advised for a reliable identification.

Thereafter, the data matrix (after lipid annotation and miss-annotation filtering) is created, data normalization should be applied in order to reduce the systematic error and improve the statistical power. There are plenty of normalization strategies and the most commonly used are internal standard-based normalization or (quality control) QC-based normalization. Several software tools are available such as internal standard-based normalization B-MIS (best-matched internal standard) [139], NOMIS (normalization using optimal selection of multiple internal standards) [140], CCMN (cross-contribution compensating multiple standard normalization) [141], which can be realized in R script independently or LipidMatch Normalizer [142] and NOREVA [143] while for QC based normalization, Batch Normalizer (based on LOESS (locally (weighted) estimated scatterplot smoothing) regression) [144] and StatTarget (a support-vector-machine-based (SVM) normalization method) [145] are also frequently used. Moreover, a combined IS based and QC based normalization method which could be performed in the "all-in-one" software MS-DIAL could also be a good choice when a combined study design with both QC samples and ISs are employed.

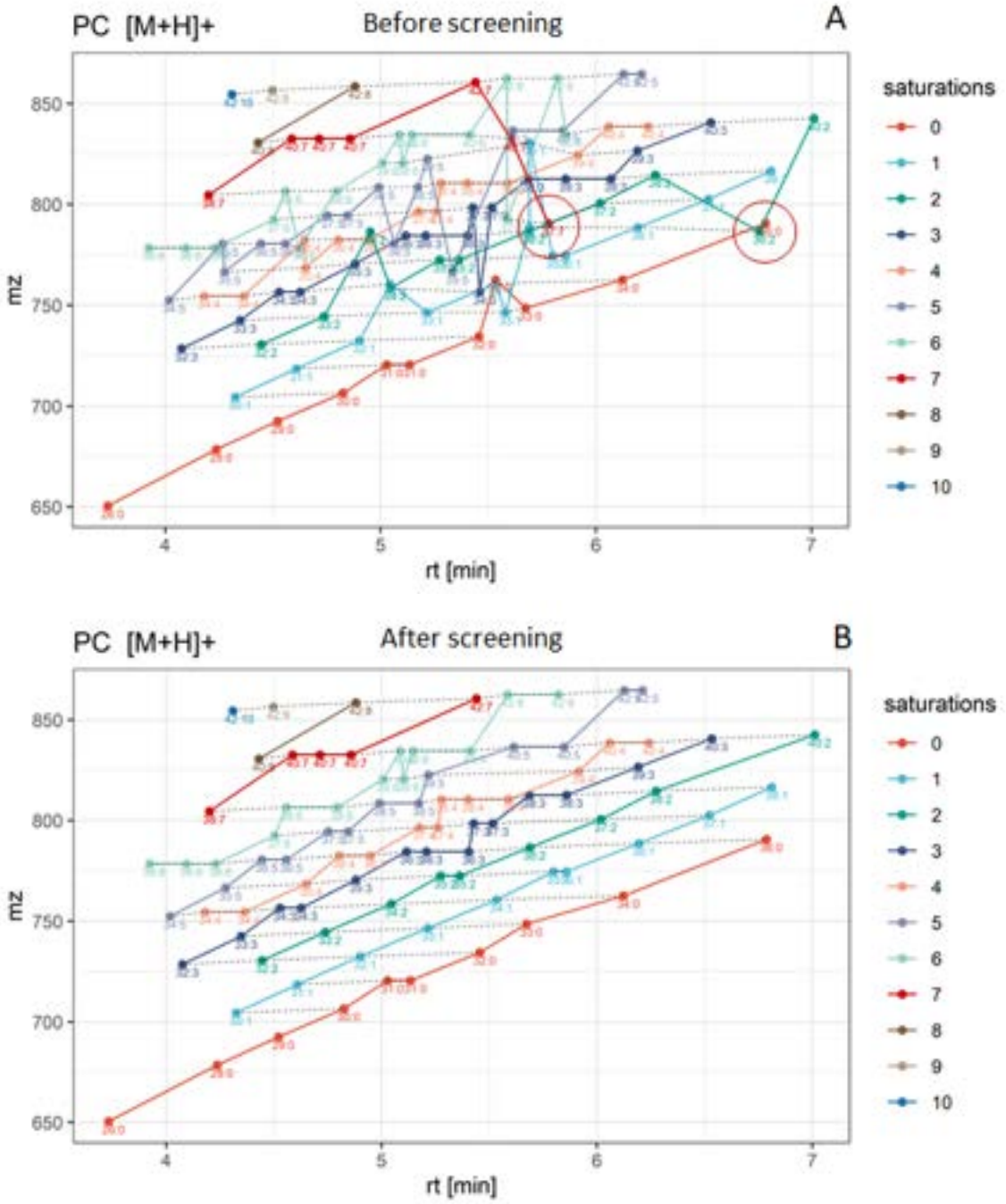

Figure 15 *Spotting maps of phosphatidylcholines (PC) showing the relation of elution order of lipids within one class with RPLC to their precursor m/z. Dots with the same colour show lipids with equal number of double bonds (DB). A: outliers (red circles) can be found based on the linear correlation between retention time to the m/z with the same double bond number. B: Outliers can be removed after mis-identification checking in order to confirm the lipids identification.*

3.3.2 Tools for biostatistics

The visualization procedures of the complex data matrix from untargeted lipidomics is one of the most important steps for biomarker discovery or pathways mapping. Generally, the

statistical analysis can be divided into parametric (when the data is normally distributed, e.g. *t*-tests) or non-parametric tests (when the data is not normally distributed, e.g. Wilcoxon-Mann-Whitney-U-test). The results of statistical hypothesis testing are usually reported as p-values to indicate the significance of any alteration (usually $p<0.05$). When the number of parallel hypothesis testing increases, there is a risk for false positive. Therefore, the p-value must be adjusted by false discovery rate evaluation (q-value) [146] or Bonferroni correction [147]. What is more, some extensive statistical tools are available to visualize classification or differences between experimental groups including principal component analysis (PCA), discriminant analysis, hierarchical clustering, volcano plots, heatmaps and boxplots. These tools together could help for evaluation of highly significant features and for potential biomarkers discovery. Commercial statistical software programs including SIMCA-p, SPSS, Origin and so on provide the possibility for all the mentioned functions. Moreover, the R language package is more powerful especially when large numbers of data need to be processed.

The aim of lipidomics is not only to detect significant alterations obtained under different experimental conditions, but also the possible metabolic pathways related to the significant features. For pathway mapping, some visualization/manipulation toolboxes e.g. Cytoscape [148], MetaboAnlayst [149], KEGG [150] and VANTED [151] are available. With the support of all these tools, a general workflow for the data processing of untargeted lipidomics can be realized.

3.4 Bioanalytical Method Validation

Bioanalytical method validation is a necessary process before an established analytical method is applied for the measurement of biological samples. Validating provides reliable data and confidence to support a quantitative evaluation of analytes in different biological matrices such as plasma, platelets, urines, serum, saliva and so on in clinical bioanalysis, industrial drug analysis or biopharmaceutics study. The American Association of Pharmaceutical Scientists (AAPS) and the United States Food and Drug Administration (FDA) [152] firstly recognized the importance of a harmonized validation guide and therefore the broadly accepted guidelines for bioanalytical method validation was summarized by FDA and in case of any requirements updated during time. The latest version was updated in November 2022 as M10 BIOANALYTICAL METHOD VALIDATION AND STUDY SAMPLE ANALYSIS [153]. Some important aspects especially the LC-MS assays relevant are briefly discussed in this thesis.

3.4.1 Selectivity and specificity

An analytical method should be selective to targeted analytes which means is able to differentiate potential interfering substances with the analytes in the blank biological matrix.

Specificity means that the analytical method should be specific for targeted analytes which can differentiate analyte-similar interferences including isomers, degradation compounds and so on in the real sample matrices. In the case of LC-MS based methods, the potential interfering related substance with the analyte should be chromatographically separated from the analytes. The criteria for both selectivity and specificity is that there is no significant response (<20% of analytes at LLOQ (low limit of quantification) and <5% of IS at LLOQ) as interfering compounds at retention of either analytes or IS.

3.4.2 Carryover

Carryover effect is a common phenomenon which can be observed during analytical method development which should be however avoided during method application since it can bring the residual analytes from a previous sample remaining in the instrument into the next injection, which leads to unprecise prediction of the analytes concentration in the following injections in LC-MS systems. Carryover effect can be overcome through needle wash and loop wash step after each injection so that method developer should pay special attention on it in order to minimize the carryover effect to acceptable criteria, which is described by FDA guideline as "Carryover in the blank samples following the highest calibration standard should not be greater than 20% of the analyte response at the LLOQ and 5% of the response for the IS".

3.4.3 Calibration curve and range

The calibration curve reflects the relationship between the analyte concentration and the instrumental response of the analytical method to the analyte. The calibration curve should possess good linearity with spiked standards in the same biological matrices covering concentration from LLOQ to ULOQ (upper limit of quantification) with at least six concentration levels and one zero sample which is the blank sample spiked with only IS in the same matrices.

Criteria is that the accuracy of at least 75% calibration standards at given levels of concentration should be within ±15% (LLOQ within ±20%).

3.4.4 Accuracy and precision

The accuracy and precision are based on the quality control samples (QCs). The QCs should be prepared in the same biological matrices with a minimum of 4 concentration levels: the LLOQ, within 3 times of the LLOQ (low QC), around 30% to 50% of the calibration curve range (medium QC) and at least 75% of the ULOQ (high QC). It is worth to mention that for the real method validation, usually a three levels QC series (low QC, medium QC and high QC) with each level 3 replicates are prepared because of the limited number of matrices, which is acceptable. It is suggested by the FDA that the QCs should be prepared from the separate stock

solution from that for calibration standards to avoid any overestimation of the accuracy and precision.

Both within-run (in each run) and between-run (in different runs, usually on three independent days) accuracy and precision should be determined for each level. Criteria is that the accuracy and precision at each level should be within ±15% except LLOQ (within ±20%).

3.4.5 Extraction recovery, matrix effect and process efficiency

"A matrix effect is defined as an alteration of the analyte response due to interfering and often unidentified component(s) in the sample matrix" [153]. The FDA guidelines include the requirements for matrix effect (ME) but not the extraction recovery (RE) and process efficiency (PE) which are also important parameters for method validation to check whether an analytical method is ready or appropriate for the application for analysing biological samples. Matuszewski 's protocol [154] provides a reference for all these parameters.

ME, RE and PE should be determined based on the three levels of QCs (low QC, medium QC and high QC) with each level 3 replicates. According to the Matuszewski 's protocol, three series of standard solution should be prepared that means for each series three levels QCs with 3 replicates in total 9 for each series and totally 27 for all series. Series 1 (neat solution) is obtained by the dilution of the calibrant stock solution in MeOH or other neat solvents without any extraction procedure. Series 2 (post-spiked) is prepared after the extraction procedure when dried extracts are reconstituted with the standard solutions before LC-MS measurement while for series 3 (pre-spiked) the standard solutions are spiked into the matrices before extraction. If the neat solution standard series 1 is designated as A, series 2 (post-spiked) as B, and series 3 (pre-spiked) as C, the values of extraction recovery, matrix effect, and process efficiency can then be calculated as follows:

$$RE\ (\%) = C/B \times 100 \quad (1)$$

$$ME\ (\%) = B/A \times 100 \quad (2)$$

$$PE\ (\%) = C/A \times 100 = (ME \times RE)/100 \quad (3)$$

There is no criteria for the ME, RE and PE because these parameters are highly dependent on the biological matrices, the extraction method and the targeted compounds. In general, a well-established analytical method should be able to reduce the interference of matrix effect and improve as much as possible the extraction recovery and process efficiency.

3.4.6 Dilution Integrity

Dilution integrity is used to confirm that the sample dilution procedure does not have an impact on the accuracy and precision of measured concentrations of analytes. Dilution QCs should be prepared with spiked analytes in matrices and diluted with different dilution factors with blank matrix, for each dilution factor 5 replicates are required and the accuracy of the dilution QCs should be within ±15% of the nominal concentration and the precision (% CV) should not exceed 15%.

3.4.7 Stability

Stability of analytes in matrix during sample storage, sample preparation and processing is of great importance which ensures the promising and convincing results. As suggested in FDA guidelines, two levels of analytes (low QC and high QC) should be used for stability test from time zero (fresh prepared) to defined time period (including short-term stability and long-term stability) at stored conditions. For biological fluids like plasma, urines, serum and so on, the freeze-thaw cycles should also be included in the stability test. Stability is a big topic in the biological method validation which involved in different aspects from sample stability itself to instrumental stability and so on. More detailed description about each kind of test can be found in FDA guidelines [153].

Criteria for the stability is that the mean concentration at each QC level should be within ±15% of the nominal concentration.

3.4.8 Proficiency testing

Proficiency testing (PT) which is also called the external quality assessment (EQA) is the evaluation of participant performance against pre-established criteria by means of interlaboratory comparisons according to ISO (International standardization organization)/IEC (International Electrotechnical Commission) 17043 [155].

The aim is to monitor the analytical performance of different methods and improve the performance of analytical laboratories. In the proficiency testing in analytical chemistry, the test samples or materials will be distributed equally to different laboratories with unknown composition of the samples. Participants analyse the samples with their own already validated method which are well documented for routine use and the results from different laboratories will be collected, reported and compared [156].

One of the most important benefits of PT is to detect and initiate biases or random variations of an analytical method for particular analytes especially when there is no external reference

and to provide an independent check on the accuracy of the analytical results for participants. This could be used as a useful tool for analytical method validation but is not mandatory during method validation.

3.5 Quantification of lipids

The quantification of lipids in biological matrices is always challenging especially for untargeted lipidomics which is common for biomarker discovery and hypothesis generation where only a relative quantification can be realized. Absolute quantification which is usually realized by targeted lipidomics approach determines the concentration level of individual lipid species especially those with significant regulation confirmed by untargeted approach so that a validation can be conducted in targeted way.

For the quantification of lipids by LC-MS strategy, the concept isotope corrections is of great importance to increase the accuracy of absolute quantification. When isomeric lipid species which have equal molar weight but differential acyl chains were analyzed by MS, the different intensity of monoisotopic peak [M] with different carbon acyl-chain length would be observed due to the differential distribution of isotopologues in those species. If the differential isotopologue distribution which is mainly depending on the number of total carbon atoms is not taken into considerations, bias can be introduced during lipid quantification [157]. There are two types of isotope correction: Type I and Type II. Type I isotope correction is introduced to correct the effect of the different isotopic distribution for different numbers of atoms in the molecule by summing up intensities of all the isotopologues for each species including the internal standard. The total ion intensity of an isotopologue cluster ([M], [M + 1], [M + 2]) of a lipid species is then applied for further quantification. Normally the type I isotopic correction factor increases with longer carbon chain length [158]. Type II isotope correction is introduced to correct the overlap of the monoisotopic signal of interest from isotopomers of the second isotopologue ([M + 2]) of a lipid with one more DB. Ideally these signals can be distinguished by high resolution MS instrument, in that case the Type II correction is not necessary any more [158]. Moreover, chromatographic separation on such species e.g. RPLC could also avoid such interferences, which is not the case for HILIC where only lipid class separation is realized and Type II isotope correction has to be applied for the co-eluted lipids. Furthermore, the isobaric interferences of different adducts e.g. [M + Na] + signal of a lipid with 3 less double bonds and 2 less carbons with the [M + H] + adduct of interest could also leads to the overestimation during quantification especially in HILIC mode where these interferences

cannot be chromatographically separated, such overestimation should also draw attention during the lipid quantification. [158].

Besides the MS aspects, other common challenges are also existing during quantification of lipids in biological samples. For many analytes, the true blank matrices are actually not available for generating a matrix-matched calibration curve. What is more, there are individual variances between each sample especially for clinical lipidomics. Samples e.g. plasma and platelets are usually in a limited amount (in microliter or a few millilitres for plasma) and for a large-scale lipidomic study the investigated samples are in large amount with over hundreds of samples which is not practical to prepare for each matrix a calibration curve [159]. All these challenges require alternative options for calibration and accurate quantification. In general, two main approaches have been proposed: external calibration and internal calibration (see Table 4).

3.5.1 External calibration

External calibration can be simply described as a calibration curve prepared by a dilution of standard mixtures in neat solution (if it is assured that matrix effects are absent or can be corrected for e.g. by isotope labelled IS). This approach is usually an alternative choice when the same matrix from the samples is not available or too limited. The results carried out by the external calibration can only be used as a reference because there will be a relatively high bias based on the accuracy since the process was carried out under far simpler matrix [159] (neat solvent instead of real biological matrices) than that of the biological extract and the matrix effect as well as the extraction loss of different analytes will be ignored which leads to the inaccuracy. Though ideally the stable MS instrument conditions are achieved, other factor including sample preparation could lead to differential recovery and the sample matrix from different donors could vary. All of these factors can contribute to the bias for the quantification based on the external calibration, which is usually not the best choice for a complex biological matrix. One possible approach for the correction of the results is to apply the matrix effect on the analyte response in neat solution or apply the process efficiency if considering the extraction procedure as well on the response of analyte in neat solution, so that the obtained calibration curve can be corrected based on the mentioned consideration. Use of a surrogate matrix which provides the same response as the real matrix is another option. Parallelism of calibration functions in surrogate matrix and real matrix needs to be proven.

3.5.2 Internal calibration

Internal calibration or in other word matrix-matched calibration with IS is nowadays the most commonly used approach. This approach takes the analyte response in real matrix into consideration that could be able to minimize the matrix effect and other detrimental factors. Different strategies are carried out for the quantification of analytes based on the matrix-matched calibration.

3.5.2.1 Single point calibration

In single point calibration, the detected analytes can be simply quantified with the relationship between the concentration (Conc.) and the response intensity (either peak height H or peak area A in MS measurement) with the spiked internal standard (IS) with known concentration.

$$Conc._{analyte} = Conc._{IS} \times A_{analyte} / A_{IS}$$

The method assumes that the response of analytes and detector is linearly correlated with the concentration of analyte [160, 161] when reflecting into the hypothetical calibration curve, it should go through (0,0) or the y intercept is 0. The bias is mainly caused by the too simple prediction model which relies on the strict linear regression through (0,0). However, in most of the case, the relationship between response of analyte and the concentration can be more complicated [161]. Thus, single point calibration is often used for semi-quantification or relative quantification, especially for untargeted lipidomic approach. However, in some researches, it shows comparable results with the multipoint calibration strategy for quantification of analytes in biological matrices [162, 163].

With single point calibration, the selection of IS should be very careful especially for untargeted lipidomics. The choice of appropriate IS for class specific lipids plays an important role for reliable quantitative workflows [77]. According to Lipidomics Standards Initiative (LSI) (https://lipidomics-standards-initiative.org/) which was initiated 2018 by Kim Ekroos and Gerhard Liebisch to develop guidelines for lipidomics, mass spectrometric quantification without ISs is not possible. An internal standard is usually an analogue of the analyte e.g. the stable isotope labelled compounds ^{13}C or deuterated compounds. They should be spiked into the matrix prior extraction during sample preparation to compensate extraction loss and ideally the matrix effect as well (note: for matrix effect correction, the IS must co-elute with the target analytes). What is more, the added amount should be in appropriate concentration which is close to the concentration of targeted analytes in matrix and the IS must be absent in the matrix. LSI summarized some requirements for ISs: (I) not present in the samples (II) addition prior lipid extraction (III) at least one per lipid class (IV) high structural similarity to analytes with

similar number of carbon and/or double bonds (V) simultaneous ionization with the analyte (VI) structural identical stable isotope labelled standards are considered as gold standard.

Ideally the IS should have the same structure and MS ionizability with the analyte so that the identical response factor could be achieved and each analyte should have one specific IS in order for single-point calibration. However, this is not practical especially when there are hundreds or thousands of targets of interest that need to be quantified in complex matrices. As a consequence, the class specific ISs are commonly used nowadays for untargeted lipidomics quantification approach based on the evidence that all the individual lipid species in the same lipid class with the same head groups share nearly identical response factor because ionization of these species is predominantly dependent on their identically charged head groups no matter the carbon chain length and the unsaturation degree in the aliphatic chain [77]. However, this is true only for the polar lipid class with the same charged head group [164] when the extraction efficiency for different polarity of species from short- until extra-long chain was considered as identical. Unfortunately, experiment claims that the extraction loss cannot be compensated by single class specific IS especially with biphasic extraction protocol for polar lipid class for the short and medium-chain polar lipids [124]. What is more, for non-polar lipid classes, there is no dominant ionizable head group for all species to have the chance to impose identical response factor (RF). In this case, response factor [165] of each analyte to the single IS should be confirmed in the neat solution. For the compound A with known concentration in neat solution, the RF to the internal standard can be calculated as follows:

RF= (peak area A/concentration A)/ (peak area IS/concentration IS)

Then, the concentration of the detected compound A in real samples can be calculated according to the equation:

Concentration A= (peak area A×concentration IS)/ (peak area IS×RF)

Moreover, although the LC-MS analysis of lipidomics brings lots of benefits e.g. the isomeric separation for different lipid species which enables the isomeric quantification, some concerns need to be considered as well. In untargeted lipidomics study, gradient elution was used in order to elute different polarity of lipids in one run. However, the gradient elution with different mobile phase composition cause variations in ionization efficiency of analytes at different elution times [166] which means the matrix effect can be different even though for the lipid species in same lipid class but with different retention time, which makes an accurate quantification more difficult. As an alternative way, at least one IS per lipid class should be included in the

untargeted lipidomics for quantitative analysis with applied response factor if possible. In the best case, three ISs covering short-, medium- and long-chain for each lipid class could help increase the accuracy for the quantification of untargeted lipidomics and single point calibration for quantitative analysis of lipids is of great importance especially when the extra matrices are not available.

3.5.2.2 Standard addition calibration

Standard addition [167] is a matrix matched method that spiking a series concentration of pure standards into the aliquots of matrices. According to the calibration curve, the endogenous concentration of analyte can be calculated from the x-intercept (Fig. 16). In order to get the real calibration curve of the analyte, the endogenous amount should be subtracted for each level so that the corrected calibration curve can be obtained which should be ideally in parallel with the original one (Fig. 12). This method is effective and accurate for one sample or only a few samples if the sample volume is high enough for several aliquots as spiking matrices. However, a high volume of samples is needed and extra work has to be done. What's more, it's not practical to use standard addition calibration method for a large-scale clinical study especially when samples are over thousands and the collected volume is low. For example, if 100 samples are collected, for each sample five or more aliquots are required for standards addition, which means 500 samples are prepared during sample preparation. This is certainly too much extra work and not applicable. As an alternative method for large-scale lipidomics, a pooled matrix was prepared and aliquoted for standard addition including one blank matrix without spiking standard to subtract the endogenous amount in matrix in order to get a matrix matched calibration curve (concentration to analyte response) which could be applied for all the measured samples [127]. This method is also called background addition. In this case, ISs spiked in each sample should be in the same concentration level for compensation of extraction loss or the loss caused by instrumental error so that the response is normally the peak area ratio of analytes to corresponding ISs. This method allows matrix-matched calibration but is not suitable when the background contains high concentration of endogenous analytes because the obtained calibration curve could be inaccurate or only suitable for quantification of analytes in a high concentration range in samples instead of those with a low abundant in samples. Moreover, the real matrix for each sample could have a small variance and the pooled matrix could not be able to simulate perfectly the matrix environment for each sample. When applying the method for untargeted lipidomics with hundreds or thousands of analytes, the selection of standards should follow similar rules as described in single point calibration for selection of ISs. At least

one standard for each lipid class should be included in the standard addition quantification in order to get a calibration curve which can be applied for the same lipid class with however three standards covering different chain length for each class the best. Standard addition method is a good choice for matrix matched calibration when the analytes are in low abundance e.g. oxylipins in biological matrix with targeted lipidomics approach [115, 168].

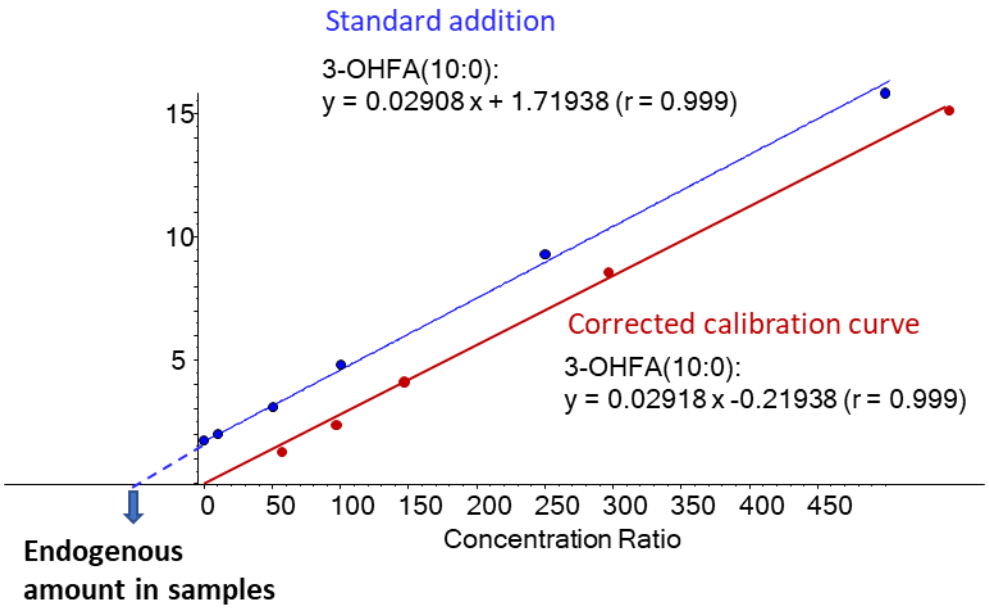

Figure 16 *Calibration curve of 3-OHFA(10:0) based on the standard addition method (blue line) and corrected calibration curve after subtracting the endogenous amount of analytes (red line) in human plasma samples. In calibration curve of standard addition method, the endogenous amount of analytes can be calculated from the x-intercept. Ideally, the two calibration curves should be in parallel.*

3.5.2.3 Surrogate calibration

Surrogate calibration [169] utilizes surrogate standards which are usually stable isotope labelled analogues of the targeted analytes that are not existing in the real matrix to create the calibration curve (Fig. 17). Analytes marked with ^{13}C-, ^{15}N-, or ^{18}O- atoms as analogues were preferred than deuterated compounds because isotope labelled ones were proven to be able to reflect the physicochemical properties including matrix effects of the target analyte in a better way [169]. In surrogate calibration, two different surrogate compounds should be prepared, one as surrogate standard and another as IS. The spiked IS in each sample always keep the same concentration level while the surrogate standard should be in a dilution series to obtain a calibration curve which should be ideally in parallel with the standard addition calibration curve (Fig. 17). It is reported [170] that the response of surrogate standards is not totally identical with the analytes, as a consequence, either the modulation of MS parameters CE or

declustering potential (DP) to balance the two signals or a response factor can be applied to the selected surrogate standards. What's more, the characterization of purchased isotope labelled analogues is necessary for the identification of unlabelled analyte as impurity so that the true concentration of labelled one can be further defined.

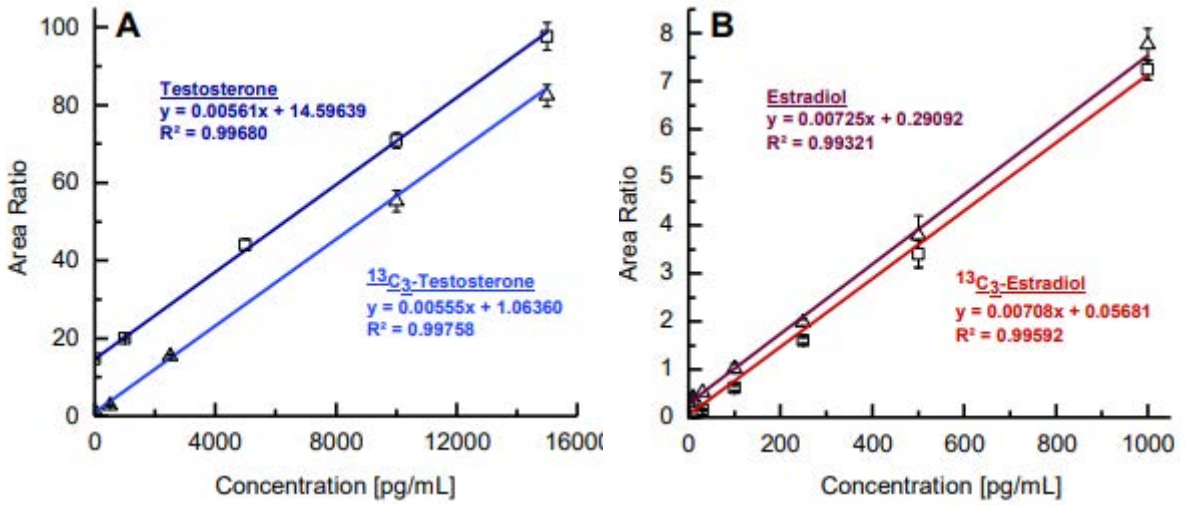

Figure 17 *Parallelism of standard addition curve and corresponding surrogate calibrant curve for (A) Testosterone & $^{13}C3$ Testosterone, (B) Estradiol & $^{13}C3$ Estradiol. Reproduced with permission from [170].Copyrights © 2018 Elsevier B.V.*

With the advantages that the endogenous interference can be ruled out and the property similarity to targeted analytes, surrogate calibration is in recent years sometimes used for quantification of lipids in targeted lipidomic assays [170].

Table 4 *Types and main distinctive features of different calibration methodologies. Modified from [171]*

Type	Calibration methodology	Calibration standard for quantification	Matrix in calibrants	Observations
External	External calibration	Analyte or surrogate	No	Applicable when there is not matrix effects
	matrix-matched calibration	Analyte or surrogate	Yes	Free-analyte matrix must be available
Internal	Single point calibration	Surrogate	Yes	Spiked internal standard should ideally be in similar cocentration range with target analytes
	Standard addition calibration	Analyte	Yes	A different calibration for each sample. When large-scale samples are measured, background addition can be applied
	Multi-points surrogate calibration	Surrogate	Yes	Surrogate and analyte must be metrologicall yand analytically very similar with at least five concentration levels.

4. Large-scale clinical platelet lipidomics study

Clinical lipidomics as the extension area of lipidomics aims to elucidate the lipid profile and investigate metabolic pathways and network in cells, organism or body fluids of patients for possible biomarker discovery or human disease diagnose [172]. The dysregulation of lipid metabolism can be closely associated with pathological state in human diseases such as Alzheimer's disease [173], type 2 diabetes [174], cardiovascular disease [175] and cancers [176]. However, the large individual variation caused by genomic or environmental aspect in patients could result in different lipid profiles in each patient which minimizes the effect of significant features in different groups. As a consequence, large-scale samples are required in order to reduce the biological variation and detect accurately the inter-group variation caused by different treatments and so on. In this thesis, the platelets lipidome will be discussed in terms of patients with cardiovascular disease.

4.1 Platelets and their role in cardiovascular disease

4.1.1 Platelet structure

Platelets or thrombocytes are small non-nuclear cellular components with a diameter of 2-4 µm in resting state and are numerous in human blood with 150,000 up to 400,000 per mm^3 [177, 178]. Since platelets have no cell nucleus, they are limited for cell mitosis and protein synthesis with a short lifetime of 8-9 days [179].

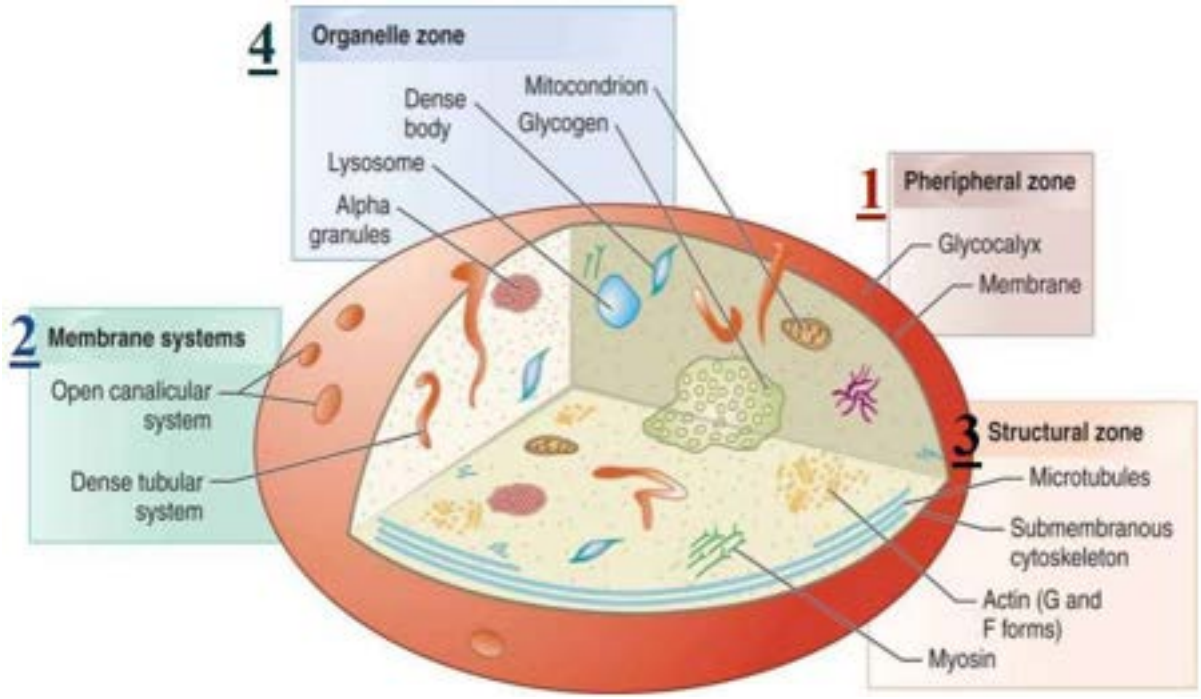

Figure 18 *Structure of platelets showing the cell organelles. Adapted from www.blogspot.com.*

Structurally the platelet can be divided into four zones (I) peripheral zone, (II) sol-gel zone, (III) organelle zone and (IV) membranous zone (Fig. 18). Peripheral zone is rich in glycoproteins (GP) e.g. GPIb/IX/V; GPVI; GPIIb/IIIa which take part in the platelet haemostasis while sol-gel zone mainly consists of microtubules and microfilaments to keep the platelets with discoid shape which is considered similar to oblate spheroids in resting state. Organelle zone is abundant with different types of platelets granules including α-granules, dense granules, lysosomes, and peroxisomes for storage of bioactive substance. The most abundant granules are α-granules with around 50-80 per platelet, which comprises 10% of the platelets volume [180]. α-granules contain clotting mediators such as factor V, factor VIII, fibrinogen, fibronectin, platelet-derived growth factor, and chemotactic agents with distinct bioactivities (pro-inflammatory or anti-inflammatory) for which the functional processes are not fully understood. Other types of granules also play their own role in platelets function: dense granules are crucial for

blood clogging with the platelet-activating mediators such as adenosine diphosphate (ADP), serotonin and Ca^{2+} cations; lysosomes have acidic pH and are important for protein and generally cell degradation because of the containing proteases as well as other enzymes participating into the process; peroxisomes are oxidative organelles with catalase activity and beta-oxidation of very long chain fatty acids (VLCFA) [180]. Membranous zone contains membranes structures organized into dense tubular system (DTS) and open canalicular system [181]. DTS is derived from parent cell endoplasmic reticulum and located within the cell's interior, which play an important role in storage of calcium and enzymes involving in prostaglandin synthesis. The open canalicular system is a complex internal network of membrane channels providing a large surface area for cellular transport and patent remaining during platelet activation with shape change [182].

4.1.2 Platelets function

One major function of platelets is to contribute to haemostasis to stop bleeding caused by vascular injury. The whole process can be divided into 3 main stages (I) adhesion (II) platelets activation (III) platelets aggregation (Fig. 19). When an injury of vascular vessel happens, platelets adhere avidly to the vascular endothelium especially the area of exposed subendothelial collagen (type I and III) and von Willebrand factor (vWF). The interaction between glycoprotein (GP) Ibα, which is a part of the GPIb/IX/V complex and vWF is created to slow down the cells and further binding from platelet GPVI and α2β1 receptors with collagen could be established [183]. Adhesion of platelets to the vascular subendothelial components is the primary response to vessel wall injury [181].

The binding of GPVI and α2β1 receptors with collagen leads to the activation of phospholipase Cγ (PLCγ) which hydrolyse phosphatidylinositol-4,5-bisphosphate (PIP_2) to form inositol-1,4,5-trisphosphate (IP_3) and diacylglycerol (DG). IP_3 further stimulates calcium mobilization from the dense tubular systems to platelet cytoplasm, and increased level of cytosolic Ca2+ and DG cause several changes: (I) the activation of phospholipase A2 (PLA2), leading to formation of thromboxane A2 (TXA2), which could be able to activate other platelets through the membrane thromboxane receptor (TP). TXA2 is a potential platelets agonist that provides platelet-mediated thrombosis. (II) the activation of protein kinase C (PKC), leading to phosphorylation of 47-kd protein. (III) secretion of granule contents. Platelets activation express several granule proteins e.g. vWF and fibrinogen of α-granules which are critical factors for platelet aggregation and granule membrane proteins P-selectin. Adenosine diphosphate (ADP) is released upon platelet activation which could bind to membrane receptor P2Y1 to produce

PLCβ2 that increase in cytosolic Ca^{2+} level. Platelet activation also increase the production of thrombin which is also important platelet agonist. (IV) change of platelet shape (Fig. 20) [184, 185].

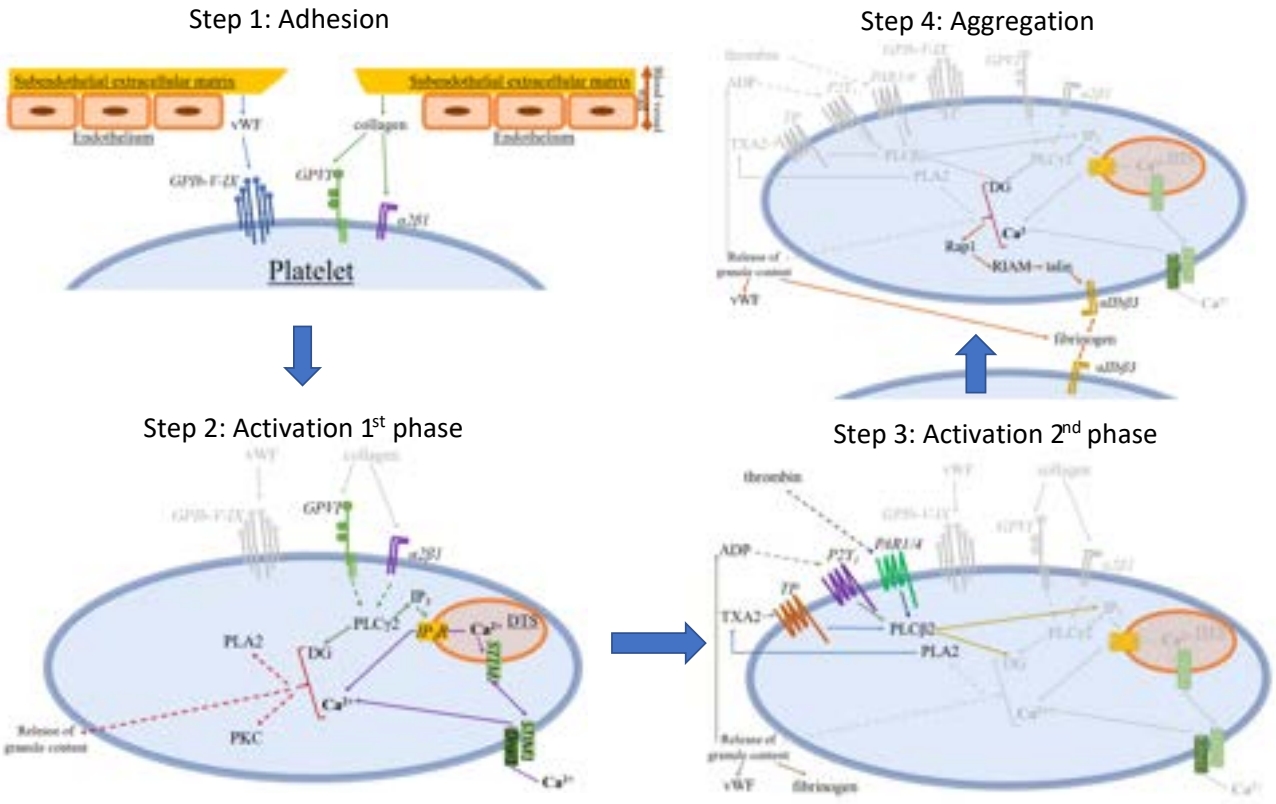

Figure 19 *Schematic overview of platelet Hemostasis: adhesion, activation (phase 1 and phase 2) and aggregation.*

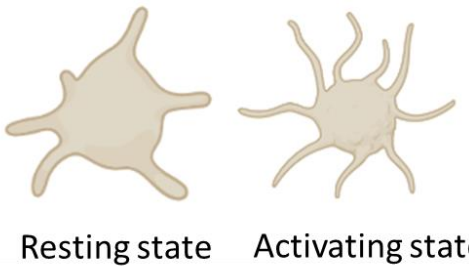

Figure 20 *Simplified platelet shape in resting state (a discoid cell shape) and after activation (a fully spread platelet). Recreated in BioRender.com.*

In the end, platelets aggregation happens through crosslinking of 2 platelets with active membrane integrin αIIbβ3 (activated by a protein complex Rap1b interacting with adaptor molecules RIAM and talin) by symmetric molecule fibrinogen [185].

4.1.3 Cardiovascular disease and platelets lipidome

On the one hand, haemostasis results in blood clot and preventing bleeding when vessel injury happens. On the other hand, it is responsible for a pathological condition called thrombosis, from which platelets aggregate around raptured atherosclerotic plaques blocking the arteries supplying major organs like the heart or brain [186] (Fig. 21). In the end, cardiovascular diseases (CVD) e.g. heart attack, angina, sudden cardiac death, and cerebral stroke are caused by improper blood circulation.

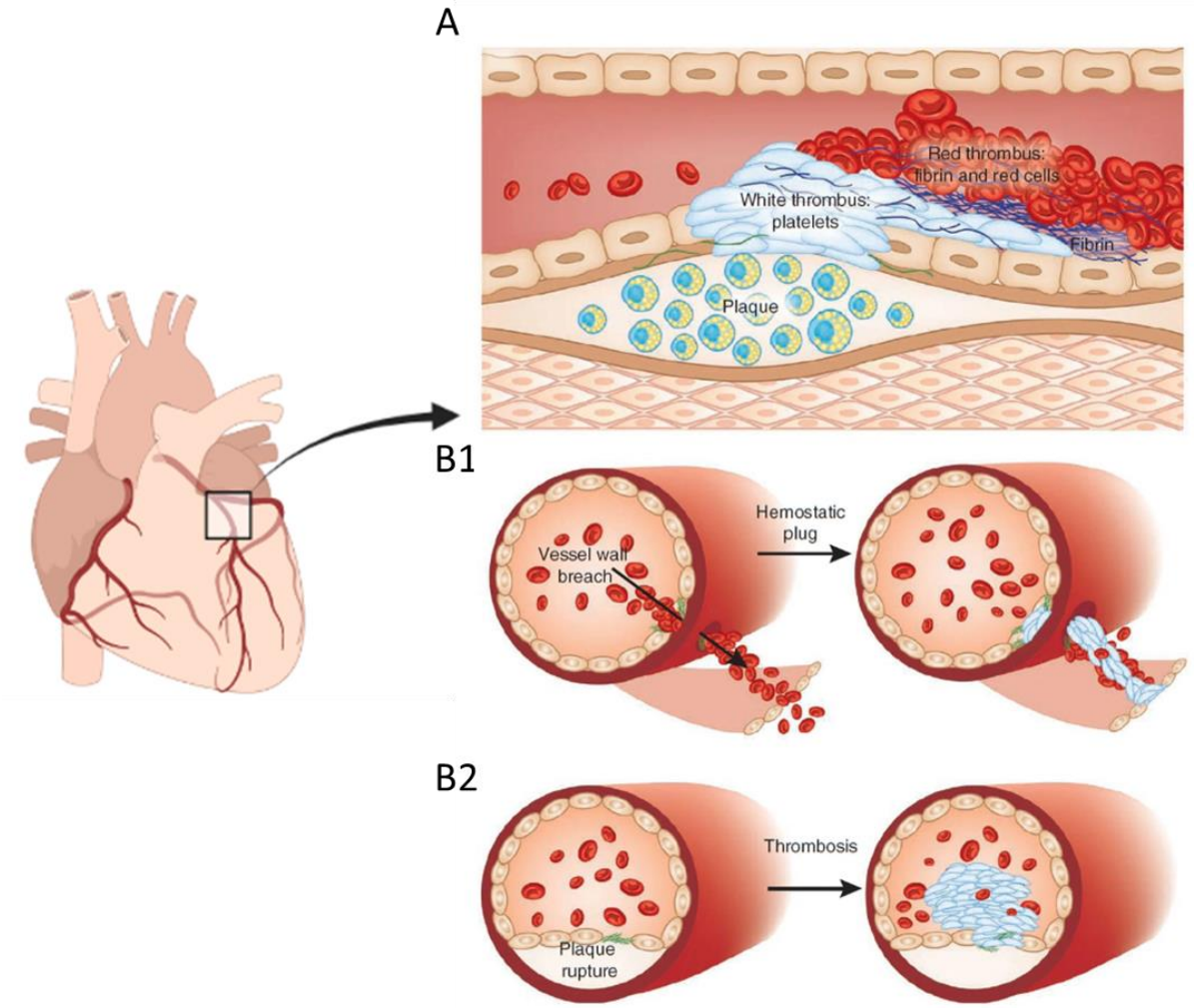

Figure 21 *A: Occlusive arterial thrombi at sites of atherosclerosis plaque rupture in cardiovascular disease. B1: The role of platelets during a primary hemostatic plug at the site of vascular injury with extravascularly aggregation. B2: The role of platelets in thrombosis with intravascular thrombus formation at a ruptured atherosclerotic plug. Reproduced with permission from[183]. Copyright © 2011, Springer Nature America, Inc.*

It is well known that hyperlipidaemia (abnormally elevated levels of any or all the lipids or lipoproteins in the blood) enhances the risk of coronary atherothrombosis. Traditionally, four major lipid categories are tracked to evaluate the CVD risk: total cholesterol, low density lipoprotein (LDL), high density lipoprotein, and triglycerides. Lipid-lowering therapies for dyslipidemia and coronary atherothrombosis suggest that circulatory lipids may modulate platelet functions [187]. Evidently, lipids play an important role in the CVD event. Since platelets are closely associated with vascular inflammation and atheroprogression, the profiling of lipids which play a fundamental role in the regulation of platelet structure, signalling, and activation while promoting thrombosis in platelets could help deeper understanding the metabolic pathway, transportation of blood lipids and the consequences for the pathophysiology of CVD.

The association of lipids with CVD has been widely improved by many studies. Activated platelets generate lysophosphatidic acid (LPA), substantially contributing to atheroprogression [188]. Lysophosphatidylcholine (LPC) has been suggested to be enriched in platelets from CAD patients at vulnerable plaque regions, evidently demonstrating its atherothrombotic attribution [189]. What's more, both pro- and anti-inflammatory lipid mediators generated by activated platelets are also associated with the pathological pathways of CVD. Platelet eicosanoids (TXA2, 12-HETE) and prostaglandins (PGE2, PGD2) regulate monocyte and neutrophil functions while pro-inflammatory leukotrienes (LTs) e.g. LTC4, LTD4 also showed elevated level at the plaque rupture site [188].

Platelet lipidome has attracted interest for several decades while the first comprehensive lipid analysis in platelet could be traced back to 1962 by Marcus and colleagues [190]. Also, with increasing interest in the role of lipids by vascular disease, some studies involving dietary uptake with lipids on platelet lipid fatty acid composition was carried out [191]. The platelet lipidomic landscape might be considered as a powerful tool for diagnostic and prognostic biomarkers for CVD. It is shown that the alteration of lipid profiling (TG, CE, SM, oxidized phospholipids oxPLs, CAR and so on) in CVD patients could be observed [175, 192, 193]. Moreover, oxylipins together with polyunsaturated fatty acids (PUFAs) profiling may also reveal the endogenous balance of prothrombotic AA-derived oxylipins with antithrombotic Dihomo-γ-linolenic acid (DGLA) derivatives [188].

4.2 Strategy in large-scale lipidomics study

For the design of a large-scale lipidomics study, different aspects from experimental to analytical and data processing workflow should be considered. Because of the large number of samples, each step from sample handling, sample preparation to analytical measurement should be

documented in standard operating procedures (SOPs) to maintain the performance for data acquisition of all samples of a cohort in order to acquire high-quality, robust, and reproducible data [194, 195] and each step especially the sample preparation should be efficient, simple to operate, time and cost effective and eco-friendly.

4.2.1 Batch design

The handling and measurements of large amounts of samples (>1000) are usually limited by the capability of extraction procedure (e.g. rack capacity of homogenizer or evaporator) and LC-MS measurements (because of the regular LC-MS instrument maintenance and the capacity for injection of column). Thus, the samples are usually conducted into multiple batches [194]. The samples should be randomly distributed into different batches and the sample amount in each batch should be confirmed at the beginning of the clinical study and followed throughout the whole batches. During sample preparation for each batch, not only the research samples but also the quality control samples (QC), blank extraction samples, NIST SRM 1950 (the National Institute of Standards and Technology Standard Reference Material) plasma and calibrants (matrix-matched calibrants that need to be extracted) should be included; during LC-MS measurement of each batch, the system control samples including blank solvent injection, system suitability test should be included as well. Moreover, the data acquisition for each batch should be performed in both positive and negative ion modes with inter-batch ion source cleaning. One example for the injection order in each batch is shown in Fig. 22.

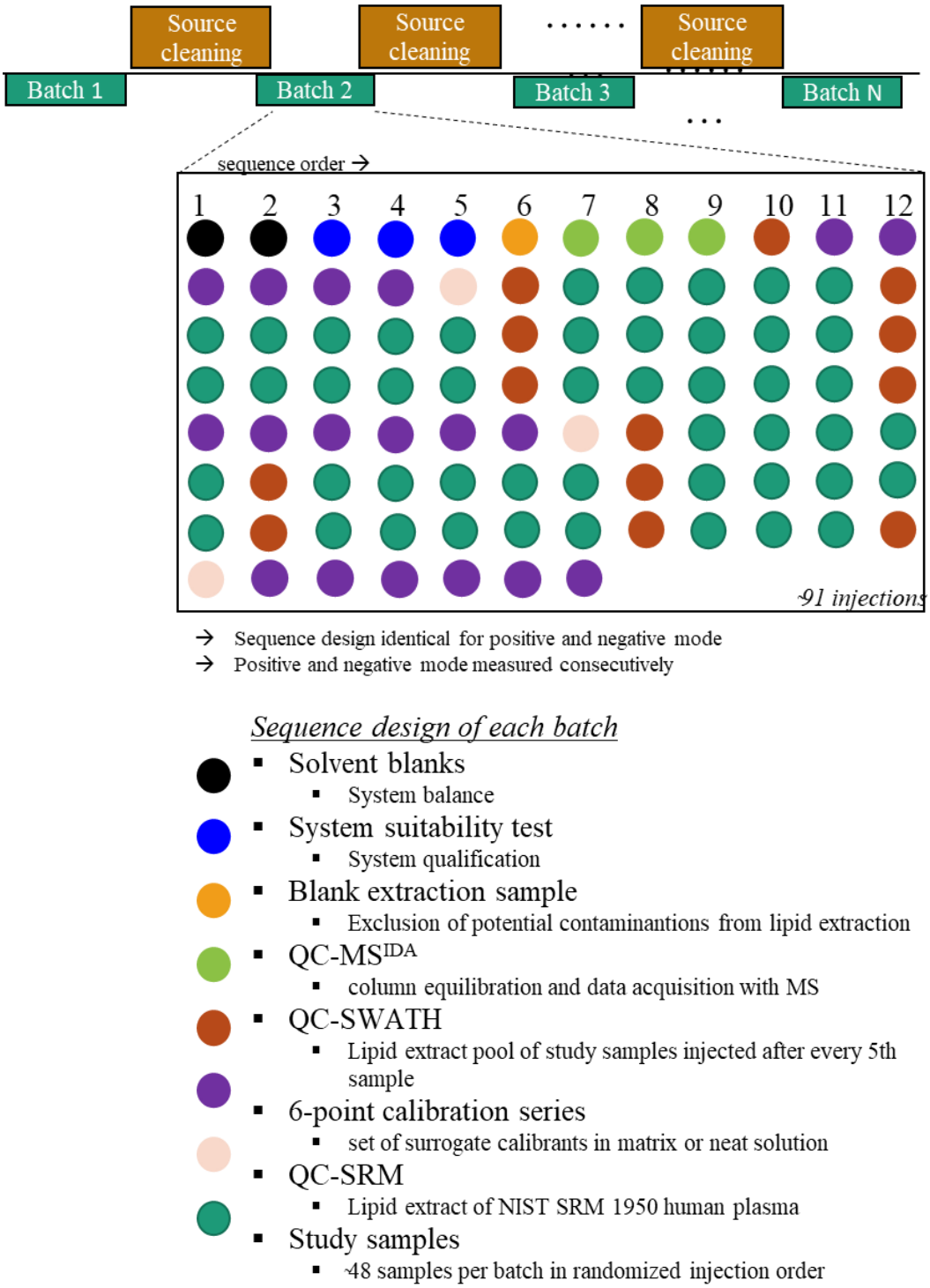

Figure 22 *The sequence of one batch during large-scale clinical lipidomic study.*

4.2.2 Quality control (QC) samples

In untargeted lipidomics assay, quality control samples (QCs) are usually defined as a pooled sample from all the measured samples in the same batch and injected regularly (e.g. every five samples) to monitor the instrumental performance and intra-batch systematic variation throughout the whole sequence [194]. When a large set of samples in several batches over a long period of study time were considered in large-scale clinical lipidomics, suitable quality assurance should be adopted for batch correction and to standardize each lipid species across batches. NIST SRM 1950 has been proposed as a suitable reference material for clinical platforms which is commercially available [196]. What's more, QCs being representative for the analysed matrix is also recommended especially with pooled matrix extracted with the same procedure as clinical samples [195, 197]. For large-scale lipidomics, the preparation of QCs should be taken into consideration at the beginning of all the batches measurements so that enough QCs could be included within each batch and during all the batches, which could be used during data processing for QC-based batch-normalization and inter-batch variation recognition.

Quality control charts were recognized as a useful tool for quality assessment especially in large-scale, long term investigations [198]. In quality control charts, the analyte response (peak area, peak height, peak width, or retention time) is plotted against the injection order either within batch (to access the intra-batch variation) or over the whole batches (inter-batch variation). The acceptance criteria are usually set to the average value with warning (± 2σ) and alert (± 3σ) levels (Fig. 23). Once any point is out of the range, the abnormal injection could be recognized for further data checking and potential removal as outlier. As can be seen from Fig. 23A, the spiked IS 12 HETE-d8 shows constant results in QC samples (injected from the same vials) indicating the good performance of instrument while some variation could be observed in different samples (spiked IS has always the same level in different samples) indicating the extraction loss of individual samples during sample preparation. From the view of QC charts, outliers can be clearly visible. What's more, QC charts could also help to identify the performance of IS for compensation of extraction loss or injection loss of instrument of target oxylipins. Fig. 23B shows the QC chart of detected 12 HETE in QC samples without signal normalization by IS 12 HETE-d8. It can be observed from Fig. 23B that the first several QC injections show decreasing signals with injection orders while this effect can be well compensated by normalization of the peak area of 12 HETE with IS 12 HETE-d8 (peak area ratio:

A/A_{IS}) in the same sample (Fig. 23C), which demonstrates the importance of IS and the QC charts to virtualize such effect in a direct way.

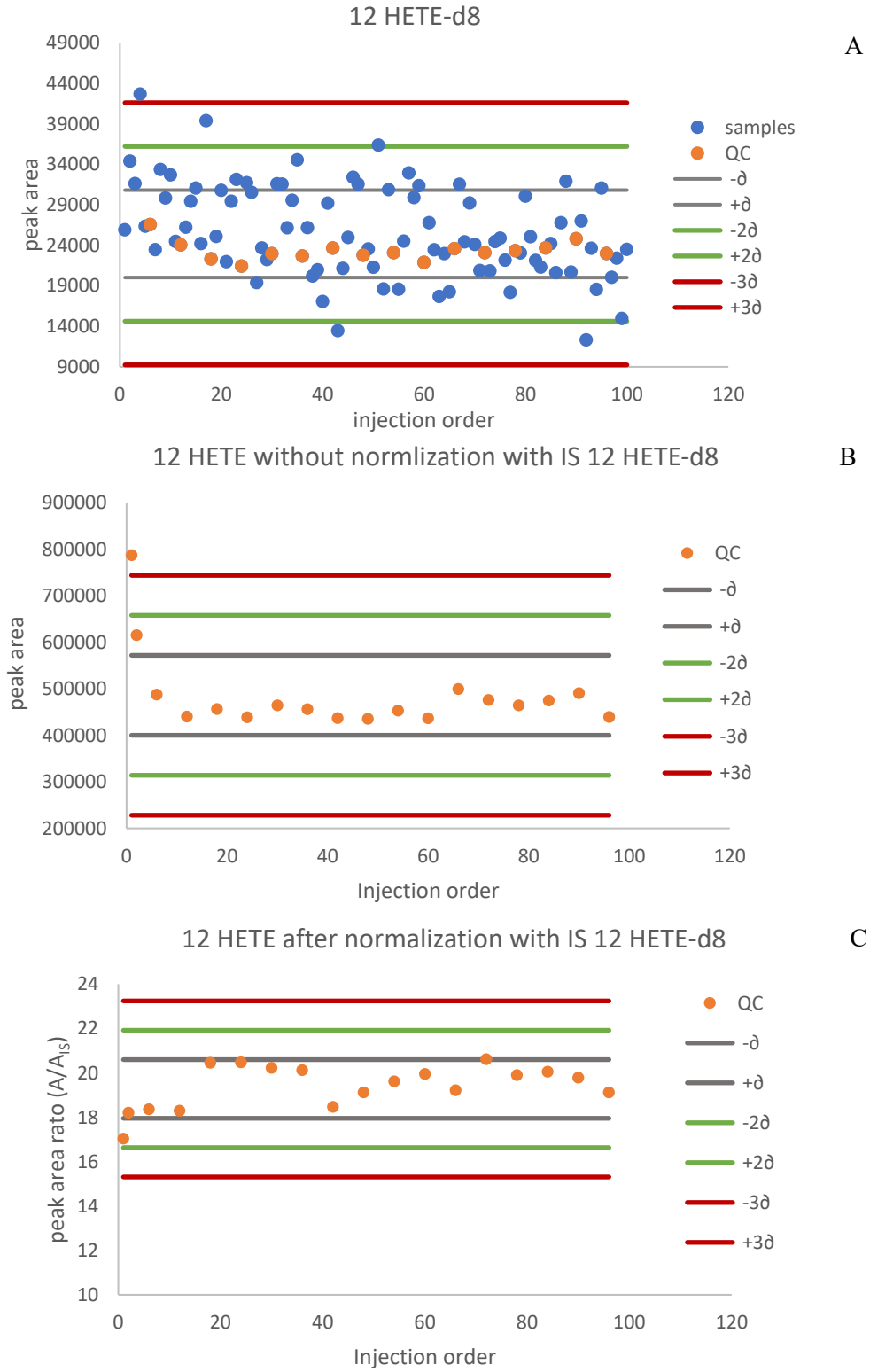

Figure 23 *Quality control chart plotting A: the peak area of the spiked internal standard 12 HETE in different types of samples (the concentration of IS is always the same in different samples) against the injection order within one batch. B: the peak area of the detected endogenous oxylipins 12 HETE in QC samples against the injection order within one batch. C: the peak area ratio (A/A_{IS} normalized by IS 12 HETE-d8) of the detected endogenous oxylipins 12 HETE in QC samples against the injection order within one batch.*

5. List of figures

6. List of tables

7. References

[1] A. Horn, J.K. Jaiswal, Structural and signaling role of lipids in plasma membrane repair, Curr Top Membr, 84 (2019) 67-98.
[2] R. Cammack, Oxford dictionary of biochemistry and molecular biology, Oxford University Press2008.
[3] E. Fahy, D. Cotter, M. Sud, S. Subramaniam, Lipid classification, structures and tools, Biochim Biophys Acta, 1811 (2011) 637-647.
[4] E. Fahy, S. Subramaniam, R.C. Murphy, M. Nishijima, C.R. Raetz, T. Shimizu, F. Spener, G. van Meer, M.J. Wakelam, E.A. Dennis, Update of the LIPID MAPS comprehensive classification system for lipids, J Lipid Res, 50 Suppl (2009) S9-14.
[5] E. Fahy, S. Subramaniam, H.A. Brown, C.K. Glass, A.H. Merrill, Jr., R.C. Murphy, C.R. Raetz, D.W. Russell, Y. Seyama, W. Shaw, T. Shimizu, F. Spener, G. van Meer, M.S. VanNieuwenhze, S.H. White, J.L. Witztum, E.A. Dennis, A comprehensive classification system for lipids, J Lipid Res, 46 (2005) 839-861.
[6] G. Liebisch, E. Fahy, J. Aoki, E.A. Dennis, T. Durand, C.S. Ejsing, M. Fedorova, I. Feussner, W.J. Griffiths, H. Köfeler, A.H. Merrill, Jr., R.C. Murphy, V.B. O'Donnell, O. Oskolkova, S. Subramaniam, M.J.O. Wakelam, F. Spener, Update on LIPID MAPS classification, nomenclature, and shorthand notation for MS-derived lipid structures, J Lipid Res, 61 (2020) 1539-1555.
[7] M. Sud, E. Fahy, D. Cotter, A. Brown, E.A. Dennis, C.K. Glass, A.H. Merrill, Jr., R.C. Murphy, C.R. Raetz, D.W. Russell, S. Subramaniam, LMSD: LIPID MAPS structure database, Nucleic Acids Res, 35 (2007) D527-532.
[8] G. Liebisch, J.A. Vizcaíno, H. Köfeler, M. Trötzmüller, W.J. Griffiths, G. Schmitz, F. Spener, M.J.O. Wakelam, Shorthand notation for lipid structures derived from mass spectrometry, Journal of Lipid Research, 54 (2013) 1523-1530.
[9] G. Liebisch, E. Fahy, J. Aoki, E.A. Dennis, T. Durand, C.S. Ejsing, M. Fedorova, I. Feussner, W.J. Griffiths, H. Köfeler, A.H. Merrill, R.C. Murphy, V.B. O'Donnell, O. Oskolkova, S. Subramaniam, M.J.O. Wakelam, F. Spener, Update on LIPID MAPS classification, nomenclature, and shorthand notation for MS-derived lipid structures, Journal of lipid research, 61 (2020) 1539-1555.
[10] The nomenclature of lipids (recommendations 1976). IUPAC-IUB Commission on Biochemical Nomenclature, J Lipid Res, 19 (1978) 114-128.
[11] O. Quehenberger, A.M. Armando, E.A. Dennis, High sensitivity quantitative lipidomics analysis of fatty acids in biological samples by gas chromatography-mass spectrometry, Biochim Biophys Acta, 1811 (2011) 648-656.
[12] C. Agostoni, M.G. Bruzzese, [Fatty acids: their biochemical and functional classification], Pediatr Med Chir, 14 (1992) 473-479.
[13] T. Řezanka, K. Sigler, Odd-numbered very-long-chain fatty acids from the microbial, animal and plant kingdoms, Progress in Lipid Research, 48 (2009) 206-238.
[14] M. Pfeuffer, A. Jaudszus, Pentadecanoic and Heptadecanoic Acids: Multifaceted Odd-Chain Fatty Acids, Adv Nutr, 7 (2016) 730-734.
[15] A.J. Dijkstra, R.J. Hamilton, W. Hamm, Trans fatty acids, John Wiley & Sons2008.
[16] J.L. Harwood, Fatty acid biosynthesis, Plant lipids, Blackwell2020, pp. 27-66.
[17] T. Kaneda, Iso- and anteiso-fatty acids in bacteria: biosynthesis, function, and taxonomic significance, Microbiol Rev, 55 (1991) 288-302.
[18] T. Kaneda, Iso-and anteiso-fatty acids in bacteria: biosynthesis, function, and taxonomic significance, Microbiological reviews, 55 (1991) 288-302.
[19] J. Nechev, W.W. Christie, R. Robaina, F. de Diego, S. Popov, K. Stefanov, Lipid composition of the sponge Verongia aerophoba from the Canary Islands, European journal of lipid science and technology, 104 (2002) 800-807.
[20] J. Jacob, A. Zeman, Das Bürzeldrüsensekret des Eissturmvogels (Fulmarus glacialis), Uropygial Gland Fat of the Fulmar, 26 (1971) 33-40.
[21] L. Zhang, W. Keung, V. Samokhvalov, W. Wang, G.D. Lopaschuk, Role of fatty acid uptake and fatty acid β-oxidation in mediating insulin resistance in heart and skeletal muscle, Biochimica et Biophysica Acta (BBA)-Molecular and Cell Biology of Lipids, 1801 (2010) 1-22.

[22] S.K. Natarajan, J.A. Ibdah, Role of 3-hydroxy fatty acid-induced hepatic lipotoxicity in acute fatty liver of pregnancy, International journal of molecular sciences, 19 (2018) 322.
[23] S.M. Houten, R.J. Wanders, A general introduction to the biochemistry of mitochondrial fatty acid β-oxidation, Journal of inherited metabolic disease, 33 (2010) 469-477.
[24] S. Uhlig, M. Negård, K.K. Heldal, A. Straumfors, L. Madsø, B. Bakke, W. Eduard, Profiling of 3-hydroxy fatty acids as environmental markers of endotoxin using liquid chromatography coupled to tandem mass spectrometry, J Chromatogr A, 1434 (2016) 119-126.
[25] F. Ianni, Z. Pataj, H. Gross, R. Sardella, B. Natalini, W. Lindner, M. Lämmerhofer, Direct enantioseparation of underivatized aliphatic 3-hydroxyalkanoic acids with a quinine-based zwitterionic chiral stationary phase, J Chromatogr A, 1363 (2014) 101-108.
[26] R. Karongo, J. Jiao, H. Gross, M. Lämmerhofer, Direct enantioselective gradient reversed-phase ultra-high performance liquid chromatography tandem mass spectrometry method for 3-hydroxy alkanoic acids in lipopeptides on an immobilized 1.6 μm amylose-based chiral stationary phase, J Sep Sci, 44 (2021) 1875-1883.
[27] N. Rifai, Tietz textbook of clinical chemistry and molecular diagnostics-e-book, Elsevier Health Sciences2017.
[28] G. Astarita, A.C. Kendall, E.A. Dennis, A. Nicolaou, Targeted lipidomic strategies for oxygenated metabolites of polyunsaturated fatty acids, Biochimica et Biophysica Acta (BBA)-Molecular and Cell Biology of Lipids, 1851 (2015) 456-468.
[29] J.D. Morrow, K.E. Hill, R.F. Burk, T.M. Nammour, K.F. Badr, L.J. Roberts, 2nd, A series of prostaglandin F2-like compounds are produced in vivo in humans by a non-cyclooxygenase, free radical-catalyzed mechanism, Proc Natl Acad Sci U S A, 87 (1990) 9383-9387.
[30] S.C. Dyall, L. Balas, N.G. Bazan, J.T. Brenna, N. Chiang, F. da Costa Souza, J. Dalli, T. Durand, J.M. Galano, P.J. Lein, C.N. Serhan, A.Y. Taha, Polyunsaturated fatty acids and fatty acid-derived lipid mediators: Recent advances in the understanding of their biosynthesis, structures, and functions, Prog Lipid Res, 86 (2022) 101165.
[31] J. Yeung, M. Hawley, M. Holinstat, The expansive role of oxylipins on platelet biology, Journal of Molecular Medicine, 95 (2017) 575-588.
[32] I. Willenberg, A.I. Ostermann, N.H. Schebb, Targeted metabolomics of the arachidonic acid cascade: current state and challenges of LC–MS analysis of oxylipins, Analytical and bioanalytical chemistry, 407 (2015) 2675-2683.
[33] V. Barquissau, R.A. Ghandour, G. Ailhaud, M. Klingenspor, D. Langin, E.-Z. Amri, D.F. Pisani, Control of adipogenesis by oxylipins, GPCRs and PPARs, Biochimie, 136 (2017) 3-11.
[34] J. Yeung, M. Hawley, M. Holinstat, The expansive role of oxylipins on platelet biology, J Mol Med (Berl), 95 (2017) 575-588.
[35] K. Kishimoto, R. Urade, T. Ogawa, T. Moriyama, Nondestructive quantification of neutral lipids by thin-layer chromatography and laser-fluorescent scanning: suitable methods for “lipidome” analysis, Biochemical and biophysical research communications, 281 (2001) 657-662.
[36] X. Han, R.W. Gross, Global analyses of cellular lipidomes directly from crude extracts of biological samples by ESI mass spectrometry: a bridge to lipidomics, Journal of lipid research, 44 (2003) 1071-1079.
[37] X. Han, R.W. Gross, The foundations and development of lipidomics, Journal of lipid research, 63 (2022).
[38] A. Fauland, H. Köfeler, M. Trötzmüller, A. Knopf, J. Hartler, A. Eberl, C. Chitraju, E. Lankmayr, F. Spener, A comprehensive method for lipid profiling by liquid chromatography-ion cyclotron resonance mass spectrometry, Journal of Lipid Research, 52 (2011) 2314-2322.
[39] T. Cajka, O. Fiehn, Comprehensive analysis of lipids in biological systems by liquid chromatography-mass spectrometry, TrAC Trends in Analytical Chemistry, 61 (2014) 192-206.
[40] K. Yang, X. Han, Lipidomics: techniques, applications, and outcomes related to biomedical sciences, Trends in biochemical sciences, 41 (2016) 954-969.
[41] S.J. Blanksby, T.W. Mitchell, Advances in mass spectrometry for lipidomics, Annual Review of Analytical Chemistry, 3 (2010) 433-465.
[42] B. Bisht, V. Kumar, P. Gururani, M.S. Tomar, M. Nanda, M.S. Vlaskin, S. Kumar, A. Kurbatova, The potential of nuclear magnetic resonance (NMR) in metabolomics and lipidomics of microalgae- a review, Archives of Biochemistry and Biophysics, 710 (2021) 108987.

[43] J. Aldana, A. Romero-Otero, M.P. Cala, Exploring the Lipidome: Current Lipid Extraction Techniques for Mass Spectrometry Analysis, Metabolites, 10 (2020).
[44] X. Han, Lipidomics: Comprehensive mass spectrometry of lipids, John Wiley & Sons2016.
[45] J.H. Gross, Mass spectrometry: a textbook, Springer Science & Business Media2006.
[46] S. Banerjee, S. Mazumdar, Electrospray Ionization Mass Spectrometry: A Technique to Access the Information beyond the Molecular Weight of the Analyte, International Journal of Analytical Chemistry, 2012 (2012) 282574.
[47] G. Hart-Smith, S.J. Blanksby, Mass analysis, Mass spectrometry in polymer chemistry, (2012) 5-32.
[48] P.L. Urban, Y.-C. Chen, Y.-S. Wang, Time-resolved mass spectrometry: from concept to applications, John Wiley & Sons2016.
[49] J. Wang, C. Wang, X. Han, Tutorial on lipidomics, Analytica Chimica Acta, 1061 (2019) 28-41.
[50] P.E. Miller, M.B. Denton, The transmission properties of an RF-only quadrupole mass filter, International journal of mass spectrometry and ion processes, 72 (1986) 223-238.
[51] S.U.A.H. Syed, S. Maher, S. Taylor, Quadrupole mass filter operation under the influence of magnetic field, Journal of Mass Spectrometry, 48 (2013) 1325-1339.
[52] S. Maher, S.U. Syed, D.M. Hughes, J.R. Gibson, S. Taylor, Mapping the Stability Diagram of a Quadrupole Mass Spectrometer with a Static Transverse Magnetic Field Applied, Journal of the American Society for Mass Spectrometry, 24 (2013) 1307-1314.
[53] R.E. March, Quadrupole ion trap mass spectrometry: a view at the turn of the century, International Journal of Mass Spectrometry, 200 (2000) 285-312.
[54] W. Paul, H. Steinwedel, Notizen: Ein neues Massenspektrometer ohne Magnetfeld, Zeitschrift für Naturforschung A, 8 (1953) 448-450.
[55] D.J. Douglas, A.J. Frank, D. Mao, Linear ion traps in mass spectrometry, Mass Spectrom Rev, 24 (2005) 1-29.
[56] Time-Of-Flight Mass Spectrometry, Instrumentation and Applications in Biological Research, Instrumentation Science & Technology, 26 (1998) 433-434.
[57] I.V. Chernushevich, A.V. Loboda, B.A. Thomson, An introduction to quadrupole–time-of-flight mass spectrometry, Journal of Mass Spectrometry, 36 (2001) 849-865.
[58] E. De Hoffmann, V. Stroobant, Mass spectrometry: principles and applications, John Wiley & Sons2007.
[59] I.V. Chernushevich, A.V. Loboda, B.A. Thomson, An introduction to quadrupole-time-of-flight mass spectrometry, J Mass Spectrom, 36 (2001) 849-865.
[60] A. Kulyyassov, M. Fresnais, R. Longuespee, Targeted liquid chromatography-tandem mass spectrometry analysis of proteins: Basic principles, applications, and perspectives, Proteomics, 21 (2021) e2100153.
[61] Y. Fillatre, D. Rondeau, A. Jadas-Hecart, P.-Y. Communal, Advantages of the scheduled selected reaction monitoring algorithm in liquid chromatography/ electrospray ionization tandem mass spectrometry multi-residue analysis of 242 pesticides: a comparative approach with classical selected reaction monitoring mode, Rapid Communications in Mass Spectrometry, 24 (2010) 2453–2461.
[62] R.L. Fitzgerald, J.D. Rivera, D.A. Herold, Broad spectrum drug identification directly from urine, using liquid chromatography-tandem mass spectrometry, Clin Chem, 45 (1999) 1224-1234.
[63] T.N. Decaestecker, K.M. Clauwaert, J.F. Van Bocxlaer, W.E. Lambert, E.G. Van den Eeckhout, C.H. Van Peteghem, A.P. De Leenheer, Evaluation of automated single mass spectrometry to tandem mass spectrometry function switching for comprehensive drug profiling analysis using a quadrupole time-of-flight mass spectrometer, Rapid Communications in Mass Spectrometry, 14 (2000) 1787-1792.
[64] J. Guo, T. Huan, Comparison of Full-Scan, Data-Dependent, and Data-Independent Acquisition Modes in Liquid Chromatography-Mass Spectrometry Based Untargeted Metabolomics, Anal Chem, 92 (2020) 8072-8080.
[65] R.S. Plumb, K.A. Johnson, P. Rainville, B.W. Smith, I.D. Wilson, J.M. Castro-Perez, J.K. Nicholson, UPLC/MS(E); a new approach for generating molecular fragment information for biomarker structure elucidation, Rapid Commun Mass Spectrom, 20 (2006) 1989-1994.

[66] B. Simons, D. Kauhanen, T. Sylvänne, K. Tarasov, E. Duchoslav, K. Ekroos, Shotgun lipidomics by sequential precursor ion fragmentation on a hybrid quadrupole time-of-flight mass spectrometer, Metabolites, 2 (2012) 195-213.
[67] L.C. Gillet, P. Navarro, S. Tate, H. Röst, N. Selevsek, L. Reiter, R. Bonner, R. Aebersold, Targeted data extraction of the MS/MS spectra generated by data-independent acquisition: a new concept for consistent and accurate proteome analysis, Molecular & Cellular Proteomics, 11 (2012).
[68] H. Tsugawa, T. Cajka, T. Kind, Y. Ma, B. Higgins, K. Ikeda, M. Kanazawa, J. VanderGheynst, O. Fiehn, M. Arita, MS-DIAL: data-independent MS/MS deconvolution for comprehensive metabolome analysis, Nat Methods, 12 (2015) 523-526.
[69] L. Krasny, P. Bland, N. Kogata, P. Wai, B.A. Howard, R.C. Natrajan, P.H. Huang, SWATH mass spectrometry as a tool for quantitative profiling of the matrisome, J Proteomics, 189 (2018) 11-22.
[70] T. Hu, J.L. Zhang, Mass-spectrometry-based lipidomics, J Sep Sci, 41 (2018) 351-372.
[71] A.T. James, A.J. Martin, Gas-liquid chromatography: the separation and identification of the methyl esters of saturated and unsaturated acids from formic acid to n-octadecanoic acid, Biochem J, 63 (1956) 144-152.
[72] A. Zanfini, E. Dreassi, A. Berardi, P. Piomboni, E. Costantino-Ceccarini, A. Luddi, GC-EI-MS analysis of fatty acid composition in brain and serum of twitcher mouse, Lipids, 49 (2014) 1115-1125.
[73] T. Cajka, O. Fiehn, Comprehensive analysis of lipids in biological systems by liquid chromatography-mass spectrometry, Trends Analyt Chem, 61 (2014) 192-206.
[74] M. Lange, Z. Ni, A. Criscuolo, M. Fedorova, Liquid chromatography techniques in lipidomics research, Chromatographia, 82 (2019) 77-100.
[75] M. Witting, T.V. Maier, S. Garvis, P. Schmitt-Kopplin, Optimizing a ultrahigh pressure liquid chromatography-time of flight-mass spectrometry approach using a novel sub-2μm core-shell particle for in depth lipidomic profiling of Caenorhabditis elegans, J Chromatogr A, 1359 (2014) 91-99.
[76] M. Ovčačíková, M. Lísa, E. Cífková, M. Holčapek, Retention behavior of lipids in reversed-phase ultrahigh-performance liquid chromatography-electrospray ionization mass spectrometry, J Chromatogr A, 1450 (2016) 76-85.
[77] M. Wang, C. Wang, X. Han, Selection of internal standards for accurate quantification of complex lipid species in biological extracts by electrospray ionization mass spectrometry—What, how and why?, Mass spectrometry reviews, 36 (2017) 693-714.
[78] M. Lange, Z. Ni, A. Criscuolo, M. Fedorova, Liquid Chromatography Techniques in Lipidomics Research, Chromatographia, 82 (2018) 77-100.
[79] A. Hartmann, M. Ganzera, Supercritical fluid chromatography–theoretical background and applications on natural products, Planta Medica, 81 (2015) 1570-1581.
[80] P. Jiang, C.A. Lucy, Coupling normal phase liquid chromatography with electrospray ionization mass spectrometry: strategies and applications, Analytical Methods, 8 (2016) 6478-6488.
[81] T. Xu, C. Hu, Q. Xuan, G. Xu, Recent advances in analytical strategies for mass spectrometry-based lipidomics, Anal Chim Acta, 1137 (2020) 156-169.
[82] Y.H. Rustam, G.E. Reid, Analytical Challenges and Recent Advances in Mass Spectrometry Based Lipidomics, Anal Chem, 90 (2018) 374-397.
[83] T.G. do Nascimento, E. de Jesus Oliveira, I.D. Basílio Júnior, J.X. de Araújo-Júnior, R.O. Macêdo, Short-term stability studies of ampicillin and cephalexin in aqueous solution and human plasma: Application of least squares method in Arrhenius equation, J Pharm Biomed Anal, 73 (2013) 59-64.
[84] L.A. Heiskanen, M. Suoniemi, H.X. Ta, K. Tarasov, K. Ekroos, Long-Term Performance and Stability of Molecular Shotgun Lipidomic Analysis of Human Plasma Samples, Analytical Chemistry, 85 (2013) 8757-8763.
[85] G.B. Reis, J.C. Rees, A.A. Ivanova, Z. Kuklenyik, N.M. Drew, J.L. Pirkle, J.R. Barr, Stability of lipids in plasma and serum: Effects of temperature-related storage conditions on the human lipidome, J Mass Spectrom Adv Clin Lab, 22 (2021) 34-42.
[86] M.J. Ryan, A. Grant-St James, N.G. Lawler, M.W. Fear, E. Raby, F.M. Wood, G.L. Maker, J. Wist, E. Holmes, J.K. Nicholson, L. Whiley, N. Gray, Comprehensive Lipidomic Workflow for Multicohort Population Phenotyping Using Stable Isotope Dilution Targeted Liquid Chromatography-Mass Spectrometry, Journal of Proteome Research, 22 (2023) 1419-1433.

[87] T. Cajka, O. Fiehn, Toward Merging Untargeted and Targeted Methods in Mass Spectrometry-Based Metabolomics and Lipidomics, Anal Chem, 88 (2016) 524-545.
[88] F.D.N. Costa, G. Jerz, P. Hewitson, F.S. Figueiredo, S. Ignatova, Laguncularia racemosa Phenolics Profiling by Three-Phase Solvent System Step-Gradient Using High-Performance Countercurrent Chromatography with Off-Line Electrospray Mass-Spectrometry Detection, Molecules, 26 (2021).
[89] Y. Shibusawa, Y. Yamakawa, R. Noji, A. Yanagida, H. Shindo, Y. Ito, Three-phase solvent systems for comprehensive separation of a wide variety of compounds by high-speed counter-current chromatography, J Chromatogr A, 1133 (2006) 119-125.
[90] J. Folch, M. Lees, G.H. Sloane Stanley, A simple method for the isolation and purification of total lipides from animal tissues, J Biol Chem, 226 (1957) 497-509.
[91] E.G. Bligh, W.J. Dyer, A rapid method of total lipid extraction and purification, Can J Biochem Physiol, 37 (1959) 911-917.
[92] H. Zhang, Y. Gao, J. Sun, S. Fan, X. Yao, X. Ran, C. Zheng, M. Huang, H. Bi, Optimization of lipid extraction and analytical protocols for UHPLC-ESI-HRMS-based lipidomic analysis of adherent mammalian cancer cells, Anal Bioanal Chem, 409 (2017) 5349-5358.
[93] C. Breil, M. Abert Vian, T. Zemb, W. Kunz, F. Chemat, "Bligh and Dyer" and Folch Methods for Solid-Liquid-Liquid Extraction of Lipids from Microorganisms. Comprehension of Solvatation Mechanisms and towards Substitution with Alternative Solvents, Int J Mol Sci, 18 (2017).
[94] A. Hara, N.S. Radin, Lipid extraction of tissues with a low-toxicity solvent, Anal Biochem, 90 (1978) 420-426.
[95] V.B. O'Donnell, R.C. Murphy, S.P. Watson, Platelet lipidomics: modern day perspective on lipid discovery and characterization in platelets, Circ Res, 114 (2014) 1185-1203.
[96] V. Matyash, G. Liebisch, T.V. Kurzchalia, A. Shevchenko, D. Schwudke, Lipid extraction by methyl-tert-butyl ether for high-throughput lipidomics, J Lipid Res, 49 (2008) 1137-1146.
[97] L. Löfgren, G.B. Forsberg, M. Ståhlman, The BUME method: a new rapid and simple chloroform-free method for total lipid extraction of animal tissue, Sci Rep, 6 (2016) 27688.
[98] B. Reichl, N. Eichelberg, M. Freytag, J. Gojo, A. Peyrl, W. Buchberger, Evaluation and optimization of common lipid extraction methods in cerebrospinal fluid samples, J Chromatogr B Analyt Technol Biomed Life Sci, 1153 (2020) 122271.
[99] S. Sarkar, T.K. Bhowmick, K. Gayen, Simultaneous extraction of chlorophylls, proteins, and carbohydrates from isolated Chlorella thermophila using a triphasic separation technique: A biorefinery approach, Biofuels, Bioproducts and Biorefining, n/a (2023).
[100] Z. Zhao, Y. Xu, An extremely simple method for extraction of lysophospholipids and phospholipids from blood samples, J Lipid Res, 51 (2010) 652-659.
[101] Y. Satomi, M. Hirayama, H. Kobayashi, One-step lipid extraction for plasma lipidomics analysis by liquid chromatography mass spectrometry, J Chromatogr B Analyt Technol Biomed Life Sci, 1063 (2017) 93-100.
[102] R.M. Pellegrino, A. Di Veroli, A. Valeri, L. Goracci, G. Cruciani, LC/MS lipid profiling from human serum: a new method for global lipid extraction, Anal Bioanal Chem, 406 (2014) 7937-7948.
[103] A. Iriondo, M. Tainta, J. Saldias, M. Arriba, B. Ochoa, F.M. Goñi, P. Martinez-Lage, B. Abad-García, Isopropanol extraction for cerebrospinal fluid lipidomic profiling analysis, Talanta, 195 (2019) 619-627.
[104] J. Zhou, C. Liu, D. Si, B. Jia, L. Zhong, Y. Yin, Workflow development for targeted lipidomic quantification using parallel reaction monitoring on a quadrupole-time of flight mass spectrometry, Anal Chim Acta, 972 (2017) 62-72.
[105] Z.H. Alshehry, C.K. Barlow, J.M. Weir, Y. Zhou, M.J. McConville, P.J. Meikle, An Efficient Single Phase Method for the Extraction of Plasma Lipids, Metabolites, 5 (2015) 389-403.
[106] M.H. Sarafian, M. Gaudin, M.R. Lewis, F.P. Martin, E. Holmes, J.K. Nicholson, M.E. Dumas, Objective set of criteria for optimization of sample preparation procedures for ultra-high throughput untargeted blood plasma lipid profiling by ultra performance liquid chromatography-mass spectrometry, Anal Chem, 86 (2014) 5766-5774.
[107] C. Calderón, C. Sanwald, J. Schlotterbeck, B. Drotleff, M. Lämmerhofer, Comparison of simple monophasic versus classical biphasic extraction protocols for comprehensive UHPLC-MS/MS lipidomic analysis of Hela cells, Anal Chim Acta, 1048 (2019) 66-74.

[108] X. Fu, C. Calderón, T. Harm, M. Gawaz, M. Lämmerhofer, Advanced unified monophasic lipid extraction protocol with wide coverage on the polarity scale optimized for large-scale untargeted clinical lipidomics analysis of platelets, Anal Chim Acta, 1221 (2022) 340155.
[109] T. Hu, C. Tie, Z. Wang, J.L. Zhang, Highly sensitive and specific derivatization strategy to profile and quantitate eicosanoids by UPLC-MS/MS, Anal Chim Acta, 950 (2017) 108-118.
[110] T. Cai, H. Ting, Z. Xin-Xiang, Z. Jiang, Z. Jin-Lan, HPLC-MRM relative quantification analysis of fatty acids based on a novel derivatization strategy, Analyst, 139 (2014) 6154-6159.
[111] S. Poschner, M. Zehl, A. Maier-Salamon, W. Jäger, Simultaneous quantification of estrogens, their precursors and conjugated metabolites in human breast cancer cells by LC-HRMS without derivatization, J Pharm Biomed Anal, 138 (2017) 344-350.
[112] T. Zhang, S. Chen, I. Syed, M. Stahlman, M.J. Kolar, E.A. Homan, Q. Chu, U. Smith, J. Boren, B.B. Kahn, A. Saghatelian, A LC-MS-based workflow for measurement of branched fatty acid esters of hydroxy fatty acids, Nat Protoc, 11 (2016) 747-763.
[113] D. Jones, J. Watson, W. Meredith, M. Chen, B. Bennett, Determination of naphthenic acids in crude oils using nonaqueous ion exchange solid-phase extraction, Analytical Chemistry, 73 (2001) 703-707.
[114] P.O. Helmer, A. Korf, H. Hayen, Analysis of artificially oxidized cardiolipins and monolyso-cardiolipins via liquid chromatography/high-resolution mass spectrometry and Kendrick mass defect plots after hydrophilic interaction liquid chromatography based sample preparation, Rapid Commun Mass Spectrom, 34 (2020) e8566.
[115] M. Cebo, X. Fu, M. Gawaz, M. Chatterjee, M. Lammerhofer, Micro-UHPLC-MS/MS method for analysis of oxylipins in plasma and platelets, J Pharm Biomed Anal, 189 (2020) 113426.
[116] I. Liakh, A. Pakiet, T. Sledzinski, A. Mika, Modern Methods of Sample Preparation for the Analysis of Oxylipins in Biological Samples, Molecules, 24 (2019).
[117] M. Shehadul Islam, A. Aryasomayajula, P.R. Selvaganapathy, A review on macroscale and microscale cell lysis methods, Micromachines, 8 (2017) 83.
[118] N. Rajapakse, K. Shimizu, M. Payne, D. Busija, Isolation and characterization of intact mitochondria from neonatal rat brain, Brain Research Protocols, 8 (2001) 176-183.
[119] L. Benov, J. Al-Ibraheem, Disrupting Escherichia coli: a comparison of methods, BMB Reports, 35 (2002) 428-431.
[120] T. Kristián, I.B. Hopkins, M.C. McKenna, G. Fiskum, Isolation of mitochondria with high respiratory control from primary cultures of neurons and astrocytes using nitrogen cavitation, Journal of neuroscience methods, 152 (2006) 136-143.
[121] S. Chaiyarit, V. Thongboonkerd, Comparative analyses of cell disruption methods for mitochondrial isolation in high-throughput proteomics study, Analytical biochemistry, 394 (2009) 249-258.
[122] J. Niklas, A. Melnyk, Y. Yuan, E. Heinzle, Selective permeabilization for the high-throughput measurement of compartmented enzyme activities in mammalian cells, Analytical biochemistry, 416 (2011) 218-227.
[123] J. Moebius, R.P. Zahedi, U. Lewandrowski, C. Berger, U. Walter, A. Sickmann, The Human Platelet Membrane Proteome Reveals Several New Potential Membrane Proteins*S, Molecular & Cellular Proteomics, 4 (2005) 1754-1761.
[124] X. Fu, C. Calderon, T. Harm, M. Gawaz, M. Lammerhofer, Advanced unified monophasic lipid extraction protocol with wide coverage on the polarity scale optimized for large-scale untargeted clinical lipidomics analysis of platelets, Anal Chim Acta, 1221 (2022) 340155.
[125] N. Danne-Rasche, C. Coman, R. Ahrends, Nano-LC/NSI MS refines lipidomics by enhancing lipid coverage, measurement sensitivity, and linear dynamic range, Analytical chemistry, 90 (2018) 8093-8101.
[126] M. Cebo, J. Schlotterbeck, M. Gawaz, M. Chatterjee, M. Lämmerhofer, Simultaneous targeted and untargeted UHPLC-ESI-MS/MS method with data-independent acquisition for quantification and profiling of (oxidized) fatty acids released upon platelet activation by thrombin, Anal Chim Acta, 1094 (2020) 57-69.
[127] X. Fu, Z. Xu, M. Gawaz, M. Lammerhofer, UHPLC-MS/MS method for chiral separation of 3-hydroxy fatty acids on amylose-based chiral stationary phase and its application for the enantioselective analysis in plasma and platelets, J Pharm Biomed Anal, 223 (2023) 115151.

[128] T. Kind, K.H. Liu, D.Y. Lee, B. DeFelice, J.K. Meissen, O. Fiehn, LipidBlast in silico tandem mass spectrometry database for lipid identification, Nat Methods, 10 (2013) 755-758.
[129] C. Guijas, J.R. Montenegro-Burke, X. Domingo-Almenara, A. Palermo, B. Warth, G. Hermann, G. Koellensperger, T. Huan, W. Uritboonthai, A.E. Aisporna, D.W. Wolan, M.E. Spilker, H.P. Benton, G. Siuzdak, METLIN: A Technology Platform for Identifying Knowns and Unknowns, Anal Chem, 90 (2018) 3156-3164.
[130] G. Hopfgartner, D. Tonoli, E. Varesio, High-resolution mass spectrometry for integrated qualitative and quantitative analysis of pharmaceuticals in biological matrices, Analytical and bioanalytical chemistry, 402 (2012) 2587-2596.
[131] R.S. Plumb, K.A. Johnson, P. Rainville, B.W. Smith, I.D. Wilson, J.M. Castro-Perez, J.K. Nicholson, UPLC/MSE; a new approach for generating molecular fragment information for biomarker structure elucidation, Rapid Communications in Mass Spectrometry: An International Journal Devoted to the Rapid Dissemination of Up-to-the-Minute Research in Mass Spectrometry, 20 (2006) 1989-1994.
[132] L.C. Gillet, P. Navarro, S. Tate, H. Röst, N. Selevsek, L. Reiter, R. Bonner, R. Aebersold, Targeted data extraction of the MS/MS spectra generated by data-independent acquisition: a new concept for consistent and accurate proteome analysis, Mol Cell Proteomics, 11 (2012) O111.016717.
[133] T. Zullig, M. Trotzmuller, H.C. Kofeler, Lipidomics from sample preparation to data analysis: a primer, Anal Bioanal Chem, 412 (2020) 2191-2209.
[134] H. Tsugawa, K. Ikeda, M. Takahashi, A. Satoh, Y. Mori, H. Uchino, N. Okahashi, Y. Yamada, I. Tada, P. Bonini, Y. Higashi, Y. Okazaki, Z. Zhou, Z.J. Zhu, J. Koelmel, T. Cajka, O. Fiehn, K. Saito, M. Arita, M. Arita, A lipidome atlas in MS-DIAL 4, Nat Biotechnol, 38 (2020) 1159-1163.
[135] H. Tsugawa, T. Cajka, T. Kind, Y. Ma, B. Higgins, K. Ikeda, M. Kanazawa, J. VanderGheynst, O. Fiehn, M. Arita, MS-DIAL: data-independent MS/MS deconvolution for comprehensive metabolome analysis, Nature methods, 12 (2015) 523-526.
[136] J. Pfeuffer, T. Sachsenberg, O. Alka, M. Walzer, A. Fillbrunn, L. Nilse, O. Schilling, K. Reinert, O. Kohlbacher, OpenMS–a platform for reproducible analysis of mass spectrometry data, Journal of biotechnology, 261 (2017) 142-148.
[137] J.P. Koelmel, N.M. Kroeger, C.Z. Ulmer, J.A. Bowden, R.E. Patterson, J.A. Cochran, C.W. Beecher, T.J. Garrett, R.A. Yost, LipidMatch: an automated workflow for rule-based lipid identification using untargeted high-resolution tandem mass spectrometry data, BMC bioinformatics, 18 (2017) 1-11.
[138] M. Cebo, C. Calderón Castro, J. Schlotterbeck, M. Gawaz, M. Chatterjee, M. Lämmerhofer, Untargeted UHPLC-ESI-QTOF-MS/MS analysis with targeted feature extraction at precursor and fragment level for profiling of the platelet lipidome with ex vivo thrombin-activation, J Pharm Biomed Anal, 205 (2021) 114301.
[139] A.K. Boysen, K.R. Heal, L.T. Carlson, A.E. Ingalls, Best-matched internal standard normalization in liquid chromatography–mass spectrometry metabolomics applied to environmental samples, Analytical chemistry, 90 (2018) 1363-1369.
[140] M. Sysi-Aho, M. Katajamaa, L. Yetukuri, M. Orešič, Normalization method for metabolomics data using optimal selection of multiple internal standards, BMC bioinformatics, 8 (2007) 1-17.
[141] H. Redestig, A. Fukushima, H. Stenlund, T. Moritz, M. Arita, K. Saito, M. Kusano, Compensation for systematic cross-contribution improves normalization of mass spectrometry based metabolomics data, Analytical chemistry, 81 (2009) 7974-7980.
[142] J.P. Koelmel, J.A. Cochran, C.Z. Ulmer, A.J. Levy, R.E. Patterson, B.C. Olsen, R.A. Yost, J.A. Bowden, T.J. Garrett, Software tool for internal standard based normalization of lipids, and effect of data-processing strategies on resulting values, BMC Bioinformatics, 20 (2019) 217.
[143] B. Li, J. Tang, Q. Yang, S. Li, X. Cui, Y. Li, Y. Chen, W. Xue, X. Li, F. Zhu, NOREVA: normalization and evaluation of MS-based metabolomics data, Nucleic Acids Res, 45 (2017) W162-w170.
[144] S.-Y. Wang, C.-H. Kuo, Y.J. Tseng, Batch Normalizer: a fast total abundance regression calibration method to simultaneously adjust batch and injection order effects in liquid chromatography/time-of-flight mass spectrometry-based metabolomics data and comparison with current calibration methods, Analytical chemistry, 85 (2013) 1037-1046.

[145] H. Luan, F. Ji, Y. Chen, Z. Cai, statTarget: A streamlined tool for signal drift correction and interpretations of quantitative mass spectrometry-based omics data, Analytica chimica acta, 1036 (2018) 66-72.
[146] J.D. Storey, The positive false discovery rate: a Bayesian interpretation and the q-value, The Annals of Statistics, 31 (2003) 2013-2035, 2023.
[147] Y. Benjamini, Y. Hochberg, Controlling the False Discovery Rate: A Practical and Powerful Approach to Multiple Testing, Journal of the Royal Statistical Society: Series B (Methodological), 57 (1995) 289-300.
[148] G. Su, J.H. Morris, B. Demchak, G.D. Bader, Biological network exploration with Cytoscape 3, Current protocols in bioinformatics, 47 (2014) 8.13. 11-18.13. 24.
[149] J. Xia, N. Psychogios, N. Young, D.S. Wishart, MetaboAnalyst: a web server for metabolomic data analysis and interpretation, Nucleic acids research, 37 (2009) W652-W660.
[150] M. Kanehisa, M. Araki, S. Goto, M. Hattori, M. Hirakawa, M. Itoh, T. Katayama, S. Kawashima, S. Okuda, T. Tokimatsu, KEGG for linking genomes to life and the environment, Nucleic acids research, 36 (2007) D480-D484.
[151] B.H. Junker, C. Klukas, F. Schreiber, VANTED: a system for advanced data analysis and visualization in the context of biological networks, BMC bioinformatics, 7 (2006) 1-13.
[152] V.P. Shah, K.K. Midha, S. Dighe, I.J. McGilveray, J.P. Skelly, A. Yacobi, T. Layloff, C. Viswanathan, C.E. Cook, R. McDowall, Analytical methods validation: bioavailability, bioequivalence, and pharmacokinetic studies, Journal of pharmaceutical sciences, 81 (1992) 309-312.
[153] I.H. Guideline, Bioanalytical method validation and study sample analysis M10, ICH Harmonised Guideline: Geneva, Switzerland, (2022).
[154] B.K. Matuszewski, M. Constanzer, C. Chavez-Eng, Strategies for the assessment of matrix effect in quantitative bioanalytical methods based on HPLC− MS/MS, Analytical chemistry, 75 (2003) 3019-3030.
[155] D.W. Tholen, Update on ISO/IEC 17043: the new international standard for proficiency testing, Accreditation and Quality Assurance, 14 (2009) 635.
[156] M. Thompson, R. Wood, International harmonized protocol for proficiency testing of (chemical) analytical laboratories, Journal of AOAC International, 76 (1993) 926-940.
[157] K. Yang, X. Han, Accurate Quantification of Lipid Species by Electrospray Ionization Mass Spectrometry — Meets a Key Challenge in Lipidomics, Metabolites, 1 (2011) 21-40.
[158] M. Lange, M. Fedorova, Evaluation of lipid quantification accuracy using HILIC and RPLC MS on the example of NIST® SRM® 1950 metabolites in human plasma, Anal Bioanal Chem, 412 (2020) 3573-3584.
[159] S. Alseekh, A. Aharoni, Y. Brotman, K. Contrepois, J. D'Auria, J. Ewald, J. C. Ewald, P.D. Fraser, P. Giavalisco, R.D. Hall, Mass spectrometry-based metabolomics: a guide for annotation, quantification and best reporting practices, Nature methods, 18 (2021) 747-756.
[160] L. Cuadros-Rodríguez, L. Gámiz-Gracia, E.M. Almansa-López, J.M. Bosque-Sendra, Calibration in chemical measurement processes. II. A methodological approach, TrAC Trends in Analytical Chemistry, 20 (2001) 620-636.
[161] M.J. Cardone, P.J. Palermo, L.B. Sybrandt, Potential error in single-point-ratio calculations based on linear calibration curves with a significant intercept, Analytical Chemistry, 52 (1980) 1187-1191.
[162] S. Wang, J.E. Magill, F.B. Vicente, A fast and simple high-performance liquid chromatography/mass spectrometry method for simultaneous measurement of whole blood tacrolimus and sirolimus, Arch Pathol Lab Med, 129 (2005) 661-665.
[163] M.K. Bjørk, M.K.K. Nielsen, L.Ø. Markussen, H.B. Klinke, K. Linnet, Determination of 19 drugs of abuse and metabolites in whole blood by high-performance liquid chromatography-tandem mass spectrometry, Anal Bioanal Chem, 396 (2010) 2393-2401.
[164] H.C. Köfeler, R. Ahrends, E.S. Baker, K. Ekroos, X. Han, N. Hoffmann, M. Holčapek, M.R. Wenk, G. Liebisch, Recommendations for good practice in MS-based lipidomics, Journal of lipid research, 62 (2021).
[165] E. Cífková, M. Holčapek, M. Lísa, M. Ovčačíková, A. Lyčka, F. Lynen, P. Sandra, Nontargeted quantitation of lipid classes using hydrophilic interaction liquid chromatography-electrospray

ionization mass spectrometry with single internal standard and response factor approach, Anal Chem, 84 (2012) 10064-10070.
[166] M. Wang, C. Wang, X. Han, Selection of internal standards for accurate quantification of complex lipid species in biological extracts by electrospray ionization mass spectrometry-What, how and why?, Mass Spectrom Rev, 36 (2017) 693-714.
[167] M. Bader, A systematic approach to standard addition methods in instrumental analysis, Journal of Chemical Education, 57 (1980) 703.
[168] M. Cebo, X. Fu, M. Gawaz, M. Chatterjee, M. Lammerhofer, Enantioselective ultra-high performance liquid chromatography-tandem mass spectrometry method based on sub-2microm particle polysaccharide column for chiral separation of oxylipins and its application for the analysis of autoxidized fatty acids and platelet releasates, J Chromatogr A, 1624 (2020) 461206.
[169] N.C. van de Merbel, Quantitative determination of endogenous compounds in biological samples using chromatographic techniques, TrAC Trends in Analytical Chemistry, 27 (2008) 924-933.
[170] B. Drotleff, M. Hallschmid, M. Lämmerhofer, Quantification of steroid hormones in plasma using a surrogate calibrant approach and UHPLC-ESI-QTOF-MS/MS with SWATH-acquisition combined with untargeted profiling, Analytica chimica acta, 1022 (2018) 70-80.
[171] L. Cuadros-Rodriguez, M.G. Bagur-Gonzalez, M. Sanchez-Vinas, A. Gonzalez-Casado, A.M. Gomez-Saez, Principles of analytical calibration/quantification for the separation sciences, J Chromatogr A, 1158 (2007) 33-46.
[172] T.G. Meikle, K. Huynh, C. Giles, P.J. Meikle, Clinical lipidomics: realizing the potential of lipid profiling, J Lipid Res, 62 (2021) 100127.
[173] A. Naudí, R. Cabré, M. Jové, V. Ayala, H. Gonzalo, M. Portero-Otín, I. Ferrer, R. Pamplona, Chapter Five - Lipidomics of Human Brain Aging and Alzheimer's Disease Pathology, in: M.J. Hurley (Ed.) International Review of Neurobiology, Academic Press2015, pp. 133-189.
[174] Z.H. Alshehry, P.A. Mundra, C.K. Barlow, N.A. Mellett, G. Wong, M.J. McConville, J. Simes, A.M. Tonkin, D.R. Sullivan, E.H. Barnes, Plasma lipidomic profiles improve on traditional risk factors for the prediction of cardiovascular events in type 2 diabetes mellitus, Circulation, 134 (2016) 1637-1650.
[175] T. Harm, A. Bild, K. Dittrich, A. Goldschmied, J. Nestele, M. Chatterjee, X. Fu, K. Kolb, T. Castor, O. Borst, T. Geisler, D. Rath, M. LaMmerhofer, M. Gawaz, Acute coronary syndrome is associated with a substantial change in the platelet lipidome, Cardiovasc Res, 118 (2022) 1904-1916.
[176] D. Wolrab, R. Jirásko, E. Cífková, M. Höring, D. Mei, M. Chocholoušková, O. Peterka, J. Idkowiak, T. Hrnčiarová, L. Kuchař, R. Ahrends, R. Brumarová, D. Friedecký, G. Vivo-Truyols, P. Škrha, J. Škrha, R. Kučera, B. Melichar, G. Liebisch, R. Burkhardt, M.R. Wenk, A. Cazenave-Gassiot, P. Karásek, I. Novotný, R. Hrstka, M. Holčapek, Lipidomic profiling of human serum enables detection of pancreatic cancer, medRxiv, (2021) 2021.2001.2022.21249767.
[177] M. Mustapha, C.M.N.C.M. Nassir, N. Aminuddin, A.A. Safri, M.M. Ghazali, Cerebral small vessel disease (CSVD)–lessons from the animal models, Frontiers in physiology, 10 (2019) 1317.
[178] K. Broos, S.F. De Meyer, H.B. Feys, K. Vanhoorelbeke, H. Deckmyn, Blood platelet biochemistry, Thrombosis research, 129 (2012) 245-249.
[179] M.E. Quach, W. Chen, R. Li, Mechanisms of platelet clearance and translation to improve platelet storage, Blood, The Journal of the American Society of Hematology, 131 (2018) 1512-1521.
[180] J.L. Fitch-Tewfik, R. Flaumenhaft, Platelet granule exocytosis: a comparison with chromaffin cells, Frontiers in endocrinology, 4 (2013) 77.
[181] R.C. Becker, Platelet Biology: The Role of Platelets in Hemostasis, Thrombosis and Inflammation, Platelets in Cardiovascular Disease, pp. 1-36.
[182] M.V. Selvadurai, J.R. Hamilton, Structure and function of the open canalicular system - the platelet's specialized internal membrane network, Platelets, 29 (2018) 319-325.
[183] S.P. Jackson, Arterial thrombosis—insidious, unpredictable and deadly, Nature medicine, 17 (2011) 1423-1436.
[184] P.E. van der Meijden, J.W. Heemskerk, Platelet biology and functions: new concepts and clinical perspectives, Nature Reviews Cardiology, 16 (2019) 166-179.
[185] J.M. Stassen, J. Arnout, H. Deckmyn, The hemostatic system, Current medicinal chemistry, 11 (2004) 2245-2260.

[186] J.G. Gribben, No longer too exhausted to run, Blood, 132 (2018) 464-465.
[187] J. Soppert, M. Lehrke, N. Marx, J. Jankowski, H. Noels, Lipoproteins and lipids in cardiovascular disease: from mechanistic insights to therapeutic targeting, Advanced drug delivery reviews, 159 (2020) 4-33.
[188] M. Chatterjee, Platelet lipidome: Dismantling the “Trojan horse” in the bloodstream, Journal of Thrombosis and Haemostasis, 18 (2020) 543-557.
[189] M. Chatterjee, D. Rath, J. Schlotterbeck, J. Rheinlaender, B. Walker-Allgaier, N. Alnaggar, M. Zdanyte, I. Müller, O. Borst, T. Geisler, T.E. Schäffer, M. Lämmerhofer, M. Gawaz, Regulation of oxidized platelet lipidome: implications for coronary artery disease, Eur Heart J, 38 (2017) 1993-2005.
[190] A.J. Marcus, H.L. Ullman, L.B. Safier, H.S. Ballard, Platelet phosphatides. Their fatty acid and aldehyde composition and activity in different clotting systems, The Journal of clinical investigation, 41 (1962) 2198-2212.
[191] V.B. O’Donnell, R.C. Murphy, S.P. Watson, Platelet lipidomics: modern day perspective on lipid discovery and characterization in platelets, Circulation research, 114 (2014) 1185-1203.
[192] M. Cebo, K. Dittrich, X. Fu, M.C. Manke, F. Emschermann, J. Rheinlaender, H. von Eysmondt, N. Ferreirós, J. Sudman, A. Witte, Platelet ACKR3/CXCR7 favors antiplatelet lipids over an atherothrombotic lipidome and regulates thromboinflammation, Blood, 139 (2022) 1722-1742.
[193] M. Chatterjee, D. Rath, J. Schlotterbeck, J. Rheinlaender, B. Walker-Allgaier, N. Alnaggar, M. Zdanyte, I. Müller, O. Borst, T. Geisler, Regulation of oxidized platelet lipidome: implications for coronary artery disease, European heart journal, 38 (2017) 1993-2005.
[194] W.B. Dunn, I.D. Wilson, A.W. Nicholls, D. Broadhurst, The importance of experimental design and QC samples in large-scale and MS-driven untargeted metabolomic studies of humans, Bioanalysis, 4 (2012) 2249-2264.
[195] E. Zelena, W.B. Dunn, D. Broadhurst, S. Francis-McIntyre, K.M. Carroll, P. Begley, S. O’Hagan, J.D. Knowles, A. Halsall, HUSERMET Consortium, Development of a robust and repeatable UPLC− MS method for the long-term metabolomic study of human serum, Analytical chemistry, 81 (2009) 1357-1364.
[196] J.A. Bowden, A. Heckert, C.Z. Ulmer, C.M. Jones, J.P. Koelmel, L. Abdullah, L. Ahonen, Y. Alnouti, A.M. Armando, J.M. Asara, Harmonizing lipidomics: NIST interlaboratory comparison exercise for lipidomics using SRM 1950–Metabolites in Frozen Human Plasma [S], Journal of lipid research, 58 (2017) 2275-2288.
[197] W.B. Dunn, D. Broadhurst, P. Begley, E. Zelena, S. Francis-McIntyre, N. Anderson, M. Brown, J.D. Knowles, A. Halsall, J.N. Haselden, Procedures for large-scale metabolic profiling of serum and plasma using gas chromatography and liquid chromatography coupled to mass spectrometry, Nature protocols, 6 (2011) 1060-1083.
[198] M.v. Bruijnsvoort, J. Meijer, C.v. den Beld, The application of control charts in regulated bioanalysis for monitoring long-term reproducibility, Bioanalysis, 9 (2017) 1955-1965.

IX. Objectives of the thesis

The aim of this thesis was to develop new LC-MS/MS analytical methods for analysis of lipids and improve the existing workflows especially the sample preparation for untargeted lipidomics in order to support the large-scale clinical lipidomics study. The works are mainly divided into two parts. Part I involved in analytical method developments including 1) the optimization of sample preparation procedure for large-scale clinical lipidomics (**publication I**), 2) the method development for targeted analysis of 3-OH-FAs in biological samples human plasma and platelets (**publication II**), 3) the method development for profiling of branched chain and straight chain saturated fatty acids in different types of biological samples including human plasma, platelets and *Staphylococcus aureus* (**publication III**), 4) the method development for targeted analysis of oxylipins with microLC coupled with MS (**publication IV**) and 5) the method development for chiral separation of oxylipins (**publication V**). Part II was involved in the application of the developed methods to clinical lipidomics study including 1) investigation of the potential of ACKR3/CXCR7 in regulating thromboinflammatory response through its impact on the platelet lipidome by targeted and untargeted lipidomics analysis (**publication VI**), 2) investigation of the platelet lipidome by untargeted approach to highlight the significant changes between acute coronary syndrome (ACS) and chronic coronary syndrome (CCS) patients (**publication VII**), 3) investigation of the platelet lipidome of CAD patients by untargeted lipidomics and highlighting significant changes between statin-treated and naïve patients (**publication VIII**).

The first part includes five projects. The first project (**publication I**) has the goal to advance the lipid extraction protocol for large-scale clinical lipidomics of platelets which are small cellular blood components. Classic liquid-liquid extraction has some limitations such as suboptimal performance for the most polar lipids (e.g. acylcarnitines), complicated handling as it requires phase separation, and is therefore non-ideal for large-scale clinical studies. After evaluation of different extraction protocols from the aspects of different extraction solvent systems, impacts of extraction cycles, different cell disruption methods and different reconstitution solvents, a modified new monophasic lipid extraction protocol for large-scale clinical lipidomics with MeOH/MTBE/IPA (1.3:1:1, v/v/v), bead homogenizer for cell disruption and MeOH/MTBE (1:1, v/v) as reconstitution solvent was reported, which shows great potential for large-scale clinical lipidomics studies.

The second to the fifth projects (**publication II-V**) focus on the analysis of fatty acids and the derivatives including 3-OH-FAs, BCFAs and oxylipins, which are important lipid components playing numerous roles in biological systems. Both 3-OH-FAs and BCFAs are involved in important biological pathways, e.g. mitochondrial β-oxidation and oxylipins are important mediators during platelets activation. For an unbiased biological interpretation, an enantioselective UHPLC-MS/MS method based on 1.6 μm particle polysaccharide column (CHIRALPAK IA-U) for chiral separation of 3-OH-FAs (**publication II**) and oxylipins (**publication V**) were established. What's more, an UHPLC-MS/MS method based on RP C18 column which allows the isomeric analysis of BCFAs with different monomethyl positions including *anteiso*, *iso* and other positions (2Me, 3Me, 4Me and so on) (**publication III**) and a new method based on superficially porous particle (2.7 μm) capillary column (0.5 mm ID) and micro-liquid chromatography coupled to tandem mass spectrometry (UHPLC-ESI-QqQ-MS/MS) method for simultaneous quantification of 42 oxylipins (**publication IV**) were developed. The goals are to develop sensitive and selective methods that could be able to detect these target lipid classes even when they are in low abundance in biological samples. These methods were successfully applied for quantitative analysis of 3-OH-FAs, BCFAs and oxylipins in human platelets and plasma samples.

The second part includes another three projects mainly involving in the clinical lipidomics application. My work in this part is the lipidomics analysis of the platelets and plasma samples in CAD patients and heathy donors. In project 6 (**publication VI**), the validated methods (**publication IV and V**) were applied for oxylipin analysis of platelets samples with different in-vitro treatments: resting platelets, activated with thrombin, treated with a selective CXCR7 agonist (with and without thrombin) in order to understand the role of the platelet CXCR7 receptor. In project 7 and 8 (**publication VII and VIII**), untargeted lipidomics analysis was performed to characterize the platelet lipidome in CAD patients in order to investigate the lipid changes between different types of CAD patients ACS and CCS and the lipid changes between ACS patients treated with statin to those naïve. The goals are to use the powerful tool of untargeted or targeted lipidomics analytical methods to elucidate the platelet lipidomic landscape for diagnostic and prognostic biomarkers discovery for CAD.

X. Results and discussion

1. Analytical methods development

1.1 Publication I

Advanced unified monophasic lipid extraction protocol with wide coverage on the polarity scale optimized for large-scale untargeted clinical lipidomics analysis of platelets

Xiaoqing Fu[a], Carlos Calderón [a,b], Tobias Harm [c], Meinrad Gawaz[c], Michael Lämmerhofer[a]*

[a]Institute of Pharmaceutical Sciences, Pharmaceutical (Bio-)Analysis, University of Tübingen, Auf der Morgenstelle 8, 72076 Tübingen, Germany

[b] Escuela de Química, Universidad de Costa Rica, San José, 11501-2060, Costa Rica

[c] Department of Cardiology and Angiology, University Hospital Tübingen, 72076 Tübingen, Germany

Reprinted with permission from Analytica Chimica Acta, Volume 1221, 15 August 2022, 340155

https://doi.org/10.1016/j.aca.2022.340155

Analytica Chimica Acta 1221 (2022) 340155

Contents lists available at ScienceDirect

Analytica Chimica Acta

journal homepage: www.elsevier.com/locate/aca

Advanced unified monophasic lipid extraction protocol with wide coverage on the polarity scale optimized for large-scale untargeted clinical lipidomics analysis of platelets

Xiaoqing Fu [a], Carlos Calderón [a,b], Tobias Harm [c], Meinrad Gawaz [c], Michael Lämmerhofer [a,*]

[a] Institute of Pharmaceutical Sciences, Pharmaceutical (Bio-)Analysis, University of Tübingen, Auf der Morgenstelle 8, 72076, Tübingen, Germany
[b] Escuela de Química, Universidad de Costa Rica, San José, 11501-2060, Costa Rica
[c] Department of Cardiology and Angiology, University Hospital Tübingen, 72076, Tübingen, Germany

HIGHLIGHTS

- Monophasic extraction protocol with bead homogenizer developed.
- Solvent mixture of methanol/methyl tert-butylether isopropanol (1.3:1:1, v/v/v).
- Extraction recoveries of endogenous lipids in platelets and IS assessed by repeated extraction.
- Close to 100% extraction recoveries for polar (acylcarnitines) and apolare lipids (TGs).
- No phase separation, eco-friendly (less and no halogenated solvent), fast (5 min for 24 samples in parallel).

GRAPHICAL ABSTRACT

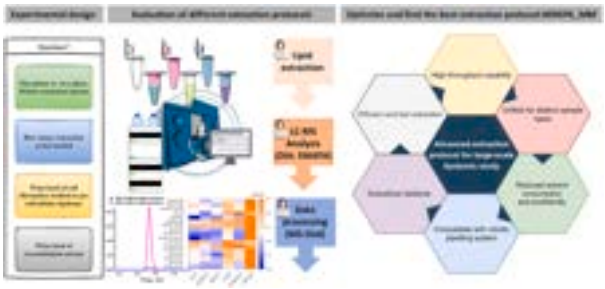

ARTICLE INFO

Keywords:
Lipidomics
Monophasic lipid extraction
Cellular/subcellular lipid extraction
Cell lysis
Green technology
Clinical analysis

ABSTRACT

Lipid extraction is a critical step in sample preparation of lipidomics studies. Biphasic liquid-liquid extraction protocol with methyl *tert*-butyl ether (MTBE)/methanol (MeOH) as organic solvents are widely adopted by researchers nowadays as an eco-friendly replacement of classic Folch, and Bligh&Dyer protocols. Yet, it has some limitations such as suboptimal performance for the most polar lipids (e.g. acylcarnitines), complicated handling as it requires phase separation, and is therefore non-ideal for large-scale clinical studies. To advance the extraction protocol for large-scale clinical lipidomics, in this study we explored i) 6 different extraction solvent systems, ii) distinct processing procedures (sonication, mechanical cell lysis and bead homogenizer), and iii) also 7 different reconstitution solvents. The extraction systems investigated included biphasic systems MTBE/MeOH/H_2O and Hexane/2-propanol (IPA)/1 M acetic acid, and monophasic systems MTBE/MeOH/$CHCl_3$, IPA/H_2O (90% IPA), MeOH/MTBE/IPA, and IPA/H_2O/MTBE as solvent system for lipid extraction of human platelets. Extraction recovery was investigated by repeated extraction cycles. Subcellular extraction efficiency was assessed by the mitochondria-specific cardiolipins. It turned out that monophasic extraction with MeOH/MTBE/IPA (1.3:1:1, v/v/v), bead homogenizer for cell disruption and MeOH/MTBE (1:1, v/v) as reconstitution solvent provide optimal cellular and subcellular extraction efficiencies for both polar (e.g. acylcarnitines) and apolar lipids (e.g. triglycerides). It is simplified (no phase separation), eco-friendly (reduced solvent consumption and

* Corresponding author.
E-mail address: michael.laemmerhofer@uni-tuebingen.de (M. Lämmerhofer).

https://doi.org/10.1016/j.aca.2022.340155
Received 9 June 2022; Received in revised form 5 July 2022; Accepted 7 July 2022
Available online 11 July 2022

no halogenated ones), fast (5 min for 24 samples in parallel), and can be easily adapted for cells, plasma, and tissue. Therefore, it has great potential for large-scale clinical lipidomics studies.

1. Introduction

Lipids as essential biomolecules play numerous roles in biological systems (energy storage, membrane function, signalling) and their alterations might be useful biomarkers for diagnosis and therapy monitoring in a variety of pathophysiological conditions such as cardiovascular disease [1]. Lipidomics as a concept to analyse the lipid profile comprehensively in biological systems [2], has made substantial progress with development of sensitive liquid chromatography-mass spectrometry (LC-MS) instruments. For targeted lipidomics, ultra-high performance liquid chromatography (UHPLC) coupled to electrospray ionization (ESI) triple quadrupole tandem MS (MS/MS) is the method of choice, while for untargeted lipidomics LC- with quadrupole time-of-flight (QToF) and Q-orbitrap, or direct-infusion with FTICR instruments are usually employed [3,4]. LC-MS based lipidomic analysis enables reliable identification of individual lipid species and effective separation of isomers and isobars [5], which advanced our ability to comprehensively study the diverse lipids in biological samples.

As a first step, both targeted and untargeted analysis require an efficient extraction of lipids from cells or other biological matrixes. A suitable extraction solvent should be able to cover as many lipids as possible including both relatively polar lipids, neutral and non-polar lipids. Meanwhile, the extraction procedure should be adapted to reduce chemical interferences and matrix effects, exhibit high extraction recoveries with good precision for sensitive and robust accurate quantitative analysis. The most commonly used protocols for lipid extraction were introduced more than 70 years ago by Folch et al. [6] and Bligh and Dyer [7] with a biphasic liquid-liquid extraction system of $CHCl_3$/MeOH/H_2O. These methods, in which lipids are collected in the lower $CHCl_3$-rich layer, have been frequently described as "gold standards" for lipid extraction [5,8–11]. Some modifications have been made by researchers to substitute $CHCl_3$ by dichloromethane (DCM) as a less toxic alternative in some studies [5]. Nevertheless, the liquid-liquid extraction systems of $CHCl_3$/MeOH/H_2O are still the most classic lipid extraction methods. Hexane-isopropanol-water (Hexane-IPA-H_2O) was proposed in 1978 by Hara et al. [12] as a less toxic option. Later this method was modified by adding acetic acid to improve extraction efficiency for acidic lipids [3]. Recently, other biphasic extraction protocols such as MTBE/MeOH/H_2O and Butanol/MeOH/H_2O were introduced by Matyash et al. [13] and Löfgren et al. [14], respectively. The former has largely replaced the classical Folch and Bligh&Dyer protocols due to its advantage that the upper layer is the lipid-rich organic phase which can be easily collected without the risk of contamination of the sample with proteins from the interface between the two layers, a problem when lipids need to be retrieved from the lower chloroform-rich layer [15,16]. To overcome inherent problems of the two-phase extraction methods, many researchers have recently propagated simple monophasic lipid extraction protocols using protein precipitation methods based on organic solvents [17–21]. In these methods, proteins are precipitated by denaturing organic solvent and then removed by centrifugation. The use of MMC (MeOH/MTBE/$CHCl_3$) [19], butanol and MeOH [22], isopropanol (IPA) with low percentage of H_2O [23,24] as organic solvent mixtures have been described to exhibit good performance and wide coverage of diverse lipid classes.

Besides the adequate extraction solvents, a suitable cell disruption method contributes to the improvement of lipid yields as it enhances the release of intracellular lipids from cell organelles. Cell disruption methods can be theoretically classified into mechanical and non-mechanical methods [25]. Reported methods for the disruption of mammalian cells include Dounce and Potter–Elvehjem homogenization [26], grinding with glass beads [27], nitrogen cavitation [28] and sonication [29,30]. In addition, chemical [31] and biological methods with enzymatic lysis have been reported as well [32]. Nevertheless, in most cases, the effectiveness of a disruption method relies on the cell type. In the context of cellular lipidomics, the integration of cell disruption methods has been rarely systematically investigated.

The present work has the goal to advance the lipid extraction protocol for large scale lipidomics of platelets which are small cellular blood components. It should cover a wide range of lipids ranging from polar lipids (such as acylcarnitines) to highly apolar lipids (like triglycerides). For lipidomic studies of platelets, the cell disruption method of platelets has not been taken into consideration so far since the membrane structure with its lipid components is considered to be dissolved in organic solvent during lipid extraction so that most lipids in cells can be extracted. Reported studies for extraction of lipids in platelets apply sonication [24,33,34] or only vortexing [35] during extraction procedure. In order to gain deeper insight into the effect of cell disruption methods on the extraction efficiencies for platelets, further investigations on several cell disruption methods were made in the present work.

Moreover, for large scale clinical studies the currently most widely established two-phase MTBE protocol is less convenient for automation. Thus, in this work the goal was to advance lipid extraction from cellular samples, such as human platelets, to improve its automation and high-throughput capability, make the protocol compatible with clinical sampling (plastic tubes) and analytical pipetting robotic workflows (solvent compatibility), reduce organic solvent consumption and improve eco-friendliness (avoid halogenated solvents), make it an efficient (also for subcellular organelles), fast and unified (for cells, plasma, tissue) protocol. To this end, we herein evaluate the extraction performance of monophasic extraction solvents (IPA/H_2O and MeOH/MTBE/$CHCl_3$) in comparison to most common biphasic extraction solvents (MTBE/MeOH/H_2O and 1 M acetic acid/IPA/Hexane) together with the impact of extraction cycles for each method as a strategy to determine extraction recoveries also of endogenous lipids. Furthermore, three cell disruption methods viz. ultrasonication, cell disruptor and cell pestle were compared with only vortexing method as suitable for small-scale sampling and ultrasonication vs homogenizer as capable for large-scale sampling based on the monophasic extraction solvent IPA/H_2O to evaluate the influence of cell lysis method on extraction efficiency. What's more, the solubility of different reconstitution solvents was discussed in the following step. Finally, the IPA based method was further optimized for a better extraction recovery for apolar lipid classes. The effect of different extraction solvent systems, cell lysis methods and reconstitution solvents will be thoroughly investigated in this study (Fig. 1).

2. Materials and methods

2.1. Materials, instruments and methods

SPLASH® LIPIDOMIX® Mass Spec Standard (composition in Table S1), EquiSPLASH™ LIPIDOMIX® Quantitative Mass Spec Internal Standard (composition in Table S2), PC 6:0–6:0 (d22), Arachidonic acid (d11) (AA (d11)), PA 15:0–18:1 (d7), Cholesterol (d7), Cholesteryl Ester 18:1 (d7) (CE 18:1 (d7)) and Lyso Sphingomyelin d18:1 (d9) (LSM d18:1 (d9)) was purchased from Avanti Polar Lipids (Alabaster, AL, USA). Octanoyl-L-carnitine (d3) (CAR 8:0 (d3)), Palmitoyl-L-Carnitine (d3) (CAR 16:0 (d3)), Sphingosine-1-phosphate d18:1 (d7) (S1P d18:1 (d7)), Eicosapentaenoic acid (d5) (EPA (d5)) and Docosahexaenoic acid (d5) (DHA (d5)) were obtained from Cayman Chemicals (Ann Arbor, MI, USA). Isopropanol (IPA, ≥ 99.98%), Acetonitrile (ACN, ≥ 99.98%),

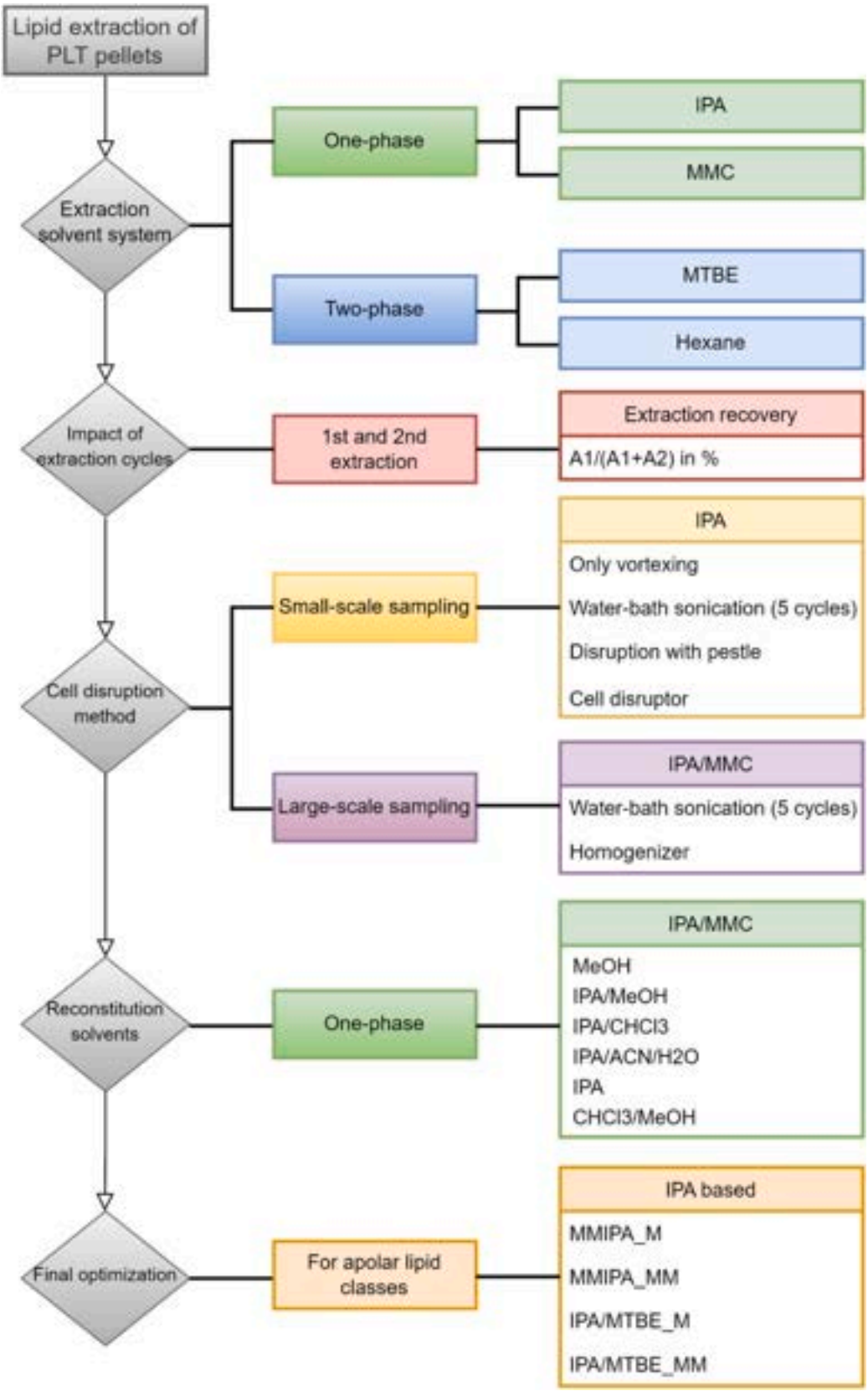

Fig. 1. Overview of the whole study design and sets of extraction experiments carried out for comparison and optimization. IPA (90% IPA and 10% H2O), MMC (MeOH/MTBE/$CHCl_3$, 1.3/1/1, v/v/v), MTBE (MTBE/MeOH/H2O, 10/3/2.5, v/v/v), Hexane (1 M acetic acid/IPA/Hexane, 2/20/30, v/v/v), MMIPA_M (MeOH/MTBE/IPA, 1.3/1/1, v/v/v as extraction solvent and MeOH as reconstitution solvent), MMIPA_MM (MeOH/MTBE/IPA, 1.3/1/1, v/v/v as extraction solvent and MeOH/MTBE, 1/1, v/v as reconstitution solvent), IPA/MTBE_M (IPA/H2O/MTBE, 18/2/5, v/v/v as extraction solvent and MeOH as reconstitution solvent), IPA/MTBE_MM (IPA/H2O/MTBE, 18/2/5, v/v/v as extraction solvent and MeOH/MTBE, 1/1, v/v as reconstitution solvent).

Methanol (MeOH, ≥ 99.98%) in Ultra LC-MS grade and formic acid (FA, ≥98%), acetic acid (HAc, supra 100%) as eluent additive were from Carl Roth (Karlsruhe, Germany). Purified water (H_2O) was produced by Elga Purelab Ultra (Celle, Germany). Extraction solvents of HPLC grade including Methyl-tert-butylether (MTBE, ≥ 99.8%), Isopropanol (IPA, ≥ 99.9%), Methanol (MeOH, ≥ 99.9%), Chloroform ($CHCl_3$, ≥99.8%) and eluent additive Ammonium formate (LC-MS, ≥ 99.0%) were from Sigma-Aldrich (Steinheim, Germany). n-Hexane in HPLC grade (≥97.0%) was purchased from Honeywell (Seelze, Germany).

The vortex mixer was from neoLab (Heidelberg, Germany); the ultrasonic bath was purchased from Bandelin (Berlin, Germany); the pellet pestle was obtained from Sigma-Aldrich (Steinheim, Germany) and the handheld ultrasonic cell disruptor was from Branson Sonifier (Cell Disruptor B15, Danbury, USA).

The lipid extracts were analyzed by UHPLC-ESI-QTOF-MS/MS as described in detail in suppl. chapter 1.2 (Table S3). Data processing was done as described in detail in suppl. chapter 1.3 (Tables S4–S6).

2.2. Platelet isolation

Platelet samples were obtained from the peripheral blood of donors at the University Hospital Tübingen, according to ethical guidelines and approved by regional authorities (number 237/2018BO2). More details can be found in suppl. chapter 1.4.

2.3. Lipid extraction

2.3.1. Lipid extraction with different extraction solvent systems

Platelet pellets were divided into 15 aliquots (each aliquot around 10^8 platelets) for 5 extraction protocols with three replicates for each. Internal standard solution (IS mix 1 in Table S7) was prepared by mixing 100 μL of LipidoMIX Solution with 20 μL AA (d11) stock solution (100 μg/mL), 20 μL EPA (d5) stock solution (100 μg/mL) and 20 μl DHA (d5) stock solution (100 μg/mL). All the extraction solvents including IS mixture were cooled down in the 4 °C fridge before lipid extraction. All extractions were carried out in 1.5 mL Eppendorf tubes. A pooled quality control (QC) sample was prepared by mixing 15 μL aliquots of each reconstituted sample from the five extraction processes.

2.3.1.1. Extraction with MTBE/MeOH/H_2O (10/3/2.5, v/v/v, "MTBE"). Lipid extraction was performed by biphasic extraction method following Matyash's protocol [13]. Internal standards (IS) solution was spiked into each aliquot of platelet pellet (3 replicates) followed by 225 μL of MeOH (4 °C) and then 750 μL MTBE (4 °C). Samples were vortexed for 30 s and incubated on the thermo shaker with temperature control at 4 °C for 1 h (500 rpm). Next, 187.5 μL of H_2O was subsequently added and samples were centrifuged (3500×*g*, 10 min without acceleration and deceleration). The upper phase was collected into a new Eppendorf tube and labelled as 1st extract, the lower phase was re-extracted with the upper phase of the following mixture: MTBE/MeOH/H_2O (10:3:2.5; v/v/v). Samples were centrifuged again and the upper layer from the 2nd extraction was collected into another Eppendorf tube labelled as 2nd extract. The extracts were then dried with an EZ2 evaporator from GeneVac (Ipswich, UK) under nitrogen protection. The residues were dissolved in 100 μL of MeOH, vortexed (10 s), sonicated (2 min), centrifuged (3500×*g*, 10 min) the resultant lipid extracts were transferred into HPLC vials and stored at −20 °C until analysis.

2.3.1.2. Extraction with 1 M acetic acid/IPA/Hexane (2/20/30, v/v/v, "Hexane"). Lipid extraction was performed by biphasic extraction method following O'Donnell's protocol [35]. Solvent mixture (1 M acetic acid/propan-2-ol/hexane; 2:20:30, v/v, 500 μL) with IS mixture solution were spiked to platelets pellets (3 replicates). Samples were vortexed and sonicated for 2 min. Hexane (500 μL) was then added and samples were incubated on the thermo shaker with a temperature control at 4 °C for 1 h (500 rpm). Samples were centrifuged (3500×*g*, 10 min without acceleration and deceleration) and the upper hexane layer was collected and labelled as 1st extract. The lower layer was re-extracted with the upper layer of the mixture 1 M acetic acid/propan-2-ol/hexane (2/20/30, v/v/v) and the upper layer from 2nd extraction was collected again into a new Eppendorf tube labelled as 2nd extract after centrifugation. The extracts were then dried and dissolved in 100 μL of MeOH as described in 2.3.1.1.

2.3.1.3. Extraction with MeOH/MTBE/$CHCl_3$ (1.33/1/1, v/v/v, "MMC"). Lipid extraction was performed by monophasic extraction method following Bischoff's protocol [36]. Internal standards (IS) mixture solutions were spiked and 500 μL of MeOH/MTBE/$CHCl_3$ (1.33:1:1, v/v/v) was then added into platelet pellets. Samples (3 replicates) were vortexed for 30 s and sonicated for 2 min. Then, samples were incubated on thermo shaker with a temperature control at 4 °C for 1 h (500 rpm) and centrifuged at 3500×*g* for 10 min. The supernatant was collected and labelled as 1st extract. The remaining pellets were re-extracted with another 500 μL of MeOH/MTBE/$CHCl_3$ (1.33:1:1, v/v/v) following the same procedure as 1st extraction and the supernatant from 2nd extraction was collected and labelled as 2nd extract. The supernatants were then dried and dissolved in 100 μL of MeOH as described in 2.3.1.1.

2.3.1.4. Extraction with IPA/H_2O (90/10, v/v, "IPA"). Lipid extraction was performed using a monophasic extraction method following the IPA/H_2O protocol [24]. Platelet pellets (2 replicates) with IS solution were suspended in 500 μL IPA/H_2O 9:1 (v/v), vortexed for 10 s and sonicated for 2 min. Then the samples were incubated on thermo shaker (4 °C, 500 rpm) for 1 h with 2 min sonication every 12 min during the incubation which means total 5 cycles sonication (each cycle 2 min). The samples were centrifuged (3500×*g*, 10 min), pellets were kept, and supernatant (lipid extract) was transferred to fresh Eppendorf tube and labelled as 1st extract. Pellets were then re-extracted as described in the 1st extraction and the supernatant from 2nd extraction was collected. Afterwards, the supernatants were dried and dissolved in 100 μL of MeOH as described in 2.3.1.1.

2.3.1.5. Extraction with tissue lyser IPA/H_2O (90/10, v/v, "IPA TL"). Internal standards (IS) solution was added to the pellets (3 replicates) followed by 500 μL IPA/H_2O 9:1 (v/v). Samples were vortexed and sonicated. After adding zirconia/glass beads (0.1 mm diameter) to each sample, the pellets were disrupted in a Fastprep-24 (MP Biomedicals) (3 cycles of 30 s, 6.5 m/s). The samples were then centrifuged (3500×*g*, 10 min) and the supernatants were collected for further drying. The remaining pellets were re-extracted by adding another 500 μL IPA/H_2O 9:1 (v/v) and extracted again using Fastprep-24 with parameters described in the 1st extraction. The 2nd supernatant was collected in new Eppendorf tubes and both supernatants from 1st and 2nd extraction were dried and reconstituted in 100 μL of MeOH as described in 2.3.1.1.

2.3.2. Lipid extraction by different cell disruption methods

2.3.2.1. Methods for small-scale sampling (with no high-throughput capability; one-by-one sample) based on IPA. Platelet pellets were divided into 12 aliquots (each aliquot around 10^8 Platelets) for 4 extraction protocols with three replicates for each. Extraction solvent was prepared by mixing 15 mL IPA/H_2O (90/10; v/v) with 75 μL of LipidoMIX Solution, 15 μL AA (d11) stock solution (100 μg/mL), 15 μL EPA (d5) stock solution (100 μg/mL) and 15 μL DHA (d5) stock solution (100 μg/mL) (IS mix 1 in Table S7). The extraction solvent was cooled down in the 4 °C fridge before lipid extraction.

Cooled extraction solvent (1 mL) was added to platelet pellets and samples were treated by either one of the following 4 extraction

protocols: 1) vortexed for 30 s (3 times) and then incubated on thermo shaker with temperature control at 4 °C for 1 h (500 rpm), 2) vortexed for 10 s followed by 2 min sonication and then incubated on thermo shaker (4 °C, 500 rpm) for 1 h with 5 cycles sonication (every 12 min one sonication cycle; each cycle 2 min), 3) vortexed for 10 s, dispersed by a pestle for 2 min and then incubated on thermo shaker with temperature control at 4 °C for 1 h (500 rpm), 4) vortexed for 10 s and a handheld ultrasonic cell disruptor was used to destroy the cell structure for 30 s (2 times after 30 s cooling, output 4, duty cycle 50%) and then incubated on thermo shaker with temperature control at 4 °C for 1 h (500 rpm). After incubation, samples were centrifuged and collected supernatants were dried and reconstituted in 100 μL MeOH as described in 2.3.1.1.

2.3.2.2. Methods for large-scale sampling (with high-throughput capability; 24 or 48 samples in parallel) based on IPA and MMC. Platelet pellets were divided into 12 aliquots (each aliquot around $2*10^8$ Platelets) for 4 extraction protocols with three replicates for each. The 5 cycles-sonication and homogenizer which can be applied for large-scale sampling were investigated in this study based on two extraction solvent systems (IPA and MMC). The extraction procedure with 5 cycles-sonication by IPA or MMC was exactly the same as described in section 2.3.1 with extended IS mixtures (IS mix2 with composition shown in Table S8). The extraction procedure with Precellys® evolution homogenizer (Bertin, Frankfurt am Main, Germany) was realized by applying 10 cycles (x 10 s and 30 s of pause between each cycle, 6800 rpm) of cell membrane disruption with platelet pellets suspended in IPA or MMC using dry ice in the cooling unit (see suppl. Fig. S1 for typical cooling performance) and 0.1 mm diameter zirconia/glass beads. Afterwards, centrifugation, evaporation and reconstitution with MeOH were performed which were the same as described in the previous section.

2.3.3. Optimization of reconstitution solvent

Platelet pellets were divided into 36 aliquots (each aliquot around $2*10^8$ platelets) for 12 extraction protocols (6 different reconstitution solvents with 2 different extraction solvents IPA and MMC) with three replicates for each using the Precellys evolution homogenizer protocol described in section 2.3.2.2. After evaporation of the extraction solvent, dried lipid extracts were then reconstituted in 100 μL of either 1) MeOH, 2) IPA/MeOH (2:1; v/v), 3) IPA/$CHCl_3$ (9:1; v/v), 4) IPA/ACN/H_2O (2:2:1; v/v/v), 5) IPA or 6) $CHCl_3$/MeOH (1:1; v/v). In the last step, reconstituted samples were vortexed (10 s), sonicated (2 min), centrifuged (3500×*g*, 10 min) and transferred to autosampler vials for storing in −20 °C before analysis.

2.3.4. Final optimization for extraction protocols

Platelet pellets were divided into 18 aliquots (each aliquot around $2*10^8$ platelets). Six (6) extraction protocols (with three different extraction solvents IPA/H_2O (9:1, v/v), MeOH/MTBE/IPA (1.33:1:1, v/v/v, MMIPA) and IPA/H_2O/MTBE (18:2:5, v/v/v, IPA/MTBE) and two reconstitution solvents MeOH (M) and MeOH/MTBE (1:1, v/v, MM)) were evaluated with three replicates for each. For sample processing in this study, the Precellys evolution homogenizer protocol described in section 2.3.2.2 with 1st and 2nd extraction cycle as described in section 2.3.1.4 was used as a further optimization step of the former IPA protocol to alleviate its shortcomings regarding extraction efficiency for apolar lipids.

2.3.5. Advanced final protocol with MMIPA_MM by homogenizer

Internal standard mix 2 (preconditioned at 4 °C, Table S8) 100 μL was spiked into platelet pellets ($2*10^8$) and then suspended in 1.5 mL extraction solvent MMIPA (preconditioned at 4 °C). Samples were vortexed (10 s) and 0.1 mm diameter zirconia/glass beads were added to each sample. Afterwards, the samples were disrupted with Precellys® evolution homogenizer by applying 10 cycles (x 10 s and 30 s of pause between each cycle, 6800 rpm) of cell membrane disruption using dry ice in the cooling unit (4 °C during the whole procedure). Then, the samples were centrifuged (3500×*g*, 10 min) and the supernatants were collected for further drying with an EZ2 evaporator from GeneVac under nitrogen protection. The residues were reconstituted in 100 μL of MeOH/MTBE (1:1, v/v), vortexed (10 s), sonicated (2 min), centrifuged (3500×*g*, 10 min) and finally the supernatant was transferred into vials for further LC-MS analysis.

3. Results and discussion

3.1. Selection of extraction solvent system

3.1.1. General lipid profiling

Acquired MS data in both positive ion mode (ESI+) and negative ion mode (ESI-) from 5 extraction protocols (Fig. 2) were processed by MS-Dial. In general, 269 features were identified (i.e. structurally annotated by MS1 and MS2 spectral match against LipidBlast library) in platelet lipid extracts of the MMC protocol with a slightly higher feature yield compared to the other four protocols (251 identified features in MTBE extracts, 246 in IPA_TL extracts, 227 in Hexane and 213 in IPA, respectively). The Venn diagram plotted in Fig. 2 shows how the identified features are distributed among all five protocols. A total number of 168 features was identified in all protocols with 38 unique features only in MMC, 22 features only in IPA_TL, 18 only in MTBE, 17 only in Hexane and 8 unique features only in IPA protocol. After carefully checking the MS spectra for each identified feature and cross-checking the features which were covered in both ESI+ and ESI- mode, a total number of 311 identified features as a sum profile for all five protocols were confirmed with high reliability for further statistical analysis (CV% < 30% in QC samples).

Normalized response (peak height of identified lipids after normalization by IS and LOWESS) was used for PCA analysis to map differences and similarities between the different extraction protocols on lipid profiling. As can be seen from the score plot in Fig. 3, the normalized data are clustered by different extraction protocols which indicates differences in lipid profiles and extraction efficiencies of the different protocols. The 12 QC injections from a pooled sample of all extraction

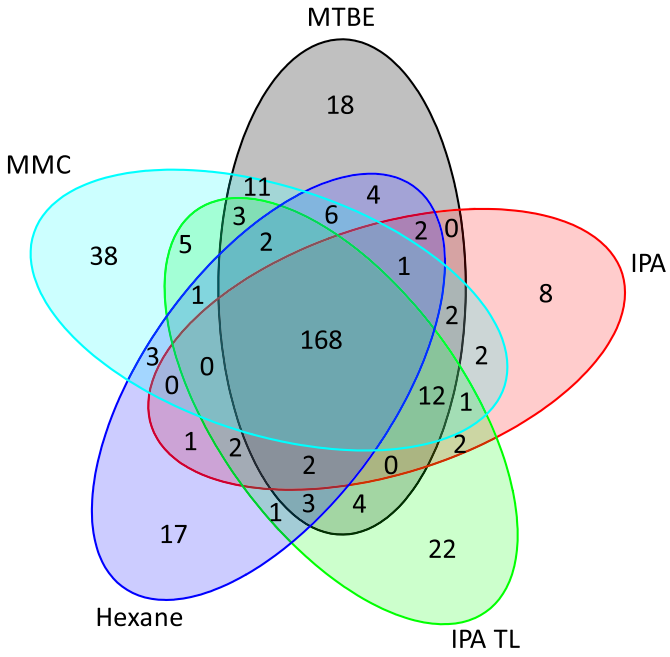

Fig. 2. Venn diagram of identified features (annotation by MS1 and MS2 spectral match with LipidBlast library) from different extraction methods from 1st extraction. For each extraction method n = 3.

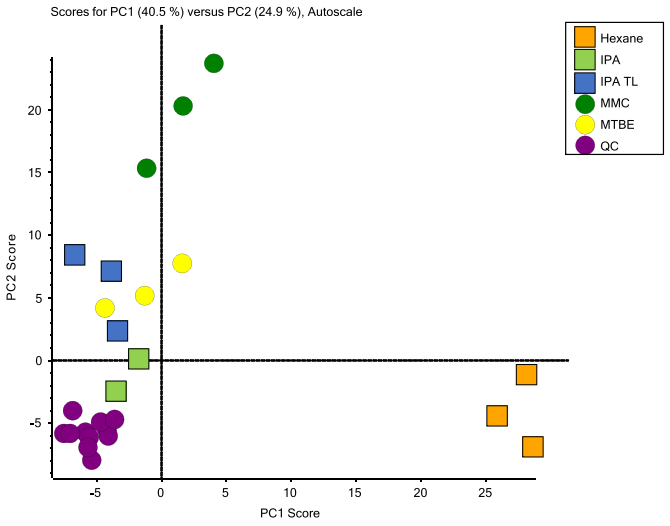

Fig. 3. PCA plots of scores plot based on five extraction protocols. Features used for PCA plot are identified lipids. For each extraction method n = 3 (IPA method n = 2).

protocols were tightly clustered which confirms a robust instrument performance during the whole measurement. This cluster may serve as reference for the relative performance of the individual protocols. It is most striking that the extraction protocol Hexane shows a significantly different distribution from the other 4 protocols in the PCA score plot, in particular it is strongly separated on the latent variable PC1. The loadings plot in Fig. S2 reveal high loadings for TGs, SMs, and FAs emphasizing their primary role in distinguishing the Hexane extraction protocol from the others. On the other hand, the IPA-based extraction protocols, IPA and IPA TL, as well as the MTBE protocol seem to show similar results for lipid extraction because of their closer proximity in the PCA score plot (especially PC1). On PC2, the MMC protocol is most distinctive from the other extraction protocols. The loadings plot (Fig. S2) indicates that LPEs, LPCs and PIs mainly contribute to the different distribution of the extraction protocols on PC2. PCs, PEs and ePCs are oriented in the direction of the pooled sample as well as extraction protocols IPA and IPA TL suggesting they are responsible for their grouping.

From the above investigation, it became evident that MTBE as two-phase extraction method revealed better extraction recoveries for apolar lipids than the IPA method while IPA as one-phase extraction showed great potential for polar lipid classes. This was studied in more depth. As a main limitation of the two-phase extraction a poor recovery of the most polar lipid classes such as Acylcarnitine (CAR) and some Glycerophosphocholines (PC) was anticipated due to the reasonable solubility of polar lipids in the aqueous phase. To document this problem, two pairs of internal standards CAR 8:0 (d3), CAR 16:0 (d3) and PC 6:0–6:0 (d22), PC 15:1–18:0 (d7) were spiked into the samples with the same concentration (500 ng/mL) during extraction with MTBE and IPA methods. It is striking that for the polar medium-chain CAR 8:0 (d3) and PC 6:0–6:0 (d22), a remarkably lower recovery (RE (%) = peak area after extraction in matrix/peak area in neat solution*100%) was observed by two-phase extraction with MTBE (CAR 8:0 (d3) of 16% and PC 6:0–6:0 (d22) of 30%) compared to monophasic IPA protocol (CAR 8:0 (d3) of 75% and PC 6:0–6:0 (d22) of 71%; Fig. 4a and Fig. 4c). In contrast, for long-chain CAR 16:0 (d3) and PC 15:1–18:0 (d7), which are less polar than the medium-chain ISs, the difference in recovery was less pronounced between the two protocols but the recovery was still better for the monophasic IPA method (CAR 16:0 (d3) of 61% with MTBE and

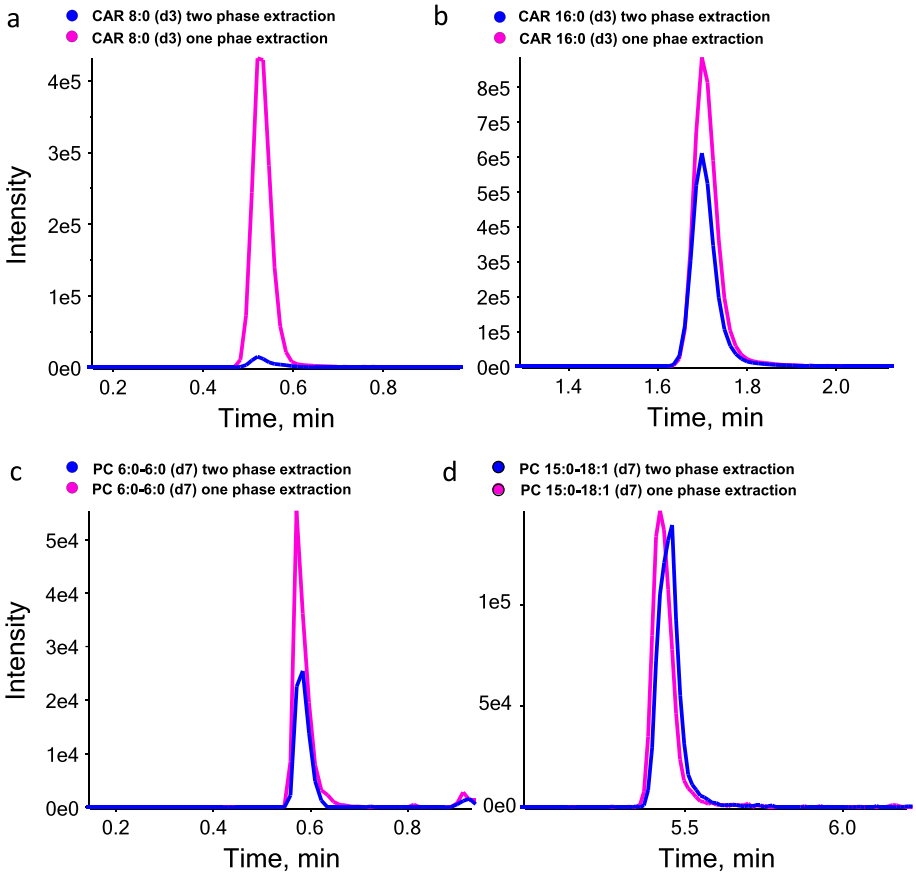

Fig. 4. XIC of (a) CAR 8:0 (d3); (b) CAR 16:0 (d3) (c) PC 6:0–6:0 (d22) and (d) PC 15:0–18:1 (d7) by different extraction methods.

86% with IPA; PC 15:1–18:0 (d22) of 89% with MTBE and 96% with IPA; Fig. 4b and d). For the two-phase extraction the more polar the compounds (like CAR 8:0 (d3) and PC 6:0–6:0 (d22)) the more they are distributed into the lower aqueous layer which will be disposed in the next step. This is not the case for the monophasic protocol for which also a slightly lower extraction recovery is observed for the short-chain vs the long-chain species for CAR (CAR 8:0 (d3) of 75% and CAR 16:0 (d3) of 86%) and for PC (PC 6:0–6:0 (d22) of 71% and PC 15:1–18:0 (d7) of 96%). This example indicates the deficiency of the two-phase extraction especially for the short-chain and medium-chain CAR class but may be the same for other polar lipid classes.

Furthermore, for two-phase extraction, the variance during transferring the organic layer could be another drawback (see Table 1). The precision (CV%) for the spiked internal standards (CAR 8:0 (d3), CAR 16:0 (d3), PC 6:0–6:0 (d22) and PC 15:1–18:0 (d7)) is much better (85%–115%) by one-phase extraction than that by two-phase LLE. Meanwhile, the accuracy (%) of CAR 8:0 (d3) (based on CAR 16:0 (d3) assuming this would be used as single class specific IS for one-point calibration) and CAR 16:0 (d3) (based on CAR 8:0 (d3)) assuming this would be used as IS for one and two-phase extraction was calculated (Table 1). The same procedure was done for internal standards of PC class. Response factors (determined with IS solutions) were corrected. It can be observed that with the one-phase extraction single-point calibration results in bias not much more than factor 1.15 while with the two-phase extraction it is around factor 2–10 in these examples. The results evidently demonstrate a serious problem when using one-point calibration for polar lipids with two-phase extraction protocol. The claim of absolute quantification with methods that allow co-ionization of the lipid class specific IS with the analytes (shotgun lipidomics, MS with lipid class separation) is in its generalized form not fully correct because the bias from extraction due to within-class recovery differences is not properly corrected with a single class specific IS, at least not for all lipid classes. A proper internal standard therefore plays a decisive role for the accurate quantification across one lipid class. For the monophasic extraction there is less bias for single IS within-class quantification.

In conclusion, all extraction protocols share a large fraction of extracted lipids, yet minor differences exist which were most pronounced for the Hexane and MMC protocols. Besides, the one phase extraction protocol evidently shows better extraction performance for the very polar lipid classes while a remarkably lower extraction recoveries of very polar lipids (CAR) can be observed during two phase extraction. Since multivariate statistics gives only a representative overview of similarities/dissimilarities of the 5 extraction protocols but no quantitative information further in-depth investigations were performed.

3.1.2. *Extraction recoveries estimated from repeated extraction cycles*

In common analytical sample preparation protocols using liquid extraction, exhaustive extraction of analytes is achieved by repeated extraction. As such a multi- or two-step extraction is hard to realize in a large-scale clinical sample batch and would be extremely tedious, it was of interest whether there is a significant gain by a 2nd extraction cycle. Thus, an independent 2nd extraction cycle after the 1st one was performed without combining the 1st and 2nd extracts. They were analyzed individually which allows to approximate extraction recoveries, even for endogenous lipids for which no standards are available.

Firstly, the extraction efficiency in the 1st cycle for each protocol was evaluated for the ISs through the peak area ratio of the 1st extraction step (A1) to the sum of the 2 cycles (A1+A2) (extraction recovery in % as determined by A1/(A1+A2)). The higher the ratio, the lower the degree of incompleteness of the extraction procedure in the first extraction step. An extraction recovery of 100% means quantitative extraction in the 1st cycle, while a 50% recovery indicates that the extraction was incomplete and a 2nd extraction cycle provided the same yield as the first one. If this was the case for a large number of lipids, it makes sense to use a (two-step) repeated extraction. Fig. 5 shows the results for extraction efficiency of ISs with the 5 extraction protocols (The results of endogenous lipids can be found in suppl. material Fig. S3). It can be observed from Fig. 5 that most of ISs including glycerophospholipid (PC 15:0–18:1 (d7), PE 15:0–18:1 (d7), PG 15:0–18:1 (d7), PI 15:0–18:1 (d7), PS 15:0–18:1 (d7), LPC 18:1 (d7) and LPE 18:1 (d7)), sphingolipid (SM d18:1–18:1 (d9)) and fatty acyls (AA (d11)) can be well extracted with a single extraction cycle as indicated by the high extraction recoveries of more than 95% for most of the extraction protocols. Solely the "Hexane" method shows significantly worse extraction efficiencies (about 50–80% recovery in the 1st step). This holds in particular for phospholipids which seem to have low solubility in the hexane layer of this two-phase extraction protocol. On the opposite, it shows equal performance for the neutral lipids like glycerolipids (TG and MG) and cholesterol as compared to MTBE and MMC. On the other hand, IPA showed the worst results for TG, MG and CE (around 60% recovery), however, similar performance for the other lipid classes as MTBE. In our formerly established IPA protocol [24,37], we increased the volume of extraction solvent (factor 5) to partly compensate the lower extraction yield of neutral lipids (TG, CE, MG). The disadvantage of the larger volume are longer solvent evaporation times, larger risk for over-drying (with problems during reconstitution), and higher solvent consumption. Herein, we tested whether mechanical cell lysis with tissue lyser can help to improve extraction efficiencies for the neutral lipids. In fact, recoveries for CE and MG could be significantly enhanced, but the effect was negligible for TGs. Overall, the MMC method showed the best results among the five extraction protocols with a high recovery for all the ISs. It has also been concluded and documented to be highly suitable for

Table 1
Precision (as % CV) and Accuracy (as % recovery) of two ISs of CAR by one and two-phase extraction.

	Precision CV%				Accuracy %[b]	
	Peak area		Normalized by IS[a]			
	CAR 8:0 (d3)	CAR 16:0 (d3)	CAR 8:0 (d3)	CAR 16:0 (d3)	CAR 8:0 (d3)	CAR 16:0 (d3)
Two-phase (MTBE)	48	17	40	44	9	1115
One phase (IPA)	15	6	14	15	89	112
	PC 6:0–6:0 (d22)	PC 15:0–18:1 (d7)	PC 6:0–6:0 (d22)	PC 15:0–18:1 (d7)	PC 6:0–6:0 (d22)	PC 15:0–18:1 (d7)
Two-phase (MTBE)	23	5	21	24	45	222
One phase (IPA)	4	4	5	5	99	101

[a] CAR: samples n = 50, for CAR 8:0 (d3), CAR 16:0 (d3) was used as IS while for CAR 16:0 (d3), CAR 8:0 (d3) was used as IS for precision CV% calculation after normalization.
[a] PC: samples n = 3, for PC 6:0–6:0 (d22), PC 15:0–18:1 (d7) was used as IS while for PC 15:0–18:1 (d7), PC 6:0–6:0 (d22) was used as IS for precision CV% calculation after normalization.
[b]Accuracy %: with response factor correction, i.e. response factors of mid and long-chain ISs of PC and CAR in neat solution and isotopic correction I were applied for further calculation of accuracy in matrix.

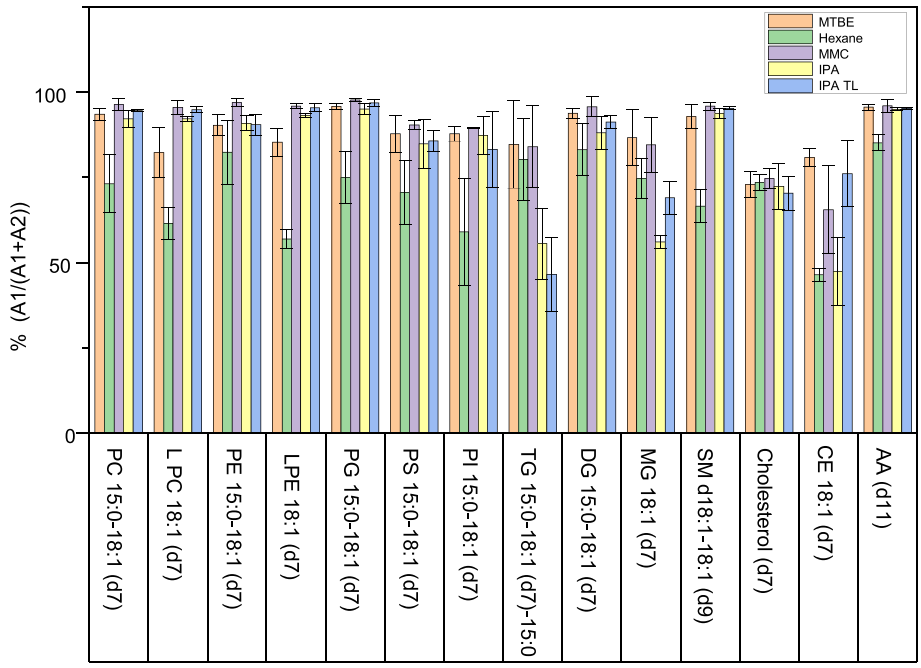

Fig. 5. Comparison of extraction recoveries (A1/(A1+A2); in %) from 2 cycles of extraction of IS with different extraction methods. All lipids were analyzed in ESI (+) mode except for AA (d11) and PS 15:0–18:1 (d7) in ESI (−). For each extraction method n = 3.

automated extraction [19,36]. From this point it seems to be most attractive. However, it requires halogenated organic solvent (chloroform) which is less eco-friendly and our automated pipetting robotics discourages its use (see Suppl. Material for solvent compatibility chart Table S9). For this reason, it was second choice in our hand.

It can be concluded that the IPA protocol compared fairly well to the MTBE and MMC protocols except for TG, CE and MGs for which bead-supported cell lysis (tissue lyser protocol) brought some improvements. Worse extraction performance for TGs is outweighed by enhanced extraction yields of polar lipids such as LPCs and LPEs as well as better eco-friendliness, better compatibility with clinical sampling devices and better compatibility with pipetting robotics.

3.2. Comparison of different methods for cell disruption

3.2.1. Methods for small-scale sampling

In an attempt to optimize the lipid extraction with the IPA protocol, various cell disruption methods were examined. Four methods 1) vortexing 2) ultrasonic bath 3) pestle (manual grinding) and 4) handheld ultrasonic cell disruptor were evaluated based on the IPA solvent system in order to understand the efficiency of cell disruption methods for total lipid extraction from platelets. Each method has its own advantages and disadvantages which are summarized in Table 2.

Cell disruption breaks the cells and improves the accessibility to the intracellular and subcellular components for increasing extraction efficiency. It may also help to overcome kinetic mass transfer limitations during extraction. On the one hand, extraction with pestle (manual grinding) and disruptor (handheld ultrasonic cell disruptor with disruptor horn) should achieve effective cell disruption. However, taking the time and efforts into consideration, these two methods are only suitable for dealing with a small number of samples. On the other hand, although vortexing and ultrasonic bath can be applied for large-scale sample preparation, the incomplete cell lysis of vortexing and the risk of radical formation by sonication which may damage and oxidize lipid molecules are problems that should be considered as well. The effectiveness of the cell disruption methods was determined by comparison of lipid intensities resulting from different extraction/cell disruption methods. For each lipid class, two or three lipids with high abundance in platelets and with good precision in QC samples (Table S10) were analyzed. Detailed results are given in suppl. material (Figs. S4–S5).

Table 2
Comparison of different cell disruption methods in terms of their advantages and disadvantages.

Cell disruption methods	Advantages	Disadvantages
Vortexing	Simplest and quickest Suitable for large-scale samples	Incomplete cell lysis
Sonication (5 cycles ultrasonic bath)	Faster extraction Suitable for all cell type and large-scale samples	High heat generation Damage chemical structure of molecules
Pestle (manual grinding)	Can be established easily Relatively effective	Time consuming High heat generation Only able to deal with one sample at one time Not suitable for large-scale sampling
Handheld Ultrasonic Cell Disruptor	Efficient and effective for cell disruption	High heat generation Only able to deal with one sample at one time Not suitable for large-scale sampling
Homogenizer	Suitable for all cell type and large-scale samples	Special falcon tubes needed Additional beads needed

In general, the results of the four cell disruption methods were comparable. Platelet activation did not take place in any of the protocols (see suppl. material 5.1). It turns out that the extraction solvent has a decisive role on extraction efficiency of lipids while the physical process has a minor effect.

3.2.2. Methods for large-scale sampling

Another set of measurements with two different cell lysis methods (5 cycles ultrasonic bath and Precellys evolution homogenizer) which are applicable for large-scale extraction based on the solvent systems MMC and IPA showing superiority for extraction efficiency was performed. As can be seen from Fig. 6, all the internal standards of phospholipids including 15:0–18:1 (d7) PC, LPC 18:1 (d7), PE 15:0–18:1 (d7), LPE 18:1

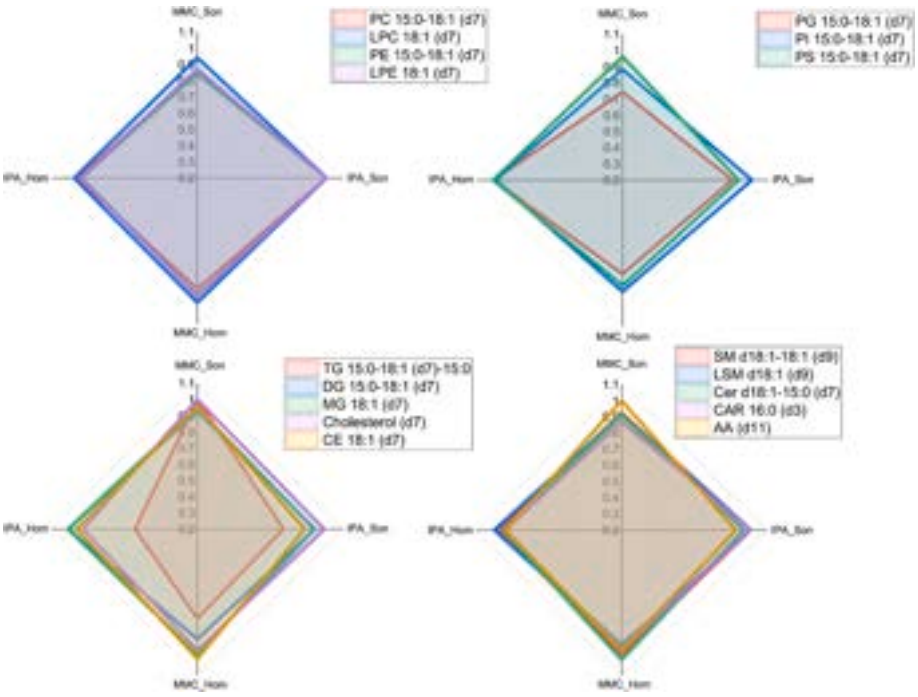

Fig. 6. Radar diagrams of peak area of IS extracted from different protocols IPA_Hom, MMC_Hom, MMC_Son and IPA_Son. The intensity was scaled to 0–1 by the maximum response of the lipid among different extraction protocols. For each extraction method n = 3.

(d7), PG 15:0–18:1 (d7), PI 15:0–18:1 (d7) and PS 15:0–18:1 (d7) which are polar lipids can be better recovered by extraction solvent of IPA compared to organic solvent mixtures MMC. The same trend could be observed as well for endogenous phospholipids extracted from platelets as a sum response of lipid species in one class (Fig. S6). On the contrary, MMC solvent showed better extraction recovery for apolar lipid classes (CE, MG, TG and DG) as well as the relevant internal standards (TG 15:0–18:1 (d7)-15:0, DG 15:0–18:1 (d7), MG 18:1 (d7), CE 18:1 (d7) and cholesterol (d7)). Meanwhile, the bead homogenizer with MMC (MMC_Hom) outperformed other methods for apolar lipid classes. For polar lipid classes IPA_Hom performed the best among all extraction methods.

When comparing the numbers of identified features in the 4 protocols, all protocols showed good extraction recoveries for lipid species. A total of 543 identified features were identified in IPA with homogenizer (IPA_Hom) while 572 identified features in IPA with sonication (IPA_Son) (note the factor 2 higher cell number used in this series of experiments compared to the one of Fig. 2). For the MMC protocols, a number of 520 identified features for homogenizer and 555 identified features for sonication methods were observed. From the Venn diagram (Fig. 7a), it can be seen that 387 identified features were found in all four protocols while each extraction protocol owns particular lipids which were not detected by any of the other protocols. To some extent, the extraction methods with sonication possessed better performance compared to the method with homogenizer in terms of numbers of identified features by MS-Dial and IPA as extraction solvent outperforms the MMC in terms of the total number of identified features. It can be observed from the OPLS-DA plot (Fig. S7a all four methods, Fig. S7b two IPA-based methods and Fig. S7c summary of fit for IPA-based methods) that the 3 replicates for each method can be well clustered and each method could be distinguished from each other, i.e. their extraction efficiency is somehow different. Evidently for most of the identified lipids especially lipid class PC, ePC, LPE, ePE, SM and TG, IPA homogenizer had better performance in terms of extraction efficiency (normalized response for each lipid) according to the score contribution plot when comparing the IPA_Son and IPA_Hom (Fig. S8). What's more,

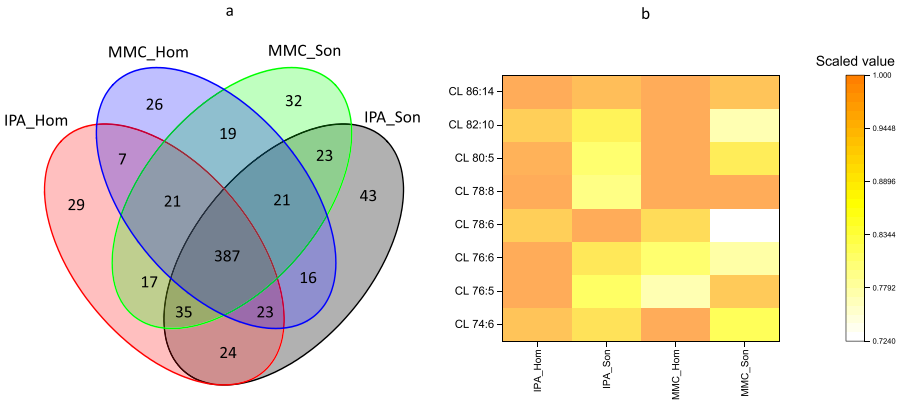

Fig. 7. (a) Venn diagram of identified features from different extraction methods IPA_Hom, MMC_Hom, MMC_Son and IPA_Son. (b) Heatmap of cardiolipins (CLs) extracted by four different protocols. Responses (normalized peak height after LOWESS + internal standard normalization) are scaled to 0–1. For each extraction method n = 3.

a few cardiolipins (CLs) which are important components of the inner mitochondrial membrane can be detected (Fig. 7b, indicating the ability of the protocols to disrupt subcellular organelles for further lipid extraction. From Fig. 7b, it can be concluded that both sonication (5-cycles water bath sonication) and homogenizer had the ability for subcellular extraction of lipids and homogenizer achieved better subcellular extraction recovery for CLs compared to sonication.

As a conclusion, both 5-cycles-sonication (in ultrasonic bath) and homogenizer showed comparable results for lipid recovery with IPA and MMC. Five-cycles-sonication outperforms slightly the homogenizer in terms of identified features while the bead homogenizer in contrast has better extraction recovery for most of the lipids and is less time consuming (5 min for 24 samples instead of 1 h incubation time based on the 5-cycle sonication) which is striking especially when a large scale of samples is required to be prepared. Since MMC contains 2 solvents (MTBE and $CHCl_3$) that are not well compatible with pipetting robotics, we finally opted for IPA with bead homogenizer as the best protocol for large scale clinical studies.

3.3. Comparison of different reconstitution solvents

The above optimized extraction with IPA and homogenizer uses only small organic solvent volume (1.5 mL). Hence, its evaporation in a high-performance evaporator (Genevac EZ2) is fast and hence avoids over-drying of samples. This limits problems during reconstitution. However, a quantitative redissolution is of great importance for a robust workflow. Thus, in the last set of measurements, the effect of 6 different reconstitution solvents including MeOH, IPA/MeOH (2:1; v/v), IPA/$CHCl_3$ (9:1; v/v), IPA/ACN/H_2O (2:2:1; v/v/v), IPA or $CHCl_3$/MeOH (1:1; v/v) on the lipid recovery after two extraction protocols monophasic IPA and MMC extraction with homogenizer (IPA_Hom and MMC_Hom) was investigated. This is of importance because not only the extraction solvent system but also the reconstitution solvents can contribute to the final lipid recovery especially when lipid extracts are dried longer than actually required.

The peak area of the spiked ISs were used to get insights into the reconstitution ability of different reconstitution solvents. The peak area was divided by the largest response amongst all reconstitution solvents, which means that a value of 1 means the best reconstitution solvent, probably equal to 100% reconstitution. The results are demonstrated in the Radar graphs in Fig. 8 for the 6 different reconstitution solvents. In the case of the four phospholipids (PC 15:0–18:1 (d7), LPC 18:1 (d7), PE 15:0–18:1 (d7) and LPE 18:1 (d7)), MeOH, IPA/MeOH (2:1; v/v), $CHCl_3$/MeOH (1:1; v/v) and the most polar combination of solvent mixtures IPA/ACN/H_2O (2:2:1; v/v/v) showed similar results with the best lipid recovery of the above ISs. In contrast, for PG 15:0–18:1 (d7), PI 15:0–18:1 (d7) and PS 15:0–18:1 (d7), the best results were achieved with MeOH as reconstitution solvent. IPA as reconstitution solvent demonstrated reasonable results as well except for PI 15:0–18:1 (d7) which showed a poor recovery. In contrast, for apolar ISs like TG 15:0–18:1 (d7)-15:0, DG 15:0–18:1 (d7), MG 18:1 (d7), CE 18:1 (d7) and cholesterol (d7), the drawbacks of polar mixtures IPA/ACN/H_2O (2:2:1; v/v/v) can be observed especially for CE 18:1 (d7). $CHCl_3$/MeOH (1:1; v/v) and IPA/MeOH (2:1; v/v) can be considered as the best choice for apolar ISs. For other ISs which were investigated in this study, $CHCl_3$/MeOH (1:1; v/v) and MeOH always showed the best lipid recovery.

These results for the ISs can reflect to a certain degree the ability and appropriateness of these investigated reconstitution solvents to dissolve the dried lipid extracts. However, single compound per lipid class may have some limitations to indicate a representative overview for the entirety of lipid species within one class. For this reason, a sum peak height from one lipid class after normalization with relevant IS was used to demonstrate the solubility of all identified lipid species in the different organic solvents which are shown in Fig. S9. Not surprisingly, MeOH showed reasonable reconstitution capable for most lipid species under IPA as extraction solvent. Also $CHCl_3$/MeOH (1:1; v/v) showed good results as reconstitution solvent with few exemptions (e.g. PGs) (Fig. S9). Interestingly, relatively similar reconstitution ability for MeOH and $CHCl_3$/MeOH (1:1; v/v) can be observed here for the lipid species CE, MG, TG and DG.

As a conclusion from the reconstitution experiments, the best reconstitution solvent could be MeOH or $CHCl_3$/MeOH (1:1; v/v). Since our institutional guidelines force us to avoid the use of $CHCl_3$, MeOH is suggested at this point as the best compromise for large scale lipidomics

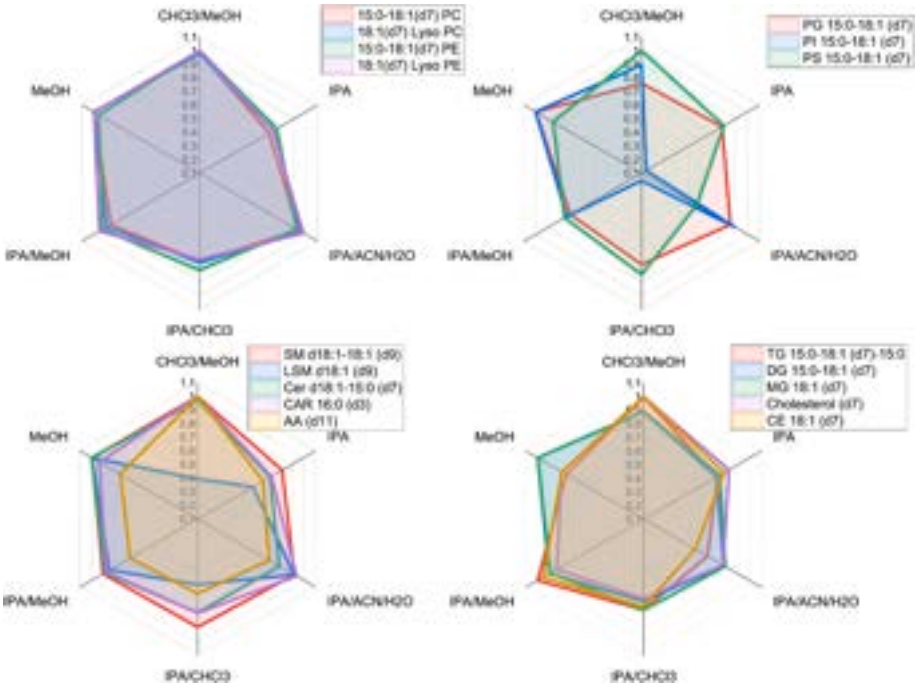

Fig. 8. Radar diagrams of peak area of IS reconstituted by different solvents based on extraction solvent IPA. The intensity was scaled to 0–1 for each internal standard by the maximum response among different extraction protocols. For each extraction method n = 3.

studies even though a slight insufficiency for apolar lipid classes may exist.

3.4. Final optimization and fine tuning of preferred extraction protocol

After the comparison of different aspects of the extraction protocols primarily based on the extraction recovery, a final extraction protocol with 90% IPA as extraction solvent and homogenizer for cell disruption with MeOH as reconstitution solvent was suggested. However, some issues remained unsolved like low extraction recovery for apolar lipid classes TG and CE. To resolve these issues, based on above insights and results we designed another series of experiments further fine-tuning the two best performing monophasic extraction protocols: the monophasic MMC protocol was modified to exclude the halogenated solvent which was replaced by IPA, MeOH/MTBE/IPA (1.33:1:1, v/v/v, MMIPA); the 90% IPA protocol was fine-tuned to improve the extraction recoveries for TGs, CEs. and cholesterol by replacing a small fraction of IPA by MTBE, IPA/H_2O/MTBE (18:2:5, v/v/v, IPA/MTBE). Furthermore, two reconstitution solvents MeOH (M) and MeOH/MTBE (1:1, v/v, MM) were evaluated, both without halogenated solvent. It can be seen from Fig. 9a that the extraction recovery (as determined by A1/(A1+A2) %) for apolar internal standards can be remarkably improved compared to the IPA protocol by replacing a small fraction of IPA by MTBE in the extraction solvent. All apolar lipids (MG, Cholesterol, CE and TG) show close to 100% extraction recoveries. The same extraction recovery (close to 100%) can be observed as well for other internal standards. What's more, by using MeOH/MTBE as reconstitution solvent, quantitative recovery can be achieved for all classes. Peak shape, even of early eluted lipids, is not compromised by MTBE in the reconstitution solvent (i.e. the sample diluent). Clearly, the MMIPA_MM protocol outperformed the other SOPs for all the internal standards (see heatmaps in Fig. 9b). The same trend can be observed for sum TG (the most apolar lipid class) and sum CAR (the most polar lipid class) as examples of endogenous lipids extracted from platelets (See Fig. S10). Finally, the peak shapes of the first eluted peaks within 3 min (both spiked ISs and endogenous lipids) were checked between MMIPA_MM protocol in comparison to other protocols for any risk of peak broadening and poor peak shape with MM as reconstitution solvent (Fig. S11). As can be seen from Fig. S11, there is no significant negative effect due to MTBE in the reconstitution solvent. Moreover, also the BPCs of blank extraction with MMIPA_MM (with IS mix spiked) were inspected for any problems with extraction of plasticisers compared with blank extraction with MTBE and IPA (Figs. S12a and b). The results are quite satisfying and the optimized protocol MMIPA_MM does not exhibit significantly more background signals compared to IPA. To conclude, the optimized protocol MMIPA_MM can achieve the best results for all lipid classes including the apolar ones.

4. Conclusions

This study has investigated the performance of different extraction systems including biphasic and monophasic extraction solvents, impact of extraction cycles, cell disruption methods and reconstitution solvents for the untargeted lipidomic study. After evaluation of the different tested protocols regarding criteria like extraction recovery and efficiency, high-throughput capability for large scale clinical study, compatibility to be combined with robotic pipetting systems and evaporation system, compatibility with clinical sampling devices (plastic tubes and containers) and also environmental friendliness aspects like reduced solvent consumption and no halogenated solvents, we suggest as the final optimized extraction protocol the solvent mixture MeOH/MTBE/IPA (1.3:1:1, v/v/v) as extraction solvent, a bead homogenizer for cell disruption, and MeOH/MTBE (1:1, v/v) as reconstitution solvent after evaporation of the above extraction solvent. This protocol provides fast (5 min for 24 samples) and efficient cellular and subcellular extraction of lipids (as confirmed by good extraction recoveries for cardiolipins which are solely present in the inner mitochondrial membrane) for a wide range of both most polar (e.g. acylcarnitines) and highly apolar lipids (e.g. triglycerides). It can be easily adapted for distinct sample types including cells, plasma, tissues, etc. furnishing a unified lipid extraction protocol. Moreover, it can be conveniently combined with automatic pipetting robotic systems. As a consequence, it is highly suitable for large-scale clinical lipidomic studies with high-throughput and reduces the sample processing times of the entire workflow (6 h for 48 samples; high performance evaporator as limiting step).

CRediT authorship contribution statement

Xiaoqing Fu: Investigation, Methodology, Formal analysis, Data curation, Visualization, Writing – original draft, Writing – review & editing. **Carlos Calderón:** Conceptualization, Supervision, Writing – review & editing. **Tobias Harm:** Investigation, Writing – review & editing. **Meinrad Gawaz:** Writing – review & editing, Funding acquisition. **Michael Lämmerhofer:** Conceptualization, Methodology, Supervision, Writing – review & editing, Resources, Funding acquisition.

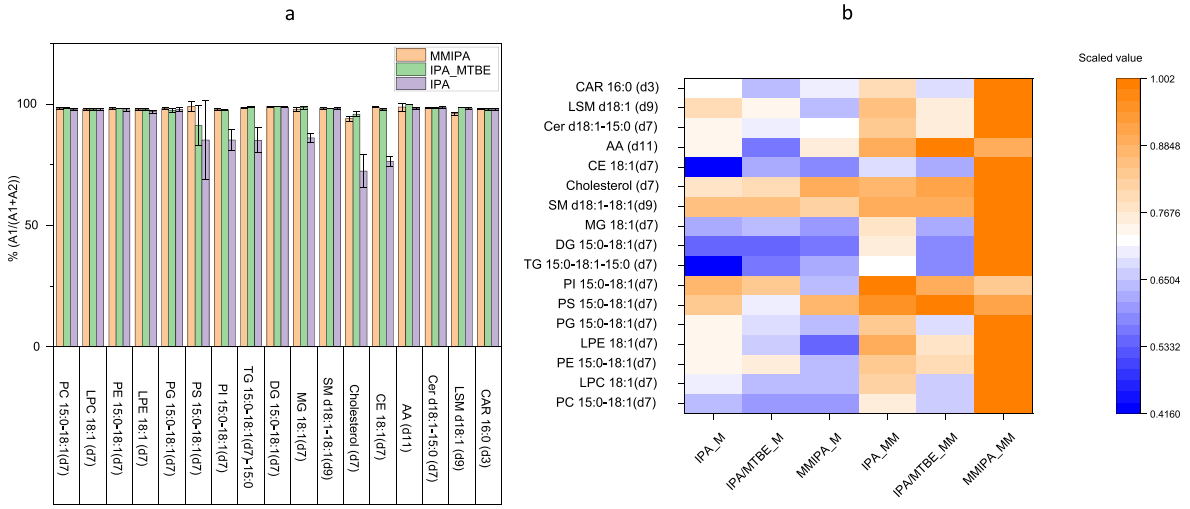

Fig. 9. (a) Comparison of extraction recoveries (A1/(A1+A2); in %) from 2 cycles of extraction of ISs with different extraction methods MMIPA, IPA/MTBE and IPA based on reconstitution solvent MeOH; (b) Heatmaps of spiked IS from 1st extraction in response to different extraction protocols IPA_M, IPA/MTBE_M, MMIPA_M, IPA_MM, IPA/MTBE_MM and MMIPA_MM. For each extraction method n = 3.

Declaration of competing interest

The authors declare that they have no known competing financial interests or personal relationships that could have appeared to influence the work reported in this paper.

Data availability

Data will be made available on request.

Acknowledgements

X.F. gratefully acknowledges the support from the China Scholarship Council (grant number 201908080155). M.L. acknowledges the support by the German Research Foundation (DFG, Deutsche Forschungsgemeinschaft), project number 374031971-TRR 240.

Appendix A. Supplementary data

Supplementary data to this article can be found online at https://doi.org/10.1016/j.aca.2022.340155.

References

[1] D. Casares, P.V. Escriba, C.A. Rossello, Membrane lipid composition: effect on membrane and organelle structure, function and compartmentalization and therapeutic avenues, Int. J. Mol. Sci. 20 (2019).
[2] S. Tumanov, J.J. Kamphorst, Recent advances in expanding the coverage of the lipidome, Curr. Opin. Biotechnol. 43 (2017) 127–133.
[3] V.B. O'Donnell, R.C. Murphy, S.P. Watson, Platelet lipidomics, Circ. Res. 114 (2014) 1185–1203.
[4] Y. Gloaguen, J.A. Kirwan, D. Beule, Deep learning-assisted peak curation for large-scale LC-MS metabolomics, Anal. Chem. 94 (2022) 4930–4937.
[5] T. Cajka, O. Fiehn, Comprehensive analysis of lipids in biological systems by liquid chromatography-mass spectrometry, Trends Anal. Chem. 61 (2014) 192–206.
[6] J. Folch, M. Lees, G.H.S. Stanley, A simple method for the isolation and purification of total lipides from animal tissues, J. Biol. Chem. 226 (1957) 497–509.
[7] E.G. Bligh, W.J. Dyer, A rapid method of total lipid extraction and purification, Can. J. Biochem. Physiol. 37 (1959) 911–917.
[8] H. Zhang, Y. Gao, J. Sun, S. Fan, X. Yao, X. Ran, C. Zheng, M. Huang, H. Bi, Optimization of lipid extraction and analytical protocols for UHPLC-ESI-HRMS-based lipidomic analysis of adherent mammalian cancer cells, Anal. Bioanal. Chem. 409 (2017) 5349–5358.
[9] C. Breil, M. Abert Vian, T. Zemb, W. Kunz, F. Chemat, Bligh and dyer" and Folch methods for solid-liquid-liquid extraction of lipids from microorganisms. Comprehension of solvatation mechanisms and towards substitution with alternative solvents, Int. J. Mol. Sci. 18 (2017) 708.
[10] T.A. Lydic, J.V. Busik, G.E. Reid, A monophasic extraction strategy for the simultaneous lipidome analysis of polar and nonpolar retina lipids, J. Lipid Res. 55 (2014) 1797–1809.
[11] R.E. Patterson, A.J. Ducrocq, D.J. McDougall, T.J. Garrett, R.A. Yost, Comparison of blood plasma sample preparation methods for combined LC-MS lipidomics and metabolomics, J. Chromatogr., B: Anal. Technol. Biomed. Life Sci. 1002 (2015) 260–266.
[12] A. Hara, N.S. Radin, Lipid extraction of tissues with a low-toxicity solvent, Anal. Biochem. 90 (1978) 420–426.
[13] V. Matyash, G. Liebisch, T.V. Kurzchalia, A. Shevchenko, D. Schwudke, Lipid extraction by methyl-tert-butyl ether for high-throughput lipidomics, J. Lipid Res. 49 (2008) 1137–1146.
[14] L. Löfgren, M. Ståhlman, G.B. Forsberg, S. Saarinen, R. Nilsson, G.I. Hansson, The BUME method: a novel automated chloroform-free 96-well total lipid extraction method for blood plasma, J. Lipid Res. 53 (2012) 1690–1700.
[15] B. Reichl, N. Eichelberg, M. Freytag, J. Gojo, A. Peyrl, W. Buchberger, Evaluation and optimization of common lipid extraction methods in cerebrospinal fluid samples, J. Chromatogr., B: Anal. Technol. Biomed. Life Sci. 1153 (2020), 122271.
[16] L. Lofgren, G.B. Forsberg, M. Stahlman, The BUME method: a new rapid and simple chloroform-free method for total lipid extraction of animal tissue, Sci. Rep. 6 (2016), 27688.
[17] Z. Zhao, Y. Xu, An extremely simple method for extraction of lysophospholipids and phospholipids from blood samples, J. Lipid Res. 51 (2010) 652–659.
[18] Y. Satomi, M. Hirayama, H. Kobayashi, One-step lipid extraction for plasma lipidomics analysis by liquid chromatography mass spectrometry, J. Chromatogr. B 1063 (2017) 93–100.
[19] R.M. Pellegrino, A. Di Veroli, A. Valeri, L. Goracci, G. Cruciani, LC/MS lipid profiling from human serum: a new method for global lipid extraction, Anal. Bioanal. Chem. 406 (2014) 7937–7948.
[20] A. Iriondo, M. Tainta, J. Saldias, M. Arriba, B. Ochoa, F.M. Goñi, P. Martinez-Lage, B. Abad-García, Isopropanol extraction for cerebrospinal fluid lipidomic profiling analysis, Talanta 195 (2019) 619–627.
[21] J. Zhou, C. Liu, D. Si, B. Jia, L. Zhong, Y. Yin, Workflow development for targeted lipidomic quantification using parallel reaction monitoring on a quadrupole-time of flight mass spectrometry, Anal. Chim. Acta 972 (2017) 62–72.
[22] Z.H. Alshehry, C.K. Barlow, J.M. Weir, Y. Zhou, M.J. McConville, P.J. Meikle, An efficient single phase method for the extraction of plasma lipids, Metabolites 5 (2015) 389–403.
[23] M.H. Sarafian, M. Gaudin, M.R. Lewis, F.P. Martin, E. Holmes, J.K. Nicholson, M. E. Dumas, Objective set of criteria for optimization of sample preparation procedures for ultra-high throughput untargeted blood plasma lipid profiling by ultra performance liquid chromatography-mass spectrometry, Anal. Chem. 86 (2014) 5766–5774.
[24] C. Calderón, C. Sanwald, J. Schlotterbeck, B. Drotleff, M. Lämmerhofer, Comparison of simple monophasic versus classical biphasic extraction protocols for comprehensive UHPLC-MS/MS lipidomic analysis of Hela cells, Anal. Chim. Acta 1048 (2019) 66–74.
[25] M. Shehadul Islam, A. Aryasomayajula, P. Selvaganapathy, A review on macroscale and microscale cell lysis methods, Micromachines 8 (2017).
[26] N. Rajapakse, K. Shimizu, M. Payne, D. Busija, Isolation and characterization of intact mitochondria from neonatal rat brain, Brain Res. Brain Res. Protoc. 8 (2001) 176–183.
[27] L. Benov, J. Al-Ibraheem, Disrupting Escherichia coli: a comparison of methods, J. Biochem. Mol. Biol. 35 (2002) 428–431.
[28] T. Kristián, I.B. Hopkins, M.C. McKenna, G. Fiskum, Isolation of mitochondria with high respiratory control from primary cultures of neurons and astrocytes using nitrogen cavitation, J. Neurosci. Methods 152 (2006) 136–143.
[29] S. Chaiyarit, V. Thongboonkerd, Comparative analyses of cell disruption methods for mitochondrial isolation in high-throughput proteomics study, Anal. Biochem. 394 (2009) 249–258.
[30] J.V. Sinisterra, Application of ultrasound to biotechnology: an overview, Ultrasonics 30 (1992) 180–185.
[31] J. Niklas, A. Melnyk, Y. Yuan, E. Heinzle, Selective permeabilization for the high-throughput measurement of compartmented enzyme activities in mammalian cells, Anal. Biochem. 416 (2011) 218–227.
[32] J. Moebius, R.P. Zahedi, U. Lewandrowski, C. Berger, U. Walter, A. Sickmann, The human platelet membrane proteome reveals several new potential membrane proteins, Mol. Cell. Proteomics 4 (2005) 1754–1761.
[33] B. Peng, D. Kopczynski, B.S. Pratt, C.S. Ejsing, B. Burla, M. Hermansson, P.I. Benke, S.H. Tan, M.Y. Chan, F. Torta, D. Schwudke, S.W. Meckelmann, C. Coman, O. J. Schmitz, B. MacLean, M.C. Manke, O. Borst, M.R. Wenk, N. Hoffmann, R. Ahrends, LipidCreator workbench to probe the lipidomic landscape, Nat. Commun. 11 (2020) 2057.
[34] J. Schlotterbeck, M. Chatterjee, M. Gawaz, M. Lammerhofer, Comprehensive MS/MS profiling by UHPLC-ESI-QTOF-MS/MS using SWATH data-independent acquisition for the study of platelet lipidomes in coronary artery disease, Anal. Chim. Acta 1046 (2019) 1–15.
[35] D.A. Slatter, M. Aldrovandi, A. O'Connor, S.M. Allen, C.J. Brasher, R.C. Murphy, S. Mecklemann, S. Ravi, V. Darley-Usmar, V.B. O'Donnell, Mapping the human platelet lipidome reveals cytosolic phospholipase A2 as a regulator of mitochondrial bioenergetics during activation, Cell Metabol. 23 (2016) 930–944.
[36] A. Gil, W. Zhang, J.C. Wolters, H. Permentier, T. Boer, P. Horvatovich, M. R. Heiner-Fokkema, D.J. Reijngoud, R. Bischoff, One- vs two-phase extraction: re-evaluation of sample preparation procedures for untargeted lipidomics in plasma samples, Anal. Bioanal. Chem. 410 (2018) 5859–5870.
[37] M. Cebo, C. Calderón Castro, J. Schlotterbeck, M. Gawaz, M. Chatterjee, M. Lämmerhofer, Untargeted UHPLC-ESI-QTOF-MS/MS analysis with targeted feature extraction at precursor and fragment level for profiling of the platelet lipidome with ex vivo thrombin-activation, J. Pharmaceut. Biomed. Anal. 205 (2021), 114301.

Supplementary information

Advanced unified monophasic lipid extraction protocol with wide coverage on the polarity scale optimized for large-scale untargeted clinical lipidomics analysis of platelets

Xiaoqing Fu[a], Carlos Calderón [a,b], Tobias Harm[c], Meinrad Gawaz[c], Michael Lämmerhofer[a]*

[a]Institute of Pharmaceutical Sciences, Pharmaceutical (Bio-)Analysis, University of Tübingen, Auf der Morgenstelle 8, 72076 Tübingen, Germany

[b] Escuela de Química, Universidad de Costa Rica, San José, 11501-2060, Costa Rica

[c] Department of Cardiology and Angiology, University Hospital Tübingen, 72076 Tübingen, Germany

*Authors for correspondence:

Prof. Dr. Michael Lämmerhofer

Pharmaceutical (Bio-)Analysis

Institute of Pharmaceutical Sciences

University of Tübingen

Auf der Morgenstelle 8

72076 Tübingen, Germany

T +49 7071 29 78793, F +49 7071 29 4565

E-mail: michael.laemmerhofer@uni-tuebingen.de

1. Experimental

1.1. Materials

Table. S1. *Composition of internal standards and their concentration in SPLASH lipidomix.*

SPLASH Lipidomix	ORIGINAL CONCENTRATION (ng/mL)	FINAL CONCENTRATION IN RECONSTITUTION SOLVENT (ng/mL)
PC 15:0-18:1 (d7)	160000	8000
PE 15:0-18:1 (d7)	5000	250
PS 15:0-18:1 (d7)	5000	250
PG 15:0-18:1 (d7)	30000	1500
PI 15:0-18:1 (d7)	10000	500
PA 15:0-18:1 (d7)	7000	350
LPC 18:1 (d7)	25000	1250
LPE 18:1 (d7)	5000	250
CE 18:1 (d7)	350000	17500
MG 18:1 (d7)	2000	100
DG 15:0-18:1 (d7)	10000	500
TG 15:0-18:1 (d7)-15:0	55000	2750
SM d18:1-18:1 (d9)	30000	1500
Cholesterol (d7)	100000	5000

Table. S2. *Composition of internal standards and their concentration in EquiSPLASH lipidomix.*

EquiSPLASH Lipidomix	ORIGINAL CONCENTRATION (ng/mL)	FINAL CONCENTRATION IN RECONSTITUTION SOLVENT (ng/mL)
PC 15:0-18:1 (d7)	100000	500
LPC 18:1 (d7)	100000	500
PE 15:0-18:1 (d7)	100000	500
LPE 18:1 (d7)	100000	500
PG 15:0-18:1 (d7) (Na Salt)	100000	500
PI 15:0-18:1 (d7) (NH4 Salt)	100000	500
PS 15:0-18:1 (d7) (Na Salt)	100000	500
TG 15:0-18:1 (d7)-15:0	100000	500
DG 15:0-18:1 (d7)	100000	500
MG 18:1 (d7)	100000	500
CE 18:1 (d7)	100000	500
SM d18:1-18:1 (d9)	100000	500
Cer d18:1-15:0 (d7)	100000	500

1.2. UHPLC-ESI-QTOF-MS/MS method

The analysis of the samples was performed with an Agilent 1290 Infinity UHPLC system (Agilent, Waldbronn, Germany) equipped with a binary pump, a PAL-HTX xt DLW autosampler (CTC Analytics AG, Switzerland) and coupled to a SCIEX TripleTOF 5600+ QTOF mass spectrometer with a DuoSpray Source (SCIEX, Concord, Ontario, Canada).

The chromatographic separation was performed on ACQUITY UPLC CSH C18 column (100 mm × 2.1 mm; particles: 1.7 µm; Waters Corporation, Millford, MA, USA) with precolumn (5 mm x 2.1 mm; 1.7 µm particles) [1, 2]. The column temperature was 65°C and the flow rate 0.6 mL/min. Mobile phase A was composed of H_2O/ACN 2:3 (v/v) containing 10 mM ammonium formate and 0.1% formic acid (v/v) while mobile phase B was IPA/ACN/H_2O 90:9:1 (v/v/v) containing 10 mM ammonium formate and 0.1% FA (v/v). The gradient elution started from 15% B to 30% B in 2 min, followed by increase of B to 48% in 0.5 min. Then mobile phase B was further increased to 82% at 11 min and quickly reached 99% in the next 0.5 min followed by holding this percentage for another 0.5 min. Afterwards, the percentage of B was back to starting conditions (15% B) in 0.1 min to re-equilibrate the column for the next injection (2.9 min).

LC-ESI-MS/MS experiments were operated in both positive and negative ion mode with injection volume of 3 µL for positive and 5 µL for negative mode. An MS full scan experiment with mass range m/z 50-1250 was selected while different SWATH windows were acquired for MS/MS experiments (see suppl. Table S1). The ion source temperature was set to 350°C with curtain gas (CUR, nitrogen), nebulizer gas (GS1, zero grade air) and heater gas (GS2, zero grade air) pressures 35 psi, 60 psi and 60 psi, respectively, for both modes. The ion spray voltage was set to 5500 V in the

positive mode and -4500 V in negative mode. The declustering potential (DP) was adjusted to 80 V and -80 V for positive and negative polarity mode, respectively. The cycle time was always 720 ms. The collision energy (CE) and collision energy spread (CES) for each experiment are shown in Table. S3.

Table. S3. *MS and MS/MS experiments of SWATH design showing precursor isolation windows with respective m/z range, accumulation time (Acc. time) and collision energy.*

			ESI (+)			ESI (-)		
Experiment	Scan typ	Acc. Time (ms)	Start (m/z)	Stop (m/z)	CE (V)	Start (m/z)	Stop (m/z)	CE (V)
1	MS Full Scan	50	50.0	1250.0	10	50	1250.0	-10
2	SWATH	31	50.0	217.6	45±15	50	213.5	-45±15
3	SWATH	31	216.6	340.3	45±15	212.5	271.4	-45±15
4	SWATH	31	339.3	441.4	45±15	270.4	314.6	-45±15
5	SWATH	31	440.4	524.9	45±15	313.6	382.6	-45±15
6	SWATH	31	523.9	571.6	45±15	381.6	427.5	-45±15
7	SWATH	31	570.6	643.4	45±15	426.5	464.3	-45±15
8	SWATH	31	642.4	687.3	45±15	463.3	501.0	-45±15
9	SWATH	31	686.3	720.1	45±15	500.0	540.8	-45±15
10	SWATH	31	719.1	740.1	45±15	539.8	617.5	-45±15
11	SWATH	31	739.1	755.0	45±15	616.5	680.3	-45±15
12	SWATH	31	754.0	764.1	45±15	679.3	697.1	-45±15
13	SWATH	31	763.1	775.1	45±15	696.1	724.0	-45±15
14	SWATH	31	774.1	786.1	45±15	723.0	749.0	-45±15
15	SWATH	31	785.1	793.1	45±15	748.0	775.6	-45±15
16	SWATH	31	792.1	806.1	45±15	774.6	793.1	-45±15
17	SWATH	31	805.1	814.2	45±15	792.1	811.0	-45±15
18	SWATH	31	813.2	829.6	45±15	810.0	832.6	-45±15
19	SWATH	31	828.6	842.7	45±15	831.6	854.1	-45±15
20	SWATH	31	841.7	903.3	45±15	853.1	861.2	-45±15
21	SWATH	31	902.3	1250.0	45±15	860.2	1050.0	-45±15

The sequence was started with three injections of IS mixture as system suitability test (SST), followed by a blank run, extraction solvent blank injection and triplicate QC injection at the beginning of the batch. The SST injections were controlled immediately, once finished before the sequence allowed to continue, or otherwise stopped if not

complying. The whole sequence was controlled by injection of QC samples after every 5 samples to allow for evaluation of the performance of the instrument and for LC-MS precision testing of detected features.

1.3. Software for data processing

MS-Dial software (version. 4.7) was used for the purpose of untargeted lipidomics profiling. The parameters can be found in Table S4 (Table S5 and S6 are files used for post-identification). In case of any targeted searching for lipids which were not identified by MS-Dial, MultiQuant (3.0) was applied as an additional tool for lipid finding. After peak alignment with MS-Dial, a list of identified and unknown lipids was obtained. Curation of the resultant peak list was done in accordance to a reference list [3] by search for outliers in trendlines of m/z vs retention plots of lipid species series differing in double bond numbers and carbon numbers (plotted by R version 4.0.2), followed by manual inspection of MS2 spectra for verification of identifications. Normalized responses of each lipid from MS-Dial were then applied for further statistical analysis including PCA plots, OPLS-DA plots (SIMCA 17), Venn diagrams and Radar plots (Origins 2020).

Table. S4. *MS-Dial parameters used for data processing in both positive and negative ion modes.*

Mode	pos	neg
	Data collection	
MS1 tolerance	0.01	0.01
MS2 tolerance	0.025	0.025
Retention time begin	0	0
Retention time end	15	15
MS1 range begin	50	50
MS1 range end	1250	1050
MS/MS range begin	50	50
MS/MS range end	1250	1050
	Peak detection	
Minimum peak height	1000	1000
Mass slice width	0.1	0.1
Smoothing method	Linear weighted moving average	Linear weighted moving average
Smoothing level	2	2
Minimum peak width	5	5
	MS2Dec	
sigma window value	0.5	0.5
MS/MS abudance cut off	0	0
	Identification	
MSP file	Msp20210527163602_converted.lbm2	Msp20210527163602_converted.lbm2
Retention time tolerance	15	15
Accurate mass tolerance (MS1)	0.01	0.01
Accurate mass tolerance (MS2)	0.05	0.05
Identification score cut off	80%	80%
	Text file and post identification (retention time and accurate mass based) setting	
Text file	SplashLipidoMix1_Pos.txt	SplashLipidoMix1_Neg.txt
Retention time tolerance	15	15
Acurrate mass tolerance	0.01	0.01
Identification score cut off	85%	85%
	Aducct	
	M+H]+, [M+NH4]+, [M+Na]+, [M+H-H2O]+	[M-H]-, [M+Cl]-, [M+FA-H]-
	Alignment	
Reference file	QC5	QC5
Retention time tolerance	0.1	0.1
MS1 tolerance	0.015	0.015
Retention time factor	0.5	0.5
MS 1 factor	0.5	0.5
Peak count filter	5%	5%
N% detcted in at least one group	35%	35%

Table. S5. *List of internal standards in positive ion mode for post-identification in MS-Dial.*

NAME	m/z	RT	Adduct	InChIKey	Formula	Ontology
PC 15:0-18:1 (d7)	753.6134	5.07	[M+H]+	ZEWLMKXMNQOCOQ-GCHPQBSENA-N	C41H73D7NO8P	PC
PE 15:0-18:1 (d7)	711.5665	5.24	[M+H]+	ADCNXGARWPJRBV-RGLIIYCRNA-N	C38H67D7NO8P	PE
PS 15:0-18:1 (d7)	755.5564	4.38	[M+H]+	KVBAVKWITJZQEG-UDKXCJCZNA-N	C39H67D7NO10P	PS
PG 15:0-18:1 (d7)	759.5877	4.63	[M+NH4]+	CAKDJPLPYOYWLK-AHOXJELVNA-N	C39H68D7O10P	PG
PI 15:0-18:1 (d7)	847.6041	4.43	[M+NH4]+	XCKYASHMOHAUQB-OAFUKSMZNA-N	C42H72D7O13P	PI
PA 15:0-18:1 (d7)	668.5248	4.00	[M+H]+	NKHIVFXDPYZIBK-WZQGNCBKSA-N	C36H62D7O8P	PA
LPC 18:1 (d7)	529.3993	1.52	[M+H]+	YAMUFBLWGFFICM-HNNXNMBSNA-N	C26H45D7NO7P	LPC
LPE 18:1 (d7)	487.3524	1.56	[M+H]+	PYVRVRFVLRNJLY-CCLUNVSZNA-N	C23H39D7NO7P	LPE
CE 18:1 (d7)	675.6779	10.94	[M+NH4]+	RJECHNNFRHZQKU-LCUGTLGDNA-N	C45H71D7O2	CE
MG 18:1 (d7)	381.3704	2.70	[M+NH4]+	RZRNAYUHWVFMIP-IJGLUQEONA-N	C21H33D7O4	MG
DG 15:0-18:1 (d7)	605.5845	6.48	[M+NH4]+	GWAPRYUVSHVZHN-ZYYJJESQNA-N	C36H61D7O5	DG
TG 15:0-18:1 (d7)-15:0	829.7985	10.43	[M+NH4]+	YUNYDLOKHYJQAT-OTEPLKBXSA-N	C51H89D7O6	TG
SM d18:1-18:1 (d9)	738.6470	4.70	[M+H]+	NBEADXWAAWCCDG-KYPZZJCONA-N	C41H72D9N2O6P	SM
Cer d18:1-15:0 (d7)	531.5477	5.15	[M+H]+	YDNKGFDKKRUKPY-ARWSMCILSA-N	C34H58D9NO3	Cer-NS
Cholesterol (d7)	376.3955	4.67	[M-H2O+H]+	HVYWMOMLDIMFJA-IFAPJKRJSA-N	C27H39D7O	CE

Table. S6. *List of internal standards in negative ion mode for post-identification in MS-Dial.*

NAME	m/z	RT	Adduct	InChIKey	Formula	Ontology
PC 15:0-18:1 (d7)	797.6043	5.07	[M+FA-H]-	ZEWLMKXMNQOCOQ-GCHPQBSENA-N	C41H73D7NO8P	PC
PE 15:0-18:1 (d7)	709.5519	5.24	[M-H]-	ADCNXGARWPJRBV-RGLIIYCRNA-N	C38H67D7NO8P	PE
PS 15:0-18:1 (d7)	753.5418	4.51	[M-H]-	KVBAVKWITJZQEG-UDKXCJCZNA-N	C39H67D7NO10P	PS
PG 15:0-18:1 (d7)	740.5466	4.61	[M-H]-	CAKDJPLPYOYWLK-AHOXJELVNA-N	C39H68D7O10P	PG
PI 15:0-18:1 (d7)	828.5626	4.43	[M-H]-	XCKYASHMOHAUQB-OAFUKSMZNA-N	C42H72D7O13P	PI
PA 15:0-18:1 (d7)	666.5097	4.00	[M-H]-	NKHIVFXDPYZIBK-WZQGNCBKSA-N	C36H62D7O8P	PA
LPC 18:1 (d7)	587.4059	1.52	[M+FA-H]-	YAMUFBLWGFFICM-HNNXNMBSNA-N	C26H45D7NO7P	LPC
LPE 18:1 (d7)	485.3378	1.56	[M-H]-	PYVRVRFVLRNJLY-CCLUNVSZNA-N	C23H39D7NO7P	LPE
SM d18:1-18:1 (d9)	782.6379	4.69	[M+FA-H]-	NBEADXWAAWCCDG-KYPZZJCONA-N	C41H72D9N2O6P	SM
Cer d18:1-15:0 (d7)	575.5386	5.15	[M+FA-H]-	YDNKGFDKKRUKPY-ARWSMCILSA-N	C34H58D9NO3	Cer-NS
AA (d11)	314.3012	2.59	[M-H]-	YZXBAPSDXZZRGB-UJZOERHRSA-N	C20H21D11O2	FA

1.4. Platelet isolation

The blood was collected in acid-citrate-dextrose (ACD) buffer as anticoagulant (12.5 g sodium citrate, 546.82 g of citric acid, 10 g glucose, 500 mL distilled water, adjusted to pH 4.69 with NaOH) (40 mL in total, ACD anticoagulant:blood 1:4, v/v) and then centrifuged (430 x g for 20 min without acceleration and deceleration). Obtained platelet-rich plasma was mixed with Tyrodes-HEPES buffer (2.5 mM HEPES, 150 mM NaCl, 1 mM KCl, 2.5 mM $NaHCO_3$, 0.36 mM NaH_2PO_4, 5.5 mM glucose, 1 mg/mL BSA, pH 6.5) and centrifuged (900 x g for 10 min without acceleration and deceleration) [4]. Platelet pellets were collected and frozen at -80°C until extraction.

The platelet pellets from different Eppendorf tubes were pooled together through re-suspending them in PBS supplemented with calcium. The pooled platelet pellets in PBS buffer were vortexed and divided into several aliquots as needed to perform different extraction protocols.

1.5. Preparation of internal standard mixtures

Table. S7. *Composition of spiked internal standard mixtures (IS mix1) during extraction.*

INTERNAL STANDARDS	FINAL CONCENTRATION IN RECONSTITUTION SOLVENT	UNIT
SPLASH Lipidomix	5	%
AA (d11)	5000	ng/mL
EPA (d5)	5000	ng/mL
DHA (d5)	5000	ng/mL

Table. S8. *Composition of spiked internal standard mixtures (IS mix2) during extraction.*

INTERNAL STANDARDS	FINAL CONCENTRATION IN RECONSTITUTION SOLVENT (ng/mL)
EquiSPLASH Lipidomix	500
AA (d11)	100
CAR 16:0 (d3)	500
PA 15:0-18:1 (d7)	500
Cholesterol (d7)	2000
CE 18:1 (d7) *	9500
LSM d18:1 (d9)	500
S1P d18:1 (d7)	500

**total conc. of CE 18:1 (d7) is 10000 ng/mL (further spiking needed to achieve sufficient concentration level for detection)*

1.6 Temperature control during lipid extraction with Precellys homogenizer

The Precellys evolution has a dry-ice cooling unit (Cryolys Evolution) which was used in this study when the homogenizer protocol was employed. The supplier gives some information about the cooling performance as documented in Fig. S1.

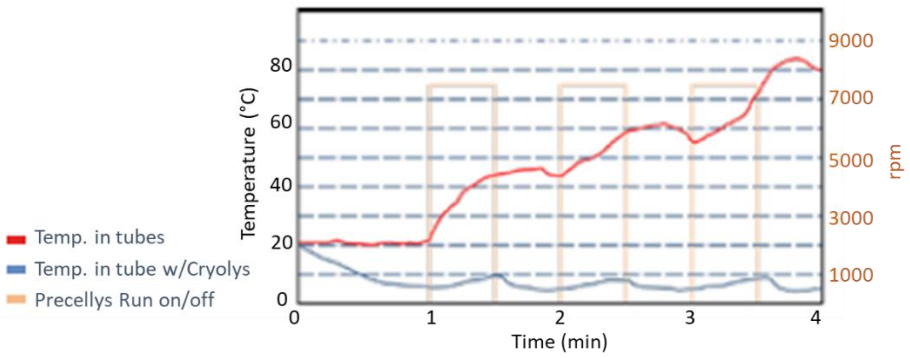

Fig. S1. *Typical tubes' temperature profile of Precellys evolution homogenizer with (red curve) and without dry-ice cooling (blue curve). Parameters: 7,500 rpm, 3 x 30 s, 30 s breaks. Source: Bertin.*

2. Selection of extraction solvent system

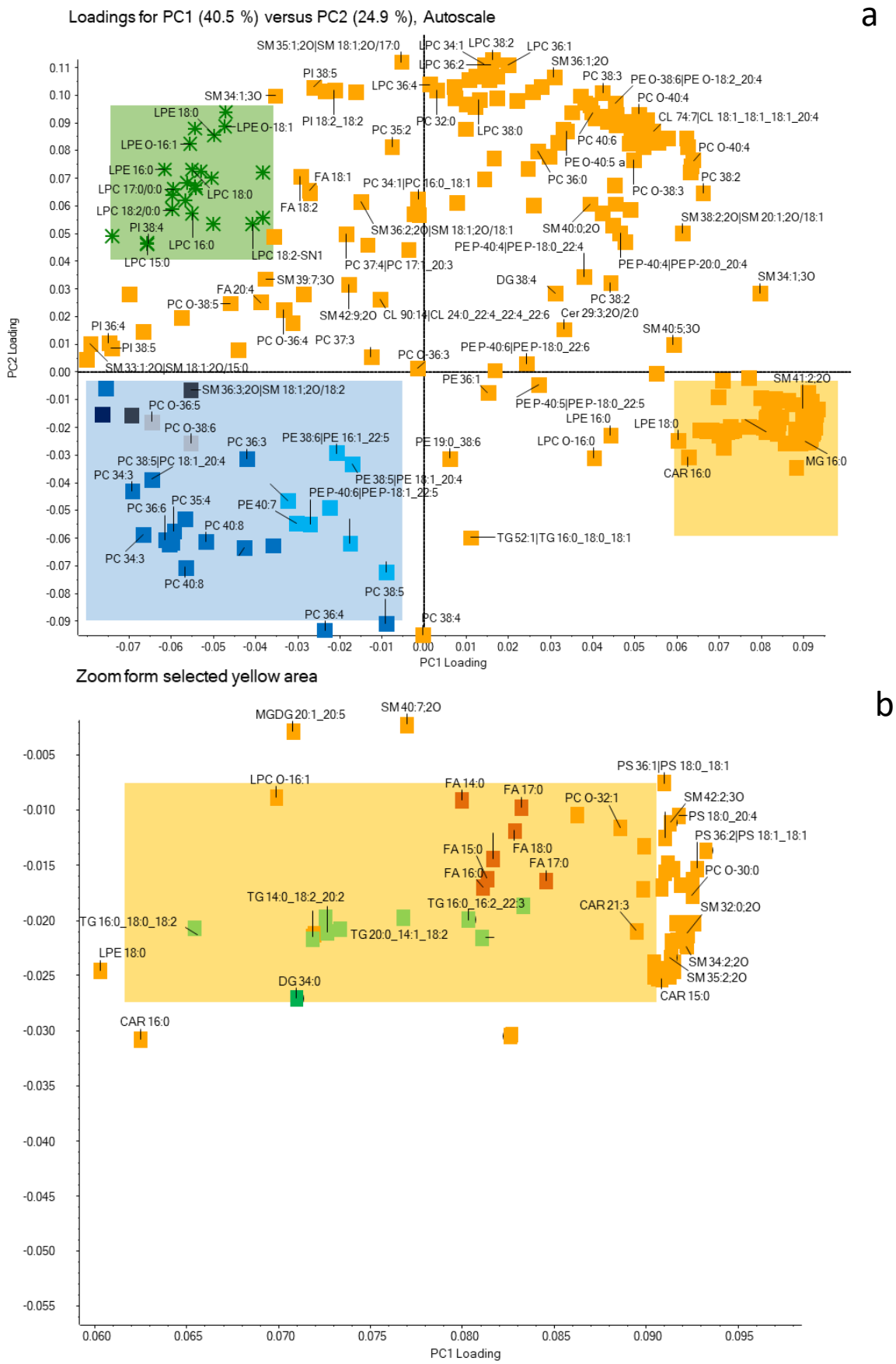

Fig. S2. *Loadings plot of identified features (a) and zoomed plot from selected yellow area (b) based on the PCA score plot of five extraction protocols.*

3. Impact of repeated extraction cycles and recoveries-endogenous lipids

After checking the results for ISs (shown in the main document), endogenous lipids extracted from platelet pellets by different protocols were also analysed in view of extraction recoveries in the first cycle of repeated extraction. From Fig. S3, it can be seen that the monophasic MMC extraction protocol exhibits over all classes the best extraction recoveries and the biphasic Hexane protocol the worst. The IPA and IPA TL methods show similar extraction recoveries as the MMC protocol for many lipid classes but shows lower extraction recovery for neutral lipids especially TG (TG 54:1 and TG 54:3), DG, MG as well as cholesterol and ceramides. In contrast, for glycerophospholipids e.g., PC 34:2, PC 36:1 and PC 38:4 which are the most abundant in platelets, similar results of high extraction recovery of over 90% for extraction protocol “MTBE”, “MMT”, “IPA” and “IPA TL” can be noticed from Fig. S3, indicating that with these extraction solvents a 2nd extraction cycle is not necessary for these lipid classes. Other glycerophospholipids like PE (PE 36:2, PE 38:4 and PE 40:7), LPE (LPE 18:0 and LPE 16:0), PI (PI 36:4, PI 38:4 and PI 38:5) and PS (PS 36:1, PS 38:4 and PS 40:6) follow the same trend as PC (Fig. S3). On the other hand, LPCs showed similar extraction recoveries for the IPA protocols as for MMC while both biphasic extraction protocols, MTBE and Hexane, were performing worse. The extraction recoveries for MTBE method were a bit higher for TGs and Ceramides compared to IPA but worse for lyso-phospholipids. For free fatty acids (FA 18:1 and FA 18:2) and cardiolipins (CL 74:3 and CL 74:7) which are detected only in ESI- mode, the difference of extraction recovery between 5 extraction protocol was not as significant as for glycerophospholipids.

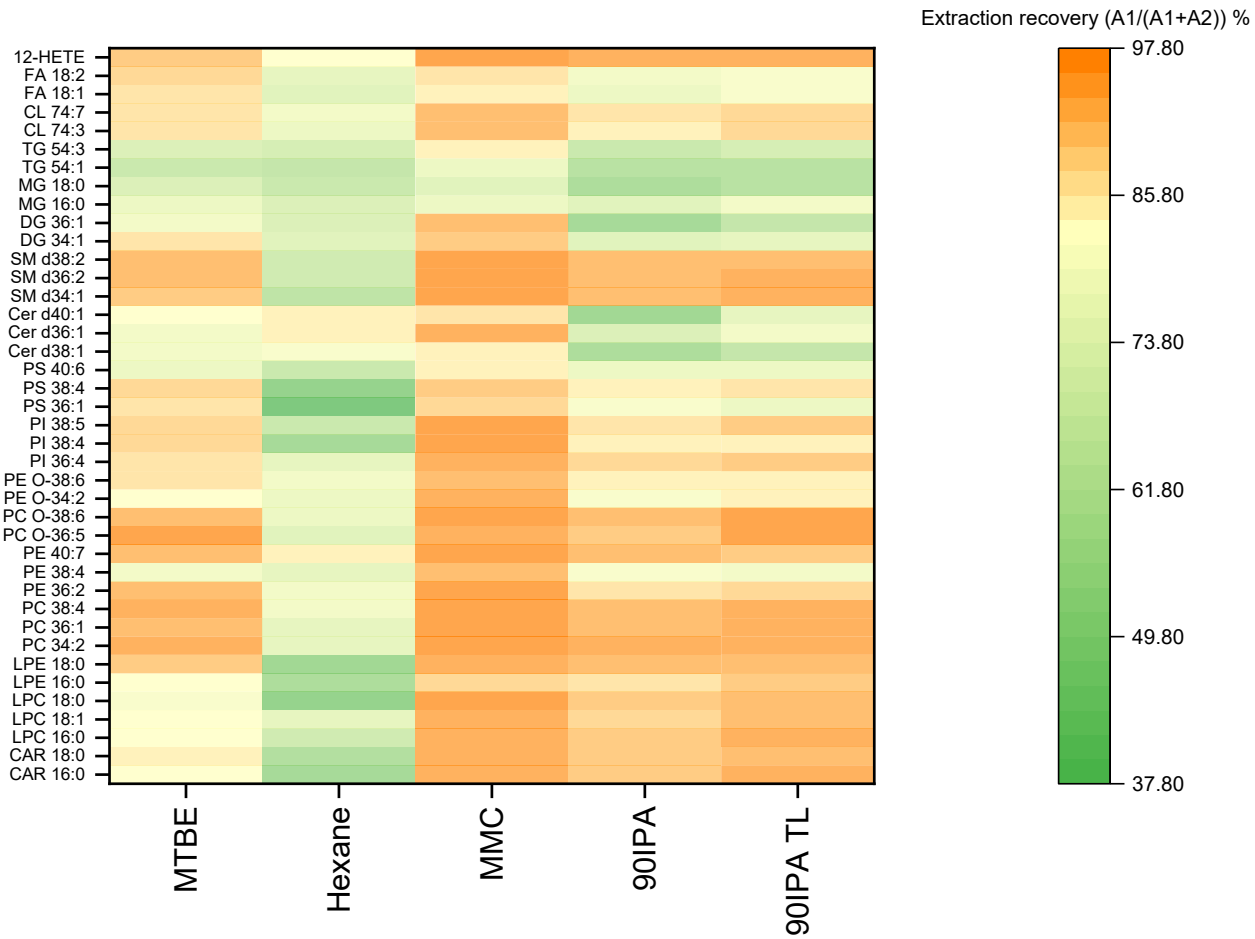

Fig. S3*. Heatmap of extraction recovery (A1/(A1+A2)) % of selected endogenous lipids in platelets with different extraction methods* (selected are a few of most abundant lipids from various classes).

4. Solvent compatibility for pipetting robotic (OT2 from Opentrons)

Table. S9. Solvent compatibility for pipetting robotic.

	PC-ABS (external & internal housing)	NBR (internal plunger O-ring)	Silicone (external O-ring)	Polypropylene (tips)
Acetone	D - Poor	D - Poor	D - Poor	A - Excellent
Ethanol	B1 - Good	C - Fair	B - Good	A - Excellent
Methanol	D - Poor	A - Excellent	A - Excellent	A2 - Excellent
Ethyl Acetate	D - Poor	D - Poor	B - Good	A1 - Excellent
MtBE	E - Unavailable	E - Unavailable	E - Unavailable	E - Unavailable
Petroleum Ether	B - Good	D - Poor	D - Poor	B1 - Good
Hexanes	D - Poor	A - Excellent	D - Poor	B1 - Good
Methylene Chloride (DCM)	D - Poor	D - Poor	D - Poor	D - Poor
1,2-Dichloroethane (DCE) methylene chloride	D - Poor	E - Unavailable	E - Unavailable	D - Poor
Acetonitrile	D - Poor	E - Unavailable	D - Poor	A1 - Excellent
Methyltetrahydrofuran (MeTHF) - Viridisol M	E - Unavailable	E - Unavailable	E - Unavailable	E - Unavailable
Dioxane	B - Good	D - Poor	D - Poor	A2 - Excellent
Tetrahydrofuran (THF)	E - Unavailable	D - Poor	D - Poor	C2 - Fair
DMF (Dimethylformamide)	D - Poor	E - Unavailable	C - Fair	A - Excellent
DMSO (dimethyl sulfoxide)	A - Excellent	C - Fair	A - Excellent	A - Excellent
DMA (dimethylacetamide)	A - Excellent	D - Poor	B - Good	E - Unavailable
Chloroform	D - Poor	D - Poor	D - Poor	C1 - Fair
Carbolic Acid (Phenol)	D - Poor	D - Poor	D - Poor	B - Good

Ratings - Chemical Effect

A - Excellent

B - Good: Minor Effect, slight corrosion, or discoloration.

C - Fair: Moderate Effect, not recommended for continuous use. Softening or loss of strength, and swelling may occur.

D - Severe Effect: Not recommended for any use.

E - Information not available.

5. Comparison of different methods for cell disruption

5.1 Small-scale sampling

Table. S10. *Precision of listed lipids in QC when comparing the normalized response (peak area ratio to IS) between different cell disruption methods.*

	Lipid	precision in QC	IS
positive mode	MG 18:0	11.9	
	MG 18:1	6.9	
	MG 16:0	13.7	MG 18:1 (d7)
	LPC 18:1	8.6	
	LPC 18:0	12.9	LPC 18:1 (d7)
	DG 16:0-18:1	7.1	
	DG 18:0-18:1	8.4	DG 15:0-18:1 (d7)
	PC 16:0-18:1	6.5	
	PC 16:0-18:2	8.5	
	PC 16:0-20:4	7.2	PC 15:0-18:1 (d7)
	PI 16:0-20:4	4.4	
	PI 18:0-20:4	13.5	
	PI 18:1-20:4	3.6	PI 15:0-18:1 (d7)
	SM d34:1	3.0	
	SM d38:1	5.6	
	SM d40:1	5.1	SM d18:1-18:1 (d9)
	TG 48:1	3.3	
	TG 54:1	9.8	TG 15:0-18:1 (d7)-15:0
	TG 54:5	4.3	
	cholesterol	20.8	Cholesterol (d7)
	CE 18:1	5.6	
	CE 18:2	4.7	
	CE 20:4	6.7	CE 18:1 (d7)
	Acar 16:0	13.8	
	Acar 18:0	14.4	MG 18:1 (d7)
	Cer d18:1-20:0	15.8	
	Cer d18:1-180	6.2	
	Cer d18:1-22:0	7.4	PI 15:0-18:1 (d7)
	Lipid	precision in QC	IS
negative mode	LPE 18:0	4.9	
	LPE 20:4	12.7	
	LPE 22:4	10.1	LPE 18:1 (d7)

	PE 16:0-18:1	3.9	
	PE 16:0-20:4	5.4	
	PE 18:0-20:4	6.7	PE 15:0-18:1 (d7)
	PS 18:0-18:1	4.8	
	PS 18:0-20:4	6.1	
	PS 18:0-22:6	9.3	PS 15:0-18:1 (d7)
	12-HETE	10.2	
	TXB2	12.8	
	12-HHT	11.3	LPE 18:1 (d7)

The evaluated response was peak area ratio to corresponding IS normalized by the highest value among the four extraction methods (corresponding to relative extraction efficiency). It can be observed from Fig. S4 that the normalized response was not significantly different from distinct cell disruption methods. For lipid class MG, it seemed that the sonication method showed the worst extraction effectivity while for LPE, CE, Cer and SM, this method yielded, however, a better result compared to the other three methods. For fatty acids and oxylipins, similar findings were observed.

For general lipids extraction from platelets with different cell disruption methods, an important aspect is to keep the resting state of platelets during the whole extraction process. In order to confirm that the investigated cell disruption methods will not activate the platelets during the extraction process, the fatty acid and oxylipin profiles extracted from different methods are presented in Fig. S5a with percentage content for each cell disruption method. Major fatty acid such as stearic acid (39.3%), palmitic acid (24.4%) and myristic acid (17.3%) were detected in platelets with all methods. Different cell disruption methods showed only minor variations for fatty acid contents. For monosaturated fatty acids (MUFAs), FA 18:1 (7-10%) was the most abundant while for polyunsaturated fatty acids (PUFAs) FA 20:4 (0.5-0.8%) yielded relatively high content (Fig. S5 b-d). Total saturated, monounsaturated and polyunsaturated fatty acid contents were 83.8-88.5%, 8.9-12.4% and 2.5-3.7% (Fig. S5e), respectively.

Furthermore, the oxylipins extracted from platelets with different methods were also analysed in order to investigate whether there was an unexpected increase of oxylipins among these four cell disruption methods indicating an activation of platelets. Three oxylipins as oxidative products of arachidonic acid including TXB2, 12-HETE and 12-HHT (Fig. S5f) were detected with similar amounts for all the four methods and the concentration is in a typical basal level of resting platelets compared to previous study [5]. What's more, there was no significant decrease on deuterated PUFAs (Fig. S5g) and no corresponding deuterated oxylipins were generated with the four cell disruption methods, which may be an evidence that with all these methods, platelets were not activated during the extraction since once the platelets are activated, the PUFAs can be oxidized to oxylipins in a certain amount.

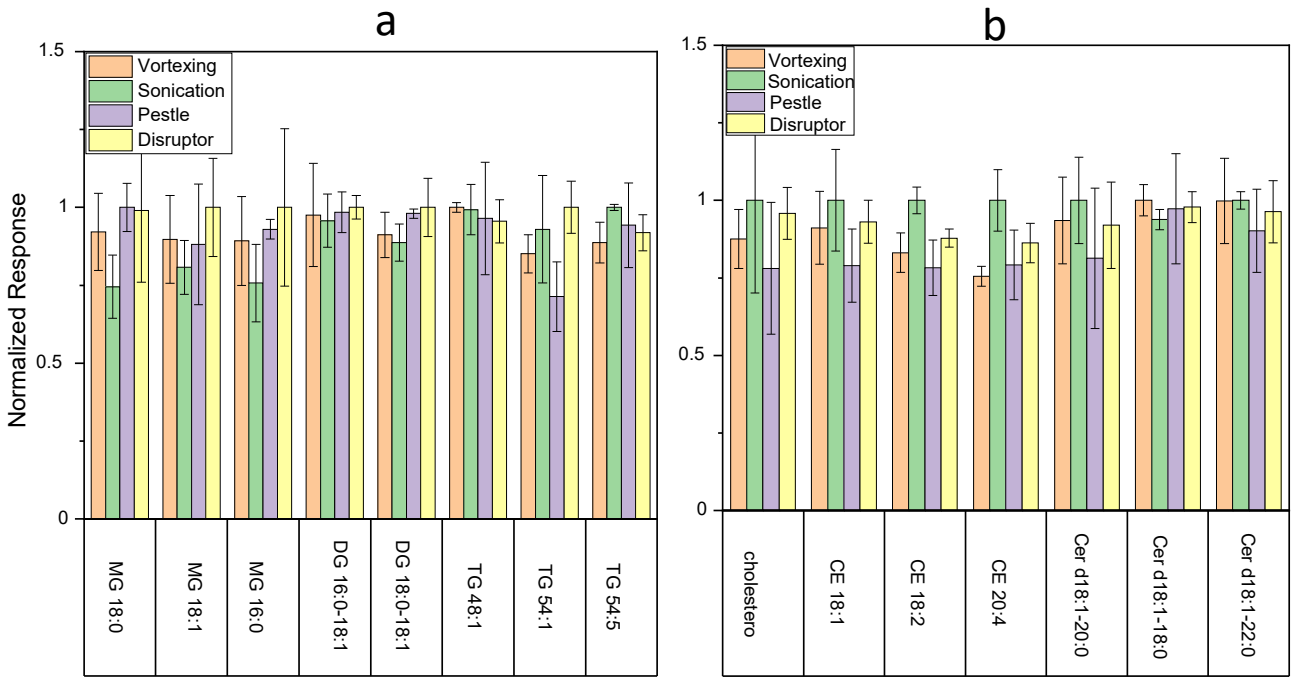

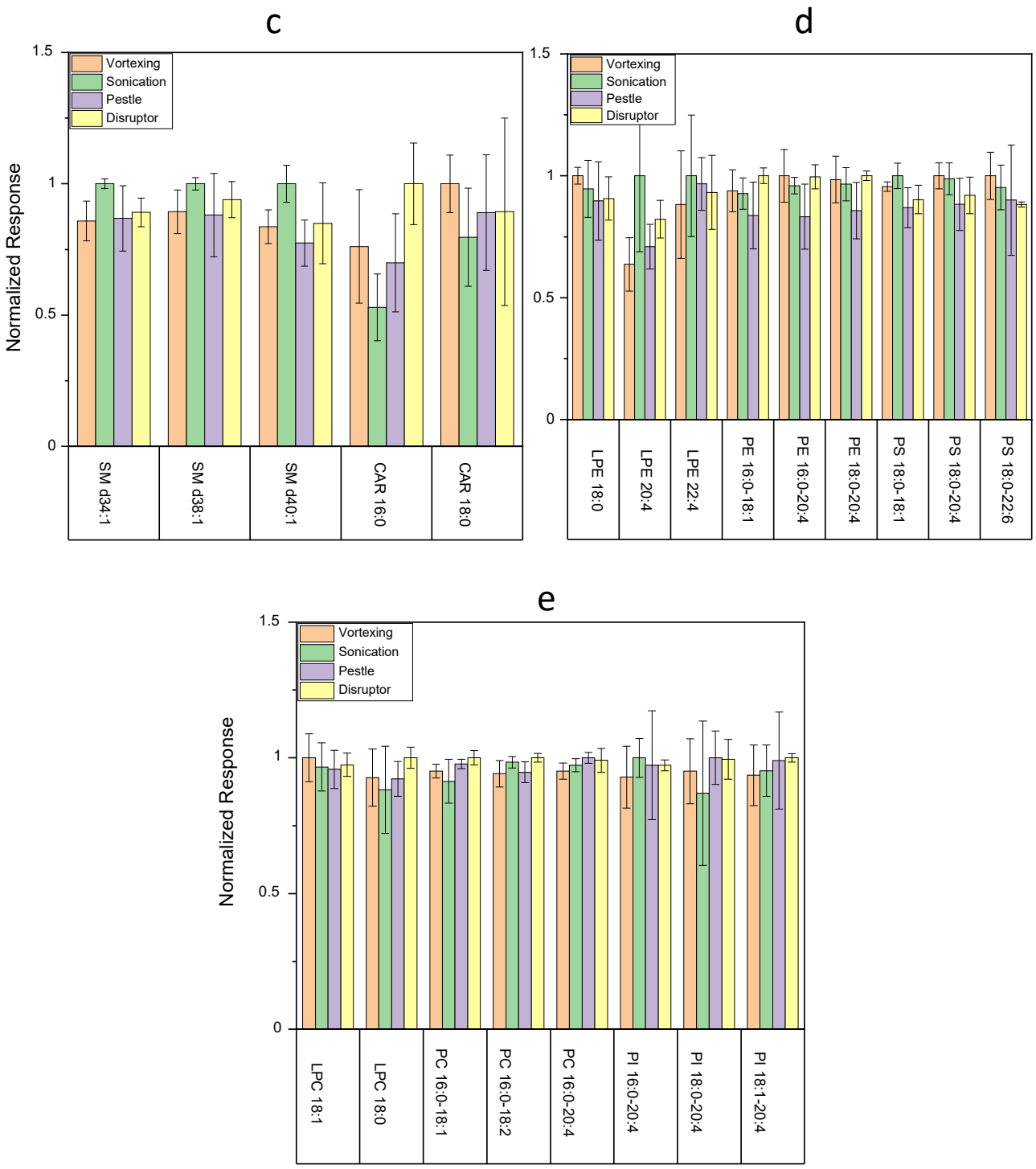

Fig. S4. *Comparison of endogenous lipids in platelets extracted by different cell disruption methods based on 90% IPA solvent. The intensity (peak area ratio to IS) of each lipid was normalized by the maximum peak area ratio of the lipid among four cell disruption methods. (a) lipid classes MG, DG and TG. (b) lipid classes CE, Cer and* cholesterol. (c) lipid classes SM and Acar. (d) lipid classes LPE, PE and PS. (e) lipid classes LPC, PC and PI.

a

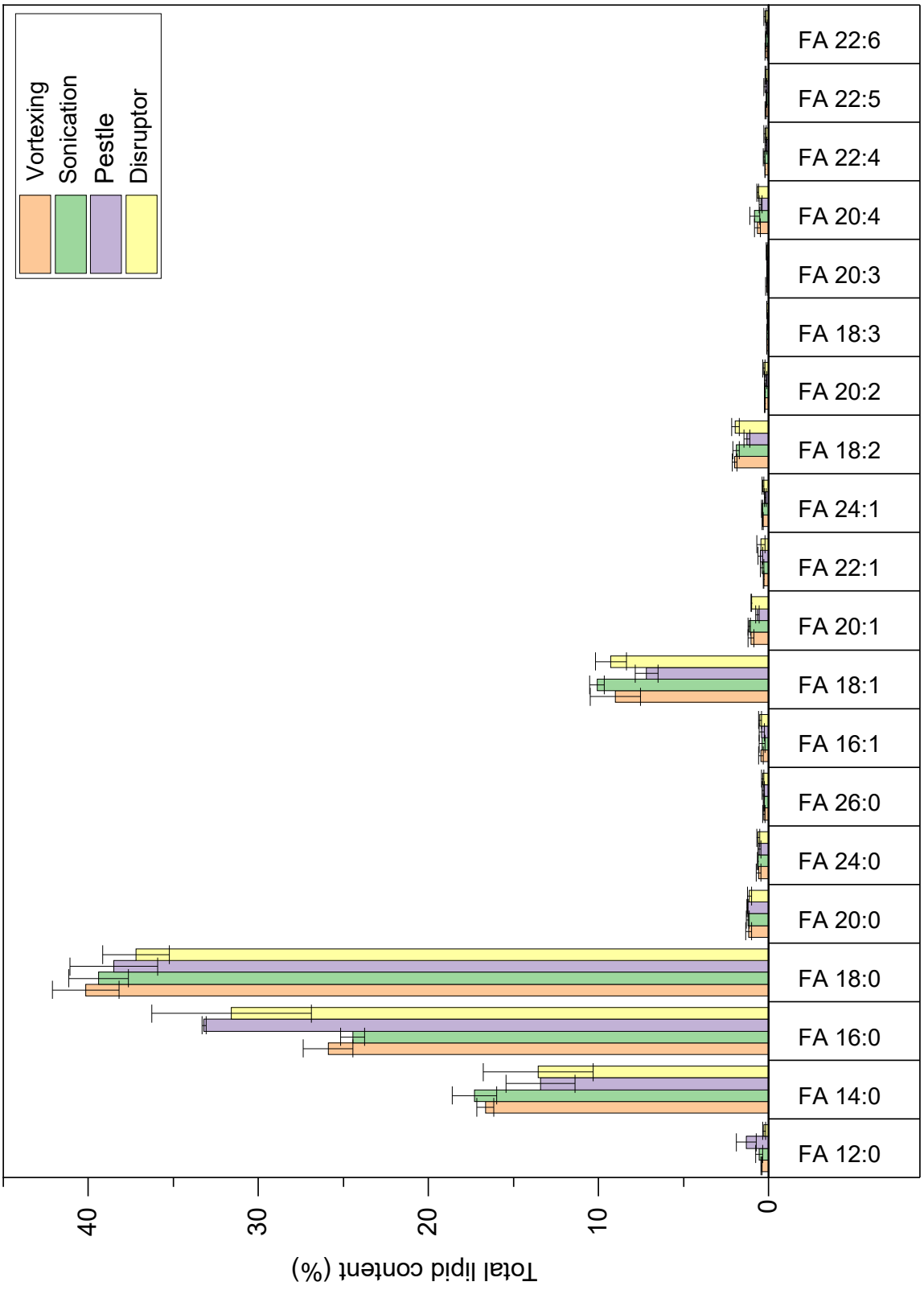
Vortexing
Sonication
Pestle
Disruptor
FA 22:6
FA 22:5
FA 22:4
FA 20:4
FA 20:3
FA 18:3
FA 20:2
FA 18:2
FA 24:1
FA 22:1
FA 20:1
FA 18:1
FA 16:1
FA 26:0
FA 24:0
FA 20:0
FA 18:0
FA 16:0
FA 14:0
FA 12:0
0
10
20
30
40
Total lipid content (%)

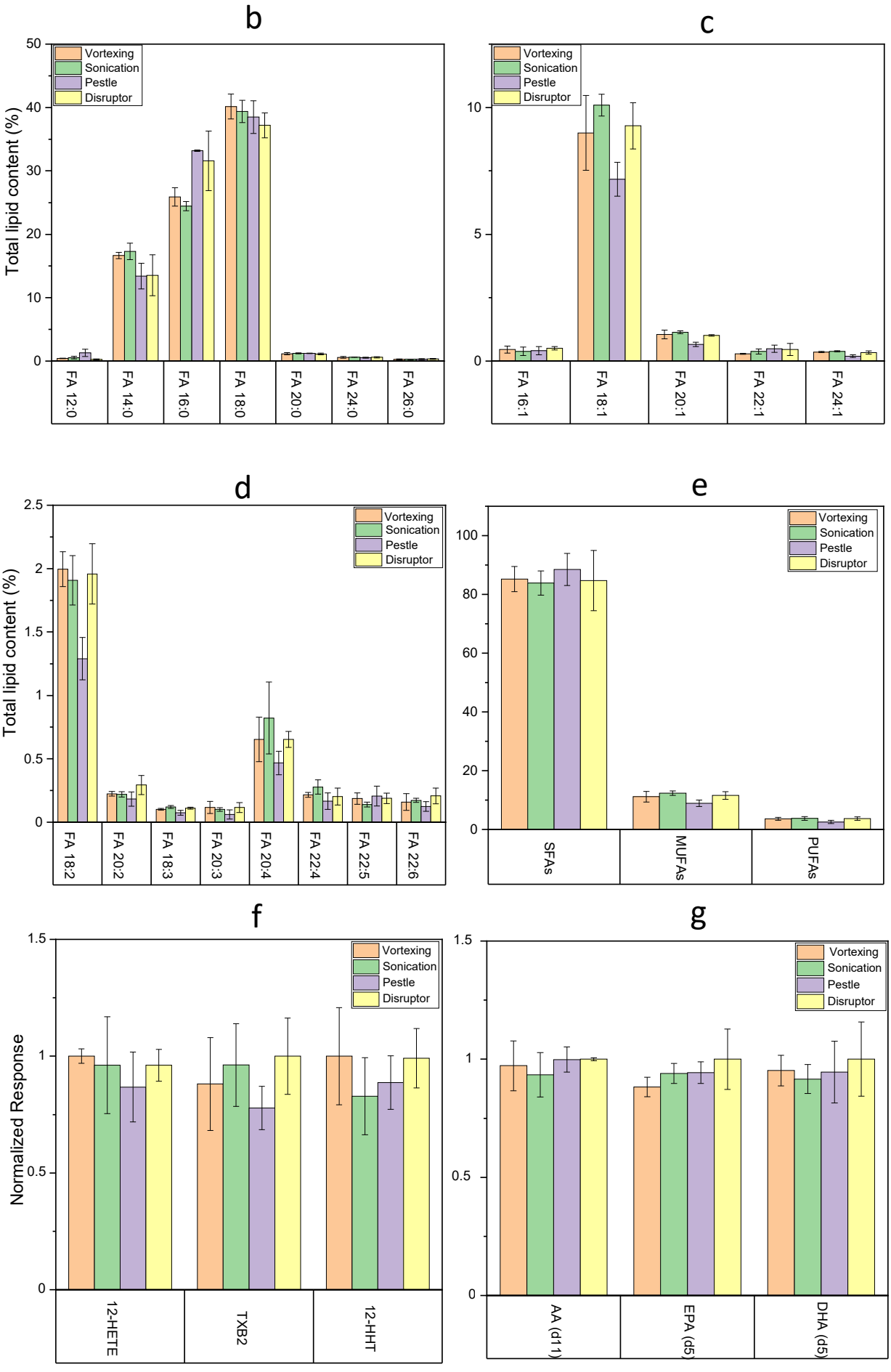
b
Total lipid content (%)
Vortexing
Sonication
Pestle
Disruptor
FA 12:0
FA 14:0
FA 16:0
FA 18:0
FA 20:0
FA 24:0
FA 26:0
c
FA 16:1
FA 18:1
FA 20:1
FA 22:1
FA 24:1
d
FA 18:2
FA 20:2
FA 18:3
FA 20:3
FA 20:4
FA 22:4
FA 22:5
FA 22:6
e
SFAs
MUFAs
PUFAs
f
Normalized Response
12-HETE
TXB2
12-HHT
g
AA (d11)
EPA (d5)
DHA (d5)

Fig. S5. *Effects of different cell disruption methods on fatty acids profile. (a) general profiles; (b) profiles in SFAs; (c) profiles in MUFAs; (d) profiles in PUFAs; (e) profiles in sum amount as SFAs, MUFAs and PUFAs. (f) Normalized response of oxylipins and (g) deuterated PUFAs.*

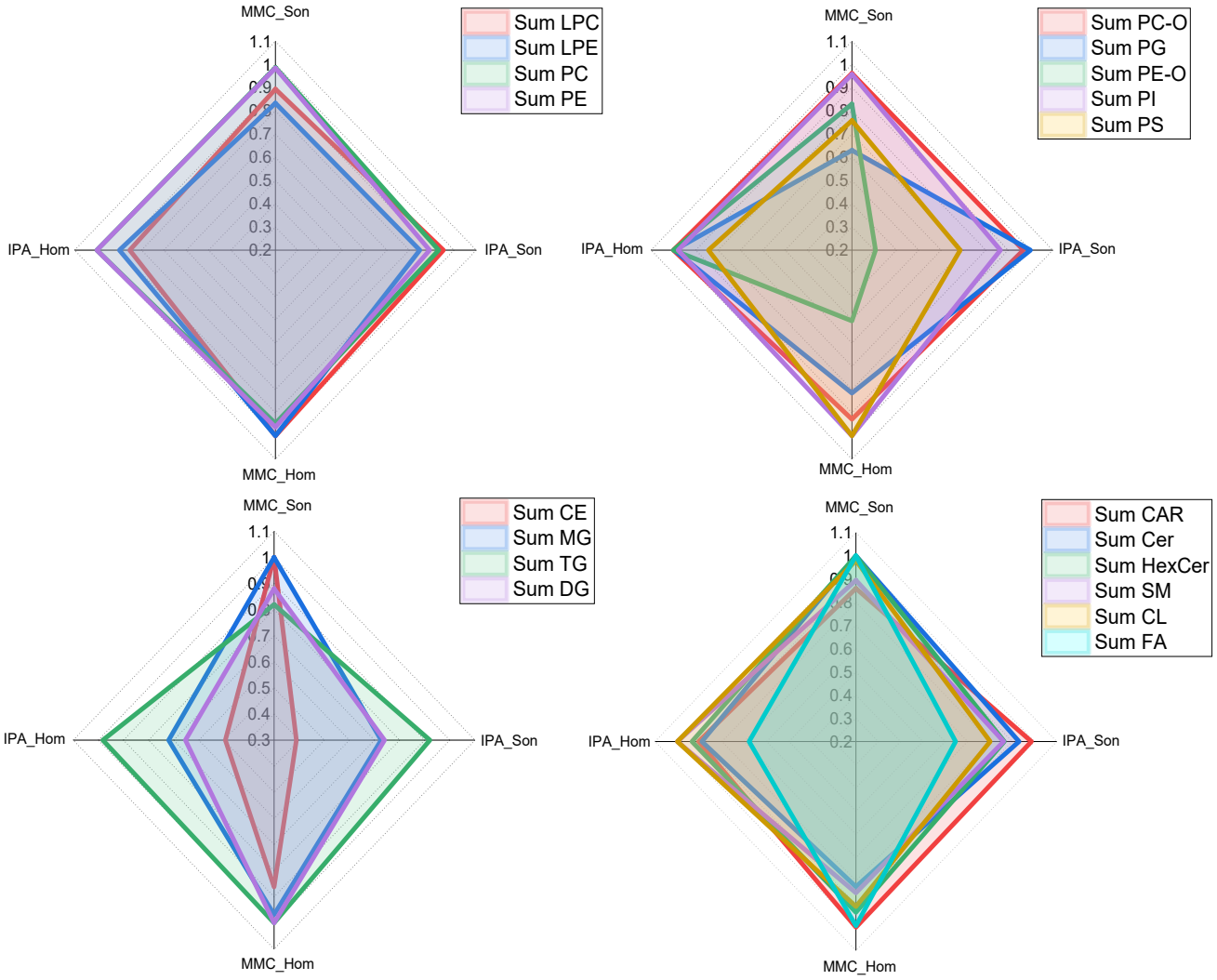

Fig. S6. *Radar diagrams of sum of normalized response (peak height) from each lipid class extracted from different protocols IPA_Hom, MMC_Hom, MMC_Son and IPA_Son. The intensity was scaled to 0-1 by the maximum response of the lipid among different extraction protocols (Hom, homogenizer; Son, multiple cycles of sonication with sonicator bath).*

5.2 Large-scale sampling-endogenous lipids

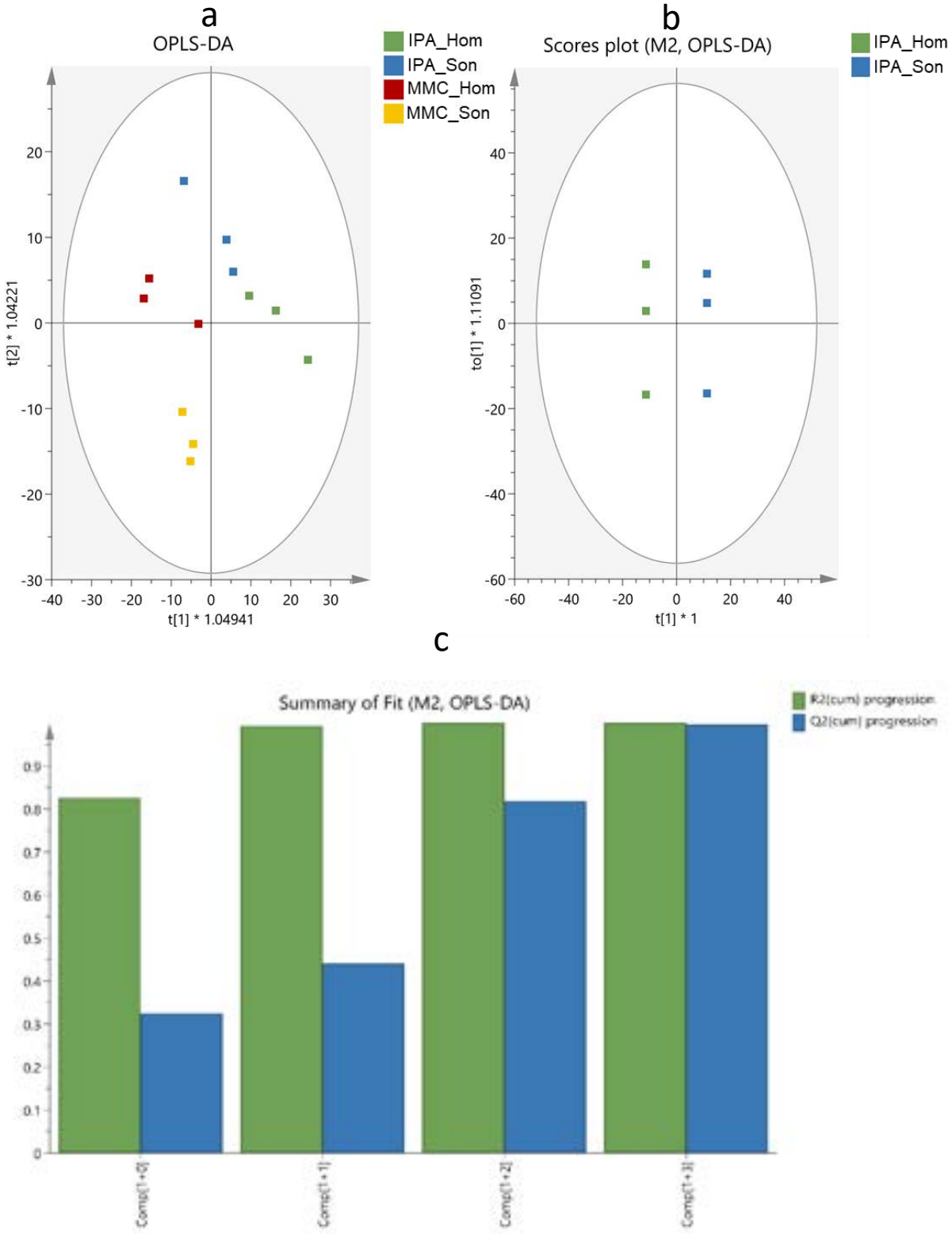

Fig. S7. *Scores plot of OPLS-DA for (a) all four protocols and (b) the sonication protocol (IPA_Son) and the homogenizer method (IPA_Hom); (c) Summary of Fit based on the OPLS-DA plot (b). SIMCA parameters: Model=M2; N=6; R2X=0.845; R2Y=1; Q2=0.996.*

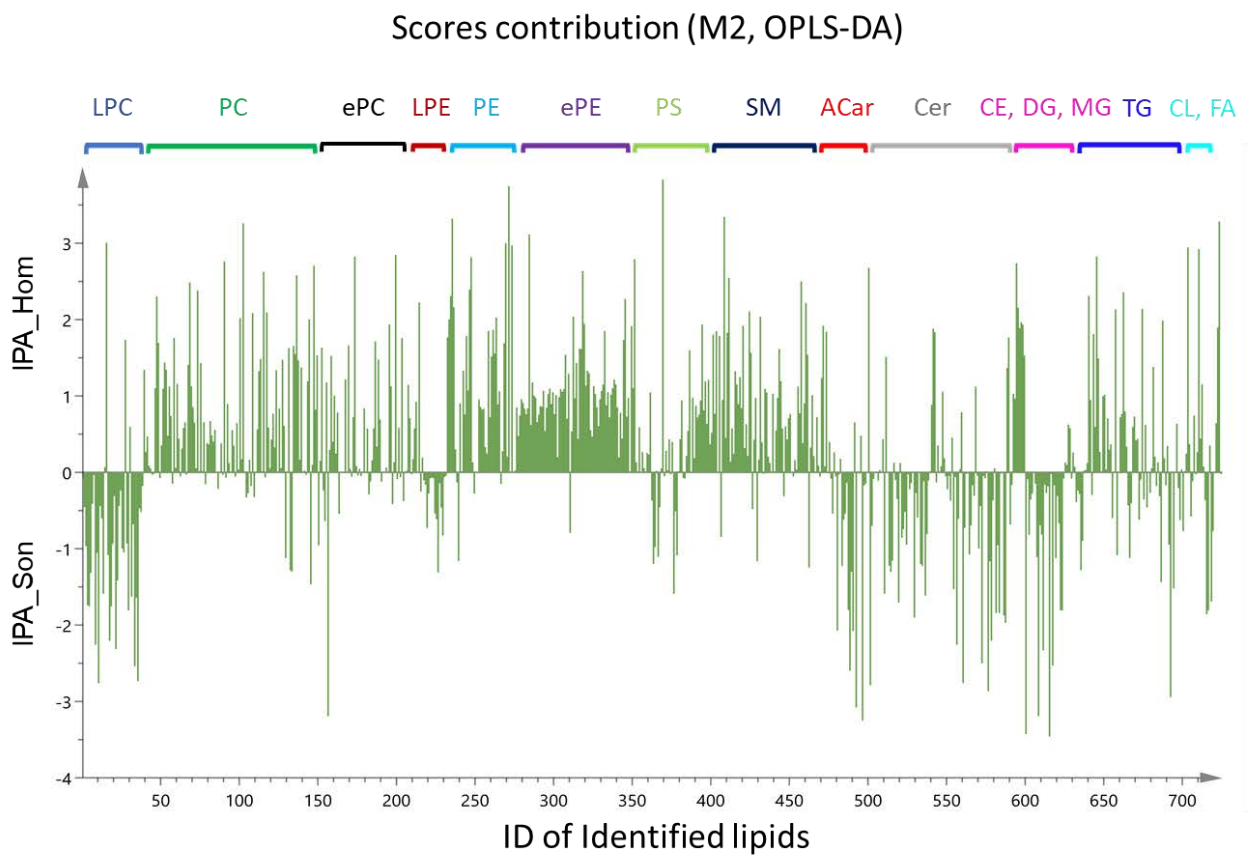

Fig. S8. Score contribution plot based on the *scores plot of OPLS-DA for the sonication protocol (IPA_Son) and the homogenizer method (IPA_Hom); SIMCA parameters: Model=M2; N=6; R2X=0.845; R2Y=1; Q2=0.996. A contribution plot highlights which variables participate in an observed deviation or differences among observations. The green line represents each lipid, when the value is positive, it means the normalized response with IPA_Hom is higher than that with IPA_Son. In the contrast, when the lipid orients to the IPA_Son (minus value) side, it means the normalized response with IPA_Son is higher than that with IPA_Hom.*

6. Comparison of different reconstitution solvents

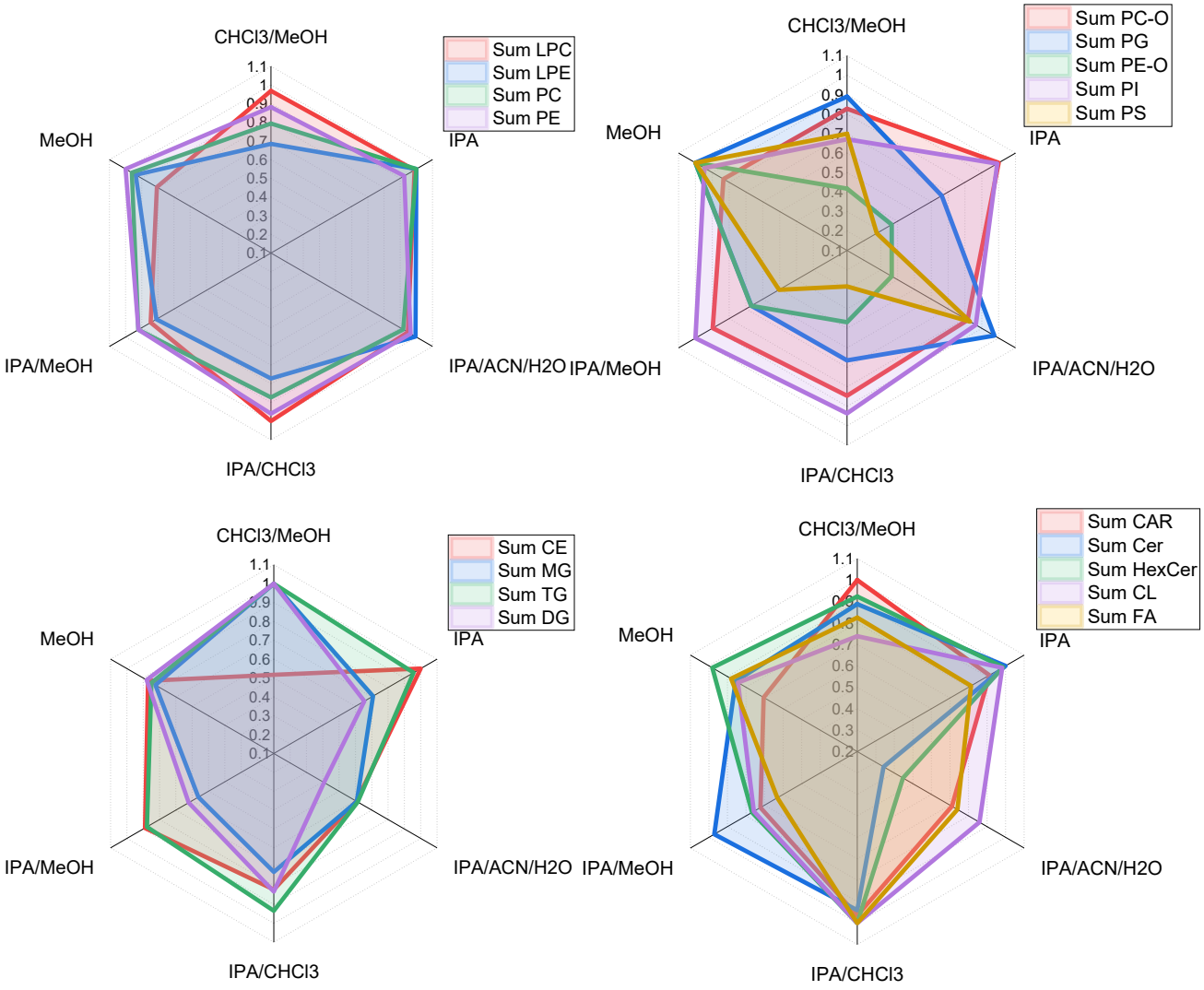

Fig. S9. *Radar diagrams of sum of normalized response (peak height) from each lipid class by different reconstitute solvents based on extraction solvent IPA. The intensity was scaled to 0-1 for each lipid class by the maximum response of the sum lipid among different extraction protocols.*

7. Final optimization for extraction protocols

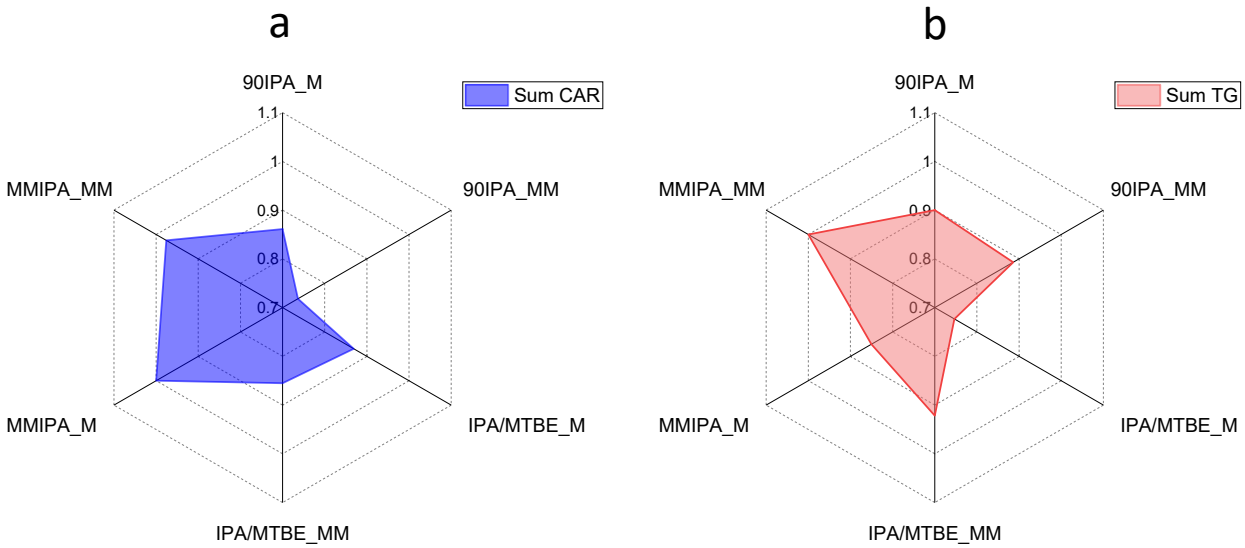

Fig. S10. *Radar diagrams of sum of normalized response (peak height) from (a)CAR and (b)TG by different extraction protocols. The intensity was scaled to 0-1 for each lipid class by the maximum response of the sum lipid among different extraction protocols.*

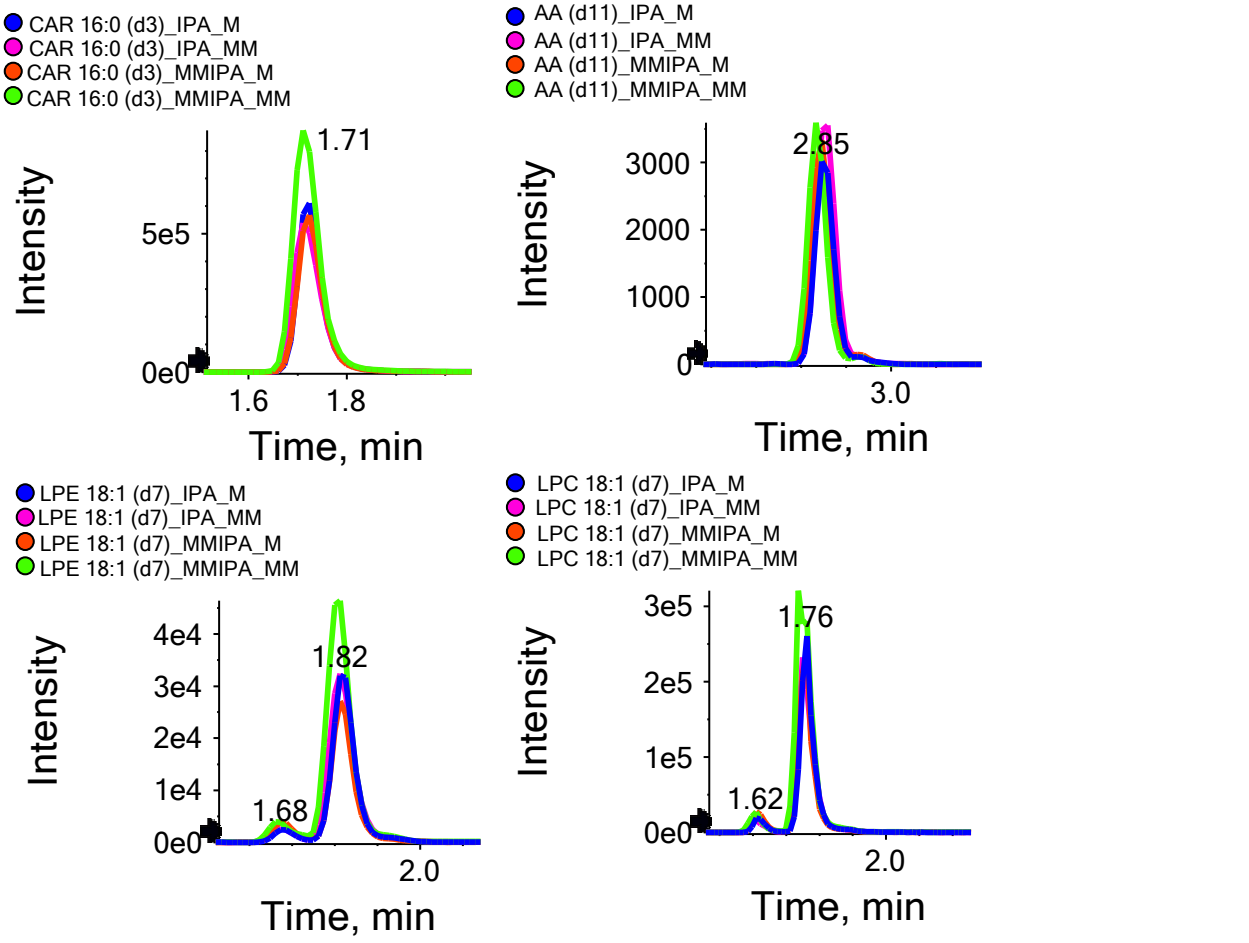

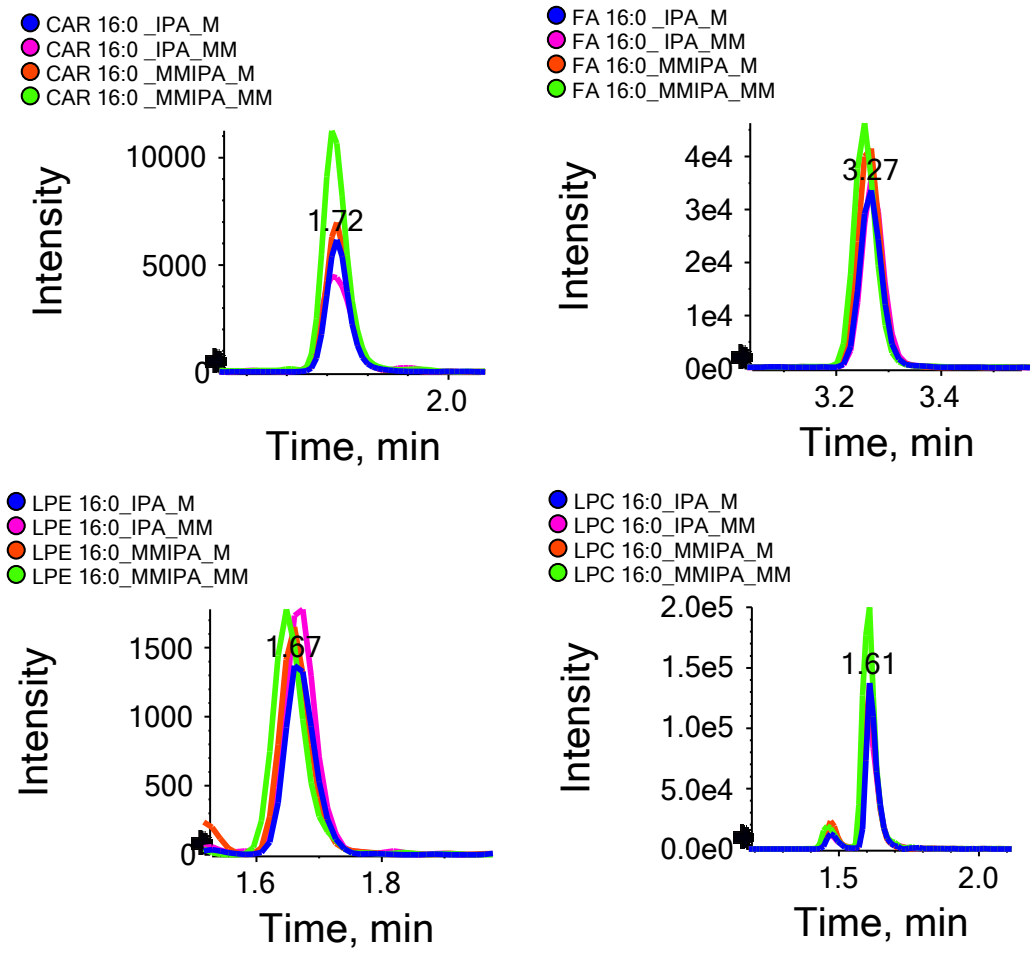

Fig. S11. *Effect of reconstitution solvents M and MM on peak shapes. XICs of early eluted peaks including spiked IS and extracted endogenous lipids with different extraction protocols are shown.*

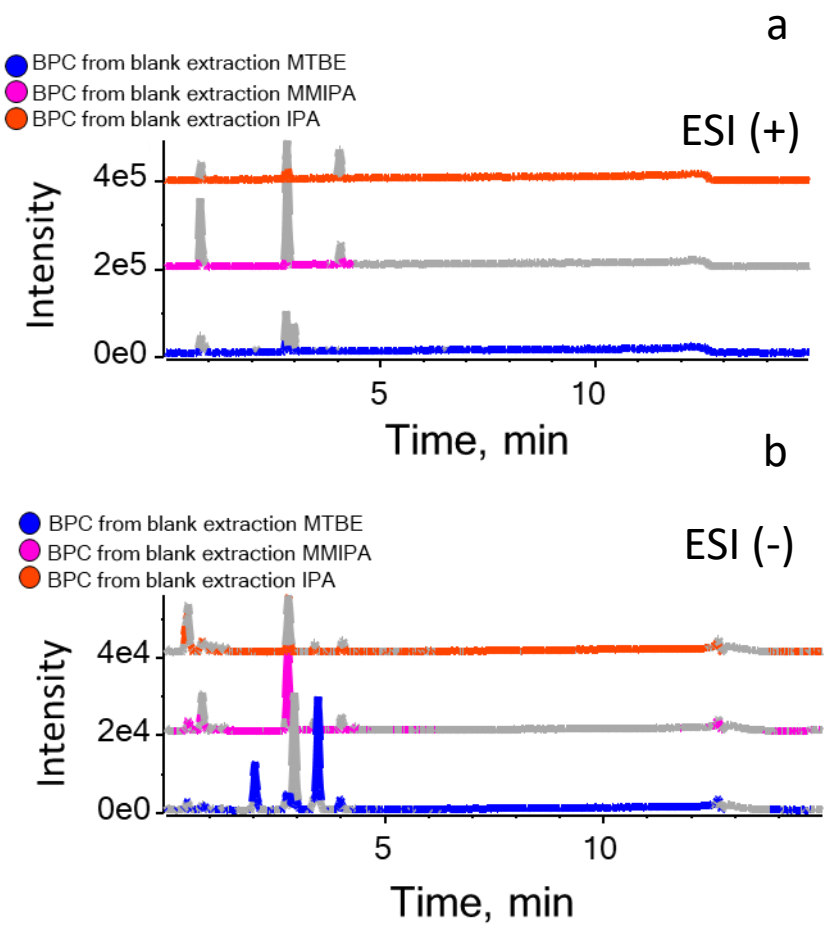

Fig. S12. *BPCs (base peak chromatograms) of blank extraction (spiked with IS) with MTBE, IPA and final optimized MMIPA_MM in (a) ESI (+) and (b) ESI (-) ion mode.*

Reference

[1] C. Calderón, C. Sanwald, J. Schlotterbeck, B. Drotleff, M. Lämmerhofer, Comparison of simple monophasic versus classical biphasic extraction protocols for comprehensive UHPLC-MS/MS lipidomic analysis of Hela cells, Anal Chim Acta, 1048 (2019) 66-74.
[2] H. Tsugawa, T. Cajka, T. Kind, Y. Ma, B. Higgins, K. Ikeda, M. Kanazawa, J. VanderGheynst, O. Fiehn, M. Arita, MS-DIAL: data-independent MS/MS deconvolution for comprehensive metabolome analysis, Nat Methods, 12 (2015) 523-526.
[3] M. Cebo, C. Calderón Castro, J. Schlotterbeck, M. Gawaz, M. Chatterjee, M. Lämmerhofer, Untargeted UHPLC-ESI-QTOF-MS/MS analysis with targeted feature extraction at precursor and fragment level for profiling of the platelet lipidome with ex vivo thrombin-activation, Journal of Pharmaceutical and Biomedical Analysis, 205 (2021) 114301.
[4] M. Cebo, J. Schlotterbeck, M. Gawaz, M. Chatterjee, M. Lämmerhofer, Simultaneous targeted and untargeted UHPLC-ESI-MS/MS method with data-independent acquisition for quantification and profiling of (oxidized) fatty acids released upon platelet activation by thrombin, Analytica Chimica Acta, 1094 (2020) 57-69.
[5] M. Cebo, K. Dittrich, X. Fu, M.C. Manke, F. Emschermann, J. Rheinlaender, H. von Eysmondt, N. Ferreirós, J. Sudman, A. Witte, L. Pelzl, O. Borst, T. Geisler, D. Rath, T. Bakchoul, M. Gawaz, T.E. Schäffer, M. Lämmerhofer, M. Chatterjee, Platelet ACKR3/CXCR7 favors antiplatelet lipids over an atherothrombotic lipidome and regulates thromboinflammation, Blood, 139 (2022) 1722-1742.

1.2 Publication II

UHPLC-MS/MS method for chiral separation of 3-hydroxy fatty acids on amylose-based chiral stationary phase and its application for the enantioselective analysis in plasma and platelets

Xiaoqing Fu[a], Zhanjian Xu[a], Meinrad Gawaz[b], Michael Lämmerhofer[a]*

[a] University of Tübingen, Institute of Pharmaceutical Sciences, Pharmaceutical (Bio-)Analysis, Auf der Morgenstelle 8, 72076 Tübingen, Germany

[b] Department of Cardiology and Angiology, University Hospital Tübingen, Otfried-Müller-Strasse 10, 72076 Tübingen, Germany

Reprinted with permission from Journal of Pharmaceutical and Biomedical Analysis Volume 223, 20 January 2023, 115151

https://doi.org/10.1016/j.jpba.2022.115151

Journal of Pharmaceutical and Biomedical Analysis 223 (2023) 115151

Contents lists available at ScienceDirect

Journal of Pharmaceutical and Biomedical Analysis

journal homepage: www.journals.elsevier.com/journal-of-pharmaceutical-and-biomedical-analysis

UHPLC-MS/MS method for chiral separation of 3-hydroxy fatty acids on amylose-based chiral stationary phase and its application for the enantioselective analysis in plasma and platelets

Xiaoqing Fu [a], Zhanjian Xu [a], Meinrad Gawaz [b], Michael Lämmerhofer [a,*,1]

[a] University of Tübingen, Institute of Pharmaceutical Sciences, Pharmaceutical (Bio-) Analysis, Auf der Morgenstelle 8, 72076 Tübingen, Germany
[b] Department of Cardiology and Angiology, University Hospital Tübingen, Otfried-Müller-Strasse 10, 72076 Tübingen, Germany

ARTICLE INFO

Keywords:
Targeted lipidomics
Mitochondrial fatty acid oxidation
Peroxysomal fatty acid oxidation
Enantioselective metabolomics
Enzyme steroselectivity
Coronary artery disease

ABSTRACT

3-Hydroxyfatty acids (3-OH-FAs) are formed in the hydration step during mitochondrial β-oxidation of saturated straight-chain fatty acids, which is a catabolic pathway that involves several enzymes. For an unbiased biological interpretation, an enantioselective analysis of 3-OH-FAs including their stereoisomers is necessary, which may contribute to the elucidation of enzymatic mechanisms in the biological pathways. In this work, an enantioselective gradient UHPLC-MS/MS method based on 1.6 μm particle polysaccharide column (Chiralpak IA-U) for chiral separation of 3-hydroxyfatty acids was developed which covers carbon chain length from C8 to C18 with a good resolution of *R* and *S* enantiomers. The method is fast and sensitive for detecting enantiomers of 3-OH-FAs by using a triple quadrupole instrument as a detector in a targeted, selected reaction monitoring (SRM) mode. A matrix matched-calibration strategy was applied for quantification of individual 3-OH-FA enantiomers. The method allows the simultaneous quantification of each enantiomer of 3-OH-FAs from C8-C18. One-phase liquid extraction with 2-propanol showed good extraction recoveries with over 90% on average. Further, the validated method was applied to investigate the alteration of 3-OH-FA enantiomers in platelets and plasma samples from human donors with different diagnoses of cardiovascular disease (acute coronary syndrome ACS, chronic coronary syndrome CCS). Both *R* and *S* enantiomers were detected in platelets and plasma samples with different predominance for *R* or *S* in dependence on carbon chain length, which might be associated with different functional enzymes of mitochondrial and peroxisomal β-oxidation. Finally, our study provides a new strategy for chiral separation and enantioselective analysis, showing great potential for targeted metabolomics in clinical biomarker discovery.

1. Introduction

3-Hydroxy fatty acids (3-OH-FAs) are fatty acid metabolites of significant importance in various biological systems, as metabolites of fatty acid oxidation (mostly in conjugated form such as CoA thioesters, yet partly in free form due to spontaneous hydrolysis or thioesterase activity) [1], constituents of lipid A which is part of endotoxins of Gram-negative bacterial outer membranes [2], as side chains of lipopeptides and other natural products [3,4]. 3-OH-FAs also gained significant practical relevance as diagnostic biomarkers of several metabolic diseases (e.g. long-chain 3-hydroxyacyl-CoA dehydrogenase LCHAD or medium/short-chain 3-hydroxyacyl-CoA dehydrogenase M/SCHAD deficiency [5]).

3-OH-FAs are metabolites resulting from fatty acid oxidation. There are three different fatty acid oxidation pathways, namely, the mitochondrial β-oxidation, peroxisomal β-oxidation, and microsomal ω-oxidation. Mitochondrial β-oxidation remains the predominant pathway for fatty acid degradation [6]. For substrates which cannot be oxidized by the mitochondrial metabolism pathway, e.g. very long chain fatty acids or branched chain fatty acids, or defective mitochondrial β-oxidation the other two pathways will compensate [7]. 3-OH-FAs are mainly formed in the hydration step during β-oxidation of saturated straight-chain fatty acids. With the aid of the fatty acid transport protein (FATPs), the long-chain fatty acids are able to enter the human cell

* Correspondence to: Pharmaceutical (Bio-)Analysis, Institute of Pharmaceutical Sciences University of Tuebingen, Auf der Morgenstelle 8, 72076 Tuebingen, Germany.
E-mail address: michael.laemmerhofer@uni-tuebingen.de (M. Lämmerhofer).
[1] http://www.bioanalysis.uni-tuebingen.de/

https://doi.org/10.1016/j.jpba.2022.115151
Received 1 October 2022; Received in revised form 4 November 2022; Accepted 7 November 2022
Available online 9 November 2022

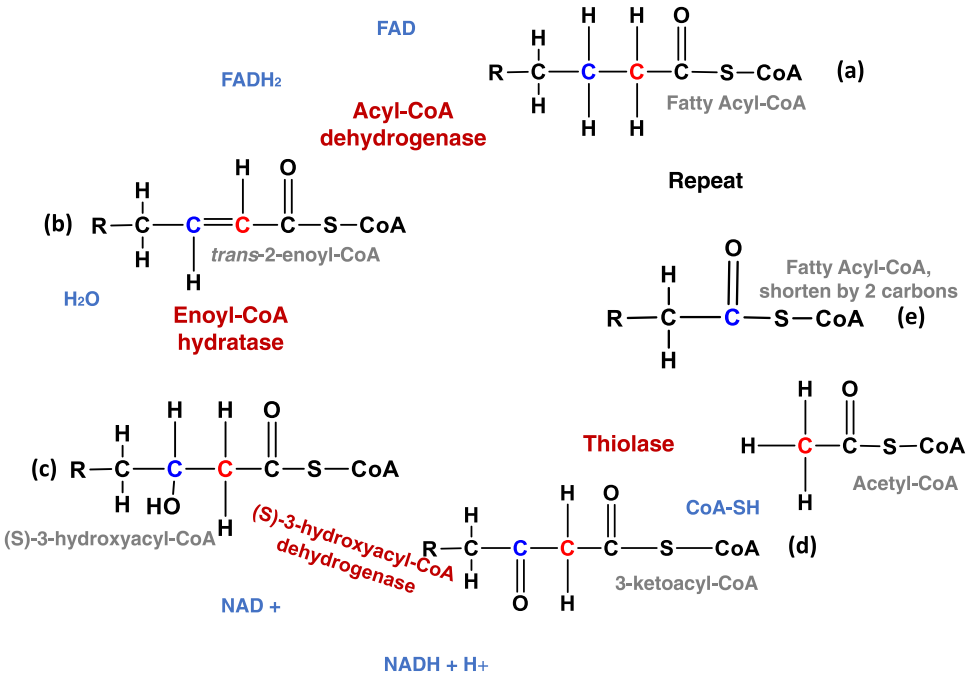

Fig. 1. Mitochondrial fatty acid oxidation (β-oxidation) cycle. The alphabet (a-e) represent the order of the cycle.

membrane and are activated to acyl-CoA. As the next step, the acyl-CoA is transported through the mitochondrial membrane into the mitochondrial matrix with aid of carnitine shuttle and ready for fatty acid β-oxidation. The complete fatty acid oxidation undergoes four repeated biochemical reactions (Fig. 1): dehydrogenation, hydration, second dehydrogenation, and thiolytic cleavage. From the perspective of acyl-CoA ester, it is firstly dehydrogenated by acyl-CoA dehydrogenase to produce *trans*-2-enoyl-CoA, resulting in the formation of a double bond in the saturated carbon chain. Then the enoyl-CoA hydratase catalyzes and hydrates the *trans*-2-enoyl-CoA into (*S*)-3-hydroxyacyl-CoA, with the addition of a hydroxyl group on the β-carbon as the second step. In the third step, the formed (*S*)-3-hydroxyacyl-CoA is catalyzed by the corresponding (*S*)-3-hydroxyacyl-CoA dehydrogenase and yields 3-ketoacyl-CoA ester. Finally, a thiolytic cleavage takes place in the 3-ketoacyl-CoA, leading to a two-carbon shortened acyl-CoA ester and an acetyl-CoA. Each cycle releases an acetyl-CoA unit from the initial acyl-CoA ester, and such cycle will repeat until the fatty acid acyl-CoA ester is decomposed into several molecules of acetyl-CoA [7,8]. From this textbook discussion, one can expect that released 3-OH-FAs are present as *S*-enantiomers in biological samples. During fasting or high energy demands FAs are the prime energy source, e.g. for liver, cardiac and skeletal muscle, platelets in the course of their activation, and fatty acid oxidation (FAO) will be enhanced. FAO disorders (FAOD) have been reported to lead to cardiomyopathies amongst others [5]. Hence, there is a specific interest in investigating this metabolic process in coronary artery disease (CAD) patients.

The comprehensive quantitative analysis of 3-OH-FAs in biological matrix including biofluids, cells and tissues is of major importance since they are involved in important biological pathways and may provide some evidence for pathophysiological states. In the past, GC-MS was the most frequently used tool for 3-OH-FA and other OH-FAs analysis [9,10]. However, GC-MS needs time-consuming derivatization during sample preparation. Eventually, LC-MS has been applied to a large extent to the 3-OH-FAs and other OH-FAs analysis with its high sensitivity and selectivity [4,11–14]. However, most of the research on 3-OH-FAs does not focus on the stereochemistry. Only a few investigations reported enantioselective analysis [3,4,15]. Enantioselective metabolomics as a well-defined research field is starting to draw attention in recent years [16–18]. Since the mitochondrial β-oxidation is associated with different functional enzymes, for an unbiased biological interpretation, an enantioselective analysis of 3-OH-FAs including their stereoisomers is necessary, which may contribute due to the information about enantiomeric composition of 3-OH-FAs and stereoselectivity of enzymatic reactions to a better understanding of the biological pathways. The chiral separation of 3-OH-FAs can be achieved by chiral stationary phases (CSP). Chromatographic separations with polysaccharide-based CSPs are nowadays widely used for enantiomer separation of oxygenated fatty acids [4,16,19] and the cellulose and amylose derivatives are the most common stationary phases. So far, a successful direct enantioseparation for underivatized 3-OH-FAs employing the polysaccharide phases was reported [4] covering carbon chain length C6-C14, which was applied for the identification of the enantiomers of 3-OH-FAs originating from a novel lipopeptide with unknown structure. However, the enantioselective analysis of 3-OH-FAs in plasma or platelets in human from sample preparation to LC-MS method was not reported yet.

Herein, we report an enantioselective UHPLC method based on the application of Chiralpak IA-U (amylose tris(3,5-dimethylphenylcarbamate) based polysaccharide chiral stationary phase immobilized on 1.6 μm silica particles) coupled with a triple quadruple mass spectrometer for 3-OH-FAs. We were able to successfully separate the enantiomers of 3-OH-FAs from C8-C18. Longer 3-OH-FAs were not detected in plasma nor platelets, shorter ones not sufficiently retained. This method was validated and optimized in terms of sample preparation and LC-MS conditions and was applied successfully to the analysis of 3-OH-FAs in plasma and platelet samples of patients suffering from CAD. Assignment of configurations of the 3-OH-FAs in plasma and platelets were for the first time realized. The stereoselective analysis of these important biomarkers of metabolic disease might be more meaningful than the achiral analysis being currently state-of-the-art in clinical analysis, because the 3-OH-FAs may result from a few distinct metabolic processes of opposite stereochemical preferences.

2. Materials and methods

2.1. Materials

The standards 3-hydroxybutyric acid (3-OH-FA (4:0)) sodium salt,

(±)-3-hydroxyhexanoic acid (3-OH-FA (6:0)), (±)-3-hydroxyoctanoic acid (3-OH-FA (8:0)), (±)-3-hydroxydecanoic acid (3-OH-FA (10:0)), (±)-3-hydroxydodecanoic acid (3-OH-FA (12:0)), and (*R*)-3-hydroxymyristic acid (3-OH-FA (14:0)) were obtained from Sigma Aldrich (Merck, Taufkirchen, Germany). The standards (±)-3-hydroxypalmitic acid (3-OH-FA (16:0)), (±)-3-hydroxystearic acid (3-OH-FA (18:0)) and the internal standards (12-hydroxy-5Z,8Z,10E,14Z-eicosatetraenoic acid-d8, 12-HETE-d8 and Resolvin D1-d5, RvD1-d5) were purchased from Cayman Chemical (Ann Arbor, MI, USA). The internal standard (arachidonic acid, AA-d11) was purchased from Avanti Polar Lipids (Alabaster, AL, USA). LC-MS grade acetonitrile (ACN), methanol (MeOH), and isopropanol (IPA) were purchased from Carl Roth (Karlsruhe, Germany). Acetic acid (HAc) was purchased from Sigma-Aldrich. Water purification was achieved by a Purelab Ultra purification system from Elga LabWater (Celle, Germany).

2.2. Sample preparation

2.2.1. Collection of plasma and platelet samples

Plasma and platelet samples were collected from the peripheral blood of donors at the Dept. of Cardiology and Angiology, University Hospital Tübingen, according to ethical guidelines of the Declaration of Helsinki. The study was approved by the local ethics committee (237/2018B02) and all patients gave written informed consent.

2.2.2. Lipid extraction from platelets

Platelets were isolated from blood of donors, as described previously [20–22]. Platelet pellets with count 2×10^8 were taken out from the − 80 °C freezer and slowly thawed on ice for about 2 h until they were completely unfrozen. Then, 10 µL of internal standard (IS) mixture (AA-d11, RvD1-d5 and 12-HETE-d8, 500 ng/mL for each with a final concentration of 50 ng/mL in reconstitution solvent) was added to platelet pellets followed by incubation (around 20 min). Afterwards, 5 mL of a cooled IPA/H_2O (9:1; v/v, 4 °C) extraction solvent mixture was added. Then, samples were vortexed for 10 s and incubated on a thermo shaker (4 °C, 500 rpm) for 1 h with 2 min sonication every 12 min during the incubation which means a total of 5 cycles sonication (each cycle 2 min). Afterwards, the samples were centrifuged (3500 x g, 10 min) and the supernatants were dried with an EZ2 evaporator from GeneVac (Ipswich, UK) under nitrogen protection. In the last step, dried extracts were reconstituted in 100 µL of MeOH, vortexed (10 s), sonicated (2 min), centrifuged (3500 x g, 10 min) and transferred into HPLC vials.

2.2.3. Lipid extraction from plasma

EDTA plasma of donors kept at − 80 °C until extraction were taken out from the freezer and slowly thawed on ice for about 3 h until the plasma was completely unfrozen. Then, 10 µL internal standard (IS) mixture (AA-d11, RvD1-d5 and 12-HETE-d8, 500 ng/mL for each with a final concentration of 50 ng/mL in reconstitution solvent) was added to each plasma aliquot (100 µL) followed by incubation. Subsequently, 1 mL of cooled IPA (4 °C) was added for protein precipitation and lipid extraction. Samples were vortexed (10 s), sonicated (2 min) and incubated on ice for 1 h (4 °C). Afterwards, the samples were centrifuged (16,000 x g, 4 °C, 10 min) and the supernatants were transferred to fresh falcon tubes. The supernatant was then dried with an EZ2 evaporator from GeneVac under nitrogen protection. The residues were dissolved in 100 µL of MeOH, vortexed (10 s), sonicated (2 min), centrifuged (16,000 x g, 10 min) the resultant lipid extracts were transferred into HPLC vials and stored at − 20 °C until analysis.

2.3. UHPLC-MS/MS method

The measurement was performed on a high-performance liquid chromatography system Agilent 1290 Infinity (Agilent Technologies, Waldbronn, Germany) comprised of a binary pump, degasser, and column oven, coupled with a CTC PAL autosampler (CTC Analytics AG, Switzerland).

As chromatographic column, Chiralpak IA-U (Daicel, supplied by Chiral Technologies Europe, Illkirch, France) with the dimension of 3.0 mm × 100 mm and particle size of 1.6 µm was used for chromatographic separation. The flow rate was 300 µL/min for all measurements, the column temperature was 40 °C, and the injection volume was 10 µL.

The mobile phase A1 was water containing 0.1% (v/v) acetic acid and the mobile phase B1 was acetonitrile containing 0.1% (v/v) acetic acid. Another mobile phase B2 was obtained by mixing acetonitrile and isopropanol (2:8, v/v), containing 0.1% (v/v) formic acid and used for a column wash step (see suppl. material).

The gradient method was started with 10% mobile phase B1 and the percentage of B1 was raised to 100% in 20 min, followed by a hold at 100% for the next 2 min, then the percentage of B1 was decreased to 10% again from 22.1 to 25 min. A wash step method started with 10% B2 and the % B2 was increased to 100% in 5 min followed by 20 min hold at 100% B2. The wash step was incorporated in the analytical batch after every 6th sample injection.

MS analysis was performed with ESI in negative mode with a triple quadruple mass spectrometry instrument API 4000 (AB Sciex, Concord, Ontario, Canada). The source voltage was − 4000 V and the source temperature was 400 °C. Nebulizer gas, heater gas and curtain gas pressures were set to 30 psi, 30 psi and 35 psi, respectively. Multiple reaction monitoring (MRM) was chosen as the scan mode. The optimized MRM transitions and parameters including dwell time, declustering potential (DP), collision energy (CE) and cell exit potential (CXP) are shown in Table. S1.

2.4. Validation of method for plasma

Method validation was performed largely following the U.S. Food and Drug Administration (FDA) guideline (Bioanalytical Method Validation Guidance for Industry). The concentration-response relationship was studied in matched matrix, limit of detection (LOD, S/N = 3) and limit of quantification (LOQ, S/N = 10), precision and accuracy of quality control samples (QCs) on three levels (QC low (0.05 ng/mL), QC mid (5 ng/mL) and QC high (50 ng/mL) for each enantiomer of 3-OH-FAs except for *R*-3-OH-FA (14:0) with QC low (0.1 ng/mL), QC mid (10 ng/mL) and QC high (100 ng/mL)) as well as their matrix effect and extraction recovery on three different days were investigated.

2.4.1. Concentration-response relationship

The goodness of fit of the concentration-response relationship, both in standard solvent and in matrix, was characterized as coefficient of determination (R^2) for the linear range of the calibration function. Stock solutions of racemic standard mixtures of (*R*+*S*)-3-OH-FA (8:0), (*R*+*S*)-3-OH-FA (10:0), (*R*+*S*)-3-OH-FA (12:0), (*R*)-3-OH-FA (14:0), (*R*+*S*)-3-OH-FA (16:0) and (*R*+*S*)-3-OH-FA (18:0) with 1000 ng/mL were prepared in MeOH and diluted with MeOH. A wide range of 9 neat calibrants from 0.1 ng/mL to 1000 ng/mL (0.1, 0.5, 1, 10, 50, 100, 250, 500, 1000 ng/mL, referring to the total concentration of the sum of *R* and *S* enantiomers except for 3-OH-FA (14:0) for which only the *R* enantiomer was available) were prepared. The QC plasma pool was divided into 10 aliquots and 9 of them were spiked with standards at different levels to prepare matrix-matched calibrants for external calibration. One aliquot was analyzed directly as blank matrix without spiking standards to determine the endogenous concentrations of the target analytes.

2.4.2. Validation of matrix effect, extraction recovery, and process efficiency

Three series of standard solution were used to calculate the matrix effect (ME %), extraction recovery (RE %), and process efficiency (PE %) following the protocol suggested in ref. [23]. Three levels of concentration of the target analytes were chosen as low, mid, and high spiking

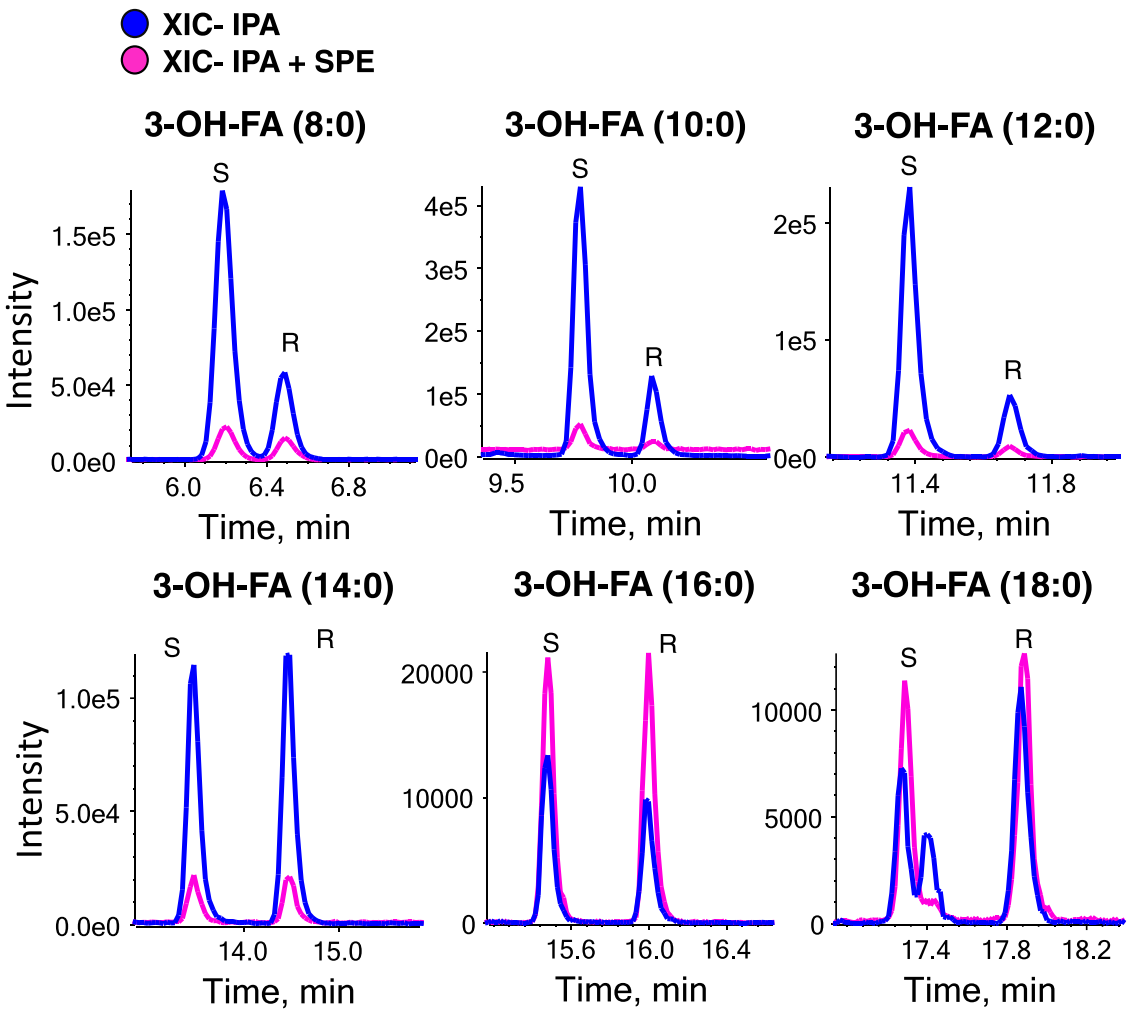

Fig. 2. Comparison of the extracted ion chromatograms (EICs) of 3-OH-FAs from C8-C18 extracted by IPA or IPA with subsequent SPE as sample preparation protocols using pooled plasma samples. Blue trace refers to extraction by IPA while pink trace to IPA+SPE.

levels (0.05, 5 and 50 ng/mL).

Series 1 (neat solution). The three levels of concentration were obtained by the dilution of the calibrant stock solution. Each level was prepared with three replicates, and the replicates were transferred into autosampler vials and were injected directly into the LC-MS/MS system.

Series 2 (post-spiked). Twelve (12) plasma aliquots with a volume of 100 μL were extracted with 1 mL cooled IPA and spiked with 100 μL MeOH instead of standards. Then the samples were incubated on ice for 1 h for protein precipitation. After centrifugation for 10 min, the supernatant was then transferred into fresh vials for evaporation. After evaporation, the extracts were reconstituted in the above three levels of neat standard solutions, respectively. Three (3) of the 12 extracts were reconstituted with 100 μL IS solution only, and used for determination of endogenous concentrations of 3-OH-FAs. In series 2, the analytes were spiked after the extraction process into plasma extracts and this series is also termed herein as post-extraction spiked.

Series 3 (pre-spiked). Twelve (12) plasma aliquots with a volume of 100 μL were prepared. Three aliquots of each of above specified three concentration levels were prepared by adding 100 μL of respective neat standard solution and each was filled up with 1 mL cooled IPA for protein precipitation and extraction. Instead of adding neat standard solutions, to 3 of the 12 aliquots 100 μL IS solution were added and used for determination of endogenous concentrations. The extraction procedure was exactly the same as described in series 2. After evaporation, the extracts were reconstituted with 100 μL MeOH. In series 3, the analytes were spiked before the extraction into plasma and this series is denoted as pre-extraction spiked.

2.4.3. *Validation of intra-batch and inter-day precision and accuracy*

Independent quality controls (QCs) were prepared in plasma at three different levels, QC low = 0.05 ng/mL, QC mid = 5 ng/mL, and QC high = 50 ng/mL for each enantiomer of 3-OH-FAs (for 3-OH-FA (14:0) only *R* is available with QC low = 0.1 ng/mL, QC mid = 10 ng/mL, and QC high = 100 ng/mL). They were used to validate precision and accuracy for each QC level on three different days, considering the endogenous concentrations of the target analytes.

2.5. *Data analysis*

Data analysis was performed with MultiQuant 3.0 (Sciex) for peak finding and integration, as well as calculation of the calibration function and in-batch precision and accuracy determination.

Further calculations were done with Excel 2010 (Microsoft, Redmond, WA, USA) and R (version 4.0.2, R-project for statistical computing). Statistical analysis and generation of plots were performed by R, Origin (Origin 2020) and MetaboAnalyst (5.0). Structures were drawn in ChemDraw Professional 16.0.

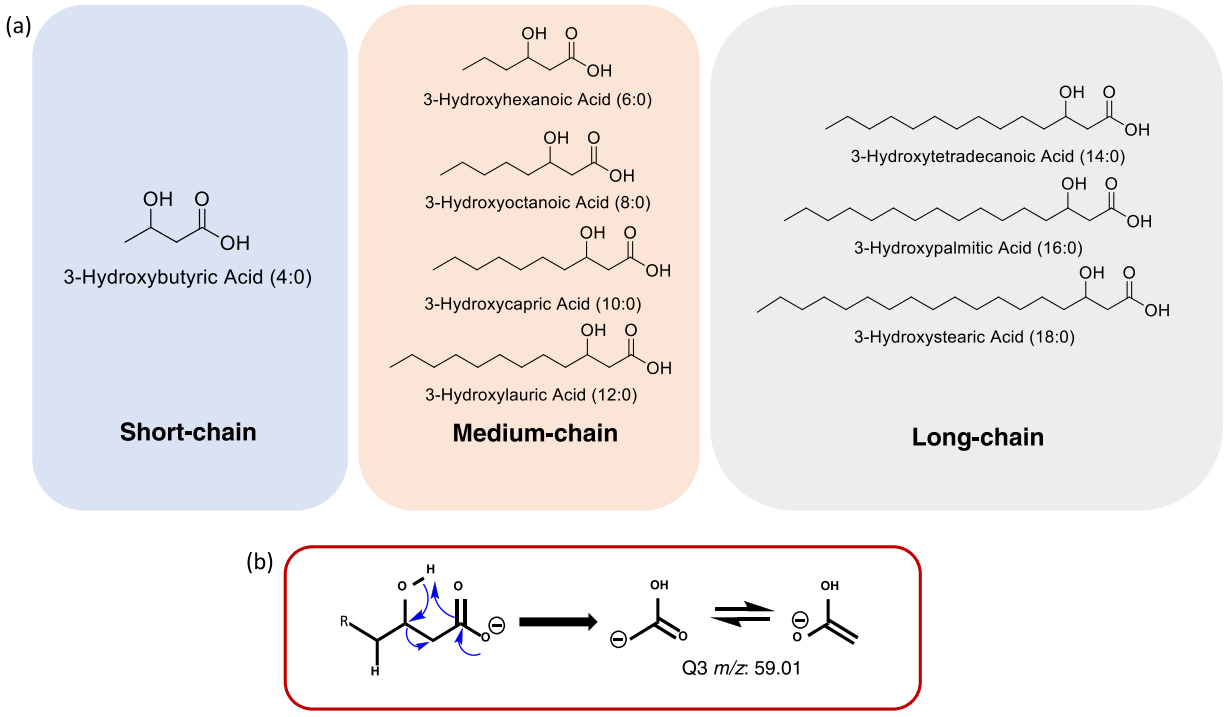

Fig. 3. (a) Structures of 3-OH-FAs from C4 to C18 (b) CID fragmentation pathway of 3-OH-FAs.

3. Results and discussion

3.1. Method development

3.1.1. Optimization of extraction method

An efficient extraction of lipids from cells or other biological matrix is the first step for a reliable targeted analysis. Here, we evaluated two extraction protocols using pooled plasma: (1) The first one, commonly used for general lipid extraction in lipidomics, was based on monophasic extraction with 2-propanol for protein precipitation (IPA) and (2) with additional subsequent SPE purification (IPA+SPE, for detailed procedure see suppl. materials). From 3-OH-FA (8:0) to 3-OH-FA (14:0) (Fig. 2), the sample using only IPA as extraction method showed significantly higher intensity than that with IPA combined with SPE, assuming that in the course of the wash step in the SPE procedure some of the 3-OH-FA with shorter chains were lost due to their higher polarity. On the contrary, the intensity improved significantly for the fatty acids with long carbon chain, when they were extracted with IPA and then purified with SPE (Fig. 2). It is concluded that for the 3-OH-FA with a longer carbon chain (16−18), a better intensity could be obtained when the extraction was performed with IPA combined with SPE. For those with a shorter carbon chain (<16), extraction with only IPA performed better. To obtain a better comparison of both extraction procedures, the extraction recovery (RE%) of 3-OH-FA 8:0 and 3-OH-FA 12:0 for both procedures and enantiomers were evaluated (Table. S2). It is noticed that the recoveries of the extraction method (IPA+SPE) of both investigated 3-OH-FAs are by far lower (30–50%) than with IPA method (80–100%). It confirmed that in the course of the SPE purification step some of the targeted compounds were lost, e.g. during wash steps, thus showing poor extraction recoveries. Taking the poor recoveries and the time-consuming step of purification by SPE into consideration, further extraction only with IPA was found more suitable for extraction.

3.1.2. LC-MS method development

The LC-MS/MS method for 3-OH-FAs requires not only adequate chromatographic enantioselectivity, but also selection of proper MRM transitions. MRM parameters were established by direct infusion of single standards of each 3-OH-FA solution with 1 μg/mL in MeOH. For each 3-OH-FA (C4-C18) (the structures of 3-OH-FAs can be found in Fig. 3a), the same group-specific product ion with *m/z* 59.01 for acetate was produced in negative ESI mode by bond cleavage between carbon-2 and carbon-3 as a result of a charge driven proton rearrangement (Fig. 3b) [13]. The compound specific MS parameters (DP, CE, CXP) were then optimized (Table. S1). This fragment was proved to be unique for 3-OH-FAs and not found for other isomeric hydroxy fatty acids substituted in other positions. A number of other potential interferences (isomeric epoxides or cyclic keto compounds) were also ruled out [24, 25]. What's more, the isobaric compounds due to [M+ 2] isotopologue such as 3-oxo-FA or 3-OH-FAs with one double bond have to be considered as potential interferences. It is proved that the 3-OH-FAs with one double bond can be detected in plasma samples, however, they can be chromatographically separated from the corresponding 3-OH-FAs without double bond, which was therefore no longer to be considered an interference in our assay (Fig. S1). To support MS/MS selectivity to differentiate these isomers, retention time was considered as another identifier. For this purpose, we employed structure-retention relationships for identification of 3-OH-FAs as retention time prediction models. It is well known that the retention behaviour of lipids is closely related to its chemical structure including the carbon chain length and the number of C=C double bonds, hence the correlation between retention time on IA-U column and *m/z* of both *R* and *S* enantiomers of different 3-OH-FAs was plotted. As can be seen from Fig. S2a, the retention time increases linearly with longer carbon chain for both *R* and *S* enantiomer with determination coefficient of R^2 0.9908 (*R*-enantiomer) and 0.9901 (*S*-enantiomer). This way, the identification of 3-OH-FAs can be more reliable.

Furthermore, the chromatographic elution conditions of different gradients were then optimized to obtain the best enantioselectivity for *R* and *S* enantiomers and also the best sensitivity for each compound. The elution order of *R* and *S* enantiomers of 3-OH-FAs was determined in the previous work for short and medium chain 3-OH-FAs [4] and confirmed herein by a standard of the *R*-enantiomer of 3-OH-FA (14:0). For all the investigated 3-OH-FAs, *S* eluted earlier than *R*. Different gradients of mobile phase B were set up with 10, 20, 30, 40 or 50% as starting

Table 1
Instrumental detection and quantification limits of 3-OH-FAs (with standard solutions).

Name	IS used	Enantiomer	LOD (ng/mL)	LOQ (ng/mL)
3-OH-FA (8:0)	RvD1 d5	*S*	0.100	0.500
		R	0.100	0.500
3-OH-FA (10:0)	RvD1 d5	*S*	0.020	0.125
		R	0.020	0.125
3-OH-FA (12:0)	RvD1 d5	*S*	0.010	0.050
		R	0.015	0.125
3-OH-FA (14:0)	12 HETE d8	*R*	0.001	0.010
3-OH-FA (16:0)	AA d11	*S*	0.010	0.050
		R	0.010	0.050
3-OH-FA (18:0)	AA d11	*S*	0.100	0.250
		R	0.100	0.250

percentages, respectively. The gradient time t_g was 20 min up to 100% B for all the different starting conditions. As can be seen from Fig. S2b, with increasing organic modifier as starting conditions, the sensitivity of 3-OH-FAs was lower along with worse enantioselectivity between *S* and *R* enantiomers of each 3-OH-FA, especially for the mid-chain 3-OH-FA (10:0) as an example. The enantioselectivity became worse and worse with higher starting %B until *S* and *R* enantiomers of 3-OH-FA (10:0) were totally co-eluted and lost resolution. The starting percentage of organic modifier had less effect on the enantioselectivity of long-chain 3-OH-FA from C14-C18 (C16 as an example in Fig. S2b). Even though, a loss of sensitivity can still be observed for long-chain 3-OH-FAs. As a consequence, an LC gradient method starting with 10% B of 25 min was confirmed. Unfortunately, *R* and *S* enantiomers of 3-OH-FA (4:0) and 3-OH-FA (6:0) with a retention close to t_0 (1.45 min) could not be separated under the employed conditions (see Fig. S3) while for the other 3-OH-FAs (C8-C18), a full baseline resolution could be observed (Fig. 2). As the next step, the flow rate for the IA-U column under experimental conditions was optimized to achieve the best sensitivity. A series of flow rates from 0.2 mL/min to 0.8 mL/min were investigated. As can be found in Fig. S4, with higher flow rate, a significant sensitivity loss can be observed (examples for first eluted C8 and last eluted C18). In the end, the flow rate of 0.3 mL/min was chosen to guarantee the sensitivity which showed good resolution (R_s >1.5) for *R* and *S* enantiomers as well (Table. S3).

As discussed above, during the optimization of extraction protocols the IPA method without SPE purification was finally chosen. It is worth mentioning that this extraction method covers a wide range of lipid classes including very apolar ones like cholesterol ester (CE) and triradylglycerol (TG), which might accumulate on the column. Acetonitrile as organic modifier in the mobile phase as under given LC conditions does not have strong enough elution ability for these apolar neutral lipids. Therefore, a wash step was incorporated after every 6 injections (5 plasma + 1 QC injections) in the analytical batch. The wash step consisted of mobile phase B2 (80% IPA and 20% ACN with 0.1% acetic acid) adopting strong elution ability due to the high IPA content. Detailed information can be found in Suppl. Materials (Fig. S5 and Table. S4).

With optimized LC-MS method, adequate selectivity and sensitivity for *R* and *S* enantiomers of 3-OH-FAs from C8-C18 can be achieved (some important parameters of resolution, gradient plate numbers as characteristic measure for column efficiency and backpressure under final experimental conditions can be found in Table. S5 and Fig. S6).

3.2. Method validation

3.2.1. Estimation of LOD and LOQ

Instrumental detection and quantification limits (LOD and LOQ, respectively) were estimated according to the response of each 3-OH-FA in neat solution. The concentration with a S/N ratio of 3 was defined as LOD and with a S/N ratio of 10 as LOQ. The results can be found in Table 1. In most of the cases, the LOQ is lower than 0.125 ng/mL except for 3-OH-FA (8:0) with a relatively high LOQ of 0.5 ng/mL.

3.2.2. Extraction recovery, matrix effect and process efficiency

Extraction recoveries (RE) and matrix effects (ME) were determined according to the protocol of Matuszewski [23]. If the neat solution standard series 1 (see 2.4.2) is designated as A, series 2 (post-spiked) as B, and series 3 (pre-spiked) as C, the values of extraction recovery, matrix effect, and process efficiency can then be calculated as follows:

$$\text{RE}\ (\%) = \text{C/B} \times 100 \quad (1)$$

$$\text{ME}\ (\%) = \text{B/A} \times 100 \quad (2)$$

$$\text{PE}\ (\%) = \text{C/A} \times 100 = (\text{ME} \times \text{RE})/100 \quad (3)$$

For this purpose, 3 levels of standards with 0.05 ng/mL (low, L), 5 ng/mL (mid, M) and 50 ng/mL (high, H) were prepared in neat, pre-spiked and post-spiked plasma. The results of RE (%), ME (%) and PE

Table 2
Intra- and inter-day Precision (CV%) and accuracy (%) in 3 QC levels (plasma).

Name		**Enantiomer**	QC low		QC mid		QC high	
			Precision CV%	Accuracy%	Precision CV%	Accuracy%	Precision CV%	Accuracy%
3-OH-FA (8:0)	**Intra-day (n = 3)**	*S*	4.8	96.0	5.8	101.6	8.0	99.0
		R	3.1	94.2	4.6	97.9	5.8	101.1
	Inter-day (n = 9)	*S*	5.1	95.8	5.6	102.1	8.7	98.5
		R	3.8	94.2	4.4	98.5	14.2	102.2
3-OH-FA (10:0)	**Intra-day (n = 3)**	*S*	3.9	93.5	5.5	101.1	5.6	102.2
		R	5.3	93.6	7.6	103.1	5.0	102.5
	Inter-day (n = 9)	*S*	3.8	94.2	5.4	101.6	7.3	99.4
		R	5.4	93.5	7.0	103.3	7.5	99.2
3-OH-FA (12:0)	**Intra-day (n = 3)**	*S*	4.1	95.1	4.9	98.9	6.7	94.6
		R	1.6	99.7	2.7	97.9	4.8	95.3
	Inter-day (n = 9)	*S*	6.2	96.2	6.9	100.1	11.6	92.2
		R	4.4	100.4	5.6	98.7	10.4	93.7
3-OH-FA (14:0)	**Intra-day (n = 3)**	*R*	2.5	98.6	5.3	99.5	2.6	103.2
	Inter-day (n = 9)	*R*	3.3	100.1	5.0	99.1	4.3	103.5
3-OH-FA (16:0)	**Intra-day (n = 3)**	*S*	2.6	104.7	9.3	95.5	3.9	96.0
		R	9.6	95.3	9.3	93.5	4.7	98.5
	Inter-day (n = 9)	*S*	7.6	89.6	10.0	90.7	8.3	102.6
		R	10.7	99.9	7.2	95.9	5.1	101.4
3-OH-FA (18:0)	**Intra-day (n = 3)**	*S*	7.4	85.4	15.7	121.8	0.9	103.7
		R	9.6	95.8	11.3	107.9	2.6	100.5
	Inter-day (n = 9)	*S*	11.2	89.6	10.9	114.1	5.9	104.6
		R	8.4	94.1	9.6	109.0	11.7	99.6

Table 3
Calibration curves of 3-OH-FAs and the slope ratio of S and R enantiomer in plasma and platelets.

Name	IS used	Enantiomer	Plasma matrix			Platelet matrix			Plasma matrix	Platelet matrix
			slope	intercept	R^2	slope	intercept	R^2	Slope ratio *k* (*S*/*R*)	Slope ratio k (*S*/R)
3-OH-FA (8:0)	RvD1 d5	*S*	0.0053	-0.0707	0.993	0.0054	-0.0711	0.997	0.88	0.87
		R	0.0060	0.0161	0.994	0.0062	-0.1383	0.993		
3-OH-FA (10:0)	RvD1 d5	*S*	0.0482	-0.0921	0.997	0.0483	-0.1451	0.994	0.83	0.92
		R	0.0577	-0.1603	0.997	0.0528	0.0265	0.989		
3-OH-FA (12:0)	RvD1 d5	*S*	0.0260	0.0770	0.997	0.0262	0.5016	0.987	0.99	0.98
		R	0.0262	0.3386	0.994	0.0267	0.4713	0.989		
3-OH-FA (14:0)	12 HETE d8	*R*	0.0321	0.2501	0.975	0.0305	0.1870	0.982	n.a	n.a
3-OH-FA (16:0)	AA d11	*S*	0.0130	0.0124	0.998	0.0115	0.0000	0.999	0.98	0.90
		R	0.0133	0.1777	0.994	0.0128	-0.0003	0.999		
3-OH-FA (18:0)	AA d11	*S*	0.0032	0.0807	0.978	0.0033	0.0031	0.996	0.95	0.94
		R	0.0034	0.0601	0.989	0.0035	0.0042	0.994		

(%) of 3-OH-FAs are summarized in Table. S6. As can be concluded from Table. S6 for most of the 3-OH-FAs the extraction recovery is over 90%, which indicates that the IPA protocol did not result in significant analyte losses during the extraction procedure. What's more, the spiked IS can well compensate the extraction loss of the targeted 3-OH-FAs in the final method and its application. A significant ion suppression for the majority of 3-OH-FAs can be observed, which is not surprising. The matrix effect for most of the 3-OH-FAs was between 60% and 80% (100% means no ME) being tantamount to ion suppression in the ESI process owing to coeluting matrix components. It seemed that the matrix effect can be stronger with longer carbon chain length. In general, due to this matrix effect and absence of stable isotope labelled IS, matrix-matched calibration was mandatory. In absence of stable isotope labelled IS, standard addition calibration curve in plasma corrected for endogenous levels was the strategy pursued in this preliminary study.

3.2.3. *Linear response function estimation, precision and accuracy*

Two sets of calibrants were prepared, 1) standards in MeOH (neat solution), 2) standards spiked to matrix (standard addition; matrix-matched calibration). The concentration range was from 0.05 to 500 ng/mL for each enantiomer except for *3R*-OH-FA (14:0) from 0.1 to 1000 ng/mL. For all the 3-OH-FAs, concentrations between 0.05 and

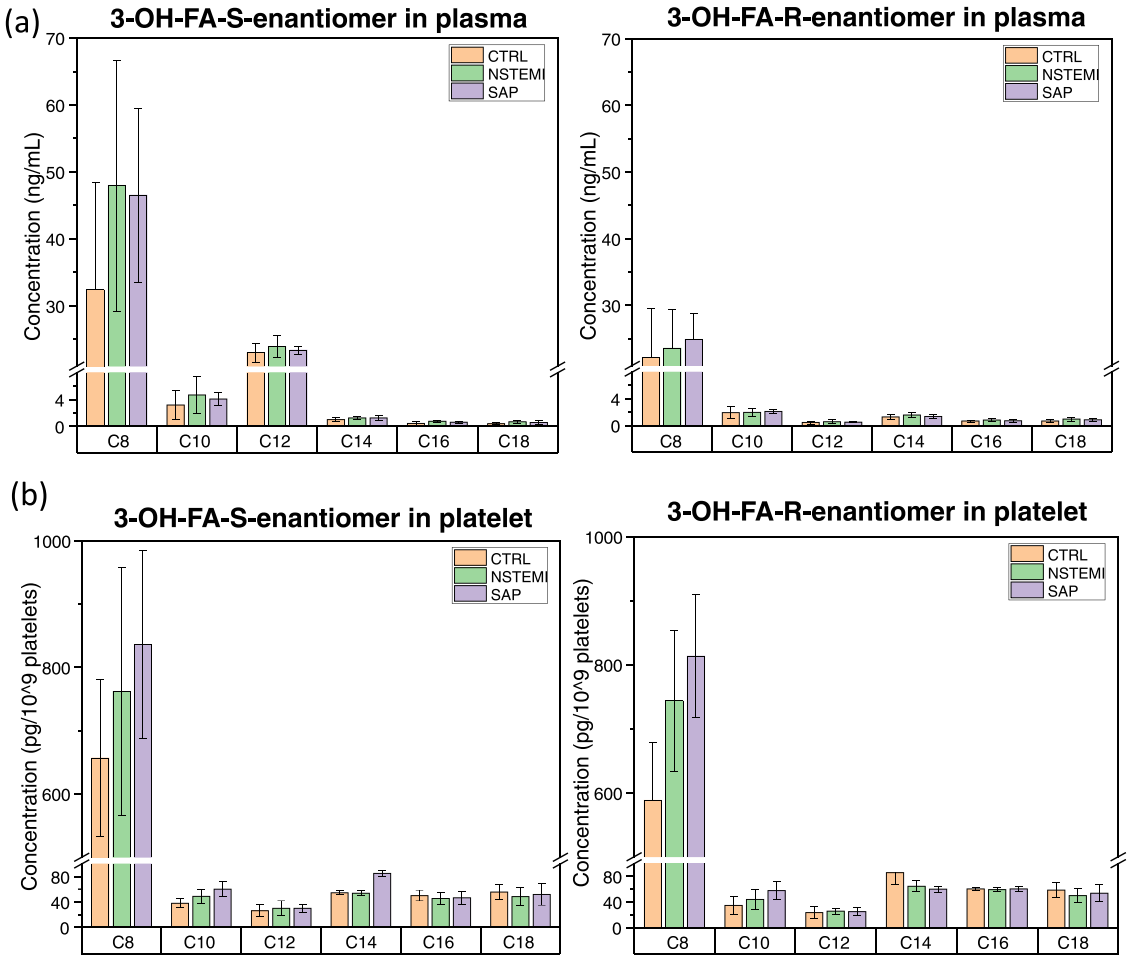

Fig. 4. The distribution of *S* and *R* enantiomer of 3-OH-FAs from C8-C18 in terms of concentration in plasma and platelets with different diagnosis groups. Shown are mean and standard deviation of the concentrations of the distinct 3-OH-FAs for each sample group (healthy control, NSTEMI and SAP; n = 6 for healthy controls and n = 10 for NSTEMI and SAP).

500 ng/mL were within the linear range of the response function of the detector. The slopes of the two kinds of calibration curve were compared. As can be seen in Table. S7 (all 3-days data), for the same 3-OH-FA, the slope varies in neat calibration curve and matrix-matched calibration curve, especially for 3-OH-FAs C8, C10 and C12 indicating that a matrix effect does have a significant influence on the response of 3-OH-FAs, as stated above, which leads to bias for final quantification if the neat calibrants were applied. Thus, a matrix-matched standard addition calibration, corrected for the endogenous levels, was required for the quantification in real samples confirming above conclusion (see 3.2.2).

Precision and accuracy were validated on 3 different days using matrix-matched calibration corrected for endogenous levels. For this purpose, quality controls (QCs) obtained by spiking standard solutions to plasma (pre-spiked standard addition approach) at 3 QC levels were employed. The results are shown in Table 2. As can be seen from Table 2, the intra- and inter-day precision (CV%) and accuracy (% recovery) at all 3 levels passed the requirement of FDA within 15% bias (20% for low level). In most of the cases, the CV% was within 10% while accuracy was between 90%− 110% for each enantiomer (*R* and *S* enantiomer) of each 3-OH-FA, which indicates the adequate performance of the method.

3.3. Method application

3.3.1. Quantitative methods

From the previous validation results, it became evident that matrix-matched calibration is necessary for a reliable quantification of 3-OH-FAs in biological samples. Classical standard addition calibration in each sample is inefficient and not readily possible in a larger number of samples. For this reason, corrected standard addition functions were established for the two types of matrices evaluated in this study, one for plasma matrix and another one for platelet matrix. Pooled plasma samples were aliquoted into 100 µL while pooled platelet samples were aliquoted into 2×10^8 cells and 3-OH-FA standard mixtures ranging from 0.1 to 250 ng/mL (7 data points, see Fig. S7) were spiked into the two different matrices. Extraction procedures were then performed as described in Sections 2.2.2 and 2.2.3. After correction of endogenous levels of each 3-OH-FA in the respective pooled matrix, the corrected calibration curves were applied for quantitation of a larger number of platelet and plasma samples in one analytical batch. As can be concluded from Fig. S7, the slopes of the same 3-OH-FA (*3S*-OH-FA (12:0) as an example) in the two different matrices were very similar with only a slight difference (0.026 in plasma and 0.028 in platelets). The slopes of other 3-OH-FAs in terms of *R* and *S* enantiomers in the two matrices can be found in Table 3.

3.3.2. Results for plasma and platelet

To understand the metabolism of hydroxy fatty acids in cardiovascular disease, plasma samples and the corresponding platelets samples from 10 SAP (stable angina pectoris), 10 NSTEMI (non-ST-segment elevation myocardial infarction) patients and 6 healthy controls were collected and analyzed by the established enantioselective quantitative analysis method with matrix-matched calibration curves corrected for endogenous levels. Exemplary chromatograms of standard solution, non-spiked plasma and platelet extracts are shown in Fig. S8. It can be noticed that both *R* and *S* enantiomers of all tested 3-OH-FAs were detected in both plasma and platelet samples. The analytes with carbon chain length till C18 were detected in plasma and platelet, the 3-OH-FAs with carbon C20 and more were not detectable (Fig. S9; RPLC-QTOF-MS analysis exhibits a full series of 3-OH-FA from C4 to C18; OH-FA with C20 was also detected in plasma but it turned out to be a 2-OH-FA). There is no limitation from the analytical method (e.g. insufficient elution strength of LC conditions), but it seems that they are not existing in our biological samples. It is known that very long-chain fatty acyl-CoA esters (>20 carbon atoms) are initially shortened by peroxisomal enzymes before they proceed into the mitochondrial network for

Table. 4
Median and IQR of 3-OH-FAs in plasma and platelets in different diagnosis groups.

Name	Enatiomer	Plasma (pmol/mL)						Platelets (pmol/10^9)					
		Control		NSTEMI		SAP		Control		NSTEMI		SAP	
		Median	IQR	Median	IQR	Median	IQR	Median	IQR	Median	IQR	Median	IQR
3-OH-FA (8:0)	S	179.75	149.82–232.13	256.11	232.25–333.89	315.80	233.25–330.49	4.27	3.90–4.47	4.45	3.78–5.53	4.78	4.22–5.49
	R	133.78	102.12–168.60	155.54	131.38–164.83	155.66	136.79–166.91	4.17	4.10–4.19	4.78	4.45–5.49	5.61	4.90–6.04
3-OH-FA (10:0)	S	13.00	11.32–18.58	21.10	15.87–30.86	20.88	18.70–25.44	0.19	0.17–0.21	0.27	0.22–0.29	0.31	0.27–0.36
	R	10.18	6.08–13.22	10.72	7.98–12.36	11.00	10.03–12.29	0.23	0.18–0.29	0.27	0.22–0.36	0.30	0.26–0.33
3-OH-FA (12:0)	S	33.76	28.51–43.13	38.63	30.24–44.13	37.83	29.89–40.54	0.10	0.09–0.12	0.14	0.09–0.17	0.14	0.11–0.17
	R	1.72	1.23–2.72	2.43	1.68–2.97	2.07	1.90–2.58	0.09	0.09–0.11	0.13	0.11–0.13	0.12	0.10–0.13
3-OH-FA (14:0)	S	3.75	3.68–4.29	4.83	4.38–5.97	5.04	4.53–5.49	0.22	0.21–0.23	0.22	0.21–0.23	0.23	0.22–0.25
	R	5.04	4.08–5.89	6.08	5.49–6.44	5.45	5.14–5.64	0.34	0.31–0.38	0.26	0.25–0.26	0.25	0.23–0.25
3-OH-FA (16:0)	S	1.33	1.18–1.79	2.71	2.35–2.88	2.23	1.89–2.48	0.18	0.17–0.20	0.17	0.16–0.18	0.18	0.13–0.20
	R	2.45	2.10–2.55	2.83	2.51–3.32	2.25	1.99–3.16	0.22	0.21–0.23	0.21	0.21–0.22	0.22	0.21–0.23
3-OH-FA (18:0)	S	1.05	0.94–1.39	2.12	1.86–2.48	1.55	1.38–2.20	0.19	0.17–0.20	0.17	0.13–0.18	0.17	0.14–0.18
	R	2.18	1.74–2.51	3.23	2.42–3.38	2.63	2.32–2.88	0.19	0.16–0.22	0.16	0.14–0.17	0.17	0.15–0.19

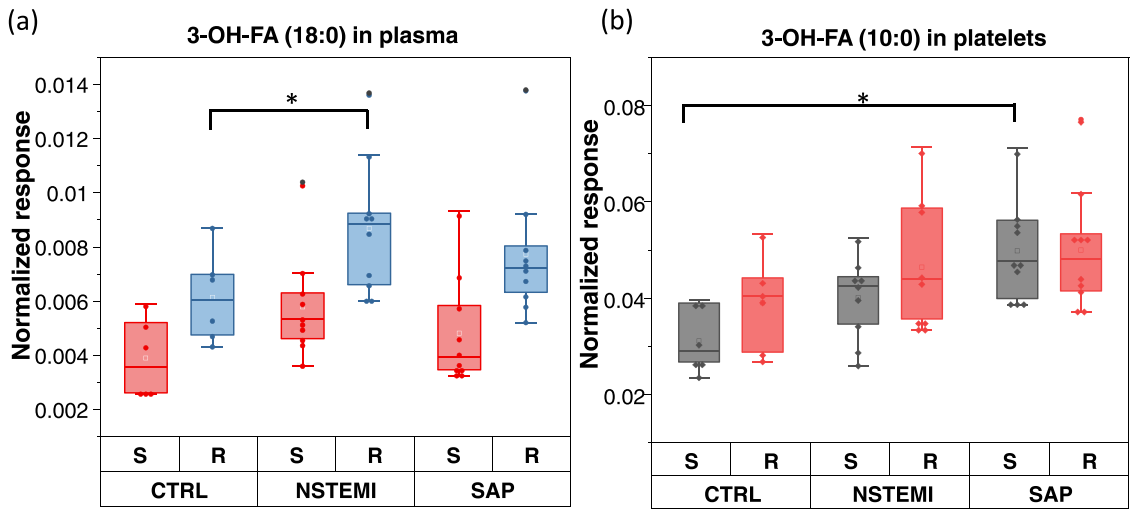

Fig. 5. Boxplots of significantly regulated 3-OH-FAs in plasma and platelet with two-groups U test. For (*R*)-3-OH-FA (18:0) in plasma, p = 0.036 (CTRL vs NSTEMI); for (*S*)-3-OH-FA (10:0) in platelets, p = 0.004 (CTRL vs SAP).

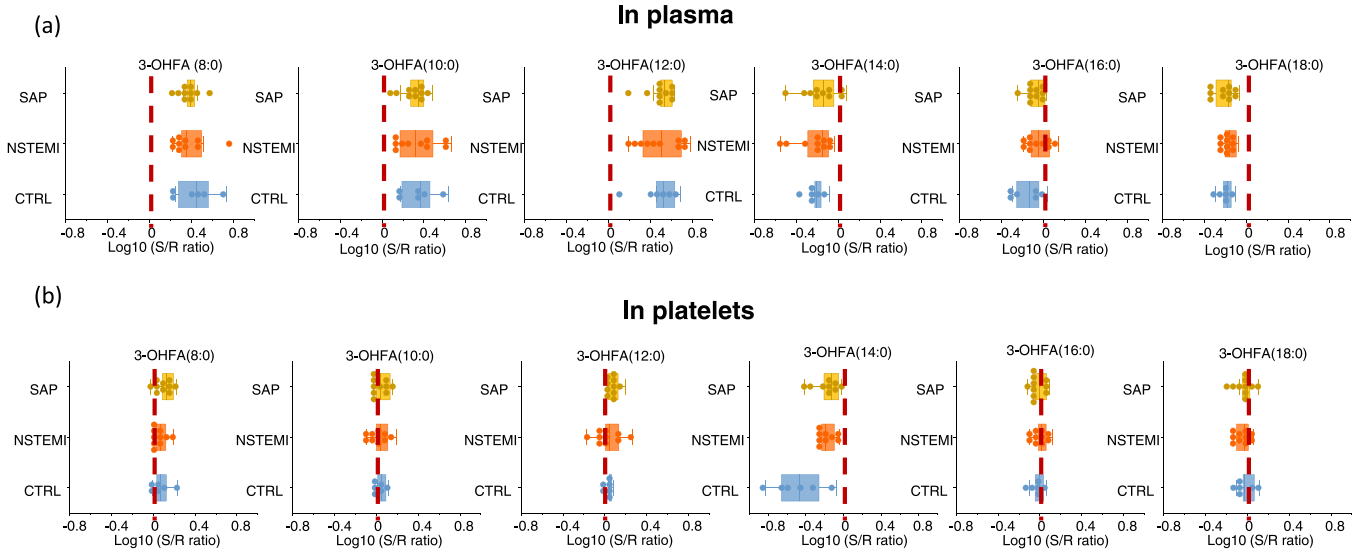

Fig. 6. Boxplots of *S/R* ratio of 3-OH-FAs in plasma (top panel) and platelets (bottom panel) compared for different sample groups. The S/R ratio was corrected by response factor *k* (*k* = slope in *S* calibration curve / slope in *R* calibration curve) and x-axis was transformed by Log10 (*S/R* ratio). The red dash line is x = 0. When x > 0, *S*>*R*; when x < 0, *S*<*R*.

β-oxidation [26]. In general, peroxisomal FAO should also lead to 3-OH FAs with preferred *S*-enantiomer resulting from the *L*-bifunctional enzyme (Ehhadh) (vide infra) [27]. The 3-OH-FA (8:0), *R*- and *S*-enantiomers, are the most abundant 3-OH-FAs in both plasma and platelet samples with a remarkably higher concentration compared to the other 3-OH-FAs (see Fig. 4). Besides 3-OH-FA (8:0), all the other 3-OH-FAs including 3-OH-FA (10:0), 3-OH-FA (12:0), 3-OH-FA (14:0), 3-OH-FA (16:0) and 3-OH-FA (18:0) were in similar concentration level except for (*S*)-3-OH-FA (12:0) in plasma samples which shows higher concentration levels (Fig. 4 and Table. 4).

To screen for valuable 3-OH-FA biomarkers, statistical analysis (*U*-test) was employed for each set. It was found that in plasma samples, (*R*)-3-OH-FA (18:0) is significantly upregulated ($p = 0.036$) in NSTEMI group when compared with the control group, while in platelet samples, (*S*)-3-OH-FA (10:0) is significantly upregulated ($p = 0.004$) in the SAP group compared to control. The boxplots of the two significantly regulated compounds are shown in Fig. 5. Due to the limited sample number in this preliminary study, it is concluded that further investigations are required to validate the findings and to give a reasonable clinical hypothesis.

3.3.3. *R to S enantiomer ratios of 3-OH-FAs*

Both enantiomers were detected successfully from 3-OH-FA (8:0) to 3-OH-FA (18:0) in our plasma and platelet samples. To illustrate the excess of either *S*- or *R*-enantiomer for the distinct sample groups (SAP, NSTEMI and control) for the two matrices plasma and platelets, the *S/R* ratio was calculated in each individual sample. The ratio was calculated by peak area ratio of *S* and *R* enantiomers in each sample (α = peak area *S*/peak area *R*) corrected by the response factor ratio of the enantiomers *k* (*k* = slope in *S* calibration curve / slope in *R* calibration curve, see Table 3) according to Eq. 4.

$$S/R \text{ ratio, corrected} = \alpha \times (1/k) \quad (4)$$

The corresponding box plots can be found in Fig. 6a for plasma and in Fig. 6b for platelets. Interestingly, it becomes evident that dependent on the carbon chain length either *S* or *R* enantiomer is present in excess in plasma (Fig. 6a): For the medium chain 3-OH-FAs (C8 – C12) the *S*-

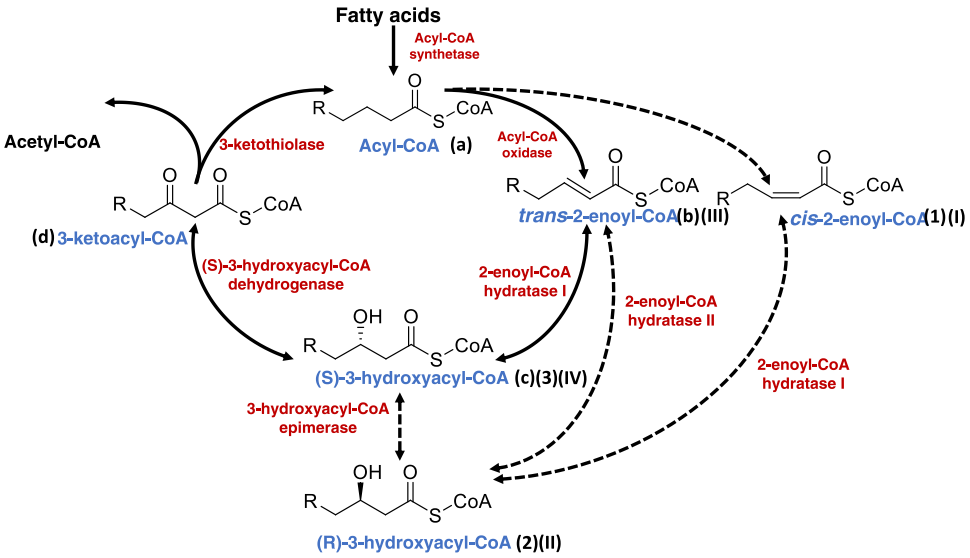

Fig. 7. Core β-oxidation cycle and enzymatic reactions involved in the synthesis of (*R*)-3-Hydroxyacyl-CoA (illustrated by dashed lines). Simplified from [29] and recreated by ChemDraw. The alphabets (a-d) represent the order of the core β-oxidation cycle. The number (1−3) and (I-IV) indicate the order of the epimerase pathway of *cis*-2-enoyl-CoA. In the epimerase pathway, conversion of *R*-3-hydroxyacyl-CoA to *S*-3-hydroxyacyl-CoA can be mediated either via a 3-hydroxyacyl-CoA epimerase (1−3) or the combined action of the 2-enoyl-CoA hydratase I and 2-enoyl-CoA hydratase II (I-IV).

enantiomer is predominant, while for the long chain 3-OH-FAs (C14 - C18) the *R*-enantiomer dominates. The trends are similar for platelets, yet less pronounced (see Fig. 6b): A higher percentage of *R*-enantiomer is present in platelets than in plasma for the medium-chain 3-OH-FAs and the excess of *R*-enantiomer is less for the long chain 3-OH-FAs (C14 - C18) in platelets compared to plasma. It becomes evident that there are some minor but significant stereoselectivity differences in the 3-OH-FA profiles of the two sample types (note, in this work platelets and plasma were from the same patient and identical blood sample, respectively). It is not surprising as platelets represent an independent metabolic compartment.

As outlined in the introduction, textbook knowledge states that mitochondrial fatty acid oxidation (by mitochondrial trifunctional protein MTP with the 2,3-enoyl-CoA hydratase and the 3-hydroxyacyl-CoA dehydrogenase activities on the α-subunit and the 3-ketoacyl-CoA thiolase activity on the β-subunit; www.uniprot.org/uniprotkb/P30084) yields the (*S*)-3-hydroxyacyl-CoA intermediates (Fig. 1) [5]. As can be seen from Fig. 6, there is a significant mismatch in this expected and experimentally determined stereoselectivities; substantial quantities of *R*-enantiomers are detected in all samples. Their origin is difficult to pinpoint but a number of metabolic processes may be responsible.

In general, 3-OH-FAs exist in biological systems in conjugated form (bound to acyl-CoA), yet spontaneous hydrolysis or thioesterase activity [28] may release a certain percentage of the intermediates into free 3-hydroxy fatty acids which we monitor in this work. Fig. 7 shows an overview of the core degradation pathways of saturated fatty acids [29]. In such a core β-oxidation cycle, four enzyme activities are required. The first enzyme acyl-CoA dehydrogenase (in the mitochondria) or acyl-CoA oxidase (in the peroxisomes) catalyzes the reaction of acyl-CoA to *trans*-2-enoyl-CoA and the 2-enoyl-CoA hydratase I converts the *trans*-2-enoyl-CoA to the *S*-isomer of 3-hydroxyacyl-CoA (also named L-β-hydroxyacyl CoA). Subsequently, (*S*)-3-hydroxyacyl-CoA is catalyzed by (*S*)-3-hydroxyacyl-CoA dehydrogenase into 3-ketoacyl-CoA (as outlined above). Finally, 3-ketothiolase cleaves the 3-ketoacyl-CoA into the two-carbon-shortened acyl-CoA [30]. This is the procedure for the core β-oxidation cycle which can lead to the formation of (*S*)-3-OH-FAs (after hydrolysis of corresponding CoAs). The core pathway cannot degrade the unsaturated even-numbered fatty acids with *cis* double bonds; however, they can be converted by 2-enoyl-CoA hydratase I to the *R*-isomers of 3-OH-FAs [31]. (*R*)-3-hydroxyacyl-CoA cannot proceed to the further steps of β-oxidation unless epimerization happens catalyzed by 3-hydroxyacyl-CoA epimerase which can be found in mammalian peroxisomes [32]. FAO can also happen in peroxisomes.

Similar to the mitochondrial trifunctional protein MTP, in the peroxisomal system the multifunctional enzymes (MFE) catalyze the hydration step of 2-enoyl-CoAs and convert the generated 3-hydroxyacyl-CoA to 3-ketoacyl-CoA. MFE-1 (also known as *L*-bifunctional protein, LBP or *L*-peroxisomal bifunctional enzyme *L*-PBE; 2-enoyl-CoA hydratase I is part of MFE-1) and MFE-2 (*D*-bifunctional protein, DBP [33] or *D*-PBE; 2-enoyl-CoA hydratase II is part of MFE-2) exert opposite stereospecificities and they exist concurrently in the mammalian peroxisomes [34]. However, both MFE-1 (inducible upon PPAR activation) and MFE-2 (constitutively expressed in peroxisomes) show broad substrate specificity [35]. MFE-1 accepts short and long chain enoyl-CoA esters while MFE-2 very-long chain FAs e.g. CoA esters of C26 fatty acids, bile-acid precursors such as di/trihydroxycholestanoic acids and 2-methyl-branched fatty acids such as pristanic acid [32]. Possibly, the higher *R*-enantiomer contents for the long-chain 3-OH-FAs in both plasma and platelet samples indicates the peroxisomal 2-enoyl-CoA hydratase II activity and its preference of very-long chain FA substrates. The elevated *R*-enantiomer levels of medium-chain 3-OH-FAs in relation to *S*-enantiomer in the platelet samples (almost equal amount of *S* and *R* enantiomer) as compared to plasma (*S*/*R*-ratios mostly > 1 with *S*-enantiomer in excess) might be an indication for enhanced peroxisomal activity in platelets. To what extent 3-OH-FAs released from acyl carrier protein of the fatty acid synthase, which have *3R*-configuration, contribute to the *R*-enantiomers in our samples, remains open. In general, the results of the current study reveal that the current stereoselective assay provides added value and additional information that might be worth for further investigations.

4. Conclusions

A new sensitive and enantioselective UHPLC-MS/MS method based on 1.6 μm particle polysaccharide column (Chiralpak IA-U) for 3-OH-FA (C8-C18) analysis has been developed. This method has been validated and can be applied for 3-OH-FAs in plasma and platelets of CAD patients and controls as biological samples from distinct metabolic compartments. The assay covers 3-OH-FAs from C8-C18 which are closely associated with mitochondrial β-oxidation cycle. A matrix-matched standard addition calibration has been applied as a reliable quantitation method for the two different biological matrices. It showed good precision and accuracy for quantitative analysis of 3-OH-FAs with high enantioselectivity between *R* and *S* enantiomers in plasma and platelets. With the use of this method, both *R* and *S* enantiomers of 3-OH-FAs (C8-C18) were identified in plasma and platelets samples. For the first time, we reported the preference of *R* and *S* isomers of 3-OH-FAs according to the carbon chain length in plasma and platelet samples. For medium-

chain C8-C12, (*S*)-3-OH-FAs are present in excess while for long-chain C14-C18, (*R*)-3-OH-FAs are slightly dominant. This method can be used as a powerful tool to investigate the stereo-mechanism behind β-oxidation pathways and enzyme stereoselectivities in FAO.

CRediT authorship contribution statement

Xiaoqing Fu: Investigation, Methodology, Formal analysis, Data curation, Visualization, Writing – original draft, Writing – review & editing **Zhanjian Xu:** Investigation, Writing – review & editing, **Meinrad Gawaz:** Writing – review & editing, Funding acquisition. **Michael Lämmerhofer:** Conceptualization, Methodology, Supervision, Writing – review & editing Resources, Funding acquisition.

Declaration of Competing Interest

The authors declare that they have no known competing financial interests or personal relationships that could have appeared to influence the work reported in this paper.

Acknowledgements

X.F. gratefully acknowledges the support from the China Scholarship Council (grant number 201908080155). M.L. acknowledges the support by the German Research Foundation (DFG, Deutsche Forschungsgemeinschaft), project number 374031971-TRR 240.

Appendix A. Supporting information

Supplementary data associated with this article can be found in the online version at doi:10.1016/j.jpba.2022.115151.

References

[1] S. Patel, S. Ahmed, Emerging field of metabolomics: big promise for cancer biomarker identification and drug discovery, J. Pharm. Biomed. Anal. 107 (2015) 63–74.
[2] S. Uhlig, M. Negård, K.K. Heldal, A. Straumfors, L. Madsø, B. Bakke, W. Eduard, Profiling of 3-hydroxy fatty acids as environmental markers of endotoxin using liquid chromatography coupled to tandem mass spectrometry, J. Chromatogr. A 1434 (2016) 119–126.
[3] F. Ianni, Z. Pataj, H. Gross, R. Sardella, B. Natalini, W. Lindner, M. Lämmerhofer, Direct enantioseparation of underivatized aliphatic 3-hydroxyalkanoic acids with a quinine-based zwitterionic chiral stationary phase, J. Chromatogr. A 1363 (2014) 101–108.
[4] R. Karongo, J. Jiao, H. Gross, M. Lammerhofer, Direct enantioselective gradient reversed-phase ultra-high performance liquid chromatography tandem mass spectrometry method for 3-hydroxy alkanoic acids in lipopeptides on an immobilized 1.6 mum amylose-based chiral stationary phase, J. Sep Sci. 44 (9) (2021) 1875–1883.
[5] N. Rifai, Tietz textbook of clinical chemistry and molecular diagnostics, Elsevier Health Sciences, 2017.
[6] L. Zhang, W. Keung, V. Samokhvalov, W. Wang, G.D. Lopaschuk, Role of fatty acid uptake and fatty acid beta-oxidation in mediating insulin resistance in heart and skeletal muscle, Biochim. Et. Biophys. Acta 1801 (1) (2010) 1–22.
[7] S.K. Natarajan, J.A. Ibdah, Role of 3-hydroxy fatty acid-induced hepatic lipotoxicity in acute fatty liver of pregnancy, Int J. Mol. Sci. 19 (1) (2018).
[8] S.M. Houten, R.J.A. Wanders, A general introduction to the biochemistry of mitochondrial fatty acid β-oxidation, J. Inherit. Metab. Dis. 33 (5) (2010) 469–477.
[9] H. Imai, K. Yamamoto, A. Shibahara, S. Miyatani, T. Nakayama, Determining double-bond positions in monoenoic 2-hydroxy fatty acids of glucosylceramides by gas chromatography-mass spectrometry, Lipids 35 (2) (2000) 233–236.
[10] A. Saraf, J.-H. Park, D.K. Milton, L. Larsson, Use of quadrupole GC-MS and ion trap GC-MS-MS for determining 3-hydroxy fatty acids in settled house dust: relation to endotoxin activity, J. Environ. Monit. 1 (2) (1999) 163–168.
[11] J. Li, J. Xu, R. Zhang, Y. Hao, J. He, Y. Chen, G. Jiao, Z. Abliz, Strategy for global profiling and identification of 2- and 3-hydroxy fatty acids in plasma by UPLC–MS/MS, Anal. Chem. 92 (7) (2020) 5143–5151.
[12] Z. Zhu, X. Li, C. Tang, J. Shen, J. Liu, Y. Ye, A derivatization strategy for comprehensive identification of 2- and 3-hydroxyl fatty acids by LC-MS, Anal. Chim. Acta 1216 (2022), 339981.
[13] Q.-F. Zhu, N. An, Y.-Q. Feng, In-depth annotation strategy of saturated hydroxy fatty acids based on their chromatographic retention behaviors and MS fragmentation patterns, Anal. Chem. 92 (21) (2020) 14528–14535.
[14] E. Koch, N. Kampschulte, N.H. Schebb, Comprehensive analysis of fatty acid and oxylipin patterns in n3-PUFA supplements, J. Agric. Food Chem. 70 (13) (2022) 3979–3988.
[15] A.M. Abdel-Mawgoud, F. Lépine, E. Déziel, A chiral high-performance liquid chromatography–tandem mass spectrometry method for the stereospecific analysis of enoyl-coenzyme A hydratases/isomerases, J. Chromatogr. A 1306 (2013) 37–43.
[16] C. Calderón, M. Lämmerhofer, Enantioselective metabolomics by liquid chromatography-mass spectrometry, J. Pharm. Biomed. Anal. 207 (2021), 114430.
[17] F. Ianni, G. Saluti, R. Galarini, S. Fiorito, R. Sardella, B. Natalini, Enantioselective high-performance liquid chromatography analysis of oxygenated polyunsaturated fatty acids, Free Radic. Biol. Med. 144 (2019) 35–54.
[18] B. Chankvetadze, Application of enantioselective separation techniques to bioanalysis of chiral drugs and their metabolites, TrAC Trends Anal. Chem. 143 (2021), 116332.
[19] M. Cebo, X. Fu, M. Gawaz, M. Chatterjee, M. Lammerhofer, Enantioselective ultra-high performance liquid chromatography-tandem mass spectrometry method based on sub-2microm particle polysaccharide column for chiral separation of oxylipins and its application for the analysis of autoxidized fatty acids and platelet releasates, J. Chromatogr. A 2020 (1624), 461206.
[20] X. Fu, C. Calderon, T. Harm, M. Gawaz, M. Lammerhofer, Advanced unified monophasic lipid extraction protocol with wide coverage on the polarity scale optimized for large-scale untargeted clinical lipidomics analysis of platelets, Anal. Chim. Acta 1221 (2022), 340155.
[21] T. Harm, A. Bild, K. Dittrich, A. Goldschmied, J. Nestele, M. Chatterjee, X. Fu, K. Kolb, T. Castor, O. Borst, T. Geisler, D. Rath, M. LäMmerhofer, M. Gawaz, Acute coronary syndrome is associated with a substantial change in the platelet lipidome, Cardiovasc. Res. 118 (8) (2021) 1904–1916.
[22] M. Cebo, K. Dittrich, X. Fu, M.C. Manke, F. Emschermann, J. Rheinlaender, H. von Eysmondt, N. Ferreirós, J. Sudman, A. Witte, L. Pelzl, O. Borst, T. Geisler, D. Rath, T. Bakchoul, M. Gawaz, T.E. Schäffer, M. Lämmerhofer, M. Chatterjee, Platelet ACKR3/CXCR7 favors antiplatelet lipids over an atherothrombotic lipidome and regulates thromboinflammation, Blood 139 (11) (2022) 1722–1742.
[23] B.K. Matuszewski, M.L. Constanzer, C.M. Chavez-Eng, Strategies for the assessment of matrix effect in quantitative bioanalytical methods based on HPLC-MS/MS, Anal. Chem. 75 (13) (2003) 3019–3030.
[24] D.K. MacMillan, R.C. Murphy, Analysis of lipid hydroperoxides and long-chain conjugated keto acids by negative ion electrospray mass spectrometry, J. Am. Soc. Mass Spectrom. 6 (12) (1995) 1190–1201.
[25] B.S. Levison, R. Zhang, Z. Wang, X. Fu, J.A. DiDonato, S.L. Hazen, Quantification of fatty acid oxidation products using online high-performance liquid chromatography tandem mass spectrometry, Free Radic. Biol. Med. 59 (2013) 2–13.
[26] M.M. Adeva-Andany, N. Carneiro-Freire, M. Seco-Filgueira, C. Fernández-Fernández, D. Mouriño-Bayolo, Mitochondrial β-oxidation of saturated fatty acids in humans, Mitochondrion 46 (2019) 73–90.
[27] S.M. Houten, S. Denis, C.A. Argmann, Y. Jia, S. Ferdinandusse, J.K. Reddy, R. J. Wanders, Peroxisomal L-bifunctional enzyme (Ehhadh) is essential for the production of medium-chain dicarboxylic acids, J. Lipid Res 53 (7) (2012) 1296–1303.
[28] T.J. Grevengoed, E.L. Klett, R.A. Coleman, Acyl-CoA metabolism and partitioning, Annu Rev. Nutr. 34 (2014) 1–30.
[29] L. Allenbach, Y. Poirier, Analysis of the alternative pathways for the beta-oxidation of unsaturated fatty acids using transgenic plants synthesizing polyhydroxyalkanoates in peroxisomes, Plant Physiol. 124 (3) (2000) 1159–1168.
[30] S.M. Houten, R.J. Wanders, A general introduction to the biochemistry of mitochondrial fatty acid β-oxidation, J. Inherit. Metab. Dis. 33 (5) (2010) 469–477.
[31] H. Schulz, W.-H. Kunau, Beta-oxidation of unsaturated fatty acids: a revised pathway, Trends Biochem. Sci. 12 (1987) 403–406.
[32] Y. Suzuki, L.L. Jiang, M. Souri, S. Miyazawa, S. Fukuda, Z. Zhang, M. Une, N. Shimozawa, N. Kondo, T. Orii, T. Hashimoto, d-3-Hydroxyacyl-CoA Dehydratase/d-3-Hydroxyacyl-CoA Dehydrogenase Bifunctional Protein Deficiency: A Newly Identified Peroxisomal Disorder, Am. J. Hum. Genet. 61 (5) (1997) 1153–1162.
[33] L.L. Jiang, T. Kurosawa, M. Sato, Y. Suzuki, T. Hashimoto, Physiological Role of D-3-Hydroxyacyl-CoA Dehydratase/D-3-Hydroxyacyl-CoA Dehydrogenase Bifunctional Protein1, J. Biochem. 121 (3) (1997) 506–513.
[34] S.A. Filppula, R.T. Sormunen, A. Hartig, W.-H. Kunau, J.K. Hiltunen, Changing stereochemistry for a metabolic pathway in vivo: experiments with the peroxisomal β-oxidation in yeast (*), J. Biol. Chem. 270 (46) (1995) 27453–27457.
[35] J. Ding, U. Loizides-Mangold, G. Rando, V. Zoete, O. Michielin, Janardan K. Reddy, W. Wahli, H. Riezman, B. Thorens, The peroxisomal enzyme L-PBE is required to prevent the dietary toxicity of medium-chain fatty acids, Cell Rep. 5 (1) (2013) 248–258.

Supplementary information
UHPLC-MS/MS method for chiral separation of 3-hydroxy fatty acids on amylose-based chiral stationary phase and its application for the enantioselective analysis in plasma and platelets

Xiaoqing Fu[a], Zhanjian Xu[a], Meinrad Gawaz[b], Michael Lämmerhofer[a]*

[a] University of Tübingen, Institute of Pharmaceutical Sciences, Pharmaceutical (Bio-)Analysis, Auf der Morgenstelle 8, 72076 Tübingen, Germany

[b] Department of Cardiology and Angiology, University Hospital Tübingen, Otfried-Müller-Strasse 10, 72076 Tübingen, Germany

***Author for correspondence:**

Prof. Michael Lämmerhofer
Pharmaceutical (Bio-)Analysis
Institute of Pharmaceutical Sciences
University of Tuebingen
Auf der Morgenstelle 8
72076 Tuebingen, Germany
T +49 7071 29 78793, F +49 7071 29 4565
e-mail: michael.laemmerhofer@uni-tuebingen.de
http://www.bioanalysis.uni-tuebingen.de/

1. MS parameters

Table. S1 MS parameters for SRM in negative mode

Analyte	Q1 [m/z]	Q3 [m/z]	Dwell time (ms)	DP (volts)	CE (volts)	CXP (volts)
3-OH-FA (8:0)	159.1	59.0	50	-53	-20	-13
3-OH-FA (10:0)	187.1	59.0	50	-59	-22	-13
3-OH-FA (12:0)	215.2	59.0	50	-65	-25	-16
3-OH-FA (14:0)	243.2	59.0	50	-57	-34	-10
3-OH-FA (16:0)	271.2	59.0	50	-80	-20	-15
3-OH-FA (18:0)	299.3	59.0	50	-80	-20	-15
RvD1 d5	380.3	140.9	50	-40	-20	-15
12 HETE d8	327.3	184.0	50	-80	-20	-15
AA d11	314.2	270.1	50	-90	-19	-12

2. Extraction protocol of IPA+SPE

When purified with an additional solid-phase extraction step (SPE) on Bond Elute Certify II (3 mL / 200 mg) (Agilent, Waldbronn, Germany) solid phase extraction cartridges, the sample preparation (i.e. lipid extraction with IPA) was the same until the first supernatant was obtained (main document 2.2.2 and 2.2.3 with IPA method). Pre-conditioning was done in 3 steps: first with 1 mL of a mixture ethyl acetate/n-hexane/acetic acid (75:24:1; v/v/v), then with 2 mL of MeOH, and the last step was 2 mL sodium acetate buffer pH 6. Then, loaded samples were washed twice with 2 mL H_2O/MeOH (4:1; v/v). Next, the cartridges were dried for 5 min, Eppendorf tubes were exchanged and the extract was eluted with 2 mL of ethyl acetate/n-hexane/acetic acid (75:24:1; v/v/v). The samples were collected and dried with GeneVac EZ-2. The following steps were the same as the extraction with IPA.

Table.S2 Comparison of extraction recovery RE (%) of 3-OH-FAs in pooled plasma extracted by IPA and IPA+SPE

Name	Configuration	RE (%)	
		IPA	IPA+SPE
3-OH-FA (8:0)	S	95	49
	R	87	42
3-OH-FA (12:0)	S	88	42
	R	78	38

3. LC-MS method optimization

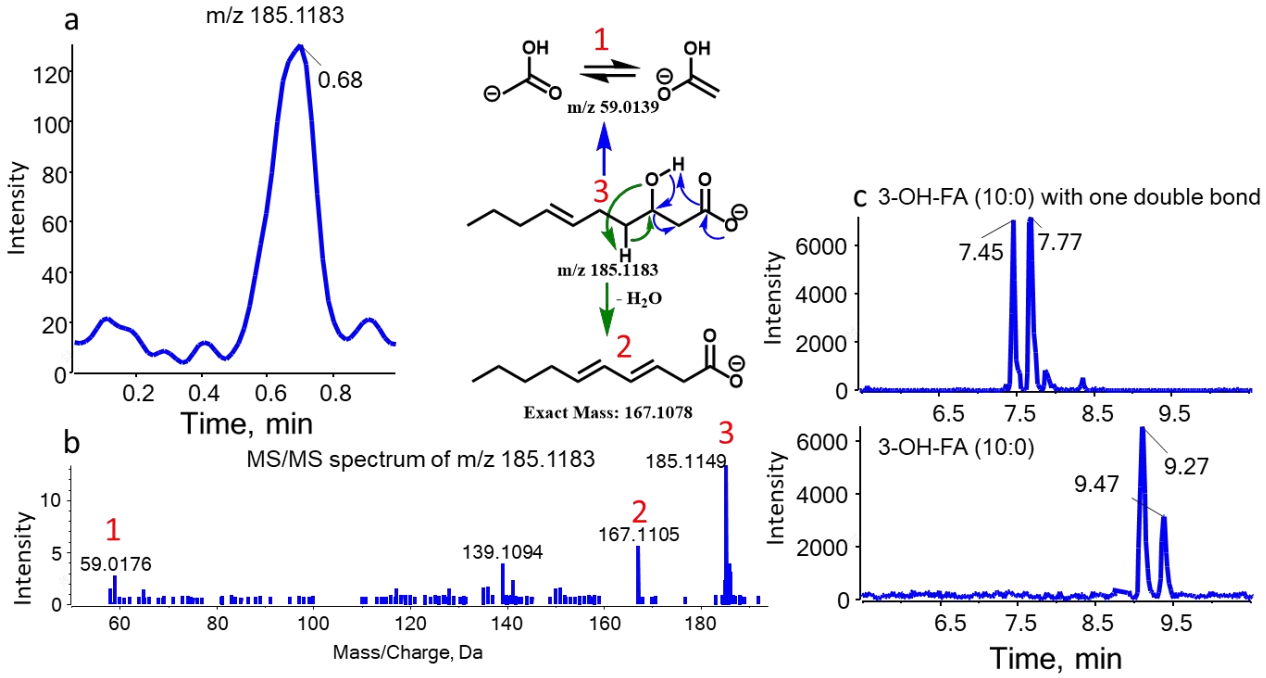

Fig. S1. *(a) EIC of compound with m/z of 185.1183 in HR-MRM scan mode with RPLC (Fiehn method, ref. [1]) in negative ion mode in pooled plasma sample. The chromatographic separation was performed on ACQUITY UPLC CSH C18 column (100 mm × 2.1 mm; particles: 1.7 µm; Waters Corporation, Millford, MA, USA) with precolumn (5 mm x 2.1 mm; 1.7 µm particles). The column temperature was 65°C and the flow rate 0.6 mL/min. Mobile phase A was composed of H_2O/ACN 2:3 (v/v) containing 10 mM ammonium formate and 0.1% formic acid (v/v) while mobile phase B was IPA/ACN/H_2O 90:9:1 (v/v/v) containing 10 mM ammonium formate and 0.1% FA (v/v). (b) MS/MS spectrum of $[M-H]^-$ of m/z 185.1183 with identified fragment ions of 1, 2 and 3. (c) EIC of 3-OH-FA (10:0) and mono-saturated 3-OH-FA (10:0) with Chiralpak IA-U column with experimental LC-MS method (see main document) in pooled plasma sample.*

In order to check for the potential isotopic interferences [M+2] in our assay which can be 3-oxo-3-FAs or 3-OH-FAs with one double bond, a HR-MRM scan mode with QToF was performed on the extracted plasma sample since no standards of 3-oxo-FAs or mono-unsaturated 3-OH-FAs were available. It can be found in Fig. S1a that a peak with *m/z* of 185.1183 referring to 3-oxo-FA or mono-unsaturated 3-OH-FA (10:0) could be detected. According to Fig. S1b, the structure was identified as mono-unsaturated 3-OH-FA (10:0) with the fragment ion *m/z* of 59.01 as well which means this [M+2] isotopologue might be an interference for the corresponding 3-OH-FAs if they co-eluted with each other. Thus, in the next step, the resolution for 3-OH-FAs and mono-

unsaturated 3-OH-FAs with IA-U column under applied experimental LC conditions (see main document) was confirmed (Fig. S1c). Both *R* or *S* enantiomer of mono-unsaturated 3-OH-FA (10:0) eluted earlier than the saturated ones and can be fully separated from *R* and *S* enantiomer of 3-OH-FA (10:0), which indicates that the potential isotopic [M+2] interference can be ruled out from consideration.

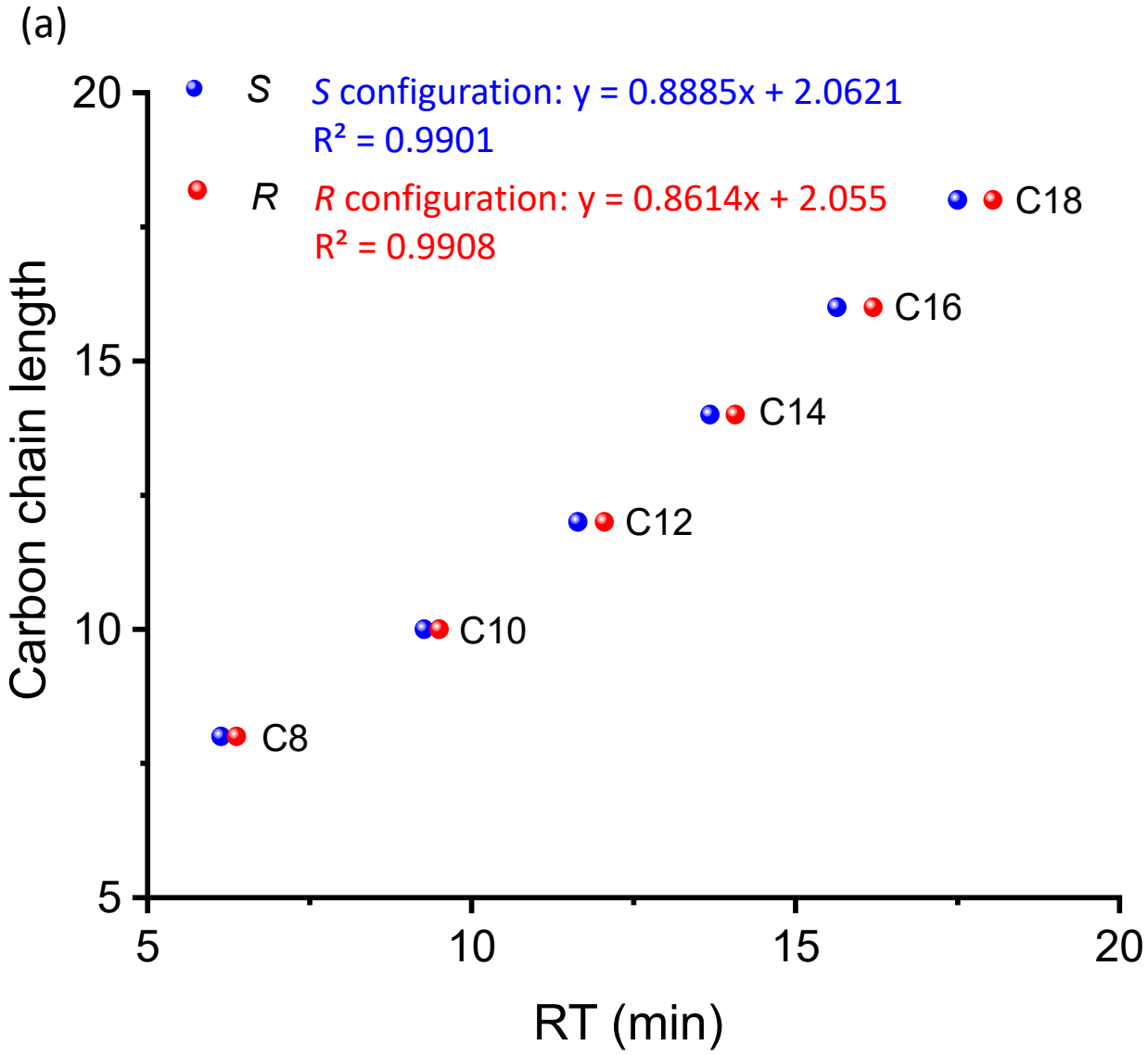

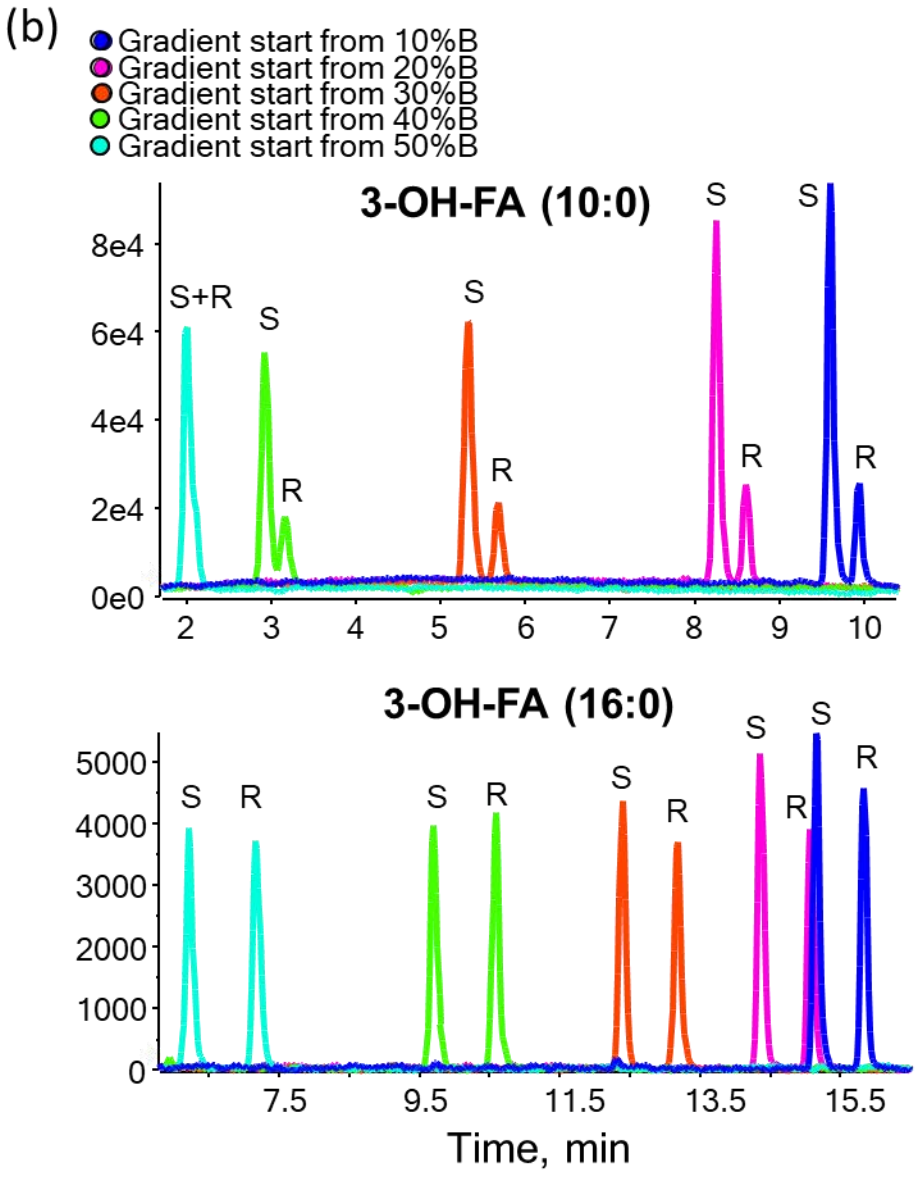

Fig. S2. *(a) Regression analysis of the retention time against the chain length (C8-C18) of saturated 3-OH-FA (DB number = 0) on Chiralpak IA-U. (b) Comparison of EICs of 3-OH-FA (10:0) and 3-OH-FA (16:0) (50 ng/mL standard mixtures spiked in plasma matrix) under different LC gradients (Gradient started from 10, 20, 30, 40 and 50% B, respectively).*

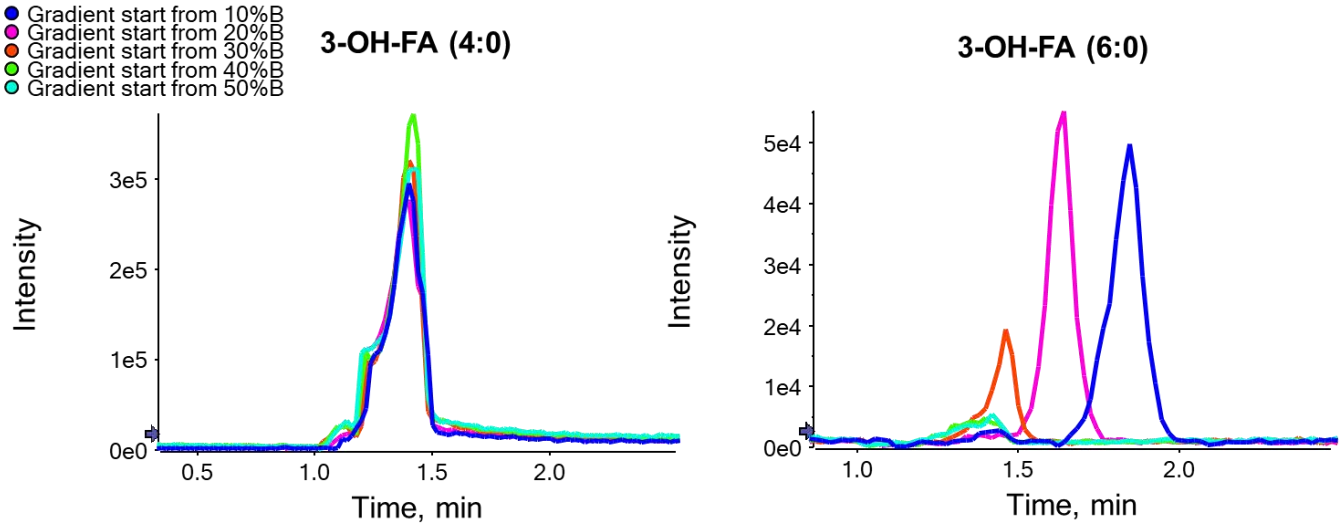

Fig. S3. *EICs of 3-OH-FA (4:0) and 3-OH-FA (6:0) under different LC conditions in pooled plasma sample. Conditions corresponding to Fig. S2b. No enantiomer separation could be achieved for this short-chain and medium chain 3-OH-FAs due to insufficient retention (t_0=1.45 min).*

4. Wash step

A wash step was incorporated after every 6 injections (5 samples+1 QC sample) in the analytical batch with mobile phase B2 (80% IPA and 20% ACN with 0.1% acetic acid) having strong elution ability in order to wash out the apolar lipid classes like CE and TG (Fig. S4). After each wash step, 2 blank injections were added to re-equilibrate the column with the same LC conditions as for samples. The batch design can be found in Table S3.

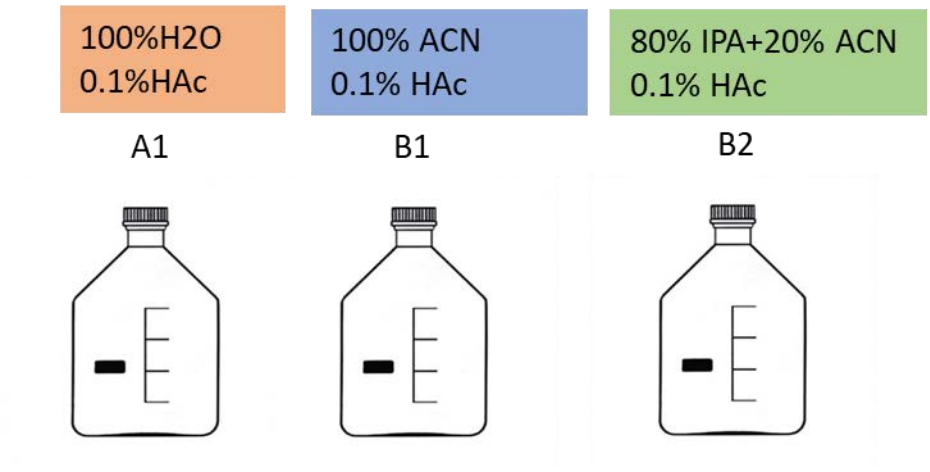

Experimental LC conditions

T(min)	A1(%)	B1(%)
0	90	10
20	0	100
22	0	100
22.01	90	10
25	90	10

Wash LC conditions

T(min)	A1(%)	B2(%)
0	90	10
5	0	100
25	0	100

Fig. S4. *Design for wash step and the mobile phase composition along with the LC conditions. For the wash step, the flow rate was 0.4 mL/min, column temperature was 40*°C with injection volume of MeOH 10 µL.

Table. S3 Analytical batch design with wash step

Injection order	Samples	Method
1	blank1	Experimental LC conditions
2	blank2	Experimental LC conditions
3	SST1	Experimental LC conditions
4	SST2	Experimental LC conditions
5	SST3	Experimental LC conditions
6	Cal0	Experimental LC conditions
7	Cal1	Experimental LC conditions
8	Cal2	Experimental LC conditions
9	Cal3	Experimental LC conditions
10	Cal4	Experimental LC conditions
11	Cal5	Experimental LC conditions
12	Cal6	Experimental LC conditions
13	Cal7	Experimental LC conditions
14	MeOH wash 1	Wash conditions
15	Equilibration 1	Experimental LC conditions
16	Equilibration 2	Experimental LC conditions
17	QC1	Experimental LC conditions
18	sample1	Experimental LC conditions
19	sample2	Experimental LC conditions
20	sample3	Experimental LC conditions
21	sample4	Experimental LC conditions
22	sample5	Experimental LC conditions
23	MeOH wash 2	Wash conditions
24	Equilibration 3	Experimental LC conditions
25	Equilibration 4	Experimental LC conditions
26	QC2	Experimental LC conditions
27	sample6	Experimental LC conditions
28	sample7	Experimental LC conditions
29	sample8	Experimental LC conditions
30	sample9	Experimental LC conditions
31	sample10	Experimental LC conditions
32	MeOH wash 3	Wash conditions
33	Equilibration 5	Experimental LC conditions
34	Equilibration 6	Experimental LC conditions
35	QCn	Experimental LC conditions
36	Cal0	Experimental LC conditions
37	Cal1	Experimental LC conditions
38	Cal2	Experimental LC conditions
39	Cal3	Experimental LC conditions
40	Cal4	Experimental LC conditions

41	Cal5	Experimental LC conditions
42	Cal6	Experimental LC conditions
43	Cal7	Experimental LC conditions
44	MeOH wash n	Wash conditions
45	Equilibration n	Experimental LC conditions
46	Equilibration n+1	Experimental LC conditions

SST (system suitability test): three injections of neat standard solution at the beginning

Equilibration: Injection of 10 µL MeOH and running a blank gradient to equilibrate the column

MeOH wash: injection of 10 µL MeOH and running wash conditions to avoid accumulation of apolar lipids.

5. Validation

Table. S4 Extraction recovery (RE%), matrix effect (ME%) and process efficiency (PE%) on 3 QC levels (in plasma)

	3-OH-FA (8:0)		3-OH-FA (10:0)		3-OH-FA (12:0)		3-OH-FA (14:0)		3-OH-FA (16:0)		3-OH-FA (18:0)	
RE (%)	***S***	***R***	***S***	***R***	***S***	***R***	***S***	***R***	***S***	***R***	***S***	***R***
L	92.7	94.7	93.5	92.7	98.2	91.1	83.2	91.3	93.9	95.0	85.9	97.4
M	103.4	101.3	99.8	95.2	103.9	95.9	90.9	97.5	89.9	91.5	86.6	89.3
H	97.0	94.9	92.8	91.5	97.9	94.2	85.7	88.2	84.5	86.1	87.2	84.1
ME (%)												
L	85.4	84.7	75.6	65.2	74.1	94.6	60.1	52.5	66.6	64.7	63.6	71.2
M	42.6	72.3	88.2	81.1	55.6	81.9	65.6	80.4	72.3	63.3	53.3	60.0
H	107.0	109.1	88.9	92.2	72.3	81.0	62.4	60.8	45.8	41.7	41.8	37.8
PE (%)												
L	79.1	80.2	70.7	60.4	72.8	86.2	50.0	47.9	62.5	61.5	54.6	69.4
M	44.0	73.3	88.0	77.2	57.8	78.6	59.7	78.4	65.0	57.9	46.1	53.6
H	103.8	103.6	82.5	84.4	70.7	76.3	53.5	53.6	38.5	35.9	36.5	31.8

Table. S5 Concentration-response relationship for matrix-matched calibration curve (plasma) and neat solution calibration curve on all three days

Day 1								
Name	**IS used**	**Enantiomer**	**standard addition method**			**neat solution calibration**		
			slope	**intercept**	**R^2**	**slope**	**intercept**	**R^2**
3-OH-FA (8:0)	RvD1 d5	S	0.0056	0.1542	0.984	0.0013	0.00148	0.998
		R	0.0062	-0.0826	0.996	0.0015	0.00193	0.999
3-OH-FA (10:0)	RvD1 d5	S	0.0468	-0.1006	0.997	0.0107	0.00433	0.988
		R	0.0474	-0.0620	0.997	0.0126	0.00524	0.998
3-OH-FA (12:0)	RvD1 d5	S	0.0263	-0.0655	0.999	0.0079	0.00143	0.998
		R	0.0274	-0.0047	>0.999	0.0080	0.00021	>0.999
3-OH-FA (14:0)	12 HETE d8	R	0.0306	-0.0120	0.999	0.0268	0.00314	>0.999
3-OH-FA (16:0)	AA d11	S	0.0089	0.0001	0.999	0.0083	0.00235	>0.999
		R	0.0089	0.0016	0.999	0.0084	0.0016	0.998
3-OH-FA (18:0)	AA d11	S	0.0029	0.0079	0.998	0.0032	0.0011	0.996
		R	0.0028	-0.0226	0.999	0.0034	0.0013	0.996
Day 2								
Name	**IS used**	**Enantiomer**	**standard addition method**			**neat solution calibration**		
			slope	**intercept**	**R^2**	**slope**	**intercept**	**R^2**
3-OH-FA (8:0)	RvD1 d5	S	0.0061	-0.1809	0.999	0.0013	0.0015	0.998
		R	0.0068	-0.0764	0.991	0.0015	0.0024	0.970
3-OH-FA (10:0)	RvD1 d5	S	0.0464	-0.0122	0.999	0.0107	0.0043	0.988
		R	0.0509	0.0414	0.999	0.0126	0.0032	0.998
3-OH-FA (12:0)	RvD1 d5	S	0.0266	-0.0618	0.999	0.0079	0.0015	0.998
		R	0.0272	-0.0090	>0.999	0.0084	-0.0010	>0.999
3-OH-FA (14:0)	12 HETE d8	R	0.0309	0.0015	0.992	0.0268	0.0031	>0.999
3-OH-FA (16:0)	AA d11	S	0.0097	0.0057	0.999	0.0083	0.0016	>0.999
		R	0.0089	0.0023	0.999	0.0084	0.0015	0.998
3-OH-FA (18:0)	AA d11	S	0.0031	0.0070	0.999	0.0032	0.0011	0.997
		R	0.0029	-0.0133	0.999	0.0033	0.0011	0.996
Day 3								
Name	**IS used**	**Enantiomer**	**standard addition method**			**neat solution calibration**		
			slope	**intercept**	**R^2**	**slope**	**intercept**	**R^2**
3-OH-FA (8:0)	RvD1 d5	S	0.0058	0.0674	0.999	0.0013	0.0015	0.998
		R	0.0060	-0.0038	0.999	0.0015	0.0019	0.999
3-OH-FA (10:0)	RvD1 d5	S	0.0441	0.0426	0.999	0.0108	0.0024	>0.999
		R	0.0471	0.0414	0.999	0.0126	0.0032	0.998
3-OH-FA (12:0)	RvD1 d5	S	0.0261	-0.0514	0.999	0.0079	0.0015	0.998
		R	0.0279	-0.0086	>0.999	0.0084	-0.0006	>0.999
3-OH-FA (14:0)	12 HETE d8	R	0.0242	-0.0127	0.995	0.0268	0.0039	0.999
3-OH-FA (16:0)	AA d11	S	0.0097	0.0014	0.999	0.0083	0.0016	0.999
		R	0.0096	0.0036	0.998	0.0084	0.0015	0.998

3-OH-FA (18:0)	AA d11	S	0.0028	0.0005	>0.999	0.0032	0.0011	0.997
		R	0.0029	-0.0168	0.999	0.0033	0.0011	0.996

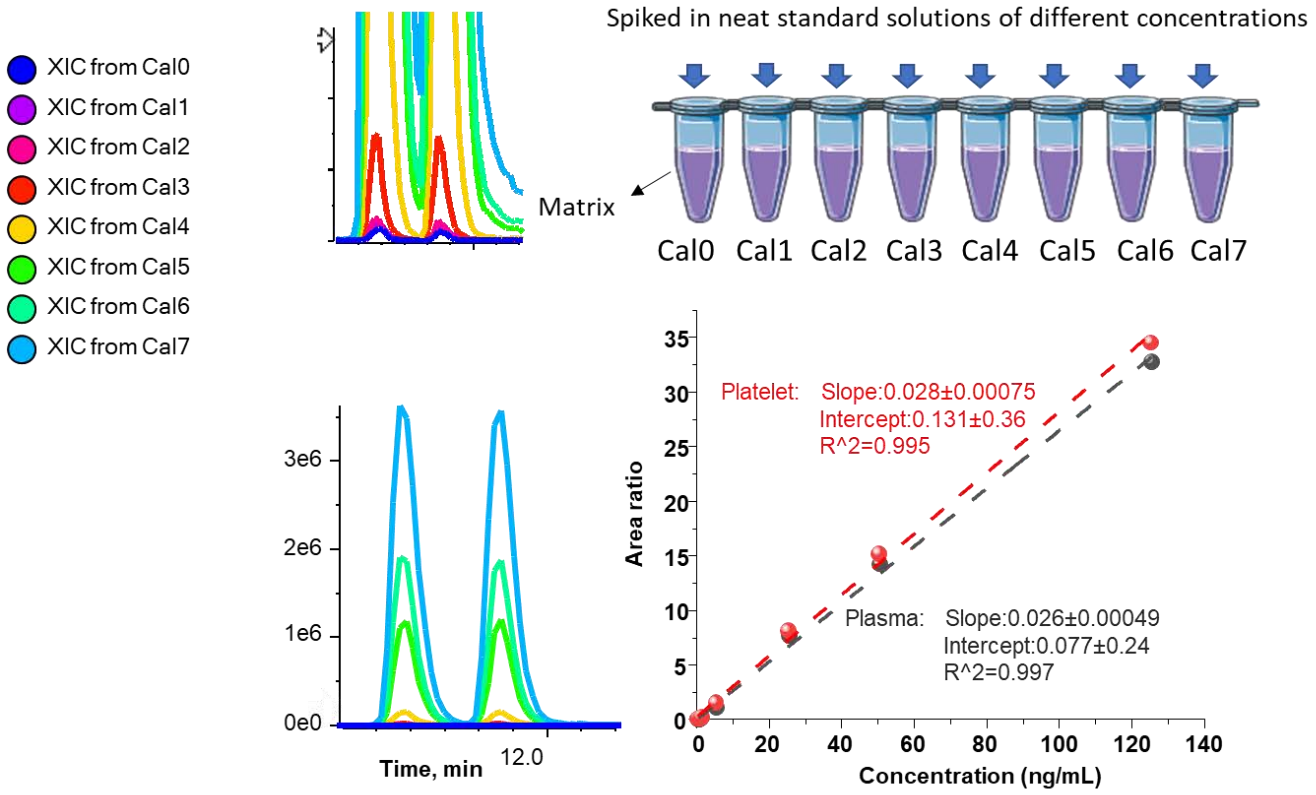

Fig. S5. *(a) EIC of 3-OH-FA (12:0) of 7 calibrants in plasma matrix. (b) Standard addition method for matrix-matched calibration. (c) Calibration curve of (S)-3-OH-FA (12:0) in plasma and platelet matrix. Area ratio is the peak area ratio of analytes to corresponding IS.*

6. Results for plasma and platelet

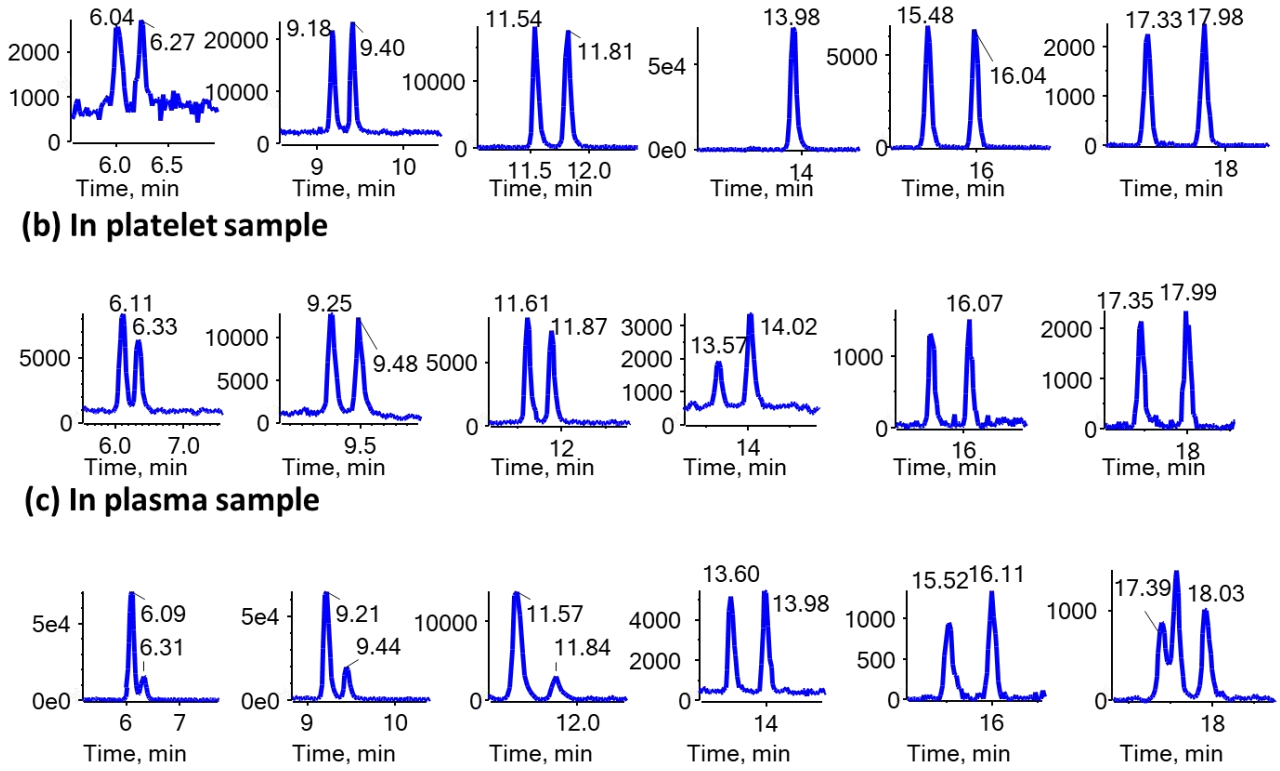

Fig. S6. *Exemplary chromatograms (EICs) of 3-OH-FAs in neat standard solution (2 ng/mL for each enantiomer except (R)-3-OH-FA (14:0) with 4 ng/mL), in extracted plasma and in extracted platelet samples.*

7. The 3-OH-FAs with carbon length C20 and more

In order to figure out whether the non-detectable 3-OH-FA C20 and more is caused by the weak LC elution condition or they are not existing in human plasma and platelets, a strong elution condition (Fiehn method [1]) was used to check the possibility. The chromatographic separation was performed on ACQUITY UPLC CSH C18 column (100 mm × 2.1 mm; particles: 1.7 µm; Waters Corporation, Millford, MA, USA) with precolumn (5 mm x 2.1 mm; 1.7 µm particles). The column temperature was 65°C and the flow rate 0.6 mL/min. Mobile phase A was composed of H_2O/ACN 2:3 (v/v) containing 10 mM ammonium formate and 0.1% formic acid (v/v) while mobile phase B was IPA/ACN/H_2O 90:9:1 (v/v/v) containing 10 mM ammonium formate and 0.1% FA (v/v) [1]. First of all, a targeted MRM scan was applied on Triple quadruple based on the C18 column since a chiral separation is not necessary in this case. The results can be found in Fig. S7. It can be seen from Fig. S7a that from C4-C18 the eluted peaks follow the retention pattern that in accordance to the longer carbon chain length, the retention time is longer. A peak of C20 can be detected, however, it doesn't fit the retention model (Fig. S7b). In order to figure out the structure of this compound, a HR-MRM with QToF was applied. After carefully checking the MS/MS spectrum, the peak might be 2-OH-FAs. According to the reference [2], a neutral loss of 46.0049 Da can be unique for 2-OH-FAs. Possible fragmentation pathways for 2-OH-FA (20:0) was shown in Fig. S7c. In this case, a conclusion can be made that with carbon length longer than 20, there are no peaks of 3-OH-FAs detectable, which verified our hypothesis that 3-OH-FAs with C20 and more are not existing above their LOD in human plasma and platelets.

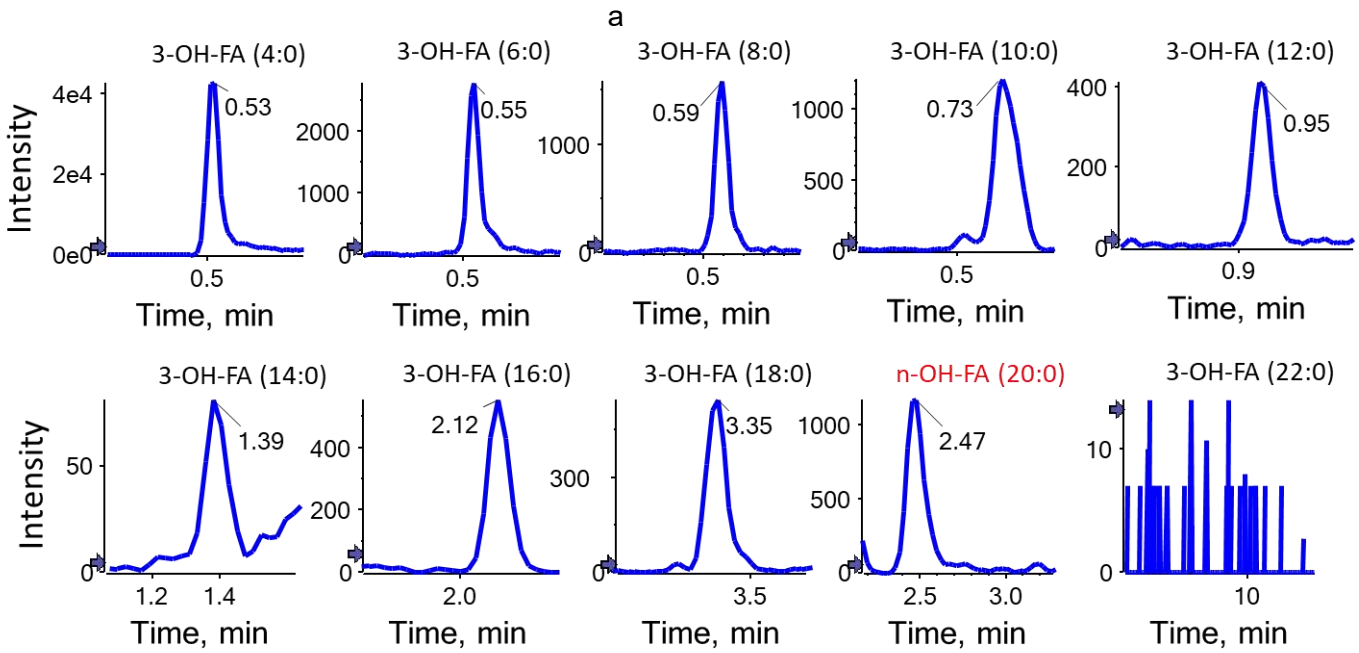

b

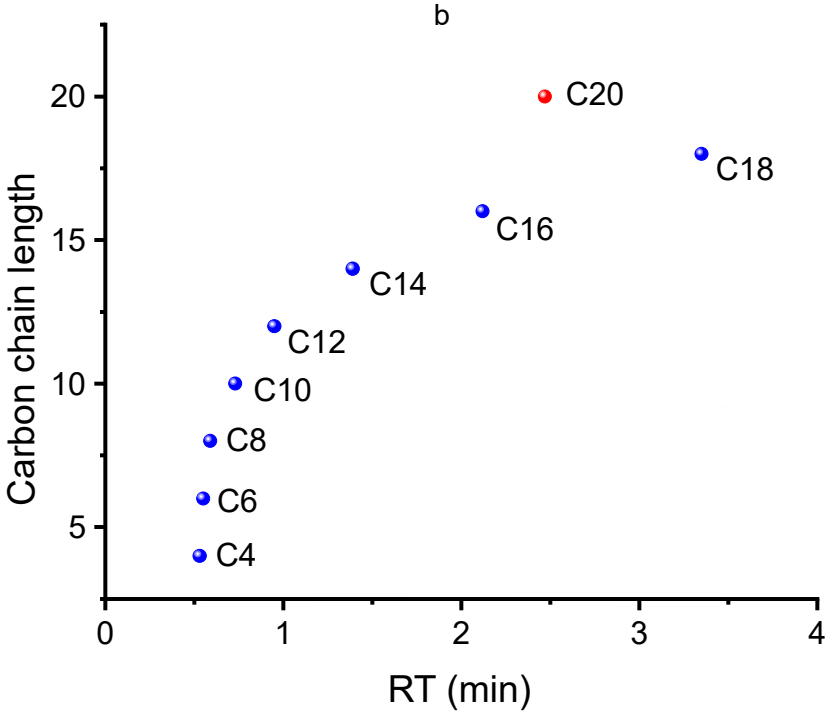

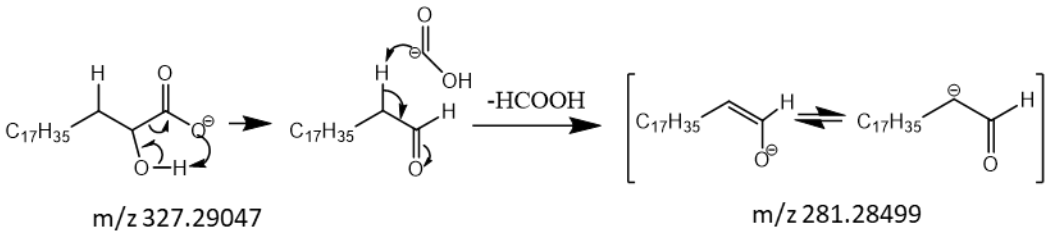

m/z 327.29047

m/z 281.28499

C

2-OH-FA (20:0)

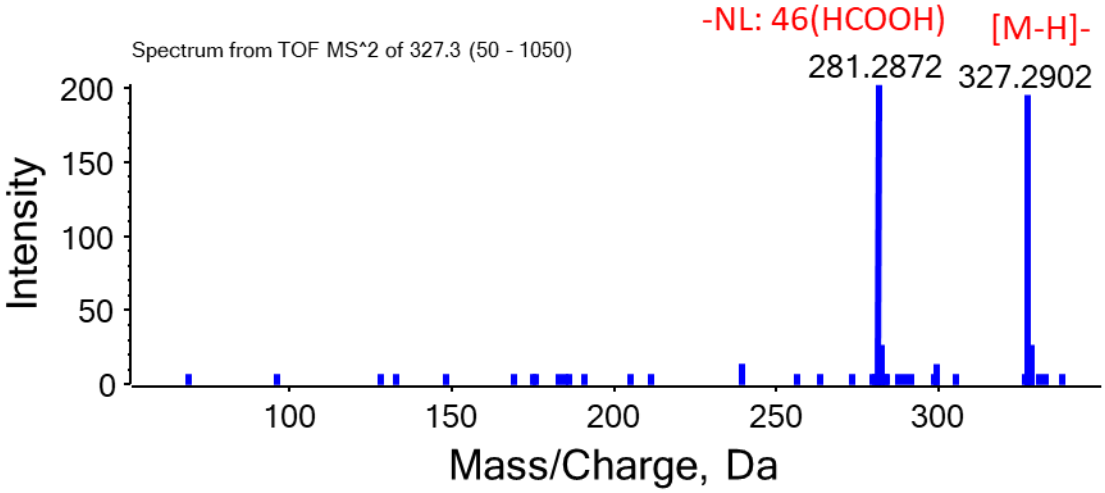

Fig. S7. *(a) EIC of 3-OH-FAs with Fiehn method (LC conditions; ref [1]) in MRM scan mode using Triple quadruple. (b) Estimation model of the retention time against the chain length (C4-C20) of 3-OH-FA (DB number = 0) with RPLC (Fiehn method). The RT is not linearly correlated to carbon number because of the LC gradient and early elution of the short chain 3-OH-FAs. (c) CID fragmentation pathway of 2-OH-FA (20:0) and MS/MS spectrum of 2-OH-FA (20:0) in plasma with HR-MRM scan mode by QTOF MS.*

Reference

[1] H. Tsugawa, T. Cajka, T. Kind, Y. Ma, B. Higgins, K. Ikeda, M. Kanazawa, J. VanderGheynst, O. Fiehn, M. Arita, MS-DIAL: data-independent MS/MS deconvolution for comprehensive metabolome analysis, Nat Methods 12(6) (2015) 523-6.
[2] J. Li, J. Xu, R. Zhang, Y. Hao, J. He, Y. Chen, G. Jiao, Z. Abliz, Strategy for Global Profiling and Identification of 2- and 3-Hydroxy Fatty Acids in Plasma by UPLC–MS/MS, Analytical Chemistry 92(7) (2020) 5143-5151.

1.3 Publication III

Profiling of branched chain and straight chain saturated fatty acids by ultra-high performance liquid chromatography-mass spectrometry

Xiaoqing Fu[a], Nourhane Hafza[b], Friedrich Götz[b], Michael Lämmerhofer[a]*

[a] University of Tübingen, Institute of Pharmaceutical Sciences, Pharmaceutical (Bio-)Analysis, Auf der Morgenstelle 8, 72076 Tübingen, Germany
[b]University of Tübingen, Interfaculty Institute for Microbiology and Infection-Medicine Tübingen, Microbial Genetics, Auf der Morgenstelle 28, 72076 Tübingen, Germany

Reprinted with permission from Journal of Chromatography A, Volume 1703, 16 August 2023, 464111

https://doi.org/10.1016/j.chroma.2023.464111

Journal of Chromatography A 1703 (2023) 464111

Contents lists available at ScienceDirect

Journal of Chromatography A

journal homepage: www.elsevier.com/locate/chroma

Profiling of branched chain and straight chain saturated fatty acids by ultra-high performance liquid chromatography-mass spectrometry ☆

Xiaoqing Fu [a], Nourhane Hafza [b], Friedrich Götz [b], Michael Lämmerhofer [a,*]

[a] University of Tübingen, Institute of Pharmaceutical Sciences, Pharmaceutical (Bio-)Analysis, Auf der Morgenstelle 8, Tübingen 72076, Germany
[b] University of Tübingen, Interfaculty Institute for Microbiology and Infection-Medicine Tübingen, Microbial Genetics, Auf der Morgenstelle 28, Tübingen 72076, Germany

ARTICLE INFO

Article history:
Received 6 April 2023
Revised 24 May 2023
Accepted 26 May 2023
Available online 26 May 2023

Keywords:
Lipidomics
Microbiome
Staphylococcus aureus
Bacterial fatty acids
Isomer

ABSTRACT

Branched chain fatty acids (BCFAs) are one of the important sub categories of fatty acids (FAs) which have unique functions in nature. They are commonly analyzed by GC–MS after derivatization to methyl esters (FAMEs). On the other hand, there is a lack of isomer-selective LC-MS methods which allow the distinction of different isomers with wide coverage of carbon chain length. In this work, a systematic retention and isomer selectivity study on seven commercially available UHPLC columns (six polysaccharide columns Chiralpak IA-U, IB-U, IC-U, ID-U, IG-U and IH-U; one Acquity UPLC CSH C18 column) was performed. Various experimental factors were evaluated including column temperatures, gradient profiles and flow rates to elucidate their effects on the separation ability of homologous series of BCFAs with distinct chain lengths, different branching types and branching positions. In general, IG-U outperformed the other columns in terms of isomer selectivity especially for the short and medium-chain BCFA isomers while RP C18 showed good potential in terms of selectivity for long-chain BCFA isomers. Furthermore, after the evaluation of the chromatographic retention pattern on the various columns and method optimization, we report a methodology for untargeted isomer-selective BCFA profiling without precolumn derivatization with UHPLC-ESI-MS/MS by quadrupole-time-of-flight instrument with SWATH acquisition. The best method provides selectivity for constitutional isomers of BCFAs covering distinct chain length (C5-C20) with different branching types (methyl or ethyl) and branching positions (2Me, 3Me, 4Me, 6Me, *anteiso* and *iso*-BCFAs) with an optimized LC condition on Acquity UPLC CSH C18 column. Finally, the optimized method was applied for the BCFAs profiling in lipid extracts of *Staphylococcus aureus* samples. Besides, pooled human platelets and pooled human plasma were evaluated as mammalian samples for presence of BCFAs as well. The new method showed strong potential for BCFA profiling in bacterial samples including different isomers *anteiso* and *iso*-BCFAs, which could be a useful tool for related subdisciplines in metabolomics and lipidomics in particular in combination with electron-activated dissociation MS. Compared to GC, the presented isomer selective LC methods can be also of great utility for preparative purposes. Equivalent (carbon) chain length numbers were calculated for RP18 and Chiralpak IG-U and compared to those of FAMEs obtained by GC.

1. Introduction

As a physiologically important class of molecules and essential building blocks, fatty acids (FAs) play an important role in energy storage, membrane structure, and various signaling pathways [1]. FAs can be classified into straight chain (SCFAs) and branched chain fatty acids (BCFAs) which have their unique functions in nature. Generally, de novo SCFAs synthesis in microorganisms and mammals starts from acetyl-CoA and malonyl-CoA that leads to the synthesis of even-chain FAs (see Fig. 1a). For odd-chain FAs, however, propionyl-CoA is required as precursor instead of acetyl-CoA in order to synthesize odd-chain FAs (see Fig. 1b) [2]. BCFAs are commonly saturated FAs substituted with one (mono-) or more (di-/oligo-) methyl-branch(es) (e.g. phytanic and pristanic acid) on the carbon chain. The monomethyl BCFAs have often either an *iso* structure where the branching point is on the penultimate carbon atom (i.e., one from the end) or an *anteiso* structure where the branching point is located on the antepenultimate carbon atom (i.e., two from the end). These monomethyl BCFAs are typically derived from branched chain amino acids (BCAAs) including valine, leucine, and isoleucine [3]. In the common biosynthetic pathways, the BCAAs are firstly transaminated to α-ketoacids and then de-

☆ http://www.bioanalysis.uni-tuebingen.de/

* Corresponding author.
E-mail address: michael.laemmerhofer@uni-tuebingen.de (M. Lämmerhofer).

https://doi.org/10.1016/j.chroma.2023.464111
0021-9673/

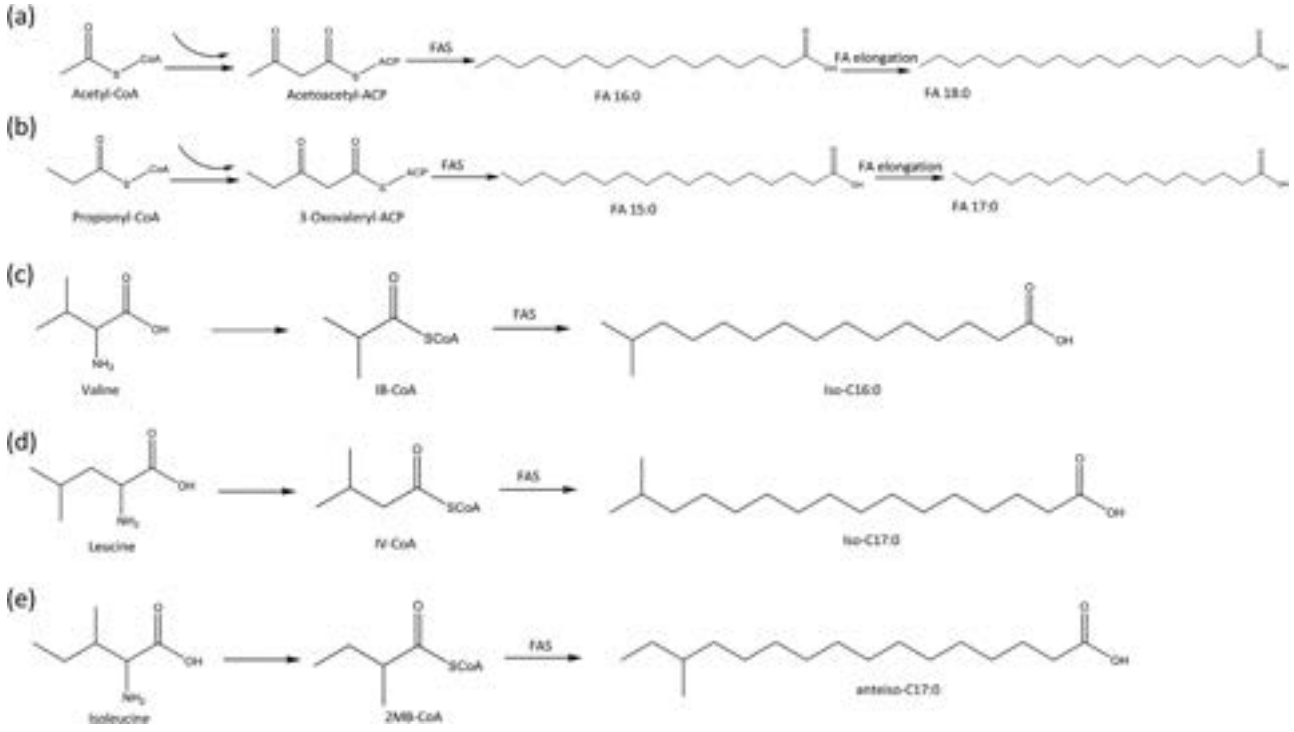

Fig. 1. Common pathways for the synthesis of (a) even straight chain fatty acids, (b) odd-chain fatty acids, (c) branched even chain fatty acids, (d) branched odd chain fatty acids with iso configuration, and (e) branched odd chain fatty acids with anteiso configuration.

carboxylated into branched short-chain carboxylic acids and finally the products are elongated by BCFA synthetase, with malonyl-CoA as the chain extender, to form the *iso*- and *anteiso*-BCFAs [3,4]. The *iso*-BCFAs with even chain length (total carbon number), for example *iso*-16:0 and *iso*-18:0, are derived from valine (see Fig. 1c) while those with odd chain length (*iso*-15:0, *iso*-17:0) from leucine (see Fig. 1d). In contrast, *anteiso*-BCFAs are derived from isoleucine (see Fig. 1e). In addition to these most common *iso* and *anteiso* methyl-positions, some other methyl-positions were also found in nature, for example 10-methyl-hexadecanoic acid (FA 16:0;10Me), 11-methyl-octadecanoic acid (FA 18:0;11Me) in the sponge *Verongia aerophoba* [5]. Furthermore, 2-, 3-, 4-, and 6-monomethyl-FAs from C7-C12 were the main BCFAs components in the preen gland of the fulmar [6]. The biosynthesis of these kinds of BCFAs remain to a large extent unknown, but most probably the structures were produced by methylmalonyl-CoA instead of malonyl-CoA for the elongation of the fatty acyl chain resulting in the insertion of a methyl branch in the chain.

BCFAs are the common constituents of the microbial lipids present in abundant quantities. In bacteria, BCFAs in membrane are utilized to increase the fluidity and lower the phase transition temperature of the lipid components. Besides, they can also be found in animals including mammals although in much lower amount. In humans, BCFAs have been detected in various tissues (like adipose tissue [7] and biofilm covering the skin of the fetus [8]) and biofluids (milk [9] and serum [10]) which are proven to be associated with energy homeostasis and insulin sensitivity in human body. In general, the analysis of BCFAs is of importance and is attracting more and more attention of researchers in different research areas including microbiology, food chemistry and clinical perspectives due to their biological effects and potential pro-health benefits thus belonging to the group of bioactive FAs. Traditionally, they have been analyzed as fatty acid methyl esters or other derivatives (e.g. picolinyl esters) by gas chromatography (GC) coupled with mass spectrometry (GC–MS) or flame ionization detection (GC-FID), which has become a routine procedure with broad application to biochemical, biomedical and industrial research [11–17]. These GC methods focus on detailed fatty acid profiling. They are not intended for general lipidomics profiling, because many lipid classes are not volatile enough even after derivatization. Eventually, liquid chromatography coupled to mass spectrometry (LC-MS) has been also applied for FAs analysis especially in lipidomics, which usually does not involve derivatization procedures and covers a wide range of lipid classes [18–20]. In most of the cases, FAs profiling by LC-MS does not distinguish between straight chain and branched chain FAs. No efforts on the improvement of chromatographic resolution of different FAs isomers including BCFAs (methyl-BCFAs at different branching positions, *anteiso*-, *iso*-BCFAs and so on) and SFAs are usually undertaken. For this purpose, a systematic study on the chromatographic resolution of isomeric FAs on different columns including the silica-based polysaccharide chiral stationary phases (CSPs) [21,22] along with the commonly used Acquity UPLC charged surface hybrid (CSH) C18 column (RP C18) was carried out. CSPs have recently shown great potential in uncommon applications like isomer separations in lipidomics [18,23-25] and were also proven to have enantioselectivity for BCFAs in many investigations [26–30]. On the other hand, RP C18 column was frequently used for lipid profiling including FAs and also Triacylglycerols (TG) isomers with BCFAs [31].

In this study, after the evaluation of different columns and optimization of LC conditions, we report an UHPLC-MS/MS method based on RP C18 column with optimized LC conditions which allows the isomeric analysis of BCFAs with different monomethyl positions including *anteiso, iso* and other positions (2Me, 3Me, 4Me and so on). Further, the method was applied for the profiling of FAs including BCFAs in *Staphylococcus aureus* samples. As mammalian samples human platelets and human plasma pools were analyzed as well for evaluating assay specificity when unsaturated FAs are present. The method was proven to be capable for BCFAs profiling in bacterial samples with good selectivity for isomeric FAs especially for saturated monomethyl-BCFAs.

2. Materials and methods

2.1. Materials

The standards 2-methyl-butanoic acid (FA 4:0;2Me), 3-methyl-butanoic acid (FA 4:0;3Me), pentanoic acid (FA 5:0), 3-methyl-pentanoic acid (FA 5:0;3Me), 4-methyl-pentanoic acid (FA 5:0;4Me), hexanoic acid (FA 6:0), 2-methyl-hexanoic acid (FA 6:0;2Me), 4-methyl-hexanoic acid (FA 6:0;4Me), heptanoic acid (FA 7:0), octanoic acid (FA 8:0), 7-methyl-octanoic acid (FA 8:0;7Me), nonanoic acid (FA 9:0), 2-ethyl-octanoic acid (FA 8:0;2Et), 4-ethyl-octanoic acid (FA 8:0;4Et), decanoic acid (FA 10:0), undecanoic acid (FA 11:0), dodecanoic acid (FA 12:0), tridecanoic acid (FA 13:0), tetradecanoic acid (FA 14:0), 12-methyl-tetradecanoic acid (FA 14:0;12Me), 13-methyl-tetradecanoic acid (FA 14:0;13Me), pentadecanoic acid (FA 15:0), hexadecanoic acid (FA 16:0), heptadecanoic acid (FA 17:0), octadecanoic acid (FA 18:0), nonadecanoic acid (FA 19:0), eicosanoic acid (FA 20:0) were obtained from Sigma Aldrich (Merck, Taufkirchen, Germany). The standards 2-ethyl-hexanoic acid (FA 6:0;2Et), 2-methyl-pentanoic acid (FA 5:0;2Me) and 4-methyl-octanoic acid (FA 8:0;4Me) were purchased from Tokyo Chemical (Toshima, Tokyo, Japan). The standards 8-methyl-decanoic acid (FA 10:0;8Me) and 6-methyl-heptanoic acid (FA 7:0;6Me) were obtained from BLD Pharmatech (Kaiserslautern, Germany) and 6-methyl-octanoic acid (FA 8:0;6Me) was from SIA Chemspace (Riga, Latvia) (see Table 1).

Table 1
Components of the complex standard mixture of isomeric saturated fatty acids.

Standards	Carbon length (total carbon number)
FA4:0;2Me	C5
FA4:0;3Me	C5
FA5:0	C5
FA5:0;2Me	C6
FA5:0;3Me	C6
FA5:0;4Me	C6
FA6:0	C6
FA6:0;2Me	C7
FA6:0;4Me	C7
FA7:0	C7
FA6:0;2Et	C8
FA7:0;6Me	C8
FA8:0	C8
FA8:0;4Me	C9
FA8:0;6Me	C9
FA8:0;7Me	C9
FA9:0	C9
FA8:0;2Et	C10
FA8:0;4Et	C10
FA10:0	C10
FA10:0;8Me	C11
FA11:0	C11
FA14:0	C14
FA15:0	C15
FA14:0;12Me	C15
FA14:0;13Me	C15
FA16:0	C16
FA17:0	C17
FA18:0	C18
FA19:0	C19
FA20:0	C20

The internal standard (arachidonic acid, AA-d11) was purchased from Avanti Polar Lipids (Alabaster, AL, USA). LC-MS grade acetonitrile (ACN), methanol (MeOH), and isopropanol (IPA) were purchased from Carl Roth (Karlsruhe, Germany). Acetic acid (HAc) was purchased from Sigma-Aldrich (Merck). Water purification was achieved by a Purelab Ultra purification system from Elga LabWater (Celle, Germany).

The chromatographic separation was performed on chiral columns (Chiralpak IA-U, IB-U, IC-U, ID-U, IG-U and IH-U) from Daicel (Osaka/Tokyo, Japan) which were supplied by Chiral Technologies Europe (Illkirch, France) with dimensions of 3.0 × 100 mm (i.d. x l.) and 1.6 µm fully porous particles or Acquity UPLC CSH C18 column (RP C18, 100 mm × 2.1 mm; fully porous particles: 1.7 μm, 130 Å; Waters Corporation, Millford, MA, USA) with precolumn (5 mm x 2.1 mm; 1.7 μm particles).

2.2. Instrumentation

The vortex mixer was from neoLab (Heidelberg, Germany); the ultrasonic bath was purchased from Bandelin (Berlin, Germany); the EZ2 evaporator was from GeneVac (Ipswich, UK) and the homogenizer was from Precellys® evolution (Bertin, Frankfurt am Main, Germany).

The lipid extracts were analyzed with an Agilent 1290 Infinity UHPLC system (Agilent, Waldbronn, Germany) equipped with a binary pump, a PAL-HTX xt DLW autosampler (CTC Analytics AG, Switzerland) and coupled to a SCIEX TripleTOF 5600+ QTOF mass spectrometer with a DuoSpray Source (SCIEX, Concord, Ontario, Canada).

2.3. Sample preparation

2.3.1. Preparation of complex fatty acid mixture

A complex fatty acid standard mixture including 31 saturated BCFAs and SCFAs (FA 4:0;2Me, FA 4:0;3Me, FA 5:0;2Me, FA 5:0;3Me, FA 5:0;4Me, FA 6:0;2Me, FA 6:0;4Me, FA 6:0;2Et, FA 7:0;6Me, FA 8:0;4Me, FA 8:0;6Me, FA 8:0;7Me, FA 8:0;2Et, FA 8:0;4Et, FA 10:0;8Me, FA 14:0;12Me, FA 14:0;13Me, FA 5:0, FA 6:0, FA 7:0, FA 8:0, FA 9:0, FA 10:0, FA 11:0, FA 14:0, FA 15:0, FA 16:0, FA 17:0, FA 18:0, FA 19:0 and FA 20:0) was prepared in MeOH with a concentration of each standard of 500 ng/mL. The components of the mixture and employed notation can be found in Table 1.

2.3.2. Collection of samples

Overnight bacterial preculture of *Staphylococcus aureus* strain USA300 JE2 was used to prepare a fresh bacterial culture in tryptic soy broth (casein peptone 17 g/L, dipotassium hydrogen phosphate 2.5 g/L, glucose 2.5 g/L, sodium chloride 5 g/L, soya peptone 3 g/L) with initial OD_{578nm}=0.1. The culture was incubated at 37 °C under shaking until mid-exponential phase. Then, the cells were collected by centrifugation at 8000 × g, 4 °C for 10 min. The cell pellet was stored at −80 °C until use.

Platelets and plasma samples were from a previous study and were obtained from the peripheral blood of donors at the University Hospital Tübingen, according to ethical guidelines and approved by regional authorities (number 237/2018BO2). The blood was collected in acid-citrate-dextrose (ACD) buffer as anticoagulant (12.5 g sodium citrate, 546.82 g of citric acid, 10 g glucose, 500 mL distilled water, adjusted to pH 4.69 with NaOH) with 40 mL in total (ACD anticoagulant:blood 1:4, v/v) and then centrifuged (430 x g for 20 min without acceleration and deceleration). Tyrodes-HEPES buffer (2.5 mM HEPES, 150 mM NaCl, 1 mM KCl, 2.5 mM $NaHCO_3$, 0.36 mM NaH_2PO_4, 5.5 mM glucose, 1 mg/mL BSA, pH 6.5) was then added into platelet-rich plasma, mixed and centrifuged (900 x g for 10 min without acceleration and deceleration) [32]. Samples were stored at −80 °C until use.

2.3.3. Lipid extraction

Lipid extraction from *Staphylococcus* samples was performed by biphasic extraction method following Matyash's protocol [33]. *Staphylococcus* pellets (with a small amount of medium) were taken out from the −80 °C freezer and slowly thawed on ice for about 80 min until they were completely unfrozen. Internal standard AA-d11 (225 µL with a concentration of 44.4 ng/mL, final concentration in reconstitution solvent is 100 ng/mL) in MeOH (4 °C) was spiked into each sample followed by 750 μL MTBE (4 °C). Samples were vortexed for 30 s and then disrupted with Precellys evolution homogenizer (Bertin) by applying 10 cycles (x 10 s and 30 s of pause between each cycle, 6800 rpm) of cell membrane disruption using dry ice in the cooling unit and 0.1 mm diameter zirconia/glass beads. Next, 187.5 μL of H_2O was subsequently added to induce phase separation and samples were centrifuged (3500 x g, 10 min without acceleration and deceleration). The upper phase was collected into a new Eppendorf tube and the lower phase was re-extracted with the upper phase of the following mixture: MTBE/MeOH/H_2O (10:3:2.5; v/v/v). Samples were centrifuged again and the upper layer from the 2nd extraction was combined with the upper layer from the 1st extraction. The combined upper layer was then dried with an EZ2 evaporator from GeneVac (Ipswich, UK) under nitrogen protection. The residues were reconstituted in 100 µL of MeOH, vortexed (10 s), sonicated (2 min), and centrifuged (3500 x g, 10 min). Ten µL from each sample were collected and pooled together as quality control (QC) sample and the remaining lipid extracts were transferred into HPLC vials and stored at −20 °C until analysis. Meanwhile, spiked QC samples were prepared by mixing the pooled QC of *Staphylococcus* with complex fatty acid mixtures (see Section 2.3.1, 1:1; v/v). For lipid extraction of plasma and platelet samples, a pooled sample from different donors was prepared. With a fixed cell count of 2×10^8 platelets, a monophasic extraction protocol using 2-propanol/water (IPA / H_2O 90:10, v/v) with 5 cycles sonication was applied. The detailed procedures can be found in reference [32]. For the lipid extraction of pooled plasma sample, a mixture of internal standards was spiked into 35 µL plasma followed by 175 µL cooled IPA for protein precipitation (2 h in 4 °C). Afterwards, the samples were centrifuged (3500 x g, 10 min) and supernatant was transferred into HPLC vials and stored at −20 °C until analysis.

It should be mentioned that the FAs extracted from different types of samples are all non-esterified FA, namely free FAs in biological samples. Experimental hydrolysis was not undertaken during the extraction procedures.

2.4. UHPLC-MS/MS method

During method optimization, the fatty acid standard mixtures were separated on different Chiralpak columns (IA-U, IB-U, IC-U, ID-U, IG-U and IH-U) and Acquity UPLC CSH C18 column at 10 °C or 40 °C with flow rate of 0.3–0.6 mL/min. Mobile phase A was composed of water containing 0.1% (v/v) acetic acid, mobile phase B of ACN containing 0.1% (v/v) acetic acid (results of other mobile phases composition can be found in Suppl. material Fig. S1). Different gradients were performed: 0 min: 10% (or 20%, 30%) B, 30 min: 100% B, 35 min: 100% B, 35.01 min: 10% (or 20%, 30%) B, 40 min: 10% (or 20%, 30%).

The lipid extracts from *Staphylococcus aureus* pellets were analyzed on RP C18 column at 10 °C with flow rate of 0.5 mL/min. Mobile phase A1 was composed of water containing 0.1% (v/v) acetic acid, mobile phase B1 of ACN containing 0.1% (v/v) acetic acid. Mobile phase B2 was obtained by mixing acetonitrile and isopropanol (2:8, v/v), containing 0.1% (v/v) acetic acid and used for a column wash step. The gradient method was started with 20% mobile phase B1 and the percentage of B1 was raised to 100% in 30 min, followed by a hold at 100% for the next 5 min, then the percentage of B1 was decreased to 20% again from 35.01 to 40 min. A wash step method with 100% B2 for 20 min was incorporated in the analytical batch after every 6th sample injection (see suppl. Material Fig. S2 and Table S1).

MS experiments were operated in negative ion mode with injection volume of 5 μL. An MS full scan experiment with mass range *m/z* 50–1250 was selected while different SWATH windows were acquired for MS/MS experiments (see suppl. Table S2). The ion source temperature was set to 350 °C with curtain gas (CUR, nitrogen), nebulizer gas (GS1, zero grade air) and heater gas (GS2, zero grade air) pressures 35 psi, 60 psi and 60 psi, respectively. The ion spray voltage was set to −4500 V. The declustering potential (DP) was adjusted to −80 V and the cycle time was always 720 ms. The collision energy (CE) and collision energy spread (CES) for each experiment are shown in Table S2. All presented data and chromatograms, respectively, were derived from the MS full scan experiment. Since the fatty acids did not fragment under selected collisional induced dissociation (CID) experiments, the MS^2 data and precursor ion chromatograms from MS^2, respectively, were used for verification only and for checking for interferences. The corresponding MS^2 chromatograms of the precursor ions from respective SWATH windows was usually of lower sensitivity.

3. Results and discussion

3.1. Preliminary tests with RP C18 column and Chiralpak IA-U column

The preliminary measurement with QC sample (from *Staphylococcus aureus* samples) was firstly carried out with RP C18 column using elution conditions commonly applied for untargeted lipidomics studies which covers all lipid classes from polar fatty acids to lipophilic triglycerides [34]. Since the acetonitrile/2-propanol-based mobile phase has strong elution ability, all the detected saturated fatty acids (SFAs) from C12 to C26 eluted within 8 min (Fig. 2a). For medium- and short-chain FAs (C<12), the elution is nearly with t_0 and they were detected with low intensity; their detection in the *Staphylococcus aureus* samples was therefore not validated. It can be seen from the *m/z* vs retention time (RT) plot (Fig. 2a) that for some SFAs, two peaks could be detected which is assumed to be the straight chain and branched chain FAs. However, from the XIC of SFA (FA 14:0 and FA 15:0 as examples in Fig. 2b) the two peaks were in most of the cases only partially resolved, which indicates that the general lipidomics method is not the perfect choice for a special focus on bacterial FAs. For this reason, we switched to Chiralpak IA-U column which is frequently used for enantioselective assays of hydroxylated FAs to check whether the selectivity for the FA isomers could be improved. Chiralpak IA-U is based on amylose tris(3,5-dimethylphenylcarbamate) which is coated and immobilized by crosslinking [35–38]. It can be used under RP-type isocratic and gradient elution conditions. The amylose backbone is helically wound and the 3,5-dimethylphenylcarbamate residues form binding clefts into which the branched chain FAs can bind isomer selectively depending on steric constraints exerted by the methyl branching position [35–38].

For IA-U column, a mobile phase of water containing 0.1% (v/v) acetic acid in channel A and ACN containing 0.1% (v/v) acetic acid in channel B was applied which has weaker elution ability compared to the above mobile phase of the general lipidomics assay with RP C18. A remarkably better selectivity for the FA isomers could be observed with the IA-U column and selected elution conditions covered FAs in the range of C5-C26. Contrary to the general lipidomics method with RP C18 and acetonitrile/2-propanol eluent, also C5-C11 FAs were additionally detected (Fig. 2c). In the *m/z* vs RT plot (Fig. 2c) and the extracted ion chromatograms (XIC) of SFA (Fig. 2d), for FAs with even carbon chain number always two peaks

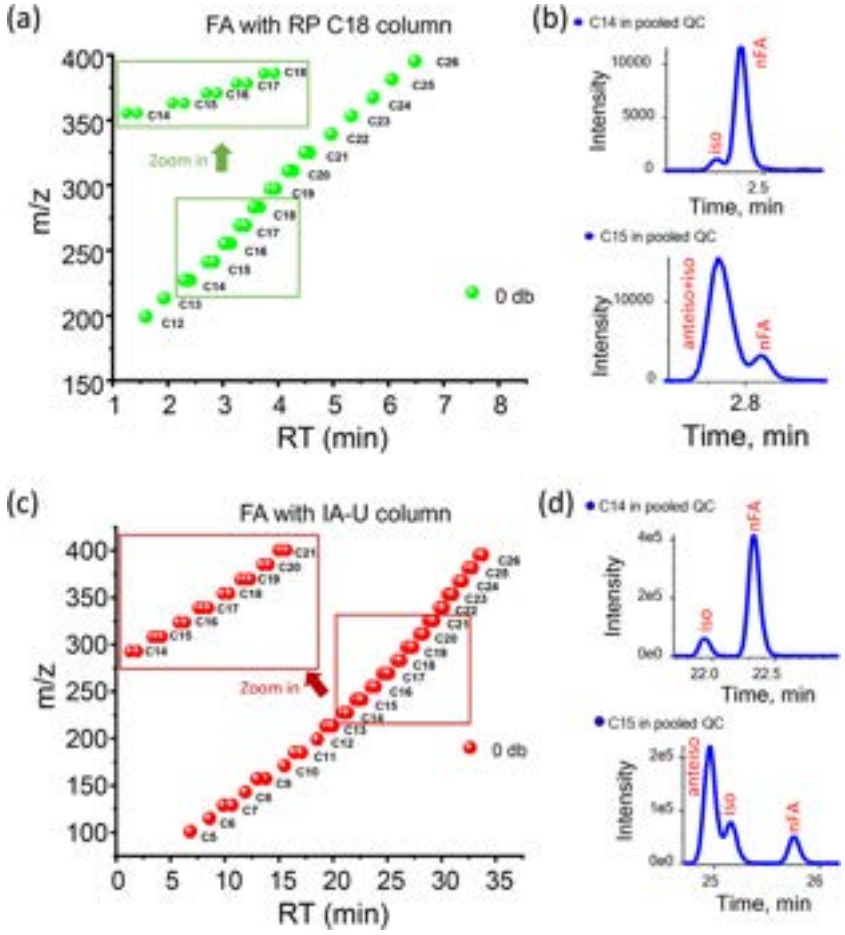

Fig. 2. Retention model by plotting *m/z* vs the retention time (RT) of saturated fatty acids (SFAs, double bond $n = 0$) in pooled quality control (QC) samples of extracts from Staphylococcus on column (a) RP C18 and (c) IA-U. Extracted ion chromatograms (XIC) of SFAs from QC samples of extracts from Staphylococcus with carbon chain length C14 and C15 on column (b) RP C18 and (d) IA-U. LC-MS method for RP C18 column: the column temperature (T) was 65 °C and the flow rate 0.6 mL/min. Mobile phase A was composed of H_2O/ACN 2:3 (v/v) containing 10 mM ammonium formate and 0.1% formic acid (v/v) while mobile phase B was IPA/ACN/H_2O 90:9:1 (v/v/v) containing 10 mM ammonium formate and 0.1% FA (v/v). The gradient refers to reference [1] and MS parameters can be found in Section 2.3. LC-MS method for IA-U column: the column temperature was 40 °C and the flow rate 0.3 mL/min. The gradient starts from 10%B and other conditions including mobile phase and MS parameters can be found in Section 2.3.

were detectable corresponding to *iso*-branched chain and straight chain FAs while for FAs with odd chain three peaks could be detected corresponding to *anteiso*- and *iso*-BCFAs and SCFAs *n*-FAs). The *iso*-BCFAs can be well separated from the SCFAs for even carbon number while the IA-U column showed also selectivity for *anteiso*- and *iso*-BCFAs (though not fully separated) as well as for BCFAs and SCFAs (fully separated).

3.2. Extension of the study

3.2.1. Column screening

From the preliminary test, we can see that the Chiralpak IA-U column has some benefits regarding selectivity for the FA isomers. In order to have an overview of a wider series of polysaccharide columns, a systematic investigation on the isomer separation ability for FA isomers for all the available sub-2 µm polysaccharide UHPLC columns (IA-U, IB-U, IC-U, ID-U, IG-U and IH-U) was carried out. These immobilized polymer stationary phases are based on distinct polysaccharide backbones, viz. amylose (IA-U, ID-U, IG-U, IH-U) and cellulose (IB-U, IC-U), as well as pendent arylcarbamate side chains with different aromatic substitutions (methyl, chloro, mixed methyl/chloro substituents). Typically, these polysaccharide columns differ by mainly two factors: i) Electronic properties control intramolecular hydrogen-bonds between adjacent carbamate groups affecting the supramolecular structure of the polymer [37] and the binding properties of analytes. It has been derived from IR spectra that electron-donating (e.g. methyl) substituents favor intramolecular hydrogen bond formation, while electron-withdrawing (e.g. chlorine) substituents have the opposite effect [39,40]. ii) Due to such supramolecular structural effects and distinct configurations of the polysaccharide backbones amylose and cellulose the binding clefts for analyte insertion spanned by three adjacent conformationally flexible aryl carbamate moieties adopt different depth, shape and size in above distinct polysaccharide phases which may lead to different intermolecular interactions of the constitutional isomers of branched chain FAs in these binding pockets [35,38]. Since the binding and molecular recognition properties of the polysaccharide phases for structural isomers of FAs are hard to predict, a screening approach was adopted herein to figure out which of these polysaccharide stationary phases shows isomer selectivity for branched-chain FAs. In a systematic study, a complex standards mixture (see Table 1) was prepared including different kinds of FA isomers (methyl-branched chain, ethyl-branched chain and straight chain) covering C5-C20 to test their isomer selectivity. In the following discussion, we may distinguish between constitutional isomer and stereoisomer (enantiomer) separations, the latter indicated with peak labels 1 and 2 for first and second eluted enantiomers.

Table 2
Resolution (Rs) of C5 isomers (between nFA5:0 and ai/iFA5:0) with different columns under different LC conditions.

Gradient (starting condition %B)	Temperature (°C)	IAU	IBU	ICU	IDU	IGU	IHU
10%	10	3.3	2.8	2.1	3.0	2.8	3.7
	40	1.7	1.7	1.7	2.2	2.0	2.9
20%	10	2.4	1.6	1.3	1.7	2.1	2.6
	40	1.0	1.0	0.9	1.2	1.2	1.2
30%	10	1.1	0.6	0.5	0.6	1.0	1.3
	40	0.4	0.3	0.6	0.3	0.7	0.7

Rs was calculated by BCFA (FA 4:0;3Me and FA 4:0;2Me coeluted as one peak) and SCFA of C5.

For each column, the LC gradient (starting from 10%, 20% and 30% B composed of ACN with 0.1% acetic acid with linear gradient to 100% B) and column temperature (10 °C and 40 °C) were investigated. On the one hand, with increasing %B as starting condition of the gradient, the selectivity for FA isomers gets worse especially for the early eluted standards C5-C7. It can be observed from Fig. S1a that for all tested columns, the selectivity for the FA isomers of C5 was worse with lower resolution between straight chain and branched-chain FAs (note, 2- and 3-methyl-branched C5 FAs are not resolved, except for IG-U which shows a partial separation for them) (Table 2). On the other hand, with increasing organic modifier the retention time of all standards were shorter, which is beneficial for the late eluted standards especially when they eluted near the end of the gradient. In general, the LC gradient starting from 10% was considered as the most appropriate method for most of the tested columns except for IA-U and IG-U on which the retention of the FA standards was a bit stronger; 20% B as starting condition was therefore favourable for IA-U and IG-U. In the case of column temperature (T), the lower the T, the better the selectivity for the FA isomers and thus Rs (Fig. S3b and resolution in Table 2). However, the better selectivity comes at expense of lower sensitivity especially for the FAs with longer carbon chain (Fig. S3b). Finally, the lower column temperature (10 °C) was chosen due to a better selectivity between BCFAs and SCFAs which is of utmost importance in our investigation.

After the optimization of the LC conditions for each tested polysaccharide column, a column comparison was made in order to determine the best column for the isomer-selective assay. For each column, the most appropriate LC conditions were applied. It is shown in Fig. 3 that ID-U and IG-U outperformed other tested columns especially for the tested FA isomers of C5, C6 and C9. IG-U provided baseline separation for the isomers of C9 between the straight-chain FA 9:0 and the BCFAs FA 8:0;7Me (*i*FA)/FA 8:0;6Me (*ai*FA). On the other hand, FA 8:0;6Me was partially separated from FA 8:0;7Me. Additionally, enantioselectivity between *R* and *S* enantiomers for FA 8:0;4Me was observed on column IG-U (indicated as peak 1 and 2 because no enantiomer standards were available). In the case of C5 FAs (Fig. S4), IG-U column was the only one that showed the selectivity for all three isomers (FA 4:0;2Me, FA 4:0;3Me and FA 5:0). On contrary, for C6 FAs (Fig. S5), all the four isomers (FA 5:0;2Me, FA 5:0;3Me, FA 5:0;4Me and FA 6:0) were separated with the ID-U column. It is worth mentioning that all the columns showed to some degree constitutional isomer selectivity. However, IG-U was unique to give enantioselectivity for some

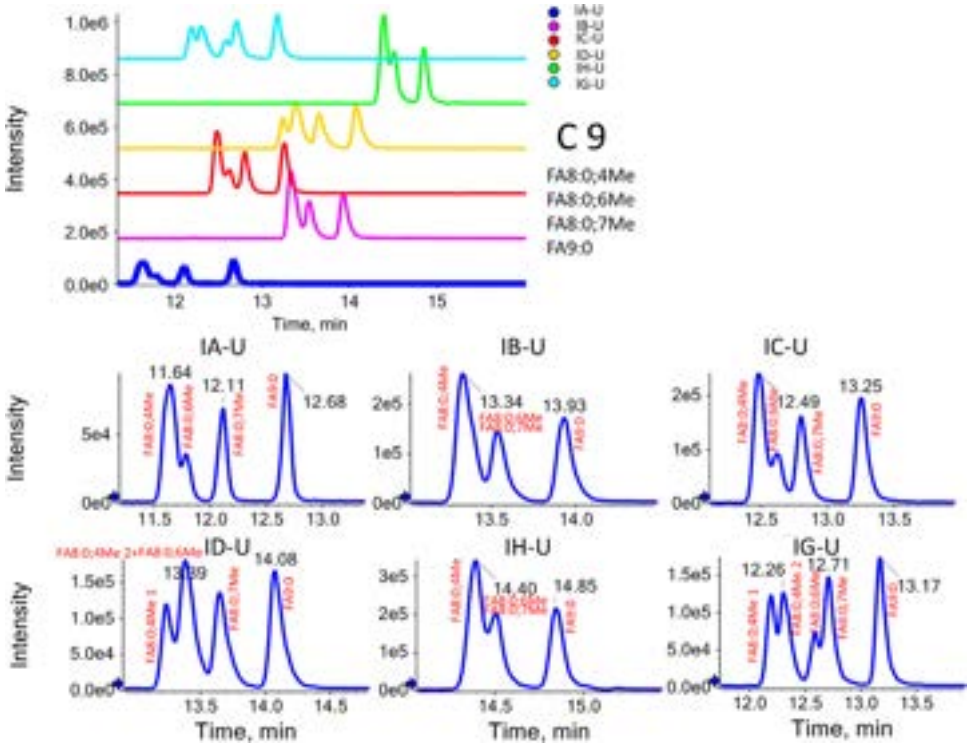

Fig. 3. XIC of C9 isomers of SFAs in complex standard mixtures on different tested Chiralpak columns (IA-U, IB-U, IC-U, ID-U, IG-U and IH-U). LC-MS method: column temperature (T) was 10 °C and the flow rate 0.3 mL/min for all columns. The gradient starts from 10%B for IB-U, IC-U, ID-U and IH-U while 20%B for IA-U and IG-U. Other conditions were the same for all columns which can be found in Section 2.3.

standards for example FA 8:0;4Me and FA 8:0;4Et with *S* and *R* enantiomer separation (Fig. S6). Unfortunately, the tested standard mixtures that were available were mainly short- and mid-chain FA isomers. For long chain FAs, the only isomer mixture that could be obtained was C15 (FA 15:0, FA 14:0;12Me and FA 14:0;13Me) and both ID-U and IG-U column showed to some degree selectivity for all three isomers (Fig. S7). Besides, IA-U column also gave isomer selectivity for C15.

Based on this screening of polysaccharide UHPLC columns, ID-U and IG-U were chosen for further optimization. Meanwhile, the RP C18 column was again tested with the same mobile phase as for above polysaccharide columns (A H_2O containing 0.1% (v/v) acetic acid and mobile phase B ACN containing 0.1% (v/v) acetic acid) instead of the strong acetonitrile/2-propanol mobile phase of the general lipidomics method that was used in the preliminary test for the comparison of the Chiralpak columns with RP C18. Interestingly, it was found that with a weaker mobile phase, the sensitivity and selectivity for FA isomers were significantly improved with over 100-fold higher intensity especially for the short chain and medium chain FAs (Fig. S8). Therefore, the three columns ID-U, IG-U and RP C18 columns were taken for further flow rate study. For RP C18, the flow rate range of 0.3–0.5 mL/min (no higher flow rate because of the column pressure limits) was tested while the flow rate range for ID-U and IG-U was 0.3–0.6 mL/min. As can be seen from Fig. S9, with increasing flow rate, the sensitivity became higher especially for long chain FAs for all three columns while for medium (and short) chain FAs the trend was not obvious. The selectivity for isomers remained similar for RP C18 with higher flow rate (for C15 it was even better) while it was a bit worse for ID-U and IG-U column. Interestingly, for IG-U column the selectivity for C8 and C9 isomers (Fig. 4) was improved dramatically with increase of flow rate while for FAs with other carbon numbers the resolution got a bit worse with increasing flow rate (C5, C7, C15). In the end, for each column the best flow rate was selected (ID-U = 0.3 mL/min, IG-U = 0.5 mL/min (instead of 0.6 mL/min due to column pressure limit), RP C18 = 0.5 mL/min) and the ability for

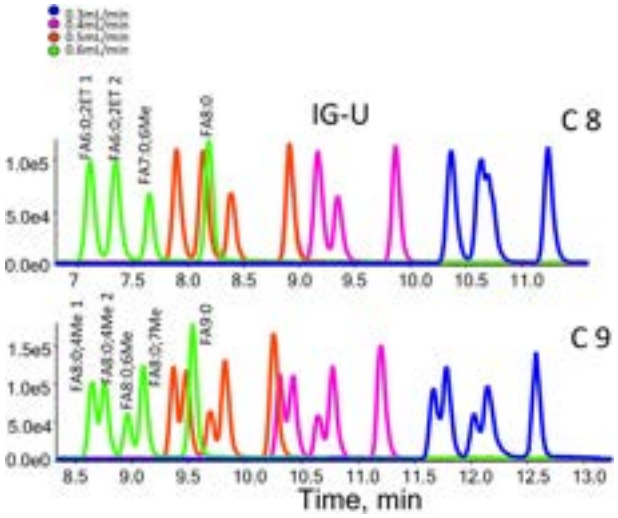

Fig. 4. *XIC of SFAs isomers of C8 and C9 in complex standard mixtures based on the IG-U column with flow rate from 0.3 to 0.6 mL/min. LC-MS conditions: column temperature (T) was 10 °C and gradient starts from 20%B. Other conditions can be found in Section 2.3.*

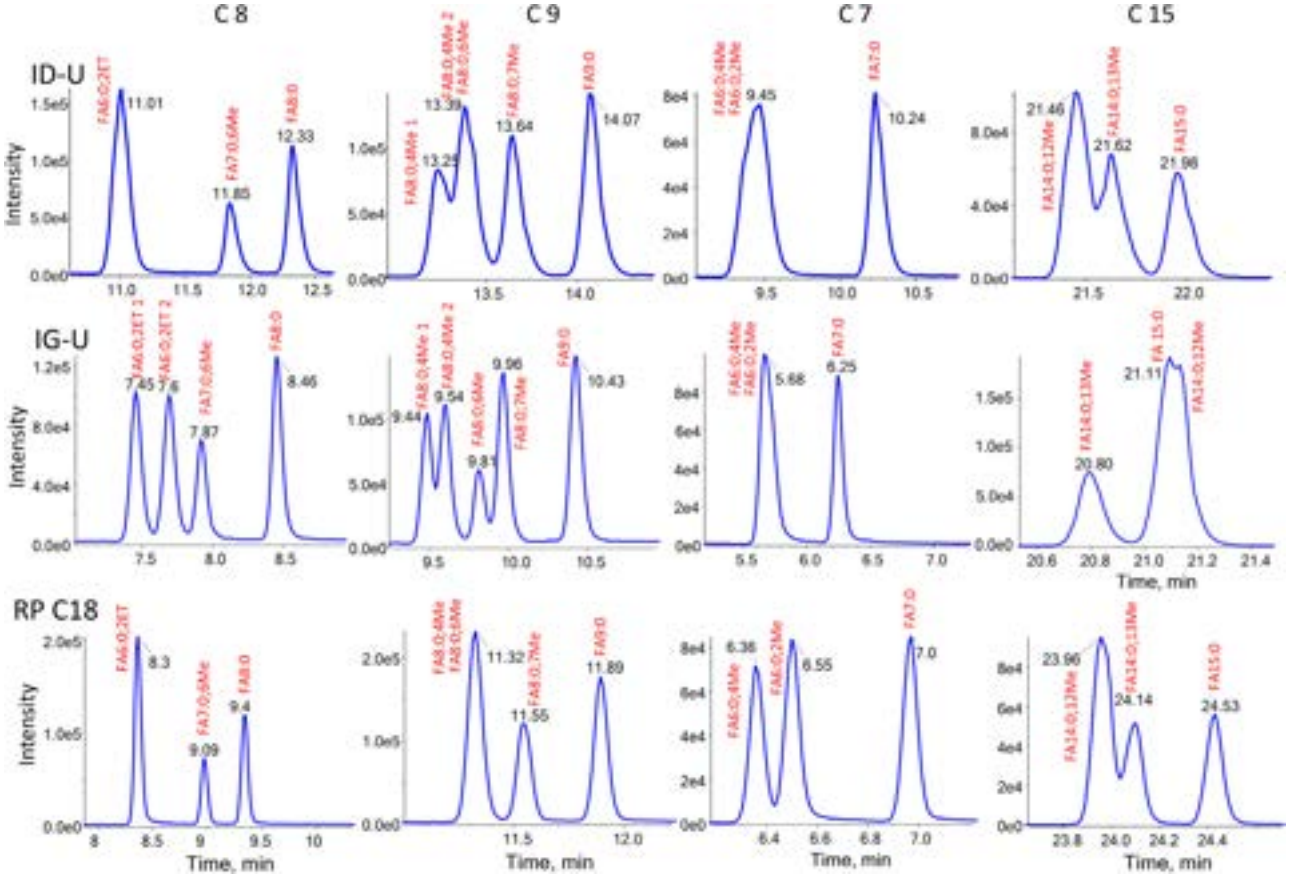

Fig. 5. XIC of SFAs isomers of C8, C9, C7 and C15 in complex standard mixtures on columns RP C18, ID-U and IG-U. LC-MS conditions: flow rate was 0.3 mL/min for ID-U, 0.5 mL/min for RP and IG-U. Column temperature (T) was 10 °C for all three columns and gradient starts from 10% for RP C18 and ID-U while 20% for IG-U. Other conditions were the same for all columns which can be found in Section 2.3.

Table 3
Comparison of isomer selectivity factor (α) for isomeric saturated fatty acids from C5 to C20 on different columns ID-U, IG-U and RP C18.

Carbon length	Isomers	IGU	RP C18	IDU
C5	ai/i	1.10	1.00	1.00
	i/n	1.24	1.13	1.22
	ai/n	1.13	1.13	1.22
C6	ai/i	1.10	1.06	1.10
	i/n	1.13	1.11	1.10
	ai/n	1.24	1.17	1.21
C7	ai/i	n.a	n.a	n.a
	i/n	n.a	n.a	n.a
	ai/n	1.12	1.08	1.10
C8	ai/i	n.a	n.a	n.a
	i/n	1.08	1.05	1.05
	ai/n	n.a	n.a	n.a
C9	ai/i	1.02	1.02	1.02
	i/n	1.05	1.04	1.04
	ai/n	1.07	1.07	1.06
C10	ai/i	n.a	n.a	n.a
	i/n	1.03	1.00	1.06
	ai/n	n.a	n.a	n.a
C11	ai/i	n.a	n.a	n.a
	i/n	n.a	n.a	n.a
	ai/n	1.02	1.04	1.03
C12	ai/i	n.a	n.a	n.a
	i/n	1.01	1.03	1.02
	ai/n	n.a	n.a	n.a
C13	ai/i	1.00	1.01	1.00
	i/n	1.02	1.03	1.02
	ai/n	1.02	1.04	1.03
C14	ai/i	n.a	n.a	n.a
	i/n	1.01	1.02	1.02
	ai/n	n.a	n.a	n.a
C15	ai/i	1.02	1.02	1.01
	i/n	1.02	1.02	1.02
	ai/n	1.00	1.04	1.03
C16	ai/i	n.a	n.a	n.a
	i/n	1.01	1.02	1.00
	ai/n	n.a	n.a	n.a
C17	ai/i	1.00	1.01	1.00
	i/n	1.01	1.02	1.02
	ai/n	1.01	1.02	1.02
C18	ai/i	n.a	n.a	n.a
	i/n	1.00	1.02	1.01
	ai/n	n.a	n.a	n.a
C19	ai/i	n.a	n.a	n.a
	i/n	1.01	1.03	1.00
	ai/n	n.a	n.a	n.a
C20	ai/i	n.a	n.a	n.a
	i/n	n.a	n.a	n.a
	ai/n	n.a	n.a	n.a

ai=*anteiso*-BCFAs (branched chain FAs)
i=*iso*-BCFAs
n=*n*FA (straight chain FAs)
n.*a*=value not available when only one peak was detected for the paired comparison
LC-MS conditions were the same as in Fig. 5.

isomer separation of the three columns was compared (Fig. 5). It is shown in Fig. 5 that for C8 and C9 isomers, IG-U outperforms the other two columns while for C7 and C15 isomers, the RP C18 column showed better resolution.

For long chain FAs, only C15 isomers were available as standards. In order to have a closer look at the selectivity of the selected columns for other long-chain FAs isomers especially C14-C18, a spiked bacterial QC sample (i.e. complex standard mixture spiked into the pooled QC sample) was prepared for further investigation since in the real bacterial samples the BCFAs including *iso*- and *anteiso*-FAs should exist. In order to have an overview about the separation performance of different columns on the isomeric SFAs, the selectivity factor (α) for paired isomers from C5-C20 were calculated (Table 3).

It can be concluded from Table 3 that IG-U provides the best selectivity for short and medium-chain FA isomers while the RP C18 column outperforms the others for long-chain FA isomers (>C12). As shown in Fig. 6 three peaks can be detected for odd chain (total carbon number) FAs with good selectivity while two peaks for even chain (total carbon number) on the RP C18 column. The methyl-branch hinders tight interaction with the alkyl-strand of C18 (for further detailed mechanistic discussion see chapter 3.2.2.2).

3.2.2. Structural assignment of fatty acids by retention model

The lack of commercial standards hinders the identification of FAs in complex biological samples. Furthermore, the alkyl chain of (branched) saturated FAs do not provide characteristic fragments in CID which would allow to pinpoint the methyl-branching position. Thus, to confirm the structure of a FA analyte, not only the MS data but also the retention time matching is necessary for the identification [41–43]. In general, in lipidomics no distinction between FA isomers is usually made. Yet, they may have distinct bioactiv-

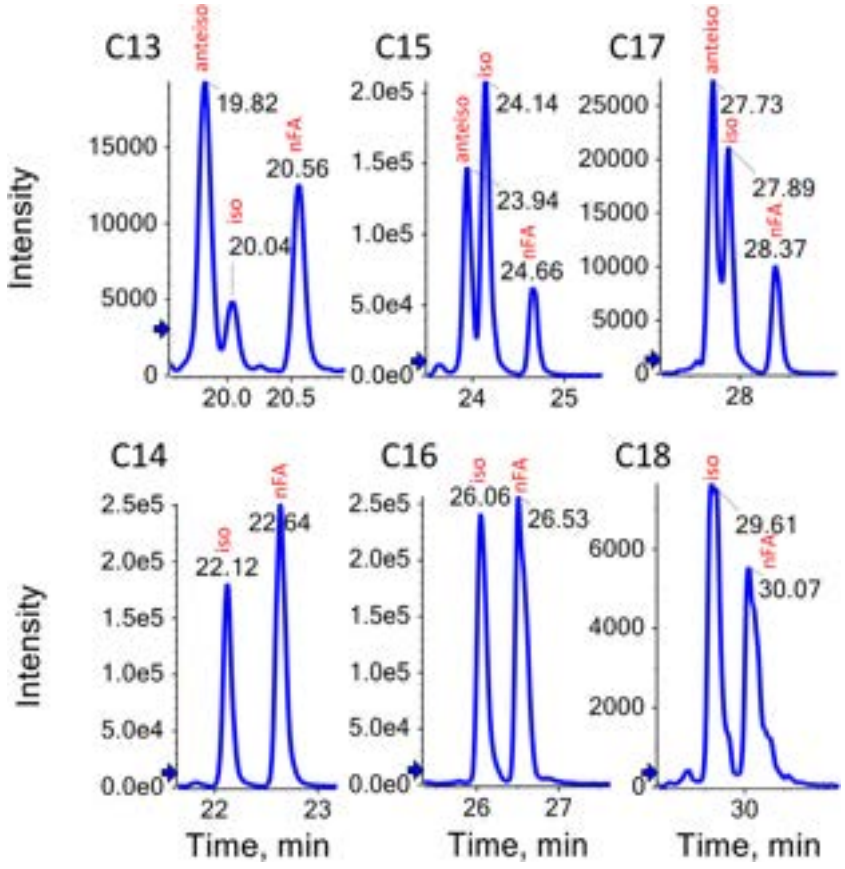

Fig. 6. XIC of SFAs isomers of even carbon number (C14-C16) and odd carbon number (C13-C17) in spiked quality control (QC) samples of extracts from Staphylococcus (complex standard mixtures + QC samples) on column RP C18. LC-MS conditions: gradient starts from 20%, others were the same as in Fig. 4.

ities and result from different biosynthetic origins, and hence a selective analysis is actually warranted. The retention behavior of (substituted) FAs is closely related to their chemical structure, including the hydroxy and methyl position, chain length, and the number of C = C double bonds. With the known standard mixtures and the detected peaks in the real QC pooled samples, the structure dependent retention time prediction model for both IGU and RP C18 column can be obtained (Fig. 7). It can be found from Fig. 7 that ethyl-branched FAs eluted earlier than methyl-branched FAs; straight chain FAs usually eluted latest. As the most common branched chain fatty acids, mono-methyl-branched FAs including the *anteiso* and *iso* BCFAs were commonly found in bacteria and to a much lesser extent in samples of mammalians. *Iso*-methyl fatty acids can be found with an even as well as odd number of carbons, while *anteiso*-forms only exist in FAs with odd carbon number. With the available standards of *anteiso, iso* and straight-chain FAs (*n*FA) of C6 (FA 5:0;2Me (*anteiso*), FA 5:0;3Me (*iso*) and nFA 6:0), C9 (FA 8:0;6Me (*anteiso*), FA 8:0;7Me (*iso*) and *n*FA 9:0) and C15 (FA 14:0;12Me (*anteiso*), FA 14:0;13Me (*iso*) and *n*FA 15:0), a conclusion can be made that the retention behavior on the RP column is RT (*n*FA) > RT (*iso*) > RT (*anteiso*). The ethyl chain BCFAs were excluded from further consideration because only two standards were available which is not enough for a prediction of the *m/z* vs RT correlation.

3.2.2.1. Retention model for anteiso-, iso- *and* n-saturated fatty acid *series.* Basically, the elution order can be confirmed from the available FA standards, but the number of isomeric FA standards was limited. With the capability for isomer selectivity of RP C18, it is possible to estimate retention times by empirical correlations due to consistent elution order in which *anteiso*-BCFAs eluted usually first followed by *iso*-BCFAs and *n*-FA usually have the longest retention on the RP column. From Fig. 7d, it can be observed that more peaks could be detected with RP C18 in cases of long-chain FAs. With odd number of carbons in total, usually three peaks were detected in the bacterial sample while for even number two peaks. The detected peaks were most probably the corresponding *anteiso*- and *iso*-BCFAs. In order to confirm the structural assignment, retention models of *m/z* vs *RT* were plotted for *anteiso*- and *iso*-BCFA. As can be seen from Fig. 8, the retention time *RT* of the standards and detected peaks matched well for both *anteiso*- (Fig. 8a) and *iso*-BCFAs (Fig. 8b) with linear regression (R^2=0.998 for both models). It indicates the possibility of structural assignment for the detected peaks in pooled QC samples by retention models. In the case of *iso*-BCFAs, besides the available standards (C5, C6, C8 and C9) and detected ones (C12-C19), the retention times for C7, C10 and C11 were estimated according to the linear regression model due to the absence of standards and because they were not detected in real samples. According to the retention model for *iso*-BCFAs with linear fitting, an estimated *RT* can be calculated so that a full series of *RT* database can be established for further structural annotations in other samples. For reliable identification in absence of authentic standards, MS hyphenation with electron-activated dissociation, or other technology like ion-mobility mass spectrometry, is required due to the small retention shifts between *ai*FAs and *i*FAs. If both BCFAs with same carbon number are present in a sample, tentative assignment is possible due to the consistent retention pattern in RPLC.

3.2.2.2. Retention model based on the methyl positions of BCFAs. There are also BCFAs with branching at other positions in biological samples, especially of bacterial origin. The positions of BCFAs

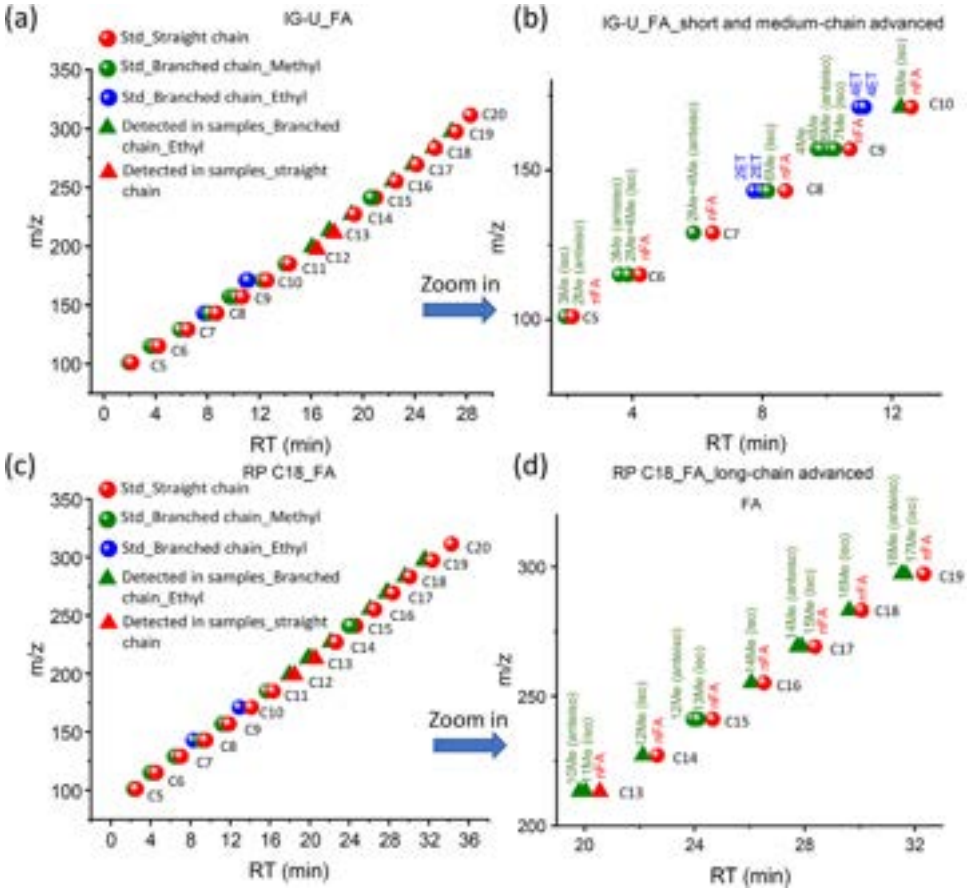

Fig. 7. Retention model obtained by plotting *m/z* vs the retention time (RT) of saturated fatty acids (SFAs, double bond $n = 0$) in spiked pooled quality control (QC) samples of extracts from Staphylococcus on column (a) IG-U and (b) zoomed in area from C5-C10; and on column (c) RP C18 and (d) zoomed in area from C13-C19. LC-MS conditions were the same as in Fig. 5.

and the chain-lengths thereby may cover a wide range, but for the monomethyl fatty acids, the branching-points are most often in positions 2 to 6. One option to deal with the branching at distinct positions is to establish separate retention models for BCFAs with the position of methyl group (2Me, 3Me, 4Me and 6Me) as indicator variable, the carbon number of the alkyl chain (*CN*) as independent variable and retention time (*RT*; in min) as dependent variable. According to *RT* of different methyl chain FAs of which standards were available, linear regression analysis with *RT* on the RP C18 column was performed by the support of SPSS statistics (Version SPSS 29.0). The variable *CN* was set to be numeric and refers to the total carbon number including methyl branch. The other variables *2Me*, *3Me*, *4Me* and *6Me* were set to be restricted numeric (0 indicates not existing and 1 existing). In this way, by linear regression the following retention model (eq. (1)) was obtained

$$RT = 2.11 \pm 0.05(CN) - 0.88 \pm 0.63(2Me) - 0.99 \pm 0.73(3Me) - 0.75 \pm 0.60(4Me) - 0.334 \pm 0.68(6Me) - 7.49 \pm 0.62 \quad (1)$$

The model shows a good fit with R^2 0.999, indicating an acceptable linear correlation (95% confidence intervals of estimated coefficients in parenthesis). Detailed statistical information about the regression model is summarized in Table 4. It can be seen that all predictors of the model are significant except for the 6Me substituent. The same procedure was performed for IG-U column using a linear regression model (see Table S3). Likewise, this approach was employed for the *iso*- and *anteiso*-FA series. The model is given in Eq. (2) (95% confidence intervals of estimated coefficients in parentheses) and the statistical parameters in suppl. Table S3.

$$RT = 2.11 \pm 0.02(CN) - 0.62 \pm 0.20(anteiso) - 0.53 \pm 0.17(iso) - 7.42 \pm 0.23 \quad (2)$$

The model indicates that the *iso*-FAs have less negative retention shift than the *anteiso*-FAs (compared to the straight chain alkane with the same total CN). With the assistance of the retention model based on the position of the methyl group of FAs, retention times can be estimated but due to the small retention shifts between different isomers (e.g. *anteiso* vs *iso*) not reliably predicted or structurally annotated without standards. When two isomers such as *anteiso*- and *iso*- are both present, the elution order provides a good indication for the structural assignment. On the other hand, LC-MS/MS with current isomer-selective chromatography in combination with electron-activated dissociation could become a reliable tool for the analysis of BCFAs, similar to GC-EI-MS of branched-chain FAMEs. Such a methodology could complement other isomer-selective methods that have already been shown to work for branched-chain FA identification, besides GC–MS as mentioned above, also by LC-MS employing photodissociation [44] and gas-phase ion/ion charge inversion reactions [45] which both, however, require the addition of reagents that might contaminate the ion-source and MS system, respectively. Besides, first experiments on ion-mobility MS analysis of branched chain fatty acids and lipids have been demonstrated previously [46], but resulted in partial resolution only. A combination of these MS and IMS technologies with the present isomer-selective LC could lead to improved

Table 4
Statistical parameters of retention model[a,b] for BCFAs for RP C18 column.
(Linear model: R = 0.999, R2 = 0.999, adj R2 = 0.998, std error of estimate = 0.411, F 3040.1, Sig. F < 0.001).

Variable	Unstandardized Coefficients	Std. Error	Standardized Coefficients	t	Sig.	95.0% Confidence Interval
(Constant)	-7.49	0.30		-25.2	<0.001	0.62
CN	2.11	0.02	0.98	95.8	<0.001	0.05
Me2	-0.88	0.30	-0.03	-2.9	0.009	0.63
Me3	-0.99	0.35	-0.03	-2.9	0.011	0.73
Me4	-0.75	0.29	-0.02	-2.6	0.017	0.60
Me6	-0.33	0.32	-0.01	-1.0	0.315	0.68

[a] Predictors: (*Constant*), *Me6*, *Me3*, *Me4*, *Me2*, *CN*.
[b] Dependent Variable: *RT*.
LC-MS conditions were the same as in Fig. 5 for RP C18 column.

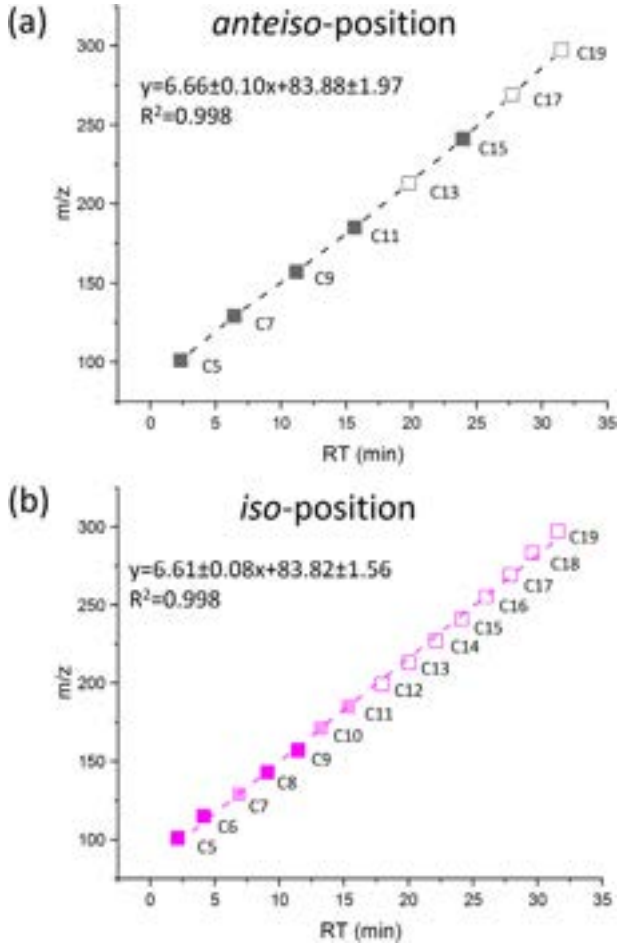

Fig. 8. Regression analysis of *m/z* vs retention time (*RT*) of (a) *anteiso*-branched chain fatty acids (*anteiso*-BCFAs) and (b) *iso*-branched chain fatty acids (*iso*-BCFAs) in spiked pooled quality control (QC) samples of extracts from Staphylococcus on column RP C18. Square with filling dark color means standards available; square without filling color means standards unavailable, however, were detected in real samples; square with filling light color means estimated *RT* based on the regression equation for those whose standards were neither available nor detected in real samples. LC-MS conditions were the same as in Fig. 5.

methodologies to decipher the role of different branched-chain FAs in biological samples.

3.2.2.3. Comparison with GC–MS FAME profiling. The above retention models already indicated that the significant retention shifts for methyl branching provide isomer-selectivity to the proposed LC-MS method for free branched chain FAs. The key question, however, is how it performs compared to the state-of-the-art methodology for FA profiling, i.e. FAME profiling by GC–MS. In GC, branched chain FAME data are often reported by their equivalent (carbon) chain length (ECL) and fractional (carbon) chain length (FCL), respectively, corresponding to the retention increment a methyl branch at a specific position in the carbon chain brings about. In a recent paper, ECLs and FCLs have been reported for an extended range of monomethyl branched FAMEs from C4–C23 of the general formula methyl x-methyl-alkane(y)-oate [47]. We calculated ECLs and FCLs for our x-methyl-y-oic acid (wherein x is the position of the methyl branch and y is the saturated alkane length) by a simple interpolation approach (eq. (3)) taking the adjacent straight chain FAs as references for the different LC systems reported herein (RP18 and IG-U) and compared them with the reported GC values for methylsilicone OV-1 stationary phase from the previous study [47].

$$ECL = CNy + FCLx = CNy + \frac{log(t_{R,\,x} - t_{Ri,\,n})}{log(t_{R,\,n+1} - t_{Ri,\,n})} \quad (3)$$

Wherein $t_{R,x}$ is the retention time of the specific branched alkane, $t_{Ri,n}$ and $t_{Ri,n+1}$ are the bracketing linear alkanes. The results are given in Table 5. An illustrative overview in form of parity plots can be found in suppl. Fig.S10. As can be derived from Table 5, *anteiso*-methyl branches have on average an FCL of 0.792 (±0.042) on IG-U and 0.688 (±0.042) on CSH C18 (suppl. Fig. S11a). Corresponding literature values of FCLs for FAMEs by GC have been calculated as 0.682 (±0.065) (or 0.705 (±0.065) without C5 outlier) on OV1 [47]. Corresponding figures for *iso*-methyl branches are 0.848 (±0.054) on IG-U and 0.771 (±0.049) on CSH C18 as well as 0.651 (±0.023) for FAMEs by GC (suppl. Fig. S11b). It can be seen that FCLs are quite comparable between CSH C18-LC and GC(OV1)-FAME although the FAs were eluted in less than 40 min in CSH C18-LC compared to about 320 min in GC for FAMEs. The FCL values do not necessarily reflect the selectivity between different monomethyl-branched FAs. To estimate selectivities of the distinct chromatographic systems for monomethyl branched FAs ratios of ECL values of corresponding *iso*- and *anteiso*-FAs were calculated. As shown in suppl. Fig. S11c, *iso*/*anteiso*-selectivity constantly drops with increasing carbon chain length on CSH C18, however, is larger over the entire tested carbon range than for IG-U and GC-FAMEs except for FAs with very low ($y = 5$) (IG-U provides the best selectivity) and high ($y = 18$) carbon numbers (GC-FAME provides better selectivity). It is also worth noting that GC-FAMEs method leads to reversed elution order for *anteiso* and *iso*-FAs as compared to CSH C18-LC, except for the FA 5:0;Me. Overall, it can be concluded that RPLC compares well in terms of selectivity with the GC-FAMEs method for FAs of the tested range. If longer run times, like in GC-FAMEs method, were acceptable, further improved resolutions may be expected.

3.3. Method application for fatty acids profiling in different types of samples

Finally, the optimized method with RP C18 column which was proven to provide the best isomeric selectivity especially for medium and long-chain FAs was applied for the saturated fatty

Table 5
Comparison of *FCL* (fractional carbon chain length) and *ECL* (equivalent carbon chain length) of RP C18 and IG-U column with reported GC-FAME method.

[M-H]⁻	X	Y	type	IG-U FCL	RP C18 FCL	GC-FAME FCL	IG-U ECL	RP C18 ECL	GC-FAME ECL
115.077	2	5		0.886	0.824	0.414	5.886	5.824	5.414
115.077	3	5	*anteiso*	0.79	0.766	0.549	5.79	5.766	5.549
115.077	4	5	*iso*	0.886	0.848	0.618	5.886	5.848	5.618
129.092	2	6		0.783	0.816	0.413	6.783	6.816	6.413
129.092	4	6		0.783	0.788	0.717	6.783	6.788	6.717
143.108	6	7	*iso*	0.785	0.841	0.634	7.785	7.841	7.634
157.123	4 (1)*	8		0.523	0.721	0.582	8.523	8.721	8.582
157.123	4 (2)*	8		0.574	0.721	0.582	8.574	8.721	8.582
157.123	6	8	*anteiso*	0.711	0.721	0.692	8.711	8.721	8.692
157.123	7	8	*iso*	0.782	0.826	0.648	8.782	8.826	8.648
185.155	8	10	*anteiso*	0.831	0.708	0.715	10.831	10.708	10.715
199.170	10	11	*iso*	0.944	0.774	0.651	11.944	11.774	11.651
213.186	10	12	*anteiso*	0.822	0.662	0.717	12.822	12.662	12.717
213.186	11	12	*iso*	0.828	0.764	0.649	12.828	12.764	12.649
227.202	12	13	*iso*	0.872	0.759	0.649	13.872	13.759	13.649
241.217	12	14	*anteiso*	0.765	0.653	0.647	14.765	14.653	14.719
241.217	13	14	*iso*	0.813	0.751	0.719	14.813	14.751	14.647
255.233	14	15	*iso*	0.869	0.759	0.648	15.869	15.759	15.648
269.249	14	16	*anteiso*	0.825	0.662	0.724	16.825	16.662	16.724
269.249	15	16	*iso*	0.825	0.747	0.647	16.825	16.747	16.647
283.264	16	17	*iso*	0.931	0.735	0.647	17.931	17.735	17.647
297.280	16	18	*anteiso*	0.797	0.646	0.729	18.797	18.646	18.729
297.280	17	18	*iso*	0.797	0.672	0.647	18.797	18.672	18.647

x is the position of the methyl branch and y is the saturated alkane length.
*(1) represent the first eluted peak and (2) the second eluted peak. Only IGU column showed the enantiomer-selectivity for R and S of FA 8:0;4Me. LC-MS conditions were the same as in Fig. 5 for IG-U and RP C18 column.

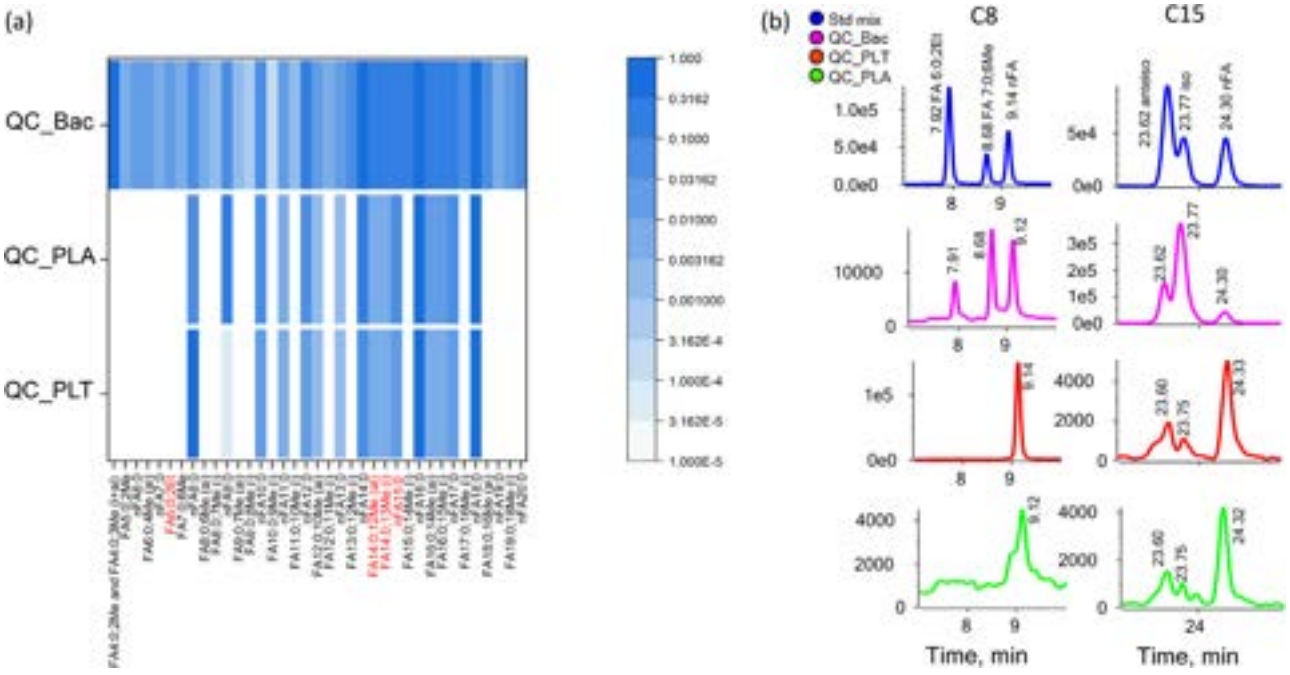

Fig. 9. (a) Heatmap of saturated fatty acids profiling in bacterial (QC_Bac), plasma (QC_PLA) and platelet (QC_PLT) samples. The normalized response is concentration divided by the maximum value in each sample type. Blank means the compound was not detected in sample. (b) XIC of SFAs isomers of C8 and C15 in neat standard solutions and real sample matrices pooled human platelets (QC_PLT), pooled human plasma (QC_PLA) and pooled *Staphylococcus aureus* (QC_Bac) on column RP C18 with optimized LC conditions. LC conditions were the same as in Fig. 5.

Table 6
Relative quantification of BCFAs in three biological matrices.

Name	Total carbon number	Concentration		
		pmol/10^9 PLT QC_PLT	pmol/mL QC_PLA	pmol/OD QC_Bac
FA4:0;2Me and FA4:0;3Me (*i*+ai)	C5	<LOD	<LOD	867.2
FA5:0;2Me	C6	<LOD	<LOD	3.1
nFA6:0	C6	<LOD	<LOD	20.6
FA6:0;4Me (ai)	C7	<LOD	<LOD	12.2
nFA7:0	C7	<LOD	<LOD	8.2
FA6:0;2Et	C8	<LOD	<LOD	12.0
FA7:0;6Me	C8	<LOD	<LOD	7.6
nFA8:0	C8	2981	2300	28.1
FA8:0;6Me (ai)	C9	<LOD	<LOD	3.0
FA8:0;7Me (i)	C9	<LOD	<LOD	1.1
nFA9:0	C9	0.36	7346	52.4
FA9:0;7Me (ai)	C11	<LOD	<LOD	2.3
FA9:0;8Me (i)	C10	<LOD	<LOD	0.4
nFA10:0	C10	133.8	2569.4	59.1
FA10:0;9Me (i)	C11	<LOD	<LOD	0.3
nFA11:0	C11	27.0	360.5	10.5
FA11:0;10Me (i)	C12	<LOD	<LOD	1.8
nFA12:0	C12	114.2	3407.3	168.0
FA12:0;10Me (ai)	C13	5.8	83.8	9.6
FA12:0;11Me (i)	C13	<LOD	<LOD	4.4
nFA13:0	C13	10.0	115.0	15.2
FA13:0;12Me (i)	C14	<LOD	<LOD	67.5
nFA14:0	C14	194.8	7368.1	314.7
FA14:0;12Me (ai)	C15	17.2	331.0	135.2
FA14:0;13Me (i)	C15	23.3	222.0	177.0
nFA15:0	C15	120.5	1665.3	110.8
FA15:0;14Me (i)	C16	<LOD	<LOD	117.9
nFA16:0	C16	2720.2	34,498.7	511.6
FA16:0;14Me (ai)	C17	21.4	1017.2	223.8
FA16:0;15Me (i)	C17	16.1	829.2	126.2
nFA17:0	C17	96.4	2437.1	104.2
FA17:0;16Me (i)	C18	<LOD	<LOD	73.2
nFA18:0	C18	4357.6	48,851.7	427.9
FA18:0;16Me (ai)	C19	<LOD	<LOD	44.1
nFA19:0	C19	<LOD	<LOD	6.8
FA19:0;18Me (i)	C20	<LOD	<LOD	13.6
nFA20:0	C20	<LOD	<LOD	67.9

Optical density (OD) at 578 nm.

acid profiling in pooled *Staphylococcus aureus* (Bac) sample but also for pooled human platelets (PLT), pooled human plasma (PLA) for comparison. A relative quantification (one-point calibration with IS AA-d11) was used for a general overview about the concentration levels of SFAs and BCFAs in different samples. Since only one FA internal standard was included in this study, a response factor approach [48] was adopted to consider the effect of distinct elution times and compound-specific (carbon number specific) ESI-MS sensitivity. For this reason, the response factor (RF) for at least each carbon chain length (C5-C20), if possible for each branched chain and straight chain FAs when the standards were available, was applied for the final relative quantification. For the compound A with known concentration in neat solution, the RF to the internal standard can be calculated as follows (Eq. (4)):

$$RF = \frac{peak\ area\ A / concentration\ A}{peak\ area\ IS / concentration\ IS} \quad (4)$$

Then, the concentration of the detected compound A in real samples can be calculated according to the equation (eq. (5)):

$$Concentration\ A = \frac{peak\ area\ A \times concentration\ IS}{peak\ area\ IS \times RF} \quad (5)$$

Mammalian samples contain also unsaturated fatty acids. Hence, the potential isotopic interference for the SFAs which is $[M + 2]$ of monounsaturated FAs (MUFAs) was checked. As can be seen from Fig. S12, the possible interference of MUFAs can be chromatographically separated from the targeted SFAs with same carbon number in our assays. For example, the FA 17:1 is separated from BCFA and *n*FA 17:0 by more than 2 min and does not interfere with BCFAs (Fig. S12). The results of the relative quantification of saturated FAs in pooled human platelet, pooled human plasma and pooled *Staphylococcus aureus* are summarized in Table 6 and Fig. 12a. BCFAs are commonly existing in bacterial samples which can be proven from the results in Table 6. BCFAs can be detected in *Staphylococcus* with different carbon chain lengths in remarkable amounts in the range of C5-C20. From the heatmap in Fig. 9a it becomes evident that the long-chain FAs from C14-C18 including the BCFAs and SFAs were the most abundant in *S. aureus*. Interestingly, quite a high amount of BCFAs of C5 (FA 4:0;2Me and FA 4:0;3Me) were detected in *S. aureus*, which was unexpected. However, it is interesting to find a high portion of short-chain FAs with only BCFAs instead of the straight chain FA 5:0 which was not detected. Unfortunately, these two BCFAs for C5 were coeluted in RPLC and only a sum quantification can be done (with IG-U column, a close to baseline separation for these two BCFAs of C5 could be achieved though, see Fig. S4). Aside from mono-methyl BCFAs, one ethyl BCFA (FA 6:0;2Et) was additionally detected in the bacterial sample with confirmed retention time by authentic standard (Fig. 9b). Unlike in *S. aureus*, in human samples (PLT and PLA), the straight chain even carbon numbered fatty acids were the dominant saturated FAs while a small amount of odd chain FAs can be detected as well which might originate from dietary intake (Fig. 9a). Similar as in *S. aureus*, the long-chain FAs with even carbon number (C14, C16 and C18) were the most abundant in both PLT and PLA

samples. The BCFAs were not the common fatty acids in human PLT and PLA, however, the *anteiso*- and *iso*-BCFA for C15 and C17 were detected with a certain amount (Fig. 9) (note, for these matrices a further optimization of the resolution from some partially interfering compounds would be beneficial). Recently, Venn-Watson et al. demonstrated that C15:0 as dietary odd-chain saturated fatty acids (OCFAs) can be associated with health benefits in human with direct roles in attenuating multiple comorbidities potentially by binding to key metabolic regulators and repairing mitochondrial function, which can be a potential essential fatty acid [49]. In this former study, it was not distinguished between the isomers of FA 15:0. Then it comes to the question whether there is associated a different effect to the distinct isomers of the FA 15:0. Our method may provide additional information for further detailed investigations allowing to differentiate between isomers concerning their association of higher circulating concentrations of OCFAs, pentadecanoic acid (C15:0) and heptadecanoic acid (C17:0) and their lower risks for cardiometabolic diseases [49].

4. Conclusions

This work demonstrated a straightforward method without pre-column derivatization for untargeted UHPLC-ESI-MS/MS based on RP C18 column for BCFAs profiling. The method enables good selectivity for constitutional isomers of BCFAs covering distinct chain lengths (C5-C20) with different branching types (methyl or ethyl) and branching positions (2Me, 3Me, 4Me, 6Me, *anteiso* and *iso*-BCFAs) with an optimized LC condition. What is more, a homologous series of short BCFA analytes with distinct chain lengths (C5-C20), branching type (methyl or ethyl), and position of branching (2, 3, 4, 6, *anteiso* and *iso*) has been systematically studied on 7 commercially available UHPLC columns (Chiralpak IA-U, IB-U, IC-U, ID-U, IG-U and IH-U; and Acquity UPLC CSH C18 column). For each column, the superiority based on the isomeric selectivity was summarized. In general, IG-U showed the best selectivity on the short and medium chain BCFAs isomers while RP C18 for the long chain BCFAs. Furthermore, the RP C18 column with optimized LC method was applied for the BCFAs profiling in three biological matrices pooled human platelets, pooled human plasma and pooled *Staphylococcus aureus* samples. To confirm the structure of an analyte, not only the MS data but also the retention time matching is necessary for the structural annotation. With the assistance of retention models, the identification of BCFAs in complex biological samples especially those without commercial standards can be more reliable. Finally, a relative quantification for each identified BCFAs and *n*FAs (one-point calibration based on the IS) was carried out with the response factor (RF) applied for each analyte. It is found that in *Staphylococcus aureus*, the BCFAs were as abundant as *n*FAs while the long chain FAs from C14-C18 (both straight chain and branched chain) possess a high portion amongst all FAs. Unlike in bacterial samples, the BCFAs were barely detected in human platelet and plasma samples. The *n*FAs and especially the long even chain nFAs (C14, C16 and C18) are the most abundant FAs in human samples. Odd chain FAs including C13, C15 and C17 were detected in human sample in a small amount which might be from the dietary intake. Interestingly, for C15 and C17 both *anteiso* and *iso*-BCFAs were identified with good selectivity for all the three isomers (*anteiso, iso, n*FAs), which could provide additional information for further investigations based on the association with health benefits in human. As a conclusion, the demonstrated method could be a powerful tool for FAs profiling not only for the straight chain FAs but also for the differentiation of constitutional isomers. The combination of these isomer selective LC methods with MS incorporating electron-activated dissociation fragmentation may provide an enhanced workflow for lipidomics profiling. Due to straightforward scalability, these isomer selective LC methods for BCFAs can be also of great value for preparative isolation of individual BCFAs.

In general, we do not want claim that the current method will replace GC–MS/FAMEs method as fatty acid profiling method of first choice. The key message is that with new developments in mass spectrometry (e.g. electron-activated dissociation and ion-mobility mass spectrometry) new technologies become available for LC-coupling which may give LC-MS profiling of free fatty acids a more prominent role than it has currently, in particular in general when the goal is to cover both free fatty acids and other more complex lipid classes with esterified FAs in lipidomics. Branched chain FA profiling might be also an important field in microbiomics.

Declaration of Competing Interest

The authors declare that they have no known competing financial interests or personal relationships that could have appeared to influence the work reported in this paper.

CRediT authorship contribution statement

Xiaoqing Fu: Investigation, Methodology, Formal analysis, Data curation, Visualization, Writing – original draft, Writing – review & editing. **Nourhane Hafza:** Investigation, Writing – review & editing. **Friedrich Götz:** Supervision, Writing – review & editing. **Michael Lämmerhofer:** Conceptualization, Methodology, Supervision, Writing – review & editing, Resources.

Data availability

Data will be made available on request.

Acknowledgments

X.F. gratefully acknowledges the support from the China Scholarship Council (grant number 201908080155). M.L. acknowledges the support by the German Research Foundation (DFG, Deutsche Forschungsgemeinschaft), project number 374031971-TRR 240.

Supplementary materials

Supplementary material associated with this article can be found, in the online version, at doi:10.1016/j.chroma.2023.464111.

References

[1] O. Quehenberger, A.M. Armando, E.A. Dennis, High sensitivity quantitative lipidomics analysis of fatty acids in biological samples by gas chromatography-mass spectrometry, Biochim. Biophys. Acta 1811 (11) (2011) 648–656, doi:10.1016/j.bbalip.2011.07.006.

[2] Y.K. Park, R. Ledesma-Amaro, J.M. Nicaud, De novo biosynthesis of odd-chain fatty acids in yarrowia lipolytica enabled by modular pathway engineering, Front. Bioeng. Biotechnol. 7 (2019) 484, doi:10.3389/fbioe.2019.00484.

[3] T. Kaneda, Iso- and anteiso-fatty acids in bacteria: biosynthesis, function, and taxonomic significance, Microbiol. Rev. 55 (2) (1991) 288–302, doi:10.1128/mr.55.2.288-302.1991.

[4] D. Eibler, H. Abdurahman, T. Ruoff, S. Kaffarnik, H. Steingass, W. Vetter, Unexpected formation of low amounts of (R)-configurated anteiso-fatty acids in rumen fluid experiments, PLoS ONE 12 (1) (2017) e0170788, doi:10.1371/journal.pone.0170788.

[5] J. Nechev, W.W. Christie, R. Robaina, F. de Diego, S. Popov, K. Stefanov, Lipid composition of the sponge Verongia aerophoba from the Canary Islands, Eur. J. Lipid Sci. Technol. 104 (12) (2002) 800–807, doi:10.1002/1438-9312(200212)104:12<800::Aid-ejlt800>3.0.Co;2-e.

[6] J. Jacob, A. Zeman, Das Bürzeldrüsensekret des Eissturmvogels (Fulmarus glacialis), Uropyg. Gland Fat Fulmar 26 (1) (1971) 33–40, doi:10.1515/znb-1971-0112.

[7] M. Wallace, C.R. Green, L.S. Roberts, Y.M. Lee, J.L. McCarville, J. Sanchez-Gurmaches, N. Meurs, J.M. Gengatharan, J.D. Hover, S.A. Phillips, T.P. Ciaraldi, D.A. Guertin, P. Cabrales, J.S. Ayres, D.K. Nomura, R. Loomba, C.M. Metallo, Enzyme promiscuity drives branched-chain fatty acid synthesis in adipose tissues, Nat. Chem. Biol. 14 (11) (2018) 1021–1031, doi:10.1038/s41589-018-0132-2.

[8] R. Ran-Ressler, S. Devapatla, P. Lawrence, J.T. Brenna, Comparison of BCFA types in vernix and meconium of healthy neonates, FASEB J. 22 (S1) (2008) 1091.1-1091.1, doi:10.1096/fasebj.22.1_supplement.1091.1.
[9] K.A. Dingess, C.J. Valentine, N.J. Ollberding, B.S. Davidson, J.G. Woo, S. Summer, Y.M. Peng, M.L. Guerrero, G.M. Ruiz-Palacios, R.R. Ran-Ressler, R.J. McMahon, J.T. Brenna, A.L. Morrow, Branched-chain fatty acid composition of human milk and the impact of maternal diet: the Global Exploration of Human Milk (GEHM) Study, Am. J. Clin. Nutr. 105 (1) (2016) 177–184, doi:10.3945/ajcn.116.132464.
[10] A. Mika, P. Stepnowski, L. Kaska, M. Proczko, P. Wisniewski, M. Sledzinski, T. Sledzinski, A comprehensive study of serum odd- and branched-chain fatty acids in patients with excess weight, Obesity (Silver Spring) 24 (8) (2016) 1669–1676, doi:10.1002/oby.21560.
[11] A. Masood, K.D. Stark, N. Salem, A simplified and efficient method for the analysis of fatty acid methyl esters suitable for large clinical studies, J. Lipid Res. 46 (10) (2005) 2299–2305, doi:10.1194/jlr.D500022-JLR200.
[12] J. Agren, A. Julkunen, I. Penttilä, Rapid separation of serum lipids for fatty acid analysis by a single aminopropyl column, J. Lipid Res. 33 (12) (1992) 1871–1876, doi:10.1016/S0022-2275(20)41345-8.
[13] T. Seppänen-Laakso, I. Laakso, R. Hiltunen, Analysis of fatty acids by gas chromatography, and its relevance to research on health and nutrition, Anal. Chim. Acta 465 (1–2) (2002) 39–62, doi:10.1016/S0003-2670(02)00397-5.
[14] J.X. Kang, J. Wang, A simplified method for analysis of polyunsaturated fatty acids, BMC Biochem. 6 (1) (2005) 1–4, doi:10.1186/1471-2091-6-5.
[15] F. Müller, T. Hammerschick, W. Vetter, Geometrical and positional isomers of unsaturated furan fatty acids in food, Lipids 58 (2) (2023) 69–79, doi:10.1002/lipd.12364.
[16] N.T. Smit, L. Villanueva, D. Rush, F. Grassa, C.R. Witkowski, M. Holzheimer, A.J. Minnaard, J.S. Sinninghe Damsté, S. Schouten, Novel hydrocarbon-utilizing soil mycobacteria synthesize unique mycocerosic acids at a Sicilian everlasting fire, Biogeosciences 18 (4) (2021) 1463–1479, doi:10.5194/bg-18-1463-2021.
[17] Z. Wang, D.H. Wang, H.G. Park, H.J. Tobias, K.S. Kothapalli, J.T. Brenna, Structural identification of monounsaturated branched chain fatty acid methyl esters by combination of electron ionization and covalent adduct chemical ionization tandem mass spectrometry, Anal. Chem. 91 (23) (2019) 15147–15154, doi:10.1021/acs.analchem.9b03912.
[18] X. Fu, Z. Xu, M. Gawaz, M. Lammerhofer, UHPLC-MS/MS method for chiral separation of 3-hydroxy fatty acids on amylose-based chiral stationary phase and its application for the enantioselective analysis in plasma and platelets, J. Pharm. Biomed. Anal. 223 (2023) 115151, doi:10.1016/j.jpba.2022.115151.
[19] T.H. Pham, M. Zaeem, T.A. Fillier, M. Nadeem, N.P. Vidal, C. Manful, S. Cheema, M. Cheema, R.H. Thomas, Targeting modified lipids during routine lipidomics analysis using HILIC and C30 reverse phase liquid chromatography coupled to mass spectrometry, Sci. Rep. 9 (1) (2019) 1–15, doi:10.1038/s41598-019-41556-9.
[20] M. Cebo, J. Schlotterbeck, M. Gawaz, M. Chatterjee, M. Lämmerhofer, Simultaneous targeted and untargeted UHPLC-ESI-MS/MS method with data-independent acquisition for quantification and profiling of (oxidized) fatty acids released upon platelet activation by thrombin, Anal. Chim. Acta 1094 (2020) 57–69, doi:10.1016/j.aca.2019.10.005.
[21] Y. Okamoto, M. Kawashima, K. Yamamoto, K. Hatada, Useful chiral packing materials for high-performance liquid chromatographic resolution. Cellulose triacetate and tribenzoate coated on macroporous silica gel, Chem. Lett. 13 (5) (1984) 739–742, doi:10.1246/cl.1984.739.
[22] Y. Okamoto, M. Kawashima, K. Hatada, Useful chiral packing materials for high-performance liquid chromatographic resolution of enantiomers: phenylcarbamates of polysaccharides coated on silica gel, J. Am. Chem. Soc. 106 (18) (1984) 5357–5359, doi:10.1021/ja00330a057.
[23] M. Cebo, X. Fu, M. Gawaz, M. Chatterjee, M. Lämmerhofer, Enantioselective ultra-high performance liquid chromatography-tandem mass spectrometry method based on sub-2µm particle polysaccharide column for chiral separation of oxylipins and its application for the analysis of autoxidized fatty acids and platelet releasates, J. Chromatogr. A 1624 (2020) 461206, doi:10.1016/j.chroma.2020.461206.
[24] P. Li, M. Lämmerhofer, Isomer selective comprehensive lipidomics analysis of phosphoinositides in biological samples by liquid chromatography with data independent acquisition tandem mass spectrometry, Anal. Chem. 93 (27) (2021) 9583–9592, doi:10.1021/acs.analchem.1c01751.
[25] F. Ianni, F. Blasi, D. Giusepponi, A. Coletti, F. Galli, B. Chankvetadze, R. Galarini, R. Sardella, Liquid chromatography separation of α- and γ-linolenic acid positional isomers with a stationary phase based on covalently immobilized cellulose tris(3,5-dichlorophenylcarbamate), J. Chromatogr. A 1609 (2020) 460461, doi:10.1016/j.chroma.2019.460461.
[26] S. Thurnhofer, G. Hottinger, W. Vetter, Enantioselective determination of anteiso fatty acids in food samples, Anal. Chem. 79 (12) (2007) 4696–4701, doi:10.1007/s11745-010-3400-9.
[27] C. Geibel, L. Zhang, K. Serafimov, H. Gross, M. Lammerhofer, Towards enantioselective ultrahigh performance liquid chromatography-mass spectrometry-based metabolomics of branched-chain fatty acids and anteiso-fatty acids under reversed-phase conditions using sub-2-mum amylose- and cellulose-derived chiral stationary phases, Chirality 34 (3) (2022) 484–497, doi:10.1002/chir.23413.
[28] C. Geibel, M. Olfert, C. Knappe, K. Serafimov, M. Lämmerhofer, Branched medium-chain fatty acid profiling and enantiomer separation of anteiso-forms of teicoplanin fatty acyl side chain RS3 using UHPLC-MS/MS with polysaccharide columns, J. Pharm. Biomed. Anal. 224 (2023) 115162, doi:10.1016/j.jpba.2022.115162.
[29] S. Hauff, G. Hottinger, W. Vetter, Enantioselective analysis of chiral anteiso fatty acids in the polar and neutral lipids of food, Lipids 45 (4) (2010) 357–365, doi:10.1007/s11745-010-3400-9.
[30] M. Lísa, M. Holčapek, Characterization of triacylglycerol enantiomers using chiral HPLC/APCI-MS and synthesis of enantiomeric triacylglycerols, Anal. Chem. 85 (3) (2013) 1852–1859, doi:10.1021/ac303237a.
[31] A. Palyzová, T. Cajthaml, T. Řezanka, Separation of regioisomers and enantiomers of triacylglycerols containing branched fatty acids (iso and/or anteiso), Electrophoresis 42 (17–18) (2021) 1832–1843, doi:10.1002/elps.202000320.
[32] X. Fu, C. Calderón, T. Harm, M. Gawaz, M. Lämmerhofer, Advanced unified monophasic lipid extraction protocol with wide coverage on the polarity scale optimized for large-scale untargeted clinical lipidomics analysis of platelets, Anal. Chim. Acta 1221 (2022) 340155, doi:10.1016/j.aca.2022.340155.
[33] V. Matyash, G. Liebisch, T.V. Kurzchalia, A. Shevchenko, D. Schwudke, Lipid extraction by methyl-tert-butyl ether for high-throughput lipidomics, J. Lipid Res. 49 (5) (2008) 1137–1146, doi:10.1194/jlr.D700041-JLR200.
[34] H. Tsugawa, T. Cajka, T. Kind, Y. Ma, B. Higgins, K. Ikeda, M. Kanazawa, J. VanderGheynst, O. Fiehn, M. Arita, MS-DIAL: data-independent MS/MS deconvolution for comprehensive metabolome analysis, Nat. Methods 12 (6) (2015) 523–526, doi:10.1038/nmeth.3393.
[35] C. Yamamoto, E. Yashima, Y. Okamoto, Structural analysis of amylose tris (3, 5-dimethylphenylcarbamate) by NMR relevant to its chiral recognition mechanism in HPLC, J. Am. Chem. Soc. 124 (42) (2002) 12583–12589, doi:10.1021/ja020828g.
[36] P. Peluso, B. Chankvetadze, Recognition in the domain of molecular chirality: from noncovalent interactions to separation of enantiomers, Chem. Rev. 122 (16) (2022) 13235–13400, doi:10.1021/acs.chemrev.1c00846.
[37] P. Peluso, V. Mamane, R. Dallocchio, A. Dessì, S. Cossu, Noncovalent interactions in high-performance liquid chromatography enantioseparations on polysaccharide-based chiral selectors, J. Chromatogr. A 1623 (2020) 461202, doi:10.1016/j.chroma.2020.461202.
[38] B.H. Kim, S.U. Lee, D.C. Moon, Chiral recognition of N-phthaloyl, N-tetrachlorophthaloyl, and N-naphthaloyl α-amino acids and their esters on polysaccharide-derived chiral stationary phases, Chirality 24 (12) (2012) 1037–1046, doi:10.1002/chir.22094.
[39] B. Chankvetadze, Recent developments on polysaccharide-based chiral stationary phases for liquid-phase separation of enantiomers, J. Chromatogr. A 1269 (2012) 26–51, doi:10.1016/j.chroma.2012.10.033.
[40] L. Chankvetadze, A.-C. Servais, M. Fillet, A. Salgado, J. Crommen, B. Chankvetadze, Comparative enantioseparation of talinolol in aqueous and non-aqueous capillary electrophoresis and study of related selector–selectand interactions by nuclear magnetic resonance spectroscopy, J. Chromatogr. A 1267 (2012) 206–216, doi:10.1016/j.chroma.2012.08.063.
[41] M. Ovcacikova, M. Lisa, E. Cifkova, M. Holcapek, Retention behavior of lipids in reversed-phase ultrahigh-performance liquid chromatography-electrospray ionization mass spectrometry, J. Chromatogr. A 1450 (2016) 76–85, doi:10.1016/j.chroma.2016.04.082.
[42] H.C. Kofeler, T.O. Eichmann, R. Ahrends, J.A. Bowden, N. Danne-Rasche, E.A. Dennis, M. Fedorova, W.J. Griffiths, X. Han, J. Hartler, M. Holcapek, R. Jirasko, J.P. Koelmel, C.S. Ejsing, G. Liebisch, Z. Ni, V.B. O'Donnell, O. Quehenberger, D. Schwudke, A. Shevchenko, M.J.O. Wakelam, M.R. Wenk, D. Wolrab, K. Ekroos, Quality control requirements for the correct annotation of lipidomics data, Nat. Commun. 12 (1) (2021) 4771, doi:10.1038/s41467-021-24984-y.
[43] F. Aicheler, J. Li, M. Hoene, R. Lehmann, G. Xu, O. Kohlbacher, Retention time prediction improves identification in nontargeted lipidomics approaches, Anal. Chem. 87 (15) (2015) 7698–7704, doi:10.1021/acs.analchem.5b01139.
[44] H.T. Pham, T. Ly, A.J. Trevitt, T.W. Mitchell, S.J. Blanksby, Differentiation of complex lipid isomers by radical-directed dissociation mass spectrometry, Anal. Chem. 84 (17) (2012) 7525–7532, doi:10.1021/ac301652a.
[45] C.E. Randolph, C.H. Beveridge, S. Iyer, S.J. Blanksby, S.A. McLuckey, G. Chopra, Identification of monomethyl branched-chain lipids by a combination of liquid chromatography tandem mass spectrometry and charge-switching chemistries, J. Am. Soc. Mass Spectrom. 33 (11) (2022) 2156–2164, doi:10.1021/jasms.2c00225.
[46] C. Freeman, H.M. Hynds, J.M. Carpenter, K. Appala, K. Bimpeh, S. Barbarek, C. Gatto, B.J. Wilkinson, K.M. Hines, Revealing fatty acid heterogeneity in staphylococcal lipids with isotope labeling and RPLC–IM–MS, J. Am. Soc. Mass Spectrom. 32 (9) (2021) 2376–2385, doi:10.1021/jasms.1c00092.
[47] R. Kubinec, J. Blaško, R. Górová, G. Addová, I. Ostrovský, A. Amann, L. Soják, Equivalent chain lengths of all C4–C23 saturated monomethyl branched fatty acid methyl esters on methylsilicone OV-1 stationary phase, J. Chromatogr. A 1218 (13) (2011) 1767–1774, doi:10.1016/j.chroma.2011.01.065.
[48] E. Cífková, M. Holčapek, M. Lísa, M. Ovčačíková, A. Lyčka, F. Lynen, P. Sandra, Nontargeted quantitation of lipid classes using hydrophilic interaction liquid chromatography-electrospray ionization mass spectrometry with single internal standard and response factor approach, Anal. Chem. 84 (22) (2012) 10064–10070, doi:10.1021/ac3024476.
[49] S. Venn-Watson, R. Lumpkin, E.A. Dennis, Efficacy of dietary odd-chain saturated fatty acid pentadecanoic acid parallels broad associated health benefits in humans: could it be essential? Sci. Rep. 10 (1) (2020) 8161, doi:10.1038/s41598-020-64960-y.

Supplementary information

Profiling of branched chain and straight chain saturated fatty acids by ultra-high performance liquid chromatography-mass spectrometry

Xiaoqing Fu[a], Nourhane Hafza[b], Friedrich Götz[b], Michael Lämmerhofer[a]*

[a] University of Tübingen, Institute of Pharmaceutical Sciences, Pharmaceutical (Bio-)Analysis, Auf der Morgenstelle 8, 72076 Tübingen, Germany

[b]University of Tübingen, Interfaculty Institute for Microbiology and Infection-Medicine Tübingen, Microbial Genetics, Auf der Morgenstelle 28, 72076 Tübingen, Germany

***Author for correspondence:**

Prof. Michael Lämmerhofer
Pharmaceutical (Bio-)Analysis
Institute of Pharmaceutical Sciences
University of Tuebingen
Auf der Morgenstelle 8
72076 Tuebingen, Germany
T +49 7071 29 78793, F +49 7071 29 4565
e-mail: michael.laemmerhofer@uni-tuebingen.de
http://www.bioanalysis.uni-tuebingen.de/

1. LC-MS method

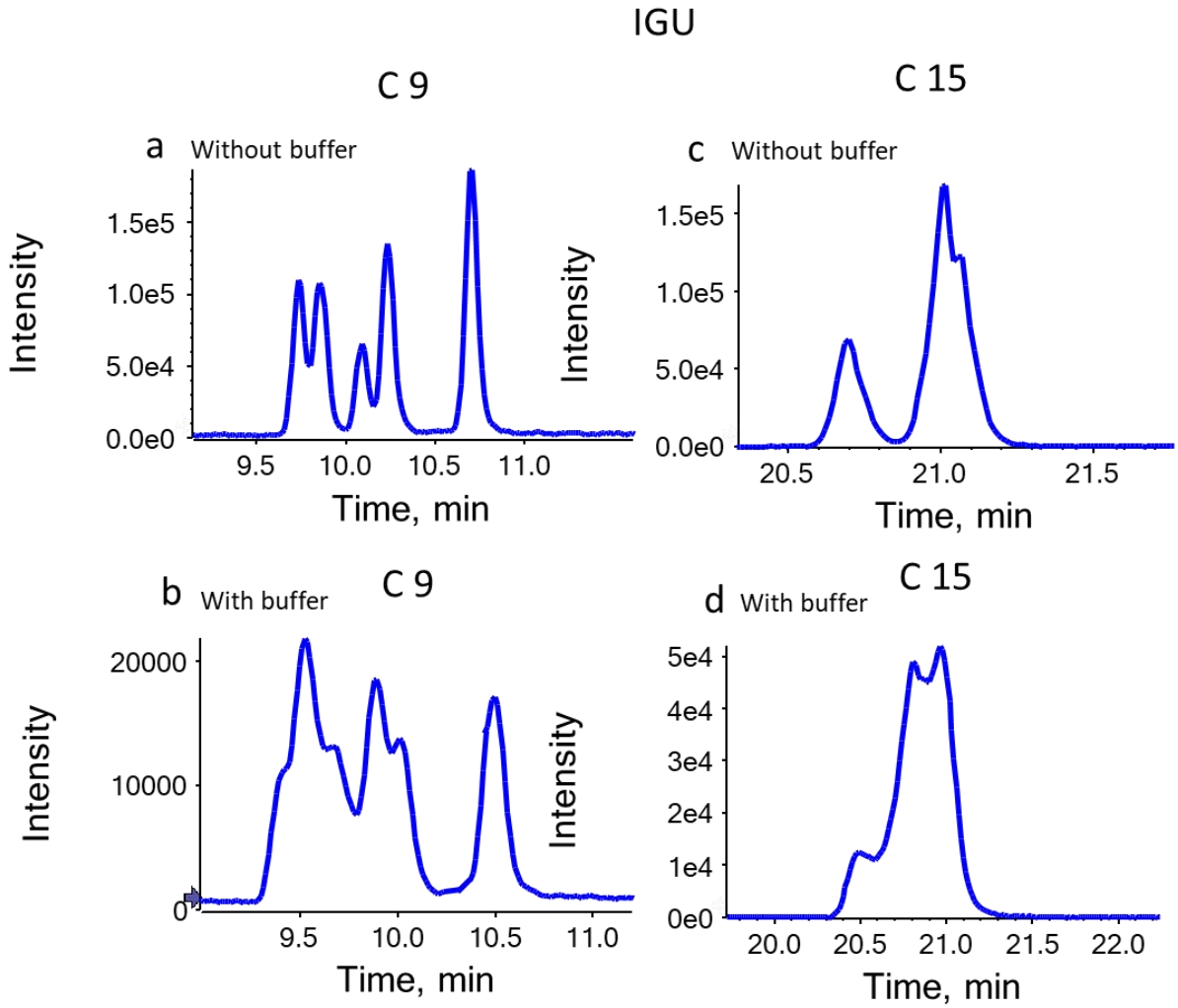

Fig. S1 *XIC of C9 and C15 isomers of SFAs in complex standard mixtures on IG-U with mobile phase A water containing 0.1% (v/v) acetic acid and mobile phase B of ACN containing 0.1% (v/v) acetic acid for (a) and (c) while with mobile phase A water containing 0.1% (v/v) acetic acid with10 mM ammounium acetate and mobile phase B of ACN containing 0.1% (v/v) acetic acid with10 mM ammounium acetate for (b) and (d). Other LC-MS method parameters were the same as described in Fig. 2 with IG-U column in main text.*

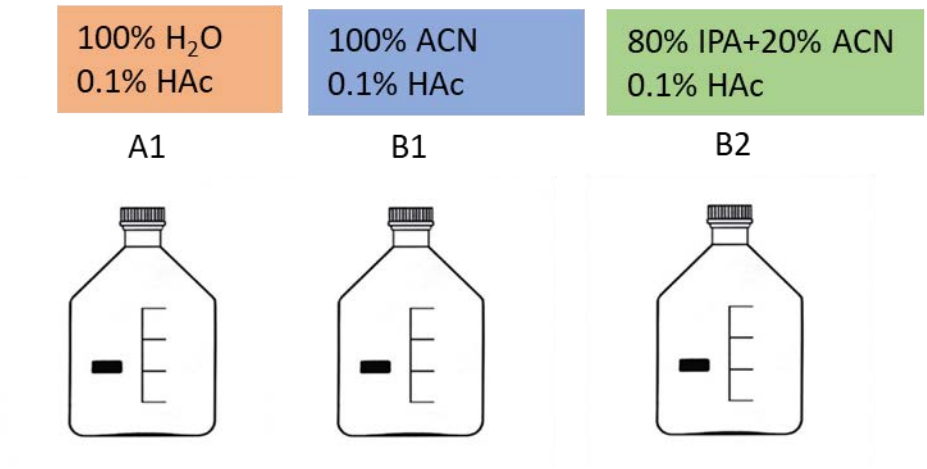

Experimental LC conditions

T(min)	A1(%)	B1(%)
0	80	20
30	0	100
35	0	100
35.01	80	20
40	80	20

Wash LC conditions

T(min)	A1(%)	B2(%)
0	0	100
20	0	100

Fig. S2 *Design for wash step and the mobile phase composition along with the LC conditions (IG-U column as an example). For the wash step, the flow rate was 0.4 mL/min, column temperature was 10°C with injection volume of MeOH 10 µL.*

Table. S1 *Analytical batch design with wash step*

Injection order	Samples	Method
1	blank1	Experimental LC conditions
2	blank2	Experimental LC conditions
3	SST1	Experimental LC conditions
4	SST2	Experimental LC conditions
5	SST3	Experimental LC conditions
6	QC1	Experimental LC conditions
7	sample1	Experimental LC conditions
8	sample2	Experimental LC conditions
9	sample3	Experimental LC conditions
10	sample4	Experimental LC conditions
11	sample5	Experimental LC conditions
12	MeOH wash 1	Wash conditions
13	Equilibration 1	Experimental LC conditions
14	Equilibration 2	Experimental LC conditions
15	QC2	Experimental LC conditions
16	sample6	Experimental LC conditions
17	sample7	Experimental LC conditions
18	sample8	Experimental LC conditions
19	sample9	Experimental LC conditions
20	sample10	Experimental LC conditions
21	MeOH wash 2	Wash conditions
22	Equilibration 3	Experimental LC conditions
23	Equilibration 4	Experimental LC conditions
24	QC n	Experimental LC conditions
25	Sample n	Experimental LC conditions
26	MeOH wash n	Wash conditions
27	Equilibration n	Experimental LC conditions
28	Equilibration n+1	Experimental LC conditions

SST (system suitability test): three injections of neat standard solution at the beginning

Equilibration: Injection of 10 µL MeOH and running a blank gradient to equilibrate the column

MeOH wash: injection of 10 µL MeOH and running wash conditions to avoid accumulation of apolar lipids.

Table. S2 *MS parameters with SWATH windows as well as collision energy (CE) and collision energy spread (CES) in negative ion mode*

			ESI (-)		
Experiment	Scan typ	Acc. Time (ms)	Start (m/z)	Stop (m/z)	CE (V)
1	MS Full Scan	50	50	1250	-10
2	SWATH	31	50	213.5	-45±15
3	SWATH	31	212.5	271.4	-45±15
4	SWATH	31	270.4	314.6	-45±15
5	SWATH	31	313.6	382.6	-45±15
6	SWATH	31	381.6	427.5	-45±15
7	SWATH	31	426.5	464.3	-45±15
8	SWATH	31	463.3	501	-45±15
9	SWATH	31	500	540.8	-45±15
10	SWATH	31	539.8	617.5	-45±15
11	SWATH	31	616.5	680.3	-45±15
12	SWATH	31	679.3	697.1	-45±15
13	SWATH	31	696.1	724	-45±15
14	SWATH	31	723	749	-45±15
15	SWATH	31	748	775.6	-45±15
16	SWATH	31	774.6	793.1	-45±15
17	SWATH	31	792.1	811	-45±15
18	SWATH	31	810	832.6	-45±15
19	SWATH	31	831.6	854.1	-45±15
20	SWATH	31	853.1	861.2	-45±15
21	SWATH	31	860.2	1050	-45±15

2. Column screening

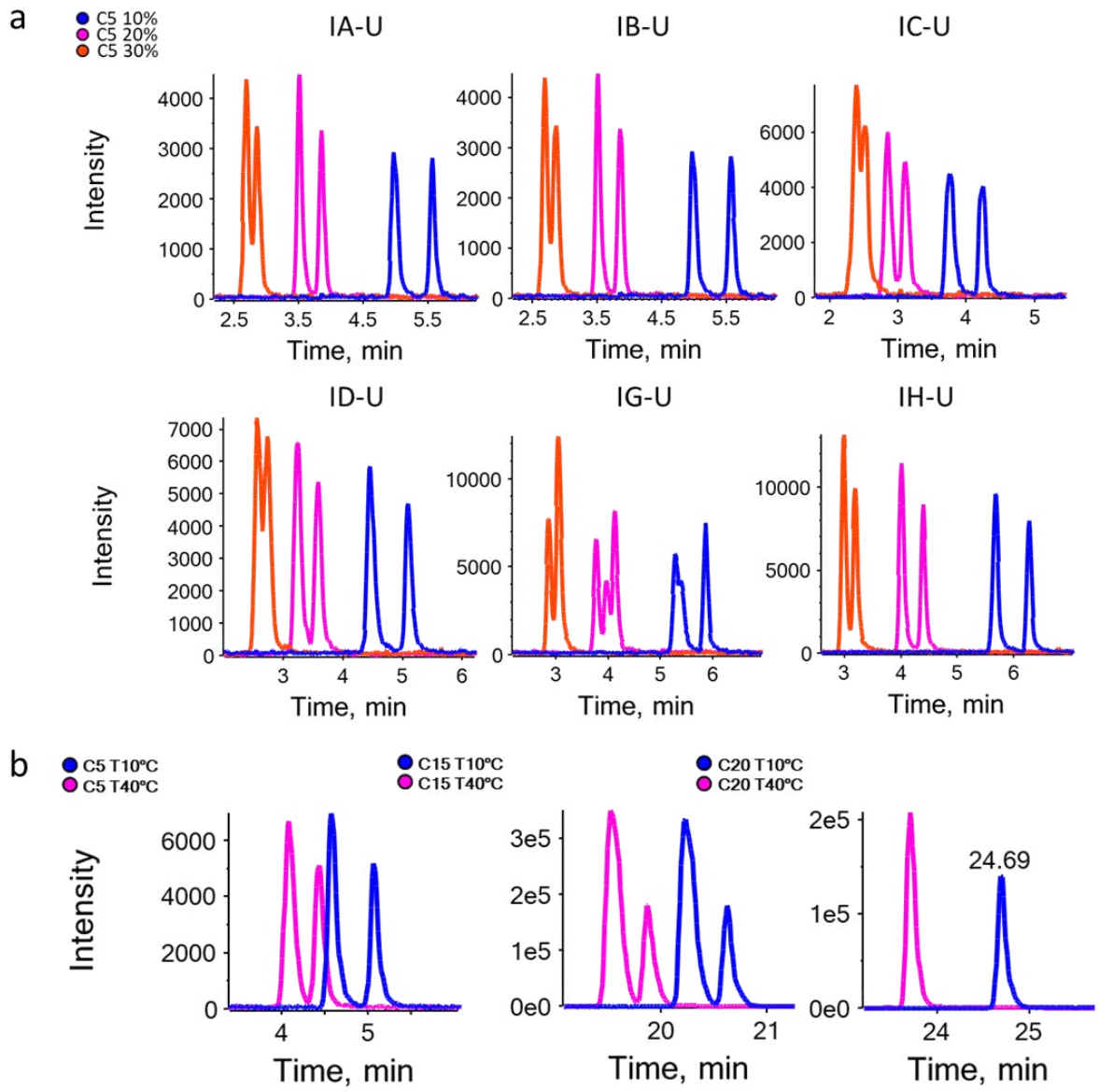

Fig. S3 (a) *Extracted ion chromatograms (XIC) of isomeric saturated fatty acids (SFAs, double bond n=0) C5 in complex standard mixtures on different Chiralpak columns (IA-U, IB-U, IC-U, ID-U, IG-U and IH-U) with different starting %B gradients. (b)XIC of isomeric SFAs C5, C15 and C20 in complex standard mixtures on column IA-U. LC-MS method: column temperature (T) was 10°C and the flow rate 0.3 mL/min for all columns. Other conditions including mobile phase and MS parameters can be found in main text section 2.3.*

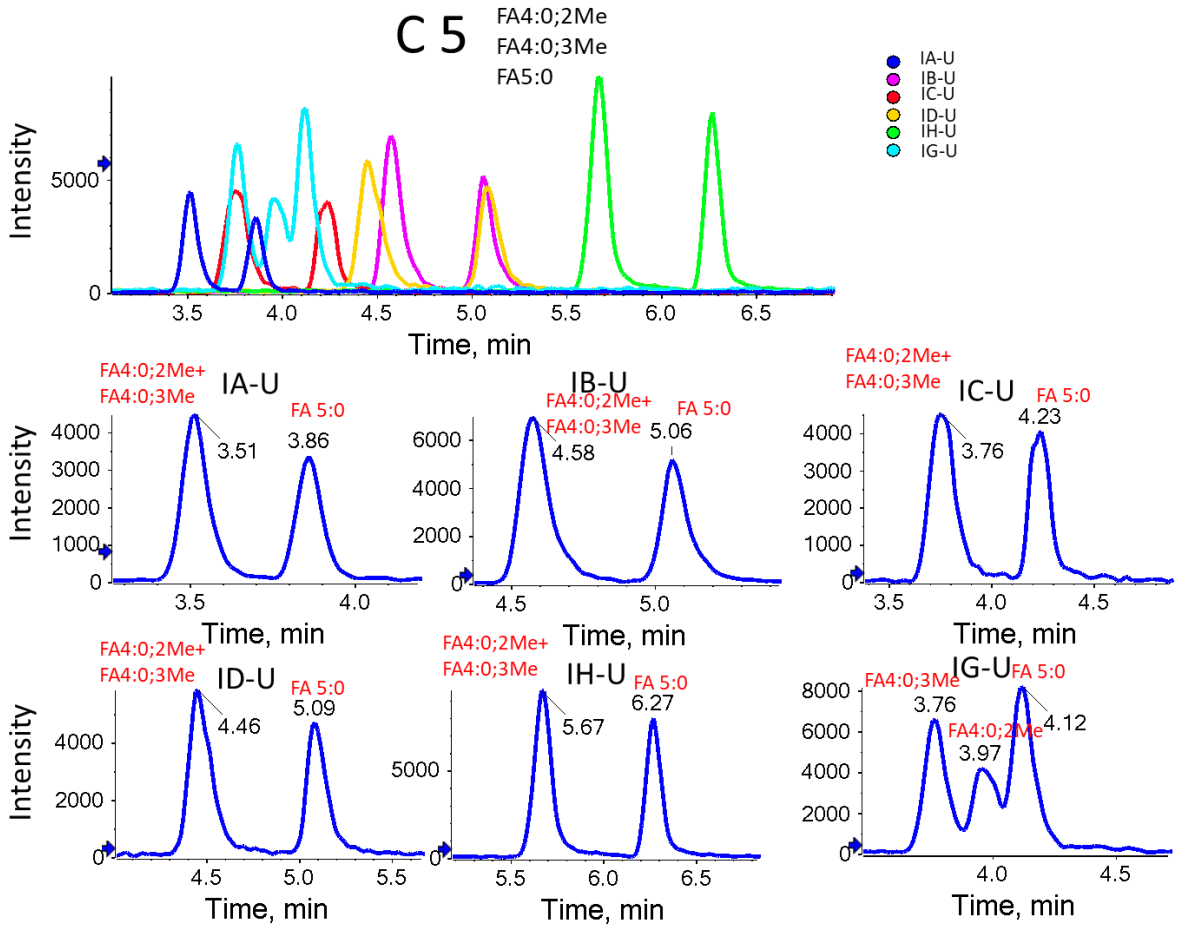

Fig. S4 *XIC of C5 isomers of SFAs in complex standard mixtures on different tested Chiralpak columns (IA-U, IB-U, IC-U, ID-U, IG-U and IH-U). LC-MS method was the same as described in Fig. 2 in main text.*

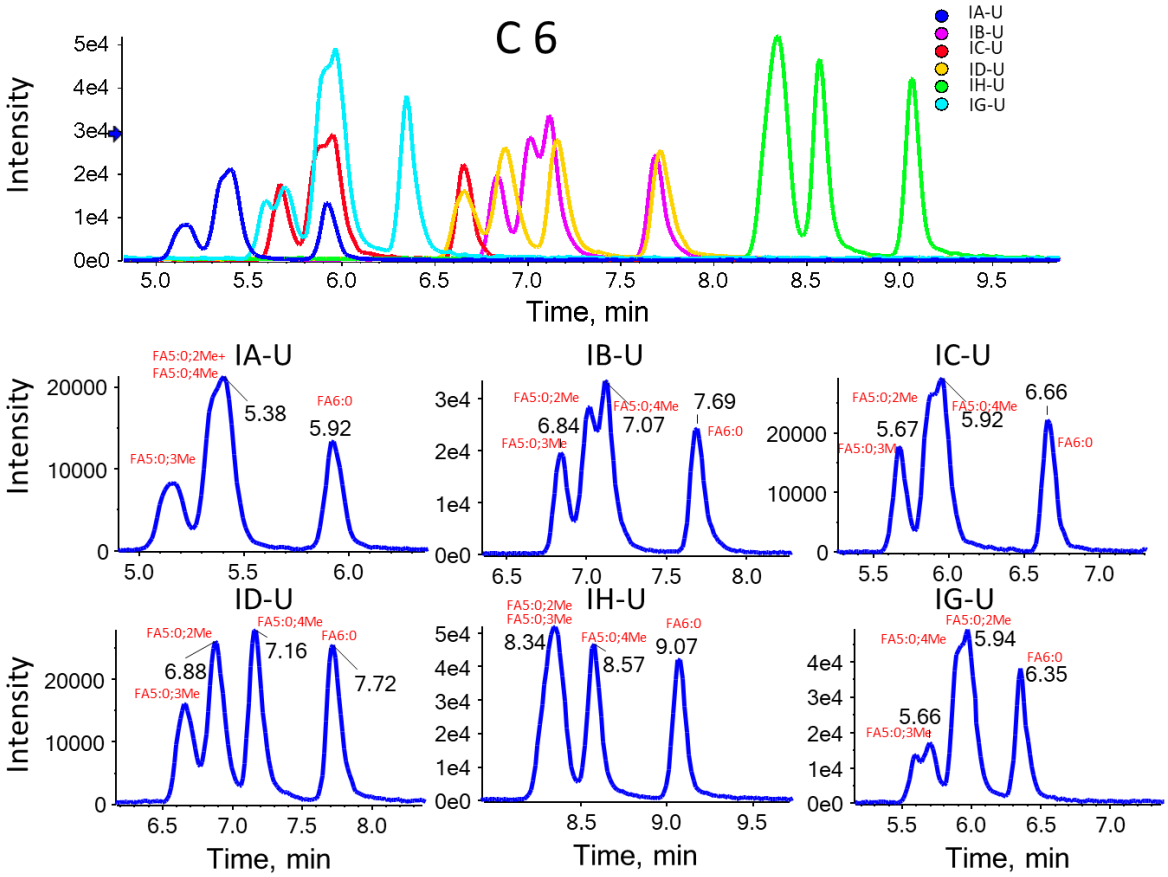

Fig. S5 *XIC of C6 isomers of SFAs in complex standard mixtures on different tested Chiralpak columns (IA-U, IB-U, IC-U, ID-U, IG-U and IH-U). LC-MS method was the same as described in Fig. 2 in main text.*

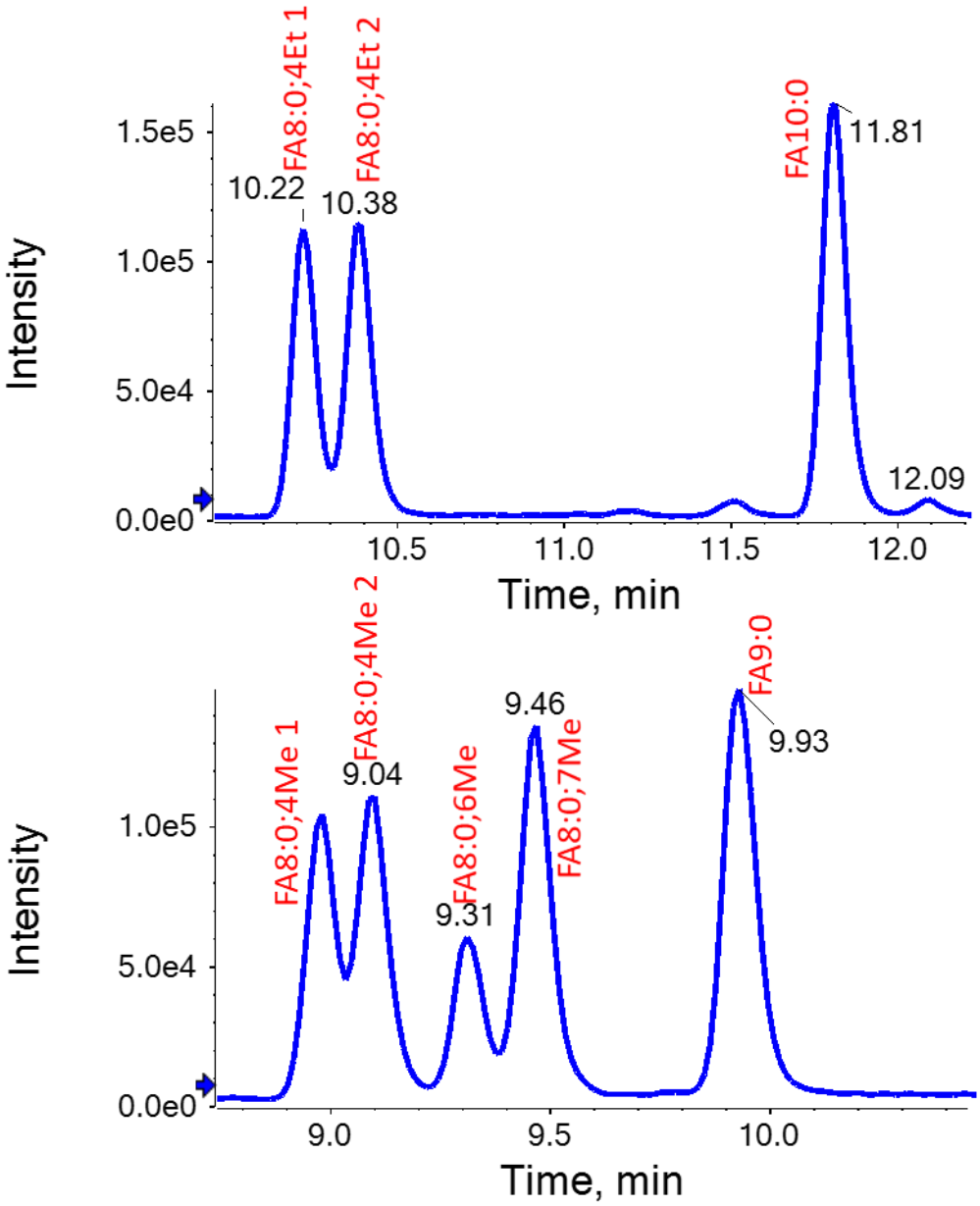

Fig. S6 *XIC of C9 and C10 isomers of SFAs in complex standard mixtures on IG-U. LC-MS method was the same as described in Fig. 2 with IG-U column in main text. Peak 1 (first eluted) and 2 (second eluted) represent the S or R enantiomers and the assignment to R and S is not available.*

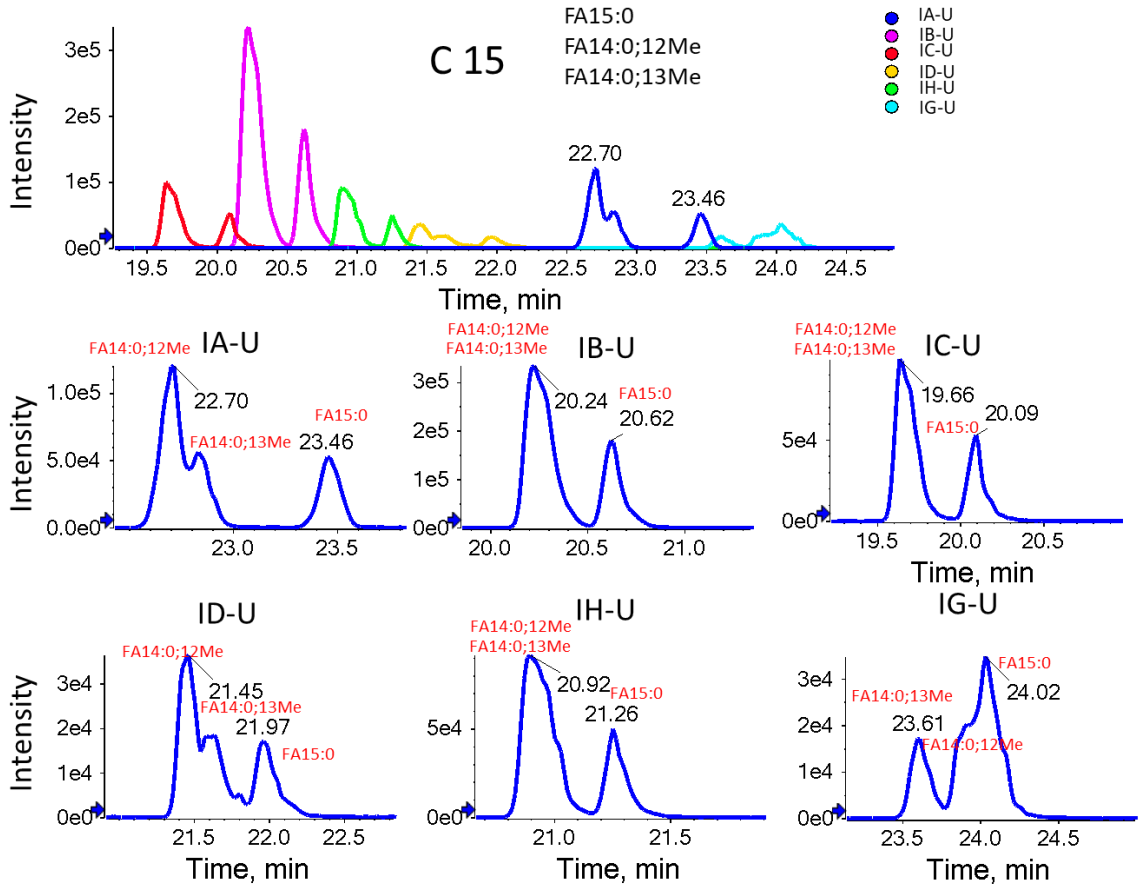

Fig. S7 *XIC of C15 isomers of SFAs in complex standard mixtures on different tested Chiralpak columns (IA-U, IB-U, IC-U, ID-U, IG-U and IH-U). LC-MS method was the same as described in Fig. 2 in main text.*

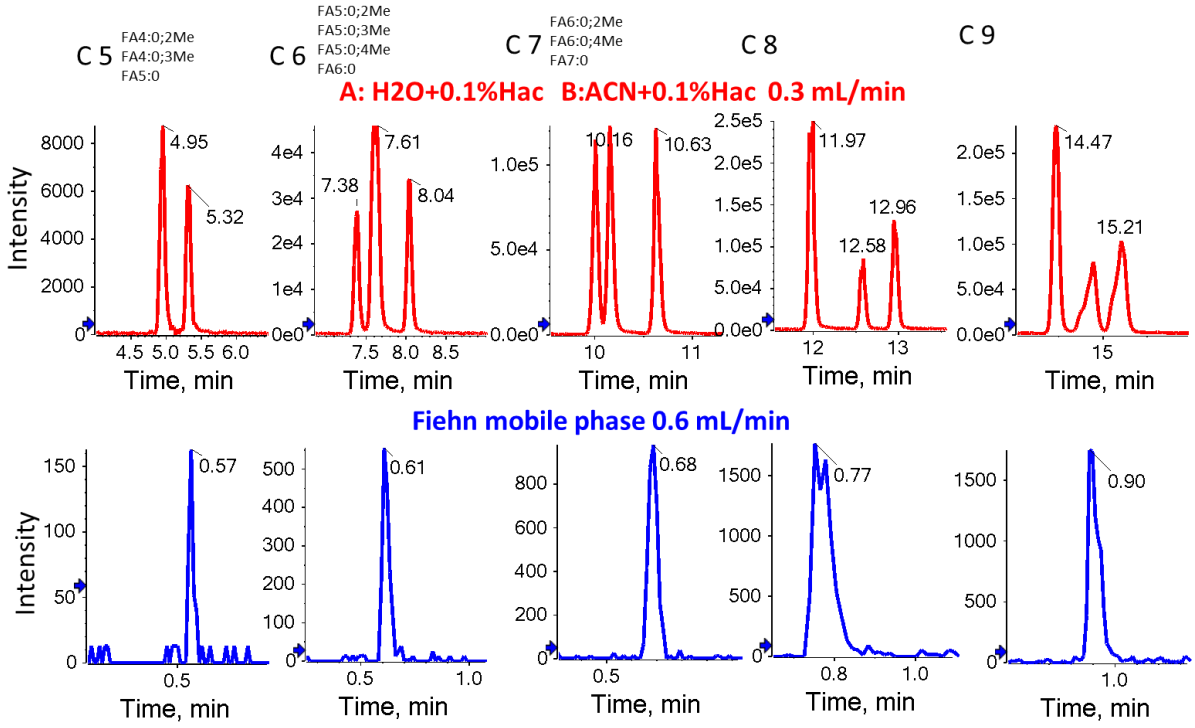

Fig. S8 *XIC of SFAs isomers of C5-C9 on columns RP C18 with different mobile phase and LC gradients. Red: mobile phase A H_2O+0.1% HAc and mobile phase B ACN+0.1% HAc, the column temperature was 40°C and the flow rate 0.3 mL/min. The gradient starts from 10%B and other conditions including MS parameters can be found in main text of section 2.3. Blue: the LC conditions were the same as in Fig. 1 for the general lipidomics method with acetonitrile/2-propanol eluent in main text.*

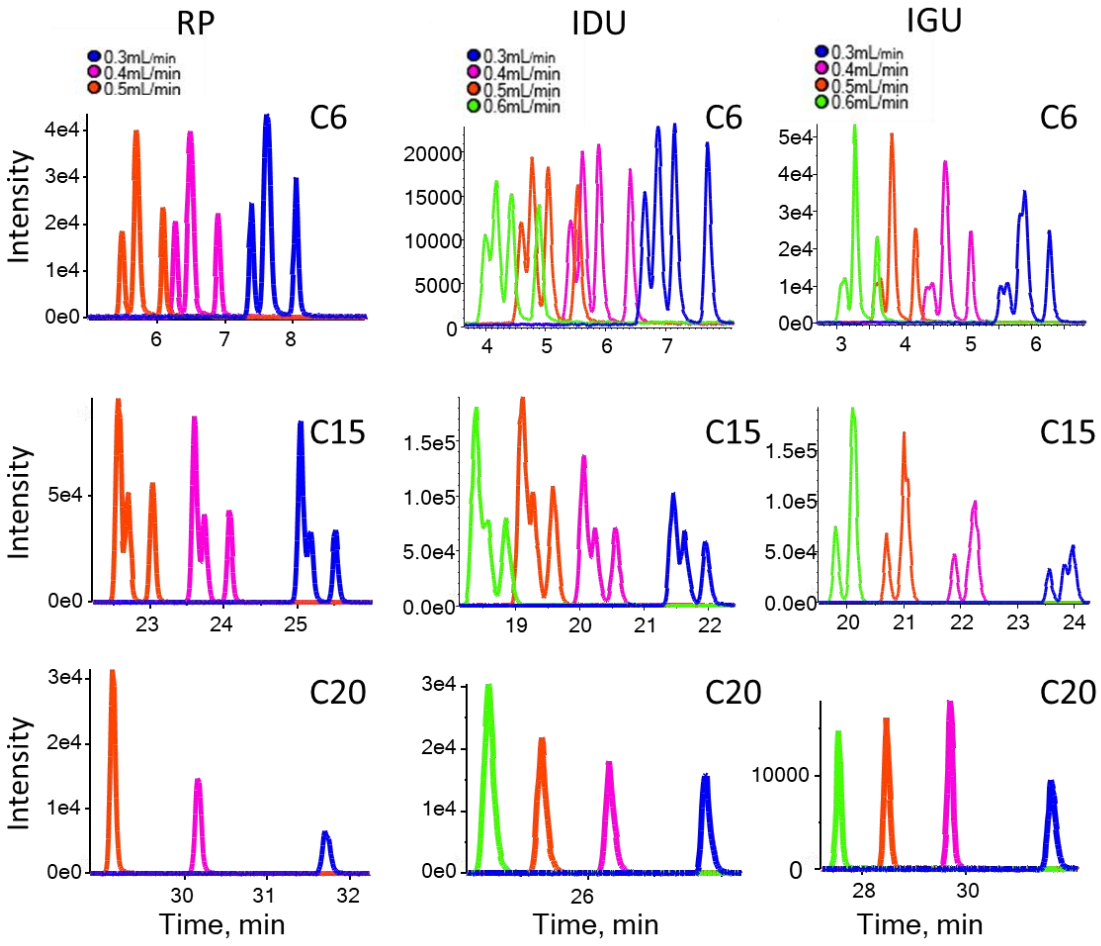

Fig. S9 *XIC of SFAs isomers of C6, C15 and C20 on columns RP C18, ID-U and IG-U under different flow rates. LC-MS conditions were the same as in Fig. 4.*

3. Retention model based on the methyl positions of BCFA

Table. S3 *Linear regression for IG-U column*

Model Summary[b]								
Model	**R**	**R Square**	**Adjusted R Square**	**Std. Error of the Estimate**	**F**	**Sig. F**		
1	0.999[a]	0.997	0.997	0.518	1315.678	<0.001		
Coefficients[b]								
Model		**Unstandardized Coefficients**		**Standardized Coefficients**	**t**	**Sig.**	**95.0% Confidence Interval for B**	
		B	**Std. Error**	**Beta**			**Lower Bound**	**Upper Bound**
1	(Constant)	-5.50	0.37		-14.7	<0.001	-6.28	-4.71
	CN	1.74	0.03	0.97	62.4	<0.001	1.68	1.79
	Me2	-0.99	0.38	-0.04	-2.6	0.017	-1.78	-0.20
	Me3	-1.28	0.44	-0.04	-2.9	0.009	-2.20	-0.37
	Me4	-0.75	0.36	-0.03	-2.1	0.052	-1.50	0.01
	Me6	-0.13	0.41	0.00	-0.3	0.752	-0.99	0.72

a. Predictors: (Constant), Me6, Me3, Me4, Me2, CN

b. Dependent Variable: RT

LC-MS conditions were the same as in Fig. 5 for IG-U column

4. Comparison with GC-MS FAME profiling

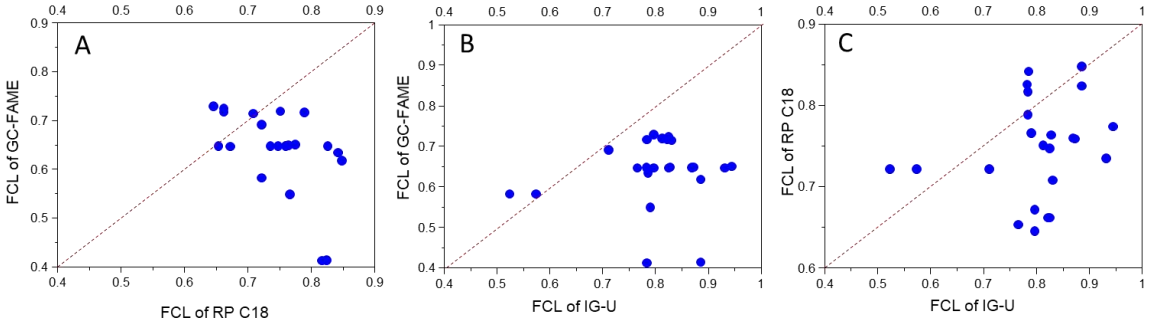

Fig. S10. *Paired comparison of FCL (fractional carbon chain length) of (a) reported GC-FAME vs. RP C18; (b) reported GC-FAME vs. IG-U and (c) RP C18 vs. IG-U. LC-MS conditions were the same as in Fig. 5. GC-FAME data were collected from ref. [47] of main document.*

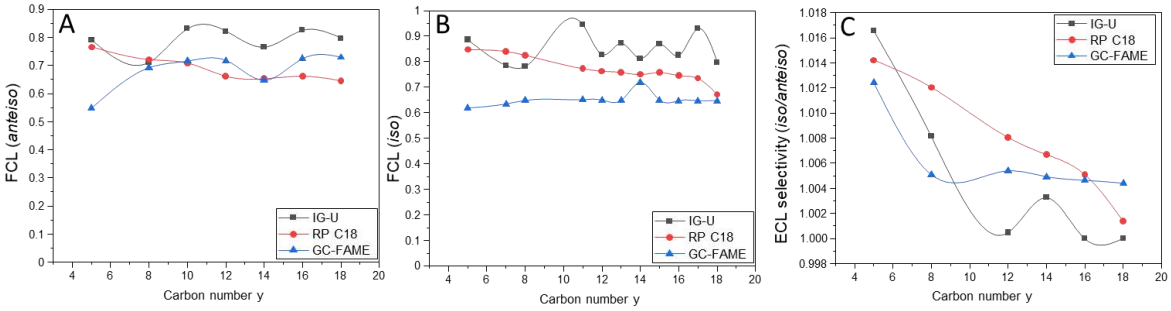

Fig. S11. FCLs in dependence on carbon number (y) in x-methyl-y-oic acid and methyl x-methyl-y-oate (with y is alkane with specific carbon number and x is branching position; for *iso*-FAs x = y-1 and for *anteiso*-FAs x = y-2). (a) FCLs of *anteiso*-FAs vs y for IG-U and CSH C18 as well as GC(OV1)-FAMEs. (b) FCLs of *iso*-FAs vs y for IG-U and CSH C18 as well as GC(OV1)-FAMEs. (c) ECL *iso*/*anteiso*-selectivity (calcuclated by the ratio of the corresponding ECLs of *iso*-FA/*anteiso*-FA with the same carbon number). *GC-FAME data were collected from ref. [47] of main document.*

5. Method application for fatty acids profiling in different types of samples

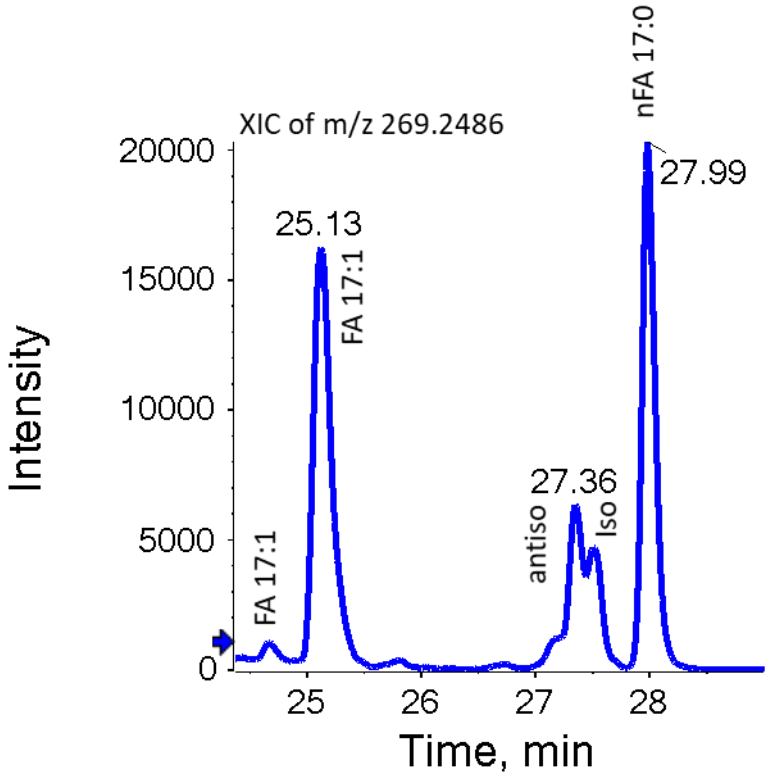

Fig. S12 *XIC of m/z 269.2486 (FA 17:0) in Staphylococcus sample. LC-MS conditions were the same as in Fig. 6 for RP C18 column.*

1.4 Publication IV

Micro-UHPLC-MS/MS method for analysis of oxylipins in plasma and platelets

Malgorzata Cebo[a], Xiaoqing Fu[a], Meinrad Gawaz[b], Madhumita Chatterjee[b], Michael Lämmerhofer[a]*

[a] University of Tübingen, Institute of Pharmaceutical Sciences, Pharmaceutical (Bio-)Analysis, Auf der Morgenstelle 8, 72076 Tübingen, Germany

[b] Department of Cardiology and Angiology, University Hospital Tübingen, Otfried-Müller-Strasse 10, 72076 Tübingen, Germany

Reprinted with permission from Journal of Pharmaceutical and Biomedical Analysis, Volume 189, 10 September 2020, 113426

https://doi.org/10.1016/j.jpba.2020.113426

Journal of Pharmaceutical and Biomedical Analysis 189 (2020) 113426

Contents lists available at ScienceDirect

Journal of Pharmaceutical and Biomedical Analysis

journal homepage: www.elsevier.com/locate/jpba

Micro-UHPLC-MS/MS method for analysis of oxylipins in plasma and platelets

Malgorzata Cebo[a], Xiaoqing Fu[a], Meinrad Gawaz[b], Madhumita Chatterjee[b], Michael Lämmerhofer[a,*,1]

[a] University of Tübingen, Institute of Pharmaceutical Sciences, Pharmaceutical (Bio-)Analysis, Auf der Morgenstelle 8, 72076, Tübingen, Germany
[b] Department of Cardiology and Angiology, University Hospital Tübingen, Otfried-Müller-Strasse 10, 72076, Tübingen, Germany

ARTICLE INFO

Article history:
Received 27 March 2020
Received in revised form 10 June 2020
Accepted 11 June 2020
Available online 20 June 2020

Keywords:
Capillary HPLC-ESI-MS/MS
Bioanalysis
Superficially porous particle capillary column
Platelet
Lipid mediator
Thromboinflammation

ABSTRACT

Oxylipins play an important role in cell signaling and they act as auto- and paracrine factors. There are numerous reports on the analysis of oxylipins in biofluids, especially in plasma. Only a limited number of studies addressed the analysis of oxylipins in platelets using modern, sensitive LC—MS methods, even though these compounds have a huge impact on platelet functions and thrombo-inflammation. In this work, a new method based on superficially porous particle (2.7 μm) capillary column (0.5 mm ID) and micro-liquid chromatography coupled to tandem mass spectrometry (μUHPLC-ESI-QqQ-MS/MS) method has been developed, optimized and validated. It has finally been successfully applied for human plasma and platelet analysis. The method allows the precise and accurate simultaneous quantification of 42 oxylipins with 13 deuterated internal standards. Solid phase extraction with Bond Elut Certify II provides good extraction recoveries (on average around 75 %). The μUHPLC-MS/MS method is selective, sensitive (LOQs between 30 and 150 pg/mL) and shows good linearity. Limits of detections for most of the compounds are between 2 and 250 fmol on column. Twenty-three oxylipins have been detected in plasma and 19 in non-activated (resting) platelets (all samples were from healthy donors). The μUHPLC-MS/MS method uses very low volume of mobile phase (less than 250 μL of organic solvents in mobile phase per analysis), and therefore is considered environmentally friendly. It also turned out to be robust enough for routine analysis.

1. Introduction

Oxylipins are oxidized polyunsaturated fatty acids (PUFAs) which are highly bioactive and play numerous important biological functions [1]. Most of the oxylipins are either chemically unstable or are metabolized very quickly. They are synthesized from PUFAs that are released from membrane phospholipids by cleavage at the sn-2 position by cytosolic phospholipase A2 (cPLA2) [1,2]. Then, free PUFAs are metabolized to oxylipins by 3 different families of enzymes: by cyclooxygenase (COX), lipoxygenase (LOX) or by cytochrome P450 (CYP450) [1,2] (Fig. 1). Oxylipins might also result from *in-vivo* or *in-vitro* non-enzymatic autoxidation.

The comprehensive quantitative analysis of oxylipins in biofluids, cells and tissues is of major importance as it might provide better insights into the biochemical changes associated with pathophysiological states [2,3]. However, analysis of oxylipins is challenging [4]. These compounds are typically present at very low concentrations in biological samples; and what is more, concentration of highest and lowest abundant analytes may differ a lot (in some cases over 10^3 fold). Also, the concentration of a particular analyte might be very different in healthy and disease state. This requires a wide linear range of detection. Some oxylipins might be unstable and usually light protection and inhibitors of further oxidation (i.e. antioxidants) are used during sample preparation; furthermore, the samples need to be stored and processed at low temperatures [5]. Many oxylipins, even if they play very different biochemical roles, have highly similar structures, hence method specificity is of high importance, but might be challenging [4,6]. Another issue is availability of standards and isotopically labeled analogues used as internal standards (IS). Their quality including purity, exact concentration (if purchased as solution) or mass (if supplied as solid material) and stability is very important for method validation and correct quantification [7]. However, in many cases suppliers of oxylipin standards provide insufficient information regarding these parameters and lot-to-lot variations may be another concern.

* Corresponding author.
E-mail address: michael.laemmerhofer@uni-tuebingen.de (M. Lämmerhofer).
[1] http://www.bioanalysis.uni-tuebingen.de/.

https://doi.org/10.1016/j.jpba.2020.113426
0731-7085/

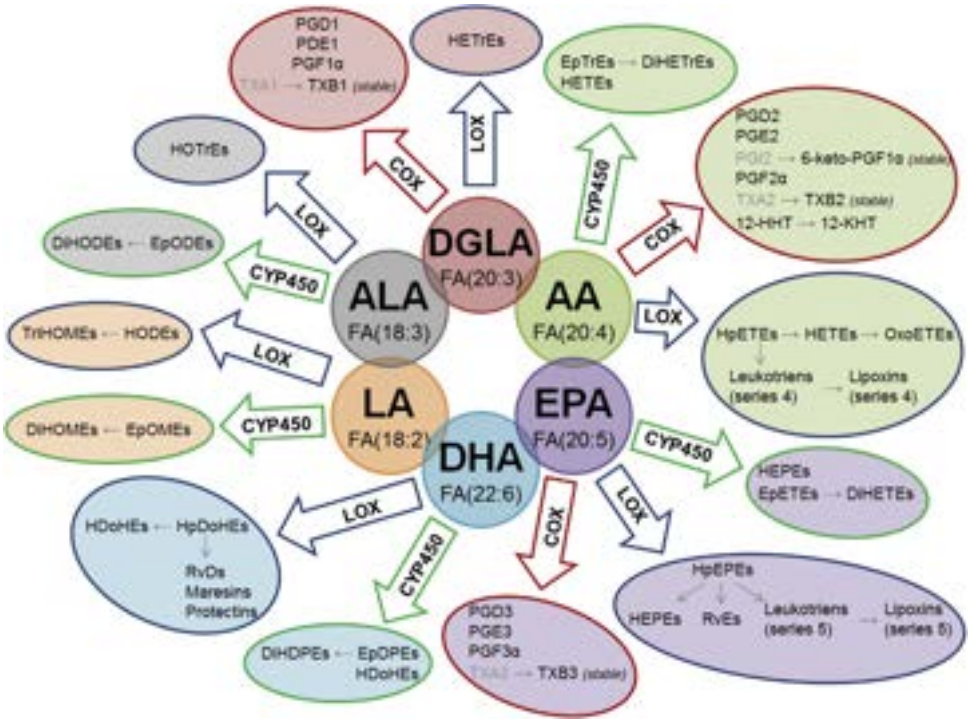

Fig. 1. Overview of enzymatic biosynthesis of oxylipins originating from the 6 most common PUFAs [10,24,28].

In the past, oxylipins were analyzed, after derivatization, with gas chromatography (GC) coupled to MS, but these GC assays were largely substituted by liquid chromatographic methods (LC) combined with tandem MS (MS/MS), which allows the analysis of oxylipins in their underivatized form [8]. Nowadays, ultra-high performance liquid chromatography (UHPLC) with reversed-phase (RP) stationary phases combined with triple quadrupole (QqQ) instruments, which feature very high sensitivity and wide linear range [9,10] or quadrupole linear ion traps (QTrap) with enhanced scan functions are most popular instrumentations for multiplexed oxylipin assays analyzing simultaneously up to 200 targets [2,11,3–16]. High resolution MS with QTOF [17] and Orbitrap gained also popularity recently and allow untargeted profiling of oxylipins. Supercritical fluid chromatography (SFC) coupled to MS is also slowly emerging in oxylipin analysis [18]. Recently, ion mobility (IMS) hyphenated to QTOF-MS has been utilized in oxylipin analysis, as it provides an additional dimension for separation of isomers [19]. In order to get a full picture of bioactivities, the chirality of oxylipins has to be considered as well. Very often only one enantiomeric form is biologically active, so it is of high importance to distinguish between racemic mixtures and pure enantiomers. MS instruments, as achiral detector, are not able to differentiate between enantiomers and only chiral separation prior to MS detection provides insight into enantiomeric composition of a sample. Nowadays, there are efficient enantioselective LC–MS/MS assays available for this purpose [20,21]. However, chiral columns give typically broader peaks and therefore might provide lower sensitivity compared to RP chromatographic methods. For this reason, in this work we describe an achiral LC–MS/MS assay for oxylipins.

There is a limited number of studies on oxylipins in platelets, even though they are highly important for platelet biochemistry [17,22]. In our studies, we established a new *ecofriendly* and robust miniaturized LC–MS method for accurate analysis of oxylipins. It utilizes μUHPLC for oxylipin separation. The method is sensitive, as the narrow column (inner diameter equal to 0.5 mm) packed with core-shell particles provides very narrow peaks with good peak resolution and enhanced signal-to-noise (S/N) ratio due to efficient ionization at low flow rates (30 μL/min). It is robust enough for routine analysis of hundreds of samples per day at significantly lower solvent costs and environmental impact. The new method has been validated for complex matrix, viz. plasma, incorporating an SPE enrichment step and was also applied to analyze platelet oxylipins.

2. Materials and methods

2.1. Materials

Arachidonic acid (AA), decanoic-2,2,3,3,4,4,5,5,6,6,7,7,8,8,9,9,10,10,10-d19 acid (FA(10:0)-d19) and undecanoic acid were purchased from Sigma Aldrich (*Merck*, Munich, Germany). All the other analytes and internal standards were obtained from Cayman Chemical (Ann Arbor, MI, USA): 5-hydroxy-6E,8Z,11Z,14Z-eicosatetraenoic acid (5-HETE), 8-hydroxy-5Z,9E,11Z,14Z-eicosatetraenoic acid (8-HETE), 9-hydroxy-5Z,7E,11Z,14Z-eicosatetraenoic acid (9-HETE), 11-hydroxy-5Z,8Z,12E,14Z-eicosatetraenoic acid (11-HETE), 12-hydroxy-5Z,8Z,10E,14Z-eicosatetraenoic acid (12-HETE), 15-hydroxy-5Z,8Z,11Z,13E-eicosatetraenoic acid (15-HETE), 20-hydroxy-5Z,8Z,11Z,14Z-eicosatetraenoic acid (20-HETE), 5-hydroxy-6E,8Z,11Z,14Z,17Z-eicosapentaenoic acid (5-HEPE), 8-hydroxy-5Z,9E,11Z,14Z,17Z-eicosapentaenoic acid (8-HEPE), 12-hydroxy-5Z,8Z,10E,14Z,17Z-eicosapentaenoic acid (12-HEPE), 15-hydroxy-5Z,8Z,11Z,13E,17Z-eicosapentaenoic acid (15-HEPE), 18-hydroxy-5Z,8Z,11Z,14Z,16E-eicosapentaenoic acid (18-HEPE), 14(15)-epoxy-5Z,8Z,11Z,17Z-eicosatetraenoic acid (14(15)-EpETE), 5,6-dihydroxy-7E,9E,11Z,14Z-eicosatetraenoic acid (5,6-DiHETE), 10-hydroxy-4Z,7Z,11E,13Z,16Z,19Z-docosahexaenoic acid (10-HDoHE), 14-hydroxy-4Z,7Z,10Z,12E,16Z,19Z-docosahexaenoic acid (14-HDoHE), 17-hydroxy-4Z,7Z,10Z,13Z,15E,19Z-docosahexaenoic acid (17-HDoHE), 9-hydroxy-10E,12Z-octadecadienoic acid (9-HODE), 13-hydroxy-9Z,11E-octadecadienoic acid (13-HODE),

12-hydroxy-5Z,8E,10E-heptadecatrienoic acid (12-HHT), 8R-hydroxy-4Z,6E,10Z-hexadecatrienoic acid (T-12-HETE), 12-hydroxy-5Z,8Z,12Z-eicosatrienoic acid (12-HETrE), 13-hydroxy-9Z,11E,15Z-octadecatrienoic acid (13-HOTrE), 5-oxo-6E,8Z,11Z,14Z-eicosatetraenoic acid (5-OxoETE), Resolvin D1 (RvD1), Resolvin D2 (RvD2), Resolvin D3 (RvD3), Resolvin D4 (RvD4), Resolvin D5 (RvD5), Resolvin E1 (RvE1), Maresin 1 (Mar1), Maresin 2 (Mar2), Lipoxin A4 (LXA4), Leukotriene B4 (LTB4), Prostaglandin D1 (PGD1), Prostaglandin E1 (PGE1), Prostaglandin D2 (PGD2), Prostaglandin E2 (PGE2), 6-keto-Prostaglandin F1α (6-keto-PGF1α), Prostaglandin F2α (PGF2α), Thromboxane B2 (TXB2), 4Z,7Z,10Z,13Z,16Z,19Z-docosahexaenoic acid (DHA), 7Z,10Z,13Z,16Z,19Z-docosapentaenoic acid (DPA), 7Z,10Z,13Z,16Z-docosatetraenoic acid (adrenic acid, ADA), 5Z,8Z,11Z,14Z,17Z-eicosapentaenoic acid (EPA), arachidonic acid (AA) and 8Z,11Z,14Z-eicosatrienoic acid (DGLA). Internal standards were also purchased from Cayman Chemical: 6Z,8E,10E,14Z,16E-eicosapentaenoic-6,7,14,15-d4 acid (RvE1-d4), 7S,8R,17S-trihydroxy-4Z,9E,11E,13Z,15E,19Z-21,21′,22,22,22-d5 docosahexaenoic acid (RvD1-d5), 9-oxo-11alpha,15S-dihydroxy-prosta-5Z,13E-dien-1-oic-3,3,4,4-d4 acid (PGE2-d4), 15S-dihydroxy-11-oxo-prosta-5Z,13E-dien-1-oic-17,17,18,18,19,19,20,20,20-d9 acid (PGD2-d9), 9alpha,11,15S-trihydroxy-thromba-5Z,13E-dien-1-oic-3,3,4,4-d4 acid (TXB2-d4), 9alpha,11alpha,15S-trihydroxy-prosta-5Z,13E-dien-1-oic-3,3,4,4-d4 acid (PGF2α-d4), 13R,14S-dihydroxy-4Z,7Z,9E,11Z,16Z,19Z-docosahexaenoic-21,21,22,22,22-d5 acid (Mar2-d5), 5S,12R-dihydroxy-6Z,8E,10E,14Z-eicosatetraenoic-6,7,14,15-d4 acid (LTB4-d4), 5S-hydroxy-6E,8Z,11Z,14Z-eicosatetraenoic-5,6,8,9,11,12,14,15-d8 acid (5-HETE-d8), 12S-hydroxy-5Z,8Z,10E,14Z-eicosatetraenoic-5,6,8,9,11,12,14,15-d8 acid (12-HETE-d8), 20-hydroxy Arachidonic Acid-d6, 20-hydroxy-5Z,8Z,11Z,14Z-eicosatetraenoic-16,16,17,17,18,18-d6 acid (20-HETE-d6), 4Z,7Z,10Z,13Z-hexadecatetraenoic-15,15,16,16,16-d5 acid (HTE-d5), 5Z,8Z,11Z,14Z-eicosatetraenoic-16,16,17,17,18,18,19,19,20,20,20-d11 acid (AA-d11), 8Z,11Z,14Z-eicosatrienoic-8,9,11,12,14,15-d6 acid (DGLA-d6), 4Z,7Z,10Z,13Z,16Z,19Z-docosahexaenoic-21,21,22,22,22-d5 acid (DHA-d5) and 5Z,8Z,11Z,14Z,17Z-eicosapentaenoic-19,19,20,20,20-d5 acid (EPA-d5). All standards were utilized as provided and with concentrations as specified by the supplier assuming appropriate quality of the supplied standard solutions and correctness of their concentrations. Validation of the quality of supplied non-certified standards and corrections for inadequate standard concentrations as suggested by N.H. Schebb and coworkers are recommended when interlaboratory studies are performed or for interstudy comparisons [7].

Solvents: methanol (MeOH), acetonitrile (ACN) and isopropanol (IPA) of LC–MS grade as well as dichloromethane (DCM) of GC grade were purchased from Carl Roth (Karlsruhe, Germany). Dess-Martin periodinane, *N*-[1-(1-Oxopropyl)-4-piperidinyl]-*N*'-[4-(trifluoromethoxy)phenyl]urea (TPPU), butylated hydroxytoluene (BHT), acetic acid (HAc), formic acid (FA), ammonium acetate (NH_4Ac), ammonium formate (NH_4FA) and sodium acetate were from Sigma Aldrich (*Merck*). Ultrapure water was produced by Elga Purelab Ultra (Celle, Germany).

Bond Elut Certify II solid phase extraction cartridges (3 mL / 200 mg) were obtained from Agilent (Waldbronn, Germany).

2.2. Synthesis of 12-KHT

12-Oxo-5Z,8E,10E-heptadecatrienoic acid (12-KHT) was synthesized from 12-HHT as described before [17]. Briefly, 50 μL of 12-HHT (100 μg/mL in ethanol) was placed together with 5 μL of undecanoic acid (100 μg/mL) as internal standard in a glass vial. Solvents were evaporated and 60 μL of DCM and 15 μL of Dess-Martin reagent solution (0.3 M in DCM) were added. The reaction was allowed to proceed at room temperature for 5 min. After that solvent was evaporated and the reaction was quenched with 500 μL MeOH. The sample was left at −80 °C for 24 h and then filtrated. The final concentration of the stock solution was determined as 8.9 μg/mL.

2.3. Sample preparation

2.3.1. Collection of plasma and platelet samples

Plasma samples were collected from the peripheral blood of healthy male donors at the Department of Medical Psychology and Behavioral Neurobiology, University Hospital Tübingen, Germany, and platelet samples were obtained from the peripheral blood of healthy donors at the Dept. of Cardiology and Angiology, University Hospital Tübingen, according to ethical guidelines and approved by regional authorities. Resting platelets were isolated from blood, as described previously [17], and samples with platelet count 2×10^8 were prepared. At the last stage of the reported protocol, phosphate-buffered saline (PBS buffer) supplemented with calcium ions was not removed. Plasma and platelets (suspended in PBS) were kept at −80 °C until extraction.

2.3.2. Oxylipin and fatty acid extraction from plasma, preparation of calibrants and quality control samples

To perform the oxylipin and fatty acid extraction, plasma was slowly thawed on ice for about 2 h. For preparation of matrix-matched calibrants and QCs, plasma was pooled and solutions of BHT as antioxidant and TPPU as soluble epoxide hydrolase (sEH) inhibitor were added: 20 μL of the mixed stock solution (200 μg/mL of each compound in MeOH, final concentration after extraction: 20 μg/mL) were added per 1 mL of plasma. Pooled plasma was then divided into 500 μL aliquots and spiked with 40 μL of internal standard (IS) mix stock solution (TXB2-d4, PGF2α-d4, PGE2-d4, PGD2-d9, RvD1-d5, RvE1-d4, Mar2-d5, LTB4-d4, 5-HETE-d8, 12-HETE-d8, 20-HETE-d6, FA(10:0)-d19, HTE-d5: each 25 ng/mL resulting in a final concentration of 10 ng/mL; except for 13-HODE-d4, DHA-d5, DGLA-d6, EPA-d5, AA-d11 for which a 2.5 μg/mL solution was added resulting in a final concentration of 1 μg/mL).

Calibrants and quality controls (QC) were prepared from above stock solutions. Calibrants were prepared at 12 different concentrations to cover sufficiently wide concentration ranges of the different analytes: oxylipin range (except 9- and 13-HODE) - 50 pg/mL of plasma to 25 ng/mL; calibrants of 9- and 13-HODE were in the range of 500 pg/mL to 250 ng/mL and fatty acids between 5 ng/mL to 2.5 μg/mL. QC samples were prepared at 3 different levels: oxylipins except 9- and 13-HODE – 160 pg/mL, 1.6 ng/mL and 4 ng/mL; 9- and 13-HODE: 16 ng/mL, 40 ng/mL and 160 ng/mL; fatty acids: 16 ng/mL, 160 ng/mL and 400 ng/mL.

Then, 1 mL of buffer pH 6 (1 M CH_3COONa in the mixture of water/MeOH (95:5; v/v) adjusted to pH 6 with HAc) was added to each sample. The samples were centrifuged (4000 x *g*, 4 °C, 5 min) in order to remove possible precipitants and solid particles from the solution, which could plug the SPE cartridge (proteins were not precipitated at this point, as only 5 % of the organic solvent MeOH were not enough to induce protein precipitation).

The Bond Elut Certify II SPE cartridges were pre-conditioned with 2 mL of a mixture of ethyl acetate/n-hexane/HAc (75:24:1; v/v/v), followed by 2 mL MeOH and in the last step with 2 mL of the 1 M CH_3COONa buffer pH 6. Then samples were loaded and washed 2 times with 2.5 mL H_2O/MeOH (4:1; v/v) mixture. Until this step, the cartridges were prevented from drying. After the second washing step the cartridges were dried for 5 min. Then the samples were

eluted with 2 times 1 mL mixture of ethyl acetate/n-hexane/HAc (75:24:1; v/v/v).

Eluates were evaporated with GeneVac (Ipswich, UK) under nitrogen protection. Evaporation time was around 1 h. After that, samples were re-dissolved in 40 μL of MeOH and 60 μL water were added. Samples were vortexed and centrifuged (4000 x g, 4 °C, 5 min) and transferred to autosampler vials for immediate LC–MS analysis.

2.3.3. Determination of matrix effects and extraction recoveries

Determination of matrix effects and extraction recoveries was performed according to Matuszewski's protocol [23]. Three sets of samples were prepared: pooled plasma spiked with standards and ISs before extraction (pre-extraction spike) (as described in the paragraph 2.2.2); pooled plasma spiked with standards and ISs after extraction, i.e. standards and ISs added with the reconstitution solvent to dried extracts; solvent (H_2O/MeOH (3:2; v/v)) spiked with standards and ISs (standard solutions). The theoretical concentration in each set was the same. ISs were spiked, as described above for QCs with the following concentrations: 10 ng/mL for TXB2-d4, PGF2α-d4, PGE2-d4, PGD2-d9, RvD1-d5, RvE1-d4, Mar2-d5, LTB4-d4, 5-HETE-d8, 12-HETE-d8, 20-HETE-d6, FA(10:0)-d19, HTE-d5, and 1 μg/mL for 13-HODE-d4, DHA-d5, DGLA-d6, EPA-d5, AA-d11. Standards were added at 3 different levels: 1.6 ng/mL, 4 ng/mL and 16 ng/mL for all oxylipins except of 9- and 13-HODE for which the concentrations were 16 ng/mL, 40 ng/mL and 160 ng/mL. For fatty acids, the concentrations were 160 ng/mL, 400 ng/mL and 1.6 μg/mL. Matrix effect was calculated as ratio of peak areas in post-extraction spiked samples and corresponding standard solution (spiked solvent). Extraction recovery was determined as ratio of peak areas in pre-extraction spiked samples and corresponding post-extraction spiked samples.

2.3.4. Oxylipin and fatty acid extraction from platelets

IPA was added to frozen platelets suspended in PBS buffer to obtain the ratio IPA/H_2O (9:1; v/v). BHT and TPPU stock solutions were added (10 μL, 200 μg/mL of each compound in MeOH). Samples were kept for 80 min in a shaker at 4 °C for thawing, protein precipitation and lipid extraction. Then, ISs were added (TXB2-d4, PGF2α-d4, PGE2-d4, PGD2-d9, RvD1-d5, RvE1-d4, Mar2-d5, LTB4-d4, 5-HETE-d8, 12-HETE-d8, 20-HETE-d6, FA(10:0)-d19, HTE-d5 at a final concentration of 10 ng/mL; 13-HODE-d4, DHA-d5, DGLA-d6, EPA-d5, AA-d11 at a final concentration of 1 μg/mL). Samples were vortexed (10 s) and sonicated (5 times, each time 2 min, samples were cooled for minimum 10 min in between). Afterwards, the samples were centrifuged (4000 × g, 4 °C, 5 min) in order to remove precipitated proteins and cell residues, and the supernatants were transferred to fresh falcon tubes. Each supernatant was diluted with 2 mL of buffer pH 6 (1 M CH_3COONa in water/MeOH (95:5;v/v) adjusted to pH 6 with HAc) and loaded onto preconditioned Bond Elut Certify II SPE cartridges, as described for plasma in the Section 2.3.2. After sample loading, the cartridges were washed 2 times with 2.5 mL H_2O/MeOH (4:1; v/v) and dried for 5 min. Samples were eluted into fresh falcon tubes with (2 times 1 mL) ethyl acetate/n-hexane/HAc (75:24:1; v/v/v). The solvent was evaporated with GeneVac under nitrogen protection. The samples were reconstituted with 20 μL MeOH and then 30 μL of water was added. The samples were vortexed (10 s), centrifuged (4000 × g, 4 °C, 5 min) and transferred to autosampler vials. A QC sample was prepared by pooling 20 μL of each sample in a separate vial. It was used to assure good quality of μLC-MS analysis and to prepare calibrants. The samples were analyzed by μUHPLC-MS/MS immediately after their preparation. The order of analysis was randomized and the QC sample was injected before, after and in between the samples.

Table 1
Binary gradient profile with eluent composition (%B) and flow rate as well as column washing program.

LC GRADIENT		
Time [min]	B [%]	Flow rate [μL/min]
During data acquisition: injection of 5 μL of sample		
0.0	15	30
9.0	99	30
10.0	99	30
Wash and re-equilibration: Injection of 5 μL IPA		
0.0	99	10
2.0	99	10
2.1	15	30
3.0	15	30

2.3.5. Calibrants for platelets

The QC pool was divided into 6 aliquots and 5 of them were spiked with standards at different levels to prepare matrix-matched external calibration. Calibration ranges of oxylipins covered concentrations from 50 pg/mL to 25 ng/mL except of 9- and 13-HODE for which concentrations ranged from 0.5 ng/mL up to 250 ng/mL. Moreover, fatty acids were calibrated at concentrations from 5 ng/mL to 2.5 μg/mL. Calibrants were analyzed in the same batch with the platelet samples and QC.

2.4. μUHPLC-MS/MS method

μUHPLC-MS/MS analysis was performed with an Eksigent μLC 200 Plus System (Sciex, Ontario, Canada) coupled to a QTrap 4500 MS instrument (Sciex) equipped with a Turbo V source and 50 μm ID hybrid electrodes – made of PEEKsil, with a 1 cm stainless steel tip. An Eksigent HALO C18 (Sciex) column (dimension 50 mm × 0.5 mm; particle size 2.7 μm, 90 Å) was used for the chromatographic separation. The column was kept at 50 °C during the analysis. The injection volume was 5 μL. Mobile phase A was H_2O with 0.1 % HAc (v/v) and mobile phase B was ACN with 0.1 % HAc (v/v). Gradient elution started with 15 % B, followed by a linear gradient to 99 % B in 9 min and subsequent hold at 99 % B for 1 min. The flow rate at this stage was equal to 30 μL/min (see Table 1). At the end of this gradient a 'solvent plug' of 5 μL IPA was injected to wash the column and remove contaminations of more apolar lipids. During this injection 99 % mobile phase B and 1 % mobile phase A were pumped through the column with reduced flow rate (10 μL/min); this step lasted 2 min. Then, the eluent composition was quickly changed (in 0.1 min) to 15 % B and the flow rate was raised to 30 μL/min to re-equilibrate the column for the next analysis (0.9 min equilibration time) (Table 1).

MS analysis was performed with ESI in negative mode. The source voltage was -4000 V and the source temperature was 400 °C. Nebulizer gas, heater gas and curtain gas pressures were set to 25 psi, 20 psi and 25 psi, respectively. The entrance potential was set to −10 V. The collision gas was used at medium pressure. Q1 and Q3 resolution was set to unit. SRMs were optimized individually for each analyte and are summarized in Table 2. Scheduled MRM mode was used with the cycle time equal to 300 ms.

2.5. Validation of method for plasma

Instrument linearity (analytes dissolved in solvent) and linearity in matrix, as well as within-batch and between-batch precision and accuracy, limit of detection (LOD) and limit of quantification (LOQ) were investigated.

Within-batch accuracy and precision was calculated based on 6 measurements of each from 3 QCs, prepared on the same day and measured in the same batch.

Table 2
SRMs (start and end RT specify the period in which the respective SRM transition was acquired).

Name	Q1 *m/z*	Q3 *m/z*	Expected RT [min]	Start RT [min]	End RT [min]	CE [V]	CXP [V]	DP [V]
PGF2a	353.1	309.2	2.5 7	2.3	10.0	−27	−12	−80
PGE1 and PGD1	353.1	317.1	2.73 and 2.77	2.5	3.5	−18	−12	−60
TXB2	369.2	195	2.35	2.0	3.7	−19	−10	−80
6-keto-PGF1a	369.2	163	1.92	0.0	2.6	−35	−10	−65
PGE2 and PGD2	351.2	315.2	2.65 and 2.76	2.3	3.7	−18	−12	−80
10-HDoHE	343.1	153	5.24	5.0	5.9	−20	−8	−70
14-HDoHE	343.1	205	5.23	4.9	5.9	−18	−10	−60
17-HDoHE	343.1	201	5.14	4.9	5.9	−20	−10	−80
5-HETE	319.1	114.9	5.4	5.1	6.1	−18	−8	−80
8-HETE	319.1	154.9	5.27	5.0	6.0	−20	−12	−75
9-HETE	319.1	151	5.33	5.1	6.0	−21	−8	−40
11-HETE	319.1	167	5.18	4.9	5.9	−22	−8	−75
12-HETE	319.1	208	5.27	5.0	6.0	−21	−10	−80
15-HETE	319.1	219	5.07	4.8	5.8	−17	−10	−40
20-HETE	319.1	245	4.66	4.4	5.4	−22	−10	−80
5-HEPE	317.1	114.9	4.91	4.6	5.6	−20	−8	−75
8-HEPE	317.1	154.8	4.79	4.5	5.5	−20	−12	−70
12-HEPE	317.1	179	4.81	4.5	5.5	−18	−8	−75
15-HEPE	317.1	219	4.71	4.4	5.4	−18	−10	−95
18-HEPE	317.1	215.1	4.56	4.3	5.3	−18	−10	−65
14(15)-EpETE	317.1	207	5.26	5.0	6.0	−16	−10	−60
5,6-DiHETE	335.1	144.9	4.19	3.9	4.9	−22	−9	−20
5-OxoETE	317.1	203	5.53	5.3	6.3	−24	−10	−85
12-OxoETE	317.1	153	5.41	5.1	6.4	−24	−10	−80
9-HODE	295.2	171	4.95	4.7	5.7	−25	−8	−80
13-HODE	295.2	195	4.91	4.6	5.6	−26	−8	−80
LXA4	351.1	114.9	3.01	2.7	3.7	−23	−8	−70
12-HHT	279.1	179	4.24	4.0	5.0	−17	−8	−80
12-KHT	277.2	113	4.46	4.2	5.2	−20	−11	−80
LTB4	335.2	195	3.87	3.6	4.6	−22	−8	−80
T-12-HETE	265.1	109	4.13	3.9	4.8	−18	−8	−50
RvD1	375.1	121.1	3.05	2.8	3.8	−35	−8	−80
RvD2	375.1	277.1	2.84	2.6	3.6	−20	−8	−70
RvD3	375.1	147	2.75	2.5	3.5	−25	−8	−40
RvD4	375.1	100.9	3.3	3.0	4.0	−26	−8	−80
RvD5	359.2	199.1	3.82	3.6	4.6	−21	−10	−40
RvE1	349.1	194.9	2	1.7	2.7	−22	−11	−65
Mar1	359.2	297.2	3.82	3.5	4.5	−22	−10	−75
Mar2	359.2	221	4.12	3.9	4.8	−16	−10	−60
12-HETrE	321.4	181	5.47	5.2	6.2	−24	−7	−40
13-HOTrE	293	224	4.54	4.3	5.2	−18	−9	−40
FA(20:4)	303	259	6.9	6.6	7.6	−20	−12	−80
FA(20:5)	301	257	6.4	6.1	7.1	−15	−12	−80
FA(20:2)	307.3	307.3	7.77	7.5	8.5	−10	−14	−80
FA(22:4)	331.3	287	7.54	7.3	8.2	−20	−12	−80
FA(20:3)	305.2	261	7.26	7.0	8.0	−25	−12	−80
FA(22:6)	327	283	6.79	6.5	7.5	−15	−12	−80
FA(22:5)	329	329	7.27	7.0	7.9	−5	−8	−80
PGE2-d4	355.2	319.2	2.64	2.4	3.3	−17	−12	−80
TxB2-d4	373.3	173.1	2.34	2.0	3.7	−24	−8	−80
12-HETE-d8	327.3	184	5.23	5.0	5.9	−20	−8	−80
13-HODE-d4	299.1	198	4.89	4.6	5.6	−24	−10	−90
RvD1-d5	380.3	140.9	3.02	2.7	3.7	−20	−8	−40
PGD2-d9	360.2	280.2	2.74	2.5	3.5	−24	−10	−80
FA(10:0)-d19	190.3	190.3	4.26	4.0	5.0	−10	−11	−70
PGF2a-d4	357.2	169.1	2.56	2.3	3.3	−35	−8	−80
HTE-d5	252.2	208.2	5.25	5.0	6.0	−20	−11	−80
AA-d11	314.2	270.1	6.87	6.6	7.5	−19	−12	−90
20-HETE-d6	325.1	281.2	4.63	4.4	5.4	−20	−13	−90
5-HETE-d8	327.1	115.9	5.36	5.1	6.1	−18	−7	−50
DHA-d5	332.1	288.1	6.77	6.5	7.5	−14	−11	−50
EPA-d5	306	262	6.38	6.1	7.1	−16	−11	−60
LTB4-d4	339.1	196.9	3.85	3.6	4.6	−22	−9	−70
Mar2-d5	364.1	221	4.11	3.8	4.8	−16	−9	−40
RvE1-d4	353.1	196.9	1.98	1.7	2.7	−22	−7	−40
DGLA-d6	311.2	267.2	7.23	7.0	7.9	−25	−11	−80

Between-batch accuracy and precision were calculated from results obtained for QCs prepared and measured on 3 different days.

LOQ and LOD were calculated from matrix-matched calibration curve. LOQ was equal to 10 times the ratio of uncertainty in calculation of peak area ratio to calibration curve (10*sigma/slope). LOD was equal to 3 times this ratio (3*sigma/slope).

Linearity, both in solvent and in matrix, was characterized as coefficient of determination (R^2) for the linear range of the calibration function.

2.6. Data analysis

Data analysis was performed with MultiQuant 3.0 (Sciex) using the algorithm MQ4. The Gaussian smooth width was set to 1.0 points, retention time half window was 5.0 s, minimal peak width was 3 points and minimum peak height was established individually for each SRM, but usually set to 500. Integration parameters included noise percentage (set to 40 %), baseline subtraction window (0.20 min) and peak splitting (usually 1 point). MultiQuant was used for peak finding and integration, as well as calculation of the calibration function by weighted linear regression (weighting was set to $1/x^2$ for all compounds). Further calculations were done with Excel 2007 (Microsoft, Redmond, WA, USA) and R (version i386 3.4.2, R-project for statistical computing).

Calibration functions were obtained by plotting peak area ratios against concentrations, except for TXB2, for which peak height ratio was used, because of the double peak caused by interconversion of hemiacetal forms. The 2 peaks of TXB2, with a plateau in between were hard to integrate accurately by peak area, but well defined by peak height. The higher, first eluted peak of TXB2 was used for calculations. The ratio of the 2 peaks was well conserved during the analysis.

3. Results and discussion

3.1. Method development

3.1.1. Optimization of μUHPLC method

Specificity of oxylipin assays can be easily compromised by numerous isobaric and isomeric interferences, if they are not properly separated. Hence, great attention was paid to the optimization of chromatographic separation to avoid coelution of oxylipins which cannot be distinguished by specific SRM transitions or get compromised due to interference from similar fragmentation pattern (Suppl. Tab. S8). On the other hand, assay sensitivity is an issue as baseline concentrations of oxylipins in plasma and resting platelets may be quite low (pg/mL to ng/mL range). While most of the reported HPLC-MS/MS assays were based on standard flow LC, in this work we selected μUHPLC. Its lower volumetric flow rates are deemed to be favorable in terms of ESI efficiency and sensitivity, respectively, while robustness is not affected significantly. To cope with high throughput requirements of clinical studies, the run time was kept short (13 min). The utilized μUHPLC system has a pressure range up to 10,000 psi (68.9 MPa). This comparably narrow pressure range limits its flexibility for use of sub-2 μm particle columns. Anyway, it was shown that 2.7 μm core-shell particle columns have a better performance/speed/back pressure compromise. They typically provide faster separations at about the same efficiency with lower back pressure as compared to sub-2 μm particle columns. Hence, a Halo C18 2.7 μm superficially porous particle column (50 mm x 0.5 mm ID) was employed in this study.

Different mobile phases were tested in order to find the most sensitive and selective chromatographic method. Mobile phase A was always water with additive and mobile phase B was 5 % of water and 95 % of either ACN or MeOH (v/v) or a mixture of both; an additive was always added also to the mobile phase B, viz. the same one and at the same final concentration as in the mobile phase A. There were 6 different additives tested: NH_4FA, NH_4Ac, FA, HAc, NH_4FA with FA and NH_4Ac with HAc (see Suppl. Material chapter 1.1 for more details).

Two standard solutions of oxylipins (each one 100 pg/mL and 1 ng/mL, respectively) were injected in triplicates with each of the mobile phases. The S/N ratios were calculated for each compound to evaluate method sensitivity. Resolution of isomeric substances like PGE2-PGD2 served to evaluate method selectivity (these 2 isomeric compounds cannot be distinguished by MS only and consequently need to be resolved chromatographically).

Generally, MeOH (especially with buffer salts as additives) provided good sensitivity; however, the peaks were much broader than with ACN. Therefore, resolution of PGE2 and PGD2 was poor with MeOH. ACN gave narrower peaks and HAc as additive was favorable in terms of detection sensitivity. As a consequence, the final mobile phase was established as: B – 100 % ACN with 0.1 % HAc (v/v) and A – 100 % H_2O with 0.1 % HAc (v/v). The gradient profile of the final method is specified in Table 1 along with flow rates and column regeneration program. S/N ratios improved with lower flow rates (tested between 20 and 50 μL/min), yet at the expense of longer run times. 30 μL/min was finally selected as the best compromise. The best chromatographic efficiencies could be achieved at the highest column temperature tested (50 °C) which represents the upper limit according to recommendations of column supplier (Suppl. Materials chapter 1.2).

In order to assure good retention time repeatability, a column regeneration step was implemented. For this purpose, a 5 μL 2-propanol (IPA) plug was injected after the end of the gradient. IPA has high elution strength for lipids and allows efficient cleaning of the column. With this column wash and subsequent re-equilibration, the method was stable and no problems with pressure increase, retention time drifts or sensitivity loss in the course of longer analysis sequences were experienced during validation and sample analysis. An exemplary separation (EICs of all oxylipins and fatty acids including internal standards) are depicted in Fig. 2.

The sensitivity gain of μUHPLC is based on the fact that MS with ESI source behaves like a concentration-dependent detector and can be maximized by maintaining a high injection volume and low volumetric flow rate. Therefore, a large injection volume of 5 μL was selected. Due to this large injection volume the composition of the sample diluent was of utmost importance. With 100 % MeOH as sample diluent peaks were distorted. When the sample diluent consisted of 40 % MeOH and 60 % water (v/v), the sample zones were efficiently refocused during gradient elution (Suppl. Fig S3).

3.1.2. MS method development

Assay specificity of LC–MS/MS methods for oxylipins is a critical parameter and requires besides adequate chromatographic selectivity, also selection of proper SRM transitions. Distinct isomeric oxylipins may share common fragment ions and only the combination of selective LC, selective Q1 precursor isolation, and specific Q3 product ion selection may guarantee adequate assay specificity. Thus, SRMs were first established by automatic compound optimization provided by Sciex' analytical software Analyst (optimization of precursor and fragment ion, DP, CE and CXP). Each compound was prepared as single solution of 1 μg/mL in MeOH and then diluted (around 1:1, v/v) with the mobile phase A in a syringe and sprayed directly to MS by direct infusion. For each compound the 3 most sensitive SRMs were chosen and then checked for selectivity by the LC–MS method. For this purpose, single standards were injected into μUHPLC-MS/MS at the highest concentration of the calibration ranges and all SRMs were recorded. The ion trace, which gave a selective signal at the expected retention time (as determined by single standard injection) for the respective analyte only was eventually chosen (Table 2). For the majority of the targets, selective SRM transitions could be found (Suppl. Tab. S8). FA(20:2) did not exhibit significant fragmentation and hence a pseudo-SRM transition was recorded i.e. the precursor ion with *m/z* 307.3 was selected in Q3 as well. As stated above, the isomer pairs PGE1 and PGD1 as well as PGE2 and PGD2 could not be distinguished by MS and required chromatographic separation which was accomplished by the described μUHPLC method (see Suppl. Table S8).

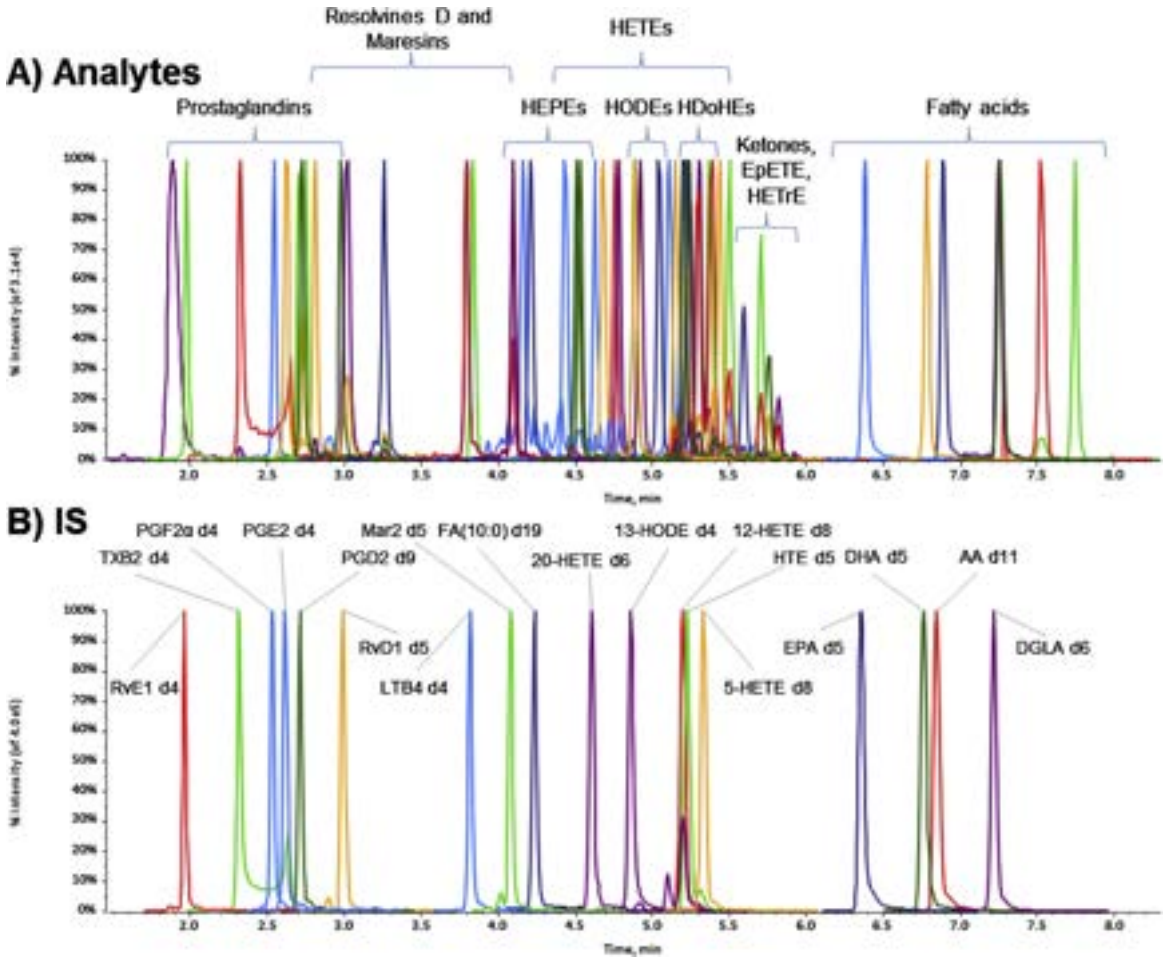

Fig. 2. Normalized chromatograms (extracted EIC) of: A) all analytes of indicated compound classes; and B) all ISs with compounds names/abbreviations.

3.1.3. Extraction protocol

Efficient extraction of targeted oxylipins with high recoveries, expedient enrichment and effective removal of interfering matrix components is of importance, especially for the current μUHPLC method. The large injection volume supports high sensitivity but at the same time amplifies the risk of matrix interferences and matrix effects. Dedicated sample preparation protocols are therefore mandatory. At the moment there is no common protocol for extraction of oxylipins, and different groups use different SPE cartridges and protocols, like Oasis HLB [10], Bond Elut Certify II [13,14], Oasis MAX [24], Strata-X [12]. One protocol reports the use of liquid-liquid extraction (with MtBE) for extraction of oxylipins from platelets [22].

Following the comparison of different extraction protocols [25] Oasis HLB was initially evaluated regarding its performance for oxylipin extraction. The results, however, were quite disappointing; especially in terms of matrix effects (strong ion suppression was observed for most compounds). Therefore, other SPE cartridges: InertSep C18, Chromabond C18 ec, Strata-X and Oasis HLB Prime (as reversed phase stationary phases), as well as Oasis MAX and Bond Elut Certify II (as mixed-mode with strong anion exchanger stationary phases) were compared with each other and with the general monophasic lipid extraction protocol with IPA. The latter lipid extraction protocol (comprising protein precipitation) gave high extraction yields but also exhibited strong matrix effects; therefore, it was not a viable option. The most promising results were obtained with Strata-X (average process efficiency equal to 35.9 %) and Bond Elut Certify II (average process efficiency 37.7 %) (see Suppl. Table S9 and S10 for more details). The latter one was selected as SPE cartridge for the final extraction method. It is an anion exchange/mixed-mode SPE sorbent which allows capture of oxylipins by both ionic and hydrophobic interactions.

Besides, different sample pre-processing methods such as no protein precipitation, protein precipitation with $ZnSO_4$ and with ACN were tested as well (for more details see Suppl. Table S11 and S12). However, it was found that the simplest method, the one without protein precipitation prior to SPE, gave reasonable results and was used for the final method. It seems that plasma protein-bound oxylipins are sufficiently liberated during the SPE process.

3.2. Calibration and validation

Method validation largely followed the guideline of the Food and Drug Administration (FDA) [https://www.fda.gov/]. Some adaptations were made in view of the given application and due to absence of analyte-free matrix.

For calibration three distinct approaches were initially evaluated (all containing ISs): i) External calibration prepared in sample diluent: H_2O/MeOH; 3:2, v/v (spiked solvent). ii) Standard-addition to plasma sample [26] (pre-extraction-spiked standard addition series), and iii) standard addition to extracted plasma sample (post-extraction spiked standard addition series). The slopes of these calibration curves were compared to each other, in order to assess the quality of each type of calibration to compensate for matrix effects and analyte losses during extraction. It was found that

Table 3
Summary of detection and quantification limits, linearity and range for oxylipin analysis in plasma.

Analyte	Internal standard	Sensitivity		Linearity range		Calibration			
		LOD in plasma	LOQ in plasma		range	R			
		[ng/mL of plasma]		[ng/mL of solvent]	R	[spiked: ng/mL of plasma]	day 1	day 2	day 3
PGF2a	PGF2a-d4	0.038	0.12	0.05 - 200	0.995	0.1 - 20	0.994	0.994	0.993
PGE1 and PGD1	PGD2-d9	0.01	0.03	0.05 - 200	0.995	0.01 - 20	0.997	0.996	0.996
TXB2	TXB2-d4	0.032	0.11	0.05 - 200	0.998	0.05 - 20	0.995	0.994	0.994
6-keto-PGF1a	RvE1-d4	0.01	0.03	0.05 - 200	0.999	0.02 - 20	0.998	0.997	0.998
PGE2	PGE2-d4	0.01	0.03	0.05 - 200	0.997	0.01 - 20	0.995	0.996	0.997
PGD2	PGD2-d9	0.01	0.03	0.05 - 200	0.994	0.01 - 20	0.996	0.998	0.996
10-HDoHE	12-HETE-d8	0.042	0.14	0.05 - 200	0.998	0.15 - 20	0.991	0.993	0.990
14-HDoHE	12-HETE-d8	0.015	0.06	0.05 - 200	0.996	0.05 - 20	0.995	0.995	0.993
17-HDoHE	12-HETE-d8	0.047	0.15	0.05 - 200	0.996	0.1 - 20	0.991	0.994	0.994
5-HETE	5-HETE-d8	0.01	0.03	0.05 - 200	0.994	0.02 - 20	0.992	0.996	0.989
8-HETE	13-HODE-d4	0.04	0.13	0.05 - 200	0.997	0.15 - 20	0.996	0.998	0.991
9-HETE	20-HETE-d6	0.055	0.18	0.05 - 200	0.997	0.15 - 20	0.993	0.986	0.999
11-HETE	12-HETE-d8	0.04	0.12	0.05 - 200	0.998	0.15 - 20	0.995	0.997	0.992
12-HETE	12-HETE-d8	0.038	0.13	0.05 - 200	0.998	0.15 - 20	0.997	0.998	0.993
15-HETE	13-HODE-d4	0.043	0.14	0.05 - 200	0.994	0.1 - 20	0.991	1.000	0.994
20-HETE	20-HETE-d6	0.01	0.03	0.05 - 200	0.995	0.01 - 20	0.993	0.996	0.994
5-HEPE	13-HODE-d4	0.01	0.03	0.05 - 200	0.990	0.05 - 20	0.997	0.994	0.997
8-HEPE	13-HODE-d4	0.011	0.04	0.05 - 200	0.995	0.01 - 20	0.988	0.994	0.995
12-HEPE	13-HODE-d4	0.01	0.03	0.05 - 200	0.997	0.05 - 20	0.997	0.997	0.996
15-HEPE	13-HODE-d4	0.021	0.06	0.05 - 200	0.996	0.02 - 20	0.997	0.987	0.987
18-HEPE	13-HODE-d4	0.08	0.27	0.05 - 200	0.994	0.2 - 20	0.997	0.996	0.995
14(15)-EpETE	HTE-d5	0.015	0.05	0.05 - 200	0.996	0.02 - 20	0.992	0.995	0.994
5,6-DiHETE	20-HETE-d6	0.022	0.07	0.25 - 200	0.996	0.15 - 20	0.994	0.983	0.993
5-OxoETE	LTB4-d4	0.01	0.03	0.05 - 200	0.998	0.01 - 20	0.992	0.997	0.996
9-HODE	13-HODE-d4	0.99	3.03	0.5 - 500	0.992	2 - 200	0.998	0.994	0.995
13-HODE	13-HODE-d4	0.921	3.08	0.5 - 500	0.997	2 - 200	0.997	0.996	0.998
LXA4	RvD1-d5	0.012	0.04	0.05 - 200	0.998	0.01 - 20	0.995	0.997	0.994
12-HHT	Mar2-d5	0.01	0.04	0.05 - 200	0.994	0.1 - 20	0.994	0.993	0.996
12-KHT	LTB4-d4	0.01	0.03	0.05 - 200	0.996	0.01 - 20	0.996	0.997	0.995
LTB4	LTB4-d4	0.01	0.03	0.05 - 200	0.999	0.01 - 20	0.997	0.996	0.996
T-12-HETE	LTB4-d4	0.04	0.12	0.05 - 200	0.999	0.05 - 20	0.996	0.997	0.993
RvD1	RvD1-d5	0.01	0.03	0.05 - 200	0.998	0.01 - 20	0.996	0.996	0.995
RvD2	RvD1-d5	0.024	0.08	0.05 - 200	0.998	0.1 - 20	0.994	0.993	0.992
RvD3	RvD1-d5	0.021	0.07	0.05 - 200	0.998	0.01 - 20	0.992	0.996	0.996
RvD4	RvD1-d5	0.013	0.04	0.05 - 200	0.997	0.01 - 20	0.995	0.995	0.995
RvD5	LTB4-d4	0.01	0.03	0.05 - 200	0.999	0.01 - 20	0.996	0.995	0.995
RvE1	RvE1-d4	0.01	0.03	0.05 - 200	0.999	0.01 - 20	0.997	0.998	0.996
Mar1	LTB4-d4	0.027	0.09	0.05 - 200	0.997	0.05 - 20	0.997	0.994	0.992
Mar2	Mar2-d5	0.014	0.05	0.05 - 200	0.998	0.01 - 20	0.996	0.996	0.994
12-HETrE	HTE-d5	0.01	0.03	0.05 - 200	0.998	0.02 - 20	0.994	0.994	0.990
13-HOTrE	13-HODE-d4	0.013	0.04	0.05 - 200	0.992	0.02 - 20	0.996	0.997	0.997

the slopes of spiked solvent and pre-extraction-spiked standard addition series matched very well for those analytes for which a compound-specific stable isotope analogue was available (e.g. RvD1 with RvD1-d5 as IS, see Suppl. Fig. S5). Analytes, for which no compound-specific stable isotope labelled ISs were available, showed a significant difference between slopes of standard solution and standard addition series (e.g. RvD2) (see Suppl. Fig. S5). It was therefore concluded that external calibration with standard solution is not adequate for the oxylipin assay in plasma, but that matrix-matched calibration is required.

The lack of blank matrix dictates more uncommon matrix-matched calibration approaches. Surrogate calibration [27] could be an option or standard addition [26]. Surrogate calibration is difficult to establish for a multiplexed assay like herein. A classical standard addition approach is not a viable option for a large clinical cohort, as samples have to be aliquoted and series of different levels of standards added to each sample have to be measured. It can be done for a limited number of samples with high accuracy requirements, but generates way too much expenditure for a clinical study. Therefore, an alternative matrix-matched standard addition approach was evaluated. A plasma pool was prepared, extracted as described in 2.3.2, and aliquots of this extract were fortified with standards at different levels affording a post-extraction spiked standard addition series (post-spiked matrix). Endogenous levels were obtained by extrapolation to the abscissa (-1×(x-intercept)). Correction of standard addition series for endogenous levels gave the working matrix-matched calibration which is suitable for quantification of a larger number of samples in an analysis sequence. This approach minimizes the expenditure for calibration and can also be carried out with cells for which matrix is limited (e.g. platelets, see below). It turned out that this 'post spiked matrix' calibration matched quite well with the one of classical standard addition corrected for endogenous levels (pre-extraction-spiked standard addition series) (see Suppl. Fig. S5). Forty (40) out of 41 analytes provided a deviation of the slope of the post-extraction spiked standard addition of less than 15 % from the classical standard addition series (see Suppl. Fig. S6). Hence, it was concluded that it is a viable option to use this simpler strategy of matrix-matched calibration. Notwithstanding, for plasma the classical standard addition approach corrected for endogenous levels was selected for calibration. However, for platelets (limited matrix available) the simplified approach of post-extraction spiked standard addition was utilized.

The method was then validated for plasma. Selectivity of the method was checked as absence of interferences from the other targeted analytes as described in 3.1.2. LOD and LOQ were calculated for each compound from the standard-addition calibration curve in plasma, based on the ratio of standard error to predict y-value (area ratio) to slope (s/S) with LOD and LOQ defined as 3 and

Table 4
Validation of extraction recoveries and matrix effects in plasma (mean and standard deviation of three distinct levels).

Analyte	Extraction recovery [%]		Matrix effect [%]	
	mean	sd	mean	sd
PGF2a	87.4	3.3	41.2	3.4
PGE1 and PGD1	83.7	11.7	35	4.6
TXB2	88.1	8.8	47.4	2.4
6-keto-PGF1a	93.1	11.2	80.2	27.2
PGE2	96.1	14	55.9	7.5
PGD2	82.6	7.1	34.5	1.6
10-HDoHE	67.1	7.6	44.8	7.2
14-HDoHE	81.8	5.5	44.1	8.2
17-HDoHE	75.3	8.4	31.4	0.7
5-HETE	102.9	7.4	53.5	11.9
8-HETE	69.6	6.4	48.5	7.5
9-HETE	79.2	12.8	37.3	4.7
11-HETE	72.9	7.9	33.3	4.7
12-HETE	66.7	8.8	54.3	0.5
15-HETE	84.1	6.6	38.3	3.1
20-HETE	44.1	4.6	48.8	3.7
5-HEPE	73.7	3.2	45.4	1.9
8-HEPE	59.7	5.7	45.8	7
12-HEPE	77.3	5.2	54.2	2
15-HEPE	69.5	3.5	40.5	2.9
18-HEPE	53	2.8	49.5	4.8
14(15)-EpETE	61.5	3.3	50.7	7.3
5,6-DiHETE	84.2	9.6	79.2	11
5-OxoETE	61.2	8.5	44.1	3.3
9-HODE	73.1	9.7	43.9	3.4
13-HODE	74.5	9.9	54.1	1.8
LXA4	71.8	9.5	38.7	5.2
12-HHT	95.1	5.3	31.1	1.1
12-KHT	66.4	2.1	42.5	2.4
LTB4	76.5	7.3	60.9	14.7
T-12-HETE	88.6	9.2	37.4	5.3
RvD1	69.6	9.7	47.9	5.2
RvD2	78.5	7.3	26.4	7.1
RvD3	67	0	54.3	4
RvD4	82.8	6.2	59.1	11.1
RvD5	75.1	5.1	55.2	10
RvE1	92.4	13	45.4	2.3
Mar1	74.1	6.2	40.1	8.7
Mar2	81.8	8.4	52	6.3
12-HETrE	38.3	4.7	58.6	3.8
13-HOTrE	68.9	6.7	50.3	7.1

10 times s/S. Only the 3 calibrants with concentrations closest to (but higher than) the intrinsic level of an analyte were considered for these calculations. In most of the cases LODs were lower than 40 pg/mL of plasma and LOQs were typically 100 pg/mL of plasma or lower (see Table 3).

The instrument linearity range was checked with standards dissolved in H_2O/MeOH (3:2; v/v). For most of the oxylipins standard solutions up to 200 ng/mL were prepared. Higher concentrations were not used, as they were considered irrelevant for biological samples. An additional reason was also the high price and restricted availability of oxylipin standards. Only 9- and 13-HODE were prepared in higher concentrations, up to 2 μg/mL. For all the oxylipins concentrations between 0.05–200 ng/mL were within the instrument linearity range. In case of the HODEs the instrument linearity range was up to 500 ng/mL (Table 3).

Extraction recoveries and matrix effects were determined for all analytes (Table 4) and also internal standards (Suppl.Tab.S12). For this purpose, QCs in plasma spiked before and after extraction, respectively, with 1.6, 5 and 16 ng per 1 mL of plasma, and 10 times more for HODEs were prepared. Extraction recoveries and matrix effects were determined according to the protocol of Matuszewski [23]. Extraction recoveries of oxylipins were mostly above 70 % (mean over all oxylipins 75.3 ± 13.3 %) (Table 4). Significant ion suppression, despite SPE purification, was observed for the majority of analytes, most probably due to the large injection volume. Matrix effect was around 40–50 % (mean 47.2 ± 11.2) (Table 4). To compensate for high matrix effect a large number of isotope-labelled ISs was included. For those compounds, for which no stable isotope labelled IS was available, the proper IS was carefully assigned.

Finally, within-batch and between-batch precision and accuracy were validated using matrix-matched calibration corrected for endogenous levels and obtained by pre-extraction standard addition approach. The results for within batch precision and accuracy are given in Suppl. Tab. S15 and the results for between batch precision and accuracy are summarized in Table 5. It can be seen in Table 5 that the employed internal standards adequately corrected for losses during extraction and matrix effects so that the results passed the requirements of FDA, which state that precision (as determined by % RSD) and accuracy (as assessed by % bias) should be less than 15 %. The assay performance should therefore be adequate, if LOQs are adequate.

Here it should be mentioned that the quality of the supplied standards was not validated, as suggested by N.H. Schebb [7], but labelled concentrations of the supplied standards were assumed to be correct. For inter-laboratory and inter-study comparisons it is, however, advised to assure the correct concentrations of supplied non-certified standard solutions by protocols as suggested.

Table 5
Between batch precision and accuracy for plasma.

	Between batch accuracy			Between batch precision		
Analyte	QC low	QC mid	QC high	QC low	QC mid	QC high
PGF2a	94.7	102.6	101.4	2.5	6.0	6.9
PGE1 and PGD1	98.0	107.6	99.5	11.8	7.3	11.4
TXB2	101.3	104.8	96.3	3.6	5.7	4.5
6-keto-PGF1a	89.9	95.4	94.4	7.9	8.5	11.4
PGE2	95.0	103.7	95.8	7.1	7.5	8.1
PGD2	94.3	106.8	99.0	4.6	5.3	6.9
10-HDoHE	96.6	105.5	92.9	2.1	10.2	2.4
14-HDoHE	106.7	105.7	96.9	3.9	12.7	11.6
17-HDoHE	99.8	103.0	93.6	5.2	10.3	6.0
5-HETE	98.6	100.9	95.8	13.2	10.0	9.9
8-HETE	88.7	110.3	93.2	3.7	12.0	5.3
9-HETE	104.5	102.9	98.0	5.1	10.0	6.4
11-HETE	92.7	101.5	93.2	6.5	7.5	7.0
12-HETE	105.2	99.3	96.2	21.1	2.0	8.2
15-HETE	97.9	109.9	103.8	11.3	2.3	7.0
20-HETE	92.9	97.4	91.2	5.6	15.5	4.7
5-HEPE	102.0	99.7	102.9	5.1	12.4	7.0
8-HEPE	89.6	101.3	92.5	3.4	6.1	2.2
12-HEPE	87.1	90.4	89.3	4.3	2.8	3.9
15-HEPE	96.4	93.9	95.0	4.2	11.4	9.2
18-HEPE	103.5	102.4	93.3	9.1	3.3	10.2
14(15)-EpETE	100.1	104.6	94.3	12.2	9.1	2.0
5,6-DiHETE	114.7	93.8	98.4	21.8	6.3	11.8
5-OxoETE	87.9	110.2	90.9	7.5	6.2	9.2
9-HODE	94.8	103.7	93.2	8.8	5.8	8.4
13-HODE	104.5	104.4	96.1	9.8	3.6	6.3
LXA4	94.1	101.9	96.0	9.7	9.4	9.2
12-HHT	94.4	101.6	89.9	11.2	5.1	1.3
12-KHT	93.2	109.3	97.4	7.3	2.8	7.0
LTB4	91.6	103.2	95.6	6.2	5.3	1.8
T-12-HETE	92.4	106.3	100.3	8.4	4.2	5.4
RvD1	103.2	108.5	104.1	12.2	1.5	10.4
RvD2	101.2	97.1	93.6	11.6	7.2	4.7
RvD3	106.0	106.7	106.1	2.5	11.0	6.9
RvD4	101.3	103.6	101.7	10.2	3.2	7.2
RvD5	90.1	100.4	90.9	4.8	2.4	4.5
RvE1	92.2	103.5	95.4	3.7	3.8	2.1
Mar1	94.1	103.3	94.8	4.2	5.6	2.8
Mar2	92.0	105.4	98.7	5.6	5.3	3.4
12-HETrE	84.0	92.3	85.1	7.8	20.4	9.9
13-HOTrE	102.3	100.0	92.6	2.8	10.1	14.0

3.3. Concentration of oxylipins in biological samples

3.3.1. Results for plasma

The validated multi-target μUHPLC-ESI-MS/MS assay was employed to determine the concentrations of the targeted oxylipins in pooled human EDTA plasma. The results are summarized in Table 6. It can be seen that several oxylipins, in particular lipoxin A4, resolvins, maresins, some less abundant HETE and HEPE constitutional isomers could not be detected (<LOD), as expected. The highest concentrations were found for 9- and 13-HODE (3.3 and 4.4 ng/mL). TXB2, 14HDoHE, 12-HETE, 15-HETE, 5,6-diHETE, 12-HHT, 12-HETrE, and 13-HOTrE were detected in a concentration range between 100 and 400 pg/mL. Other oxylipins such as PGE2, PGD2, 5-HETE, 20-HETE, 5-HEPE, and 12-HEPE were found in the range between LOQ and 100 pg/mL. Evidently, for many oxylipins LOQs were adequate to allow quantification of these important lipid mediators in plasma samples of healthy donors. These findings clearly document the practical applicability of the newly developed μUHPLC-ESI-MS/MS assay.

3.3.2. Results for platelets

The ultimate goal of this study was to establish a targeted lipidomics workflow to accurately measure oxylipins in platelets. Thus, the method which was first developed for readily available plasma was adapted for platelets isolated from peripheral blood. Some adjustments in sample preparation had to be made. Oxylipins were first extracted from platelets with IPA and then subjected to SPE. Due to limited amounts of matrix in case of platelets, matrix-matched calibration was done by post-extraction spiked standard addition series as described above. For this purpose, the platelet samples of 5 donors (each 2×10^8 platelets) were extracted with IPA and then aliquoted for calibrant and (spiked and non-spiked) QC preparation (see Suppl. Materials chapter 6 for more details); one aliquot of each sample was kept for analysis of oxylipins concentrations in the platelet samples under resting (non-activated) state from 5 healthy donors. Endogenous levels of oxylipins in the pooled platelet extract were obtained from the x-intercept of the standard addition series. Matrix-matched calibration functions for platelets were then constructed and used to determine endogenous concentration of oxylipins in samples from each donor, as well as method LOD and LOQ (in the same way as described above for plasma). The non-spiked QC injections allowed deriving information on the precision of the μUHPLC-MS/MS method for this matrix. The results of this preliminary validation are summarized in Suppl. Tab. S16.

The concentrations of oxylipins measured in non-activated (resting) platelet samples from 5 distinct donors are given in Table 7. It can be seen that the baseline levels of many oxylipins are very low, in many cases undetectable. However, some donors clearly show elevated baseline concentrations, e.g. donor 2 (D2). Resolvins, maresins, and lipoxin A4 were not detected. The major platelet activation factor Thromboxan A2 (analyzed as the more stable analog TXB2) was found above LOQ in the platelet samples

Table 6
Concentration (together with standard deviation) of oxylipins in pooled plasma.

Analyte	Concentration [pg/mL of plasma]	sd	Analyte	Concentration [pg/mL of plasma]	sd
PGF2a	<LOD		14(15)-EpETE	<LOD	
PGE1 and PGD1	<LOD		5,6-DiHETE	236	82
TXB2	131	17	5-OxoETE	<LOD	
6-keto-PGF1a	<LOD		9-HODE	3331	419
PGE2	38	3	13-HODE	4210	436
PGD2	33	2	LXA4	<LOD	
10-HDoHE	<LOQ		12-HHT	133	17
14-HDoHE	139	11	12-KHT	<LOD	
17-HDoHE	<LOQ		LTB4	<LOD	
5-HETE	61	6	T-12-HETE	<LOQ	
8-HETE	<LOQ		RvD1	<LOD	
9-HETE	<LOD		RvD2	<LOD	
11-HETE	<LOQ		RvD3	<LOD	
12-HETE	353	39	RvD4	<LOD	
15-HETE	184	23	RvD5	<LOD	
20-HETE	29	11	RvE1	<LOD	
5-HEPE	40	4	Mar1	<LOD	
8-HEPE	<LOD		Mar2	<LOD	
12-HEPE	45	2	12-HETrE	107	13
15-HEPE	<LOQ		13-HOTrE	142	5
18-HEPE	<LOQ				

Table 7
Concentrations of oxylipins in non-activted (resting) platelets (Targeted analytes, which are not found in the table, were not detected in the samples).

	Estimated concentration				
	[ng/1 × 10^8 platelets]				
	Donor				
Analyte	D1	D2	D3	D4	D5
TXB2	11.95	8.36	2.47	2.43	12.97
PGE2	< LOQ	0.69	< LOD	< LOD	< LOQ
10-HDoHE	< LOQ	0.98	< LOQ	< LOQ	< LOQ
14-HDoHE	< LOQ	33.44	< LOQ	< LOD	< LOD
17-HDoHE	0.39	1.22	< LOD	< LOD	< LOD
8-HETE	0.05	0.36	0.09	< LOD	< LOD
9-HETE	< LOQ	6.71	< LOQ	< LOQ	< LOQ
11-HETE	0.38	0.63	< LOQ	< LOQ	0.36
12-HETE	< LOQ	44.58	< LOQ	< LOD	< LOQ
15-HETE	< LOQ	0.37	< LOD	< LOD	< LOQ
12-HEPE	3.34	23.59	2.73	< LOQ	< LOQ
15-HEPE	< LOQ	0.72	0.57	0.32	0.44
9-HODE	< LOQ	4.22	< LOQ	< LOQ	< LOQ
13-HODE	6.06	18.33	5.94	4.46	4.52
12-HHT	54.34	16.98	5.28	6.39	15.1
12-KHT	1.2	< LOD	< LOD	< LOD	0.35
T-12-HETE	0.09	2.0	< LOD	< LOD	< LOD
12-HETrE	< LOD	11.9	< LOQ	< LOD	< LOD
13-HOTrE	0.27	1.83	0.3	< LOQ	< LOQ

of all donors (between 2 and 15 ng/100 Mio platelets corresponding to about 20–150 atto gram per platelet). The assay was found to be suitable and will be utilized to determine oxylipin concentrations in experimental platelet samples of a pharmacolipidomics project as well as in patients of a clinical CAD cohort.

3.4. Discussion of assay performance

Some recent reviews discussed the general performance of assays for oxylipins in biofluids, particularly in plasma [4,6,28]. In any case, most of the LC–MS/MS assays employed SPE to extract and enrich oxylipins, in order to reach required LOQs down to the low pg/mL range. Gladine et al. reported a summary of LC–MS/MS assays, which is quite useful to assess the performance of our assay in comparison to previously published works (see Table 2 of Ref. [4] and suppl. Table S18). LOQs were typically in the range of 0.5–600 fmol injected on-column [4,10,12,24,29]. In our work, these values were between 2.0 and 250 fmol on-column for plasma and between 0.7 and 8.4 fmol on-column for standard solution (Suppl. Tab. S17). It allowed to quantitate important oxylipins down to the low pg/mL range, e.g. PGE2 and PGD2 down to 30 pg/mL (LOQ) corresponding to 0.085 nM in plasma. On the other hand, run times were typically between 10 and 30 min in those reported assays. Our μUHPLC-ESI-MS/MS assay eluted all target compounds within 8 min and took only 13 min together with column regeneration and re-equilibration. While other assays partly cover more analytes (up to 175 oxylipins), the coverage of the current method is reasonable, in particular for its application to platelets. Overall, the current μUHPLC-MS/MS assay for oxylipins compares fairly well with recently published assays using standard flow HPLC and UHPLC format.

4. Conclusions

A new sensitive and highly economic μUHPLC-ESI-MS/MS assay for oxylipin analysis in terms of solvent usage (less than 250 μL

of organic solvent in the mobile phase per sample) has been developed. It has been validated for plasma and documented its suitability to analyze baseline levels in plasma and platelets as real biological test samples. The assay covers 42 oxylipins. It shows good precision and accuracy for quantitative analysis in plasma and platelets. The microflow regime may be a good compromise between nano-HPLC with its higher sensitivity due to reduced volumetric flow rates in the nL/min range and standard HPLC with its robustness in several 100 μL/min flow regime. The current μUHPLC assay may also be regarded as ecofriendly. If implemented in routine analysis in clinical laboratories, limited use of toxic acetonitrile of the mobile phase may help to reduce organic waste.

CRediT authorship contribution statement

Malgorzata Cebo: Investigation, Methodology, Formal analysis, Data curation, Visualization, Writing - original draft, Writing - review & editing. **Xiaoqing Fu:** Investigation, Data curation, Writing - review & editing. **Meinrad Gawaz:** Writing - review & editing, Funding acquisition. **Madhumita Chatterjee:** Investigation, Writing - review & editing, Funding acquisition. **Michael Lämmerhofer:** Conceptualization, Methodology, Supervision, Writing - review & editing, Resources, Funding acquisition.

Declaration of Competing Interest

The authors declare no conflict of interests.

Acknowledgements

This project was funded by the Deutsche Forschungsgemeinschaft (DFG, German Research Foundation) – Project number 374031971 – TRR 240.

Appendix A. Supplementary data

Supplementary material related to this article can be found, in the online version, at doi:https://doi.org/10.1016/j.jpba.2020.113426.

References

[1] J. Yeung, M. Hawley, M. Holinstat, The expansive role of oxylipins on platelet biology, J. Mol. Med. (Berl.) 95 (2017) 575–588, http://dx.doi.org/10.1007/s00109-017-1542-4.The.
[2] G. Astarita, A.C. Kendall, E.A. Dennis, A. Nicolaou, Targeted lipidomic strategies for oxygenated metabolites of polyunsaturated fatty acids, Biochim. Biophys. Acta - Mol. Cell Biol. Lipids 1851 (2015) 456–468, http://dx.doi.org/10.1016/j.bbalip.2014.11.012.
[3] B. Peng, S. Geue, C. Coman, P. Münzer, D. Kopczynski, C. Has, N. Hoffmann, M.C. Manke, F. Lang, A. Sickmann, M. Gawaz, O. Borst, R. Ahrends, M. Patrick, D. Kopczynski, C. Has, N. Hoffmann, M.C. Manke, F. Lang, A. Sickmann, M. Gawaz, O. Borst, R. Ahrends, P. Münzer, D. Kopczynski, C. Has, N. Hoffmann, M.C. Manke, F. Lang, A. Sickmann, M. Gawaz, O. Borst, R. Ahrends, M. Patrick, D. Kopczynski, C. Has, N. Hoffmann, M.C. Manke, F. Lang, A. Sickmann, M. Gawaz, O. Borst, R. Ahrends, Identification of key lipids critical for platelet activation by comprehensive analysis of the platelet lipidome, Blood 132 (2018) e1–e12, http://dx.doi.org/10.1182/blood-2017-12-822890.
[4] C. Gladine, A.I. Ostermann, J.W. Newman, N.H. Schebb, MS-based targeted metabolomics of eicosanoids and other oxylipins: analytical and inter-individual variabilities, Free Radic. Biol. Med. 144 (2019) 72–89, http://dx.doi.org/10.1016/j.freeradbiomed.2019.05.012.
[5] H.S. Jonasdottir, H. Brouwers, R.E.M.M. Toes, A. Ioan-Facsinay, M. Giera, Effects of anticoagulants and storage conditions on clinical oxylipid levels in human plasma, Biochim. Biophys. Acta - Mol. Cell Biol. Lipids 1863 (2018) 1511–1522, http://dx.doi.org/10.1016/j.bbalip.2018.10.003.
[6] I. Willenberg, A.I. Ostermann, N.H. Schebb, Targeted metabolomics of the arachidonic acid cascade: current state and challenges of LC-MS analysis of oxylipins, Anal. Bioanal. Chem. 407 (2015) 2675–2683, http://dx.doi.org/10.1007/s00216-014-8369-4.
[7] N.M. Hartung, M. Mainka, N. Kampschulte, A.I. Ostermann, N.H. Schebb, A strategy for validating concentrations of oxylipin standards for external calibration, Prostaglandins Other Lipid Mediat. 141 (2019) 22–24, http://dx.doi.org/10.1016/j.prostaglandins.2019.02.006.
[8] D. Tsikas, A.A. Zoerner, Analysis of eicosanoids by LC-MS/MS and GC-MS/MS: a historical retrospect and a discussion, J. Chromatogr. B Anal. Technol. Biomed. Life Sci. 964 (2014) 79–88, http://dx.doi.org/10.1016/j.jchromb.2014.03.017.
[9] P. Le Faouder, V. Baillif, I. Spreadbury, J.P. Motta, P. Rousset, G. Chêne, C. Guigné, F. Tercé, S. Vanner, N. Vergnolle, J. Bertrand-Michel, M. Dubourdeau, N. Cenac, LC-MS/MS method for rapid and concomitant quantification of pro-inflammatory and pro-resolving polyunsaturated fatty acid metabolites, J. Chromatogr. B Anal. Technol. Biomed. Life Sci. 932 (2013) 123–133, http://dx.doi.org/10.1016/j.jchromb.2013.06.014.
[10] K. Strassburg, A.M.L.L. Huijbrechts, K.A. Kortekaas, J.H. Lindeman, T.L. Pedersen, A. Dane, R. Berger, A. Brenkman, T. Hankemeier, J. Van Duynhoven, E. Kalkhoven, J.W. Newman, R.J. Vreeken, Quantitative profiling of oxylipins through comprehensive LC-MS/MS analysis: Application in cardiac surgery, Anal. Bioanal. Chem. 404 (2012) 1413–1426, http://dx.doi.org/10.1007/s00216-012-6226-x.
[11] J.T. English, P.C. Norris, R.R. Hodges, D.A. Dartt, C.N. Serhan, Identification and profiling of specialized pro-resolving mediators in human tears by lipid mediator metabolomics, Prostaglandins Leukot. Essent. Fatty Acids 117 (2017) 17–27, http://dx.doi.org/10.1016/j.plefa.2017.01.004.
[12] M. Chocholoušková, R. Jirásko, D. Vrána, J. Gatěk, B. Melichar, M. Holčapek, Reversed phase UHPLC/ESI-MS determination of oxylipins in human plasma: a case study of female breast cancer, Anal. Bioanal. Chem. 411 (2019) 1239–1251, http://dx.doi.org/10.1007/s00216-018-1556-y.
[13] A.I. Ostermann, T. Greupner, L. Kutzner, N.M. Hartung, A. Hahn, P. Schuchardt, N. Helge, Intra-individual variance of the human plasma oxylipin pattern: low inter-day variability in fasting blood samples versus high variability during the day, Anal. Methods 19 (2018), http://dx.doi.org/10.1039/c8ay01753k.
[14] K.M. Rund, A.I. Ostermann, L. Kutzner, J.M. Galano, C. Oger, C. Vigor, S. Wecklein, N. Seiwert, T. Durand, N.H. Schebb, Development of an LC-ESI(-)-MS/MS method for the simultaneous quantification of 35 isoprostanes and isofurans derived from the major n3- and n6-PUFAs, Anal. Chim. Acta 1037 (2018) 63–74, http://dx.doi.org/10.1016/j.aca.2017.11.002.
[15] R.A. Colas, M. Shinohara, J. Dalli, N. Chiang, C.N. Serhan, Identification and signature profiles for pro-resolving and inflammatory lipid mediators in human tissue, Am. J. Physiol. - Cell Physiol. 307 (2014) 39–54, http://dx.doi.org/10.1152/ajpcell.00024.2014.
[16] L. Kutzner, K.M. Rund, A.I. Ostermann, N.M. Hartung, J. Galano, L. Balas, T. Durand, M.S. Balzer, S. David, N.H. Schebb, Development of an optimized LC-MS method for the detection of specialized pro-resolving mediators in biological samples, Front. Pharmacol. 10 (2019), http://dx.doi.org/10.3389/fphar.2019.00169.
[17] M. Cebo, J. Schlotterbeck, M. Gawaz, M. Chatterjee, M. Lämmerhofer, Simultaneous targeted and untargeted UHPLC-ESI-MS/MS method with data-independent acquisition for quantification and profiling of (oxidized) fatty acids released upon platelet activation by thrombin, Anal. Chim. Acta 1094 (2020) 57–69, http://dx.doi.org/10.1016/j.aca.2019.10.005.
[18] R. Berkecz, M. Lísa, M. Holčapek, Analysis of oxylipins in human plasma: comparison of ultrahigh-performance liquid chromatography and ultrahigh-performance supercritical fluid chromatography coupled to mass spectrometry, J. Chromatogr. A 1511 (2017) 107–121, http://dx.doi.org/10.1016/j.chroma.2017.06.070.
[19] C. Hinz, S. Liggi, G. Mocciaro, S. Jung, I. Induruwa, M. Pereira, C.E. Bryant, S.W. Meckelmann, V.B. O'Donnell, R.W. Farndale, J. Fjeldsted, J.L. Griffin, A comprehensive UHPLC ion mobility quadrupole time-of-flight method for profiling and quantification of eicosanoids, other oxylipins, and fatty acids, Anal. Chem. 91 (2019) 8025–8035, http://dx.doi.org/10.1021/acs.analchem.8b04615.
[20] M. Cebo, X. Fu, M. Gawaz, M. Chatterjee, M. Lämmerhofer, Enantioselective ultra-high performance liquid chromatography-tandem mass spectrometry method based on sub-2μm particle polysaccharide column for chiral separation of oxylipins and its application for the analysis of autoxidized fatty acids and platelet r, J. Chromatogr. A 1624 (2020), 461206, http://dx.doi.org/10.1016/j.chroma.2020.461206.
[21] F. Ianni, G. Saluti, R. Galarini, S. Fiorito, R. Sardella, B. Natalini, Enantioselective high-performance liquid chromatography analysis of oxygenated polyunsaturated fatty acids, Free Radic. Biol. Med. 144 (2019) 35–54, http://dx.doi.org/10.1016/j.freeradbiomed.2019.04.038.
[22] B. Peng, S. Geue, C. Coman, P. Münzer, D. Kopczynski, C. Has, N. Hoffmann, M.C. Manke, F. Lang, A. Sickmann, M. Gawaz, O. Borst, R. Ahrends, Identification of key lipids critical for platelet activation by comprehensive analysis of the platelet lipidome, Blood 132 (2018) e1–e12, http://dx.doi.org/10.1182/blood-2017-12-822890.
[23] B.K. Matuszewski, M.L. Constanzer, C.M. Chavez-Eng, Strategies for the assessment of matrix effect in quantitative bioanalytical methods based on HPLC – MS/MS, Anal. Chem. 75 (2003) 3019–3030.
[24] A.M. Wolfer, M. Gaudin, S.D. Taylor-Robinson, E. Holmes, J.K. Nicholson, Development and validation of a high-throughput ultrahigh-performance liquid chromatography-mass spectrometry approach for screening of oxylipins and their precursors, Anal. Chem. 87 (2015) 11721–11731, http://dx.doi.org/10.1021/acs.analchem.5b02794.
[25] A.I. Ostermann, I. Willenberg, N.H. Schebb, Comparison of sample preparation methods for the quantitative analysis of eicosanoids and other oxylipins in plasma by means of LC-MS/MS, Anal. Bioanal. Chem. 407 (2015) 1403–1414, http://dx.doi.org/10.1007/s00216-014-8377-4.

[26] A. Hauswaldt, O. Rienitz, R. Ja, N. Fischer, D. Schiel, G. Labarraque, B. Magnusson, Uncertainty of Standard Addition Experiments: A Novel Approach to Include the Uncertainty Associated with the Standard in the Model Equation, 2012, pp. 129–138, http://dx.doi.org/10.1007/s00769-011-0827-5.
[27] B. Drotleff, M. Hallschmid, M. Lämmerhofer, Quantification of steroid hormones in plasma using a surrogate calibrant approach and UHPLC-ESI-QTOF-MS/MS with SWATH-acquisition combined with untargeted profiling, Anal. Chim. Acta 1022 (2018) 70–80, http://dx.doi.org/10.1016/j.aca.2018.03.040.
[28] L. Kortz, J. Dorow, U. Ceglarek, Liquid chromatography-tandem mass spectrometry for the analysis of eicosanoids and related lipids in human biological matrices: a review, J. Chromatogr. B Anal. Technol. Biomed. Life Sci. 964 (2014) 1–11, http://dx.doi.org/10.1016/j.jchromb.2014.01.046.
[29] G. Chen, Q. Zhang, Comprehensive analysis of oxylipins in human plasma using reversed-phase liquid chromatography-triple quadrupole mass spectrometry with heatmap-assisted selection of transitions, Anal. Bioanal. Chem. 411 (2019) 367–385, http://dx.doi.org/10.1007/s00216-018-1446-3.

Supplementary information

Micro-UHPLC-MS/MS method for analysis of oxylipins in plasma and platelets

Malgorzata Cebo[a], Xiaoqing Fu[a], Meinrad Gawaz[b], Madhumita Chatterjee[b], Michael Lämmerhofer[a]*

[a] University of Tübingen, Institute of Pharmaceutical Sciences, Pharmaceutical (Bio-)Analysis, Auf der Morgenstelle 8, 72076 Tübingen, Germany

[b] Department of Cardiology and Angiology, University Hospital Tübingen, Otfried-Müller-Strasse 10, 72076 Tübingen, Germany

***Author for correspondence:**

Prof. Michael Lämmerhofer
Pharmaceutical (Bio-)Analysis
Institute of Pharmaceutical Sciences
University of Tuebingen
Auf der Morgenstelle 8
72076 Tuebingen, Germany
T +49 7071 29 78793, F +49 7071 29 4565
e-mail: michael.laemmerhofer@uni-tuebingen.de
http://www.bioanalysis.uni-tuebingen.de/

1. LC-MS method development.

1.1 LC method development

1.1.1 Comparison of mobile phases.

Different mobile phases were tested to figure out which one will give the best sensitivity (as assessed by the S/N ratio for selected oxylipins) and the best selectivity (i.e. resolution between PGE2 and PGD2).

In the first round, AcN and MeOH were compared as mobile phase B (mobile phase B consisted of 95% of organic solvent and 5% of water (v/v)). Six different types of additives were added: 5 mM NH_4FA, 5 mM NH_4Ac, 0.1% FA (v/v), 0.1% HAc (v/v), 5 mM NH_4FA with 0.1% FA (v/v) and 5 mM NH_4Ac with 0.1% HAc (v/v). Mobile phase A was prepared separately for each type of mobile phase B and it consisted of water with the same additive in the same concentration as in the matching mobile phase B. Preparation of each mobile phase is shown in Suppl. Table S1.

Table S1. *Preparation of mobile phases for the first round of comparison*.

Mobile phase		H_2O	AcN	MeOH	200 mM NH_4Ac in H_2O	200 mM NH_4FA in H_2O	HAc	FA
		mL	mL	mL	mL	mL	µL	µL
A	1	97.5			2.5			
B	1	2.5	95		2.5			
A	2	97.5				2.5		
B	2	2.5	95			2.5		
A	3	97.5			2.5		100	
B	3	2.5	95		2.5		100	
A	4	97.5				2.5		100
B	4	2.5	95			2.5		100
A	5	100					100	
B	5	5	95				100	
A	6	100						100
B	6	5	95					100
A	7	97.5			2.5			
B	7	2.5		95	2.5			
A	8	97.5				2.5		
B	8	2.5		95		2.5		
A	9	97.5			2.5		100	
B	9	2.5		95	2.5		100	
A	10	97.5				2.5		100
B	10	2.5		95		2.5		100
A	11	100					100	
B	11	5		95			100	
A	12	100						100
B	12	5		95				100

A short 3.5 min chromatographic method with linear gradient from 10% to 50% B when AcN was used and 40% to 80% when MeOH was used was programmed to compare the performances of the mobile phases.

Table S2. *Comparison of S/N ratios for 3 prostaglandins with different mobile phases. The best result for each compound is marked with dark green background and the second-best result with light green.*

Mobile phase	**PGE2** (100 pg/mL)		**PGD2** (100 pg/mL)		**PGF2a** (1 ng/mL)	
	S/N	*st. dev.*	*S/N*	*st. dev.*	*S/N*	*st. dev.*
1	10.9	1.6	6.1	1.4	16.9	6.0
2	9.2	4.9	5.7	1.7	14.3	2.7
3	14.6	2.1	6.3	0.3	16.0	3.5
4	8.8	0.5	6.0	2.7	15.5	2.7
5	22.2	5.5	9.1	1.5	11.2	3.1
6	10.8	1.7	4.5	1.6	12.9	1.7
7	23.9	4.8	11.9	3.5	26.4	3.1
8	Not separated				21.0	4.1
9	Not separated				25.6	1.5
10	Not separated				16.7	2.1
11	Not separated				13.8	2.3
12	Not separated				3.7	4.4

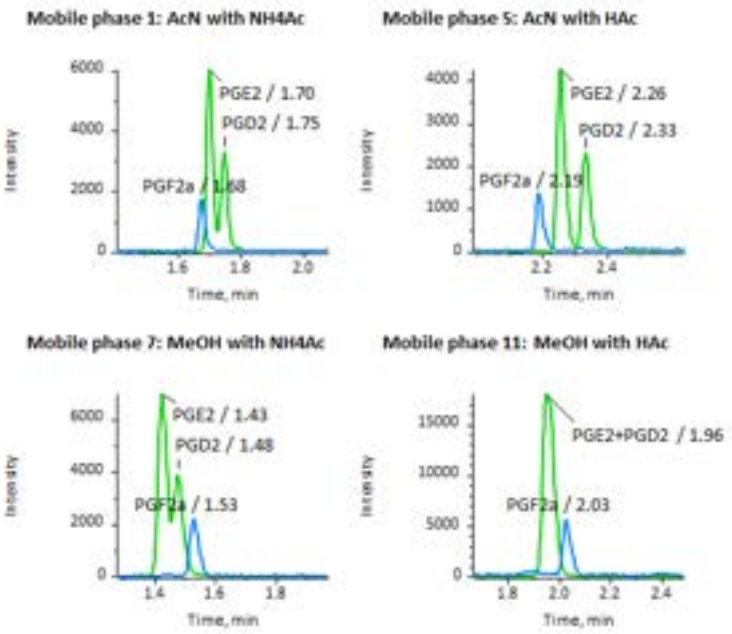

Figure S1. *EIC of 3 prostaglandins with 4 selected methods.*

Table S3. *Preparation of mobile phases for the second round of comparison.*

Mobile phase			H_2O mL	AcN mL	MeOH mL	200 mM NH_4OAc in H_2O mL	200 mM NH_4FA in H_2O mL	HAc µL	FA µL
A	13		95			5			
B	13	a		95		5			
B	13	b		70	25	5			
B	13	c		50	45	5			
A	14		95			5		100	
B	14	a		95		5		100	
B	14	b		70	25	5		100	
B	14	c		50	45	5		100	
A	15		95					100	
B	15	a		95				100	
B	15	b		70	25			100	
B	15	c		50	45			100	
A	16		95				5		
B	16	a		95			5		
B	16	b		70	25		5		
B	16	c		50	45		5		
A	17		100				5		100
B	17	a	5	95			5		100
B	17	b	5	70	25		5		100
B	17	c	5	50	45		5		100
A	18		100						100
B	18	a	5	95					100
B	18	b	5	70	25				100
B	18	c	5	50	45				100

Two mixtures of selected prostaglandins (PGE2, PGD2 and PGF2a) in MeOH were prepared, one with concentration of 100 pg/mL of each prostaglandin and the other 1 ng/mL of each prostaglandin. The mixtures were injected in triplicates with each mobile phase. PGE2 and PGD2 gave higher peaks and therefore the lower concentration (100 pg/mL) was used for comparison. PGF2a, which gave smaller peaks, was compared at higher concentration (1 ng/mL). The comparison of the sensitivity for the different mobile phases is shown in Suppl. Tab. S2.

These preliminary results showed that the best sensitivity was obtained with MeOH with salt (in particular 5 mM ammonium acetate, eluent 7) as additive (also acids with salts gave good results). However, mobile phases containing MeOH gave also quite broad peaks with worse

separation of PGE2 and PGD2, when compared to AcN (examples are shown in Suppl. Fig. S1).

The second round of comparison involved mixtures of AcN and MeOH to check if it is possible to obtain narrow peaks (as for AcN) with great sensitivity of MeOH (Suppl. Tab. S3). The LC gradient for this comparison was as follows: 10% to 70% B in 5 min. More compounds were added at this point to obtain broader knowledge about sensitivity (2 mixtures in MeOH: 100 pg/mL of each compound and 1 ng/mL of each compound; PGE2, PGD2, PGF2a, HHT, 5-HETE, 12-HETE, 9-HODE and 13-HODE).

Table S4. *Comparison of S/N ratios for oxylipins at concentration* ***1 ng/mL*** *with different mobile phases. The best result for each compound is marked with dark green background and the second-best result with light green.*

Mobile phase	PGE2		PGD2		PGF2a		HHT		5-HETE		12-HETE		9-HODE		13-HODE	
	S/N	*Sd*	*S/N*	*sd*	*S/N*	*sd*	*S/N*	*sd*	*S/N*	*sd*	*S/N*	*sd*	*S/N*	*sd*	*S/N*	*sd*
13a	25	3	36	4	46	3	22	2	73	10	210	16	167	11	126	3
13b	23	1	38	6	40	7	22	4	90	8	273	17	198	10	173	12
13c	23	1	35	2	47	4	50	8	146	9	475	9	329	13	330	12
14a	31	2	60	7	71	13	40	3	93	5	318	33	268	3	269	2
14b	41	7	80	3	73	3	65	6	147	14	504	30	410	25	388	16
14c	48	5	97	7	118	8	70	5	153	10	534	19	441	7	407	23
15a	220	17	601	10	368	11	284	13	489	39	1764	101	1662	73	1581	54
15b	168	25	527	44	254	29	267	23	485	40	1638	51	1556	18	1357	107
15c	207	7	569	39	580	118	188	20	431	35	1230	75	1333	50	1208	142
16a	34	6	34	6	41	10	12	2	45	8	118	17	99	14	98	10
16b	40	5	40	5	52	13	31	3	68	4	236	14	185	9	186	23
16c	58	3	58	3	59	8	33	4	83	7	238	21	186	10	191	13
17a	31	2	55	5	56	8	22	2	65	10	193	17	158	2	147	8
17b	39	3	79	2	95	10	31	3	95	6	277	10	199	13	199	18
17c	99	8	99	8	129	5	28	9	105	16	276	28	186	2	191	17
18a	94	16	203	24	229	20	83	14	315	23	781	91	608	38	559	29
18b	128	13	264	21	291	40	118	9	369	13	1277	54	745	53	703	31
18c	143	13	309	42	342	28	108	17	350	18	985	25	729	8	697	13

Table S5. *Comparison of S/N ratios for oxylipins at concentration* ***100 pg/mL*** *with different mobile phases. The best result for each compound is marked with dark green background and the second-best result with light green.*

Mobile phase	PGE2		PGD2		PGF2a		HHT		5-HETE		12-HETE		9-HODE		13-HODE	
	S/N	*Sd*	*S/N*	*sd*	*S/N*	*sd*	*S/N*	*sd*	*S/N*	*sd*	*S/N*	*sd*	*S/N*	*sd*	*S/N*	*sd*
13a									7.2	1.1	21.7	4.6	26.7	0.3	21.5	0.5
13b									11.6	3.4	34.0	6.2	27.3	2.5	26.2	2.1
13c									15.9	3.7	46.0	3.0	37.0	2.0	57.2	4.7
14a									14.5	4.0	39.0	2.0	35.7	4.5	34.3	5.3
14b									18.5	7.8	48.5	2.1	48.5	3.5	49.5	2.1
14c									18.2	3.8	62.7	10.0	53.7	7.1	55.8	8.0
15a	30.1	0.6	55.3	3.5	56.8	2.0	26.4	7.3	61.0	3.6	200.9	11.8	212.0	12.9	199.8	4.8
15b	21.6	1.5	47.0	1.0	36.0	2.7	30.5	4.1	59.8	3.0	188.5	5.5	187.6	11.7	189.7	13.9
15c	18.7	7.6	42.3	3.1	203.1	42.4	25.8	3.0	59.8	11.5	183.0	9.0	184.4	9.2	172.7	21.7
16a	5.3	2.5	5.3	2.5	5.6	0.9			7.9	2.1	11.7	1.5	14.3	1.2	16.6	2.2
16b	6.3	1.2	6.3	1.2	8.4	1.6			11.6	4.5	27.0	4.0	34.0	1.7	37.7	7.5
16c	7.7	1.5	7.7	1.5	11.3	4.5			13.0	3.0	30.3	3.1	32.3	7.5	40.3	4.2
17a	8.0	5.2	8.0	5.2	9.2	3.8			9.4	1.2	24.7	3.2	19.7	2.9	21.7	2.1
17b	9.0	1.7	9.0	1.7	12.9	0.9			13.7	3.0	32.0	5.2	25.0	4.4	32.0	5.0
17c	11.3	2.1	11.3	2.1	18.7	3.1			16.9	4.7	27.7	2.3	28.3	4.2	30.0	9.5
18a	10.3	0.6	24.0	2.6	28.2	3.3	8.9	0.9	38.3	10.2	85.3	13.1	76.7	8.6	63.5	4.0
18b	18.0	2.0	28.7	1.5	33.9	4.7	12.5	1.9	44.2	9.3	140.7	1.5	91.7	9.8	88.3	6.7
18c	16.7	5.1	37.0	0.0	55.1	16.3	14.2	1.4	37.1	1.8	98.0	3.0	94.7	5.5	93.2	2.3

The best results were obtained when 0.1% HAc was used (Table S4 and S5). As earlier shown, peaks were broader the more MeOH was in the mobile phase (Fig. S2).

In the next step, different gradient methods were evaluated for mobile phases 15a, 15b and 15c (data not shown). The best results in terms of sensitivity and PGE2-PGD2 resolution were obtained with AcN and without addition of MeOH.

The final mobile phase was chosen as: A – 100% H_2O with 0.1% HAc and B – 100% AcN with 0.1% HAc.

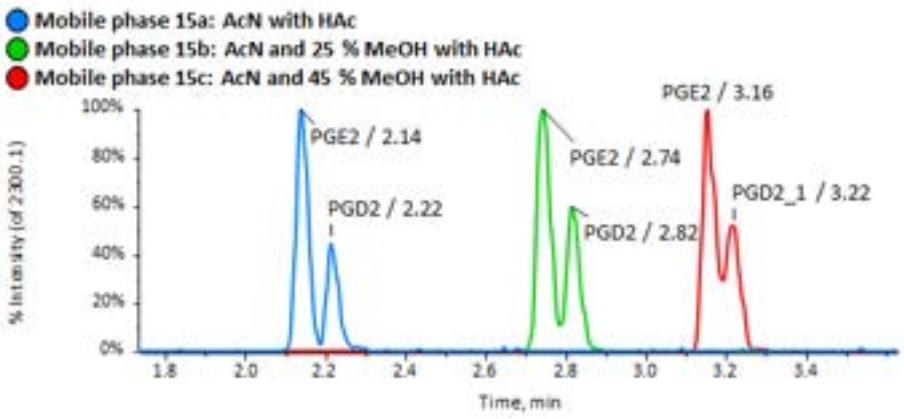

Figure S2. *EIC of PGE2 and PGD2 with 3 selected mobile methods.*

1.1.2 Adjustment of column temperature and flow rate

Seven different flow rates between 20 and 50 µL/min were tested to compare sensitivity (S/N) (Suppl. Table S6). For most of the compounds the sensitivity was the best when a low flow rate was used (20 – 35 µL/min). The flow rate for the final method was chosen as 30 µL/min as a compromise between efficiency and run time.

Table S6. *Comparison of S/N ratio for oxylipins at concentration 100 pg/mL with different* ***flow rates****. The best result for each compound is marked with dark green background and the second-best result with light green.*

Flow rate	PGE2		PGD2		PGF2a		HHT		5-HETE		12-HETE		9-HODE		13-HODE	
[uL/min]	*S/N*	*sd*	*S/N*	*sd*	*S/N*	*sd*	*S/N*	*sd*	*S/N*	*sd*	*S/N*	*sd*	*S/N*	*sd*	*S/N*	*sd*
20	36.3	2.3	61.7	4.7	130.7	21.0	38.6	4.2	22.7	0.6	94.0	7.9	151.0	1.7	158.7	14.0
25	30.3	4.0	65.3	9.9	132.2	14.7	36.3	3.8	42.0	9.2	149.7	12.7	167.1	12.6	157.1	27.2
30	29.7	3.2	52.7	4.2	118.2	9.9	31.0	3.5	45.0	7.0	139.3	9.7	178.3	22.3	175.6	14.9
35	21.7	1.2	47.7	4.0	90.2	2.4	26.3	4.0	46.7	7.0	143.3	8.6	166.4	4.1	147.6	23.0
40	22.0	2.0	41.3	5.1	81.9	6.3	23.0	1.7	43.0	3.6	124.4	9.8	158.0	11.5	139.7	5.9
45	21.3	3.1	39.3	1.5	78.5	8.0	19.7	2.5	45.7	3.5	124.3	8.1	132.2	1.8	125.9	13.2
50	19.0	0.0	42.7	3.8	69.8	11.4	16.7	1.5	40.7	4.6	125.0	2.0	122.6	23.1	118.2	9.5

In the next step the column temperature was adjusted. Five different temperatures between 30 and 50°C were compared. As always, higher S/N was used as parameter for the decision.

Table S7. *Comparison of S/N ratio for oxylipins at concentration 100 pg/mL with different* ***temperatures****. The best result for each compound is marked with dark green background and the second-best result with light green.*

Temperature [°C]	PGE2		PGD2		PGF2a		HHT		5-HETE		12-HETE		9-HODE		13-HODE	
	S/N	*sd*	*S/N*	*sd*	*S/N*	*sd*	*S/N*	*sd*	*S/N*	*sd*	*S/N*	*sd*	*S/N*	*sd*	*S/N*	*sd*
30	37.3	5.1	55.7	3.2	132.6	7.8	51.7	8.1	64.7	8.0	208.7	3.2	249.0	14.1	206.6	3.0
35	36.7	1.5	65.0	6.1	147.0	4.1	58.7	2.1	64.3	4.5	243.7	14.5	275.4	36.0	239.7	18.7
40	41.7	6.5	67.7	7.8	147.0	6.1	51.9	3.0	82.0	5.3	261.7	8.3	290.5	31.1	253.9	12.0
45	36.7	8.5	67.0	12.8	143.7	3.9	52.5	6.4	79.7	6.0	290.3	9.1	303.2	40.8	294.7	36.7
50	40.7	2.5	65.7	7.6	152.4	6.4	57.5	6.5	83.7	1.2	301.7	17.6	316.8	21.2	301.1	51.2

The highest temperature gave the best results for most of the compounds. No temperature higher than 50°C was tested, because of the column usage guideline discourages use of higher temperatures.

The temperature 50°C was used in the final method.

1.1.3 Comparison of injection solvents

Standards solutions of oxylipins in different injection solvents with different H_2O-MeOH ratios were prepared. On the one hand, the injection solvent should match well with the gradient starting conditions i.e. it should not have higher elution strength and, on the other hand, it should provide good solubility of analytes. The first requirement is better fulfilled with high water content (the RP method starts with 15% AcN in H_2O). For the second requirement more MeOH is better, especially when common lipid extraction protocols are used, as apolar lipids extracted with such procedures might not be fully soluble in high water content solvents.

It is especially important for microLC to carefully select the injection solvent as the injected sample volume, here 5 µL, is quite large. This large injection volume was selected in favor of high sensitivity of the method. It means that the column is filled to a significant extent with the sample plug and efficient refocusing on the stationary phase is mandatory to avoid extra peak broadening which is possible only with a weakly eluting sample solvent (diluent).

Peaks, especially early eluted ones, showed significant peak broadening when solvent with high MeOH content was used for sample reconstitution. No negative effects were observed for low MeOH contents. However, poor solubility of real extracts was giving some problems. The final method used therefore a H_2O/MeOH (3:2; v/v) mixture as injection solvent as a good compromise (Suppl. Fig. S3).

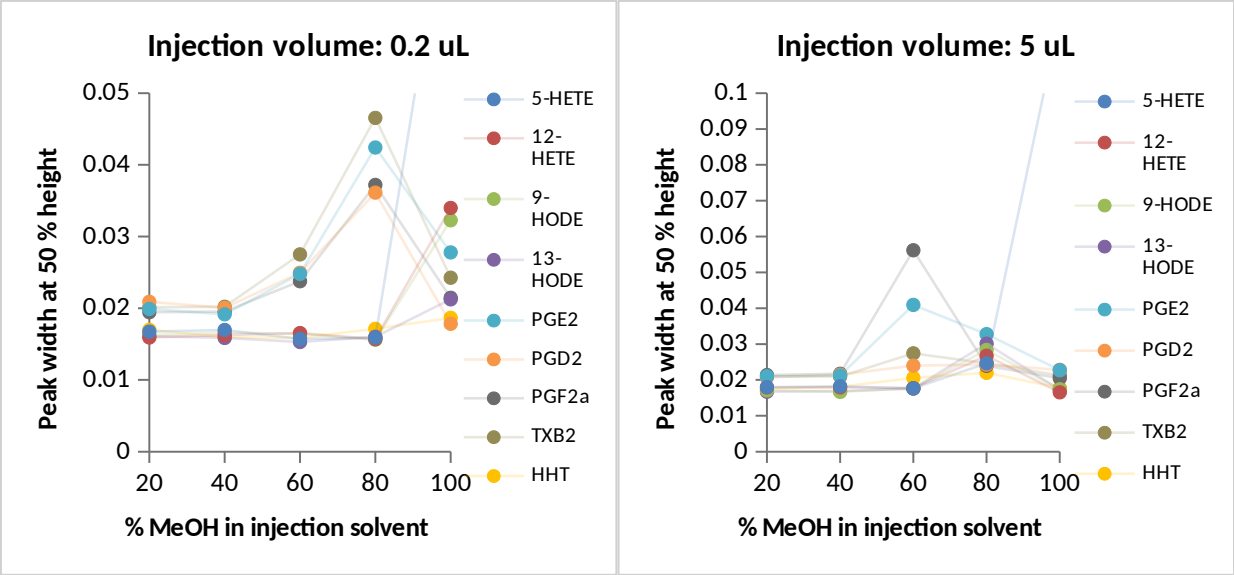

Figure S3. *Comparison of peak width (at 50% of peak height) with different injection solvents for 2 injection volumes (left: 0.2 µL and right: 5 µL) and 9 oxylipins.*

2. Extraction protocol.

2.1 Comparison of different SPE protocols and liquid extraction.

Extraction efficiency was compared for different SPE methods studying both matrix effects and extraction recoveries as performance parameters. For this purpose, 3 sets of samples were prepared: pre-extraction spiked, post-extraction spiked and standards spiked to H_2O/MeOH (3:2; v/v) (standard solutions). Deuterated oxylipins were used for this purpose as standards, because they do not appear naturally in plasma, which was the matrix in this study. Seven compounds were used for these experiments (PGE2-d4, PGD2-d9, PGF2a-d4, TXB2-d4, 12-HETE-d8, 13-HODE-d4 and AA-d11). Six different reversed phase or mixed mode SPEs were tested: InertSep C18, Chromabond C18 ec, Strata X, Oasis HLB Prime, Oasis Max and Bond Elut Certify II. Also monophasic liquid extraction with 90% (v/v) IPA in water was used for comparison.

The employed protocol was unified for all SPE cartridges. EDTA plasma from different donors was pooled and BHT and TPPU solutions were added (10 µL, 200 µg/mL of each compound in MeOH, final concentration: 20 µg/mL). Then, the plasma was aliquoted (250 µL) to falcon tubes. For pre-extraction spiked samples, deuterated oxylipins were added. The plasma was diluted 1:1 (v/v) with the final solvent for SPE conditioning (Suppl. Tab. S8). The samples were centrifuged at 4°C and the supernatant was loaded onto pre-conditioned SPE cartridges (Suppl. Tab. S8). Afterwards, the charged SPE cartridges were washed and then analytes were eluted to clean falcon tubes (as described in detail in Suppl. Tab. S8). The eluates were dried with a Gene-Vac (2-3 h) under nitrogen protection. For post-extraction spiked samples deuterated oxylipins were added after the extraction procedure at the same concentrations. All samples

were reconstituted by H_2O/MeOH (3:2; v/v). For mere standard solutions, the deuterated oxylipins were spiked at the same concentrations to H_2O/MeOH (3:2; v/v). All 3 sets were analyzed immediately by µUHPLC-MS/MS in randomized sample order.

Table S8. *Overview of extraction methods with different SPE cartridges and liquid extraction.*

	SPE cartridge	Size	SPE conditioning	SPE wash	SPE elution
Reversed phase	InertSep C18	3 mL / 200 mg	MeOH **2.5 mL** H_2O **2.5 mL** MeOH/H_2O/HOAc 5:95:0.1 **2.5 mL**	MeOH/H_2O/HAc 20:80:0.1 2 x **2.5 mL**	MeOH **2 x 2 mL**
	Chromabond C18 ec	3 mL / 200 mg			
	Strata-X	3 mL / 200 mg			
	Oasis HLB Prime	3 cc / 60 mg			
Mixed mode anion .	Oasis MAX	3 cc / 60 mg	MeOH **2.5mL** H_2O **2.5 mL**	2 % NH_4OH in water **2.5 mL** H_2O/MeOH 4:1 **2.5 mL**	MeOH/FA 95:5 **2 x 2 mL**
	Bond Elut Certify II	3 mL / 200 mg	MeOH **2.5mL** 1 M NaAc in water Adjusted to pH 6 **2.5 mL**	H_2O/MeOH 4:1 2 x **2.5 m** Dried: 5 min	Hexane/ethyl acetate/HAc 25:75:1 **2 x 2 mL**
Liquid extractio	IPA/H_2O 9:1 (v/v)	2.5 mL			

Monophasic liquid extraction using IPA was performed as described previously (ref. [1] of main document). Plasma was pooled, BHT and TPPU (as specified in main document) were added and samples were divided into 250 µL aliquots For pre-extraction spiked samples deuterated oxylipins were added. 2.25 mL of IPA was added to each sample (final extraction solvent: IPA/H_2O 9:1 (v/v)). Samples were shaken for 20 min at 4°C and then centrifuged. The supernatants were transferred to fresh falcon tubes and samples were dried with a Gene-Vac. The dried lipid extract was reconstituted in MeOH, because it was not possible to dissolve it in

H_2O/MeOH (3:2; v/v) (most probably because of a high content of apolar TGs and CEs). For the post-extraction spiked set and the set in MeOH deuterated oxylipins were spiked either to matrix (plasma extracted with IPA protocol and dried) or MeOH. All samples were analyzed immediately after preparation in randomized order

Table S9. *Results of extraction recoveries and matrix effects for different extraction methods.*

	Extraction recovery [%]						
SPE	**PGE2-d4**	**PGD2-d9**	**PGF2a-d4**	**TXB2-d4**	**12-HETE-d8**	**13-HODE-d4**	**AA-d11**
InertSep C18	104.8	32.1	102.2	84.9	5.7	15.6	3.1
Chromabond C18 ec	107.6	138.9	102.7	80.2	64	111.8	14.1
Strata X	70.8	61.2	76	68.8	132.3	67.6	56.7
Oasis HLB Prime	83.5	82	104.1	58.4	13.8	21.1	23
Oasis Max	36	6.6	72.2	58.8	50.7	31.5	12.2
Bond Elut Certify II	83	88.7	82.5	95.2	67.7	69.5	14.8
IPA (liquid extraction)	100.6	30	109	109.5	104.1	108.4	114.6
	Matrix effect [%]						
SPE	**PGE2-d4**	**PGD2-d9**	**PGF2a-d4**	**TXB2-d4**	**12-HETE-d8**	**13-HODE-d4**	**AA-d11**
InertSep C18	41.8	53.5	46.2	61.6	46	26.3	25.2
Chromabond C18 ec	36.9	21.4	46.3	49.3	47.5	16.8	15.4
Strata X	61.6	71.2	60.7	63.4	24.2	34.8	32.5
Oasis HLB Prime	24.6	27.2	23.5	23.7	49.6	40.2	3.2
Oasis Max	63.9	52.2	61	44.7	48.3	55.1	46.7
Bond Elut Certify II	50.2	57.8	50.3	40.2	50.8	62.6	88
IPA (liquid extraction)	27	19.4	13.4	30.1	28.5	32.7	33.6
	Process efficiency [%]						
SPE	**PGE2-d4**	**PGD2-d9**	**PGF2a-d4**	**TXB2-d4**	**12-HETE-d8**	**13-HODE-d4**	**AA-d11**
InertSep C18	43.8	17.2	47.2	52.3	2.6	4.1	0.8
Chromabond C18 ec	39.7	29.7	47.6	39.5	30.4	18.8	2.2
Strata X	43.6	43.6	46.1	43.6	32.0	23.5	18.4
Oasis HLB Prime	20.5	22.3	24.5	13.8	6.8	8.5	0.7
Oasis Max	23.0	3.4	44	26.3	24.5	17.4	5.7
Bond Elut Certify II	41.7	51.3	41.5	38.3	34.4	43.5	13.0
IPA (liquid extraction)	27.2	5.8	14.6	33.0	29.7	35.4	38.5

The biggest problem for all SPE protocols was a serious matrix effect with strong ion suppression (Suppl. Tab. S9). In this regard, Bond Elut Certify II showed the best results with a mean value for matrix effect of 57.1%. The strongest matrix effect was obtained with Oasis HLB Prime, especially for late eluted AA-d11, and also liquid extraction with 90% IPA. The best

extraction recoveries were obtained with Chromabond C18 ec, Strata X, Bond Elut Certify II and also liquid extraction. Overall most promising results were obtained with Bond Elut Certify II and Strata X, and the first one was chosen as the final extraction method.

2.2 Different methods of protein precipitation.

Furthermore, protein precipitation prior to extraction was examined as a possibility to improve extraction results. Three different methods were compared: no protein precipitation, precipitation with aqueous $ZnSO_4$ solution and with AcN. These experiments were done at the early stage of SPE testing with Oasis HLB, and later repeated (only no precipitation and precipitation with AcN) with Bond Elut Certify II.

Table S10. *Results of extraction recoveries and matrix effects for different extraction methods.*

	Extraction recovery [%]						
SPE	**PGE2-d4**	**PGD2-d9**	**PGF2a-d4**	**TXB2-d4**	**12-HETE-d8**	**13-HODE-d4**	**AA-d11**
Oasis HLB Prime	83.5	82	104.1	58.4	13.8	21.1	23
Oasis HLB Prime ZnSO4	50.6	74.1	95.6	64.5	15.8	19.9	20.6
Oasis HLB Prime AcN	74.7	68.4	54.5	45.4	98	89.5	111.8
Bond Elut Certify II	74.3	34.9	77	90.5	45.2	50.9	11.6
Bond Elut Certify II AcN	3	3.2	3	1.6	22.1	17.1	35.8
	Matrix effect [%]						
SPE	**PGE2-d4**	**PGD2-d9**	**PGF2a-d4**	**TXB2-d4**	**12-HETE-d8**	**13-HODE-d4**	**AA-d11**
Oasis HLB Prime	24.6	27.2	23.5	23.7	49.6	40.2	3.2
Oasis HLB Prime ZnSO4	57.1	15.2	26.3	22.7	67	70.5	26.6
Oasis HLB Prime AcN	56.3	27.8	44.2	20.8	21.7	32.3	10.8
Bond Elut Certify II	55.6	50.3	47.7	45.6	55.8	62.6	80.5
Bond Elut Certify II AcN	57.5	47.2	48	48.6	21.8	22.5	20.5
	Process efficiency [%]						
SPE	**PGE2-d4**	**PGD2-d9**	**PGF2a-d4**	**TXB2-d4**	**12-HETE-d8**	**13-HODE-d4**	**AA-d11**
Oasis HLB Prime	20.5	22.3	24.5	13.8	6.8	8.5	0.7
Oasis HLB Prime ZnSO4	28.9	11.3	25.1	14.6	10.6	14.0	5.5
Oasis HLB Prime AcN	42.1	19.0	24.1	9.4	21.3	28.9	12.1
Bond Elut Certify II	41.3	17.6	36.7	41.3	25.2	31.9	9.3
Bond Elut Certify II AcN	1.7	1.5	1.4	0.8	4.8	3.8	7.3

The experiment without protein precipitation was done as described above. The protocol for protein precipitation with $ZnSO_4$ was as follows: plasma was diluted 2.5 times with $ZnSO_4$ water solution (56 mg/mL). The samples were shaken on ice for 20 min and then centrifuged. The supernatant was loaded onto SPE and the general protocol described in the former paragraph was followed. To precipitate proteins with AcN, plasma samples were diluted 9 times with AcN (250 µL of plasma with 2,250 µL of AcN) and stored at -20°C for 30 min. After centrifugation the supernatant was transferred to a new falcon tube and was diluted with the solution of the final step of SPE conditioning (Suppl. Tab. S8): 8.75 mL of the solution was added to each sample. Then, diluted samples were loaded (stepwise) to SPE cartridges.

The method without protein precipitation was chosen (with Bond Elut Certify II as SPE cartridge), as it gave good results and was the simplest procedure, hence presumably the least error-prone to perform in larger clinical studies.

3. Calibration.

Three distinct calibration sets were prepared and compared to each other in terms of their performance to compensate for losses and matrix effect: i) pre-extraction spiked standard addition in plasma (post-spiked matrix), ii) post-extraction-spiked standard addition to plasma (classical standard addition approach), and ii) standards in plain solvent (H_2O/MeOH 3:2 (v/v)) (spiked solvent). Endogenous analyte concentrations in the employed plasma matrix employed for pre- and post-extraction spiked standard addition were calculated from the x-intercept of the standard addition calibration functions (-1(x-intercept)). Respective matrix-matched calibration functions corrected for endogenous levels were then prepared and used for this study.

The method using spiked solvent is straightforward and does not need any additional biological samples. However, this method failed for compounds, which did not have their real compound-specific isotopically labeled analogues. The post-extraction spiked standard addition method has the advantage over the classical ‘standard addition method’, because it does not require high volume of precious biological matrix and generates much less samples for extraction and LC-MS analysis. The approach with post-spiked samples was devised, because it is possible to apply it later for platelet cell pellets. If there is not enough matrix (like for platelet cell pellets) to prepare calibration curves, the real samples might be extracted and after extraction small aliquots of each extract can be pooled together. Then, the pooled extract can be aliquoted and used for calibrant preparation. The ‘post-spiked matrix’ method showed good results with slopes well matching the ones from the classical ‘standard addition’ approach (pre-extraction spiked standard addition assumed to be the most accurate way of calibration).

Table S11. Accuracies as determined by the slope ratios of post-spiked matrix and spiked solvent vs. pre-extraction spiked standard addition (classical standard addition) (slope ratio*100 assuming that the standard addition represents 100% of the true value). Blue background indicates compounds for which their deuterated real analogues ware used as IS.

Accuracy of slope in:					
Compound	Post-spiked matrix	Spiked solvent	Compound	Post-spiked matrix	Spiked solvent
PGF2a	99.8	98.1	14(15)-EpETE	86.5	115.6
PGE1 and PGD1	92.3	149.9	5,6-DiHETE	89.1	89.6
TXB2	97.5	104.7	5-OxoETE	100.2	160.8
6-keto-PGF1a	96	52	9-HODE	93.7	110.7
PGE2	94	87.3	13-HODE	92.5	97.7
PGD2	96.3	121.6	LXA4	104.9	119.8
10-HDoHE	100.6	107.7	12-HHT	109.4	173.6
14-HDoHE	103.7	111.4	12-KHT	95.4	158.8
17-HDoHE	107.2	181.4	LTB4	104	102.1
5-HETE	85.8	75.1	T-12-HETE	90.2	157.9
8-HETE	104	100	RvD1	107.5	100.4
9-HETE	96.4	157.6	RvD2	103.4	155.2
11-HETE	108.6	150.9	RvD3	90.9	77.4
12-HETE	110.7	111.8	RvD4	99.8	71.8
15-HETE	85.7	130.8	RvD5	103.4	117.9
20-HETE	96.6	97.2	RvE1	90	109.3
5-HEPE	93.1	105.6	Mar1	103.8	107.7
8-HEPE	107.6	166	Mar2	109.7	95.8
12-HEPE	105.2	106.3	12-HETrE	125.4	174.9
15-HEPE	98.9	125.4	13-HOTrE	102.4	92.6
18-HEPE	109	105.4			

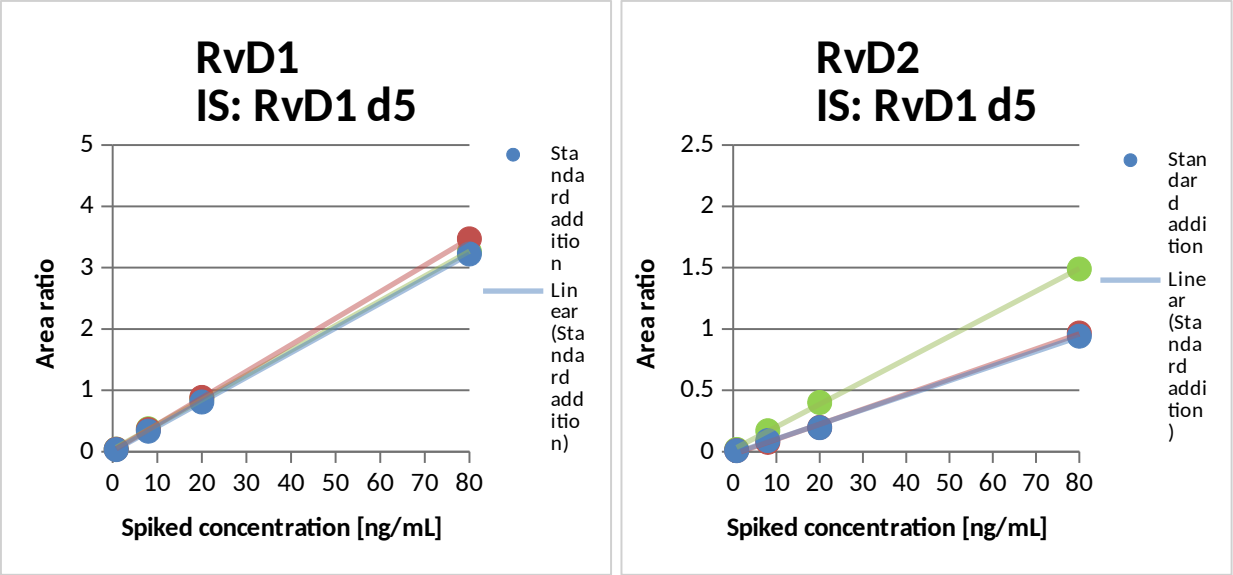

Figure S4. *Comparison of calibration curves for different methods. Left plot: RvD1, which uses its deuterated analogue for normalization (RvD1-d5) and right: RvD2, which lacks its deuterated analogue. Standard addition means pre-extraction-spiked standard addition series, and post-spiked matrix means post-extraction spiked standard addition series. Spiked solvent means standards dissolved in* H_2O/MeOH 3:2 (v/v).

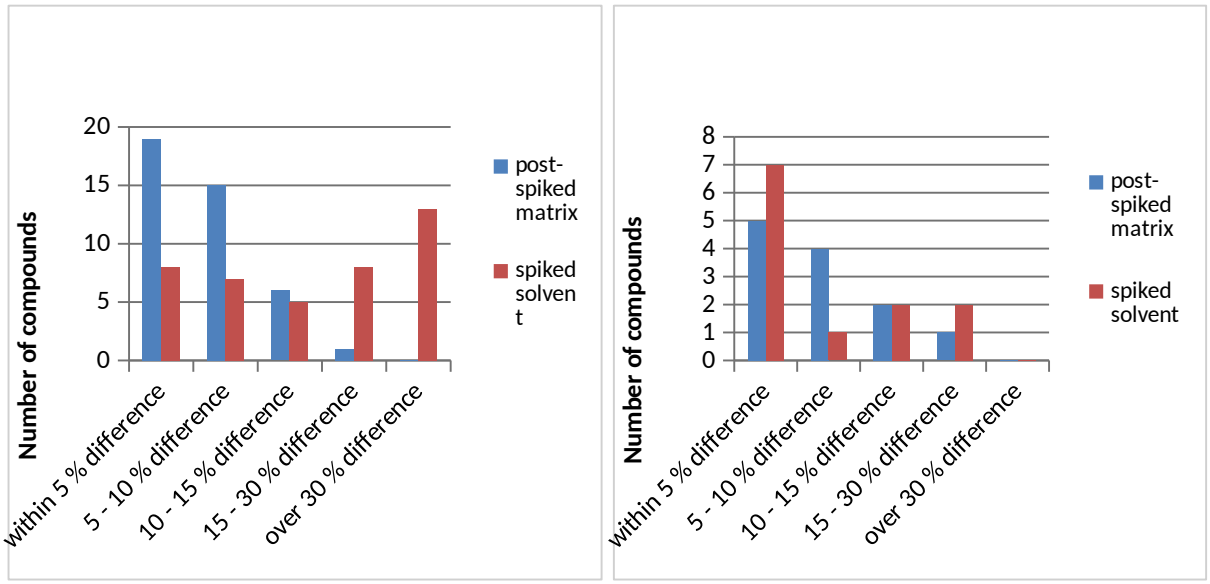

Figure S5. *Bias of calibration by post-extraction-spiked standard addition series (post-spiked matrix) (blue bars) and standard solutions (spiked solvent) (red bars) as compared to pre-extraction-spiked standard addition series. Left graph: All compounds including those for which no compound-specific stable isotope labelled IS was available. Right graph: Only compounds considered for which compound-specific stable isotope labelled IS (deuterated analogues) were available. 'Within 5% difference' means accuracy between 95 and 105% (or bias between -5 and 5%), assuming that the classical pre-extraction-spiked standard addition series gives fully accurate results (100%). Bias (%) was calculated from the slopes of the distinct calibration*

*functions, i.e. (slope ratio of post-extraction-spiked standard addition series and pre-extraction-spiked standard addition series – 1)*100 (%) as well as (slope ratio of standard solution series and pre-extraction-spiked standard addition series – 1)*100 (%).*

4. Extraction recovery and matrix effect for IS with the final method

The extraction recovery and matrix effect for ISs were also determined with the final method during the method validation. The results are summarized in Suppl. Table S12.

The extraction recovery showed good results for oxylipins, as for most of them it exceeded 70%. The results were much worse for fatty acids, for all of them the recovery was below 50% and for DGLA-d6 the result was only 2.7%. This suggests that the current SPE method is not adequate for fatty acids. They were therefore not further considered as they are covered by another assay.

The results for the matrix effect indicated high ion suppression for oxylipins (around 50%, but sometimes even lower than 30%). The matrix effect was much better for fatty acids, probably because matrix components of similar polarity and similar retention time were poorly removed from SPE.

Table S12. *Extraction recovery and matrix effect for ISs obtained with the final method (mean and standard deviation of three levels investigated;* 1.6, 5 and 16 ng per 1 mL of plasma*).*

	Extraction recovery [%]		Matrix effect [%]	
	mean	sd	mean	sd
PGF2a-d4	83.4	12.5	46.9	6.7
PGE2-d4	82.0	11.1	53.1	7.3
PGD2-d9	79.8	13.2	37.4	3.9
TXB2-d4	97.1	8.3	41.4	3.1
5-HETE-d8	71.2	20.5	35.7	5.2
12-HETE-d8	69.2	9.3	47.9	2.4
20-HETE-d6	56.3	23.2	41.0	6.8
13-HODE-d4	71.8	14.0	60.6	6.0
LTB4-d4	86.4	19.6	29.7	3.2
RvD1-d5	72.5	10.0	28.3	3.3
RvE1-d4	91.9	4.5	34.7	5.1
Mar2-d5	85.1	10.4	47.0	5.1
FA(10:0)-d19	46.3	7.2	29.9	8.9
HTE-d5	49.9	12.6	62.4	7.7
DGLA-d6	2.7	0.4	89.1	8.4
AA-d11	13.0	0.9	87.3	26.4
EPA-d5	27.6	3.1	72.5	10.6
DHA-d5	14.7	2.2	104.2	30.9

5. Validation of within batch precision and accuracy for plasma

Table S13. *Within batch precision and accuracy for plasma.*

	Within batch accuracy								
Analyte	**QC low**			**QC mid**			**QC high**		
	day 1	**day 2**	**day 3**	**day 1**	**day 2**	**day 3**	**day 1**	**day 2**	**day 3**
PGF2a	92.1	96.6	95.4	108.3	103.6	96	94.2	108.1	102
PGE1/ PGD1	86.7	109.9	97.5	109.4	114.4	99	94.2	112.5	91.8
TXB2	97.1	102.9	103.9	103.4	111.3	99.6	94.1	101.3	93.5
6-keto-PGF1a	91.7	82.1	96	103.2	87.1	95.9	100.4	82	100.9
PGE2	87.5	100.5	96.9	105.9	110.2	95.1	90.9	104.7	91.8
PGD2	90.3	98.9	93.8	110.7	109.3	100.3	97.5	106.4	93
10-HDoHE	95.3	95.5	98.9	114.6	108.3	93.7	91.9	95.5	91.3
14-HDoHE	102.2	110.3	107.7	114.5	112.3	90.3	94.3	109.3	87.2
17-HDoHE	97.8	95.8	105.7	112.1	105.7	91.3	87.2	97.2	96.5
5-HETE	83.7	105	107.2	106.8	106.6	89.3	86.3	105.2	95.8
8-HETE	87.3	86.4	92.5	124.8	107.3	98.9	89.9	98.9	90.9
9-HETE	108.6	98.5	106.5	110.2	91.1	107.5	94.4	94.3	105.2
11-HETE	89.9	99.6	88.6	106.8	104.9	92.8	98.2	95.7	85.8
12-HETE	90.4	94.4	130.7	98	101.5	98.3	87.5	98.5	102.7
15-HETE	85.8	100.2	107.6	112.8	108.3	108.5	97.3	111.6	102.6
20-HETE	88.5	91.5	98.6	114.9	88.4	89	91.3	86.9	95.5
5-HEPE	96.2	103.8	106.1	107.8	105.8	85.5	103.9	109.6	95.3
8-HEPE	86.1	91.3	91.4	107.9	100.4	95.6	94.8	91	91.8
12-HEPE	86.2	83.9	91.3	93	87.9	90.4	91.4	85.3	91.2
15-HEPE	98.2	99.2	91.7	105.8	90.9	85.1	104.6	92.8	87.5
18-HEPE	112.8	103.7	94	103.5	105.1	98.6	89.3	104.2	86.5
14(15)-EpETE	88.5	98.9	112.8	102.9	114.9	96.1	93.5	96.5	92.9
5,6-DiHETE	102	98.6	143.5	98.6	87.2	95.6	100.2	86	108.9
5-OxoETE	80.3	91.1	92.2	114.7	102.4	113.5	81.3	96.4	94.9
9-HODE	100.7	98.5	85.3	108.2	106.1	96.9	88.7	88.6	102.2
13-HODE	113.3	106.9	93.3	103.3	108.6	101.4	93.2	92.1	103.1
LXA4	85	103.3	94.1	105.5	109.2	91.1	94.5	105.5	88.1
12-HHT	86.8	106.4	89.9	104.1	105.1	95.6	90	91	88.7
12-KHT	85.4	96.3	97.8	110.7	105.8	111.5	89.6	102.4	100.3
LTB4	85.9	91.6	97.2	107.7	104.7	97.1	95.2	97.5	94.1
T-12-HETE	85	91.6	100.5	111.4	104.7	102.8	96.8	97.5	106.5
RvD1	88.8	109.1	111.8	106.6	109.6	109.2	91.6	109.6	111
RvD2	107.8	87.6	108.2	98.6	89.5	103.3	93.8	89.1	97.9
RvD3	108.5	106.4	103.2	112.3	114.7	93.2	99.2	113.8	105.2
RvD4	100.4	91.4	112	100.6	102.9	107.2	94.1	102.3	108.8

RvD5	86.2	89.4	94.7	102.6	100.7	97.9	86.3	94.2	92.2
RvE1	88.2	94.5	93.8	106.9	104.3	99.2	94.1	97.7	94.4
Mar1	93.8	90.3	98.2	110	100	99.9	93.4	97.9	93.2
Mar2	86.4	96.5	93.1	110.4	106.4	99.4	95.2	101.8	99.2
12-HETrE	76.4	87.8	87.8	75.1	89.3	112.4	81.2	79.3	94.7
13-HOTrE	99.3	102.6	105.1	104.1	107.5	88.5	96.9	102.9	78

	Within batch precision								
Analyte	**QC low**			**QC mid**			**QC high**		
	day 1	**day 2**	**day 3**	**day 1**	**day 2**	**day 3**	**day 1**	**day 2**	**day 3**
PGF2a	7.4	7.8	6.7	6.1	4	8.8	6.1	3.9	6.3
PGE1/PGD1	1.8	4.6	5.7	7.2	0.3	8.6	6.2	1.1	6.3
TXB2	9.1	8.8	1.9	3.2	1.9	2	3.3	3.8	8.2
6-keto-PGF1a	5.3	2.1	6.4	3.6	1.5	6.8	3.7	1	11
PGE2	7.8	5	6	2.8	1.9	6.8	12.2	5.6	5.4
PGD2	4.9	10.1	7	3.7	5.8	7.4	3.3	5.8	3.5
10-HDoHE	12.3	14.2	12.6	2.5	3.9	4.6	8.2	4.1	6.6
14-HDoHE	7.9	6.6	12.7	0.2	4.7	3.5	4.1	1.1	11.4
17-HDoHE	10.4	12	3.7	8.8	2.8	7.6	7.3	6	9.4
5-HETE	6.3	5.8	10.2	3.9	1.6	7.4	2.8	4.1	6.4
8-HETE	7.5	13.5	12.8	2.5	6.1	8.6	6	6.8	14.1
9-HETE	2.9	13.1	4.4	3.4	12.5	8.4	6	10.5	6.1
11-HETE	10.2	9.7	7	2.6	13.2	5.6	8.7	4.9	7.7
12-HETE	22.7	11.2	18.8	7.3	5.6	3.9	6.4	8.1	7.3
15-HETE	18.6	6.5	4.4	7	3.1	7.3	6.3	7	9.3
20-HETE	6.6	11.4	7.4	2.9	12.3	8.5	5.6	7.7	14
5-HEPE	8.1	6	19.8	4.6	4.2	4.5	4.6	4.6	10.4
8-HEPE	7.5	8.3	12.6	8.4	5	6.2	4.6	9.2	6.9
12-HEPE	5.3	8.1	12.5	6.2	5.7	7.8	7.5	9.9	3.1
15-HEPE	12.6	6.8	13.5	9.2	5.8	4.1	7.8	7.8	4.3
18-HEPE	10.8	2.4	11.2	5.5	5.1	9.3	4.2	7.5	5.3
14(15)-EpETE	12.7	10.6	3.2	3.5	1.9	11.5	5	5.3	11.1
5,6-DiHETE	8.2	9.4	60.5	10.7	9.2	14.7	6.6	11.5	7.9
5-OxoETE	3.9	9.4	10.7	3.9	3.2	7.4	4.3	9.2	8
9-HODE	8.2	5.1	8	4.4	5.5	11.1	5.6	8.3	14.3
13-HODE	7	4	4.2	2.2	2.2	9.4	3.5	3.7	4.2
LXA4	8.2	7.6	7.3	8	3.5	7.6	9.9	5.3	4.5
12-HHT	12.8	8.2	7.2	5.7	2.8	6.9	5.3	8.2	7.1
12-KHT	4.1	10.1	11.1	3.7	3.5	1.8	3.6	6.8	8.4
LTB4	0.7	3.4	7.9	3.7	2.3	6.3	2.9	3.2	12.1
T-12-HETE	5.9	3.4	12	7.9	2.3	11.4	5.7	3.2	12.2

RvD1	4.5	2.7	6.7	5.6	2.4	4	4.5	3.6	3.1
RvD2	8.5	8	8.3	9.6	8.4	9.4	8.1	10.2	12.3
RvD3	10.6	10.5	11.4	8.3	1.9	9.7	8.3	3.6	9.5
RvD4	5.2	4	9.4	6.1	3.9	7	6.7	3.7	3.3
RvD5	1.1	3.3	8.6	7.3	2.9	8.1	1.7	1.8	10.9
RvE1	4.1	2.2	9	4.9	4.6	6.1	3.3	2.9	6.7
Mar1	4.6	2.2	7.6	3.5	4.9	8.8	4.7	4.9	9.9
Mar2	1.5	5	10	4.2	2.9	4	3.4	6.8	5
12-HETrE	7.1	4.2	13.7	2.3	5.1	2.5	1.6	8.7	10.3
13-HOTrE	14.4	10.3	12.3	10.2	2.7	7.8	1.9	5.8	7.8

6. Estimated concentrations of oxylipins in platelets.

Suppl. Table S14 shows the results of linearity and sensitivity for the quantification of oxylipins in platelets (calibration performed in pooled QC by post-extraction standard addition). To document adequate performance of the method for platelets, a pooled QC sample was prepared and was injected before and after the sequence as well as within the sequence. Precision of the results were calculated for these multiple injections of the same sample and are also included in the Table S14.

Table S14. *Limits of detection and quantification, linearity and precision for platelet samples.*

Analyte	LOD	LOQ	Linearity [R]	Precision in QC
	[ng/1 x 10^8 platelets]			[%]
PGF2a	1.101	3.67	0.9989	N/A
PGE1	0.206	0.69	0.9989	N/A
PGD1	2.635	8.78	0.9986	N/A
TXB2 (peak 1, height)	0.305	1.02	0.9990	6.2
6-keto-PGF1a	0.888	2.96	0.9997	N/A
PGE2	0.104	0.35	0.9997	12.5
PGD2	0.254	0.85	0.9988	N/A
10-HDoHE	0.089	0.30	1.0000	15.4
14-HDoHE	2.357	7.86	0.9920	4.7
17-HDoHE	0.073	0.24	0.9999	19.9
5-HETE	0.089	0.30	0.9995	N/A
8-HETE	0.003	0.01	0.9988	11.0
9-HETE	0.500	1.67	0.9995	27.3
11-HETE	0.098	0.33	1.0000	11.6
12-HETE	4.709	15.70	0.9461	4.2
15-HETE	0.072	0.24	1.0000	15.8
20-HETE	0.130	0.43	0.9999	N/A
5-HEPE	0.214	0.71	0.9999	N/A
8-HEPE	0.082	0.27	0.9998	N/A

12-HEPE	0.589	1.96	0.9996	4.5
15-HEPE	0.073	0.24	0.9996	24.0
18-HEPE	0.079	0.26	1.0000	N/A
14(15)-EpETE	0.075	0.25	0.9987	N/A
5,6-DiHETE	0.497	1.66	1.0000	N/A
5-OxoETE	0.417	1.39	0.9999	N/A
12-OxoETE	1.751	5.84	0.9990	20.6
9-HODE	1.328	4.43	0.9985	8.9
13-HODE	0.878	2.93	0.9996	6.4
LXA4	0.044	0.15	0.9981	N/A
12-HHT	0.102	0.34	0.9984	7.6
12-KHT	0.118	0.39	0.9991	20.4
LTB4	0.051	0.17	0.9998	N/A
T-12-HETE	0.011	0.04	0.9995	7.0
RvD1	0.095	0.32	0.9996	N/A
RvD2	0.108	0.36	0.9993	N/A
RvD3	0.060	0.20	0.9983	N/A
RvD4	0.048	0.16	0.9996	N/A
RvD5	0.033	0.11	0.9998	N/A
RvE1	0.041	0.14	0.9989	N/A
Mar1	1.054	3.51	0.9989	23.4
Mar2	0.060	0.20	0.9995	N/A
12-HETrE	1.583	5.28	0.9978	7.2
13-HOTrE	0.024	0.08	0.9990	8.5

1.5 Publication V

Enantioselective UHPLC-MS/MS method based on sub-2µm particle polysaccharide column for chiral separation of oxylipins and its application for the analysis of autoxidized fatty acids and platelet releasates

Malgorzata Cebo[a], Xiaoqing Fu[a], Meinrad Gawaz[b], Madhumita Chatterjee[b], Michael Lämmerhofer[a]*

[a] University of Tübingen, Institute of Pharmaceutical Sciences, Pharmaceutical (Bio-)Analysis, Auf der Morgenstelle 8, 72076 Tübingen, Germany

[b] Department of Cardiology and Angiology, University Hospital Tübingen, Otfried-Müller-Strasse 10, 72076 Tübingen, Germany

Reprinted with permission from Journal of Chromatography A, Volume 1624, 2 August 2020, 461206

https://doi.org/10.1016/j.chroma.2020.461206

Journal of Chromatography A 1624 (2020) 461206

Contents lists available at ScienceDirect

Journal of Chromatography A

journal homepage: www.elsevier.com/locate/chroma

Enantioselective ultra-high performance liquid chromatography-tandem mass spectrometry method based on sub-2µm particle polysaccharide column for chiral separation of oxylipins and its application for the analysis of autoxidized fatty acids and platelet releasates

Malgorzata Cebo[a], Xiaoqing Fu[a], Meinrad Gawaz[b], Madhumita Chatterjee[b], Michael Lämmerhofer[a,*]

[a] University of Tübingen, Institute of Pharmaceutical Sciences, Pharmaceutical (Bio-)Analysis, Auf der Morgenstelle 8, 72076 Tübingen, Germany
[b] Department of Cardiology and Angiology, University Hospital Tübingen, Otfried-Müller-Strasse 10, 72076 Tübingen, Germany

ARTICLE INFO

Article history:
Received 2 March 2020
Revised 1 May 2020
Accepted 4 May 2020
Available online 16 May 2020

Keywords:
Chiral separation
Oxylipin enantiomer
Targeted lipidomics
Polyunsaturated fatty acid
Autoxidation
Chiral stationary phase

ABSTRACT

Oxylipins, the oxidation products of polyunsaturated fatty acids, are important signaling molecules in living organisms. Some of them have pro-inflammatory properties, while others act as pro-resolving agents. Oxylipins also play a major role in platelet biology and the progression of thrombo-inflammation. Depending on their structure, they may be pro-thrombotic or anti-thrombotic. For an unbiased biological interpretation, a detailed analysis of a broad spectrum of oxylipins including their stereoisomers is necessary. In our work, we developed for the first time an enantioselective UHPLC-ESI-MS/MS assay which allows quantifying individual oxylipin enantiomers. The assay made use of a sub-2µm particle-based amylose-(3,5-dimethylphenylcarbamate) chiral stationary phase (Chiralpak IA-U) under MS-compatible reversed-phase conditions. It covered 19 enantiomeric pairs of oxylipins and one diasteromeric pair of a lipid mediator: 2 pairs of hydroxyoctadecadienoic acids (HODE), 6 pairs of hydroxyeicosatetraenoic acids (HETE), 5 pairs of hydroxyeicosapentaenoic acids (HEPE), 3 pairs of hydroxydocosahexaenoic acids (HDoHE) and one pair of each: resolvins D1, hydroxyeicosatrienoic acid (HETrE), hydroxyoctadecatrienoic acid (HOTrE) and dihydroxyeicosatetraenoic acid (DiHETE). The new method is fast and showed outstanding peak resolution for most of the isomeric pairs. Excellent method sensitivity (average LOD was equal to 2.7 pg on column) was obtained by using a triple quadrupole instrument as a detector in a targeted, selected reaction monitoring (SRM) mode. The applicability of the method was verified by preliminary validation. It was then applied to analyze oxylipins produced by autoxidation of polyunsaturated fatty acids (PUFA) in air. Multiple oxylipins were found in each of the samples as racemic mixtures and served as reference substances for identification. Finally, the new enantioselective UHPLC method was applied to analyze releasates from platelets in resting state, and following activation with thrombin. The highest abundant oxylipin in the platelet releasate was 12(*S*)-HETE, but many other oxylipins were found in the thrombin activated samples, usually as single enantiomers (e.g. 12(*S*)-HEPE, 11(*R*)-HETE, 9(*R*)-HODE, 13-(*S*)-HODE, 14(*S*)-HDoHE). The latter was detected at about similar concentration in resting platelet releasates as well. 15-HETE showed elevated levels for both *R*-and *S*-enantiomers in releasates of thrombin-activated platelets. 12-HETrE was found presumably as both enantiomers, however, retention time inconsistencies indicate that the *R*-enantiomer is actually a different compound, maybe another constitutional isomer with different double-bond configuration.

1. Introduction

Oxylipins, the oxidation products of polyunsaturated fatty acids (PUFA), play a crucial role in several pathophysiological conditions e.g. metabolic disorders, cardiovascular diseases or cancer,

* Corresponding author: T +49 7071 29 78793, F +49 7071 29 4565;
E-mail address: michael.laemmerhofer@uni-tuebingen.de (M. Lämmerhofer).
URL: http://www.bioanalysis.uni-tuebingen.de/ (M. Lämmerhofer)

https://doi.org/10.1016/j.chroma.2020.461206
0021-9673/

regulating inflammatory processes [1]. They are also important regulators of platelet functions, whereby their autocrine and paracrine mode of actions and intraplatelet signaling is mediated by members of this class of compounds [2–4]. Oxylipins are major players of thrombo-inflammation and have influence on the progression of cardiovascular disease (CVD) risk and thrombosis [5,6]. It is well-known that some members of the oxylipin class are pro-inflammatory, while others are anti-inflammatory [7]. As a consequence, the full understanding of thrombo-inflammatory processes requires a detailed analysis of these lipid mediators.

In general, oxylipins can originate from autoxidation of PUFAs, oxidative stress and enzymatic synthesis. Autoxidation and lipid oxidation by reactive oxygen species (ROS) due to oxidative stress are non-stereospecific and therefore lead to racemic mixtures of products [8]. Enzymatic production of oxylipins occurs by 3 main families of enzymes: cyclooxygenases (COXs), lipoxygenases (LOXs) and cytochrome P450 (CYP450). These enzymatic reactions proceed enantioselectively due to the chiral nature of the enzymes and they result in production of pure enantiomers.

The stereochemical differences of products from autoxidation/oxidative stress, and enzymatic reactions (i.e. racemate *vs.* pure enantiomer) might be used to determine the level of oxidative stress in tissues. Moreover, non-enzymatically derived oxylipins might serve as markers of autoxidation or biomarkers of oxidative stress [9].

The biological activity of oxylipins is most often related to only one enantiomeric form. To get unbiased insight into biochemical processes, it is advisable to perform the analysis of oxylipins in biological samples by enantioselective assays. However, routine analysis of oxylipins typically use achiral reversed-phase ultra-high performance liquid chromatography (UHPLC) [3,10–14] or, less commonly, achiral supercritical fluid chromatography (SFC) [15]. These chromatographic methods coupled to a mass spectrometer (MS) provide concentrations of 10s to 100s for oxylipins with high sensitivity. However, they are unable to separate enantiomers, so the information about enantiomeric composition of oxylipins in the samples is lost.

Such information about individual oxylipin enantiomers can be obtained by enantioselective liquid chromatography. There are many chiral stationary phases (CSP) available for enantioselective liquid chromatographic separation [16,17].

Chiral separations of short-chain and long-chain hydroxycarboxylic acids have been reported with quinine- and quinidine carbamate-derived brush-type CSPs [18–20]. The selectivity of these CSPs turned out to depend on the hydroxycarboxylic acid structure, especially on the position of the OH group with respect to the carboxylic acid group. Good chiral recognition and enantiomer separation could be obtained for 2- and 3-hydroxy carboxylic acids. Hydroxy carboxylic acid enantiomer separations for such compounds have also been reported for macrocyclic antibiotic CSPs [21].

However, in the case of oxylipins, the position of the hydroxy group is farther away from the carboxylic acid group than α and β, and it varies from compound to compound. Therefore, a more generally applicable method with enantioselectivity for a variety of distinct hydroxy fatty acids is required. In the recent decades, the polysaccharide-based CSPs have gained enormous popularity, because of their versatility. These CSPs can be used in various elution modes, most commonly in normal-phase LC, reversed-phase LC and supercritical fluid chromatography mode, but also in polar organic LC, and hydrophilic interaction liquid chromatography (HILIC) mode [22,23]. Chromatographic separations with polysaccharide-based CSPs are nowadays the most common methods for enantiomer separation of oxylipins and especially the columns with tris(methylbenzoate) and tris(3,5-dimethylphenylcarbamate) derivatives of cellulose [24,25] and amylose [26–28] have been widely used. Most of the recent chiral separations of oxylipins have been reviewed by Mesaros et al. [29], and more recently by Ianni et al. [16].

The commercially available polysaccharide-based CSPs were originally produced as polysaccharide-coated CSPs [22,23]. These columns are less flexible where the usage of mobile phases is concerned, as some solvents cause dissolution or swelling of the chiral selector. The newer generation of columns is the immobilized type of columns with the chiral selector covalently bonded to silica. They can be safely used with extended set of solvents and conveniently switched between elution modes [30,31]. Oxylipin enantiomer separations on polysaccharides were initially performed mainly in normal-phase mode due to excellent enantioselectivities [32]. However, normal-phase LC is not very well compatible with electrospray ionization (ESI) and therefore reversed-phase mode HPLC separations dominate the field of bioanalytical applications with mass spectrometric detection [33]. The columns employed are typical standard HPLC columns based on 5 µm, or more recently also 3 µm, particle based polysaccharide CSPs.

Herein, we report the first UHPLC enantiomer separations of oxylipins on polysaccharide-type sub-2µm particle columns which can be used for fast UHPLC separations. We used them to develop a selective and sensitive enantioselective UHPLC-MS/MS method for chiral separation of multiple oxylipins of different types in biological samples. The method utilized the newest generation of polysaccharide-based CSP columns, in particular Chiralpak IA-U with sub-2µm particles and immobilized amylose tris(3,5-dimethyl-phenylcarbamate) as the chiral selector. The new enantioselective UHPLC-MS/MS method was then successfully employed for the analysis of oxylipins in autoxidized PUFA samples and in platelet releasates after thrombin activation.

2. Materials and methods

2.1. Materials

All the oxylipins, fatty acid standards and deuterated internal standards (IS) (5(*S*)-HETE-d8, 12(*S*)-HETE-d8 and 13(*S*)-HODE-d4) were purchased from Cayman Chemical (Ann Arbor, MI, USA). Their structures, IUPAC and common names are displayed in the supplementary information (section 1). Acetonitrile (ACN) and methanol (MeOH) of LC-MS grade were obtained from Carl Roth (Karlsruhe, Germany). Acetic acid (HAc), formic acid (FA), sodium acetate, butylated hydroxytoluene (BHT), Dulbecco's phosphate-buffered saline (PBS buffer) as well as solvents of HPLC grade (MeOH, ethyl acetate and n-hexane) were all purchased from Sigma Aldrich (Merck, Munich, Germany). Purified water was produced by Elga Purelab Ultra (Celle, Germany).

The preparation of the autoxidation samples is reported in Suppl. Material (section 2.1). Platelet releasates were from a previous study [3] and were prepared from blood collected from healthy donors at the Department of Cardiology and Angiology, University Hospital Tübingen in accordance with ethical guidelines. The extraction procedure of oxylipins from platelet releasates is described in detail in Suppl. Material (section 2.2).

2.2. Test mixtures

Two mixtures of standards were prepared in order to test the chromatographic enantiomer separation of the compounds. The mixtures were comprised of 15 pairs of enantiomeric monohydroxy fatty acids, 2 pairs of positional isomers (2 pairs of prostaglandins) and 1 pair of diastereoisomers (2 resolvins).

The mixture A (Mix A) contained (±)9-HODE, (±)13-HODE, (±)5-HETE, (±)8-HETE, (±)11-HETE, (±)12-HETE, (±)15-HETE, (±)5-HEPE, (±)12-HEPE, (±)15-HEPE, (±)18-HEPE, (±)10-HDoHE, (±)17-

HDoHE, RvD1, 17(*R*)-RvD1, PGD1, PGE1, PGD2 and PGE2 (for structures see Suppl. Information, section 1.1).

The mixture B (Mix B) contained 9(*S*)-HODE, 13(*S*)-HODE, (±)9-HETE, (±)8-HEPE, 17(*R*)-RvD1, PGE1 and PGE2.

The concentration of each substance in the mixtures was 50 ng/mL and the compounds were dissolved in MeOH.

2.3. LC methods

2.3.1. Screening methods

All the measurements were done with an Agilent 1290 Infinity UHPLC system (Agilent, Waldbronn, Germany) comprised of a binary pump, degasser and column oven and coupled to CTC PAL HTS autosampler (CTC Analytics AG, Switzerland).

Two immobilized polysaccharide UHPLC columns with sub-2µm particles were used for method screening to find suitable conditions for enantiomer separation, namely Chiralpak IA-U and Chiralpak IC-U (Daicel, Osaka, Japan) with identical dimensions of 3.0 mm x 100 mm and identical particle size of 1.6 µm.

Four different gradient methods with different mobile phases were used. Each mobile phase consisted of water with 0.1% (v/v) of acid as the component A. The component B was organic solvent (either ACN or MeOH) with 0.1% (v/v) of the same acid as in A. HAc and FA were used as the acid additives.

The gradient method for screening with ACN as the B component of the mobile phase started with 50% B and the percentage of B was raised to 95% in 5 min, followed by a hold at 95% for the next 2.5 min, then %B quickly dropped to 50% (in 0.1 min) and it stayed at this level for the last 2.4 min for column re-equilibration.

Due to a weaker elution strength, the gradient methods with MeOH started with 90% B and the fraction of B increased to 100% in 5 min, then it was kept at this level for 2.5 min, followed by re-equilibration for 2.4 min.

For all the screening methods the flow rate was equal to 0.3 mL/min, column temperature was kept at 25°C and the injection volume was 10 µL.

2.3.2. Final method

The final method thus developed utilized the Chiralpak IA-U column (3.0 mm x 100 mm, 1.6 µm). The mobile phase was composed of water with 0.1% (v/v) HAc as the component A and ACN with 0.1% (v/v) HAc as the component B. Gradient elution was performed from 50% B to 100% B in 5 min, followed by a hold at 100%%B for 5 min. Then, the B level was decreased to 50% in 0.1 min and kept at 50% for the next 1.9 min. The flow rate was 0.3 mL/min and column temperature was kept at 40°C. Injection volume was always 10 µL.

2.4. MS method

For detection, an AB SCIEX API 4000^{TM} MS/MS mass spectrometer with TurboIonSpray (SCIEX, Ontario, Canada) was utilized. Selected reaction monitoring (SRM) ion pairs were individually optimized for each compound and checked for possible interferences. The list of SRMs of the components of Mix A and Mix B is displayed in Tab. 1.

All the measurements were done with ESI in negative polarity mode. Cell exit potential was set to –15 V, entrance potential was -10 V, source voltage was equal to -4,000 V, source temperature was kept at 400°C, heater gas pressure and nebulizer gas pressure were both equal to 50 psi, curtain gas pressure was 35 psi and the collision gas pressure was set to medium. Dwell time for each SRM in Tab. 1 was 20 ms and the total cycle time was 378 ms.These parameters were identical for the screening methods and the final method.

Table 1
SRMs for components of Mix A and Mix B. The selected precursor ions in quadrupole 1 (Q1 *m/z*) and chosen fragment ion (Q3 *m/z*) as well as collision energy (CE) and declustering potential (DP) for each compound is shown.

Name	Q1 *m/z*	Q3 *m/z*	CE [V]	DP [V]
9-HODE	295.2	171.2	-24	-85
13-HODE	295.2	195.1	-27	-90
5-HETE	319.2	115.1	-20	-70
8-HETE	319.2	155.0	-19	-70
9-HETE	319.2	151.0	-20	-60
11-HETE	319.2	167.2	-24	-70
12-HETE	319.2	179.2	-20	-70
15-HETE	319.2	219.4	-19	-70
5-HEPE	317.2	115.1	-22	-70
8-HEPE	317.2	161.1	-26	-70
12-HEPE	317.2	179.2	-19	-70
15-HEPE	317.2	219.4	-19	-65
18-HEPE	317.2	259.5	-19	-70
10-HDoDE	343.2	153.0	-22	-60
17-HDoDE	343.2	201.0	-20	-40
RvD1	375.1	215.1	-27	-40
PGD1 & PGE1	353.0	317.2	-22	-40
PGD2 & PGE2	351.0	271.1	-25	-80

The parameters used for the extended set of oxylipins are summarized in the supplementary information (Suppl. Tab. S5).

2.5. Data processing

The data were processed with PeakView 2.1 and MultiQuant 3.0 (both from Sciex, Ontario, Canada). The following parameters were used for peak integration: Gaussian smooth width: 1 point, minimum peak width: 3 points, minimum peak height: 100, noise percentage: 40%, baseline subtraction window: 0.5 min. Peak splitting points were adjusted individually depending on peak shape and how close the isomers eluted to each other, but usually was set to 1 point.

Microsoft Office 2010 (Microsoft, Redmond, WA, USA) and R (version i386 3.4.2; R-project for statistical computing) were used for further calculations and figure preparation.

Chromatographic resolution Rs was calculated by the peak width at half height method.

3. Results and discussion

3.1. Screening of methods

Column selection is the most critical factor in analytical process development for enantioselective methods. Rational column selection based on prediction of chiral recognition mechanisms has turned out illusive. Consequently, method development in enantioselective chromatography typically starts with the screening of a number of distinct promising chiral stationary phases with broad selectivity using a variety of different mobile phases [34,35]. For the current application, MS detection was mandatory and hence columns with MS compatibility (reversed-phase elution mode) were prioritized. Polysaccharide CSPs have the broadest application spectra and since recently are available as stable-bonded phases with immobilized selectors on sub-2µm particle basis. Two members of this family (one amylose, one cellulose based CSP) with complementary enantioselectivity profiles were tested: Chiralpak IA-U, based on amylose tris(3,5-dimethylphenylcarbamate), and Chiralpak IC-U (cellulose tris(3,5-dichlorophenylcarbamate). Eighteen pairs of structural isomers were analyzed with different screening methods using these two columns. The resolution values between each pair of corresponding isomers were calculated and

Table 2
Resolution between isomeric peak pairs obtained with different screening methods (for corresponding values of Chiralpak IC-U see Suppl. Table S1 and for corresponding retention times see Suppl. Table S2).

	Column IA-U			
Compounds	ACN + HAc	ACN + FA	MeOH + HAc	MeOH + FA
9-HODE	9.53	9.63	5.48	5.61
13-HODE	14.97	14.69	11.70	11.76
5-HETE	3.55	3.57	7.50	7.46
8-HETE	4.35	4.42	6.39	6.36
9-HETE	2.36	2.52	3.01	2.93
11-HETE	4.07	4.06	4.17	4.12
12-HETE	2.73	2.83	4.99	4.84
15-HETE	5.96	6.21	8.73	8.82
5-HEPE	2.44	2.49	6.57	6.45
8-HEPE	3.35	3.42	5.79	5.65
12-HEPE	2.94	3.04	4.95	4.87
15-HEPE	2.34	2.45	5.92	5.70
18-HEPE	1.81	1.95	3.76	3.44
10-HDoDE	3.29	3.51	5.33	5.32
17-HDoDE	2.08	2.09	5.28	5.12
Resolvins D1	2.59	2.65	2.63	2.55
PGD1 and PGE1	2.67	2.73	1.70	1.72
PGD2 and PGE2	1.12	1.14	0.00	0.00

they are summarized in Tab. 2. The obtained chromatograms are illustrated in Fig 1.

Overall, better results in terms of resolution between isomers were obtained with the IA-U column (i.e. with amylose based CSP) for all of the compounds except for prostaglandins (PGD1/E1 and PGD2/E2). These two constitutional isomer pairs can be separated by RPLC with C18 phase but are actually often poorly resolved in RPLC, especially the PGD1/E1 isomer pair. As can be seen from Fig. 1, the IC-U column (with the cellulose CSP) gives exceptional resolution values (>3.0) when ACN was used as organic modifier. However, in the current studies the main focus was on separation of enantiomeric mono- and polyhydroxycarboxylic acids and the IA-U column was chosen for further method development. Prostaglandins were removed from further comparisons and discussions.

In terms of organic solvent comparison, both ACN and MeOH provided resolution over 1.5, so baseline separations were achieved for all the isomer pairs except for PGD2/PGE2. Generally, higher resolution values were obtained with MeOH mainly due to larger separation factors (Suppl. Fig S1). However, peaks were broader with MeOH (Suppl. Table S3), which was considered disadvantageous with regard to detection sensitivities. Moreover, methods with MeOH were considered less flexible in terms of adjustments of mobile phase elution strengths (the gradient started already with 90% B) and flow rate (higher backpressure in the system was observed with MeOH; a comparison is provided in the Suppl. Fig. S2). Therefore, ACN was chosen for final method fine tuning.

Last but not the least, the type of acid additive (acetic vs formic acid) was examined as it could show some effect on isomer resolution, but also on detection sensitivity. It was found that the acid additive did not exert a strong influence neither on the retention time, nor peak shape, and therefore resolution as well. Method sensitivity was then compared for these 2 acids and the results were also very similar with slightly better sensitivity obtained with HAc (data provided in the Suppl. Tab. S4). Therefore, this acid was selected for the final method adjustment.

3.2. Final method adjustment (fine tuning of gradient profile)

The final gradient profile of the method was adjusted for obtaining good isomer separations, avoiding interferences from structurally related oxylipins in order to secure satisfactory assay specificity, and finally assuring complete elution of other possible components of the oxidized PUFAs and the platelet releasate samples. Had they accumulated on the column, problems with assay specificity and method ruggedness might have occurred.

The final gradient was slightly steeper with channel B varying from 50 to 100% B (instead of to 95% B as in the screening method) in 5 min. Then the washing step of 100% B was extended to 5 min in order to elute possible other more lipophilic compounds (for example fatty acids) from the column, which might show stronger retention. For the same reason, the column temperature was increased to 40°C.

At this point, different MS source parameters were also tested by automated optimization with flow injection, but the initial conditions performed very well and were not changed for the final method. The fully optimized final method is given in the experimental section.

3.3. Preliminary validation for quantification of oxylipins from autoxidation of PUFAs

Several parameters were determined in the pre-validation studies to prove that the method can give reliable results when real samples are analyzed. For this reason, instrumental limit of detection (LOD) as the lowest concentration of an analyte (dissolved in MeOH), which gives signal-to-noise (S/N) ratio of minimum 3 was determined. Similarly, the desired lower limit of quantification (LOQ) was confirmed to give S/N ratio of at least 10. Method linearity in the calibration range was determined, as well as intra-assay method accuracy and precision for 2 independent concentration levels was measured: 2.5 ng/mL and 12.5 ng/mL for all the analytes except of 14(S)-HDoHE, 12(S)-HETrE and 13(S)-HOTrE, for which the spiked concentration was two times higher (5.0 and 25.0 ng/mL) The results were satisfying and are displayed in Tab. 3.

3.4. Results of autoxidation of PUFAs

Six different PUFAs (LA, AA, EPA, DHA, ALA, DGLA) were oxidized in air at 3 different time points: 18 h, 24 h and 48 h. All the compounds used for method development were monitored in this experiment: 2 pairs of HODEs, 6 pairs of HETEs, 5 pairs of HEPEs, 2 pairs of HDoHEs and a pair of resolvins D1. Additionally, 4 more SRMs were added to monitor 3 other hydroxy fatty acids, viz. 12-HETrE, 13-HOTrE and 14-HDoHE (pure *S* enantiomers were used as standards, but no *R* nor racemic mixture were available for comparison) as well as 5,6-DiHETE (the standard was a racemic mixture of the two *cis*-enantiomers, but not all 4 stereoisomers were available). The results of the oxidation are shown in Fig. 2 (compounds above LOQ) and a table with all the results is displayed in the Supplementary Information (Suppl. Table S6).

As shown in Fig. 2 several compounds were found in the oxidized samples. Oxidation of AA produced high amounts of 15-HETE and lower concentrations of other HETEs. For all HETEs the maximal amount was observed at 24 h of oxidation and it dropped or was not detected anymore when the arachidonic acid was oxidized for 48 h. It seems that these compounds are further degraded to secondary oxidation products. As expected, the two enantiomers were always produced in equal quantities (within the error limits) and no stereoselectivity was observed due to the absence of chiral catalyst.

HEPEs, which are products of EPA oxidation, were found at minute amounts, always below LOQ. Similarly to HETEs, they usually appeared after 24 h of oxidation and were not detected anymore in the sample after 48 h of oxidation. 5,6-DiHETE, which also originates from EPA, was not detected in air-oxidized samples.

HODEs, oxylipins originating from LA, were found in high amounts around 1 ng of each enantiomer of the hydroxy fatty acid from 1 µg of the PUFA (LA). They were highly abundant already

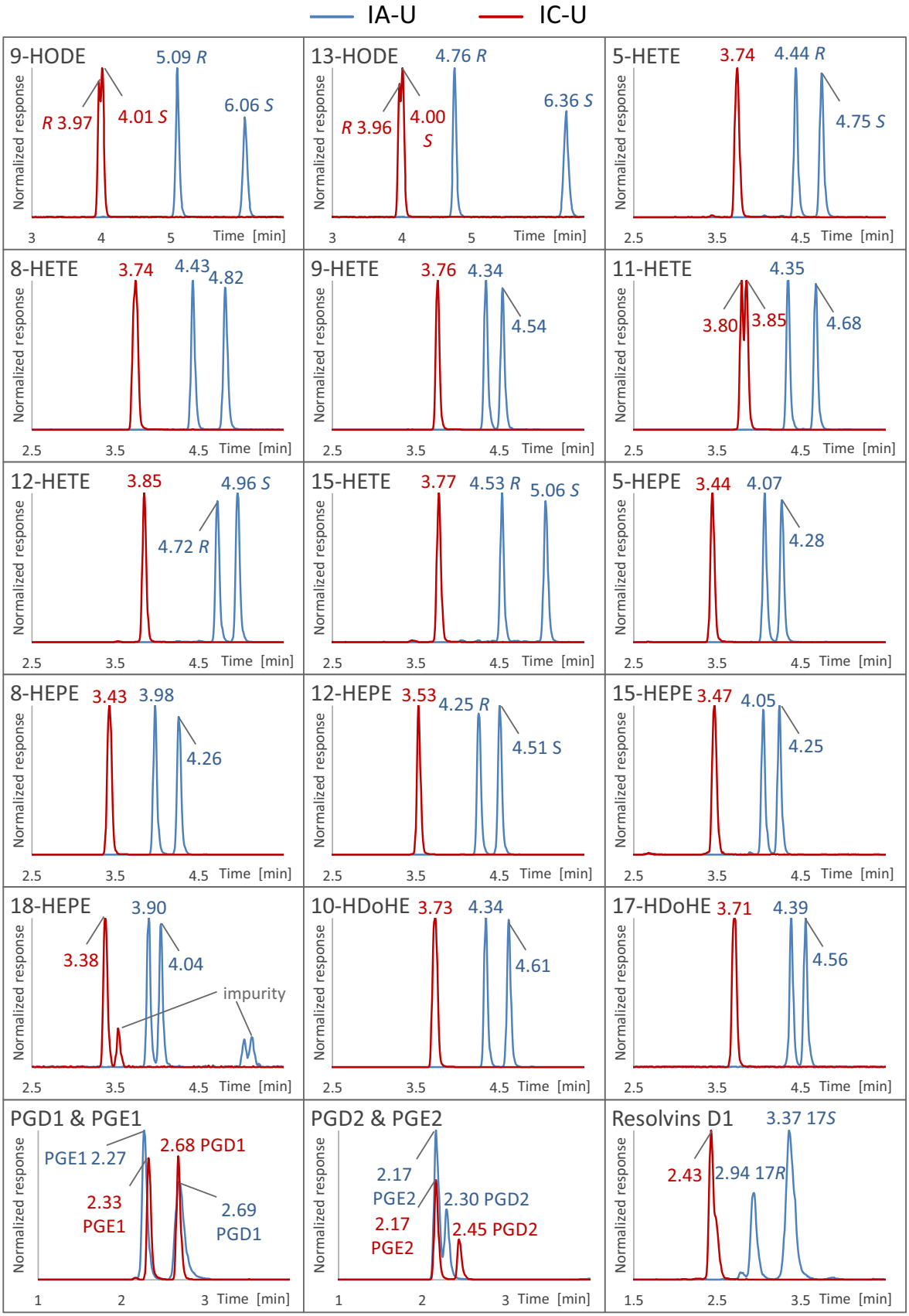

Figure 1. Comparison of chromatograms obtained with Chiralpak IA-U column (blue) and Chiralpak IC-U column (red). Chromatographic conditions: A: H_2O+0.1% (v/v) HAc, B: ACN+0.1% (v/v) HAc, 50-95% B in 5 min, 95% B for 2.5 min, 95-50% B in 0.1 min, 50% for 2.4 min; flow rate: 3 mL/min; column temperature 25°C.

Table 3
Preliminary validation results for quantification of oxylipins from autoxidation of PUFAs.

PUFA	Compound	LOD [pg on column]	LOQ [pg on column]	Range [pg per 1 µg of PUFA]	R	Accuracy [%][a] QC low	Accuracy [%][a] QC high	Precision [%][b] QC low	Precision [%][b] QC high
LA	9(*R*)-HODE	2.5	5	50-5,000	0.989	114.1	98.3	1.2	5.0
	9(*S*)-HODE	2.5	5	50-5,000	0.991	107.7	97.7	8.0	10.7
	13(*R*)-HODE	2.5	5	50-5,000	0.985	111.1	104.2	0.9	3.2
	13(*S*)-HODE	2.5	5	50-5,000	0.990	108.1	102.5	2.0	9.3
AA	5(*S*)-HETE	0.5	5	50-5,000	0.991	112.2	105.7	7.0	5.2
	5(*R*)-HETE	0.5	5	50-5,000	0.983	113.3	105.2	9.1	4.2
	8-HETE p1	2.5	5	50-5,000	0.991	115.0	104.6	2.6	6.7
	8-HETE p2	2.5	5	50-5,000	0.988	112.6	102.5	3.1	2.3
	9-HETE p1	2.5	5	50-5,000	0.990	113.9	101.8	5.4	1.3
	9-HETE p2	2.5	5	50-5,000	0.987	110.5	102.8	1.5	1.0
	11-HETE p1	0.25	5	50-5,000	0.990	114.8	101.8	6.2	3.1
	11-HETE p2	0.25	5	50-5,000	0.988	114.2	105.8	11.5	7.4
	12(*R*)-HETE	2.5	5	50-5,000	0.991	114.1	105.2	6.3	2.6
	12(*S*)-HETE	2.5	5	50-5,000	0.990	114.0	104.4	6.0	8.9
	15(*R*)-HETE	2.5	5	50-5,000	0.992	113.9	100.7	8.8	5.7
	15(*S*)-HETE	2.5	5	50-5,000	0.993	112.6	102.6	5.7	3.9
EPA	5-HEPE p1	2.5	5	50-5,000	0.983	112.3	110.4	7.7	6.6
	5-HEPE p2	2.5	5	50-5,000	0.992	111.9	101.7	0.3	5.0
	8-HEPE p1	2.5	5	50-5,000	0.993	112.0	102.6	3.4	4.3
	8-HEPE p2	2.5	5	50-5,000	0.991	114.4	101.1	6.0	3.8
	12(*R*)-HEPE	2.5	5	50-5,000	0.994	110.2	99.3	0.2	5.5
	12(*S*)-HEPE	2.5	5	50-5,000	0.993	114.7	100.3	3.7	4.5
	15-HEPE p1	2.5	5	50-5,000	0.989	111.6	102.7	0.1	3.4
	15-HEPE p2	2.5	5	50-5,000	0.994	110.7	97.0	3.7	0.6
	18-HEPE p1	5	25	250-5,000	0.997	97.4	99.9	6.2	0.2
	18-HEPE p2	5	25	250-5,000	0.993	87.7	92.4	6.1	0.2
DHA	10-HDoHE p1	0.5	5	50-5,000	0.991	114.9	100.3	2.8	6.7
	10-HDoHE p2	0.5	5	50-5,000	0.991	113.4	103.3	1.2	7.2
	17-HDoHE p1	5	25	250-5,000	0.995	94.6	97.4	8.1	6.3
	17-HDoHE p2	5	25	250-5,000	0.995	86.8	95.7	5.0	7.4
	RvD1	5	25	250-5,000	0.986	113.6	94.8	7.2	9.8
	17(*R*)-RvD1	5	25	250-5,000	0.986	113.6	94.8	7.2	9.8
ALA	13(*R*)-HOTrE	1	10	100-10,000	0.989	N/A	N/A	N/A	N/A
	13(*S*)-HOTrE	1	10	100-10,000	0.878	113.0	103.3	3.5	5.9
DGLA	12(*R*)-HETrE	1	10	100-10,000	0.989	N/A	N/A	N/A	N/A
	12(*S*)-HETrE	1	10	100-10,000	0.989	114.9	99.2	4.0	6.4
DHA	14(*R*)-HDoHE	1	10	100-10,000	0.990	N/A	N/A	N/A	N/A
	14(*S*)-HDoHE	1	10	100-10,000	0.990	113.5	101.5	2.6	2.1
EPA	5,6-DiHETE p1	10	50	500-5,000	0.987	95.3	102.1	3.6	13.0
	5,6-DiHETE p2	10	50	500-5,000	0.992	108.9	99.1	11.2	1.4

[a] Accuracy given as % recovery (n=3)
[b] precision given as % RSD (n=3)

after 18 h of oxidation and their levels remained more or less constant throughout the oxidation experiments. We have reported amounts of oxidation only for the *R* enantiomers as there were interfering signals eluting close to the *S* enantiomers. Due these interferences correct quantification of these enantiomers is cumbersome and some further chromatographic optimization is recommended. However, as it is shown for other autoxidation products, equal amounts of *S* and *R* enantiomers were expected and accurate quantification of one enantiomer allowed conclusion on the second one.

No oxidation products of DHA with selected SRMs were found above the LOQ levels and only minor amounts of 10-HDoHE and 14-HDoHE close to LOD were detected.

12-HETrE and 13-HOTrE, which are formed from DGLA and ALA respectively, were observed in the corresponding samples. 12-HETrE reached the maximum level at 24 h and was not detected after 48 h of oxidation. 13-HOTrE showed the highest abundance already after 18 h of oxidation. The calibration function was only available for the *S* enantiomers, but equal concentration of *R* enantiomers can be validly assumed in the absence of a chiral catalyst as supported by equal peak area ratios.

All of the newly added compounds - 12-HETrE, 13-HOTrE, 14-HDoHE and 5,6-DiHETE, were well separated, which shows that the method can be conveniently extended to other mono and polyhydroxy fatty acids. Three of the compounds (12-HETrE, 13-HOTrE and 14-HDoHE) were found as pairs of enantiomers (with similar area ratio *R* to *S* enantiomer in the respective samples) in the corresponding autoxidized PUFAs. 5,6-DiHETE was not detected in the oxidation samples, but the standard was a pair of *cis*-enantiomers, which were well separated. The chromatograms are showed in Fig. 3.

3.5. Preliminary validation for the quantification of oxylipins in platelet releasates

Released hydroxy fatty acids from resting and thrombin-activated platelets were extracted and analyzed by UHPLC-MS/MS using a matrix-matched calibration and three stable isotope labelled internal standards. The analytical method was extended by addition of 12-HETrE, 13-HOTrE, 14-HDoHE and 5,6-DiHETE (compared to the screening method).

Similarly to previously described quantification, the analysis of platelet releasates was also pre-validated to show that the method gives satisfying results and can be used for quantification of the analytes in platelet supernatant studies. Instrumental LOD (as analytes dissolved in MeOH, not in matrix because of lack of an analyte-free-matrix for all compounds) was established with minimal value of S/N as 3. LOQ was determined in matrix with minimal S/N ratio equal to 10. Calibration functions were established using area ratios (peak area of an analyte divided by peak area

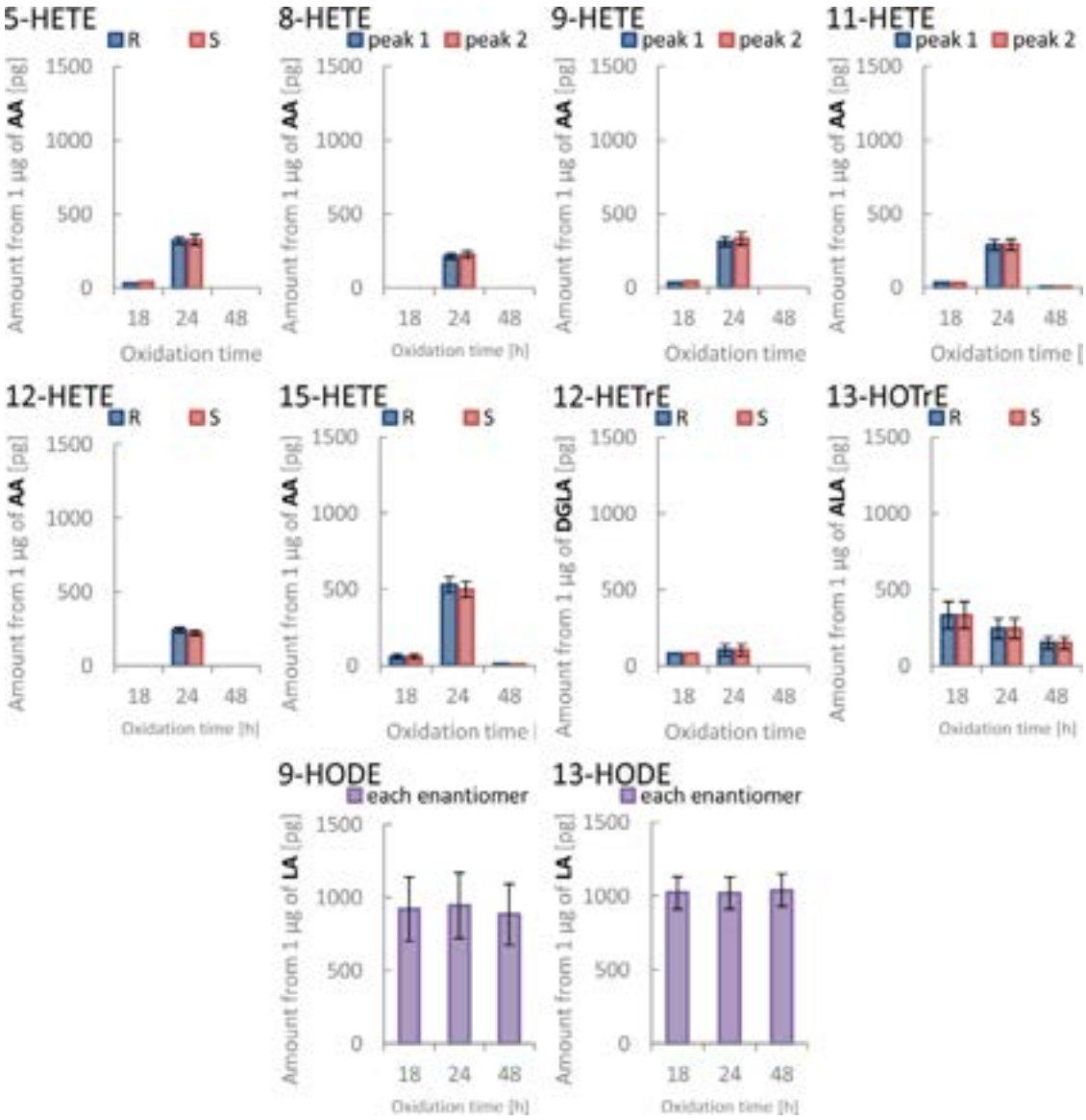

Figure 2. Bar graphs showing mass [in pg] of hydroxy fatty acids produced by oxidation of 1 µg of a corresponding PUFA. Compounds were analyzed at 3 different time points of oxidation: exposure to air for 18, 24 and 48 h. Blue bars show the amount of the first eluted enantiomer (specified in legend as *R* or *S* if identified), and the red bars display the later eluted enantiomer; In case of HODEs the purple bar graphs show amount of the *R* enantiomer and the *S* enantiomer is assumed to be equal. The y scale is unified for all the bar graphs to 1,500 pg.

of an internal standard), by weighted linear regression using $1/x^2$. Good linearity was confirmed over the calibration range specified in Tab. 4 by correlation coefficients $R > 0.98$. Intra-assay accuracy and precision were determined for two independent concentration levels: platelet release spiked with 2.5 ng/mL and 12.5 ng/mL of all analytes accept of 14(*S*)-HDoHE, 12(*S*)-HETrE and 13(*S*)-HDoHE, which were spiked with 2 times higher concentration. The final results are presented in Tab. 4.

3.6. Results of the analysis of platelet releasates

Several oxylipins were detected in the platelet releasates and for many of them an increased level in thrombin-activated platelets was observed. Importantly, in most of the cases one of the enantiomers was elevated, while the other was not detected or detected in minute concentrations, which is indicative for enzymatic oxidation. Box plots of the oxylipins with concentrations higher than LOQ are illustrated in Fig. 4, while all the results are summarized in the supplementary information (Suppl. Tab. S7).

The highest concentration of the hydroxy fatty acids released from activated platelets was that of 12(*S*)-HETE. This compound exceeded over 15 times the concentration of any other oxylipin analyzed in this study. 12(*S*)-HETE was present in the releasate from resting platelets only at very minor concentrations and highly increased with thrombin activation. It is a product of 12-LOX activity and it is one of the main metabolites generated when platelets are activated by factors like thrombin, calcium or collagen. The role of free 12(*S*)-HETE remains unknown, but it has been shown that significant amounts of this hydroxy fatty acid are re-esterified into membrane phospholipids [36,37].

The production of other 12-hydroxy fatty acids was also observed. 12-HEPE, which originates from EPA, was also detected as *S* enantiomer, while 12-HETrE from DGLA was seemingly present in both forms as *R* and *S* enantiomers (*vide infra*), and their concentration was very similar.

In case of 11-HETE the first eluted peak, which is supposed to be the *R* enantiomer, increased upon activation. Both enantiomers

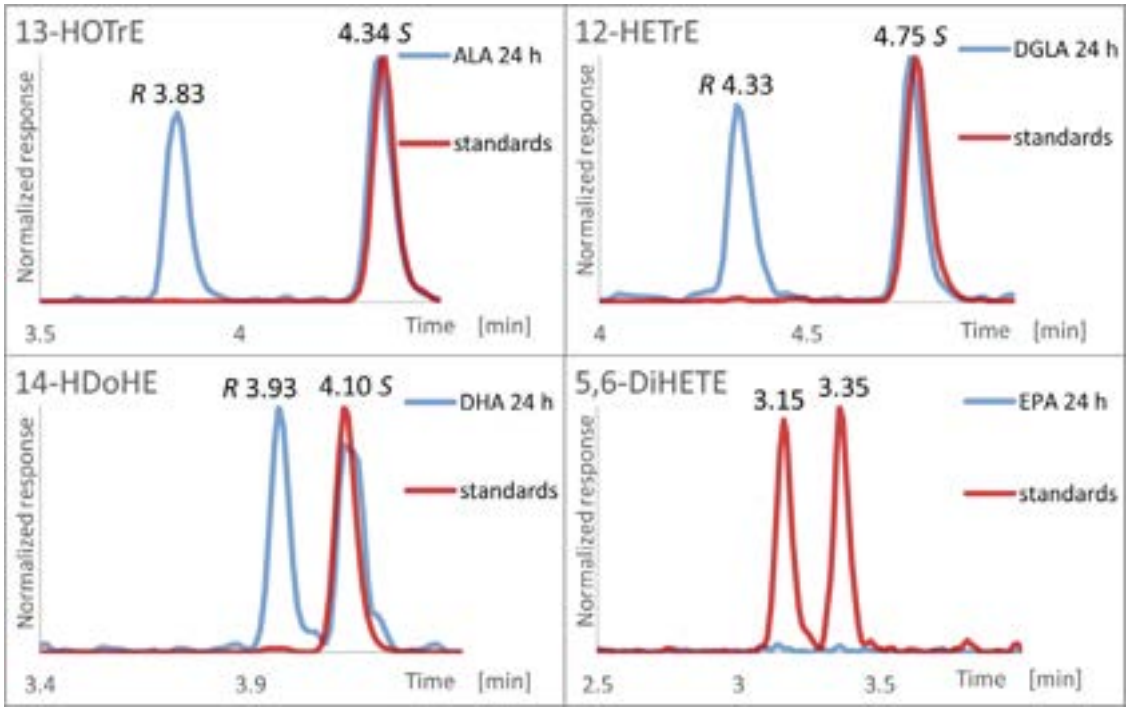

Figure 3. Separation of enantiomers of 13-HOTrE, 12-HETrE, 14-HDoHE and 5,6-DiHETE. Blue line shows chromatogram from a corresponding oxidized PUFA and red trace shows chromatogram from a pure standard (in case of 13-HOTrE, 12-HETrE and 14-HDoHE standards were pure *S* enantiomers and 5,6-DiHETE was a racemic mixture of *cis*-enantiomers).

of 15-HETE were elevated in the samples of thrombin-activated platelets.

Opposite observations were made for 9- and 13-HODE: for 9-HODE mostly the *R* enantiomer increased upon activation, while 13-HODE was detected mostly as the *S* enantiomer in thrombin activated samples.

14(*S*)-HDoHE was present already in resting platelets and its level remained quite the same in activated platelets. The *R* enantiomer was not observed.

3.7. Practical implications of the current results and discussion on their biological effects

The vast majority of methods used nowadays for oxylipin analysis are non-enantioselective targeted assays (e.g. [38]). These assays often cover a wide variety of lipid mediators. However, they do not give the entire picture of oxylipin synthesis in biological systems like platelets, as they cannot distinguish whether the products are originating from autoxidation, cellular ROS-triggered oxidation (which is undoubtedly faster than oxidation in air due to the reactive potential of the transiently generated radicals) or enzymatic biotransformation. Enantioselective assays are more powerful as they create additional information which allows for a more differentiated interpretation of the results in terms of biochemical pathways. The following discussion should document this for platelet activation, however, has been already reported for other biological questions on other columns (mostly Chiralpak AD-H) [39].

3.7.1. Distinction between autoxidation, oxidative stress and enzymatic biotransformation

One particular problem of PUFAs and PUFA-containing lipids is their ease of autoxidation. PUFA-autoxidation products cannot be distinguished from enzymatic PUFA metabolites by achiral LC-MS/MS assays. Enantioselective UHPLC-MS/MS does provide this information. For example, human platelet-type 12-lipoxygenase (12-LOX) plays an important role in the regulation of human platelet function. Autoxidation produces both enantiomers (Fig. 5A1), while 12-LOX action generates the *S*-enantiomer of 12-HETE only (Fig. 5A2). In Fig. 5A2 we see that there was no 12(*R*)-HETE present in the activated platelet sample and therefore we could conclude that autoxidation was absent. If both enzymatic and autoxidation products had been present at the same time, non-racemic mixtures would have been the result and the enantiomeric excess of *S*-enantiomer (ee% = (*S*-*R*)/(*S*+*R*)) would have indicated the 12-LOX product while the *R*-enantiomer peak would have been considered as a marker of autoxidation. The same principal picture of enantiomer ratios as elaborated for autoxidation is expected for hydroxyl PUFA metabolites that are formed from oxidative stress due to cellular ROS which also generates the racemic mixture. Distinction between autoxidation (in course of sample preparation) and ROS-triggered oxidation becomes possible if the corresponding isotope labelled PUFA is added as an internal standard.

3.7.2. Contamination of platelet isolate with leukocytes

A distinctive problem of the purity of isolated platelet preparations is their contamination with leukocytes. Leukocytes express 5-LOX, while platelets are deficient in 5-LOX [40]. 5-HETE, if present in platelet samples, is therefore due to autoxidation/ROS-oxidation (both enantiomers present at same concentration level), or if present as *S*-enantiomer (or as enantiomeric excess of *S*-enantiomer) might indicate leukocyte contamination. If autoxidation was the problem the entire PUFA oxidation profile for AA is expected to be present in similar levels as shown in Fig. 5C. If a single 5(*S*)-HETE enantiomer is detected, it might indicate leukocyte activity. It can be seen that in our platelet samples (both resting and thrombin–activated) 5-HETE is completely absent as expected (Fig. 5B2). It documents a good quality of our platelet isolates.

Table 4
Preliminary validation results for quantification of oxylipins in platelet releasates.

Compound	IS	LOD [pg on column]	LOQ [pg on column]	Range [fg/1e6 platelets]	R	Accuracy [%][a] QC low	Accuracy [%][a] QC high	Precision [%][b] QC low	Precision [%][b] QC high
9(*R*)-HODE	13(*S*)-HODE d4	2.5	6	20-1500	0.987	85.8	93.0	3.5	5.0
9(*S*)-HODE	13(*S*)-HODE d4	2.5	6	20-1500	0.982	110.9	90.5	12.6	2.0
13(*R*)-HODE	13(*S*)-HODE d4	2.5	6	20-1500	0.986	86.6	88.2	3.8	8.3
13(*S*)-HODE	13(*S*)-HODE d4	2.5	6	20-1500	0.987	87.6	91.5	3.8	14.5
5(*S*)-HETE	5(*S*)-HETE d8	0.5	5	20-1500	0.991	91.4	97.4	8.0	5.5
5(*R*)-HETE	5(*S*)-HETE d8	0.5	5	20-1500	0.992	87.1	98.3	11.2	1.7
8-HETE p1	12(*S*)-HETE d8	2.5	6	20-1500	0.996	86.1	96.2	3.3	2.6
8-HETE p2	12(*S*)-HETE d8	2.5	6	20-1500	0.997	85.1	93.9	6.1	3.9
9-HETE p1	12(*S*)-HETE d8	2.5	6	20-1500	0.998	91.4	93.5	11.6	7.5
9-HETE p2	12(*S*)-HETE d8	2.5	6	20-1500	0.986	88.0	99.1	5.2	4.6
11-HETE p1	12(*S*)-HETE d8	0.25	5	20-1500	0.991	86.6	90.0	4.8	2.0
11-HETE p2	12(*S*)-HETE d8	0.25	5	20-1500	0.995	87.4	91.9	3.9	1.1
12(*R*)-HETE	12(*S*)-HETE d8	2.5	6	20-1500	0.991	86.6	93.6	2.5	2.8
12(*S*)-HETE	12(*S*)-HETE d8	2.5	6	20-1500	0.993	88.9	93.8	2.1	5.4
15(*R*)-HETE	12(*S*)-HETE d8	2.5	6	20-1500	0.990	86.8	87.0	4.6	2.0
15(*S*)-HETE	12(*S*)-HETE d8	2.5	6	20-1500	0.993	92.8	89.1	9.0	6.7
5-HEPE p1	5(*S*)-HETE d8	2.5	6	20-1500	0.985	94.8	98.9	8.1	5.3
5-HEPE p2	5(*S*)-HETE d8	2.5	6	20-1500	0.984	86.0	91.9	2.1	7.8
8-HEPE p1	12(*S*)-HETE d8	2.5	6	20-1500	0.993	86.6	95.7	1.1	7.2
8-HEPE p2	12(*S*)-HETE d8	2.5	6	20-1500	0.987	86.4	90.7	7.0	1.8
12(*R*)-HEPE	12(*S*)-HETE d8	2.5	6	20-1500	0.992	85.8	91.3	3.6	2.4
12(*S*)-HEPE	12(*S*)-HETE d8	2.5	6	20-1500	0.991	88.6	91.3	5.0	4.6
15-HEPE p1	12(*S*)-HETE d8	2.5	6	20-1500	0.986	85.9	90.5	1.9	8.2
15-HEPE p2	12(*S*)-HETE d8	2.5	6	20-1500	0.989	86.5	90.9	4.3	4.2
18-HEPE p1	12(*S*)-HETE d8	5	25	90-1500	0.994	< LOQ	94.1	< LOQ	3.0
18-HEPE p2	12(*S*)-HETE d8	5	25	90-1500	0.996	< LOQ	85.6	< LOQ	3.3
10-HDoHE p1	12(*S*)-HETE d8	0.5	5	20-1500	0.983	85.0	94.6	4.7	3.6
10-HDoHE p2	12(*S*)-HETE d8	0.5	5	20-1500	0.992	88.3	91.5	7.2	4.1
17-HDoHE p1	12(*S*)-HETE d8	5	25	90-1500	0.989	< LOQ	87.7	< LOQ	8.6
17-HDoHE p2	12(*S*)-HETE d8	5	25	90-1500	0.969	< LOQ	94.9	< LOQ	11.4
RvD1	5(*S*)-HETE d8	5	25	90-1500	0.995	< LOQ	101.2	< LOQ	5.2
17(*R*)-RvD1	5(*S*)-HETE d8	5	25	90-1500	0.990	< LOQ	103.9	< LOQ	7.4
13(*R*)-HOTrE	13(*S*)-HODE d4	1	10	40-3000	0.999	N/A	N/A	N/A	N/A
13(*S*)-HOTrE	13(*S*)-HODE d4	1	10	40-3000	0.999	87.6	92.6	2.5	8.9
12(*R*)-HETrE	12(*S*)-HETE d8	1	10	40-3000	0.993	N/A	N/A	N/A	N/A
12(*S*)-HETrE	12(*S*)-HETE d8	1	10	40-3000	0.993	90.1	89.9	3.1	4.5
14(*R*)-HDoHE	12(*S*)-HETE d8	1	10	40-3000	0.987	N/A	N/A	N/A	N/A
14(*S*)-HDoHE	12(*S*)-HETE d8	1	10	40-3000	0.987	88.1	90.0	6.4	2.8
5,6-DiHETE p1	12(*S*)-HETE d8	10	50	200-1500	0.972	< LOQ	92.2	< LOQ	3.7
5,6-DiHETE p2	12(*S*)-HETE d8	10	50	200-1500	0.995	< LOQ	87.0	< LOQ	0.4

[a] Accuracy given as % recovery (n=3)
[b] precision given as % RSD (n=3)

3.7.3. 12-HETrE case

12-HETrE is the oxidation product of DGLA (Fig. 3, top right chromatogram). In a recent study on substrate specificity of human platelet-type 12-LOX, it has been shown that DGLA is comparable as substrate to AA and EPA [41]. However, as can be seen from Fig. 4, top row, the stereoselectivity pattern is different from that of AA (12-HETE as product) and EPA (12-HEPE as product). The product of DGLA formed by 12-LOX is 12(*S*)-hydroperoxy-8Z,10E,14Z-eicosatrienoic acid and its reduced form 12(*S*)-hydroxy-8Z,10E,14Z-eicosatrienoic acid (12(*S*)-HETrE). As can be seen in Fig. 6A1, 12(S)-HETrE could be detected in thrombin-activated platelet releasates (peak at 4.75 min, also detected in 12(*S*)-HETrE standard (peak at 4.73 min, Fig. 6A4) and in racemate from oxidized DGLA (peak at 4.73 min, Fig. 6A3)). The *R*-enantiomer 12(*R*)-HETrE is eluted at 4.32 min (Fig. 6A3). In the activated platelet sample, also a second peak was eluted before the *S*-enantiomer (peak at 4.44 min in Fig. 6A1). This peak could be misleadingly identified as 12(*R*)-HETrE, but the retention time did not match with the one of the racemate from oxidized DGLA (0.12 min difference is too much to be within the experimental error of this enantioselective UHPLC method). Hence, MeOH was also evaluated as modifier in the mobile phase with the Chiralpak IA-U column (Fig. 6B1-3) and the complementary enantioselective UHPLC column Chiralpak IC-U was tested as well by injection of the same samples (Fig. 6C1-3). Using the same elution conditions with AcN on the IC-U column, the racemate of 12-HETrE was not resolved; the two enantiomers eluted both at 3.92 min (Fig. 6C3). However, in the thrombin-activated platelet releasate sample, a second peak was observed, which eluted slightly earlier (peak at 3.56 min in Fig. 6C1). These results suggest that there is another compound formed which is structurally similar to 12(*R*)-HETrE. Indeed, it was reported earlier that besides platelet 12(*S*)-HETrE (with 8Z,10E,14Z double bond configurations) another HETrE, viz. 12(*R*)-hydroxy-5Z,8Z,14Z-eicosatrienoic acid exists [41]. In fact, this compound differs just by the position and configuration of double bonds (Fig. 7) and may therefore show similar retention time as 12(*R*)-hydroxy-8Z,10E,14Z-eicosatrienoic acid and the same SRM transitions (m/z 321.4→181.0). The slight shift in retention times on Chiralpak IA-U and IC-U columns could be explained by the different double bond positions and double bond configurations, respectively, and this shift therefore could be indicative for the other 12(*R*)-HETrEs (without conjugated double bonds). However, this compound has not been detected yet in platelets, but seems to be specific for epithelium cells [41]. To clarify this issue and inconsistency in structural assignment is of importance because the two 12(*R*)-HETrEs have not only different structure and different origin (DGLA and AA), but also elicit distinct biological actions. The 12-LOX metabolite of DGLA i.e. 12(*S*)-hydroxy-8Z,10E,14Z-eicosatrienoic acid has

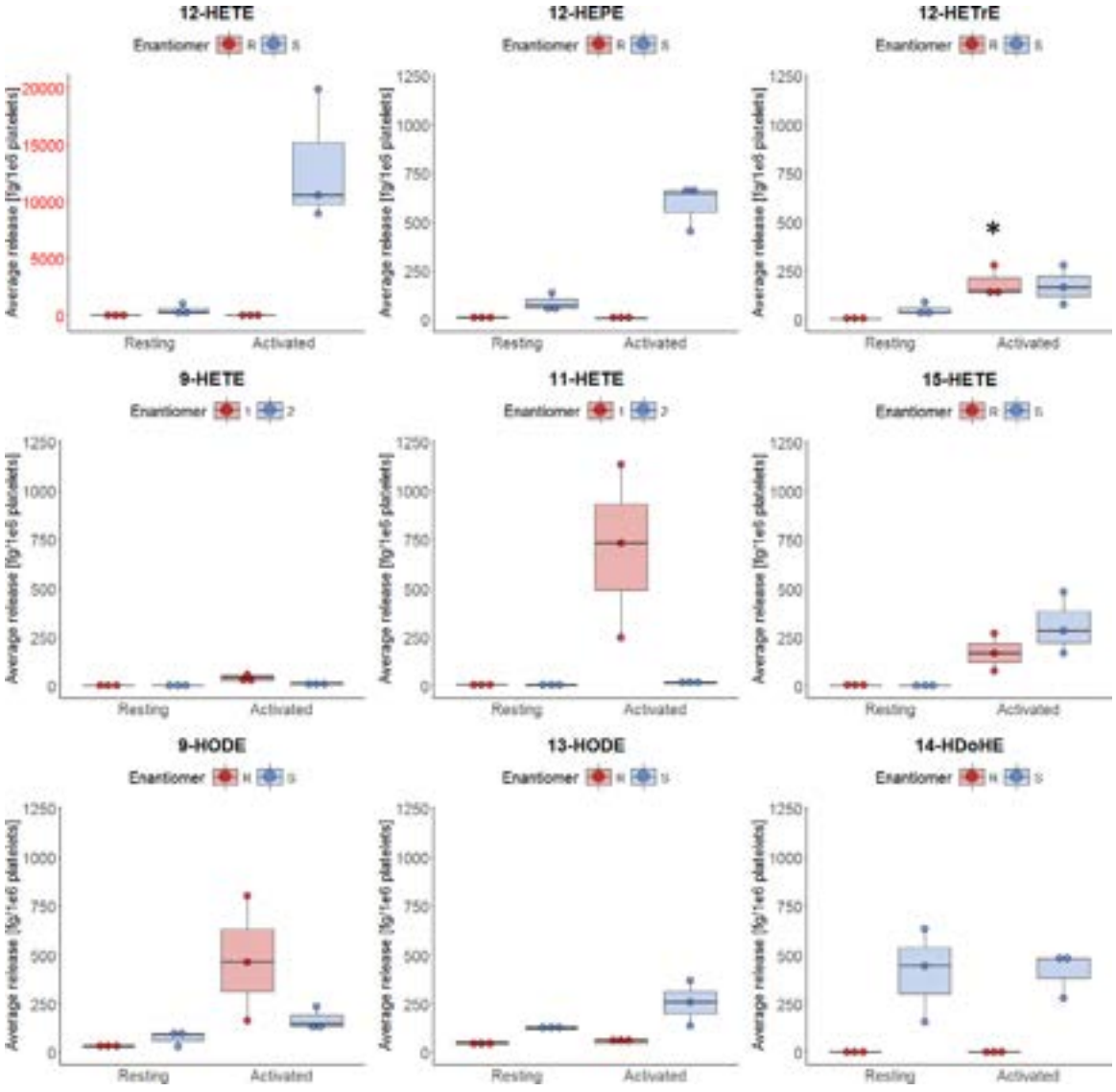

Figure 4. Box bots of the average release (n=3) of oxylipins [in fg] from 1 million platelets (estimated release for 12-HETE, whose concentration highly exceeded ULOQ). Red color shows levels of the first eluted peak and blue color represents the second eluted peak (*R* and *S* annotation is present if enantiomers are identified). The y-axis scale is unified for all the compounds except 12-HETE. The left part of the plots represents release for resting platelets and the right part from thrombin-activated platelets. 12(*R*)-HETrE detected in activated platelets (*) is most probably an isomer with different double bond composition.

been shown to inhibit platelet activation and thrombosis [42]. The AA metabolite 12(*R*)-hydroxy-5Z,8Z,14Z-eicosatrienoic acid demonstrated biological activities that are typical for inflammatory mediators including increased membrane permeability, vasodilation, chemotaxis and angiogenesis [43]. Unfortunately, this compound is currently not available commercially, for which reason a full identification could not be provided at present and our hypothesis could not be proven in this manuscript. We are currently working, however, on its clarification to provide experimental evidence via custom synthesized standard and more selective chromatography.

3.7.4. 8-, 9-, and 11-HETE

For all of these three PUFA metabolites, the first eluted peak (presumably *R*-configuration) dominated, while the second eluted peak (presumably *S*) was present at much lower concentration or essentially absent (see Suppl. Fig. S7). From this we could conclude that these oxidation products were not generated by autoxidation or ROS, but were products of enzymatic reactions. 8- and 9-HETE were detected only at very low concentrations. However, 11-HETE was detected in the platelet releasates in significant concentrations (see Fig. 4 and Suppl. Fig. S7C2). There is not much known about the 11-HETE stereochemistry in human platelets and their releasates. Our data indicate that 11(*R*)-HETE is formed upon platelet activation with thrombin. In a study with cultured bovine coronary artery endothelial cells it was reported previously that 11(*R*)-HETE is probably derived from cyclooxygenase [44]. This could explain the different stereochemistry with respect to 12-LOX but was not discussed hitherto for releasates from thrombin-activated platelets.

3.7.5. 15-HETE

The enantioselective analysis of 15-HETE in thrombin-activated releasates showed the presence of both enantiomers with a slight excess of the *S*-enantiomer (Suppl. Fig. S7D2). In the work cited above on bovine coronary artery endothelial cells 15(*S*)-HETE was found predominantly formed by 15-LOX [44]. Platelets reportedly do not express 15-LOX or 5-LOX but have 12-LOX. Although we did not observe any autoxidation in our platelet samples through-

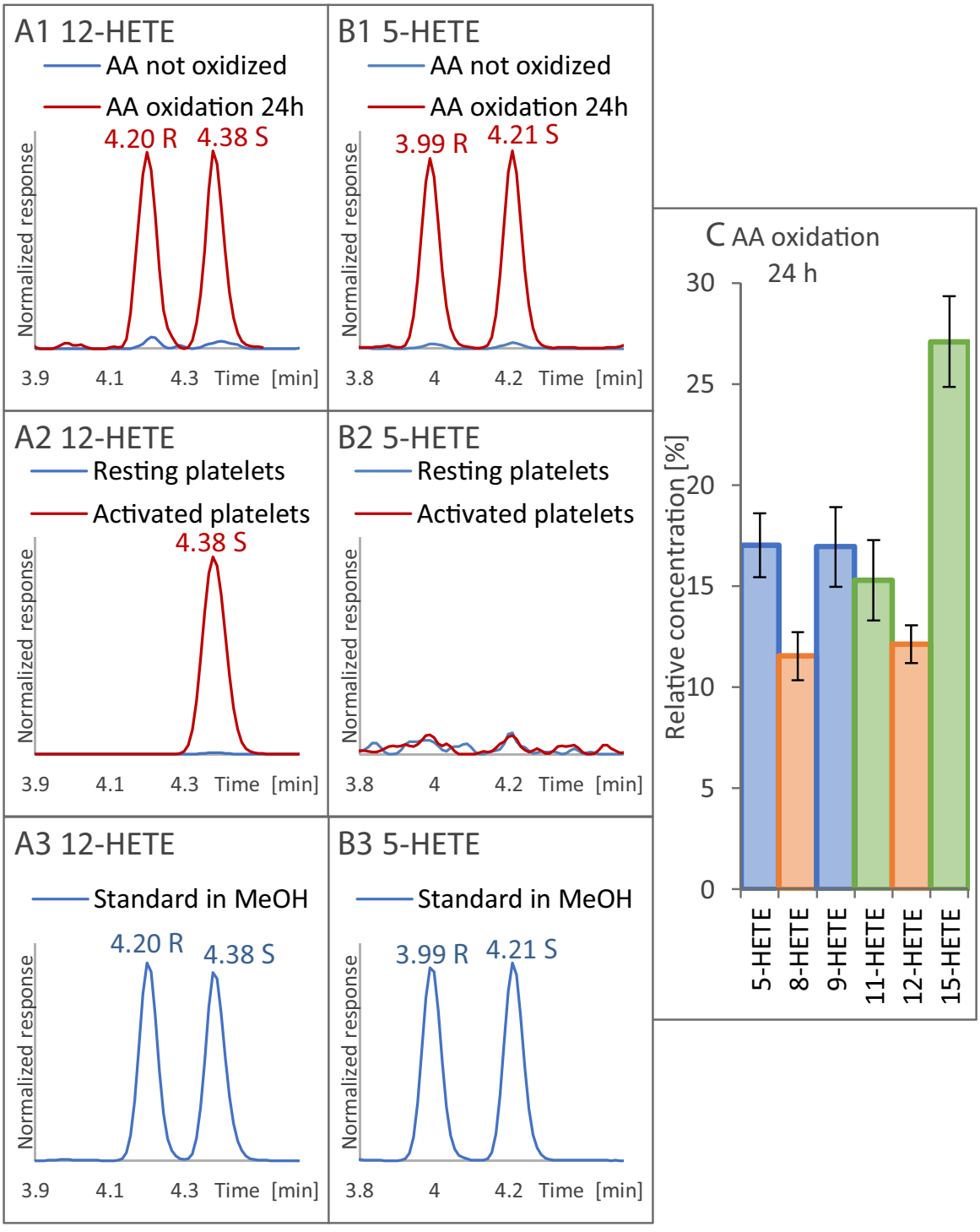

Figure 5. Comparison of oxylipins from different origins. EIC of 12-HETE in oxidized PUFA (**A1**), platelets (**A2**) and standard solution (**A3**); EIC of 5-HETE in oxidized PUFA (**B1**), platelets (**B2**) and standard solution (**B3**); and a boxplot showing distribution of HETEs obtained after 24 h of AA oxidations (**C**), the same colors indicate the same initial position of a free radical. Analyzed with the final method.

out this work, lipid peroxidation is detected in activated platelets [40] which could account for the presence of 15-HETE. However, in this case a racemic mixture was expected. Previous studies have also detected these 15-HETE enantiomers in whole blood in a similar enantiomeric ratio [38]. Thus, we hypothesize that the enantiomers of 15-HETE are formed through enzymatic contribution from either COX [45] or Cytochrome P450 [46] as reported previously. Further experimental studies are required to validate the exact source and mode of 15-HETE formation in platelets.

3.7.6. 9-HODE and 13-HODE

9- and 13-HODE are the oxidation products of LA. They show some peculiar stereochemistries. In releasates from thrombin-activated platelets, the *R*-enantiomer prevails for 9-HODE while the *S*-enantiomer is present in excess for 13-HODE. Little is

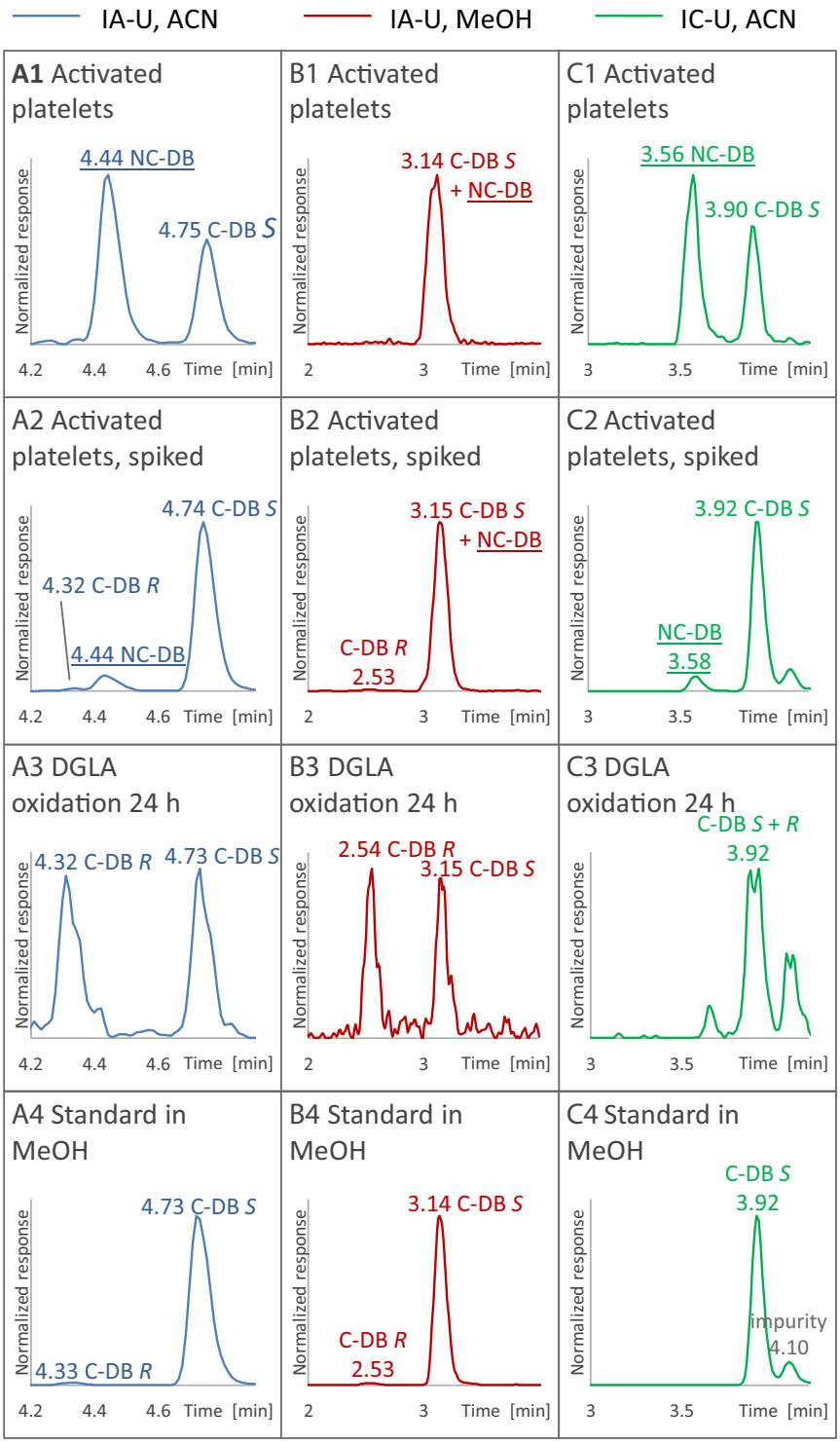

Figure 6. Separation of 12-HETrEs: with conjugated double bonds (C-DB *S* and C-DB *R*) and with non-conjugated double bonds (NC-DB) with different chromatographic conditions. **A1-4** and **B1-4**: separation with IA-U column; **C1-4**: separation with IC-U column. Mobile phase A: H_2O + 0.1% HAc (v/v), B: ACN + 0.1% HAc (v/v) for **A1-4** and **C1-4** or MeOH + 0.1% HAc (v/v) for **B1-4**. Gradient for ACN methods: 50-100% B in 5 min, 100% for 5 min, 50 % for 1.9 min. Gradient for MeOH methods: 90-100% B in 5 min, 100% for 5 min, 90 % for 1.9 min. Column temperature: 40°C, flow rate: 0.3 mL/min, injection volume: 10 µL. Concentration of 12-HETrE in the oxidized DGLA (**A3, B3** and **C3**) was very low, that is why the chromatograms showed poor quality.

known about the stereochemical preference of 9- and 13-HODE in platelets and their releasates. However, a few studies have investigated the stereochemical preference of LA biotransformation by 12-LOX. In a recent work, linoleic acid metabolism by intestinal tissues of Min mice, an animal model for intestinal neoplasia, showed that LA was converted to an equal mixture of 9(*S*) and 13(*S*)-HODE [47]. In another study, positional isomer selectivity and stereoselectivity of HODE oxidation by mouse 12(*S*)-lipoxygenase isoenzymes was investigated [48]. For 13-HODE mainly *S*-enantiomers were formed. For 9-HODE platelet- and epidermis-type isoenzymes generated the *R*-enantiomer while leukocyte-type 12(*S*)-lipoxygenase yielded the *S*-enantiomer. Our findings (Fig. 8) agree

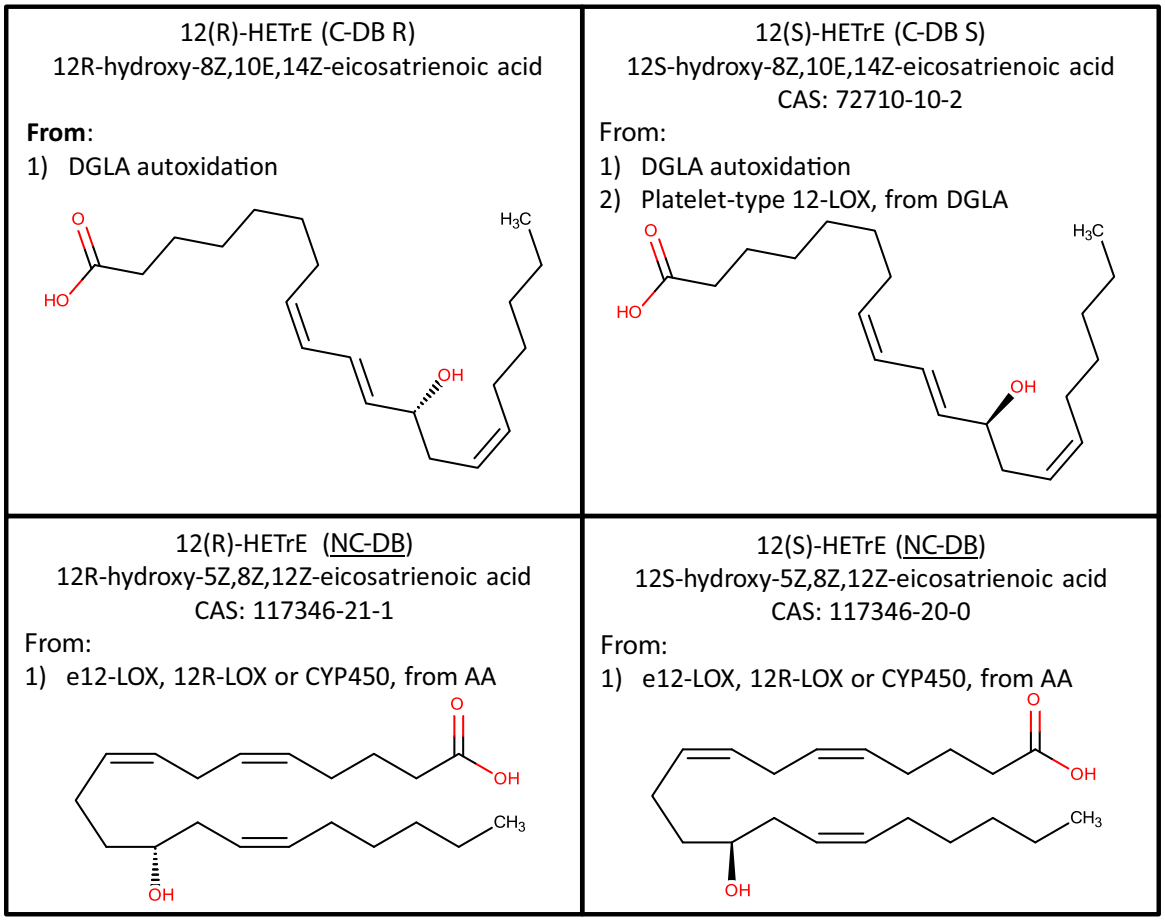

Figure 7. Structures of 12-HETrEs and their origins. The coding next to names (e.g. **C-DB *R***) is related to the peak naming in Fig. 6.

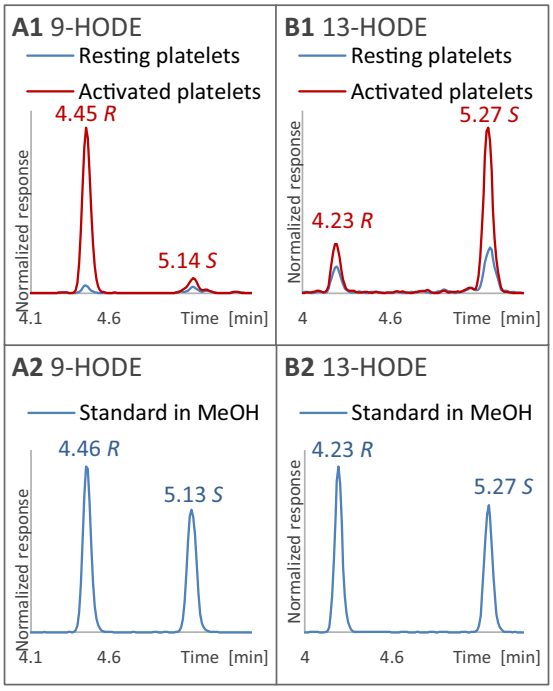

Figure 8. Stereoselectivity of 9- and 13-HODE formed upon platelet activation by thrombin as analyzed in releasates and compared to resting platelets (**A1** and **B1**); and separation of 9- and 13-HODE enantiomers in racemic standard solution (**A2** and **B2**). Analyzed with the final method.

well with the results of the platelet type isoenzymes of this study.

3.7.7. 14-HDoHE

10-, 14-, and 17-HDoHE are metabolites of DHA oxidation and were included in our stereoselective assay. 17-HDOHE was not detected at all and 10-HDoHE was detected below LOQ in activated platelet supernatants. However, 14-HDoHE was present in significant amounts in platelet supernatants and only the *S*-enantiomer was found (Suppl. Fig. S7E2). Interestingly, the levels in releasates from non-activated resting platelets were essentially the same as in thrombin-activated platelets. Yet, it must be emphasized that this fact cannot be attributed to autoxidation because of the finding that only the *S*-enantomer was present indicative of an enzymatic process. If autoxidation was the reason for 14-HDoHE, also other HDoHE isomers would have been formed and the racemic mixture would have been obtained for all of them.

4. Conclusions

Enantioselective UHPLC-ESI-MS/MS based on sub-2µm particle-based polysaccharide CSPs using reversed-phase elution conditions was used for the first time to develop a highly selective and sensitive assay for analyzing enantiomers and diastereoisomers of different types of oxylipins in platelet samples and autoxidized PUFAs. Autoxidation of PUFAs yielded racemic mixtures, as expected and provided reference samples of both enantiomers and regioisomers for method development. For several analytes the enantiomer elution order could be determined and seems to be

preferentially *R*- before *S*-enantiomer on Chiralpak IA-U. The new method was finally utilized for enantioselective analysis of releasates from resting and thrombin-activated human platelets. In the majority of the cases, single enantiomers of oxylipins were produced in thrombin-activated platelet samples by enzymatic oxidation, e.g. 12(*S*)-configuration in case of 12-LOX products (12(*S*)-HETE and 12-(*S*)-HEPE). Other oxylipins had *R*-configurations such as 11(*R*)-HETE. In several cases, both enantiomers were present, although not as racemic (50:50) mixtures. In any case, for a meaningful biological interpretation of oxylipin formation, enantioselective assays are indispensable and currently employed Chiralpak IA-U column has the performance to set the state-of-art in this field.

CRediT authorship contribution statement

Malgorzata Cebo: Investigation, Methodology, Formal analysis, Data curation, Visualization, Writing - original draft, Writing - review & editing. **Xiaoqing Fu:** Investigation, Data curation, Writing - review & editing. **Meinrad Gawaz:** Writing - review & editing, Funding acquisition. **Madhumita Chatterjee:** Investigation, Writing - review & editing, Funding acquisition. **Michael Lämmerhofer:** Conceptualization, Methodology, Supervision, Writing - review & editing, Resources, Funding acquisition.

Declaration of conflict of interests

The authors declare no conflict of interests.

Acknowledgements

This project was funded by the Deutsche Forschungsgemeinschaft (DFG, German Research Foundation) – Project number 374031971 – TRR 240. We would like to acknowledge support by the master students of the Univeristy of Tuebingen, Master in Pharmaceutical Sciences & Technologies, Florian Stahl, Jiayue Xu and Anita Bär.

Supplementary materials

Supplementary material associated with this article can be found, in the online version, at doi:10.1016/j.chroma.2020.461206.

References

[1] C.N. Serhan, P.A. Ward, D.W. Gilroy, Fundamentals of Inflammation, Cambridge University Press, 2010 https://doi.org/10.1017/CBO9781139195737.
[2] K. Broos, S.F. De Meyer, H.B. Feys, K. Vanhoorelbeke, H. Deckmyn, Blood platelet biochemistry, Thromb. Res. 129 (2012) 245–249 https://doi.org/10.1016/j.thromres.2011.11.002.
[3] M. Cebo, J. Schlotterbeck, M. Gawaz, M. Chatterjee, M. Lämmerhofer, Simultaneous targeted and untargeted UHPLC-ESI-MS/MS method with data-independent acquisition for quantification and profiling of (oxidized) fatty acids released upon platelet activation by thrombin, Anal. Chim. Acta. 1094 (2020) 57–69 https://doi.org/10.1016/j.aca.2019.10.005.
[4] J. Schlotterbeck, M. Chatterjee, M. Gawaz, M. Lämmerhofer, Comprehensive MS/MS profiling by UHPLC-ESI-QTOF-MS/MS using SWATH data-independent acquisition for the study of platelet lipidomes in coronary artery disease, Anal. Chim. Acta. 1046 (2019) 1–15 https://doi.org/10.1016/j.aca.2018.08.060.
[5] B.E. Tourdot, I. Ahmed, M. Holinstat, The emerging role of oxylipins in thrombosis and diabetes, Front. Pharmacol. 4 JAN (2014) 1–9 https://doi.org/10.3389/fphar.2013.00176.
[6] M. Chatterjee, D. Rath, J. Schlotterbeck, J. Rheinlaender, B. Walker-Allgaier, N. Alnaggar, M. Zdanyte, I. Müller, O. Borst, T. Geisler, T.E. Schäffer, M. Lämmerhofer, M. Gawaz, Regulation of oxidized platelet lipidome: Implications for coronary artery disease, Eur. Heart J. 38 (2017) 1993–2005 https://doi.org/10.1093/eurheartj/ehx146.
[7] J. Yeung, M. Hawley, M. Holinstat, The expansive role of oxylipins on platelet biology, J Mol Med (Berl) 95 (2017) 575–588 https://doi.org/10.1007/s00109-017-1542-4.The.
[8] J.D. Morrow, T.M. Harris, L. Jackson Roberts, Noncyclooxygenase oxidative formation of a series of novel prostaglandins: Analytical ramifications for measurement of eicosanoids, Anal. Biochem. 184 (1990) 1–10 https://doi.org/10.1016/0003-2697(90)90002-Q.
[9] P. Montuschi, P.J. Barnes, L.J. Roberts, Isoprostanes: Markers and mediators of oxidative stress, FASEB J 18 (2004) 1791–1800 https://doi.org/10.1096/fj.04-2330rev.
[10] L. Kortz, J. Dorow, U. Ceglarek, Liquid chromatography-tandem mass spectrometry for the analysis of eicosanoids and related lipids in human biological matrices: A review, J. Chromatogr. B Anal. Technol. Biomed. Life Sci. 964 (2014) 1–11 https://doi.org/10.1016/j.jchromb.2014.01.046.
[11] A.M. Wolfer, M. Gaudin, S.D. Taylor-robinson, E. Holmes, J.K. Nicholson, Development and Validation of a High-Throughput Ultrahigh- Performance Liquid Chromatography – Mass Spectrometry Approach for Screening of Oxylipins and Their Precursors, (2015). https://doi.org/10.1021/acs.analchem.5b02794.
[12] G. Astarita, A.C. Kendall, E.A. Dennis, A. Nicolaou, Targeted lipidomics strategies for oxygenated metabolites of polyunsaturated fatty acids, Biochim Biophys Acta 1851 (2015) 456–468 https://doi.org/10.1016/j.bbalip.2014.11.012.
[13] K.M. Rund, A.I. Ostermann, L. Kutzner, J.M. Galano, C. Oger, C. Vigor, S. Wecklein, N. Seiwert, T. Durand, N.H. Schebb, Development of an LC-ESI(-)-MS/MS method for the simultaneous quantification of 35 isoprostanes and isofurans derived from the major n3- and n6-PUFAs, Anal. Chim. Acta. 1037 (2018) 63–74 https://doi.org/10.1016/j.aca.2017.11.002.
[14] B. Peng, S. Geue, C. Coman, M. Patrick, D. Kopczynski, C. Has, N. Hoffmann, M.C. Manke, F. Lang, A. Sickmann, M. Gawaz, O. Borst, R. Ahrends, P. Münzer, D. Kopczynski, C. Has, N. Hoffmann, M.C. Manke, F. Lang, A. Sickmann, M. Gawaz, O. Borst, R. Ahrends, Identification of key lipids critical for platelet activation by comprehensive analysis of the platelet lipidome, Blood 132 (2018) e1–e12 https://doi.org/10.1182/blood-2017-12-822890.
[15] R. Berkecz, M. Lísa, M. Holčapek, Analysis of oxylipins in human plasma: Comparison of ultrahigh-performance liquid chromatography and ultrahigh-performance supercritical fluid chromatography coupled to mass spectrometry, J. Chromatogr. A. 1511 (2017) 107–121 https://doi.org/10.1016/j.chroma.2017.06.070.
[16] F. Ianni, G. Saluti, R. Galarini, S. Fiorito, R. Sardella, B. Natalini, Enantioselective high-performance liquid chromatography analysis of oxygenated polyunsaturated fatty acids, Free Radic. Biol. Med. 144 (2019) 35–54 https://doi.org/10.1016/j.freeradbiomed.2019.04.038.
[17] M. Lämmerhofer, Chiral recognition by enantioselective liquid chromatography: Mechanisms and modern chiral stationary phases, J. Chromatogr. A. 1217 (2010) 814–856 https://doi.org/10.1016/j.chroma.2009.10.022.
[18] F. Ianni, Z. Pataj, H. Gross, R. Sardella, B. Natalini, W. Lindner, M. Lämmerhofer, Direct enantioseparation of underivatized aliphatic 3-hydroxyalkanoic acids with a quinine-based zwitterionic chiral stationary phase, J. Chromatogr. A. 1363 (2014) 101–108 https://doi.org/10.1016/j.chroma.2014.03.060.
[19] C. Calderón, C. Santi, M. Lämmerhofer, Chiral separation of disease biomarkers with 2-hydroxycarboxylic acid structure, J. Sep. Sci. 41 (2018) 1224–1231 https://doi.org/10.1002/jssc.201701243.
[20] C. Calderón, M. Lämmerhofer, Chiral separation of short chain aliphatic hydroxycarboxylic acids on cinchonan carbamate-based weak chiral anion exchangers and zwitterionic chiral ion exchangers, J. Chromatogr. A. 1487 (2017) 194–200 https://doi.org/10.1016/j.chroma.2017.01.060.
[21] D. Norton, B. Crow, M. Bishop, K. Kovalcik, J. George, J.A. Bralley, High performance liquid chromatography-tandem mass spectrometry (HPLC/MS/MS) assay for chiral separation of lactic acid enantiomers in urine using a teicoplanin based stationary phase, J. Chromatogr. B Anal. Technol. Biomed. Life Sci. 850 (2007) 190–198 https://doi.org/10.1016/j.jchromb.2006.11.020.
[22] T. Ikai, Y. Okamoto, Structure control of polysaccharide derivatives for efficient separation of enantiomers by chromatography, Chem. Rev. 109 (2009) 6077–6101 https://doi.org/10.1021/cr8005558.
[23] B. Chankvetadze, Recent developments on polysaccharide-based chiral stationary phases for liquid-phase separation of enantiomers, J. Chromatogr. A. 1269 (2012) 26–51 https://doi.org/10.1016/j.chroma.2012.10.033.
[24] U. Garscha, T. Nilsson, E.H. Oliw, Enantiomeric separation and analysis of unsaturated hydroperoxy fatty acids by chiral column chromatography-mass spectrometry, J. Chromatogr. B Anal. Technol. Biomed. Life Sci. 872 (2008) 90–98 https://doi.org/10.1016/j.jchromb.2008.07.013.
[25] M. Blum, I. Dogan, M. Karber, M. Rothe, W.H. Schunck, Chiral lipidomics of monoepoxy and monohydroxy metabolites derived from long-chain polyunsaturated fatty acids, J. Lipid Res. 60 (2019) 135–148 https://doi.org/10.1194/jlr.M089755.
[26] M. Bayer, A. Mosandl, D. Thaçi, Improved enantioselective analysis of polyunsaturated hydroxy fatty acids in psoriatic skin scales using high-performance liquid chromatography, J. Chromatogr. B Anal. Technol. Biomed. Life Sci. 819 (2005) 323–328 https://doi.org/10.1016/j.jchromb.2005.02.008.
[27] C. Schneider, Z. Yu, W.E. Boeglin, Y. Zheng, A.R. Brash, Enantiomeric Separation of Hydroxy and Hydroperoxy Eicosanoids by Chiral Column Chromatography, Enantiomeric Sep. Hydroxyand Hydroperoxy Eicosanoids by Chiral Column Chromatography, Methods in Enzymology 433 (2007) 145–157 https://doi.org/10.1016/S0076-6879(07)33008-5.
[28] H.L. Seon, M.V. Williams, I.A. Blair, Targeted chiral lipidomics analysis, Prostaglandins Other Lipid Mediat 77 (2005) 141–157 https://doi.org/10.1016/j.prostaglandins.2004.01.009.
[29] C. Mesaros, S.H. Lee, I.A. Blair, Targeted quantitative analysis of eicosanoid lipids in biological samples using liquid chromatography-tandem mass spectrometry, J. Chromatogr. B Anal. Technol. Biomed. Life Sci. 877 (2009) 2736–2745 https://doi.org/10.1016/j.jchromb.2009.03.011.
[30] R. Sardella, F. Ianni, A. Lisanti, M. Marinozzi, S. Scorzoni, B. Natalini, The effect of mobile phase composition in the enantioseparation of pharmaceutically rel-

evant compounds with polysaccharide-based stationary phases, Biomed. Chromatogr. 28 (2014) 159–167 https://doi.org/10.1002/bmc.3015.
[31] T. Zhang, P. Franco, Analytical and Preparative Potential of Immobilized Polysaccharide-Derived Chiral Stationary Phases, 2007. https://doi.org/10.1002/9783527611737.ch3.
[32] A.R. Brash, W.E. Boeglin, J.H. Capdevila, S. Yeola, I.A. Blair, 7-HETE, 10-HETE, and 13-HETE are major products of NADPH-dependent arachidonic acid metabolism in rat liver microsomes: Analysis of their stereochemistry, and the stereochemistry of their acid-catalyzed rearrangement, Arch. Biochem. Biophys. 321 (1995) 485–492 https://doi.org/10.1006/abbi.1995.1421.
[33] K.V. Penmetsa, C.D. Reddick, S.W. Fink, B.L. Kleintop, G.C. Didonato, K.J. Volk, S.E. Klohr, Development of reversed-phase chiral HPLC methods using mass spectrometry compatible mobile phases, J. Liq. Chromatogr. Relat. Technol. 23 (2000) 831–839 https://doi.org/10.1081/JLC-100101492.
[34] W. Schafer, T. Chandrasekaran, Z. Pirzada, C. Zhang, X. Gong, M. Biba, E.L. Regalado, C.J. Welch, Improved Chiral SFC Screening for Analytical Method Development, Chirality 25 (2013) 799–804 https://doi.org/10.1002/chir.22218.
[35] F.T. Mattrey, A.A. Makarov, E.L. Regalado, F. Bernardoni, M. Figus, M.B. Hicks, J. Zheng, L. Wang, W. Schafer, V. Antonucci, S.E. Hamilton, K. Zawatzky, C.J. Welch, Current challenges and future prospects in chromatographic method development for pharmaceutical research, TrAC - Trends Anal. Chem. 95 (2017) 36–46 https://doi.org/10.1016/j.trac.2017.07.021.
[36] F. Sekiya, J. Takagi, T. Usui, K. Kawajiri, Y. Kobayashi, F. Sato, Y. Saito, 12S-hydroxyeicosatetraenoic acid plays a central role in the regulation of platelet activation, Biochem. Biophys. Res. Commun. 179 (1991) 345–351 https://doi.org/10.1016/0006-291X(91)91376-N.
[37] D.A. Slatter, P.W. Collins, V.B.O. Donnell, D.A. Slatter, C.L. Percy, K. Allenredpath, J.M. Gajsiewicz, N.J. Brooks, A. Clayton, V.J. Tyrrell, M. Rosas, S.N. Lauder, A. Watson, M. Dul, Y. Garcia-diaz, M. Aldrovandi, M. Heurich, J. Hall, P.W. Collins, V.B.O. Donnell, Enzymatically oxidized phospholipids restore thrombin generation in coagulation factor deficiencies, JCI Insight 3 (6) (2018) e98459 https://doi.org/10.1172/jci.insight.98459.
[38] L. Kutzner, K.M. Rund, A.I. Ostermann, N.M. Hartung, J. Galano, L. Balas, T. Durand, M.S. Balzer, S. David, N.H. Schebb, Development of an Optimized LC-MS Method for the Detection of Specialized Pro-Resolving Mediators in Biological Samples, Front. Pharmacol. 10 (2019) https://doi.org/10.3389/fphar.2019.00169.
[39] J. Homann, C. Lehmann, A.S. Kahnt, D. Steinhilber, M.J. Parnham, G. Geisslinger, N. Ferreirós, Chiral chromatography-tandem mass spectrometry applied to the determination of pro-resolving lipid mediators, J. Chromatogr. A. 1360 (2014) 150–163 https://doi.org/10.1016/j.chroma.2014.07.068.
[40] M. Chatterjee, Platelet lipidome: Dismantling the “Trojan horse” in the bloodstream, J. Thromb. Haemost. (2020) jth.14721 https://doi.org/10.1111/jth.14721.
[41] J. Yeung, M. Holinstat, Who is the real 12-HETrE? Prostaglandins Other Lipid Mediat 132 (2017) 25–30 https://doi.org/10.1016/j.prostaglandins.2017.02.005.
[42] J. Yeung, B.E. Tourdot, R. Adili, A.R. Green, C.J. Freedman, P. Fernandez-Perez, J. Yu, T.R. Holman, M. Holinstat, 12(S)-HETrE, a 12-lipoxygenase oxylipin of dihomo-γ-linolenic acid, inhibits thrombosis via $G\alpha s$ signaling in platelets, Arterioscler. Thromb. Vasc. Biol. 36 (2016) 2068–2077 https://doi.org/10.1161/ATVBAHA.116.308050.
[43] M. Laniado-Schwartzman, M.W. Dunn, Cytochrome P450-Derived Eicosanoids are Mediators of Ocular Surface Inflammation, in: Adv. Prostaglandin, Leukot. Other Bioact. Lipid Res., 2003, pp. 47–54. https://doi.org/10.1007/978-1-4419-9194-2_10.
[44] M. Rosolowsky, W.B. Campbell, Synthesis of hydroxyeicosatetraenoic (HETEs) and epoxyeicosatrienoic acids (EETs) by cultured bovine coronary artery endothelial cells, Biochim. Biophys. Acta - Lipids Lipid Metab. 1299 (1996) 267–277 https://doi.org/10.1016/0005-2760(95)00216-2.
[45] C. Schneider, A.R. Brash, Lipoxygenase-catalyzed formation of R-configuration hydroperoxides, Prostaglandins Other Lipid Mediat 68–69 (2002) 291–301 https://doi.org/10.1016/S0090-6980(02)00041-2.
[46] J. Capdevila, P. Yadagiri, S. Manna, J.R. Falck, Absolute configuration of the hydroxyeicosatetraenoic acids (HETEs) formed during catalytic oxygenation of arachidonic acid by microsomal cytochrome P-450, Biochem. Biophys. Res. Commun. 141 (1986) 1007–1011 https://doi.org/10.1016/S0006-291X(86)80144-9.
[47] H. Kawajiri, L.C. Hsi, H. Kamitani, H. Ikawa, M. Geller, T. Ward, T.E. Eling, W.C. Glasgow, Arachidonic and linoleic acid metabolism in mouse intestinal tissue: Evidence for novel lipoxygenase activity, Arch. Biochem. Biophys. 398 (2002) 51–60 https://doi.org/10.1006/abbi.2001.2685.
[48] F. BÜRGER, P. KRIEG, F. MARKS, G. FÜRSTENBERGER, Positional- and stereo-selectivity of fatty acid oxygenation catalysed by mouse (12S)-lipoxygenase isoenzymes, Biochem. J. 348 (2000) 329–335 https://doi.org/10.1042/bj3480329.

Supplementary information

Enantioselective UHPLC-MS/MS method based on sub-2µm particle polysaccharide column for chiral separation of oxylipins and its application for the analysis of autoxidized fatty acids and platelet releasates

Malgorzata Cebo[a], Xiaoqing Fu[a], Meinrad Gawaz[b], Madhumita Chatterjee[b],Michael Lämmerhofer[a]*

[a] University of Tübingen, Institute of Pharmaceutical Sciences, Pharmaceutical (Bio-)Analysis, Auf der Morgenstelle 8, 72076 Tübingen, Germany

[b] Department of Cardiology and Angiology, University Hospital Tübingen, Otfried-Müller-Strasse 10, 72076 Tübingen, Germany

***Author for correspondence:**

Prof. Michael Lämmerhofer
Pharmaceutical (Bio-)Analysis
Institute of Pharmaceutical Sciences
University of Tuebingen
Auf der Morgenstelle 8
72076 Tuebingen, Germany
T +49 7071 29 78793, F +49 7071 29 4565
e-mail: michael.laemmerhofer@uni-tuebingen.de
http://www.bioanalysis.uni-tuebingen.de/

1. Structures and names of standards and internal standards used in this study

1.1 Compounds in Mix A and Mix B

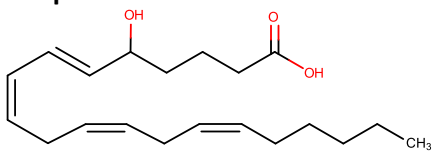

(±)5-HETE
5-hydroxy-6E,8Z,11Z,14Z-eicosatetraenoic acid

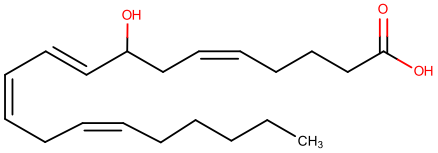

(±)8-HETE
8-hydroxy-5Z,9E,11Z,14Z-eicosatetraenoic acid

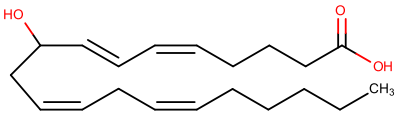

(±)9-HETE
9-hydroxy-5Z,7E,11Z,14Z-eicosatetraenoic acid

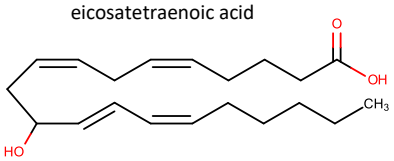

(±)11-HETE
11-hydroxy-5Z,8Z,12E,14Z-eicosatetraenoic acid

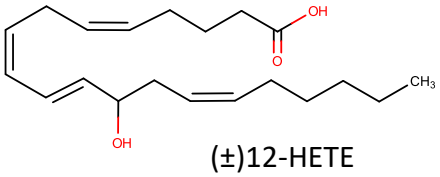

(±)12-HETE
12-hydroxy-5Z,8Z,10E,14Z-eicosatetraenoic acid

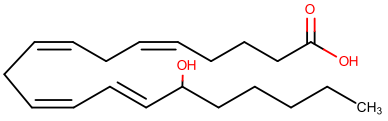

(±)15-HETE
15-hydroxy-5Z,8Z,11Z,13E-eicosatetraenoic acid

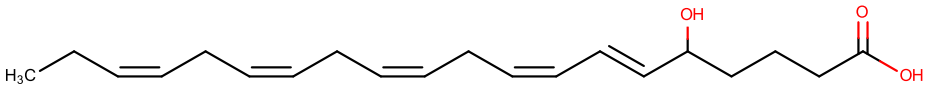

(±)5-HEPE
5-hydroxy-6E,8Z,11Z,14Z,17Z-eicosapentaenoic acid

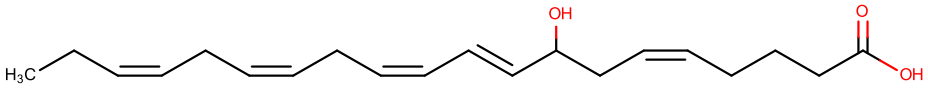

(±)8-HEPE
8-hydroxy-5Z,9E,11Z,14Z,17Z-eicosapentaenoic acid

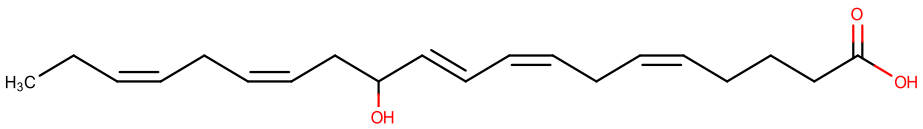

(±)12-HEPE
12-hydroxy-5Z,8Z,10E,14Z,17Z-eicosapentaenoic acid

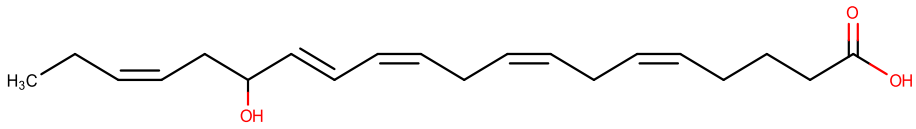

(±)15-HEPE
15-hydroxy-5Z,8Z,11Z,13E,17Z-eicosapentaenoic acid

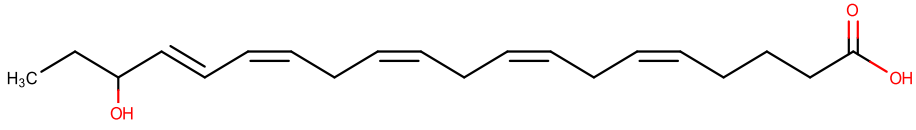

(±)18-HEPE
18-hydroxy-5Z,8Z,11Z,14Z,16E-eicosapentaenoic acid

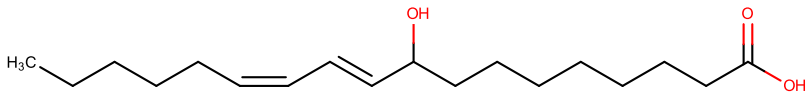

(±) 9-HODE
9-hydroxy-10E,12Z-octadecadienoic acid

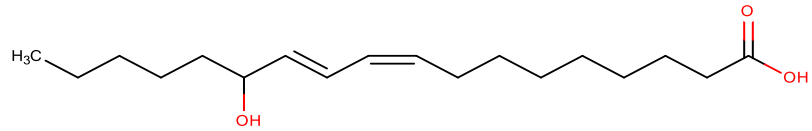

(±) 13-HODE
13-hydroxy-9Z,11E-octadecadienoic acid

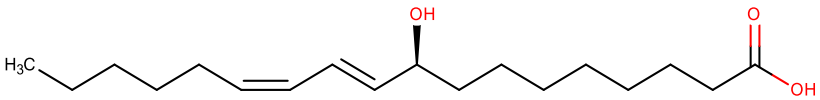

9(S)-HODE
9-hydroxy-10E,12Z-octadecadienoic acid

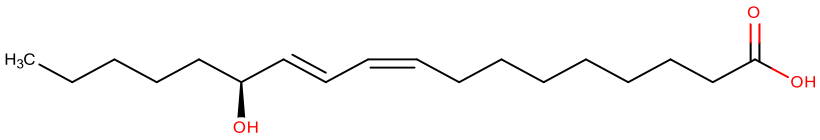

13(S)-HODE
13-hydroxy-9Z,11E-octadecadienoic acid

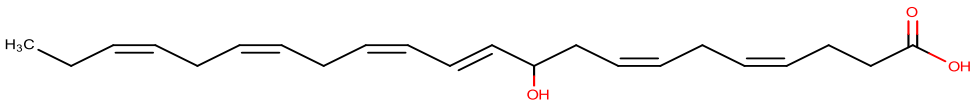

(±)10-HDoHE
10-hydroxy-4Z,7Z,11E,13Z,16Z,19Z-docosahexaenoic acid

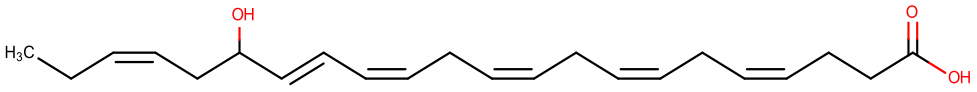

(±)17-HDoHE
17-hydroxy-4Z,7Z,10Z,13Z,15E,19Z-docosahexaenoic acid

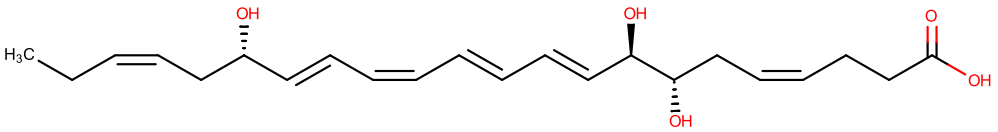

RvD1
Resolvin D1
7S,8R,17S-trihydroxy-4Z,9E,11E,13Z,15E,19Z-docosahexaenoic acid

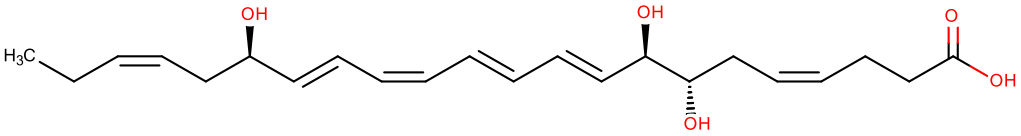

17(R)-RvD1
17(R)-Resolvin D1
7S,8R,17R-trihydroxy-4Z,9E,11E,13Z,15E,19Z-docosahexaenoic acid

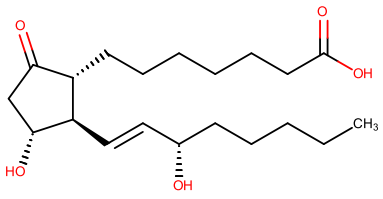

PGE1
Prostaglandin E1
9-oxo-11R,15S-dihydroxy-13E-prostaenoic acid

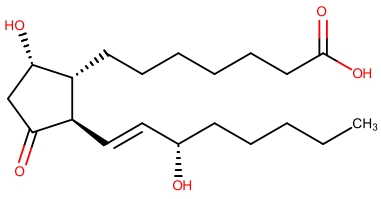

PGD1
Prostaglandin D1
9S,15S-dihydroxy-11-oxo-13E-prostaenoic acid

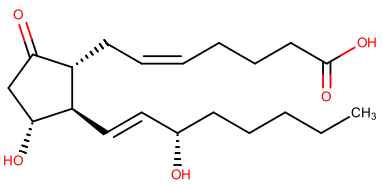

PGE2
Prostaglandin E2
9-oxo-11R,15S-dihydroxy-5Z,13E-prostadienoic acid

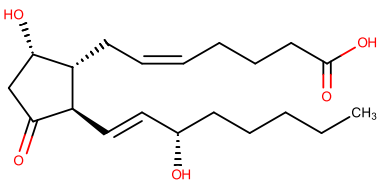

PGD2
Prostaglandin D2
9S,15S-dihydroxy-11-oxo-5Z,13E-prostadienoic acid

1.2 PUFAs used for auto-oxidation

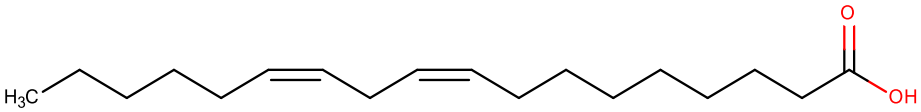

Linoleic acid (LA)
9Z,12Z-octadecadienoic acid

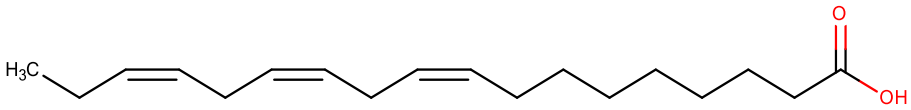

α-Linolenic acid (ALA)
9Z,12Z,15Z-octadecatrienoic acid

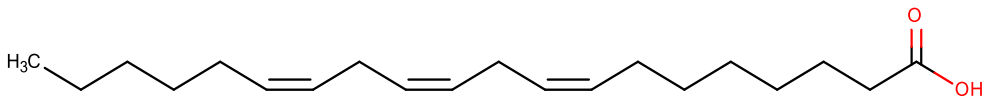

Dihomo-γ-linolenic acid (DGLA)
8Z,11Z,14Z-eicosatrienoic acid

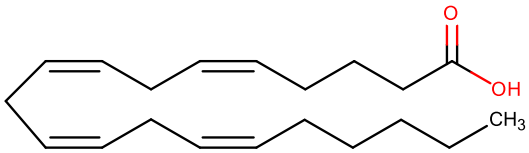

Arachidonic acid (AA)
5Z,8Z,11Z,14Z-eicosatetraenoic acid

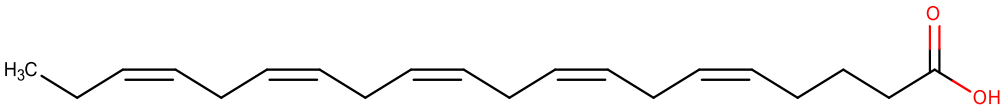

5Z,8Z,11Z,14Z,17Z-eicosapentaenoic acid (EPA)

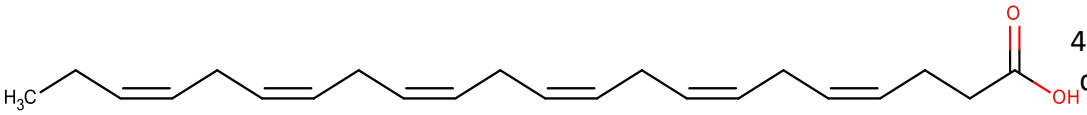

4Z,7Z,10Z,13Z,16Z,19Z-docosahexaenoic acid (DHA)

1.3 Additional oxylipins in the extended set

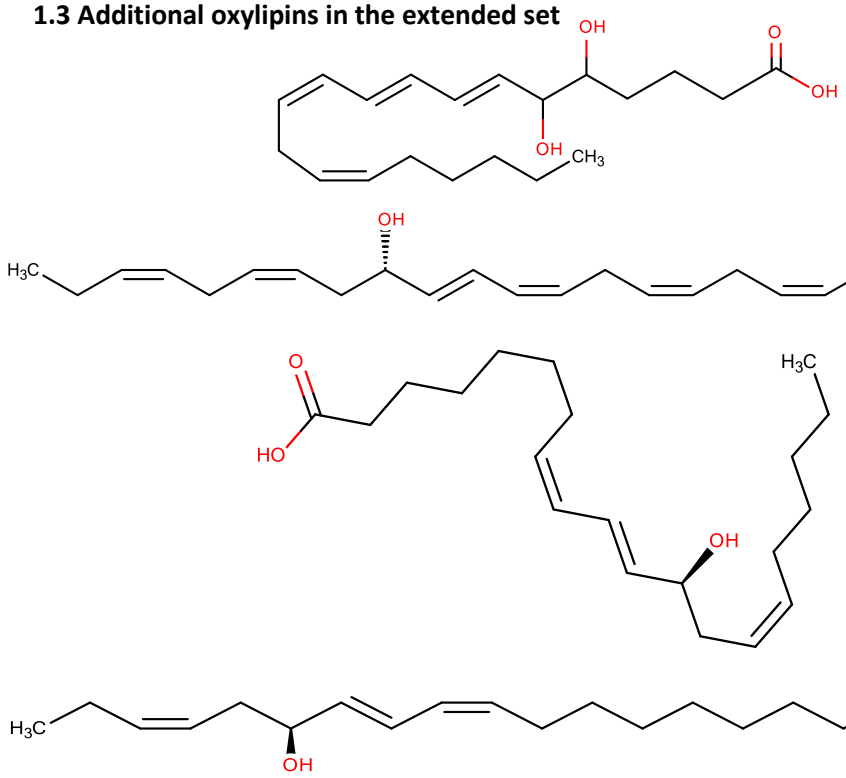

(±)5,6-DiHETE
cis-5,6-dihydroxy-7E,9E,11Z,14Z-eicosatetraenoic acid

14(S)-HDoHE
14-hydroxy-4Z,7Z,10Z,12E,16Z,19Z-docosahexaenoic acid

12(S)-HETrE
12-hydroxy-5Z,8Z,12Z-eicosatrienoic acid

13(S)-HOTrE
13-hydroxy-9Z,11E,15Z-octadecatrienoic acid

1.4 IS used in platelet releasate analysis

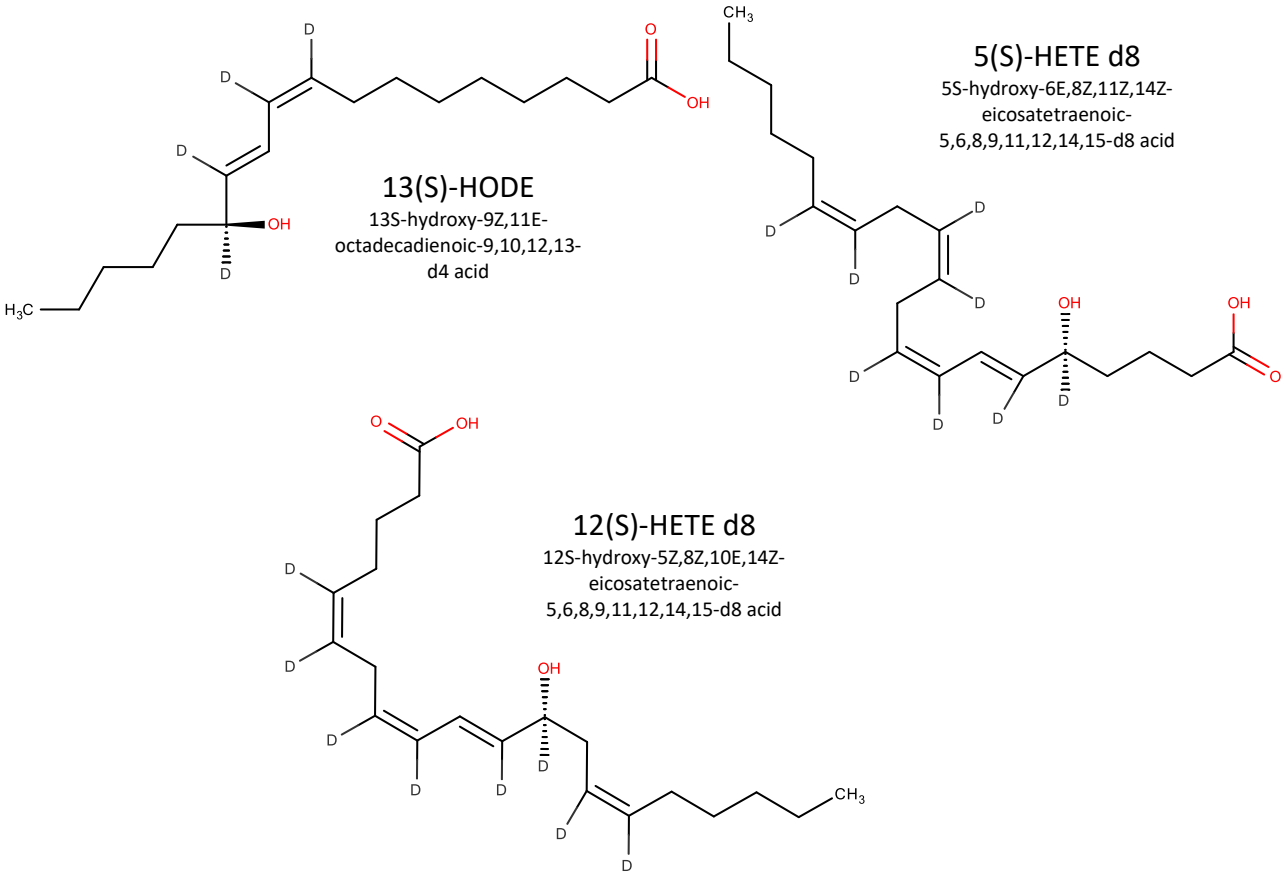

13(S)-HODE
13S-hydroxy-9Z,11E-octadecadienoic-9,10,12,13-d4 acid

5(S)-HETE d8
5S-hydroxy-6E,8Z,11Z,14Z-eicosatetraenoic-5,6,8,9,11,12,14,15-d8 acid

12(S)-HETE d8
12S-hydroxy-5Z,8Z,10E,14Z-eicosatetraenoic-5,6,8,9,11,12,14,15-d8 acid

2. Screening methods

Polysaccharide CSPs can be used in different elution conditions, viz. normal-phase, polar organic, reversed-phase (RP) and SFC elution conditions. In this work, RP elution conditions were chosen. Two columns, 2 organic solvents used as mobile phase component B and 2 acidic additives were screened for finding a suitable method for separation of isomers of oxylipins. That gave all together 8 different separation conditions.

The results of the column screening were already depicted in the main document. Fig. S1 shows the comparison of separations obtained with MeOH and ACN as organic modifiers on the preferable Chiralpak IA-U column. Tab. S3 displays sensitivities of methods as signal-to-noise ratio (S/N) with different acid additives (HAc *vs.* FA). The data for the IA-U column and ACN as organic component in the mobile phase were chosen for this comparison.

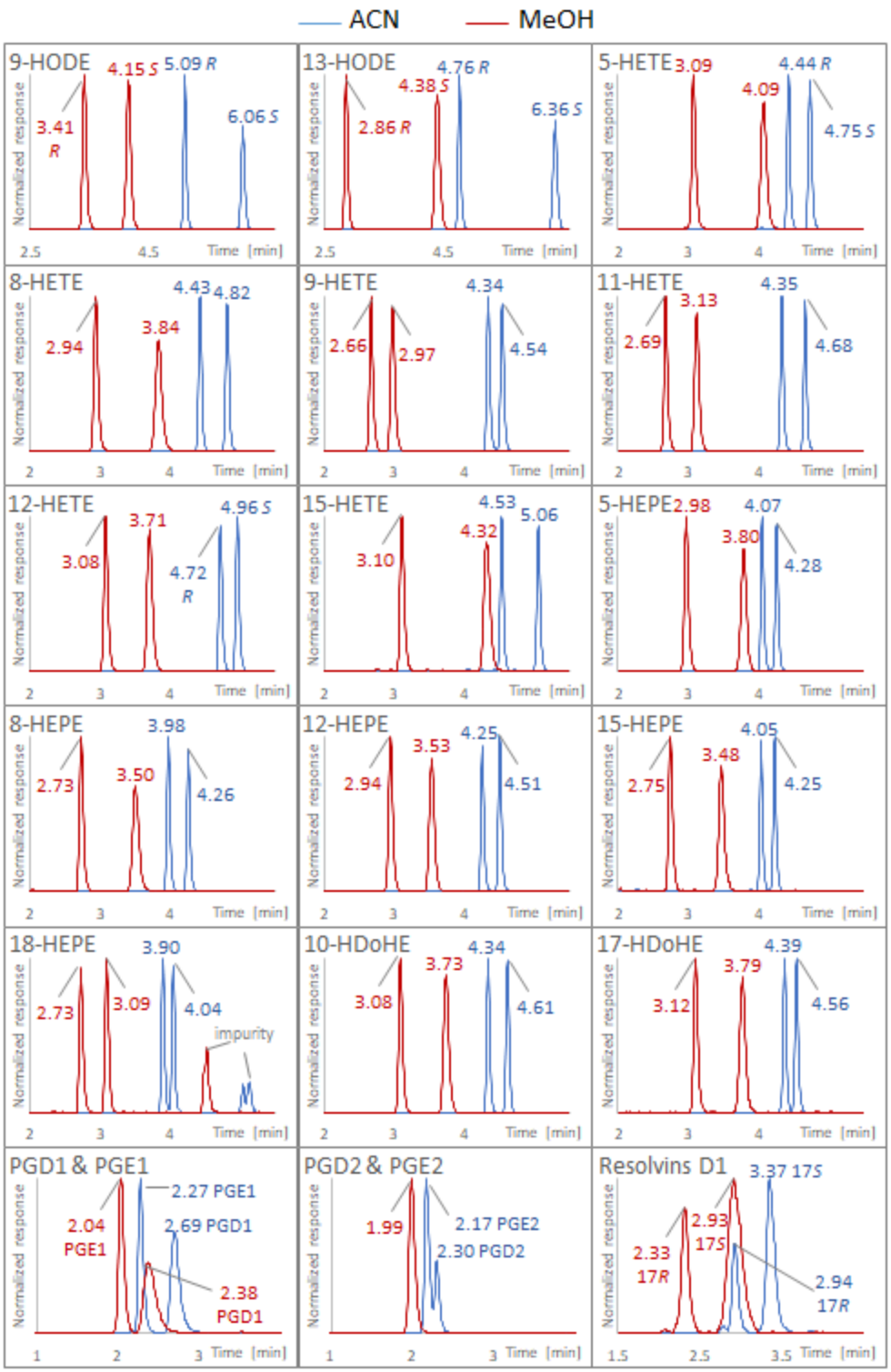

Suppl. Figure S1. Comparison of chromatograms obtained with ACN (blue) and MeOH(red). Chromatographic conditions: Column: Chiralpak IA-U, flow rate: 3 mL/min; column temperature 25°C; gradient for ACN: A: H_2O+0.1% (v/v) HAc, B: ACN+0.1% (v/v) HAc, 50-95% B in 5 min, 95% B for 2.5 min, 95-50% B in 0.1 min, 50% for 2.4 min; gradient for MeOH: A: H_2O+0.1% (v/v) HAc, B: MeOH+0.1% (v/v) HAc, 90-100% B in 5 min, 100% B for 2.5 min, 100-90% B in 0.1 min, 90% for 2.4 min;

Suppl. Table S1. Retention times [min] of analytes obtained with screening methods.

Compounds	Column IA-U				Column IC-U			
	ACN + HAc	ACN + FA	MeOH + HAc	MeOH + FA	ACN + HAc	ACN + FA	MeOH + HAc	MeOH + FA
9(R)-HODE	5.09	5.12	3.41	3.37	3.97	3.97	2.29	2.28
9(S)-HODE	6.06	6.10	4.15	4.11	4.01	4.01	2.29	2.28
13(R)-HODE	4.76	4.78	2.86	2.83	3.96	3.96	2.28	2.27
13(S)-HODE	6.36	6.39	4.38	4.34	4.00	4.01	2.28	2.27
5(R)-HETE	4.44	4.46	3.09	3.06	3.74	3.74	2.20	2.19
5(S)-HETE	4.75	4.78	4.09	4.04	3.74	3.74	2.20	2.19
8-HETE peak 1	4.43	4.45	2.94	2.91	3.74	3.74	2.18	2.17
8-HETE peak 2	4.82	4.84	3.84	3.77	3.74	3.74	2.18	2.17
9-HETE peak 1	4.34	4.36	2.66	2.66	3.76	3.75	2.17	2.18
9-HETE peak 2	4.54	4.56	2.97	2.96	3.76	3.75	2.17	2.18
11-HETE peak 1	4.35	4.37	2.69	2.67	3.80	3.80	2.20	2.20
11-HETE peak 2	4.68	4.71	3.13	3.10	3.85	3.85	2.20	2.20
12(R)-HETE	4.72	4.75	3.08	3.05	3.85	3.85	2.20	2.19
12(S)-HETE	4.96	4.99	3.71	3.66	3.85	3.85	2.20	2.19
15-HETE peak 1	4.53	4.55	3.10	3.07	3.77	3.78	2.19	2.19
15-HETE peak 2	5.06	5.08	4.32	4.26	3.77	3.78	2.19	2.19
5-HEPE peak1	4.07	4.09	2.98	2.95	3.44	3.45	2.13	2.13
5-HEPE peak2	4.28	4.30	3.80	3.76	3.44	3.45	2.13	2.13
8-HEPE peak 1	3.98	4.00	2.73	2.72	3.43	3.42	2.11	2.11
8-HEPE peak 2	4.26	4.29	3.50	3.47	3.43	3.42	2.11	2.11
12-HEPE peak1	4.25	4.27	2.94	2.92	3.53	3.53	2.13	2.12
12-HEPE peak2	4.51	4.53	3.53	3.48	3.53	3.53	2.13	2.12
15-HEPE peak 1	4.05	4.07	2.75	2.73	3.47	3.47	2.12	2.11
15-HEPE peak 2	4.25	4.27	3.48	3.43	3.47	3.47	2.12	2.11
18-HEPE peak 1	3.90	3.92	2.73	2.71	3.38	3.39	2.12	2.12
18-HEPE peak 2	4.04	4.06	3.09	3.06	3.38	3.39	2.12	2.12
10-HDoDE peak 1	4.34	4.36	3.08	3.05	3.73	3.73	2.19	2.19
10-HDoDE peak 2	4.61	4.64	3.73	3.68	3.73	3.73	2.19	2.19
17-HDoDE peak 1	4.39	4.41	3.12	3.09	3.71	3.71	2.19	2.18
17-HDoDE peak 2	4.56	4.58	3.79	3.73	3.71	3.71	2.19	2.18
17(R)-RvD1	2.94	2.95	2.33	2.32	2.43	2.44	1.84	1.85
RvD1	3.37	3.39	2.93	2.89	2.43	2.44	1.84	1.85
PGE1	2.27	2.28	2.04	2.03	2.33	2.34	2.20	2.17
PGD1	2.69	2.70	2.38	2.37	2.68	2.69	2.31	2.28
PGE2	2.17	2.17	1.99	1.99	2.17	2.18	2.04	2.03
PGD2	2.30	2.30	1.99	1.99	2.45	2.46	2.13	2.11

Suppl. Table S2. Peak width at 50% of peak height [min] obtained with screening methods

Compounds	Column IA-U				Column IC-U			
	ACN + HAc	ACN + FA	MeOH + HAc	MeOH + FA	ACN + HAc	ACN + FA	MeOH + HAc	MeOH + FA
9(R)-HODE	0.053	0.054	0.075	0.070	0.046	0.046	0.076	0.069
9(S)-HODE	0.067	0.066	0.084	0.085	0.050	0.050	0.076	0.069
13(R)-HODE	0.052	0.052	0.063	0.059	0.043	0.042	0.079	0.076
13(S)-HODE	0.075	0.078	0.091	0.092	0.052	0.053	0.079	0.076
5(R)-HETE	0.050	0.050	0.064	0.064	0.062	0.060	0.061	0.057
5(S)-HETE	0.053	0.054	0.094	0.091	0.062	0.060	0.061	0.057
8-HETE peak 1	0.050	0.050	0.064	0.061	0.073	0.073	0.060	0.060
8-HETE peak 2	0.055	0.055	0.102	0.098	0.073	0.073	0.060	0.060
9-HETE peak 1	0.049	0.047	0.055	0.056	0.048	0.047	0.052	0.054
9-HETE peak 2	0.051	0.047	0.065	0.065	0.048	0.047	0.052	0.054
11-HETE peak 1	0.047	0.047	0.057	0.055	0.051	0.052	0.072	0.070
11-HETE peak 2	0.049	0.051	0.068	0.067	0.052	0.052	0.072	0.070
12(R)-HETE	0.051	0.050	0.066	0.065	0.052	0.052	0.059	0.058
12(S)-HETE	0.053	0.052	0.083	0.083	0.052	0.052	0.059	0.058
15-HETE peak 1	0.048	0.047	0.066	0.065	0.055	0.050	0.058	0.059
15-HETE peak 2	0.056	0.053	0.098	0.093	0.055	0.050	0.058	0.059
5-HEPE peak1	0.050	0.048	0.061	0.061	0.054	0.056	0.056	0.055
5-HEPE peak2	0.050	0.050	0.087	0.086	0.054	0.056	0.056	0.055
8-HEPE peak 1	0.048	0.048	0.059	0.058	0.062	0.066	0.060	0.062
8-HEPE peak 2	0.053	0.051	0.099	0.097	0.062	0.066	0.060	0.062
12-HEPE peak1	0.051	0.049	0.062	0.061	0.048	0.048	0.057	0.054
12-HEPE peak2	0.050	0.050	0.078	0.077	0.048	0.048	0.057	0.054
15-HEPE peak 1	0.049	0.046	0.061	0.060	0.063	0.060	0.053	0.058
15-HEPE peak 2	0.049	0.049	0.085	0.084	0.063	0.060	0.053	0.058
18-HEPE peak 1	0.046	0.045	0.056	0.057	0.056	0.057	0.057	0.055
18-HEPE peak 2	0.049	0.044	0.060	0.064	0.056	0.057	0.057	0.055
10-HDoDE peak 1	0.048	0.046	0.063	0.061	0.069	0.068	0.061	0.059
10-HDoDE peak 2	0.051	0.048	0.082	0.078	0.069	0.068	0.061	0.059
17-HDoDE peak 1	0.049	0.048	0.063	0.063	0.064	0.065	0.056	0.052
17-HDoDE peak 2	0.049	0.049	0.087	0.085	0.064	0.065	0.056	0.052
17(R)-RvD1	0.081	0.084	0.096	0.095	0.064	0.057	0.281	0.271
RvD1	0.117	0.113	0.176	0.171	0.064	0.057	0.281	0.271
PGE1	0.067	0.068	0.074	0.072	0.053	0.051	0.058	0.054
PGD1	0.118	0.114	0.164	0.156	0.053	0.051	0.057	0.056
PGE2	0.066	0.066	0.081	0.080	0.054	0.053	0.064	0.070
PGD2	0.065	0.065	0.081	0.080	0.055	0.054	0.074	0.072

Suppl. Table S3. Comparison of S/N ratio obtained with HAc and FA as acid additives for 3 different concentrations of analytes: 10 ng/mL, 1 ng/mL and 0.1 ng/mL. Chromatographic conditions: column: IA-U, flow rate: 3 mL/min; column temperature 25°C; A: H_2O+0.1% (v/v) acid, B: ACN+0.1% (v/v) acid, 50-95% B in 5 min, 95% B for 2.5 min, 95-50% B in 0.1 min, 50% for 2.4 min.

Concentration [ng/mL]:	10		1		0.1	
Compound	HAc	FA	HAc	FA	HAc	FA
9(R)-HODE	297.0	297.0	42.5	21.3	4.3	6.5
9(S)-HODE	566.1	327.5	52.7	21.3	6.8	6.5
13(R)-HODE	105.6	96.8	25.7	23.1	7.3	5.3
13(S)-HODE	325.0	129.7	34.4	28.4	10.3	4.5
5(S)-HETE	311.7	311.7	65.0	65.0	13.0	4.3
5(R)-HETE	721.2	357.0	133.5	71.0	28.0	6.7
8-HETE	293.7	176.2	30.0	120.0	4.3	8.5
8-HETE	681.3	197.6	56.4	160.0	6.8	6.0
9-HETE p1	370.3	309.7	64.5	62.0	8.8	6.0
9-HETE p2	878.9	350.3	117.4	72.0	19.2	6.2
11-HETE p1	276.0	193.2	138.0	69.0	13.5	13.5
11-HETE p2	619.2	206.1	255.5	73.3	29.5	15.5
12(R)-HETE	765.0	765.0	60.0	40.0	10.0	2.0
12(S)-HETE	1849.7	875.0	108.5	38.7	26.0	1.8
15-HETE p1	205.0	102.5	29.5	16.0	3.0	1.5
15-HETE p2	523.0	116.0	33.0	17.0	5.5	1.3
5-HEPE	124.0	93.0	17.7	26.5	4.3	7.0
5-HEPE	342.1	102.8	32.0	29.0	4.7	11.0
8-HEPE p1	86.2	101.0	21.3	39.5	7.1	5.3
8-HEPE p2	215.4	110.9	40.5	44.4	10.1	7.5
12-HEPE p1	113.4	189.0	40.0	80.0	14.0	7.5
12-HEPE p2	252.4	206.7	81.5	92.0	20.0	10.0
15-HEPE	21.2	20.9	6.2	12.1	3.0	1.5
15-HEPE	51.6	23.1	8.1	12.3	5.5	1.5
18-HEPE	21.0	12.0	2.5	1.7	1.0	1.5
18-HEPE	28.0	12.0	4.5	2.0	1.5	0.5
10-HDoHE p1	746.0	149.2	89.5	46.0	3.3	5.0
10-HDoHE p2	1690.6	165.8	91.5	51.5	9.0	10.0
17-HDoHE p1	38.1	54.2	2.5	8.2	0.6	1.7
17-HDoHE p2	94.6	63.3	4.8	7.0	1.4	1.8
RvD1	12.9	15.2	2.5	4.2	1.6	1.2
17(R)-RvD1	31.8	19.3	4.2	3.7	1.9	0.8

One of the arguments to choose ACN over MeOH as an organic modifier for the mobile phase of the final analytical method was the higher backpressure observed when MeOH was used. The backpressure was higher even though the gradient method always contained high amounts of the organic solvent (90-100% B). Fig. S2 compares pressure profiles during gradient runs of the screening methods. If the MeOH method had contained higher amounts of water, the pressure would have been even higher.

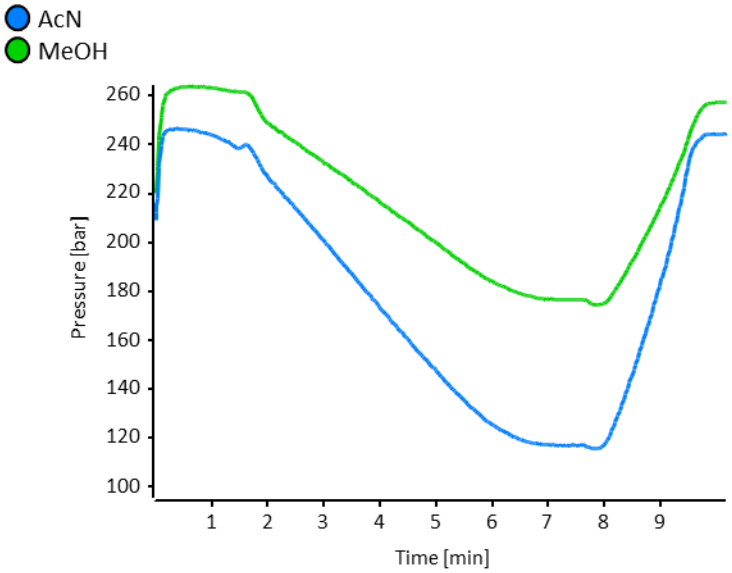

Suppl. Figure S2. Comparison of pressure profiles for gradient methods. Injection: 10 µL of MeOH in both cases. Mobile phase ACN or MeOH with 0.1% (v/v) HAc, and methods as described in paragraph 2.3.1. of the main document.

3. MS method for extended set of oxylipins

All the SRMs used for analysis are shown in Suppl. Tab. S4.

Suppl. Table S4. SRMs for extended set of analytes. The ion transitions with precursor ion selection in quadrupole 1 (Q1 m/z) and chosen fragment ion (product ion) (Q3 m/z) as well as collision energy (CE) and declustering potential (DP) for each compound are shown.

Name	Q1 *m/z*	Q3 *m/z*	CE [V]	DP [V]
10-HDoHE	343.1	153.0	-20	-70
14-HDoHE	343.1	205.0	-18	-60
17-HDoHE	343.1	201.0	-20	-80
5-HETE	319.1	114.9	-18	-80
8-HETE	319.1	154.9	-20	-75
9-HETE	319.1	151.0	-21	-40
11-HETE	319.1	167.0	-22	-75
12-HETE	319.1	208.0	-21	-80
15-HETE	319.1	219.0	-17	-40
5-HEPE	317.1	114.9	-20	-75
8-HEPE	317.1	154.8	-20	-70
12-HEPE	317.1	179.0	-18	-75
15-HEPE	317.1	219.0	-18	-95
18-HEPE	317.1	215.1	-18	-65
5,6-DiHETE	335.1	144.9	-22	-20
9-HODE	295.2	171.0	-25	-80
13-HODE	295.2	195.0	-26	-80
RvD1	375.1	121.1	-35	-80
12-HETrE	321.4	181.0	-24	-40
13-HOTrE	293.0	224.0	-18	-40
12-HETE-d8	327.3	184.0	-20	-80
13-HODE-d4	299.1	198.0	-24	-90
5-HETE-d8	327.1	115.9	-18	-50

4. Autoxidation of PUFAs.

4.1 Results of autoxidation of PUFAs.

Suppl. Tab. S5 shows detailed results of autoxidation of PUFAs. Limit of detection (LOD), lower limit of quantification (LOQ) and upper limit of quantification (ULOQ) are summarized together with oxylipin amount observed at each time point of PUFA oxidation.

Suppl. Table S5. Results of PUFA autoxidation.

		Amount from 1 µg of PUFA [pg]					
		Limits			Oxidation time [h]		
Corresponding PUFA	Compound	LOD	LOQ	ULOQ	18	24	48
LA	9(R)-HODE	25	50	5000	920 ± 220	945 ± 225	881 ± 210
	9(S)-HODE	25	50	5000	N/A	N/A	N/A
	13(R)-HODE	25	50	5000	1020 ± 110	1018 ± 110	1038 ± 110
	13(S)-HODE	25	50	5000	N/A	N/A	N/A
AA	5(S)-HETE	5.0	50	5000	< LOQ	321 ± 25	< LOD
	5(R)-HETE	5.0	50	5000	< LOQ	325 ± 35	< LOD
	8-HETE peak 1	25	50	5000	< LOD	211 ± 20	< LOD
	8-HETE peak 2	25	50	5000	< LOD	227 ± 25	< LOD
	9-HETE peak 1	25	50	5000	< LOQ	312 ± 30	< LOD
	9-HETE peak 2	25	50	5000	< LOQ	332 ± 45	< LOD
	11-HETE peak 1	2.5	50	5000	< LOQ	290 ± 35	< LOQ
	11-HETE peak 2	2.5	50	5000	< LOQ	291 ± 40	< LOQ
	12(R)-HETE	25	50	5000	< LOD	240 ± 20	< LOD
	12(S)-HETE	25	50	5000	< LOD	220 ± 15	< LOD
	15-HETE peak 1	25	50	5000	55 ± 2	530 ± 50	< LOQ
	15-HETE peak 2	25	50	5000	55 ± 3	500 ± 35	< LOQ
EPA	5-HEPE peak 1	25	50	5000	< LOD	< LOQ	< LOD
	5-HEPE peak 2	25	50	5000	< LOD	< LOQ	< LOD
	8-HEPE peak 1	25	50	5000	< LOD	< LOQ	< LOD
	8-HEPE peak 2	25	50	5000	< LOD	< LOQ	< LOD
	12-HEPE peak 1	25	50	5000	< LOQ	< LOQ	< LOD
	12-HEPE peak 2	25	50	5000	< LOQ	< LOQ	< LOD
	15-HEPE peak 1	25	50	5000	< LOD	< LOQ	< LOD
	15-HEPE peak 2	25	50	5000	< LOD	< LOQ	< LOD
	18-HEPE peak 1	50	250	5000	< LOD	< LOQ	< LOD
	18-HEPE peak 2	50	250	5000	< LOD	< LOQ	< LOD
DHA	10-HDoHE peak 1	5.0	50	5000	< LOQ	< LOQ	< LOQ
	10-HDoHE peak 2	5.0	50	5000	< LOQ	< LOQ	< LOQ
	17-HDoHE peak 1	50	250	5000	< LOD	< LOD	< LOD
	17-HDoHE peak 2	50	250	5000	< LOD	< LOD	< LOD
	RvD1	50	250	5000	< LOD	< LOD	< LOD
	17(R)-RvD1	50	250	5000	< LOD	< LOD	< LOD
ALA	13(R)-HOTrE	10	100	10000	331 ± 90	243 ± 65	148 ± 40
	13(S)-HOTrE	10	100	10000	331 ± 90	243 ± 65	148 ± 40
DGLA	12(R)-HETrE	10	100	10000	< LOQ	102 ± 40	< LOD
	12(S)-HETrE	10	100	10000	< LOQ	102 ± 40	< LOD
DHA	14(R)-HDoHE	10	100	10000	< LOQ	< LOQ	< LOQ
	14(S)-HDoHE	10	100	10000	< LOQ	< LOQ	< LOQ
EPA	5,6-DiHETE peak 1	100	500	5000	< LOD	< LOD	< LOD
	5,6-DiHETE peak 2	100	500	5000	< LOD	< LOD	< LOD

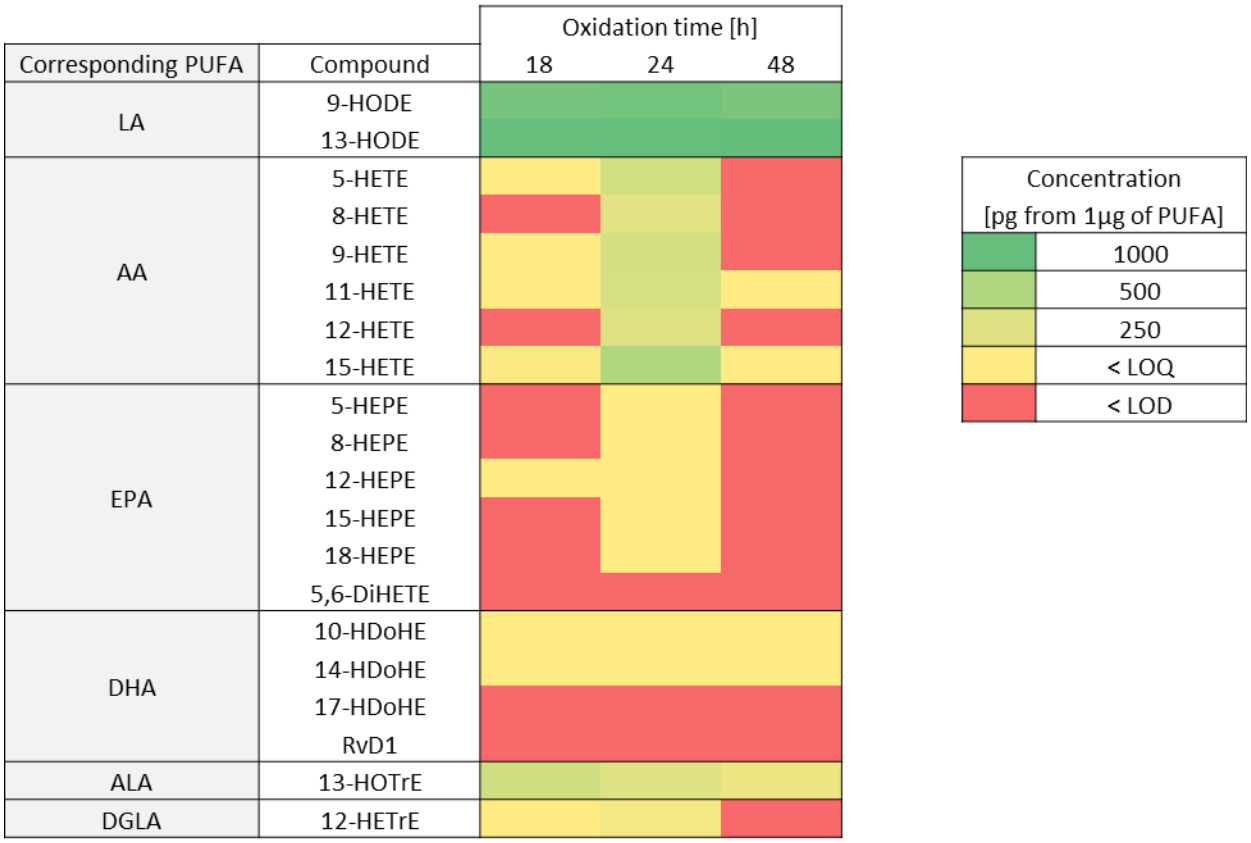

Suppl. Fig. S3. Heat map showing abundance of compounds created during PUFAs autoxidation.

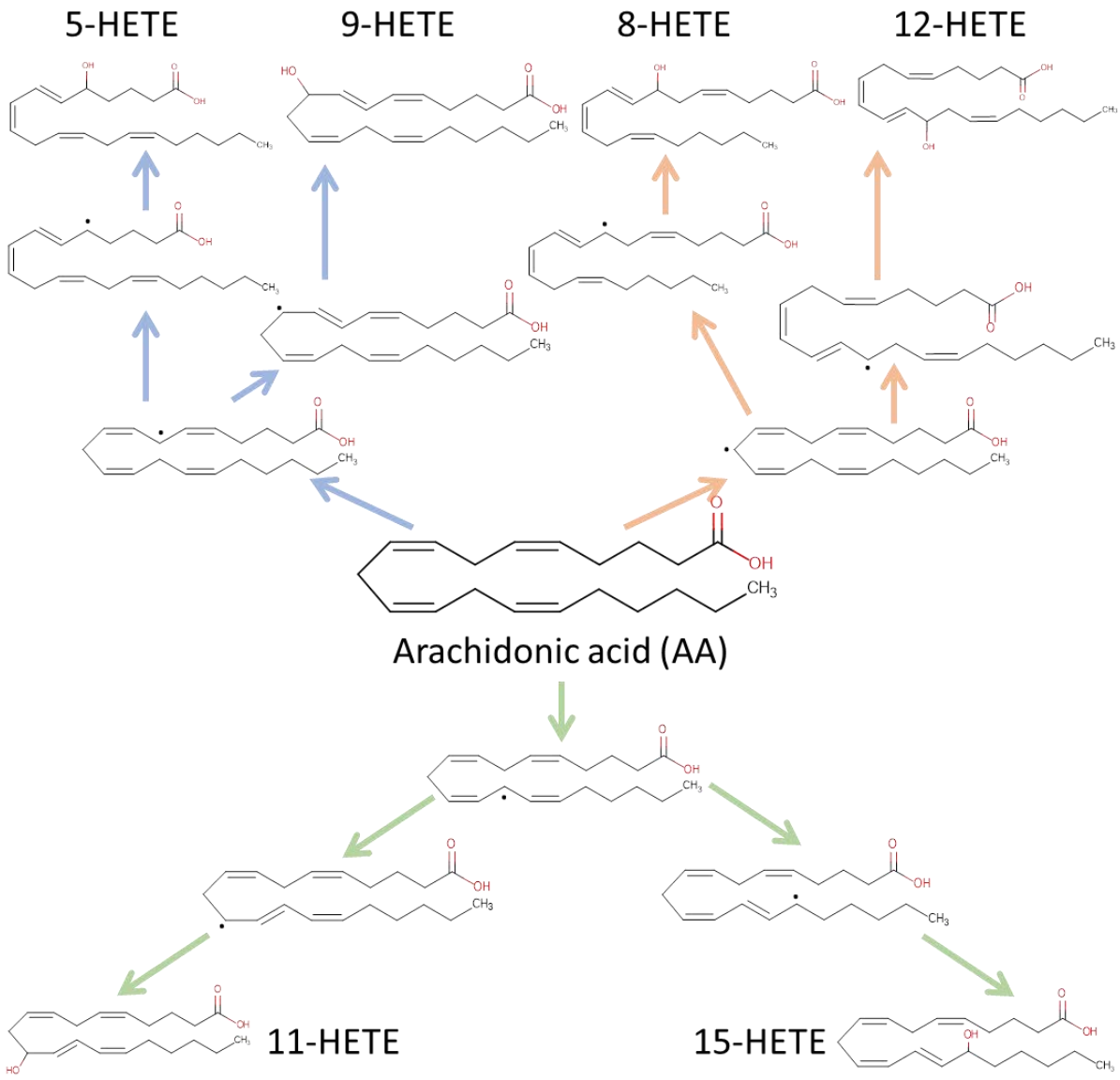

Suppl. Fig. S4. Scheme of autoxidation of AA to monohydroxy fatty acids.

4.2 Interference in 9- and 13-HODE.

Potential interferences, which partially co-eluted with 9(S)-HODE and 13(S)-HODE were detected in oxidized LA. None of these interferences were present in standards and in the extracts from platelet releasates.

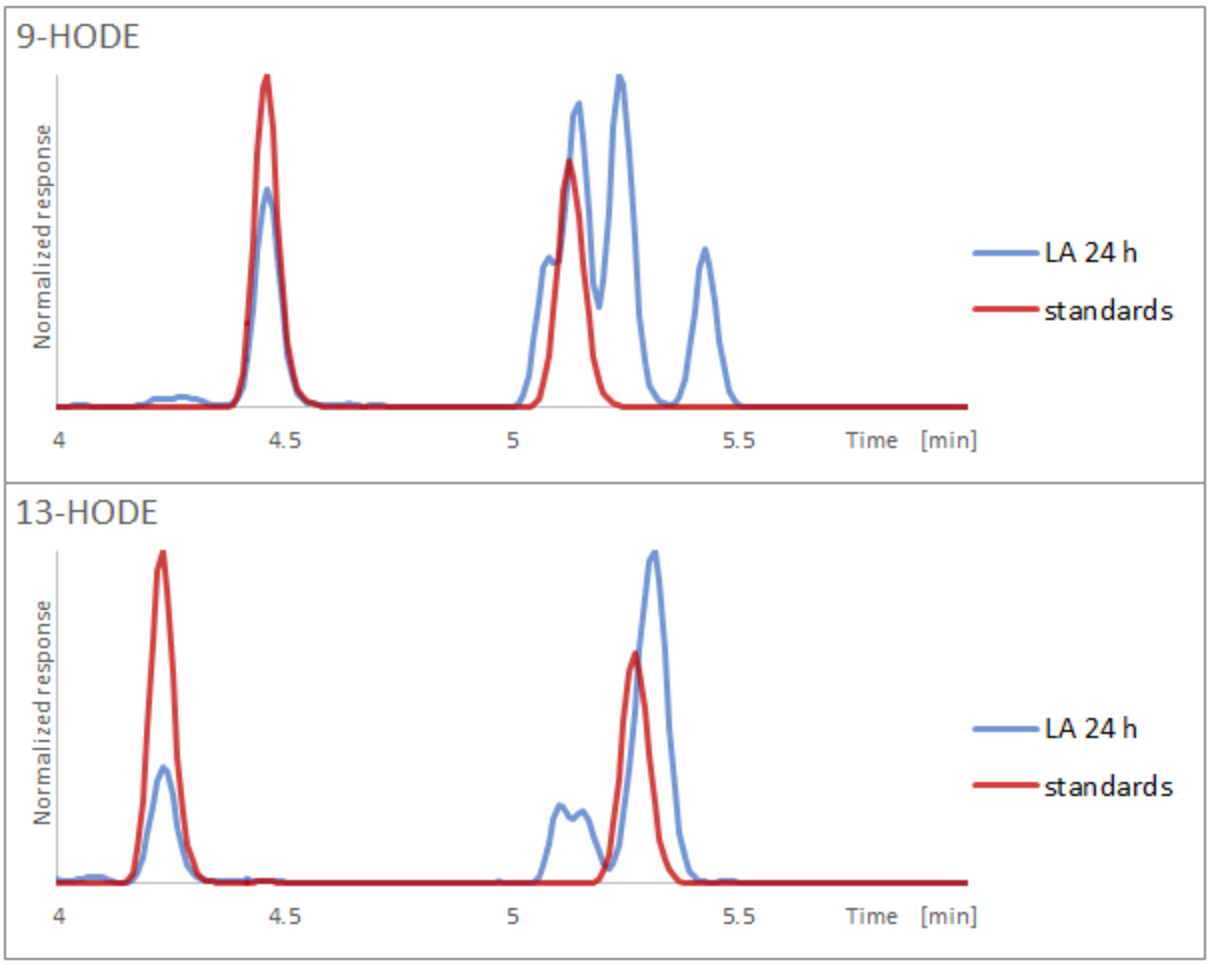

Suppl. Fig. S5. Extracted ion chromatograms of SRM for 9-HODE (top) and 13-HODE (bottom). Blue line shows the signals in oxidized LA in which potential interferences to the S enantiomers were detected. Red line displays the signals for standard solution.

5. Results from the analysis of platelet releasate.

Suppl. Table S6. Results of platelet releasates.

	Release [fg/1e6 platelets]								
	Limits			Resting			Thrombin activated		
Compound	LOD	LOQ	ULOQ	Donor 1	Donor 2	Donor 3	Donor 1	Donor 2	Donor 3
9(R)-HODE	9	20	1500	32 ± 4	42 ± 6	23 ± 4	163 ± 25	801 ± 120	463 ± 70
9(S)-HODE	9	20	1500	90 ± 8	101 ± 9	31 ± 3	115 ± 10	236 ± 21	149 ± 13
13(R)-HODE	9	20	1500	58 ± 7	51 ± 6	28 ± 4	59 ± 8	78 ± 10	41 ± 5
13(S)-HODE	9	20	1500	123 ± 9	140 ± 9	116 ± 7	137 ± 11	368 ± 25	259 ± 20
5(S)-HETE	2	20	1500	< LOD	< LOD	< LOD	< LOD	< LOD	< LOD
5(R)-HETE	2	20	1500	< LOD	< LOD	< LOD	< LOD	< LOD	< LOD
8-HETE	9	20	1500	< LOD	< LOD	< LOD	< LOQ	< LOQ	< LOQ
8-HETE	9	20	1500	< LOD	< LOD	< LOD	< LOD	< LOD	< LOD
9-HETE p1	9	20	1500	< LOD	< LOD	< LOD	< LOQ	58 ± 1	44 ± 1
9-HETE p2	9	20	1500	< LOD	< LOD	< LOD	< LOD	21 ± 1	< LOQ
11-HETE p1	1	20	1500	< LOQ	< LOQ	< LOQ	247 ± 47	1134 ± 215	732 ± 139
11-HETE p2	1	20	1500	< LOQ	< LOQ	< LOQ	< LOQ	25 ± 5	< LOQ
12(R)-HETE	9	20	1500	< LOD	< LOD	< LOD	< LOQ	47 ± 3	< LOD
12(S)-HETE	9	20	1500	302 ± 12	187 ± 7	1041 ± 41	10,000*	20,000*	10,000*
15-HETE p1	9	20	1500	< LOQ	< LOD	< LOD	78 ± 3	270 ± 13	167 ± 8
15-HETE p2	9	20	1500	< LOQ	< LOQ	< LOD	166 ± 8	484 ± 24	281 ± 14
5-HEPE	9	20	1500	< LOD	< LOD	< LOD	< LOD	< LOD	< LOD
5-HEPE	9	20	1500	< LOD	< LOD	< LOD	< LOD	< LOD	< LOD
8-HEPE p1	9	20	1500	< LOQ	< LOD	< LOD	< LOD	< LOD	< LOD
8-HEPE p2	9	20	1500	< LOD	< LOD	< LOD	< LOD	< LOD	< LOD
12-HEPE p1	9	20	1500	< LOQ	< LOQ	< LOD	< LOD	< LOD	< LOQ
12-HEPE p2	9	20	1500	136 ± 5	44 ± 2	71 ± 3	643 ± 25	678 ± 27	452 ± 18
15-HEPE	9	20	1500	< LOD	< LOD	< LOD	< LOD	< LOD	< LOD
15-HEPE	9	20	1500	< LOD	< LOD	< LOD	< LOD	< LOD	< LOD
18-HEPE	20	90	1500	< LOD	< LOD	< LOD	< LOD	< LOD	< LOD
18-HEPE	20	90	1500	< LOD	< LOD	< LOD	< LOD	< LOD	< LOD
10-HDoHE p1	2	20	1500	< LOQ	< LOQ	< LOQ	< LOQ	< LOQ	< LOQ
10-HDoHE p2	2	20	1500	< LOQ	< LOQ	< LOQ	< LOQ	< LOQ	< LOQ
17-HDoHE p1	20	90	1500	< LOD	< LOD	< LOD	< LOD	< LOD	< LOD
17-HDoHE p2	20	90	1500	< LOD	< LOD	< LOD	< LOD	< LOD	< LOD
RvD1	20	90	1500	< LOD	< LOD	< LOD	< LOD	< LOD	< LOD
17(R)-RvD1	20	90	1500	< LOD	< LOD	< LOD	< LOD	< LOD	< LOD
13(R)-HOTrE	4	40	3000	< LOD	< LOD	< LOD	< LOD	< LOD	< LOD
13(S)-HOTrE	4	40	3000	< LOD	< LOD	< LOD	< LOD	< LOQ	< LOD
12(R)-HETrE	4	40	3000	< LOD	< LOD	< LOQ	132 ± 10	277 ± 22	149 ± 11
12(S)-HETrE	4	40	3000	< LOQ	< LOQ	88 ± 7	76 ± 6	277 ± 22	165 ± 13
14(R)-HDoHE	4	40	3000	< LOD	< LOD	< LOD	< LOD	< LOD	< LOD
14(S)-HDoHE	4	40	3000	444 ± 25	157 ± 9	633 ± 35	278 ± 16	483 ± 28	480 ± 28
5,6-DiHETE	40	200	1500	< LOD	< LOD	< LOD	< LOD	< LOD	< LOD
5,6-DiHETE	40	200	1500	< LOD	< LOD	< LOD	< LOD	< LOD	< LOD

* estimated value

Suppl. Fig. S6. Heat map showing release of oxylipins from platelets in resting and activated states, logarithmic scale.

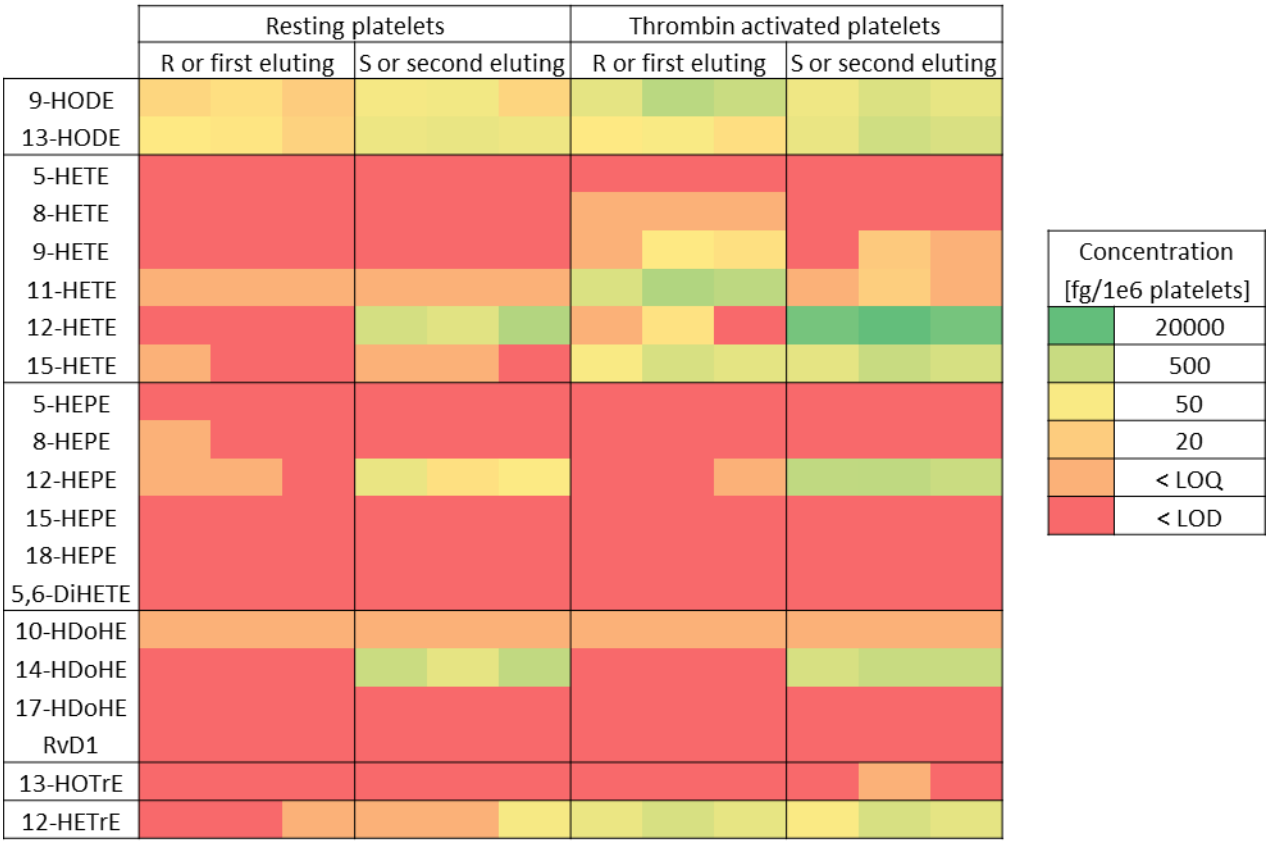

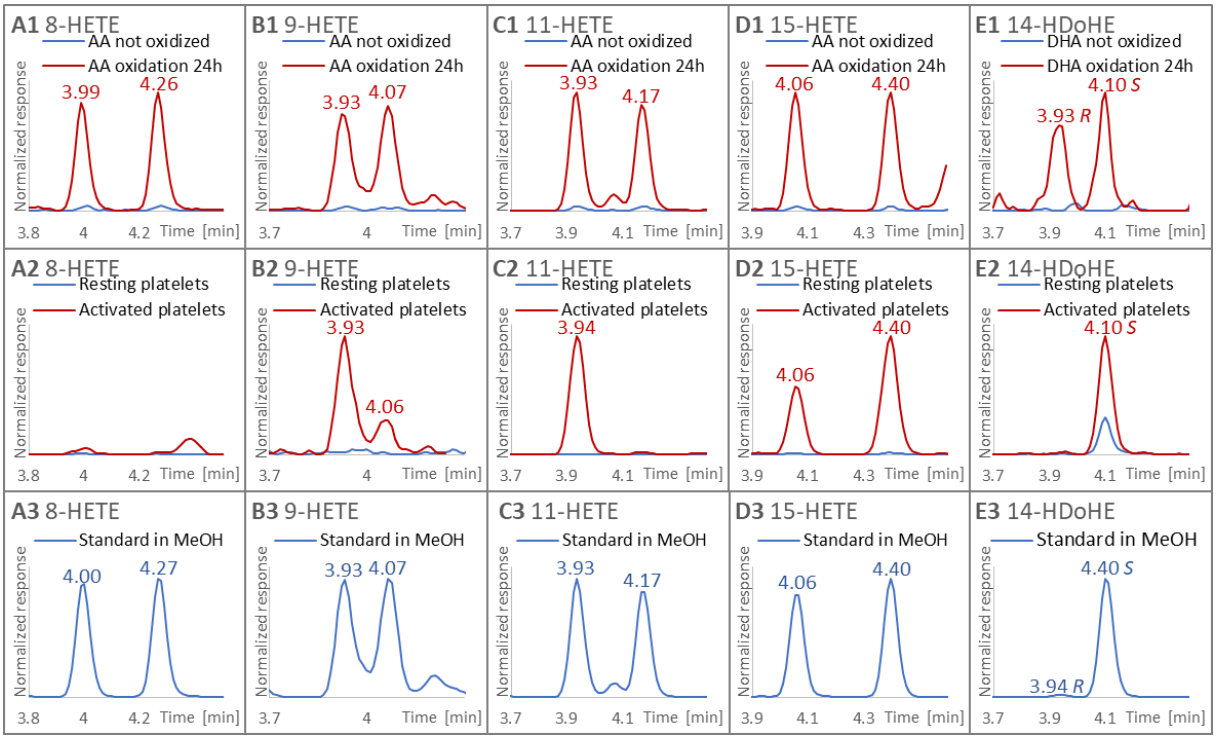

*Suppl. Fig. S7. Comparison of oxylipins from different sources. EIC of 8-HETE in oxidized PUFA (**A1**), platelets (**A2**) and standard solution (**A3**); EIC of 9-HETE in oxidized PUFA (**B1**), platelets (**B2**) and standard solution (**B3**); EIC of 11-HETE in oxidized PUFA (**C1**), platelets (**C2**) and standard solution (**C3**); EIC of 15-HETE in oxidized PUFA (**D1**), platelets (**D2**) and standard solution (**D3**); EIC of 14-HDoHE in oxidized PUFA (**E1**), platelets (**E2**) and standard solution (**E3**). Analyzed with the final method.*

2. Application to clinical lipidomics

2.1 Publication VI

Platelet ACKR3/CXCR7 favors antiplatelet lipids over an atherothrombotic lipidome and regulates thromboinflammation

Malgorzata Cebo[1#], Kristina Dittrich[1#], Xiaoqing Fu[1], Mailin C. Manke[2,3], Frederic Emschermann[2], Johannes Rheinlaender[4], Hendrik von Eysmondt[4], Nerea Ferreirós[5], Jessica Sudman[2], Alexander Witte[2], Lisann Pelzl[6], Oliver Borst[2,3], Tobias Geisler[2], Dominik Rath[2], Tamam Bakchoul[6], Meinrad Gawaz[2], Tilman E. Schäffer[4], Michael Lämmerhofer[1], Madhumita Chatterjee[2*]

[1]Institute of Pharmaceutical Sciences, University of Tübingen, [2]Department of Cardiology and Angiology, [3]DFG Heisenberg Group Thrombocardiology, University Hospital Tübingen, [4]Institute of Applied Physics, University of Tübingen, [5]Pharmazentrum Frankfurt, University Hospital Frankfurt, [6]Institute for Clinical and Experimental Transfusion Medicine (IKET), University Hospital Tübingen, Germany

#share equal contribution as first authors

Reprinted with permission from *Blood* (2022) 139 (11): 1722–1742.

https://doi.org/10.1182/blood.2021013097

blood®
Regular Article

THROMBOSIS AND HEMOSTASIS

Platelet ACKR3/CXCR7 favors antiplatelet lipids over an atherothrombotic lipidome and regulates thromboinflammation

Malgorzata Cebo,[1,*] Kristina Dittrich,[1,*] Xiaoqing Fu,[1] Mailin C. Manke,[2,3] Frederic Emschermann,[2] Johannes Rheinlaender,[4] Hendrik von Eysmondt,[4] Nerea Ferreirós,[5] Jessica Sudman,[2] Alexander Witte,[2] Lisann Pelzl,[6] Oliver Borst,[2,3] Tobias Geisler,[2] Dominik Rath,[2] Tamam Bakchoul,[6] Meinrad Gawaz,[2] Tilman E. Schäffer,[4] Michael Lämmerhofer,[1] and Madhumita Chatterjee[2]

[1]Institute of Pharmaceutical Sciences, University of Tübingen, Tübingen, Germany; [2]Department of Cardiology and Angiology and [3]Deutsche Forschungsgemeinschaft (DFG) Heisenberg Group Thrombocardiology, University Hospital Tübingen, Tübingen, Germany; [4]Institute of Applied Physics, University of Tübingen, Tübingen, Germany; [5]Pharmazentrum Frankfurt, University Hospital Frankfurt, Frankfurt, Germany; and [6]Institute for Clinical and Experimental Transfusion Medicine (IKET), University Hospital Tübingen, Tübingen, Germany

KEY POINTS

- **ACKR3/CXCR7 ligation regulates COX-1 and 12-LOX–derived prothrombotic lipids but favors antiplatelet lipids that trigger platelet inhibition.**
- **Contrary to prothrombotic CXCR4, ACKR3/CXCR7 modulates thrombotic and thromboinflammatory functions without affecting hemostasis.**

Platelet ACKR3/CXCR7 surface expression is enhanced and influences prognosis in coronary artery disease (CAD) patients, who exhibit a distinct atherothrombotic platelet lipidome. Current investigation validates the potential of ACKR3/CXCR7 in regulating thromboinflammatory response through its impact on the platelet lipidome. CAD patients with enhanced platelet ACKR3/CXCR7 expression exhibited reduced aggregation. Pharmacological CXCR7 agonist (VUF11207) significantly reduced prothrombotic platelet response in blood from acute coronary syndrome patients ex vivo. CXCR7 agonist administration reduced thrombotic functions and thromboinflammatory plateletleukocyte interactions post–myocardial infarction and arterial injury in vivo. ACKR3/CXCR7 ligation did not affect surface availability of surface receptors, coagulation profile, bleeding time, plasma-dependent thrombin generation (thrombinoscopy), or clot formation (thromboelastography) but counteracted activation-induced phosphatidylserine exposure and procoagulant platelet-assisted thrombin generation. Targeted (micro-UHPLC-ESI-QTrap-MS/MS) and untargeted (UHPLCESI-QTOF-MS/MS) lipidomics analysis revealed that ACKR3/CXCR7 ligation favored generation of antithrombotic lipids (dihomo-γ-linolenic acid [DGLA], 12-hydroxyeicosatrienoic acid [12-HETrE]) over cyclooxygenase-1 (COX-1) or 12-lipoxygenase (12-LOX) metabolized prothrombotic and phospholipase-derived atherogenic lipids in healthy subjects and CAD patients, contrary to antiplatelet therapy. Through 12-HETrE, ACKR3/CXCR7 ligation coordinated with Gαs-coupled prostacyclin receptor to trigger cyclic adenosine monophosphate/protein kinase A–mediated platelet inhibition. ACKR3/CXCR7 ligation reduced generation of lipid agonists and lipid signaling intermediates, which affected calcium mobilization, intracellular signaling, and consequently platelet interaction with physiological matrices and thromboinflammatory secretome. This emphasized its functional dichotomy from prothrombotic CXCR4. Moreover, CXCR7 agonist regulated heparin-induced thrombocytopenia–sera/immunoglobulin G–triggered platelet and neutrophil activation, heparin-induced platelet aggregation, generation of thromboinflammatory lipids, platelet-neutrophil aggregate formation, and thromboinflammatory secretion ex vivo. Therefore, ACKR3/CXCR7 may offer a novel therapeutic strategy in acute/chronic thromboinflammation exaggerated cardiovascular pathologies and CAD.

Introduction

Thromboinflammatory attributes of platelets are widely investigated in cardiovascular disease to find novel therapeutic interventions.[1,2] Immunothrombosis resulting from FcγRIIA-mediated[3] platelet activation and involving thromboinflammatory platelet-leukocytes associations[4] may manifest venous, arterial, and pulmonary microvascular thrombosis,[5,6] as well as thromboischemic complications.[5] Platelet-monocyte interactions in acute coronary syndrome (ACS)[7] and platelet-neutrophil associations in heparin induced thrombocytopenia (HIT)[8] aggravate disease severity and thrombotic disposition. Platelet-derived thromboinflammatory mediators (eg, IL-1β,sCD40L) add to circulatory levels during acute inflammation[6,9] and chronic atheroprogression.[10] Given the unmet need for better antiplatelet

strategies in thromboischemic pathologies to overcome the drawbacks of current therapeutics[10] and inefficacy of aspirin (ASA)[11] in immunothrombosis-associated mortality, innovative antithromboinflammatory approaches[1,5,10] are warranted.

Thromboinflammatory platelet functions propagate vascular and microvascular thrombosis in veins,[8] arteries,[12] and pulmonary micro-capillaries,[13] as well as influence the severity of target organ damage also subsequent regeneration, remodeling, and functional recovery.[1,14] Coronary artery disease (CAD) patients show increased surface expression of the chemokine stromal cell–derived factor CXCL12/SDF1α[15] and its receptors, CXCR4 and ACKR3/CXCR7, on platelets.[16] ACKR3/CXCR7 surface expression is particularly enhanced in ACS patients and associated with improved left ventricular ejection fraction (LVEF) and prognosis.[16,17] Interestingly, ACKR3/CXCR7 is richly expressed by cardiomyocytes; it is significantly enhanced at the infarct border zone of the affected myocardium in mice[18] and in heart failure patients.[18] Endothelial deletion of ACKR3/CXCR7 increases infarct size and mortality and aggravates functional impairment post-MI,[19] whereas targeted delivery of *cxcr7* gene[19] and administration of CXCR7 agonist AMD3100[20] (CXCR4 antagonist) or TC14012[18,19,21] (CXCR4 inverse agonist) offers cardio-protective benefits[19,21] in mice. However, the implications of enhanced platelet ACKR3/CXCR7 availability among ACS patients[16,17] in modulating thrombotic and thromboinflammatory actions post–myocardial infarction/reperfusion injury (MI/RI) remained unexplored. This is of significance because activated platelets infiltrate the myocardium with either deleterious or regenerative consequences, as well as cause recurrent atherothrombotic and thromboischemic complications.[22]

Plasma levels of physiological ligands CXCL12/SDF1α[23,24] and macrophage migration inhibitory factor (MIF)[25] are progressively elevated with disease severity in ACS patients, which may influence platelet CXCR4 and ACKR3/CXCR7 availability[26,27] and thereby their pathophysiological engagement post-MI. CXCL12/SDF1α and MIF promote platelet survival through ACKR3/CXCR7.[26,27] Plasma-CXCL12/SDF1α may exert a prothrombotic effect through platelet CXCR4, but MIF does not regulate platelet response to external stimuli.[27,28] However, it reduces externalization of thrombogenic phospholipid phosphatidylserine on procoagulant platelets, which consequently exercises an antithrombotic effect, counteracted upon blocking ACKR3/CXCR7.[27] On the contrary, prothrombotic CXCL12/SDF1α[29] promotes collagen-induced platelet aggregation, adenosine triphosphate (ATP) release, thromboxane production and thrombus formation[30] through intracellular calcium mobilization, triggering activatory signaling cascade involving phosphoinositide 3-kinase (PI3K), Akt, PDK1, glycogen synthase kinase 3 beta, and myosin light chain phosphorylation.[31] These studies suggest the functional dichotomy of CXCR4 and ACKR3/CXCR7, the balance of which may direct the course of thromboinflammation and thrombotic propensity in cardiovascular pathologies arising from chronic[10] and acute inflammation.[5]

Previous investigators have employed cyclic peptide (TC14012), allosteric agonist (AMD3100), and agonist (CCX771)[32] to demonstrate the therapeutic implications of ACKR3/CXCR7 in myocardial infarction,[19,21] pulmonary fibrosis,[33] and atherosclerosis.[34] We have used the high-affinity (pKi = 8.1)[32,35-37] CXCR7 agonist (VUF11207) instead of proinflammatory physiological ligands to validate the potential of ACKR3/CXCR7 in governing thrombotic and thromboinflammatory platelet functions post-MI, following arterial injury, and those induced by HIT-sera/immunoglobulin G (IgG) acting through FcγRIIA. In search of its mechanism of action we also revealed its regulatory impact on the platelet lipidome.

Methods

A detailed description is provided in supplemental Methods; experimental conditions are specified in figure legends.

Platelet functions

Degranulation (CD62P, CD63 surface expression by flow cytometry, ATP release by lumi-aggregometry[38]), αIIbβ3-integrin activation (flow cytometry),[1,8] spreading, elastic modulus[39] (scanning ion conductance microscopy [SICM]), aggregation (impedance[29] and lumi-aggregometry[38]), procoagulant platelets (flow cytometry),[27] thrombus formation[1,40] (total thrombus analysis system [T-TAS]), intraplatelet calcium mobilization (flow cytometry),[41] platelet-leukocyte aggregates (flow cytometry), and thromboinflammatory platelet release (cytometric bead array) were evaluated in presence/absence of CXCR7 agonist/vehicle control.

Hemostatic and coagulation parameters

Tail bleeding time,[42] plasma coagulation (activated partial thromboplastin time [APTT], prothrombin time [PT]),[29] thrombin generation (thrombinoscopy),[14] and clot formation (thromboelastography)[40] were ascertained.

Lipidomics

Untargeted (UHPLC-ESI-QTOF-MS/MS) and targeted (micro-UHPLC-ESI-QTrap-MS/MS) lipidomics analyses for oxylipins[43,44] were performed for resting and thrombin-activated platelets[45] and platelet supernatant/releasates[46] in presence/absence of CXCR7 agonist/vehicle control. Lipid extraction from platelet releasate was done with MTBE/MeOH/H_2O; from platelet pellet in a monophasic extraction with isopropanol/water 9:1 (vol/vol), followed by solid-phase extraction on Bond Elut Certify II cartridges (Agilent) with ethyl acetate/*n*-hexane/acetic acid 75:24:1 (vol/vol/v) for oxylipins. 1290-Agilent UHPLC instrument, PAL-HTX xt DLW autosampler (CTC Analytics) and SCIEX TripleTOF 5600+ were used for untargeted lipidomics; Eksigent MicroLC 200 Plus System (Sciex) and QTrap 4500 MS instrument (Sciex) were used for targeted (micro-UHPLC-ESI-QTrap-MS/MS) lipidomics analysis. MS-Dial[47] was used for peak picking, lipid identification supported with confirmation of correct retention time,[45] manual curation, and peak integration.

cAMP levels

Time-dependent increase in intraplatelet cyclic adenosine monophosphate (cAMP) levels following CXCR7 agonist treatment was ascertained by LC-ESI-MS/MS.

Immunoblots

Western blots for phosphorylated phospholipase C gamma (PLCγ), Src Family Tyr416, protein kinase C (PKC), PI3K, Akt, and p38MAPK were performed in collagen-related peptide (CRP)-activated platelets in presence/absence of CXCR7 agonist/vehicle control.[26,27]

Table 1. Baseline characteristics of CAD patients enrolled for platelet aggregation test and surface expression of CXCR4 and ACKR3/CXCR7

CAD patients' characteristics	CAD (n = 230)
Age (mean ± SD)	67.1 (± 11.9)
Male gender	170 (73.9%)
LVEF % at admission (mean ± SD)	50.6 (± 11.0)
Cardiovascular risk factors	
Arterial hypertension	200 (87.0%)
Hyperlipidemia	134 (58.3%)
Diabetes mellitus type 2	60 (26.1%)
Smoking	104 (45.2%)
Medication on admission	
ASA	123 (53.5%)
Clopidogrel	27 (11.7%)
Prasugrel	4 (1.7%)
Ticagrelor	10 (4.3%)
ACE inhibitors	90 (39.1%)
ARBs	38 (16.5%)
β blockers	117 (50.9%)
Ca-channel inhibitors	45 (19.6%)
Diuretics	74 (32.1%)
Statins	99 (43.0%)
Reason of admission/clinical diagnosis	
ACS	142 (61.7%)
CCS	88 (38.3%)
Plasma lipid profile	
Total cholesterol (mg/dl)	177.1 (± 46.5)

We included n = 230 consecutive patients with symptomatic CAD to analyze platelet ACKR3/CXCR7 surface expression and aggregation response to ADP and TRAP in whole blood samples.

CAD patient cohort

Blood was collected from femoral arterial access site of patients during coronary angiography[16,48] (Tables 1-3). All patients admitted to the Department of Cardiology and Angiology gave written informed consent. The study was approved by the institutional ethics committee (270/2011BO1, 237/2018BO2) and complied with the Declaration of Helsinki and Good Clinical Practice guidelines.

HIT-associated thromboinflammation

Sera and corresponding IgG fractions from 3 patients with clinically and serologically confirmed HIT-associated thrombosis (using 4Ts score 4-6, enzyme-linked immunosorbent assay (ELISA), heparin-induced platelet aggregation [HIPA]-positive) were collected to evaluate platelet and neutrophil activation (flow cytometry), platelet-neutrophil aggregates (flow cytometry) thromboxane A2 (TxA2), 12-HETE generation (lipidomics), and platelet thromboinflammatory release (cytometric bead array).

Animal experimentations

Eight- to 10-week-old C57BL/6J mice of either sex (Jackson Laboratories) were used for ex vivo platelet function assays, tail-bleeding time, coagulation profile (PT, APTT), FeCl3-induced arterial thrombosis,[27,29] and MI/RI model by left anterior descending artery ligation.[49] All experimentations were conducted according to the German law for welfare of animals, following Animal Research: Reporting of In Vivo Experiments guidelines, and approved by local authorities.

Statistical analysis

Experimental studies Data (mean ± standard error of the mean [SEM]/standard deviation [SD]) were analyzed using GraphPad Prism software (GraphPad Software, Inc.; San Diego, CA, USA) at $P < 0.05$ statistical significance with analysis of variance (ANOVA) for >2 groups; Mann-Whitney *U* test, Welch's *t* test, and Wilcoxon matched-pairs signed rank test for 2 groups.

Clinical cohort Data (median ± SD) were analyzed using SPSS version 21.0 (SPSS, Inc.; Chicago, IL, USA). Nonnormally distributed data were compared using the Mann-Whitney *U* test.

Results

ACKR3/CXCR7 may exert antithrombotic actions post-MI/RI

Increased platelet ACKR3/CXCR7 surface expression in ACS patients is associated with improved prognosis.[16,17] Symptomatic CAD patients (n = 230; Table 1) with relatively enhanced platelet ACKR3/CXCR7 surface expression showed significantly lower aggregation response to adenosine 5′-diphosphate (ADP) and TRAP (Figure 1A), which paved the way to assess the antithrombotic influence of platelet ACKR3/CXCR7. Pharmacological CXCR7 agonist (VUF11207) induced a dose- and time-dependent internalization of ACKR3/CXCR7 (Figure 1Bi-Bii) in vitro, as expected,[35] but contrary to CXCL12/SDF-1α,[26,27] which externalizes ACKR3/CXCR7. However, unlike CXCL12/SDF-1α,[26,27] CXCR7 agonist (VUF11207) neither internalized CXCR4 (supplemental Figure 1Ai-ii) nor affected the surface expression of other CXCR-GPCRs (ie, CXCR1, CXCR2, CXCR6) on human platelets vs vehicle control (supplemental Figure 1Biiii), suggesting an ACKR3/CXCR7-specific effect. Similarly, a time-dependent internalization of murine platelet ACKR3/CXCR7 was observed in vitro (supplemental Figure 1C) and among circulatory platelets following CXCR7 agonist administration (until 3 hours) in vivo (supplemental Figure 1D), without affecting CXCR4 surface expression (supplemental Figure 1C-D) vs vehicle control.

CXCR7 agonist showed a dose-dependent (10-200 μg/mL) inhibitory effect on CRP-induced CD62P surface expression, PAC-1 binding (supplemental Figure 2A), collagen-induced aggregation (supplemental Figure 2B), and thrombus formation (supplemental Figure 2C-D) ex vivo. We further explored thrombus formation over collagen-coated (Figure 1Ci; supplemental Videos 1-6) and collagen + tissue factor (TF)-coated chips (Figure 1Cii; supplemental Videos 7-8) with T-TAS. CXCR7 agonist (100 μg/mL) reduced thrombus formation (Figure 1Ci) and

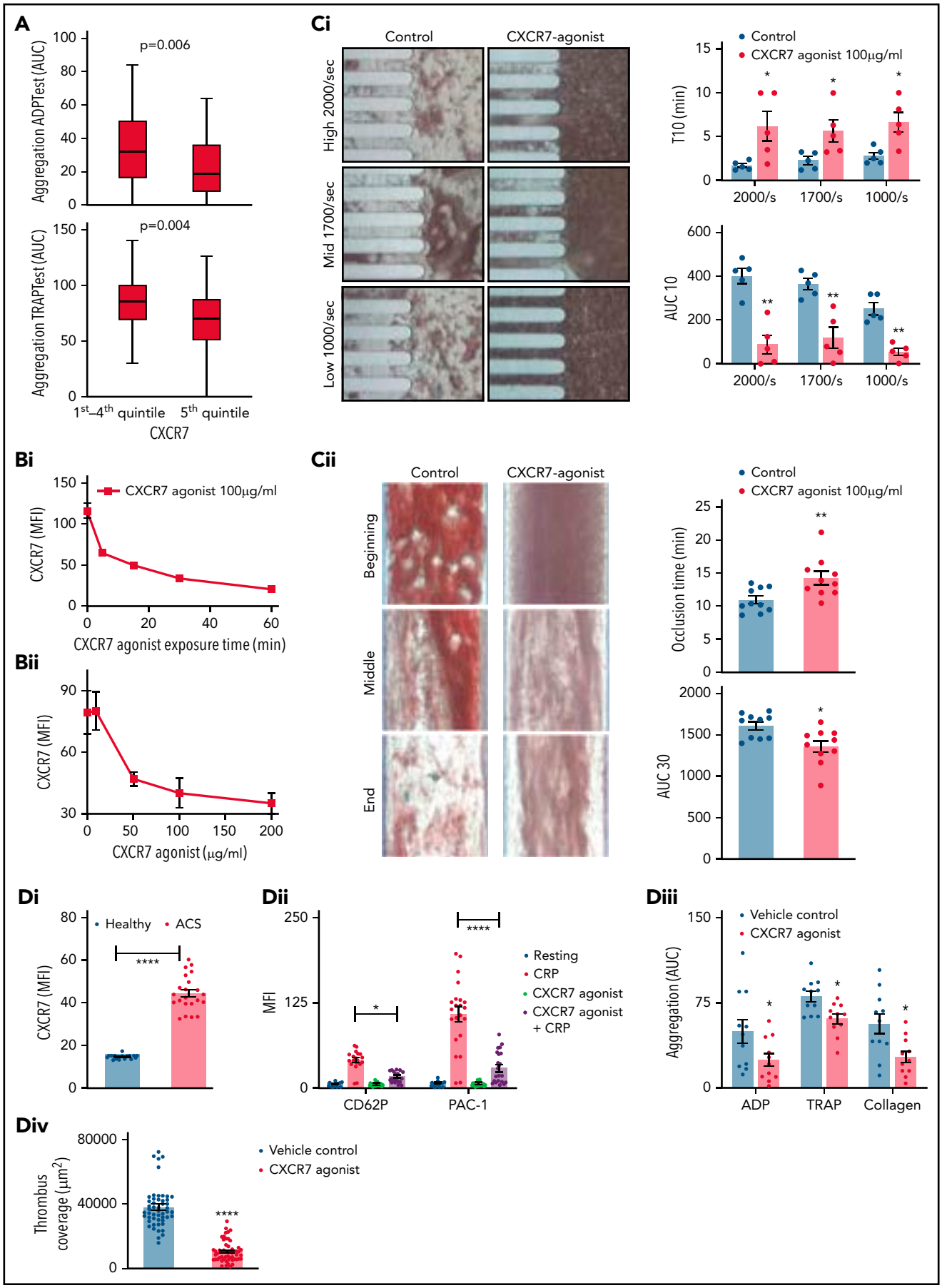

Figure 1.

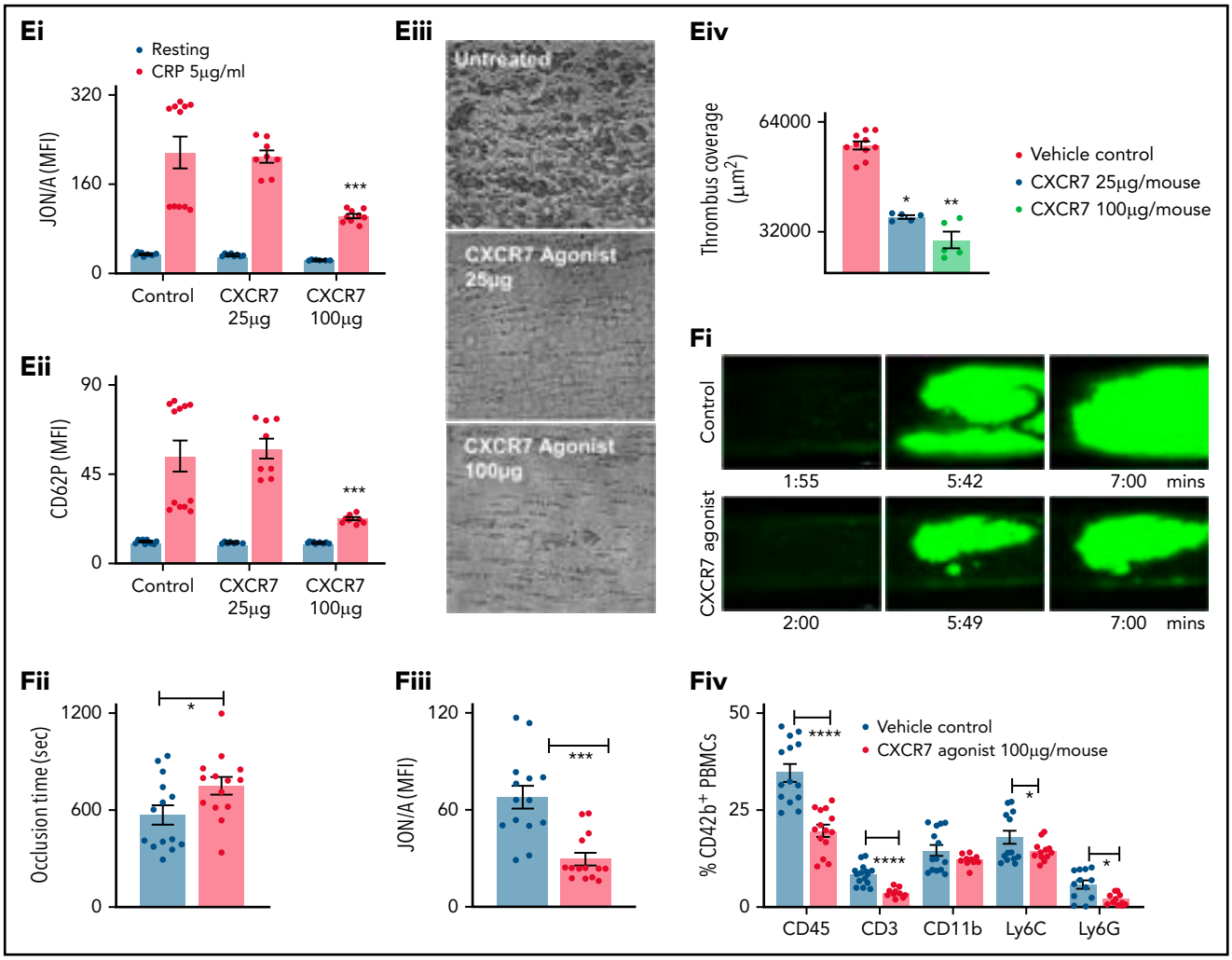

Figure 1. ACKR3/CXCR7 exerts antithrombotic effects. (A) Aggregation response to ADP (ADPTest, Roche) and TRAP-6 (TRAPTest, Roche) evaluated by impedance aggregometry in whole blood samples acquired in hirudinized tubes (Sarstedt) from CAD (n = 230; ACS, n = 142; CCS, n = 88) patients. *P* values using Mann-Whitney *U* test (line in box plots denote median). Flow cytometric detection of ACKR3/CXCR7 (mouse anti-human/mouse ACKR3/CXCR7-PE) internalization from the platelet surface following CXCR7 agonist treatment in a (Bi) time and (Bii) dose-dependent manner, gating for platelet-specific marker CD42b (anti-human CD42b-FITC) in whole blood. Data in the graphs are mean ± SEM from 4 healthy donors. T-TAS (Fujimori Kogyo Co Ltd, Shinjuku, Japan) data showing (Ci) thrombus coverage (AUC) and time to attainment of 10 kPa (T10) pressure over collagen (PL-chip) using 320 µL of hirudin anticoagulated blood and (Cii) thrombus coverage (AUC) and time to occlusion over collagen + tissue factor (AR-chip) using 450 µL of recalcified citrated human blood at arterial shear rates in presence/absence of CXCR7 agonist (100 µg/mL) or vehicle control incubated for 30 minutes at room temperature before perfusion. Data in the graphs are mean ± SEM from 5 experiments with healthy donors. *$P < .05$, **$P < .01$ using Mann-Whitney test. (Di) Surface expression of ACKR3/CXCR7 on platelets in n = 11 ACS patients as compared with healthy subjects (n = 11). Data in the graphs are mean ± SEM. **** $P < .0001$ using Mann-Whitney *U* test. Ex vivo whole blood functional assays performed with blood collected from ACS patients (n = 11) showing (Dii) surface expression of CD62P (anti-human CD62P-FITC) and PAC-1 (PAC-1–FITC) binding detected by flow cytometry gating for $CD42b^+$-platelet (anti-human CD42b-PE) population; (Diii) aggregation response to ADP (ADPTest), TRAP-6(TRAPTest), and collagen(ColTest) in hirudinized blood; and (Div) thrombus formation over collagen coated (100 µg/mL) surface in parallel plate flow chamber assay in presence/absence of CXCR7 agonist (100 µg/mL)/vehicle control preincubated for 30 minutes at room temperature. *$P < .05$, **** $P < .0001$ using Mann-Whitney *U* test between 2 groups and ANOVA followed by Sidak's multiple comparison test for >2 groups. Ex vivo analysis of murine platelet functions performed 1 hour after administration of CXCR7 agonist (100 µg/mL)/vehicle control (1% DMSO) showing (Ei) JON/A (JON/A-PE) response, (Eii) CD62P (anti-mouse CD62P-FITC) surface expression by whole blood flow cytometry gating for platelet-specific marker CD42b (anti-mouse CD42b-Dylight-649), and (Eiii-Eiv) thrombus coverage over collagen-coated surface (100 µg/mL) in ex vivo parallel plate flow chamber assay. Data in the graphs are mean ± SEM from 5 mice per group. CXCR7 agonist (100 µg per mouse) or vehicle control (1% DMSO) along with in vivo platelet-labeling antibody (GPIbβ-Dylight 488, 0.1 µg/gm by body weight) was administered IV 1 hour prior to surgical procedures to inflict carotid artery injury. Intravital microscopy (IVM) with NIS-Elements (Nikon) microscope was carried out using a 10x objective following carotid artery injury inflicted by application of a filter paper soaked in 15% $FeCl_3$ for 1 minute. (Fi) Reduced thrombus formation (green fluorescence from platelets in circulation stained in vivo with GPIbβ-Dylight 488) and (Fii) time to vessel occlusion (*$P = .034$). Following IVM analysis, blood was collected to perform further ex vivo analysis of platelet functions. Flow cytometric detection of (Fiii) JON/A response, (Fiv) platelet (anti-mouse GPIbβ-Dylight 488) aggregate formation with leukocytes (anti-mouse CD45-APC), lymphocytes (anti-mouse CD3-APC), monocytes, and neutrophils (anti-mouse Ly6C-APC, anti-mouse Ly6G-PE, anti-mouse CD11b-APC) following carotid artery injury in CXCR7 agonist/vehicle control–administered mice. In panels Ei through Fiii, *$P < .05$, **$P < .01$, ***$P < .001$ using an unpaired Student *t* test with Welch's correction; in panel Fiv, *$P < .05$, ****$P < .0001$ using Mann-Whitney *U* test for each surface marker. Data in the graphs are mean ± SEM from 14 mice per group. AUC, area under the curve; APC, apocyanin; DMSO, dimethyl sulfoxide; FITC, fluorescein isothiocyanate.

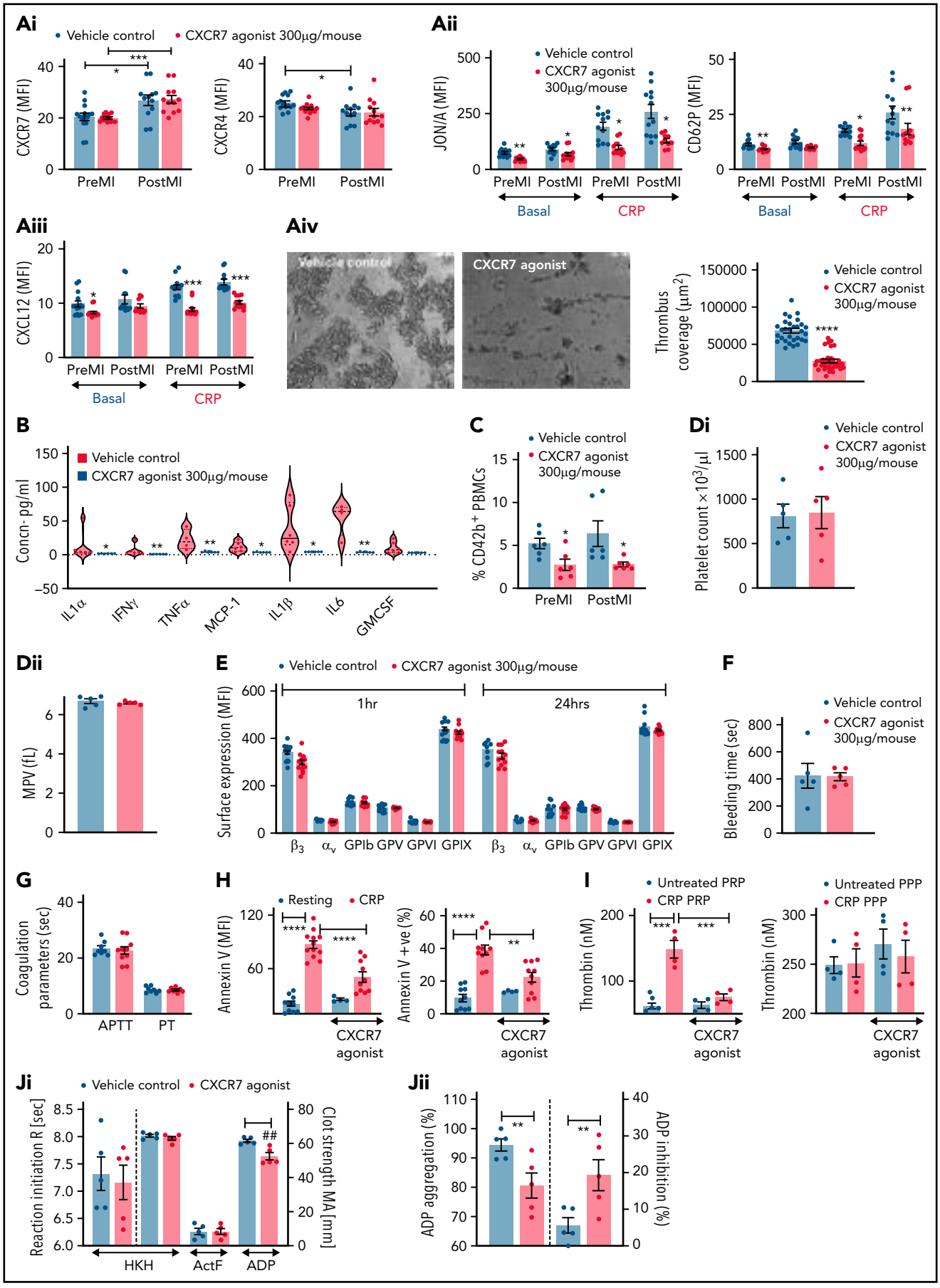

Figure 2.

decelerated (time to 10 kPa pressure attainment) thrombus build-up over collagen. Similarly, CXCR7 agonist decreased thrombus coverage and prolonged time to occlusion (Figure 1Cii) over collagen++ TF-coated surface.

Next, we assessed the antithrombotic efficacy of CXCR7 agonist in whole blood platelet function assays among ACS patients (n = 11) ex vivo, who exhibited significantly enhanced platelet ACKR3/CXCR7 surface expression (Figure 1Di). CXCR7 agonist counteracted CRP-induced degranulation (CD62P), $\alpha_{IIb}\beta_3$-integrin activation (PAC-1) (Figure 1Dii), ADP-, collagen-, TRAP-induced aggregation (Figure 1Diii), and thrombus formation (Figure 1Div). Therefore, enhanced platelet ACKR3/CXCR7 availability in ACS patients[16] post-myocardial infarction (MI) may possibly be used to regulate platelet response.

ACKR3/CXCR7 ligation modulates thrombotic and thromboinflammatory functions

We assessed the antithrombotic potential of platelet ACKR3/CXCR7 in regulating arterial thrombosis and platelet functions post-MI using murine models. Since CXCR7 agonist showed a dose-dependent antithrombotic efficacy with murine blood (supplemental Figure 2E) in vitro, we administered CXCR7 agonist at suboptimal (25 μg per mouse) and optimal (100 μg per mouse) doses in vivo and after 1 hour analyzed platelet functions ex vivo. CXCR7 agonist (100 μg per mouse) administration significantly counteracted subsequent CRP-induced $\alpha_{IIb}\beta_3$-integrin activation (JON/A-response) (Figure 1Ei), degranulation (CD62P) (Figure 1Eii), and thrombus formation (Figure 1Eiii-Eiv) ex vivo, as well as reduced arterial thrombus formation, significantly prolonging time to vessel occlusion (Figure 1Fi-ii; supplemental Videos 9-10), and countered $\alpha_{IIb}\beta_3$-integrin activation (Figure 1Fiii) in vivo. Platelet-leukocyte interactions in circulation substantiate atherothrombosis[14] and mediate acute thromboinflammation,[4,13] necessitating adequate antiplatelet strategies. CXCR7 agonist administration reduced circulatory platelet-leukocyte aggregate formation (Figure 1Fiv) following arterial injury.

Antiplatelet therapies are cornerstone in preventing platelet hyper-reactivity causing recurrent thromboischemic complications in ACS patients.[50,51] Corroborating previous reports using TC14012 (10 mg/kg)[19,21] and AMD3100,[20] administration of VUF11207 (300 μg per mouse) at a comparable/similar dose reduced infarct size (supplemental Figure 2F) and showed less deteriorated LVEF in mice 24 hours post-MI (ejection fraction/infarct size: vehicle control 2.35 ± 0.82 vs CXCR7 agonist 3.45 ± 1.01, $P = .037$; infarct area/area at risk: vehicle control 46.65 ± 6.740 vs CXCR7 agonist 33.21 ± 4.087, $P = .0005$). Circulatory platelet ACKR3/CXCR7 surface expression was enhanced, whereas CXCR4 expression was reduced (Figure 2Ai) 24 hours post-MI, contrary to increment in both CXCR4-ACKR3/CXCR7 on platelets from CAD patients as compared with healthy subjects and significantly increased expression of ACKR3/CXCR7 in ACS patients as compared with stable CAD.[16,48] This suggests interspecies differences in relative platelet surface availability of CXCR4-ACKR3/CXCR7. In addition to its known therapeutic effect on the ischemic heart,[18,19] CXCR7 agonist administration reduced $\alpha_{IIb}\beta_3$-integrin activation (Figure 2Aii), CD62P exposure, platelet surface expression of prothrombotic, inflammatory CXCL12/SDF-1α (Figure 2Aiii) in vivo, and decreased activation potential/responsiveness of circulatory platelets ascertained by CRP-induced activation ex vivo. CXCR7 agonist–treated mice showed reduced thrombotic potential (Figure 2Aiv), declined plasma levels of proinflammatory mediators (IL1α, IL1β, TNFα, IFNγ, IL-6, MCP-1) derived from different cellular origins (eg, circulatory cells), and not exclusively platelets (Figure 2B), as well as decreased thromboinflammatory platelet-leukocyte aggregates in circulation (Figure 2C). However, platelet counts, mean platelet volume (Figure 2Di-ii), and surface expression of receptors glycoprotein Ibα, GPV, GPVI, GPIX, α_v-integrin, and β_3-integrin (Figure 2E) remained unaffected. These experimental (in vivo) and clinical data from ACS patients (ex vivo) suggest that enhanced platelet ACKR3/CXCR7 availability post-MI may be used to counter thrombotic and thromboinflammatory functions.

Figure 2. CXCR7 agonist modulates thrombotic and thromboinflammatory platelet response without compromising plasma dependent coagulation. CXCR7 agonist (300 μg/mouse) or vehicle control (2% DMSO) was administered IV 1 hour prior to the surgical procedure. Surface expression of (Ai) ACKR3/CXCR7 (anti-human/mouse CXCR7-PE) and CXCR4 (anti-mouse CXCR4-Fluorescein) on circulating murine platelets. (Aii) Platelet JON/A response (JON/A-PE) and CD62P (anti-mouse CD62P-FITC) surface expression and (Aiii) surface expression of CXCL12/SDF-1α (anti human/mouse CXCL12/SDF-1α- Fluorescein) (denoting degranulation) in basal and CRP-activated (incubated ex vivo for 30 minutes at room temperature) state were evaluated by flow cytometry using blood collected pre-MI (before beginning the surgical procedure) and 24 hours post-MI/RI. (Aiv) Thrombus coverage ex vivo. (B) Levels of proinflammatory mediators in plasma (violin plot with median line) measured with cytometric bead arrays (Legendplex murine 13-plex inflammation panel) 24 hours post-MI/RI. (C) Percentage of $CD42b^+$ (anti-mouse CD42b-FITC)-$CD45^+$ (anti-mouse CD45-APC) platelet-leukocyte aggregates in blood collected pre-MI and 24 hours post-MI/RI. In panels A through C, $^*P < .05$, $^{**}P < .01$, $^{***}P < .001$, $^{****}P < .0001$ using Mann-Whitney *U* test. (Di-Dii) Platelet count and mean platelet volume (MPV) 24 hours post-MI/RI. CXCR7 agonist (300 μg/mouse) or vehicle control (2% DMSO) was administered IV, and experiments depicted in (E-G) performed 1 hour post-administration. (E) Surface availability of receptors glycoprotein Ibα, glycoprotein V (GPV), glycoprotein VI (GPVI), glycoprotein IX (GPIX), α_v-integrin, and β_3-integrin on murine platelets detected by whole blood flow cytometry (using anti-mouse CD42b/GPIbα-Dylight 649, anti-mouse GPV-FITC, anti-mouse GPVI-FITC, anti-mouse GPIX-FITC, anti-mouse β_3-FITC, and anti-mouse α_v-FITC). Data in the graphs are presented as mean ± SEM derived from 6 mice per group. (F) Tail bleeding time and (G) plasma coagulation profile (PT, APTT) was evaluated using the START4 platform. Data are mean ± SEM from 5 mice per group. (H) Phosphatidylserine exposure (annexin V-FITC MFI) on human platelets and percentage of annexin V^+ platelets under basal resting condition and following CRP (5 μg/mL) stimulation for 1 hour at room temperature in presence/absence of CXCR7 agonist (100 μg/mL)/vehicle control (1% DMSO) given as a pretreatment of 30 minutes at room temperature. Data are mean ± SEM of 4 experiments with healthy donors. I. Thrombin generation under basal condition and in the presence of platelet-activating CRP in platelet-rich plasma (PRP) and platelet-poor plasma (PPP) evaluated by calibrated automated thrombinoscopy (Stago) in presence/absence of CXCR7 agonist (100 μg/mL)/vehicle control (1% DMSO) given as a pretreatment of 30 minutes at room temperature. Data are mean ± SEM of independent experiments performed with n = 4 healthy donors. (H-I) $^{**}P < .01$, $^{***}P < .001$, $^{****}P < .0001$ using ANOVA followed by Sidak's post hoc test. (J) Thromboelastographic analysis (Whole Blood Hemostasis System) using the TEG6s PlateletMapping cartridges (Haemonetics, Germany) evaluating (Ji) the time to initiation of the appearance of first clot (R) and clot strength deciphered as maximum amplitude (MA). (Jii) Percentage of ADP aggregation; percentage of (extent of) inhibition imposed on ADP-induced aggregation, ascertained separately in the HKH (kaolin with heparinase); ActF (ActivatorF); and ADP assays using blood from healthy subjects in presence/absence of CXCR7 agonist (100 μg/mL)/vehicle control (1% DMSO). Data are shown as mean ± SEM of 5 independent experiments. $\#\#P = .002$, $^{**}P = .003$ using a paired Student *t* test. APC, apocyanin; DMSO, dimethyl sulfoxide; FITC, fluorescein isothiocyanate; MFI, mean fluorescence intensity; PE, phosphatidylethanolamine.

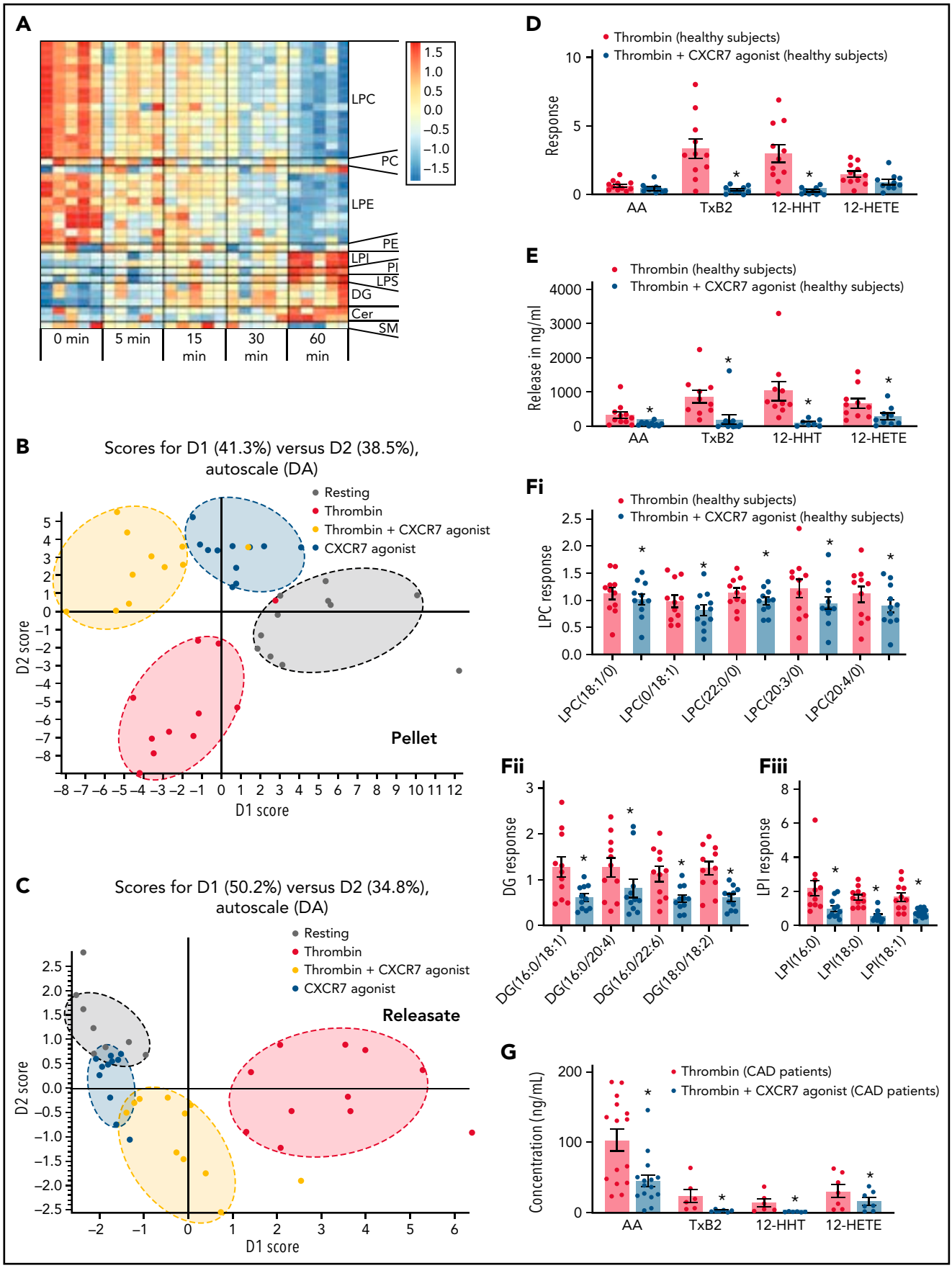

Figure 3.

Targeting ACKR3/CXCR7 does not affect basal hemostatic or coagulation response

CXCR7 agonist administration in vivo neither altered bleeding time (Figure 2F) nor plasma coagulation profile (APTT, PT)[29] (Figure 2G) of mice. We further verified these observations in human systems in vitro. Phosphatidylserine (PS) exposure on procoagulant platelets support thrombin generation driving coagulation,[52] which is severely affected in Scott syndrome, leading to enhanced bleeding.[53,54] Increased PS exposure on procoagulant platelets during acute inflammation, as in intensive care unit–admitted COVID-19 patients, correlates with sequential organ failure assessment score and D-dimer levels. COVID-19 patients with thrombotic complications exhibit higher PS externalization.[3] Like physiological ligands (CXCL12/SDF1α, MIF),[26,27] pharmacological CXCR7 agonist reduced the extent of PS exposure (annexin V mean fluorescence intensity) and percentage of annexin V^+ procoagulant platelets (Figure 2H) following CRP stimulation, without affecting basal status. Consequently, CXCR7 agonist counteracted only CRP-induced thrombin generation in PRP without affecting basal thrombin generation in PRP or in PPP (Figure 2I). Thromboelastographic (TEG6s) analysis using PlateletMapping assay confirmed that CXCR7 agonist did not affect clot formation (R) or clot strength (MA) (Figure 2Ji) in kaolin with heparinase activation test or MA in Activator F test. However, it significantly reduced ADP-activated platelet-dependent clot formation (MA), as well as decreased percent of ADP-induced aggregation and increased the extent of aggregation inhibition (Figure 2Jii). Therefore, targeting ACKR3/CXCR7 may regulate activated platelet-driven procoagulant and hemostatic functions without affecting plasma coagulation and basal hemostatic response.

ACKR3/CXCR7 ligation modulates the platelet lipidome

Next, we investigated the molecular mechanisms driving these inhibitory effects. Platelet CXCR4 or ACKR3/CXCR7 surface expression is not altered by activating stimuli but by physiological ligands[26,27] and lipoproteins.[29] Higher plasma low-density lipoprotein (LDL) levels in CAD patients correspond with significantly increased platelet CXCR4 and relatively enhanced ACKR3/CXCR7 expression (supplemental Figure 6A). Intraplatelet oxidized LDL levels correlate differentially with platelet CXCR4 and ACKR3/CXCR7 surface expression[29] in CAD patients, who exhibit a distinctively altered platelet lipidome enriched in atherogenic oxidized phospholipids and ceramides.[29] Platelet activatory signaling cascade also engages lipid mediators, while lipid agonists (eg, TxA2) released upon activation substantiate functional response.[38,55,56]

Current lipidomics evaluation in healthy subjects (Figure 3A-F) revealed a significant influence of ACKR3/CXCR7 ligation on the basal platelet lipidome over time, showing significantly reduced levels of several lipid classes including phosphatidylethanolamine, phosphatidylcholine, lysophosphatidylethanolamine (LPE), lysophosphatidylcholine (LPC), and sphingomyelin (Figure 3A). Thrombin-induced activation considerably alters the platelet lipidome.[57] Distinct clustering of resting and thrombin-activated platelets (Figure 3B), as well as platelet releasates (Figure 3C), in the presence/absence of CXCR7 agonist in principal components analysis-discriminant analysis (PCA-DA) score plots distinctly demonstrated that ACKR3/CXCR7 ligation may alter basal and counteract thrombin-driven changes to the platelet lipidome in healthy subjects. Thrombin-induced generation (Figure 3D) and release of (Figure 3E) prothrombotic arachidonic acid (AA), 12-hydroxyheptadecatrenoic acid (12-HHT), thromboxane-$TxA(B)_2$ through cyclooxygenase-1 (COX-1), and 12-HETE through 12-lipoxygenase (12-LOX) were reduced upon ACKR3/CXCR7 ligation. 12-HETE promotes platelet activation downstream of FcγRIIA,[58] whereas HETE phospholipids promote coagulation in a calcium- and phosphatidylserine-dependent manner.[59]

Platelets from CAD patients show increased levels of phospholipase-A_2 (LPC, lyophosphatidylinositol [LPI]) and phospholipase-C (diacylglycerol [DG]) metabolites.[29] LPCs, a major constituent of platelet-derived microvesicles,[60] induce platelet activation and platelet-monocyte aggregate formation. LPCs influence plaque instability and are richly deposited at unstable areas of atherosclerotic plaques[60] that may support atherothrombosis. CXCR7 agonist reduced generation of LPCs (Figure 3Fi), DGs (Figure 3Fii), and LPIs (Figure 3Fiii) in thrombin-activated platelets from healthy subjects. This was a unique regulatory influence of a chemokine receptor (ACKR3/CXCR7) on the generation of prothrombotic (eg, LPI, DG, TxA2, 12-HETE) and atherogenic (eg, LPC) lipids in platelets, which may deliver them at the site of vascular inflammation/injury during atheroprogression. As in platelets from healthy donors,

Figure 3. ACKR3/CXCR7 ligation modulates the platelet lipidome: observation from healthy subjects and CAD patients. (A) Washed platelets (200×10^6/sample) from n = 5 healthy donors were treated with CXCR7 agonist (100 μg/mL) for 0, 5, 15, 30, and 60 minutes at room temperature. Heat map showing significant changes in lipid concentration upon treatment with CXCR7 agonist (100 μg/mL) for a period of (0-60) minutes; linear regression model; the significance level for the corrected (false discovery rate correction [FDR]) *P* values was 0.05. The data were normalized by z-scores for each donor separately and derived from 5 independent experiments performed with 5 healthy donors. Washed platelets (300×10^6/sample) from n = 11 healthy donors were pretreated with CXCR7 agonist (100 μg/mL) or vehicle control (1% DMSO) for 30 minutes at room temperature. Platelets were then either kept under resting condition or activated with thrombin (0.1 U/mL) for 15 minutes at room temperature. The supernatants were separated from the platelet pellets by centrifugation, and both were used for lipid extraction and subsequent lipidomics analysis. PCA-DA score plots showing distinct grouping or clustering of resting platelets, thrombin-activated platelets, CXCR7 agonist plus thrombin-treated platelets, and CXCR7 agonist–treated platelets as analyzed in (B) platelet pellet and (C) platelet releasate/platelet supernatant. Relative abundance reflecting generation of (D) AA, $TxA(B)_2$, 12-HHT, and 12-HETE in thrombin (0.1 U/mL)-activated platelet pellet from n = 11 healthy subjects plus CXCR7 agonist (100 μg/mL) or vehicle control and (E) release of AA, $TxA(B)_2$, 12-HHT, and 12-HETE in thrombin-activated platelet supernatant of healthy subjects plus CXCR7 agonist (100 μg/mL) or vehicle control. Metabolism of (Fi) LPCs, (Fii) diacylglycerol (DGs), and (Fiii) LPIs in thrombin-activated platelets from healthy subjects is significantly reduced by CXCR7 agonist (100 μg/mL) pretreatment with respect to vehicle control. The significance levels for the corrected (FDR) *P* values are given using nonparametric paired Wilcoxon signed rank test with statistical significance $P < .05$. Response in the Y-axis of panels D and F refers here to relative signal intensities and were calculated from the raw data (peak heights) after LOWESS normalization. (G) Washed platelets (300×10^6/sample) from CAD patients (Table 2; n = 15 for untargeted analysis of AA and n = 7 for targeted analysis of oxylipins) were pretreated with CXCR7 agonist (100 μg/mL) or vehicle control (1% DMSO) for 30 minutes at room temperature. Platelets were then activated with thrombin (0.1 U/mL) for 15 minutes at room temperature. Generation of platelet-activating prothrombotic lipid mediators AA, $TxA(B)_2$, 12-HHT, and 12-HETE in thrombin (0.1 U/mL)-activated platelets was significantly reduced upon ex vivo pretreatment with CXCR7 agonist (100 μg/mL) with respect to vehicle control. The significance levels for the corrected (FDR) *P* values are given using nonparametric paired Wilcoxon signed rank test with statistical significance $P < .05$. DMSO, dimethyl sulfoxide; LOWESS, locally weighted scatterplot smoothing; PCA-DA, principal components analysis-discriminant analysis.

Table 2. Baseline characteristics of CAD patients enrolled for the analysis of platelet lipidome and functions following ex vivo treatment with CXCR7 agonist

CAD patient characteristics	CAD (n=20)
Age (mean ± SD)	71.9 (± 11.2)
Male gender	14 (70%)
LVEF% at admission (mean ± SD)	51.7 (± 7.8)
Cardiovascular risk factors	
Arterial hypertension	18 (90%)
Hyperlipidemia	11 (55%)
Diabetes mellitus type 2	9 (45%)
Smoking	4 (20%)
Medication on admission	
ASA	9 (45%)
Clopidogrel	3 (15%)
Prasugrel	0 (0%)
Ticagrelor	0 (0%)
ACE inhibitors	7 (35%)
ARBs	7 (35%)
β blockers	10 (50%)
Ca-channel inhibitors	6 (30%)
Diuretics	6 (30%)
Statins	11(55%)
Reason of admission/clinical diagnosis	
ACS	4 (20%)
CCS	16 (80%)
Plasma lipid profile	
Total cholesterol	170.1 (± 59.8)
LDL cholesterol	109.3 (± 49.9)
HDL cholesterol	47.8 (± 17.2)
Triglycerides	134.6 (± 91)

Arterial blood was collected from CAD (n = 20) patients during the percutaneous coronary intervention (PCI) procedure as previously described.70 Administration of antiplatelet therapy and statin were considered from the record of medications upon admission.

CXCR7 agonist treatment ex vivo significantly counteracted subsequent thrombin-induced generation of prothrombotic lipid mediators (AA, 12-HHT, $TxA(B)_2$, 12-HETE) in platelets from CAD patients (Table 2; Figure 3G), who also showed significantly increased platelet ACKR3/CXCR7 surface expression as compared to healthy subjects (supplemental Figure 6B).

By comparison, levels of DGs, LPCs, and LPIs (Figure 4A; supplemental Figure 6Ci-Cv) in platelets from CAD patients (n = 107; Table 3) were not significantly regulated by APT, even in combination with statin (68.2% patients) (Figure 4A; supplemental Excel File 1). Although ASA inhibits COX-1–metabolized TxA2 generation, it might not influence generation of upstream phospholipase metabolites (eg, LPCs), warranting alternate strategies to modulate the atherothrombotic platelet lipidome. Thrombin-induced ex vivo changes to the platelet lipidome was observed in CAD patients (n = 15) (Figure 4Bi-Bii) despite 5 out of 15 patients being on ASA. Treatment of platelets from these CAD patients (Table 2) with CXCR7 agonist ex vivo significantly counteracted subsequent thrombin-induced changes to the platelet lipidome (Figure 4Bi-Bii), particularly atherogenic LPCs, lipid mediator DGs, (Figure 4C-D), and to a certain extent, LPIs (Figure 4Diii). Combined with its effects on lipid agonists (AA, TxA2, 12-HETE) (Figure 3G), this may account for the antithrombotic effects of CXCR7 agonist.

Reduced generation of lipid mediators affects platelet activatory signaling cascade and functions

Signaling events triggered by external stimuli at the membrane receptors (TRAP/thrombin-PARs, collagen/CRP-xl-GPVI, ADP-P2Y12) converge downstream at the level of phospholipases.[38,55] Because ACKR3/CXCR7 ligation significantly altered the lipidome of both resting and activated platelets, we assessed some prime components of the platelet activatory signaling cascade. CXCR7 agonist reduced CRP-GPVI–induced phosphorylation/activation of PLCγ and Src family kinases (Figure 5A). A decrease in thrombin-induced LPI generation (Figure 3Fiii) corroborated with reduced intracellular calcium mobilization in the presence of CXCR7 agonist (Figure 5B), whereas reduced PLCγ activation, and consequently DG production (Figure 3Fii), corresponded with compromised PKC activation following CRP-GPVI stimulation (Figure 5C). CRP-GPVI–induced phosphorylation of PI3K, Akt, and p38MAPK in the activatory signaling network were also affected (Figure 5C).

By influencing the lipidome, ACKR3/CXCR7 ligation may modulate the activatory signaling cascade that mediates platelet responsiveness to external stimuli (eg, interaction with physiological matrices, aggregation, and thromboinflammatory secretion). Live imaging of single platelet response by SICM demonstrated that CXCR7 agonist pretreatment affected adhesion to collagen and fibrinogen (Figure 5D-E). Recording of dynamic platelet response showed reduced initial spreading rate on collagen (Figure 5D) and a significantly decreased final spreading area on collagen and fibrinogen (Figure 5E). Although CXCR7 agonist administration did not alter the surface availability of receptors (Figure 2E), a regulation on receptor-mediated signaling events affected platelet interaction with physiological matrices. A gradual increase in cellular stiffness accompanies platelet adhesion and spreading.[39] The elastic modulus ("stiffness") of platelets adhering to fibrinogen was also reduced (Figure 5F) by CXCR7 agonist pretreatment, in accordance with its impact on platelet adhesion and spreading.

Similar to its effect on CD62P, CXCR7 agonist reduced CD63 surface expression (Figure 5G), and ATP release from δ-granules (Figure 5H) of CRP (GPVI)- and TRAP (PAR1)-activated platelets. Combined with reduced release of lipid agonists (eg, TxA2) (Figure 3), it affected aggregation response to CRP and TRAP (Figure 5I). CXCR7 agonist also reduced degranulation of inflammatory cytokines and chemokines in vitro from α-granules of CRP-activated human (Figure 5J) and thrombin-activated murine platelets (Figure 5K) that mediate atheroprogression[14]

and contribute (eg, IL-1β, IL-6, IFN-γ) to plasma levels in acute thromboinflammatory conditions.[6]

Favoring generation of antiplatelet lipids, ACKR3/CXCR7 ligation triggers negative modulators of platelet response

We also explored the influence of ACKR3/CXCR7 ligation on platelet inhibitory signaling. Although ACKR3/CXCR7 is a noncanonical GPCR,[32] we observed an unexpected increase in cAMP (Figure 6A), in contrast to Gαi-coupled CXCR4, which decreases cAMP levels to facilitate thrombotic functions.[30] Moreover, G-protein coupling antagonist peptide and Gαs-coupling inhibitor (melittin) counteracted the inhibitory effects of CXCR7 agonist on CRP-GPVI–induced degranulation, integrin activation (supplemental Figure 7Ai-Aii), collagen-induced aggregation (supplemental Figure 7Aiii), and thrombus formation (supplemental Figure 7Aiv) without affecting basal response to activating stimuli (supplemental Figure 7Ai-Aiv). However, in case of melittin, in addition to preventing Gαs coupling, a stimulatory effect on Gαi[61] and inhibitory effect on adenylyl cyclase[62] could also have contributed to this counteracting influence. Neither G-protein coupling antagonist nor melittin triggered release of lipid mediators (AA, TxA2, 12-HHT, 12-HETE, 12-HETrE)

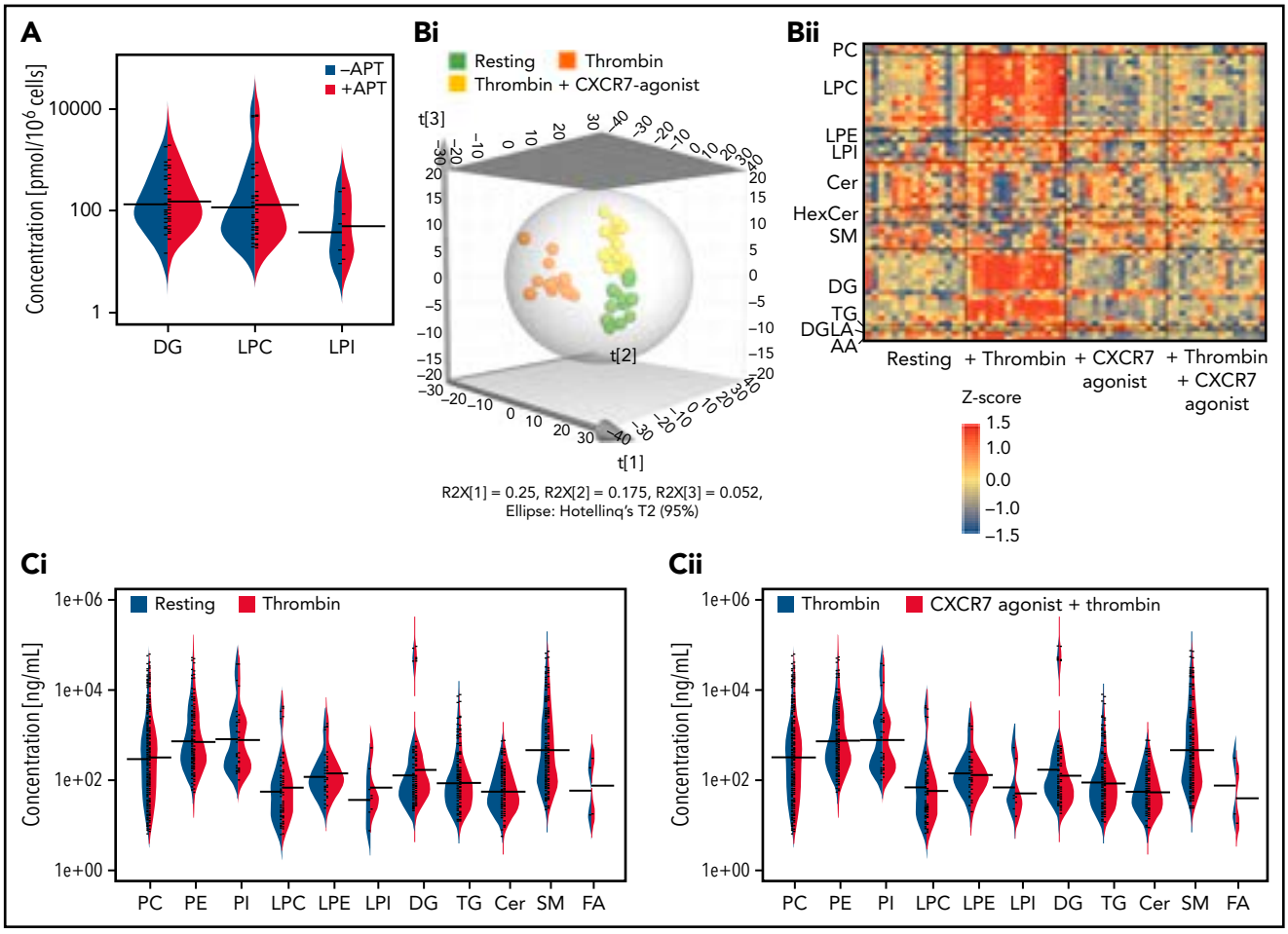

Figure 4. Effect of antiplatelet therapy in clinical practice and ex vivo CXCR7 agonist treatment on the platelet lipidome of CAD patients. Data are derived from untargeted lipidomics analysis of platelets. The asymmetric beanplot in (A) is derived from data on the basal platelet lipidome of CAD (n = 107, Table 3) patients. It represents the distribution of the concentration levels of individual lipid species within each of the lipid classes DG, LPC, and LPI among CAD patients treated with antiplatelet therapy (APT) (n = 46) and those without APT (n = 61). Smaller lines indicate concentration levels of individual lipid species within a group; the larger lines mark the average concentration of all detected lipid species within each class and group. (Bi-Diii) Lipidomics analysis of platelets from n = 15 CAD patients (Table 2) in their resting status and after thrombin (0.1 U/mL)-induced activation for 15 minutes at room temperature in presence/absence of ex vivo pretreatment with CXCR7 agonist (100 μg/mL) or vehicle control (1% DMSO) for 30 minutes at room temperature. Lipid concentrations were scaled for each donor by a z-score calculation. The 3D representation of a PLS-DA model in panel Bi shows clear clustering of platelet samples in accordance with their resting status, thrombin-induced activation, and thrombin plus CXCR7 agonist treatment conditions (six components with $R^2X(cum) = 0.566$, $R^2Y(cum) = 0.971$, and $Q2(cum) = 0.780$). The heat map in panel Bii is based on lipids with a variable importance in projection (VIP) score (which is a measure of a variable's importance in the PLS-DA model) >1.5 in the PLS-DA model further illustrates alterations in the lipidome, especially in thrombin-activated platelets. (C) Asymmetric beanplots indicate changes in the platelet lipidome for the different lipid classes phosphatidylcholine (PC), phosphatidylethanolamine (PE), phosphatidylinositol (PI), LPC, lysophosphatidylethanolamine (LPE), LPI, DG, triacylglycerol (TG), ceramides (Cer), sphingomyelin (SM), and fatty acids (FA), either comparing (Ci) resting vs thrombin-activated platelets or (Cii) thrombin-activated vs thrombin plus CXCR7 agonist–treated platelets (small lines denote individual lipid species and larger markings denote average concentration per lipid class and group). (Di-Dii) Boxplots depict changing concentration levels of significantly altered lipids in thrombin vs thrombin plus CXCR7 agonist–treated platelets (nonparametric paired Wilcoxon signed rank test with FDR correction, significance level: q-value < 0.05), which belong to the DG and LPC lipid classes. (Diii) The boxplots of 4 LPI species (showing a trend of reduced generation in the presence of CXCR7 agonist as compared with thrombin alone, without reaching statistical significance). All lipid concentrations were determined by relative quantification using class-specific isotope labeled internal standard (ILIS) related to 100 μL lipid extract from 3×10^8 platelets. DMSO, dimethyl sulfoxide; PLS-DA, partial least square-discriminant analysis.

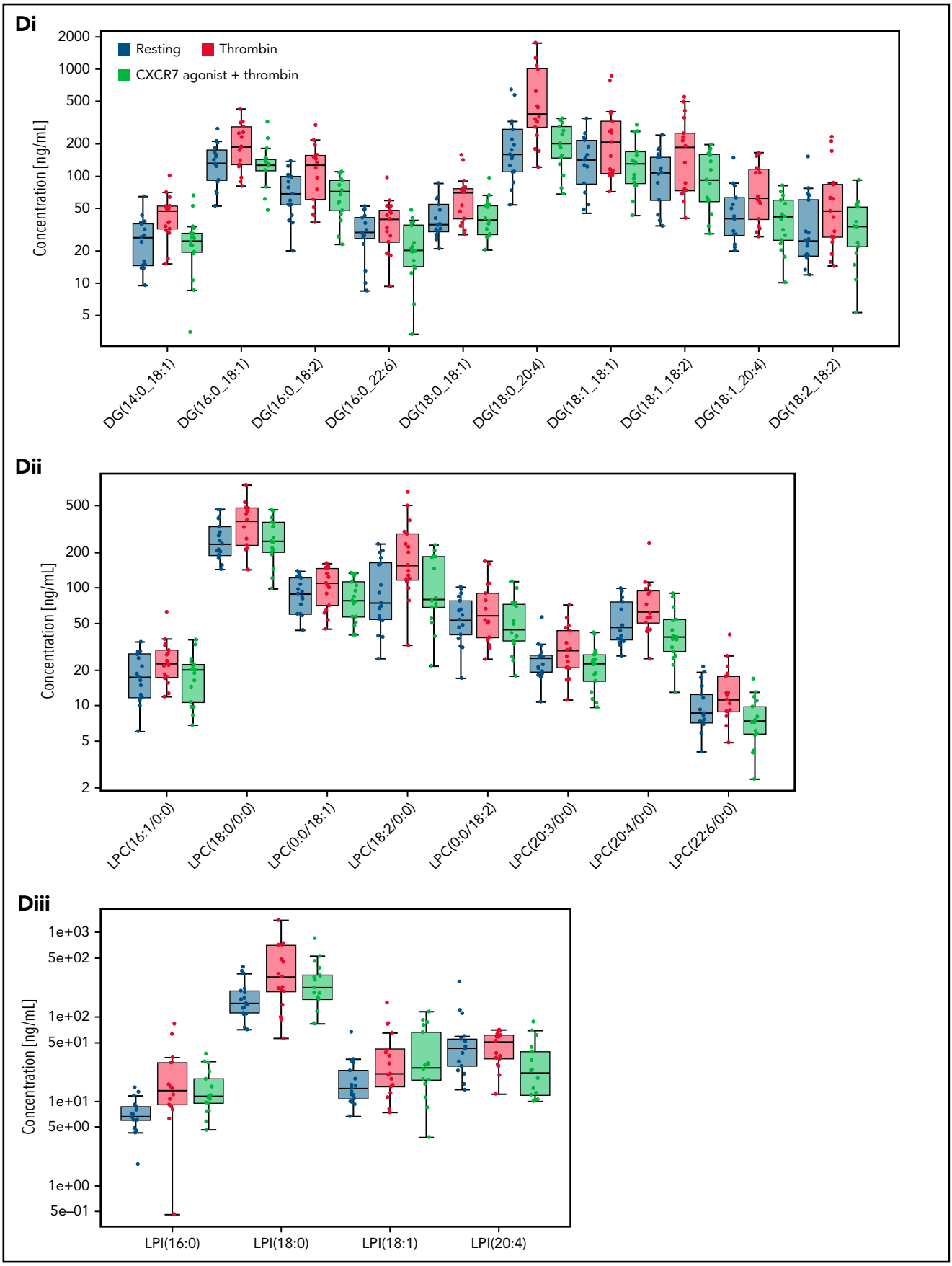

Figure 4. (continued)

Table 3. Baseline characteristics of CAD patients enrolled for analysis of the basal platelet lipidome

CAD patient characteristics	CAD (n = 107)
Age (mean ± SD)	71.2 (± 10.7)
Male gender	79 (73.8%)
LVEF% at admission (mean ± SD)	51.9 (± 11.2)
Cardiovascular risk factors	
Arterial hypertension	86 (80.4%)
Hyperlipidemia	52 (48.6%)
Diabetes mellitus type 2	31 (29.0%)
Smoking	19 (17.8%)
Medication on admission	
ASA	54 (50.5%)
Clopidogrel	12 (11.2%)
Prasugrel	4 (3.7%)
Ticagrelor	12 (11.2%)
ACE inhibitors	56 (52.3%)
ARBs	26 (24.3%)
β blockers	73 (68.2%)
Statins	73 (68.2%)
Reason of admission/clinical diagnosis	
ACS	26 (24.3%)
CCS	81 (75.7%)
Plasma lipid profile	
Total cholesterol (mg/dL)	161.3 (± 45.4)
LDL cholesterol (mg/dL)	96.2 (± 34.4)
HDL cholesterol (mg/dL)	48.6 (± 17.4)
Triglycerides (mg/dL)	145.3 (± 84.5)

CAD (n = 107) patients were enrolled separately for lipidomic analysis of washed platelets isolated from arterial blood collected during percutaneous coronary intervention (PCI) procedure.[70] Administration of antiplatelet therapy and statin were considered from the record of medications upon admission.

(supplemental Figure 7Bi) or altered the platelet lipidome to a significant extent (supplemental Figure 7Bii).

The apparent paradox of cAMP elevation was clarified by exploring the platelet lipidome following ACKR3/CXCR7 ligation using a targeted approach for oxylipins.[43] We observed a time-dependent increase in intraplatelet levels of linoleic acid, AA, the antiplatelet lipid dihomo-γ-linolenic acid (DGLA) (Figure 6Bi), and a subsequent rise in the levels of DGLA-derived 12-LOX metabolite 12-HETrE (Figure 6Bii). Levels of linoleic acid–derived CytP450 or COX-1 metabolite 13-hydroxyoctadecadienoic acid (13-HODE) (Figure 6Biii) and eicosapentanoic acid (EPA)-derived 12-LOX metabolite 12-HEPE (Figure 6Biv) with reported antiplatelet effects[63] were also increased but that of AA-derived prothrombotic COX-1 metabolite $TxA(B)_2$ remain unaltered (Figure 6Bv).

Platelet membranes contain more AA than DGLA,[63] which may be metabolized into prothrombotic or antithrombotic lipids. To get a translational perspective, we checked the relative levels of thrombogenic AA and antiplatelet DGLA in platelets from CAD (n = 107) patients receiving APT and statin. Comparative levels of AA (mean ± SD, without APT: 513 ± 297 ng/mL, with APT: 661 ± 455 ng/mL) and DGLA (without APT: 61 ± 37 ng/mL, with APT: 76 ± 63 ng/mL) were observed in CAD patients despite APT (supplemental Figure 6Di), as well as among those undergoing statin therapy (supplemental Figure 6Dii). Neither DGLA (CCS: 70 ± 53 ng/mL, ACS: 59 ± 33 ng/mL) nor AA (CCS: 600 ± 384 ng/mL, ACS: 526 ± 335 ng/mL) levels altered with disease severity (supplemental Figure 6Ei), irrespective of APT administration (supplemental Figure 6Eii) (DGLA: CCS, 75 ± 57 ng/mL, ACS, 59 ± 43 ng/mL; AA: CCS, 647 ± 406 ng/mL, ACS, 576 ± 467 ng/mL) (supplemental Excel File 1).

The antithrombotic actions of 12-HETrE released from platelets are mediated through Gαs-coupled prostacyclin receptor (IP).[64] We observed a time-dependent increase in generation and release of 12-HETrE from CXCR7 agonist–treated platelets (Figure 6C). Moreover, presence of IP antagonist prevented 12-HETrE from binding back to the IP receptor, which consequently increased levels of 12-HETrE in the platelet supernatant. This clarified the unexpected rise in cAMP as mediated by 12-HETrE acting through Gαs-coupled IP receptor in coordination with ACKR3/CXCR7 ligation. Therefore, IP antagonist decreased the inhibitory effects of CXCR7 agonist on-platelet activation (Figure 6Di-Dii), aggregation (Figure 6E), and thrombus formation (Figure 6F) without affecting basal platelet response to activating stimuli or the platelet lipidome (supplemental Figure 7Bi-Bii). Inhibitors of adenylyl cyclase (SQ22536) (supplemental Figure 8A) and cAMP-dependent kinases (KT5720) (supplemental Figure 8B) also counteracted the inhibitory actions of CXCR7 agonist on-platelet activation, aggregation, and thrombus formation. As in platelets from healthy subjects (Figure 6B-C), CXCR7 agonist treatment ex vivo induced 12-HETrE generation in platelets from CAD patients (Figure 6Gi) whereas IP antagonist counteracted the inhibitory actions of CXCR7 agonist on-platelet activation (Figure 6Gii) and aggregation (Figure 6Giii). Therefore, an alternate antiplatelet strategy through ACKR3/CXCR7 ligation counteracting generation of thrombogenic COX-1 (TxA2, HHT) or 12-LOX (12-HETE) metabolites in favor of antiplatelet lipids (12-HETrE, 13-HODE, 12-HEPE) might be considered advantageous.

CXCR7 agonist regulates HIT-associated thrombotic and thromboinflammatory response

Thrombo-inflammation exaggerates micro/macrothrombotic consequences.[5] Since ACKR3/CXCR7 ligation counteracted inflammatory release and platelet-leukocyte interactions, we verified its regulatory potential against thrombotic and thromboinflammatory challenges inflicted by HIT^+ sera/IgG. HIT is a drug-induced thromboinflammatory adversity that may cause venous/arterial thrombosis. Upon heparin administration in emergency during a thromboischemic event (MI), susceptible individuals develop anti–PF4-heparin antibodies that activate platelets through FcγRIIA, necessitating heparin replacements.

Sera from HIT^+ patients significantly enhanced platelet (Figure 7A-D) and neutrophil (Figure 7F) activation. CXCR7 agonist

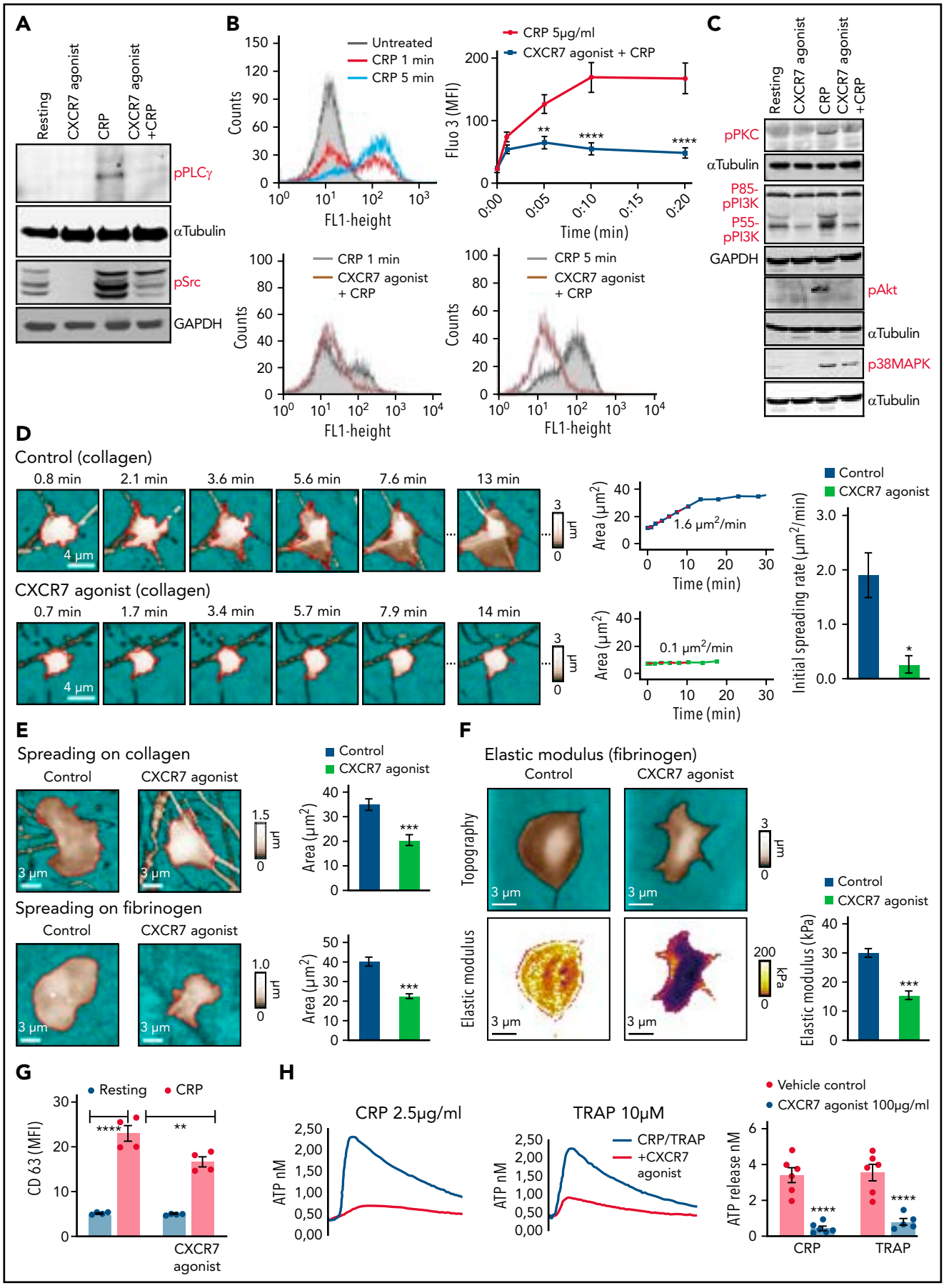

Figure 5.

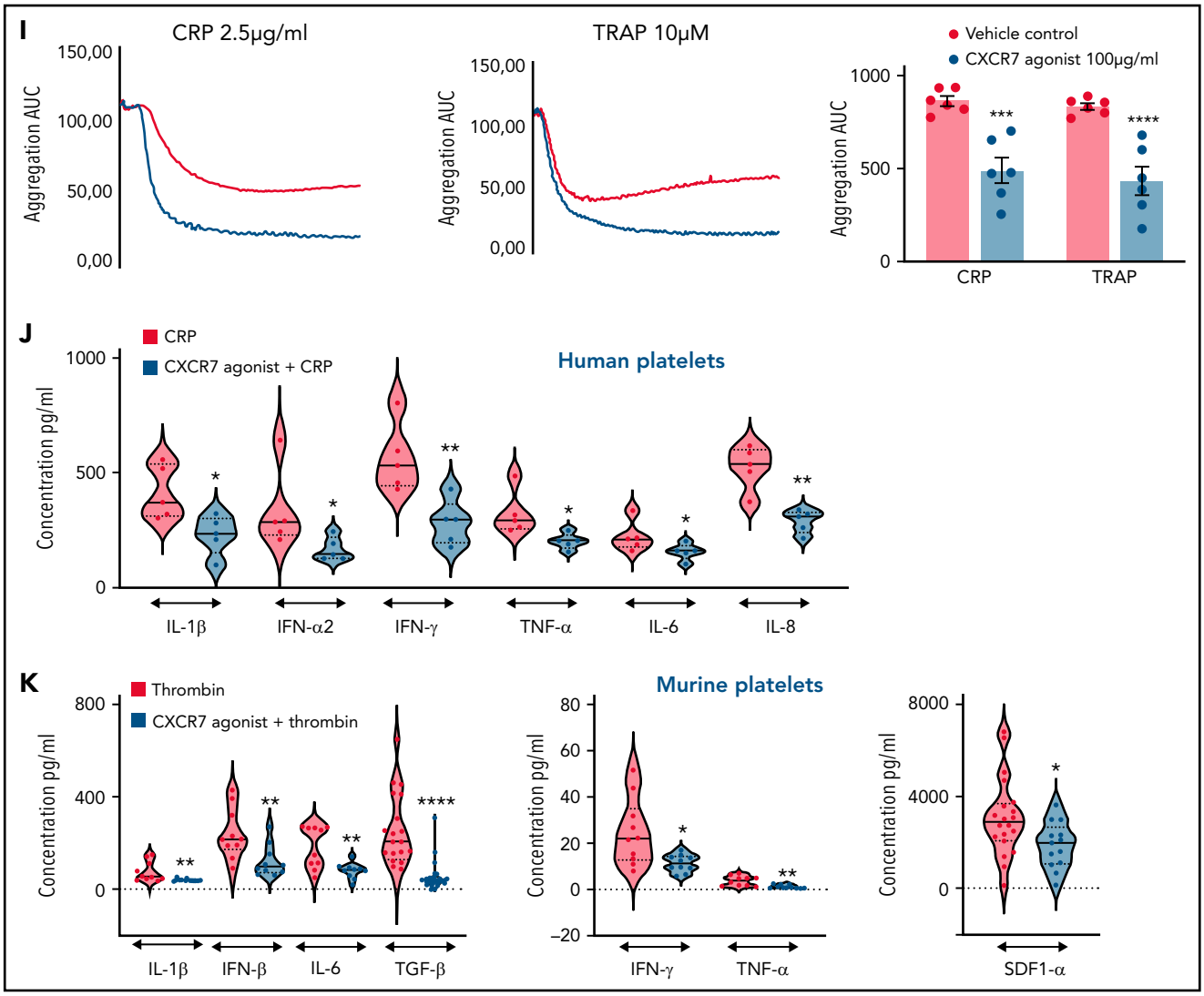

Figure 5. CXCR7 agonist–induced changes in platelet lipidome affect activatory mediators and functional response. (A) Western blot analysis showing phosphorylation of PLCγ and Src family kinases in response to CRP (5 µg/mL) stimulation for 10 minutes at room temperature in presence/absence of CXCR7 agonist (100 µg/mL) or vehicle control (1% DMSO) given as a pretreatment of 15 minutes at room temperature. (B) Flow cytometric histogram overlays and data showing CRP (5 µg/mL)-induced intraplatelet calcium mobilization detected with Fluo-3 AM (5 µM) in presence/absence of CXCR7 agonist (100 µg/mL)/vehicle control in whole blood assay gating for platelet-specific marker CD42b (anti-human CD42b-PE). Data are mean ± SEM from 5 experiments; $^{**}P < .0077$, $^{****}P < .0001$ vs CRP using ANOVA followed by Bonferroni's multiple comparison test. (C) Phosphorylation of PKC, PI3K, Akt, and p38MAPK triggered by CRP (5 µg/mL) in presence/absence of CXCR7 agonist (100 µg/mL)/vehicle control (1% DMSO). In panels A and C, data are representative of 3 western blots. (D) SICM imaging showed reduced initial spreading rate on collagen (100 µg/mL)-coated surfaces in presence/absence of CXCR7 agonist (50 µg/mL) or vehicle control (0.1% DMSO). (E) Decreased final spreading area of CXCR7 agonist (50 µg/mL)-treated platelets on collagen- and fibrinogen (100 µg/mL)-coated surfaces with respect to vehicle control. Data are mean ± SEM from 3 experiments. Student *t* test; $^{*}P < .05$, $^{***}P < .001$. (F) SICM stiffness mapping showing reduced elastic modulus of platelets pretreated with CXCR7 agonist (50 µg/mL) while interacting with fibrinogen-coated surfaces. Plots show geometric mean ± SEM from 3 experiments. Student *t* test, $^{***}P < .001$. Number of platelets: 5 to 6 in panel D, 18 to 24 in panel E, and 25 to 31 in panel F. (G) Surface expression of CD63 (δ-granule release, anti-human CD63-FITC) detected by flow cytometry following CRP (5 µg/mL)-induced activation for 30 minutes at room temperature in presence/absence of CXCR7 agonist (100 µg/mL)/vehicle control (1% DMSO) given as a pretreatment of 30 minutes at room temperature. Data are mean ± SEM from 4 experiments; $^{**}P < .002$, $^{****}P < .0001$ using ANOVA followed by Sidak's multiple comparison text. (H) CRP (2.5 µg/mL) and TRAP (10 µM) induced release of ATP from δ-granules in presence/absence of CXCR7 agonist (100 µg/mL)/vehicle control ascertained by lumi-aggregometry. Extracellular ATP released from activated platelets was assessed employing the luciferase bioluminescent assay, and the amount of ATP release was calculated using the exogenously added ATP standard with aggrolink-8 software (ChronoLog). (I) Corresponding aggregatory response to CRP (2.5 µg/mL) and TRAP (10 µM) for a duration of 10 minutes at 37°C and under a stirring speed of 1000 revolutions per minute (RPM) in presence/absence of CXCR7 agonist (100 µg/mL)/vehicle control. In panels H through I, data are mean ± SEM from 6 experiments with healthy donors; $^{***}P = .0002$, $^{****}P < .0001$ using ANOVA followed by Sidak's multiple comparison text. Washed human (200×10^6/sample) and murine (100×10^6/sample) were preincubated with CXCR7 agonist (100 µg/mL) or vehicle control (1% DMSO) for 30 minutes and thereafter stimulated with platelet agonists as specified below for 30 and 15 minutes, respectively, at room temperature. Samples were then centrifuged to collect activated platelet supernatant. Violin plots (line denotes median) showing release of inflammatory mediators from (J) CRP (5 µg/mL)-activated human (Legendplex human 13-plex inflammation panel) and (K) thrombin (0.1 U/mL)-activated murine platelets (Legendplex murine 13-plex inflammation panel) evaluated by cytometric bead arrays. In panels J and K, $^{*}P < .05$, $^{**}P < .01$, $^{****}P < .0001$ using Mann-Whitney *U* test for each analyte. Data are plotted as mean ± SEM from 5 healthy donors in panel J and from 10 mice in panel K. DMSO, dimethyl sulfoxide.

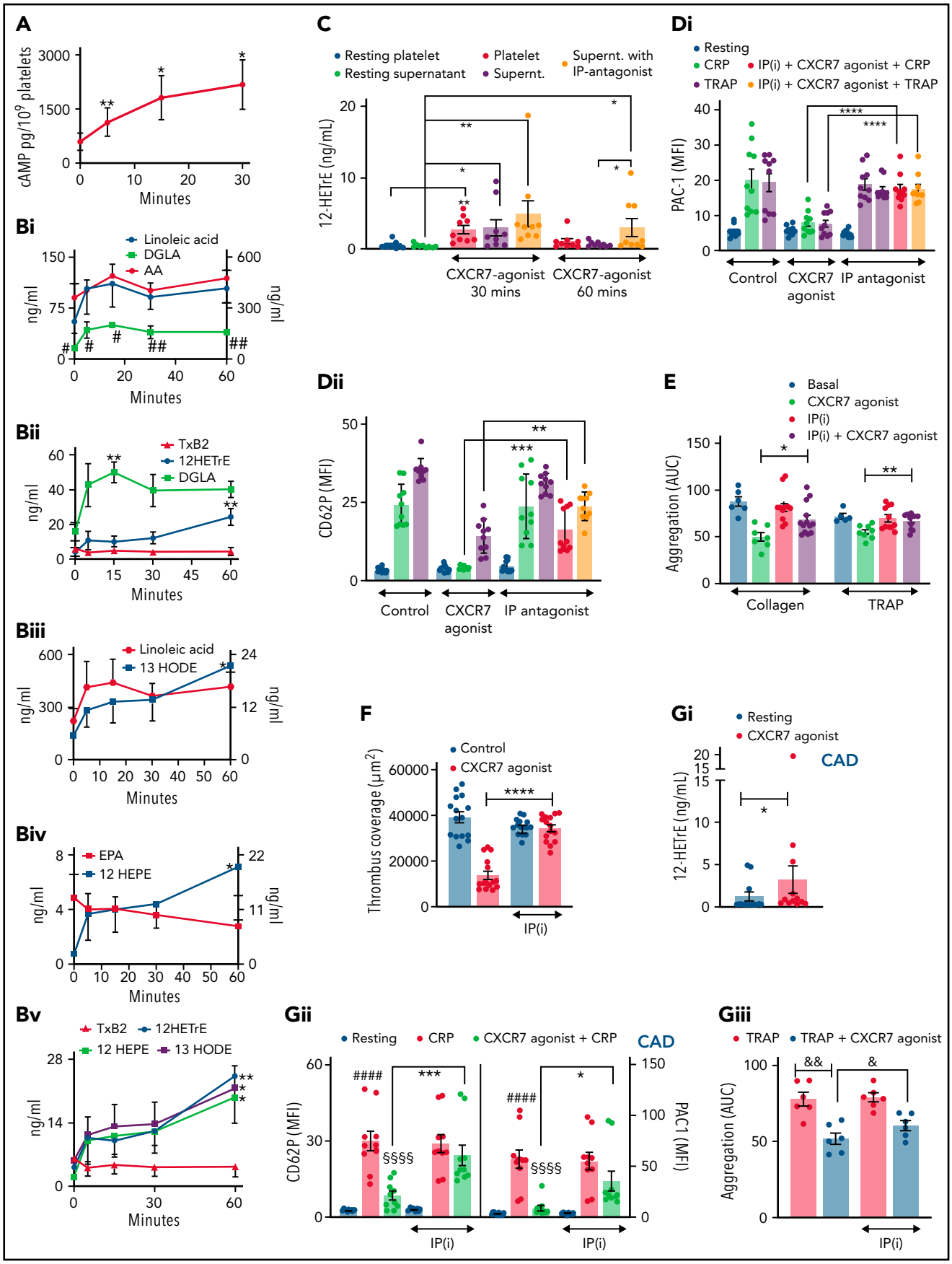

Figure 6.

reduced CD62P expression (Figure 7A), $\alpha_{IIb}\beta_3$-integrin activation (Figure 7B), platelet response in HIPA test (Figure 7C), and thrombus formation (Figure 7D) triggered by HIT^+ sera ex vivo. 12-LOX plays a vital role in mediating prothrombotic response triggered through FcγRIIA.[58,65] Moreover, both TxA2[66] and 12-HETE[67] have prominent proinflammatory attributes. Therefore, 12-LOX is a potential antiplatelet drug target,[63] like COX-1. CXCR7 agonist significantly reduced HIT sera-induced generation of thromboinflammatory COX-1–derived TxA2 and platelet 12-LOX-derived 12-HETE (Figure 7E), which could have contributed to its antithrombotic effects (Figure 7A-D) in identical experimental settings ex vivo.

Neutrophils aggravate HIT-associated thrombotic complications.[8] CXCR7 agonist significantly decreased neutrophil CD11b activation (Figure 7F) triggered by HIT^+ sera. Combined with its effect on platelet CD62P exposure and $\alpha_{IIb}\beta_3$-integrin activation that engage in interaction with P-selectin glycoprotein ligand (PSGL-1) and Mac-1 complex (CD11b/CD18), CXCR7 agonist significantly reduced platelet-neutrophil aggregate formation triggered by HIT^+ sera and IgG fractions (Figure 7Gi-Gii; supplemental Figure 9); moreover, it counteracted release of thromboinflammatory mediators (eg, IL-1β, IFN-γ, sCD40L, TNF-α, sP-selectin, neutrophil chemoattractant IL-8, and thrombogenic TF) from HIT^+ IgG-treated platelets (Figure 7H). Therefore, therapeutics targeting ACKR3/CXCR7 may be useful to cope with HIT-associated thromboinflammation, as well as in acute inflammatory pathologies that trigger platelet FcγRIIA, as in vaccine-induced immune thrombotic thrombocytopenia[68] that closely resembles HIT or antibodies against SARS-CoV2.[3,6]

Discussion

Capitalizing on our extensive work exploring platelet CXCL12/SDF1α-CXCR4- ACKR3/CXCR7 axis in experimental[26,27] and clinical studies,[16,17,29,48] novel translational findings of the current investigation are (1) Platelet ACKR3/CXCR7 surface expression is enhanced post-MI, which could be therapeutically targeted by a CXCR7 agonist to reduce thrombotic response post-MI in vivo (murine model) and ex vivo (ACS patients). (2) CXCR7 agonist checked arterial thrombosis in vivo without compromising basal hemostasis. (3) CXCR7 agonist also regulated thromboinflammatory platelet response triggered by HIT^+ sera/IgG ex vivo and in peripheral circulation of mice post-MI and arterial injury in vivo. (4) ACKR3/CXCR7 ligation modulated the platelet lipidome to limit metabolism and release of thrombotic and atherogenic lipid mediators while favoring the generation of antiplatelet lipids in healthy subjects and CAD patients ex vivo. (5) 12-HETrE–mediated engagement of Gαs-coupled IP receptor following ACKR3/CXCR7 ligation triggered the platelet inhibitory AC-cAMP–protein kinase A cascade to regulate thromboinflammatory functions.

ACKR3/CXCR7 primarily as an atypical/noncanonical GPCR shows cell- and ligand-specific functional response.[32] Recently, the cardiovascular significance of ACKR3/CXCR7 has become evident in the hematopoietic-vascular niche,[33] platelets,[16,17,26,27,48] atherosclerosis,[34] and CAD.[16,17,29,48] Its therapeutic potential has been shown in murine models of myocardial infarction,[18,19,21] atherosclerosis,[34] and in impeding pulmonary fibrosis[33] by employing pharmacological CXCR7 agonists[32] and lineage-specific *cxcr7*-deficient mice.[19,34] Systemic administration of CXCR7 agonist in the current investigation may have exerted significant impact on both the target organ (myocardium), as previously described,[19,21] and cells in peripheral circulation, including platelets. The currently observed antithrombotic effect adds to its therapeutic value. Differences in relative platelet CXCR4 and ACKR3/CXCR7 availability between murine MI models, stable CAD, and ACS patients put aside, platelet ACKR3/CXCR7 surface expression is low under physiological conditions,[26,27] as are levels of its physiological ligands (CXCL12/SDF1-α, MIF). However, a significant increment in platelet ACKR3/CXCR7 is observed post-MI in mice and ACS patients. ACKR3/CXCR7 is not directly involved in executing thrombotic-hemostatic platelet functions. Therefore, deletion of *cxcr7* from murine platelets may not exhibit a drastic platelet-centered phenotype under physiological conditions. Attempting to close the translational gap between experimental and clinical research, we validated our observations in CAD patients exhibiting increased platelet ACKR3/CXCR7 surface expression[16,17,48] with experimental evidence from human system ex vivo/in vitro and murine models in vivo. Antithrombotic effects of CXCR7 agonist ascertained in whole blood from ACS patients, closely resembling physiological conditions ex vivo, corroborated with

Figure 6. CXCR7 agonist–induced generation of antiplatelet lipid 12-HETrE and platelet inhibitory mediator cAMP. Washed platelets (200×10^6/sample) from n = 5 healthy donors were treated with CXCR7 agonist (100 μg/mL) for 0, 5, 15, and 30 minutes at room temperature. Thereafter platelet pellets were collected by centrifugation and used for detection of cAMP levels by LC-ESI-MS/MS analysis. (A) Gradual elevation in intraplatelet cAMP in response to CXCR7 agonist (100 μg/mL); $^*P < .05$, $^{**}P < .01$ vs 0 minute by Wilcoxon matched-pairs signed rank test, n = 5 donors. Washed human platelets (200×10^6/sample) from n = 5 healthy donors were treated with CXCR7 agonist (100 μg/mL) for 0, 5, 15, 30, and 60 minutes at room temperature. Intraplatelet levels of (Bi) linoleic acid (right y-axis), AA, and DGLA (left y-axis); (Bii) DGLA, 12-HETrE, and $TxA(B)_2$; (Biii) linoleic acid (left y-axis) and 13-HODE (right y-axis); (Biv) EPA (left y-axis) and 12-HEPE (right y-axis); and (Bv) 12-HETrE, 12-HEPE, and 13-HODE as compared with $TxA(B)_2$. $\#P < .05$ and $\#\#P < .01$ vs AA; $^*P < .05$, $^{**}P < .01$ vs 0 minute using Welch's *t* test. (C) Washed platelets (300×10^6/sample) from n = 9 healthy donors were treated with CXCR7 agonist (100 μg/mL) or vehicle control (1% DMSO) for 30 and 60 minutes at room temperature. IP receptor antagonist (RO-1138452 10 μM) was given as a pretreatment before CXCR7 agonist for 15 minutes at room temperature. At the end of incubation period, the supernatants were separated from the platelet pellets by centrifugation, and both were used for lipid extraction and subsequent targeted lipidomics analysis for 12-HETrE. Data are mean ± SEM. The significance levels for the corrected (FDR) *P* values are given using nonparametric paired Wilcoxon signed rank test with statistical significance $^*P < .05$, $^{**}P < .01$. Experiments done with blood from healthy donors (n = 5) showing inhibitory effect of CXCR7 agonist (100 μg/mL) on CRP (5 μg/mL) and TRAP (25 μM)-induced platelet (Di) PAC-1 binding, (Dii) CD62P surface expression (flow cytometry), (E) collagen and TRAP-induced aggregation (whole blood impedance aggregometry), and (F) thrombus formation was counteracted by IP receptor antagonist (RO-1138452 10 μM) given as a pretreatment before CXCR7 agonist for 15 minutes at room temperature. Data are mean ± SEM from 5 experiments with healthy donors. $^*P < .05$, $^{**}P < .01$, $^{***}P < .001$, $^{****}P < .0001$ with ANOVA followed by Sidak's multiple comparison test. (Gi) Washed platelets from CAD patients (Table 2; n = 12) were treated with vehicle control (1% DMSO) or CXCR7 agonist (100 μg/mL) for 30 minutes at room temperature and processed for targeted lipidomics analysis for 12-HETrE. CXCR7 agonist treatment to CAD patient platelets ex vivo significantly increased 12-HETrE levels. Data are mean ± SEM. The significance levels for the FDR corrected *P* values are given using nonparametric paired Wilcoxon signed rank test with statistical significance $^*P < .05$. (Gii-Giii) Inhibitory effect of CXCR7 agonist (100 μg/mL) observed in CAD patients on (Gii) platelet CD62P surface expression, PAC-1 binding (n = 5), and (Giii) TRAP induced aggregation (n = 6) was counteracted in presence of IP receptor antagonist (RO-1138452 10 μM) given as a pretreatment before CXCR7 agonist for 15 minutes at room temperature. In panels Gii through Giii, data are mean ± SEM; $\#\#\#\#P < .0001$ vs resting; §§§§$P < .0001$ vs CRP, $^*P < .02$, $^{***}P < .001$; &&$P < .002$, &$P < .02$ with ANOVA followed by Sidak's multiple comparison test. DMSO, dimethyl sulfoxide; Supernt., supernatant.

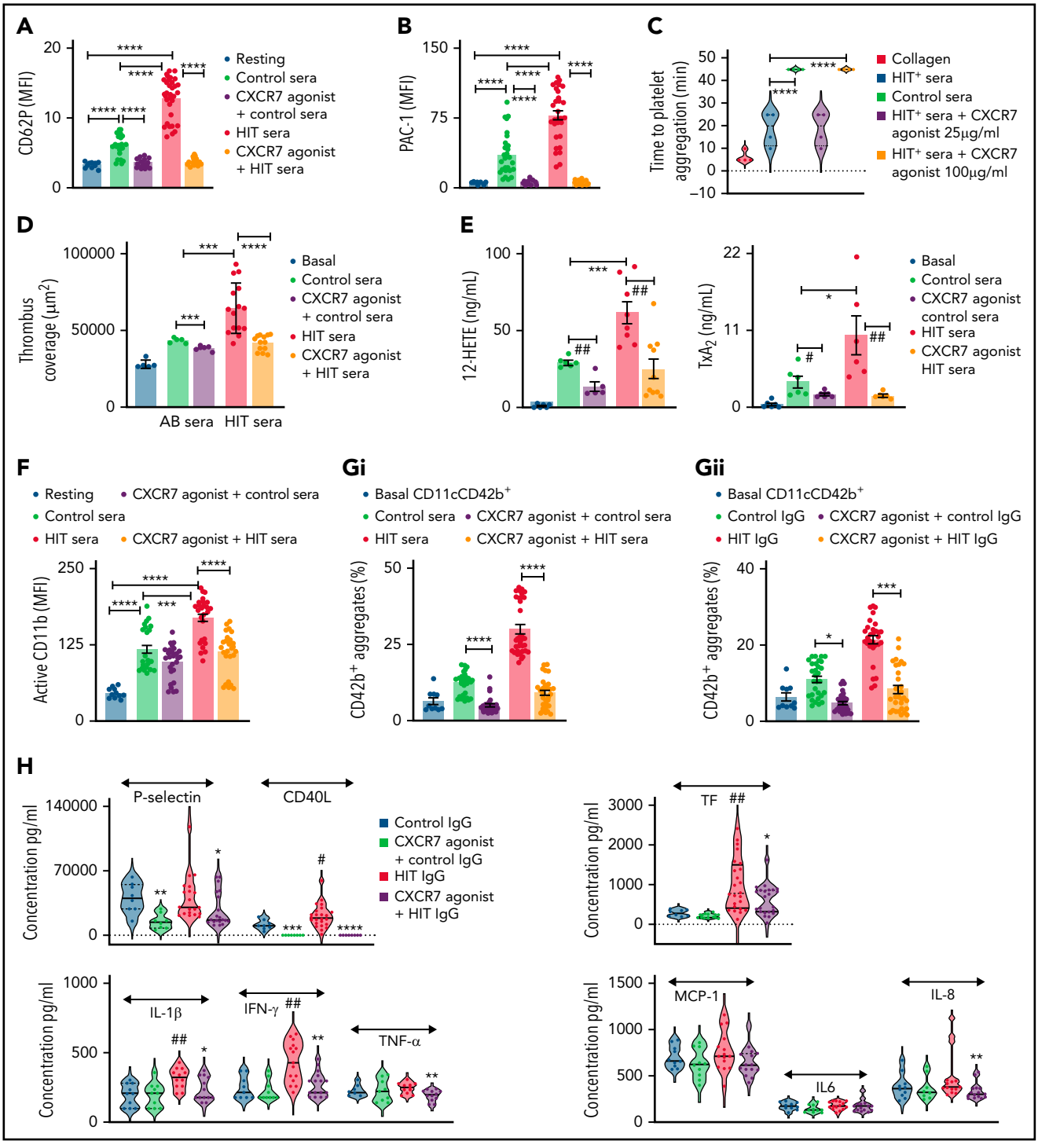

Figure 7. CXCR7 agonist counteracts thrombotic and thromboinflammatory response elicited by HIT sera/IgG. Whole blood assays with heparinized (0.2 IU/mL) blood from healthy donors (n = 5) was carried out in presence of control sera (n = 3) and HIT$^+$ patient sera (n = 3) incubated at 1:10 vol/vol dilution for 1 hour at room temperature. CXCR7 agonist (100 µg/mL) or vehicle control (1% DMSO) was given as a pretreatment for 30 minutes at room temperature. HIT$^+$ patient sera induced (A) platelet CD62P surface expression and (B) PAC-1 binding denoting $\alpha_{IIb}\beta_3$-integrin activation ex vivo. (C) HIPA assay performed with isolated washed platelets from 3 healthy donors in presence/absence of CXCR7 agonist (25 and 100 µg/mL) or vehicle control shows an inhibitory effect of CXCR7 agonist. (D) Ex vivo thrombus formation was performed in heparinized (0.2 IU/mL) blood from healthy donors (n = 5) over collagen-coated surface in presence of control sera (n = 3) and HIT$^+$ patient sera (n = 3) in presence/absence of CXCR7 agonist (100 µg/mL) or vehicle control. In panels A through D, *P < .05, ***P < .001, ****P < .0001 using ANOVA followed by Sidak's multiple comparison test. (E) Targeted lipidomics analysis for oxylipins showed that ex vivo treatment with control sera (n = 3), HIT$^+$ patient sera (n = 3), HIT$^+$ patient sera (n = 3) for 1 hour at room temperature induced generation of COX-1–derived TxA2 and platelet 12-LOX–derived 12-HETE, which was significantly counteracted in the presence of CXCR7 agonist (100 µg/mL) given as a pretreatment of 30 minutes at room temperature. *P < .05, #P < .05, ##P < .01, ***P < .001 with Wilcoxon signed rank test. (F) Neutrophil CD11b (anti-human active CD11b-FITC) activation ex vivo in heparinized (0.2 IU/mL) blood from healthy donors (n = 5) in response to control sera (n = 3) or sera from HIT$^+$ patients (n = 3) (at 1:10 vol/vol dilution) in presence/absence of CXCR7 agonist (100 µg/mL) or vehicle control. Diagram showing formation of CD42b$^+$ (anti-human CD42b-FITC)-CD11c$^+$ (anti-human CD11c-APC) platelet-neutrophil aggregates ex vivo in heparinized (0.2 IU/mL) blood from healthy donors (n = 5 donors) treated with (Gi) sera or (Gii) corresponding isolated IgG fractions from control healthy subjects and HIT$^+$ patients

those detected post-MI and arterial injury in CXCR7 agonist administered mice in vivo, offering the possibility of preclinical validation. Enhanced platelet ACKR3/CXCR7 availability post-MI may regulate platelet response and reduce thromboinflammatory platelet-leukocyte interactions in circulation in presence of an adequate ligand. Considering increased formation of platelet-monocyte aggregates in ACS patients, attributed to elevated sP-selectin, IL-6 levels, and its association with enhanced risk of ACS,[7] CXCR7 agonist offered regulation on platelet CD62P, plasma IL-6, and platelet-leukocyte aggregate formation post-MI seem favorable.

Cxcr7-deficient hyperlipidemic mice show increased neointima formation and macrophage accumulation at carotid lesions, whereas administration of CXCR7 agonist (CCX771) ablates atheroprogression[34] and reduces plasma cholesterol by prompting uptake of very-low-density lipoproteins in the adipose tissue.[34] Currently, we evidenced an unprecedented influence of ACKR3/CXCR7 ligation on the platelet lipidome in reducing the generation of prothrombotic LPCs, LPIs, and DGs, levels of which are elevated in platelets from CAD patients,[29] notwithstanding antiplatelet or statin therapy. In thrombin-activated platelets from healthy subjects and CAD patients alike, CXCR7 agonist also reduced the generation and release of AA, HHT, TxA2, and 12-HETE. Such a unique influence of ACKR3/CXCR7 may check atherothrombosis by regulating generation of prothrombotic lipids and atherogenic LPCs carried by platelets and platelet-derived microvesicles.[60] However, this needs to be experimentally validated in atherosclerosis-prone murine models. Apparently, CXCR7 agonist–mediated effects have an unexpected advantage over ASA, which inhibits COX-1 metabolism downstream of phospholipases, whereas levels of LPIs, LPCs, and DGs remain elevated in CAD patients,[29] and thrombogenic 12-HETE and HETE phospholipids can be formed by 12-LOX.[59] Moreover, CXCR7 agonist potentiated the generation of antiplatelet lipids (DGLA, 12-HETrE,[64] 13-HODE, 12-HEPE),[63] interestingly limiting 12-LOX–metabolized prothrombotic, procoagulatory AA-derived 12-HETE but promoting DGLA- and EPA-derived antiplatelet 12-LOX products (ie, 12-HETrE and 12-HEPE, respectively). Although mechanistic reason behind this preference remains to be deciphered, a deliberate shift favoring antiplatelet lipids seems promising. Attributed to 12-HETrE, ACKR3/CXCR7 ligation coordinated with Gαs-coupled IP receptor to elevate cAMP levels and regulate thrombotic functions, an effect contrary to the prothrombotic actions of platelet CXCR4.[29-31] Gαi-coupled CXCR4 triggers a canonical signaling cascade following CXCL12/SDF-1α binding that decreases cAMP levels[30,31] while inducing intracellular calcium mobilization, PI3K-Akt activation, and release of ATP and TxA2, which is contrary to the influence of ACKR3/CXCR7 on platelet activatory signaling cascade (visual/graphical abstract).

Acute or chronic thromboinflammatory processes may cause cardiovascular complications.[1,2,5] Impact of antiplatelet therapies on inflammatory mediators like hsCRP, IL-6, and TNF-α has been deduced in clinical studies.[14] Currently, CXCR7 agonist decreased thromboinflammatory release from CRP (GPVI)- and thrombin (PAR)-activated platelets and those triggered by HIT^+ IgG (FcγRIIA). ACKR3/CXCR7 ligation also counteracted HIT^+ sera/IgG-induced platelet and neutrophil activation, platelet-neutrophil interactions, and generation of proinflammatory oxylipins TxA2[66] and 12-HETE.[67] Apart from its antiplatelet effects, CXCR7 agonist may also influence inflammatory functions of ACKR3/CXCR7-expressing immune cells, epithelium, and endothelium,[69] much like the effect of antiplatelet ASA on COX-expressing cells. Considering the inhibitory impact of CXCR7 agonist (VUF11207) on thrombotic and thromboinflammatory functions, this opens a new vista of investigation in validating the therapeutic potential of ACKR3/CXCR7 in acute/chronic inflammatory pathologies that trigger thrombotic complications.[5]

Presently, we have substantiated our previously recognized[16,17,23,27] translational implications of ACKR3/CXCR7 in platelet pathophysiology. In CAD patients, increased platelet CXCR4 and ACKR3/CXCR7 expression is associated with improved prognosis.[16,17] CXCR4 is relatively more abundant on platelets under physiological conditions,[26] whereas ACKR3/CXCR7 might be transiently induced post-MI[16] by circulatory or platelet-associated CXCL12/SDF1α in ACS patients[15,24] as observed in experimental studies.[26] ACKR3/CXCR7 may offer a novel therapeutic paradigm to fine-tune thrombotic and thromboinflammatory platelet response without affecting physiological/basal hemostasis or antagonizing the function and surface availability of platelet receptors. There is no evidence that ACKR3/CXCR7 interacts with these receptors or their respective ligands. Therefore, pharmacological targeting of ACKR3/CXCR7 to overcome platelet-driven thromboinflammation may diverge from the direct inhibitory effects of antiplatelet therapeutics that act as receptor antagonists (P_2Y_{12}, $GP_{IIbIIIa}$, PAR-1 antagonists). Translational implications of exploiting ACKR3/CXCR7 may be realized by (a) assessing the therapeutic "time window" of increased ACKR3/CXCR7 availability as a potential drug target on circulating platelets post-MI in longitudinal clinical studies with ACS patients and (b) by extending its therapeutic validation in HIT and other thromboinflammatory pathologies.

Acknowledgments

This work was supported by funding from the German Research Foundation (DFG) project number 374031971-TRR240, Deutsche Stiftung für Herzforschung (DSHF-F/22/17) to M. Chatterjee, and DFG project number BO3786/3-1 to O.B.

Authorship

Contribution: M. Cebo, K.D., and X.F. performed lipidomics analysis; M.C.M. performed intravital microscopy (IVM); F.E. performed thromboelastography and Legendplex analysis; J.R. and H.v.E. performed SICM; N.F. analyzed cAMP levels; J.S. analyzed the MI/RI model; A.W. analyzed tail bleeding time; L.P. characterized HIT patients; D.R. analyzed clinical data; T.E.S. supervised SICM; M.L. supervised lipidomics analysis with

Figure 7 (continued) (n = 3 each) at 1:10 vol/vol dilution for 1 hour at room temperature in presence/absence of CXCR7 agonist (100 μg/mL). In panels F through G, $*P < .05$, $***P < .001$, $****P < .0001$ using ANOVA followed by Sidak's multiple comparison test. Washed human platelets (200×10^6/sample) from n = 5 donors were pretreated with CXCR7 agonist (100 μg/mL) or vehicle control for 30 minutes at room temperature and then with IgG fractions from control or HIT^+ patient sera (n = 3 each) at 1:10 vol/vol for 1 hour at room temperature. Activated platelet supernatants were collected and analyzed by cytometric bead array (Legendplex 13-plex human inflammation panel, 10-plex human thrombosis panel). (H) Violin plots (solid line denotes median) showing levels of proinflammatory mediators and chemoattractants in platelet releasate. Data represent mean ± SEM; $\#P < .05$, $\#\#P < .01$ vs control IgG; $*P < .05$, $**P < .01$, $***P < .001$, $****P < .0001$ vs HIT^+ IgG using Mann-Whitney *U* test for each inflammatory mediator.

M. Chatterjee; O.B. (IVM), T.G. (CAD cohort), T.B. (HIT), and M.G. (MI/RI model) collaborated in the project; and M. Chatterjee was involved in the project design, supervision, experimentation, data analysis, and manuscript writing.

Conflict-of-interest disclosure: The authors declare no competing financial interests.

ORCID profiles: M.C.M., 0000-0001-9197-4940; F.E., 0000-0002-9564-2000; J.R., 0000-0002-1976-9245; H.v.E., 0000-0003-0759-2056; T.E.S., 0000-0001-5643-8384; M.L., 0000-0002-1318-0974; M. Chatterjee, 0000-0002-3428-4107.

Correspondence: Madhumita Chatterjee, Department of Cardiology and Angiology, University Hospital Tübingen, Otfried-Müller-Straße 10, 72076, Tübingen, Germany; e-mail: madhumita.chatterjee@med.uni-tuebingen.de.

Footnotes

Submitted 25 June 2021; accepted 30 November 2021; prepublished online on *Blood* First Edition 14 December 2021. DOI 10.1182/blood.2021013097.

*M. Cebo and K.D. are joint first authors.

For original data, please contact madhumita.chatterjee@med.uni-tuebingen.de.

The online version of this article contains a data supplement.

There is a *Blood* Commentary on this article in this issue.

The publication costs of this article were defrayed in part by page charge payment. Therefore, and solely to indicate this fact, this article is hereby marked "advertisement" in accordance with 18 USC section 1734.

REFERENCES

1. d'Alessandro E, Becker C, Bergmeier W, et al; Scientific Reviewer Committee. Thrombo-inflammation in cardiovascular disease: an Expert Consensus Document from the Third Maastricht Consensus Conference on Thrombosis. *Thromb Haemost.* 2020;120(4):538-564.
2. Rayes J, Bourne JH, Brill A, Watson SP. The dual role of platelet-innate immune cell interactions in thrombo-inflammation. *Res Pract Thromb Haemost.* 2019;4(1):23-35.
3. Althaus K, Marini I, Zlamal J, et al. Antibody-induced procoagulant platelets in severe COVID-19 infection. *Blood.* 2021;137(8):1061-1071.
4. Manne BK, Denorme F, Middleton EA, et al. Platelet gene expression and function in patients with COVID-19. *Blood.* 2020;136(11):1317-1329.
5. McFadyen JD, Stevens H, Peter K. The emerging threat of (Micro)thrombosis in COVID-19 and its therapeutic implications. *Circ Res.* 2020;127(4):571-587.
6. Zaid Y, Puhm F, Allaeys I, et al. Platelets can associate with SARS-Cov-2 RNA and are hyperactivated in COVID-19. *Circ Res.* 2020;127(11):1404-1418.
7. Wang J, Zhang S, Jin Y, Qin G, Yu L, Zhang J. Elevated levels of platelet-monocyte aggregates and related circulating biomarkers in patients with acute coronary syndrome. *Int J Cardiol.* 2007;115(3):361-365.
8. Perdomo J, Leung HHL, Ahmadi Z, et al. Neutrophil activation and NETosis are the major drivers of thrombosis in heparin-induced thrombocytopenia. *Nat Commun.* 2019;10(1):1322.
9. Guo L, Rondina MT. The era of thromboinflammation: platelets are dynamic sensors and effector cells during infectious diseases. *Front Immunol.* 2019;10:2204.
10. Weber C, Badimon L, Mach F, van der Vorst EPC. Therapeutic strategies for atherosclerosis and atherothrombosis: past, present and future. *Thromb Haemost.* 2017;117(7):1258-1264.
11. Salah HM, Mehta JL. Meta-analysis of the effect of aspirin on mortality in COVID-19. *Am J Cardiol.* 2021;142:158-159.
12. Elia E, Montecucco F, Portincasa P, Sahebkar A, Mollazadeh H, Carbone F. Update on pathological platelet activation in coronary thrombosis. *J Cell Physiol.* 2019;234(3):2121-2133.
13. Middleton EA, He XY, Denorme F, et al. Neutrophil extracellular traps contribute to immunothrombosis in COVID-19 acute respiratory distress syndrome. *Blood.* 2020;136(10):1169-1179.
14. Oikonomou E, Leopoulou M, Theofilis P, et al. A link between inflammation and thrombosis in atherosclerotic cardiovascular diseases: clinical and therapeutic implications. *Atherosclerosis.* 2020;309:16-26.
15. Wurster T, Stellos K, Haap M, et al. Platelet expression of stromal-cell-derived factor-1 (SDF-1): an indicator for ACS? *Int J Cardiol.* 2013;164(1):111-115.
16. Rath D, Chatterjee M, Borst O, et al. Expression of stromal cell-derived factor-1 receptors CXCR4 and CXCR7 on circulating platelets of patients with acute coronary syndrome and association with left ventricular functional recovery. *Eur Heart J.* 2014;35(6):386-394.
17. Rath D, Chatterjee M, Meyer L, et al. Relative survival potential of platelets is associated with platelet CXCR4/CXCR7 surface exposure and functional recovery following STEMI. *Atherosclerosis.* 2018;278:269-277.
18. Ishizuka M, Harada M, Nomura S, et al. CXCR7 ameliorates myocardial infarction as a β-arrestin-biased receptor [published correction appears in *Sci Rep.* 2021;11(1):12340]. *Sci Rep.* 2021;11(1):3426.
19. Hao H, Hu S, Chen H, et al. Loss of endothelial CXCR7 impairs vascular homeostasis and cardiac remodeling after myocardial infarction: implications for cardiovascular drug discovery. *Circulation.* 2017;135(13):1253-1264.
20. Hu X, Dai S, Wu WJ, et al. Stromal cell derived factor-1 alpha confers protection against myocardial ischemia/reperfusion injury: role of the cardiac stromal cell derived factor-1 alpha CXCR4 axis. *Circulation.* 2007;116(6):654-663.
21. Zhang S, Yue J, Ge Z, Xie Y, Zhang M, Jiang L. Activation of CXCR7 alleviates cardiac insufficiency after myocardial infarction by promoting angiogenesis and reducing apoptosis. *Biomed Pharmacother.* 2020;127:110168.
22. Walsh TG, Poole AW. Do platelets promote cardiac recovery after myocardial infarction: roles beyond occlusive ischemic damage. *Am J Physiol Heart Circ Physiol.* 2018;314(5):H1043-H1048.
23. Rath D, Chatterjee M, Bongartz A, et al. Platelet surface expression of SDF-1 is associated with clinical outcomes in the patients with cardiovascular disease. *Platelets.* 2017;28(1):34-39.
24. Stellos K, Ruf M, Sopova K, et al. Plasma levels of stromal cell-derived factor-1 in patients with coronary artery disease: effect of clinical presentation and cardiovascular risk factors. *Atherosclerosis.* 2011;219(2):913-916.
25. Müller II, Müller KA, Schönleber H, et al. Macrophage migration inhibitory factor is enhanced in acute coronary syndromes and is associated with the inflammatory response. *PLoS One.* 2012;7(6):e38376.
26. Chatterjee M, Seizer P, Borst O, et al. SDF-1α induces differential trafficking of CXCR4-CXCR7 involving cyclophilin A, CXCR7 ubiquitination and promotes platelet survival. *FASEB J.* 2014;28(7):2864-2878.
27. Chatterjee M, Borst O, Walker B, et al. Macrophage migration inhibitory factor limits activation-induced apoptosis of platelets via CXCR7-dependent Akt signaling. *Circ Res.* 2014;115(11):939-949.
28. Strüßmann T, Tillmann S, Wirtz T, Bucala R, von Hundelshausen P, Bernhagen J. Platelets are a previously unrecognised source of MIF. *Thromb Haemost.* 2013;110(5):1004-1013.
29. Chatterjee M, Rath D, Schlotterbeck J, et al. Regulation of oxidized platelet lipidome:

implications for coronary artery disease. *Eur Heart J*. 2017;38(25):1993-2005.

30. Walsh TG, Harper MT, Poole AW. SDF-1α is a novel autocrine activator of platelets operating through its receptor CXCR4. *Cell Signal*. 2015;27(1):37-46.

31. Ohtsuka H, Iguchi T, Hayashi M, et al. SDF-1α/CXCR4 signaling in lipid rafts induces platelet aggregation via PI3 kinase-dependent Akt phosphorylation. *PLoS One*. 2017;12(1):e0169609.

32. Wang C, Chen W, Shen J. CXCR7 targeting and its major disease relevance. *Front Pharmacol*. 2018;9:641.

33. Cao Z, Lis R, Ginsberg M, et al. Targeting of the pulmonary capillary vascular niche promotes lung alveolar repair and ameliorates fibrosis. *Nat Med*. 2016;22(2):154-162.

34. Li X, Zhu M, Penfold ME, et al. Activation of CXCR7 limits atherosclerosis and improves hyperlipidemia by increasing cholesterol uptake in adipose tissue. *Circulation*. 2014; 129(11):1244-1253.

35. Wijtmans M, Maussang D, Sirci F, et al. Synthesis, modeling and functional activity of substituted styrene-amides as small-molecule CXCR7 agonists. *Eur J Med Chem*. 2012;51:184-192.

36. Adlere I, Caspar B, Arimont M, et al. Modulators of CXCR4 and CXCR7/ACKR3 function. *Mol Pharmacol*. 2019;96(6):737-752.

37. Lounsbury N. Advances in CXCR7 modulators. *Pharmaceuticals (Basel)*. 2020; 13(2):33.

38. Peng B, Geue S, Coman C, et al. Identification of key lipids critical for platelet activation by comprehensive analysis of the platelet lipidome. *Blood*. 2018;132(5):e1-e12.

39. Rheinlaender J, Vogel S, Seifert J, et al. Imaging the elastic modulus of human platelets during thrombin-induced activation using scanning ion conductance microscopy. *Thromb Haemost*. 2015;113(2):305-311.

40. Borst O, Münzer P, Alnaggar N, et al. Inhibitory mechanisms of very low-dose rivaroxaban in non-ST-elevation myocardial infarction. *Blood Adv*. 2018;2(6):715-730.

41. Monteiro MD, Goncalves MJ, Sansonetty F, O'Connor JE. Flow cytometric analysis of calcium mobilization in whole-blood platelets. *Curr Protoc Cytom*. 2003;Chapter 9:Unit 9.20.

42. Münzer P, Borst O, Walker B, et al. Acid sphingomyelinase regulates platelet cell membrane scrambling, secretion, and thrombus formation. *Arterioscler Thromb Vasc Biol*. 2014;34(1):61-71.

43. Cebo M, Fu X, Gawaz M, Chatterjee M, Lämmerhofer M. Micro-UHPLC-MS/MS method for analysis of oxylipins in plasma and platelets. *J Pharm Biomed Anal*. 2020; 189:113426.

44. Cebo M, Fu X, Gawaz M, Chatterjee M, Lämmerhofer M. Enantioselective ultra-high performance liquid chromatography-tandem mass spectrometry method based on sub-2μm particle polysaccharide column for chiral separation of oxylipins and its application for the analysis of autoxidized fatty acids and platelet releasates. *J Chromatogr A*. 2020;1624:461206.

45. Calderón C, Rubarth L, Cebo M, Merfort I, Lämmerhofer M. Lipid atlas of keratinocytes and betulin effects on its lipidome profiled by comprehensive UHPLC-MS/MS with data independent acquisition using targeted data processing. *Proteomics*. 2020;20(11): e1900113.

46. Cebo M, Schlotterbeck J, Gawaz M, Chatterjee M, Lämmerhofer M. Simultaneous targeted and untargeted UHPLC-ESI-MS/MS method with data-independent acquisition for quantification and profiling of (oxidized) fatty acids released upon platelet activation by thrombin. *Anal Chim Acta*. 2019;2094:57-69.

47. Tsugawa H, Cajka T, Kind T, et al. MS-DIAL: data-independent MS/MS deconvolution for comprehensive metabolome analysis. *Nat Methods*. 2015;12(6):523-526.

48. Rath D, Chatterjee M, Borst O, et al. Platelet surface expression of stromal cell-derived factor-1 receptors CXCR4 and CXCR7 is associated with clinical outcomes in patients with coronary artery disease. *J Thromb Haemost*. 2015;13(5):719-728.

49. Ziegler M, Elvers M, Baumer Y, et al. The bispecific SDF1-GPVI fusion protein preserves myocardial function after transient ischemia in mice. *Circulation*. 2012;125(5): 685-696.

50. Capodanno D, Bhatt DL, Eikelboom JW, et al. Dual-pathway inhibition for secondary and tertiary antithrombotic prevention in cardiovascular disease. *Nat Rev Cardiol*. 2020;17(4):242-257.

51. Sibbing D, Aradi D, Jacobshagen C, et al; TROPICAL-ACS Investigators. A randomised trial on platelet function-guided de-escalation of antiplatelet treatment in ACS patients undergoing PCI. Rationale and design of the Testing Responsiveness to Platelet Inhibition on Chronic Antiplatelet Treatment for Acute Coronary Syndromes (TROPICAL-ACS) Trial. *Thromb Haemost*. 2017;117(1):188-195.

52. van der Meijden PEJ, Heemskerk JWM. Platelet biology and functions: new concepts and clinical perspectives. *Nat Rev Cardiol*. 2019;16(3):166-179.

53. Agbani EO, Poole AW. Procoagulant platelets: generation, function, and therapeutic targeting in thrombosis. *Blood*. 2017;130(20):2171-2179.

54. Lhermusier T, Chap H, Payrastre B. Platelet membrane phospholipid asymmetry: from the characterization of a scramblase activity to the identification of an essential protein mutated in Scott syndrome. *J Thromb Haemost*. 2011;9(10):1883-1891.

55. Chatterjee M. Platelet lipidome: dismantling the 'Trojan horse' in the bloodstream. *J Thromb Haemost*. 2020;18(3):543-557.

56. O'Donnell VB, Murphy RC, Watson SP. Platelet lipidomics: modern day perspective on lipid discovery and characterization in platelets. *Circ Res*. 2014;114(7):1185-1203.

57. Slatter DA, Aldrovandi M, O'Connor A, et al. Mapping the human platelet lipidome reveals cytosolic phospholipase A2 as a regulator of mitochondrial bioenergetics during activation. *Cell Metab*. 2016;23(5): 930-944.

58. Yeung J, Tourdot BE, Fernandez-Perez P, et al. Platelet 12-LOX is essential for FcγRIIa-mediated platelet activation. *Blood*. 2014; 124(14):2271-2279.

59. Lauder SN, Allen-Redpath K, Slatter DA, et al. Networks of enzymatically oxidized membrane lipids support calcium-dependent coagulation factor binding to maintain hemostasis. *Sci Signal*. 2017; 10(507):eaan2787.

60. Diehl P, Nienaber F, Zaldivia MTK, et al. Lysophosphatidylcholine is a major component of platelet microvesicles promoting platelet activation and reporting atherosclerotic plaque instability. *Thromb Haemost*. 2019;119(8):1295-1310.

61. Fukushima N, Kohno M, Kato T, et al. Melittin, a metabostatic peptide inhibiting Gs activity. *Peptides*. 1998;19(5):811-819.

62. Kajita S, Iizuka H. Melittin-induced alteration of epidermal adenylate cyclase responses. *Acta Derm Venereol*. 1987;67(4):295-300.

63. Tourdot BE, Ahmed I, Holinstat M. The emerging role of oxylipins in thrombosis and diabetes. *Front Pharmacol*. 2014;4:176.

64. Yeung J, Tourdot BE, Adili R, et al. 12(S)-HETrE, a 12-lipoxygenase oxylipin of dihomo-γ-linolenic acid, inhibits thrombosis via gαs signaling in platelets. *Arterioscler Thromb Vasc Biol*. 2016;36(10):2068-2077.

65. Yeung J, Holinstat M. 12-Lipoxygenase: a potential target for novel anti-platelet therapeutics. *Cardiovasc Hematol Agents Med Chem*. 2011;9(3):154-164.

66. Capra V, Bäck M, Angiolillo DJ, Cattaneo M, Sakariassen KS. Impact of vascular thromboxane prostanoid receptor activation on hemostasis, thrombosis, oxidative stress, and inflammation. *J Thromb Haemost*. 2014; 12(2):126-137.

67. Kulkarni A, Nadler JL, Mirmira RG, Casimiro I. Regulation of tissue inflammation by 12-lipoxygenases. *Biomolecules*. 2021;11(5):717.

68. Greinacher A, Thiele T, Warkentin TE, Weisser K, Kyrle PA, Eichinger S. Thrombotic thrombocytopenia after ChAdOx1 nCov-19 vaccination. *N Engl J Med*. 2021;384(22): 2092-2101.

69. Koenen J, Bachelerie F, Balabanian K, Schlecht-Louf G, Gallego C. Atypical chemokine receptor 3 (ACKR3): a comprehensive overview of its expression and potential roles in the immune system. *Mol Pharmacol*. 2019;96(6):809-818.

70. Burkhart JM, Vaudel M, Gambaryan S, et al. The first comprehensive and quantitative analysis of human platelet protein composition allows the comparative analysis of structural and functional pathways. *Blood*. 2012;120(15):e73-e82.

Supplemental Material

Manuscript title: Platelet ACKR3/CXCR7 Favors Anti-Platelet Lipids over an Atherothrombotic Lipidome and Regulates Thrombo-inflammation

Short title for the running head: CXCR7 regulates platelet lipidome and functions

Authors: Malgorzata Cebo[1#], Kristina Dittrich[1#], Xiaoqing Fu[1], Mailin C. Manke[2,3], Frederic Emschermann[2], Johannes Rheinlaender[4], Hendrik von Eysmondt[4], Nerea Ferreirós[5], Jessica Sudman[2], Alexander Witte[2], Lisann Pelzl[6], Oliver Borst[2,3], Tobias Geisler[2], Dominik Rath[2], Tamam Bakchoul[6], Meinrad Gawaz[2], Tilman E. Schäffer[4], Michael Lämmerhofer[1], Madhumita Chatterjee[2]*.

Authors Affiliations: [1]Institute of Pharmaceutical Sciences, University of Tübingen, [2]Department of Cardiology and Angiology, [3] DFG Heisenberg Group Thrombocardiology, University Hospital Tübingen, [4]Institute of Applied Physics, University of Tübingen, [5]Pharmazentrum Frankfurt, University Hospital Frankfurt, [6]Institute for Clinical and Experimental Transfusion Medicine (IKET), University Hospital Tübingen, Germany

#share equal contribution as first authors

***Corresponding Author:** Madhumita Chatterjee, Dept. of Cardiology and Angiology, University Hospital Tübingen. Address: Otfried-Müller-Straße 10, 72076, Tübingen, Germany. Phone: +49-7071-2982888, Email: madhumita.chatterjee@med.uni-tuebingen.de

Supplemental material

1. **Supplemental materials and methods**
2. **Supplemental figures and video files**
3. **Supplemental Excel file**

Figure S1: Effect of CXCR7-agonist on surface expression of CXCR4, ACKR3/CXCR7 and other CXCR receptors on platelets

Figure S2: Dose dependent effect of CXCR7-agonist on platelet response in human and murine systems

Supplemental Video S3A-F: Anti-thrombotic effects of CXCR7-agonist over collagen observed in T-TAS *ex vivo*

Supplemental Video S4A-B: Anti-thrombotic effects of CXCR7-agonist over collagen + tissue factor-coated surface seen in T-TAS *ex vivo*

Supplemental Video S5A-B: Anti-thrombotic effects of CXCR7-agonist administration in occlusive thrombus formation model in mice.

Figure S6: Platelet CXCR4 and ACKR3/CXCR7 surface expression in hyperlipidemia and platelet lipidome under the influence of anti-platelet therapy in CAD patients.

Figure S7: Involvement of Gαs-coupled IP receptor in anti-thrombotic actions of CXCR7-agonist

Figure S8: Adenylyl cyclase (AC) and cAMP dependent protein kinase (PKA) contribute to the anti-thrombotic effects of CXCR7-agonist.

Figure S9: CXCR7- agonist reduces thrombo-inflammatory platelet-neutrophil interaction induced by HIT sera and IgG fractions

Visual/graphical abstract: Anti-thrombotic mode of action downstream of platelet ACKR3/CXCR7-ligation and its functional dichotomy from CXCR4

Supplemental Excel file 2 (Lipidomics analysis)

Materials and methods

Chemicals and antibodies: Pharmacological ACKR3/CXCR7 agonist VUF11207 was procured from Calbiochem. AC inhibitor (SQ22536), PKA inhibitor (KT5720), melittin, G-protein coupling antagonist peptide (Glp-Gln-D-Trp-Phe-D-Trp-D-Trp-Met-NH2), and IP receptor antagonist (RO1138452) were purchased from Tocris. Anti-human CD42b-FITC, anti-human CD62P-FITC, anti-human CD63-FITC were purchased from Beckman Coulter; anti-human CD42b-PE and PAC-1-FITC from BD Biosciences; mouse monoclonal anti-human CXCR4-PE, mouse monoclonal anti-human ACKR3/CXCR7-PE, mouse anti-human/mouse ACKR3/CXCR7-PE, mouse anti human CXCR1/IL-8RA-PE, mouse anti human CXCR2/IL-8RB-PE, mouse anti human CXCR6-PE, anti-human/mouse CXCL12/SDF-1-Fluorescein, rat anti-mouse CXCR4-Fluorescein, and anti-human CD14-APC antibodies were from R&D systems. Anti-mouse CD42b-Dylight 649, anti-mouse CD42b-FITC, anti-mouse CD62P-FITC, anti-mouse-active $\alpha_{IIb}\beta_3$-PE-(JON/A)-PE, anti-mouse GPV-FITC, anti-mouse GPVI-FITC, anti-mouse GPIX-FITC, anti-mouse β_3-FITC, anti-mouse α_v-FITC, respective fluorochrome (FITC, PE or Dylight 649) conjugated isotype controls, and GPIbβ-X488 *in vivo* platelet labelling antibody were obtained from Emfret analytics. Anti-human CD11b(activ)-FITC, anti-human CD11b-APC, anti-human CD3-APC, anti-human CD45-APC, anti-mouse CD45-APC, anti-mouse CD3-APC, anti-mouse Ly6C-APC, anti-mouse Ly6G-PE, anti-mouse CD11b-APC, anti-mouse CD14-APC, were bought from Biolegend. Respective fluorochrome (FITC, PE or Dylight 649) conjugated isotype controls for murine antibodies were obtained from Emfret analytics; other antibody specific isotype controls as suggested by the manufacturer were from Biolegend, R&D Systems, BD Biosciences, and Beckman Coulter. Annexin V-FITC was obtained from Immuno Tools. Horm Collagen was from Takeda Austria GmbH; fibrinogen was from Sigma Aldrich. Thrombin, ADPTest, TRAPTest, and COLTest reagents for whole blood impedance aggregometry were from Roche. Specified reagents and kits for coagulation analysis (PT and APTT) with START4™; and reagents for thrombinoscopy (CAT) analysis

(thrombin generation) were procured from Stago; PlateletMapping® catridges for thromboelastographic (TEG6s® whole blood hemostasis system) analysis were purchased from Haemonetics. IgG-EIA was from Zymutest HIA, IgG, Hyphen BioMed, Neuville-sur-Oise, France, and IgG purification kit -MelonTM-Gel IgG Spin Purification Kit, from Thermo Fisher Scientific. Antibodies against phosphorylated- PLCγ, Src, PKC, PI3K, Akt, p38MAPK, anti-α-tubulin, anti-β-actin, anti-GAPDH, the protease-phosphatase inhibitor cocktail, and lysis buffer were procured from cell signaling technologies. Legendplex® human and murine 13-plex inflammation panel, Legendplex® murine 13-plex chemokine panel, Legendplex® human 10-plex thrombosis panel were purchased from Biolegend.

Specific materials for cAMP analysis: Water, methanol, acetonitrile (LC-MS grade) and ammonium acetate (purity ≥97.0%) were purchased from Carl Roth (Karlsruhe, Germany). Acetic acid (99.8%) was from Fischer Chemicals (Schwerte, Germany). Adenosine 3', 5'-cyclic monophosphate (3', 5'-cAMP) was purchased from Sigma-Aldrich (Munich, Germany). The internal standard (IS) adenosine-3', 5'-cyclic-^{13}C5 monophosphate (^{13}C5-cAMP) was obtained from Toronto Research Chemicals (Ontario, Canada).

Specific materials for lipidomics analysis: Isopropanol, methanol and acetonitrile in ultra LC-MS grade were purchased from Carl Roth (Karlsruhe, Germany). Ammonium formate, ammonium acetate, formic acid, acetic acid and methyl tert-butyl ether (MTBE) were from Merck (Darmstadt, Germany). SPLASH® Lipidomix® (mixture of deuterated lipids) was obtained from Avanti Polar Lipids (Alabaster, AL, USA). All oxylipin and fatty acid standards and deuterated internal standards were purchased from Cayman Chemical (Ann Arbor, MI, USA). Ultrapure water was produced in-house by Elga Purelab Ultra (Celle, Germany).

Account of samples used for platelet function tests: Most functional analyses (platelet activation, degranulation, aggregation, thrombus formation, T-TAS, intracellular calcium mobilization, surface expression of CXCR4, ACKR3/CXCR7, platelet-leukocyte aggregate formation) were performed in whole blood assays, which closely resembles physiological

condition *ex vivo*. However due to technical limitations and experimental demands platelet aggregation and ATP release, platelet apoptosis (Annexin V exposure) were performed in platelet rich plasma (PRP) samples; whereas SICM, collection of resting and activated platelet supernatant, cAMP analysis, lipidomics analysis, Western blot analysis were performed with isolated washed platelet preparations.

Animal experimentation: (8-10) weeks old wild-type C57BL/6J mice of either sex (supplier Jackson laboratories) were used for *ex vivo* platelet function assays, tail-bleeding time, coagulation assays (PT, APTT), to inflict $FeCl_3$ induced arterial (carotid artery) injury and thrombus formation *in vivo*. Wild-type C57BL/6J mice were also used to generate myocardial ischemia-reperfusion injury (MI/RI) model by left anterior descending artery (LAD) ligation. Randomization of the control and CXCR7-agonist treated groups was done and the experimenter was blinded to the treatments during the course of experiments until final data analysis and statistical evaluation. For surgical procedures mice were anesthetized by injection of midazolame (5 mg/kg body weight), medetomidine (0.5 mg/kg body weight) and fentanyl (0.05 mg/kg body weight). Blood collection from retro-orbital plexus of mice was done under Isofluran. All animal experimentations were conducted according to the German law for the welfare of animals; following ARRIVE guidelines and were approved by local authorities (Regierungsprasidium Tübingen, approval M5/17, M20/15, M08-14 and M18-14).

Surface expression of CXCR4, ACKR3/CXCR7, CXCR1, CXCR2 CXCR6, on human platelets by flow cytometry: Platelets in whole blood from CAD patients (n=230; ACS=142, CCS=88) and healthy subjects (for experimental studies) were analyzed for the surface expression of CXCR4, and ACKR3/CXCR7 gating for the platelet specific marker CD42b (GPIbα). Blood collected in CPDA was diluted 1:50 with PBS and incubated with the respective fluorochrome-conjugated antibodies- mouse monoclonal anti-human CXCR4-PE, mouse monoclonal anti-human ACKR3/CXCR7-PE and anti-human CD42b/GPIbα-FITC. Threshold cytometer settings had been adjusted using individual isotype controls. Clinical samples were

incubated for 30 minutes at room temperature in the dark, fixed with 0.5% paraformaldehyde and analyzed by flow cytometry (FACS-Calibur flow cytometer, Becton-Dickinson)[1, 2].

Experimental blood samples collected in CPDA anticoagulant from healthy donors were treated with CXCR7-agonist at (0, 10, 50, 100, and 200)µg/mL for 30 minutes or for (0, 5, 15, 30, and 60) minutes with 100µg/mL of CXCR7-agonist or vehicle control (1% DMSO); and stained for the surface expression of CXCR4 and ACKR3/CXCR7 on platelets as mentioned. Samples were fixed in 0.5% paraformaldehyde and analyzed by flow cytometry. All analyses were carried out in duplicates for each biological sample. Data are presented as mean±S.E.M from n=4 independent experiments with healthy donors.

To evaluate the impact of CXCR7-agonist on the surface expression of CXCR1, CXCR2 and CXCR6 on platelets, CPDA anticoagulant from healthy donors (n=5) were treated with CXCR7-agonist (100µg/mL) for (0, 5, 15, 30, and 60) minutes and stained for the surface expression of CXCR1 (mouse anti human CXCR1/IL-8RA-PE), CXCR2 (mouse anti human CXCR2/IL-8RB-PE) and CXCR6 (mouse anti human CXCR6-PE) on platelets with respective fluorochrome conjugated antibodies against these receptors as mentioned. Samples were fixed in 0.5% paraformaldehyde and analyzed by flow cytometry. All analyses were carried out in duplicates for each biological sample. Data are presented as mean±S.E.M from n=5 independent experiments with healthy donors.

Surface expression of CXCR4 and ACKR3/CXCR7, on murine platelets by flow cytometry:

In vitro evaluation: Blood was collected from the retro-orbital plexus of mice in ACD (1:4) anti-coagulant, diluted 1:20 in PBS+$CaCl_2$ and incubated with vehicle control (1% DMSO) or CXCR7-agonist (150µg/mL) for (0,5,15,30 and 60) minutes at room temperature in the dark in the presence of respective fluorochrome conjugated antibodies against ACKR3/CXCR7 (anti-mouse/human ACKR3/CXCR7-PE) and CXCR4 (anti-mouse CXCR4-FITC) and platelet

specific marker anti-mouse CD42b/GPIbα-Dylight 649. At the end of incubation period samples were acquired by flow cytometry gating for platelet specific marker CD42b.

In vivo evaluation: Mice we injected (i.v.) with 300µg/mouse of CXCR7-agonist or vehicle control (2% DMSO). Blood was collected from the retro-orbital plexus of mice in ACD (1:4) anticoagulant 30 mins, 1, 3, 6, 8 and 24hrs post-administration. Blood was diluted 1:20 in PBS+$CaCl_2$ and incubated with respective fluorochrome conjugated antibodies against CXCR4, ACKR3/CXCR7, and platelet specific marker anti-mouse CD42b for 30 minutes at room temperature in the dark. At the end of incubation period samples were acquired by flow cytometry as described.

Platelet activation (degranulation from α-granules and $\alpha_{IIb}\beta_3$-integrin activation) by flow cytometry: Whole blood collected in CPDA anticoagulant from ACS patients (n=11) or healthy subjects (n=5 for each experimental investigation) was diluted 1:50 in PBS supplemented with $CaCl_2$+$MgCl_2$. Samples were either kept under resting condition or treated with vehicle control (1% DMSO) or CXCR7-agonist (10, 25, 50,100, or 200µg/mL of CXCR7-agonist for dose-response analysis and 100µg/mL for other experiments) for 30 minutes at room temperature. Thereafter samples were treated with platelet-activating stimulus collagen related peptide (CRP) (5µg/mL) for a further 30 minutes at room temperature in the presence of anti-human CD62P-FITC or PAC-1-FITC and platelet specific anti-human CD42b-PE. Where specified, blood was pre-treated with pharmacological inhibitors, e.g. AC inhibitor (SQ-22536-10µM), PKA inhibitor (KT-5720-2µM), G protein coupling antagonist peptide (10µM), Gαs protein coupling inhibitor (melittin-5µM), IP-receptor antagonist (RO-1138452 10µM), or vehicle control for 15 minutes at room temperature, before the samples were treated with CXCR7-agonist (100µg/mL). At the end of incubation period, samples were fixed with 0.5% paraformaldehyde and analyzed immediately for the surface expression of CD62P (degranulation) or PAC-1 binding ($\alpha_{IIb}\beta_3$-integrin activation) by flow cytometry.[1,8] All experimental sets were carried out in duplicates. Data are presented as mean±S.E.M.

Platelet aggregation by impedance aggregometry: Multi-electrode impedance aggregometry is a whole blood platelet function assay that was used to monitor platelet aggregation. 600µL blood/sample from CAD patients (n=230, ACS=142, CCS=88), ACS patients (n=11) or healthy subjects (n=5-8 donors) acquired in hirudinized tubes (Sarstedt) was used to perform ADP(ADPTest), TRAP-6(TRAPTest), collagen(ColTest) -induced aggregation as indicated. In the CAD cohort, aggregation test was performed with ADP and TRAP. In *ex vivo* analysis of blood from ACS patients (n=11) or from healthy donors, whole blood was pre-treated with vehicle control (1% DMSO) or pharmacological CXCR7-agonist (10, 25, 50, 100, 200µg/mL) as specified for 30 minutes at room temperature before starting aggregation with ADP, TRAP or collagen. Where mentioned, blood was incubated with pharmacological inhibitors e.g. AC inhibitor (SQ-22536-10µM), PKA inhibitor (KT-5720-2µM), G protein coupling antagonist peptide (10µM), Gαs protein coupling inhibitor/antagonist (melittin-5µM), IP-receptor antagonist (RO-1138452-10µM), or respective vehicle control for 15 minutes at room temperature before the samples were treated with CXCR7-agonist (100µg/mL). The area under the aggregation curve (AUC) was used as a measure of overall platelet aggregation[1]. All experimental sets were carried out in duplicates. Data represent mean±S.E.M.

Platelet aggregation and ATP release: Aggregation of platelets ($250x10^3$/µl) in platelet rich plasma (PRP) was estimated from light transmission, estimated with a lumi-aggregometer Modell 700 (ChronoLog). Briefly, blood from healthy donors was collected in citrate anti-coagulant and centrifuged at 200xg for 20 minutes without break or acceleration. PRP was collected from the upper 2/3 layer. Platelet poor plasma (PPP) was collected following a further centrifugation at 1000xg, for 10 minutes. Platelet count was evaluated with Sysmex® and adjusted according to experimental demand with PPP.

Platelets in PRP were pre-treated with vehicle control (1% DMSO) or CXCR7-agonist (100µg/mL) for 30 minutes at room temperature and then activated with CRP (2.5µg/mL) or TRAP (10µM) to record aggregation response for a duration of 10 minutes, at 37°C and under

a stirring speed of 1000 revolutions per minute (r.p.m.). Analysis was performed with the aggrolink-8 software (ChronoLog)[3]. Data are mean±S.E.M derived from n=6 healthy donors.

Simultaneous ATP release was determined in the samples to study secretion of dense granules as described previously[3]. Platelet counts were adjusted to $250x10^3$ platelets/µl of PRP. After calibration with ATP standard (ChronoLog), the ATP concentration was determined utilizing the ChronoLume luciferin assay (ChronoLog, Havertown, USA) on a lumi-aggregometer (Modell 700, ChronoLog) according to the manufacturer's instructions. Platelets pre-treated with vehicle control (1% DMSO) or CXCR7-agonist (100µg/mL) for 30 minutes at room temperature were activated with CRP (2.5µg/mL) or TRAP (10µM) for 10 minutes, at 37°C and a stirring speed of 1000r.p.m during the course of aggregation and ATP release. Extracellular ATP released from activated platelets was assessed employing the luciferin/luciferase bioluminescent assay and amount of ATP release was calculated using the exogenously added ATP standard with aggrolink-8 software (ChronoLog)[3]. All experimental sets were carried out in duplicates. Data are mean±S.E.M derived from n=6 healthy donors.

Dense-(δ)-granule release by flow cytometry: Release of dense (δ) granules was also confirmed by flow cytometric detection of CD63 exposure on the platelet surface. Blood collected in CPDA anticoagulant from healthy subjects (n=4 healthy donors) was diluted 1:50 in PBS supplemented with $CaCl_2$+$MgCl_2$. Samples were either kept under resting condition or treated with vehicle control (1% DMSO) or CXCR7-agonist (100µg/mL) for 30 minutes at room temperature, following which platelets were activated with CRP (5µg/mL) for a further 30 minutes at room temperature in the presence of anti-human CD63-FITC and platelet specific marker anti-human CD42b-PE. At the end of incubation period, samples were fixed in 0.5% paraformaldehyde and analyzed immediately for the surface expression of CD63 by flow cytometry. All experimental analyses were carried out in duplicates. Data are mean±S.E.M.

***Ex vivo* thrombus formation in parallel plate flow chamber assay:** Blood from healthy human subjects (n=11 ACS patients, and n=5 healthy donors for each experimental

investigation) collected in CPDA anticoagulant, or heparinized murine blood collected from the retro-orbital plexus of C57BL/6J mice (n=5-6 mice/group) was pre-treated with vehicle control (1% DMSO) or CXCR7-agonist (10, 25, 50,100, or 200)µg/mL (for dose dependent response), or CXCR7-agonist at 100µg/mL for 30 minutes at room temperature and perfused through a transparent parallel plate flow chamber (slit depth 50µm) over a collagen (100µg/mL)-coated surface at 1700s^{-1} (human) and 1000s^{-1} (murine) wall shear rates as specified. Where mentioned blood was incubated with pharmacological inhibitors, e.g. AC inhibitor (SQ-22536-10µM), PKA inhibitor (KT-5720-2µM), G protein antagonist peptide (10µM), Gαs protein coupling inhibitor (melittin-5µM), IP-receptor antagonist (RO-1138452-10µM), or respective vehicle control for 15 minutes at room temperature before the samples were treated with CXCR7-agonist (100µg/mL). After blood perfusion, the chamber was rinsed for 5 minutes by perfusing PBS, and images were captured from at least 6 different randomly chosen microscopic areas (Axiovert 200, Carl Zeiss, optical objective 20x). Analysis of thrombus area was done offline using acquired images with AxioVision software (Carl Zeiss).[1] Data are mean±S.E.M.

***Ex vivo* thrombus formation with T-TAS:** Thrombus formation was determined using the most recent and advanced total thrombus formation analysis system/T-TAS (Fujimori Kogyo Co Ltd, Shinjuku, Japan). Measurements were performed on a collagen+tissue factor-coated chip (AR-chip, Fujimori Kogyo Co. Ltd), using 450µL of recalcified citrated human blood, or on a collagen-coated chip (PL-chip, Fujimori Kogyo Co Ltd), using 320µL of hirudin anticoagulated blood, according to the manufacturer's instructions. Blood samples were pre-treated with vehicle control (1% DMSO) or CXCR7-agonist (100µg/mL) for 30 minutes at room temperature before perfusion through the specified chips. The experiment was monitored continuously throughout the course of blood perfusion and both video recordings and images were captured at regular time intervals during blood flow through the chips. Data analysis was performed with total thrombus-formation analysis (T-TAS) software (Fujimori Kogyo Co Ltd), calculating the time to the start of chip occlusion i.e. time to 10kPa pressure attainment (T_{10} for

PL-chip), occlusion time (OT for AR chip), and the AUC[4] (thrombus coverage on both PL and AR-chips). Respective video recordings are provided as supplemental data (**supplemental video 3A-F and 4A-B**) and available online. Data are mean±S.E.M from 5 independent experiments with healthy donors.

Platelet interaction with physiological matrices (collagen and fibrinogen) by scanning ion conductance microscopy (SICM): SICM topography images of platelets were recorded with a custom-built SICM setup as described previously[5]. Briefly, platelets from healthy subjects (n=3 experiments with healthy donors) were incubated for 30 minutes at room temperature with 50µg/mL CXCR7-agonist or 0.1% DMSO (vehicle control), then added to collagen- or fibrinogen-coated (coating done using 100µg/mL of collagen or 100µg/mL of fibrinogen for 1h at 37°C) culture dishes (Greiner 627160) containing Tyrode buffer (supplemented with 1mM $CaCl_2$, CXCR7-agonist or DMSO depending on the experimental set up; for fibrinogen also with 0.1U/mL thrombin). Platelets were then imaged live directly after adhesion (for initial spreading rate) or imaged after fixation (in 2% formaldehyde + 1% glutaraldehyde in PBS for 10 minutes) to estimate final spreading area following 30 minutes of adhesion time, or imaged live (for elastic modulus) throughout the course of the experiment at room temperature. SICM imaging was performed in backstep/hopping mode with nanopipettes made of borosilicate glass with a typical opening radius of approximately 50-100 nm, allowing a lateral resolution of about 150-300 nm[5]. Scan area was typically chosen as $(12 \times 12)\mu m^2$ and pixel resolution between (20×20) and (96×96)px, depending on the required time resolution. Platelet shape was quantified from topography images with custom-written software using Igor Pro (Wavemetrics, Lake Oswego, Oregon). Briefly, platelets were manually selected in the images and analyzed for their shape after binarizing the topography images with a height threshold of 50 nm. The initial spreading rate was quantified from absolute area change during the first 10 minutes. The elastic modulus of live platelets was measured and quantified as described previously[5] using 20 kPa pressure applied to the nanopipette.

Evaluation of phosphatidylserine exposure by Annexin V binding: Activation induced platelet procoagulant property was evaluated by phosphatidylserine (PS) externalization (Annexin V binding) as reported previously by flow cytometry[6]. PRP platelets (10^6/sample) from healthy subjects (n=4) were either pre-treated with vehicle control (1% DMSO) or CXCR7-agonist (100µg/mL) for 30 minutes at room temperature and then either kept under resting condition or treated with CRP (5µg/mL) for 1hr at room temperature. PS exposure was ascertained as an increase in Annexin V binding as previously described[6]. Data are mean±S.E.M.

Monitoring intracellular calcium levels in whole blood platelets by flow cytometry: Flow cytometric detection for intraplatelet calcium mobilization estimated as free calcium levels was done with the calcium sensitive dye fluo-3 acetomethyl ester (fluo-3AM-5µM) and the platelet-specific antibody anti-CD42b-PE in whole blood samples. We chose this whole blood assay firstly, to be consistent with the functional analysis done in whole blood preparation and to assure minimum manipulation otherwise caused during isolation of platelets and subsequent sample handling. Briefly, whole blood collected (n=5 healthy donors) in citrate-anticoagulant (135mM tribasic sodium citrate, pH 7.4) was diluted 1:10 in modified Tyrode's buffer (137mM NaCl, 2.8mM KCl, 1mM $MgCl_2$-$6H_2O$, 12mM $NaHCO_3$, 0.4 mM Na_2HPO_4-$2H_2O$, 10mM HEPES, pH 7.4 adjusted with 0.1N NaOH). Platelets in 500µL of diluted blood samples were loaded with the calcium indicator fluo-3AM (5µM) by incubating for 15 minutes at room temperature in the dark. Samples were subsequently stained with platelet specific marker CD42b-PE. Thereafter samples were treated with vehicle control or 100µg/mL of CXCR7-agonist. The blood samples were run on a flow cytometer in kinetic mode [7]. Flow cytometer settings were adjusted as described previously[7]. After the initial acquisition of baseline fluo-3 fluorescence, sample acquisition was briefly stopped to add platelet activating stimulus CRP (5µg/mL) and real-time changes in fluo-3 fluorescence were observed. Data are mean±S.E.M from 5 independent experiments.

***In vivo* thrombus formation in mice: arterial thrombosis model**

CXCR7-agonist showed significant anti-thrombotic effects *in vitro*, in most mice as compared to vehicle control starting from a dose of 50µg/mL (**Supplementary Figure S2E**). Considering approximately 2mL of blood volume in mice on average, we administered an optimal dose of CXCR7-agonist at 100µg/mouse (corresponding to 50µg/mL per mouse) and lower dose of 25µg/mouse (corresponding to 12.5µg/mL per mouse) to compare with and nullify any unspecific off-target effects. CXCR7-agonist administered at 100µg/mouse showed significant and consistent anti-thrombotic effect in *ex vivo* flow chamber assay, platelet CD62P surface exposure and JON/A response (**Figure1Ei-Eiv**) with respect to vehicle control. Therefore, subsequent thrombus formation assay *in vivo* in $FeCl_3$-induced arterial thrombosis model was performed following administration of CXCR7-agonist at 100µg/mouse.

To evaluate the anti-thrombotic impact of CXCR7-agonist on arterial thrombus formation *in vivo*, (8-10) weeks old C57BL/6J wild type mice (n=14 mice/group) were administered with vehicle control (1% DMSO in 100µl of 0.9% NaCl i.v.) or CXCR7-agonist (100µg/mouse in 100µl of 0.9% NaCl i.v.) under anaesthesia. The platelets in circulation were stained *in vivo* with GPIbβ-Dylight488 (Emfret Analytics) (0.1µg/gm b.wt.) administered i.v. along with vehicle control or CXCR7-agonist. After 1hr, the surgical procedure was started. Following an incision, the carotid artery was exteriorized and injured by topical application of a filter paper soaked in 15% $FeCl_3$ for 1 minute. Thrombus formation in the artery was monitored for 20 minutes or until complete occlusion (blood flow stopped for > 1 minute) with NIS-Elements (Nikon) microscope using a 10x objective. Digital images were recorded and analyzed off-line.[1, 6] Respective video recordings are provided as supplemental online data (**Supplementary material online, video 6A-B**).

Platelet function tests following carotid artery injury:

$\alpha_{IIb}\beta_3$-intergrin activation: To assess the status of platelet activation in circulation following carotid artery injury and thrombus formation, blood was collected after the IVM procedure in

ACD (1:4) anti-coagulant to assess JON/A response by whole blood flow cytometry. Blood samples diluted 1:20 in PBS+$CaCl_2$ were incubated with JON/A-PE for 30 minutes at room temperature. At the end of incubation period, samples were further diluted with 300µL of PBS+$CaCl_2$ and acquired immediately by flow cytometry gating for platelet specific marker GPIbβ-Dylight 488 (used for *in vivo* labelling of platelets).

Platelet-leukocyte aggregate formation: To assess the formation of platelet (CD42b)-neutrophil (Ly6G, CD11b), monocyte (Ly6C), T lymphocyte (CD3), leukocyte (CD45) aggregates in peripheral circulation of mice, blood samples collected after the IVM procedure, were incubated with respective antibodies against distinct leukocyte population-e.g. anti-CD45-APC (pan leukocyte marker), anti-CD3-APC, anti-CD11b-APC, anti-Ly6C-APC, anti-Ly6G-PE for 30 minutes at room temperature. Samples were thereafter treated with BD-lysis solution (1:10) to lyse the RBCs and fix them; then washed once in PBS by centrifugation at 1000xg for 5 minutes and acquired by flow cytometry. The percentage of $CD42b^+$ population was assessed for each cell type, to evaluate formation of platelet-leukocyte aggregates in the peripheral circulation of mice following thrombus build-up in the carotid artery.

Myocardial infarction model in mice: C57BL/6J wild type mice were used for this study. CXCR7-agonist VUF11207 was administered at 300µg/mouse i.v. (similar to previously shown for allosteric CXCR7 agonist and CXCR4 antagonist AMD3100[8, 9] and comparable to CXCR7 agonist TC14012 administered at 10mg/Kg body weight[10, 11]) 1hr prior to the surgical procedure. CXCR7-agonist or respective vehicle control (2% DMSO) administered mice were anaesthetized by intraperitoneal injection of a solution of 5mg midazolam, 0.5mg medetomidine, and 0.05 mg fentanyl each per kilogram of body weight. Myocardial ischemia was induced by ligation of the left anterior descending artery (LAD) for 30 minutes as described previously[12]. 1 day after MI/RI echocardiography was performed, and infarct size was determined using AxioVision software (Carl Zeiss), expressed as the percentage of total left ventricular (LV) volume. Analysis of left ventricular ejection fraction was performed with Vevo

2100 software Software (VevoLAB und VevoStrain; Vevo2100, FUJIFILM VisualSonics Version 3.1 (VisualSonics, Toronto, ON, Canada).

Platelet function test pre-MI and 24hrs post-MI/RI:

Surface expression of receptors: Blood was collected from the retro-orbital plexus of mice in ACD (1:4) anti-coagulant pre-MI (1hr after CXCR7-agonist or vehicle control administration and before surgery) and 24hrs post MI/RI. Platelet surface expression of the major functional receptors- GPIbα, GPV, GPVI, GPIX, α_v-integrin, β_3-integrin, also CXCR4 and ACKR3/CXCR7 were evaluated by whole blood flow cytometry. Briefly blood was diluted 1:20 in PBS+$CaCl_2$ and incubated with respective fluorochrome conjugated antibodies against the surface receptors- anti-mouse CD42b/GPIbα-Dylight 649, anti-mouse GPV-FITC, anti-mouse GPVI-FITC, anti-mouse GPIX-FITC, anti-mouse β_3-FITC, anti-mouse α_v-FITC, anti-mouse CXCR4-FITC, or anti-mouse/human ACKR3/CXCR7-PE, for 30 minutes at room temperature in the dark. Thereafter samples were further diluted with 300µL of PBS+$CaCl_2$ and acquired immediately by flow cytometry gating for platelet specific marker CD42b.

Surface expression/degranulation of CXCL12/SDF1α: Platelet surface expression of CXCL12/SDF1α is enhanced in ACS patients[13]. To evaluate the surface expression of CXCL12/SDF1α on circulating murine platelets by whole blood flow cytometry, blood was collected from the retro-orbital plexus of mice pre-MI/surgery and 24hrs post MI/RI in ACD (1:4) anti-coagulant. Blood samples diluted 1:20 in PBS+$CaCl_2$ were either kept under resting condition or incubated with platelet agonist CRP (5µg/mL) in the presence of anti-human/mouse CXCL12/SDF1α-Fluorescein and, anti-mouse CD42b-Dylight 649-antibodies for 30 minutes at room temperature. At the end of incubation period samples were further diluted with 300µL of PBS+$CaCl_2$ and acquired immediately by flow cytometry gating for the $CD42b^+$ platelet population.

Platelet activation status: To assess basal platelet activation status and responsiveness or activation potential, blood was collected pre-MI and 24hrs post MI/RI in ACD (1:4) anti-

coagulant to assess surface expression of CD62P, and JON/A response by whole blood flow cytometry. Blood samples diluted 1:20 in PBS+$CaCl_2$ were either kept under resting condition or incubated with platelet agonist CRP (5µg/mL) in the presence of anti-CD62P-FITC and JON/A-PE, anti-CD42b-Dylight 649-antibodies for 30 minutes at room temperature. Following incubation, samples were further diluted with 300µL of PBS+$CaCl_2$ and acquired immediately by flow cytometry gating for $CD42b^+$ platelets.

Thrombus formation potential: To ascertain thrombotic propensity post-MI, blood was collected 24hrs post-MI/RI in heparin anticoagulant (1:3) from the retro-orbital plexus of mice and perfused through a transparent flow chamber (slit depth 50µm) over a collagen (100µg/mL)-coated surface at 1000 s^{-1} shear rate. After perfusion, the chamber was rinsed with PBS and images were captured from at least 6 different randomly chosen microscopic areas (Axiovert 200, Carl Zeiss, and optical objective 20x). Assessment of thrombus area during offline analysis of acquired images was done with AxioVision software (Carl Zeiss).[1]

Thrombo-inflammatory platelet-leukocyte interaction: To determine the presence of platelet leukocyte aggregates in peripheral circulation of mice before and 24hrs post-MI/RI, blood samples collected in ACD anticoagulant (1:4) were incubated with platelet specific antibody anti-CD42b-FITC and pan leukocyte marker anti-CD45-APC for 30 minutes at room temperature. Because limited amount of blood (<50µL) was collected before surgery, a detailed analysis for different leukocyte subsets could not be performed for the MI/RI model as we have performed in the arterial thrombosis model. Samples were treated with BD-lysis solution (1:10) to lyse the RBCs and fix the samples. Thereafter samples were washed once in PBS by centrifugation at 1000xg for 5 minutes, and acquired by flow cytometry. The percentage of $CD42b^+CD45^+$ population was assessed to evaluate platelet leukocyte aggregates.

Inflammatory mediators in circulation: Remaining blood samples collected 24hrs post-MI were centrifuged at 2,500xg for 10 minutes at 4°C to collect plasma and perform cytometric

bead array for inflammatory mediators (Legendplex® murine 13-plex inflammation panel from Biolegend) according to manufacturer's instructions.

Tail bleeding time in mice: To assess the impact of CXCR7-agonist on bleeding time, (8-10) weeks old C57BL/6J mice (n=5 mice/experimental group) were administered with DMSO (2%) as vehicle control or CXCR7-agonist (300µg/mouse i.v.; the maximum dose of CXCR7-agonist administered in MI/RI models) under anaesthesia. After 1hr, a 3-mm segment of the tail tip was removed with a scalpel from anesthetized mice. Tail bleeding was monitored by gentle absorption of blood onto a filter paper at 20 seconds intervals without making direct contact with the wound site. When no blood was absorbed on the filter paper, bleeding was determined to have been ceased.[14] Data are mean±S.E.M.

Coagulation parameters (Pro-thrombin time-PT and activated partial thromboplastin time- APTT): To evaluate the impact of CXCR7-agonist on coagulation profile *in vivo*, (8-10) weeks old C57BL/6J wild type mice (n=5 mice/experimental group) were administered with vehicle control (2% DMSO) or CXCR7-agonist (300µg/mouse i.v.) under anaesthesia. Blood was obtained after 1hr and centrifuged at 2500xg for 10 minutes to collect platelet poor plasma (PPP). Plasma coagulation parameters PT and APTT were analyzed with PPP samples from these mice using the START4™ platform as per manufacturer's instructions and described previously [1]. All samples were run in duplicates and the data are mean±S.E.M derived from 5 mice/group.

Thrombin generation by calibrated automated thrombinoscopy (CAT): Platelet dependent thrombin generation in response to tissue factor, in platelet rich plasma (PRP), and platelet independent thrombin generation in platelet poor plasma (PPP) was evaluated in 4 healthy human subjects by calibrated automated thrombinoscopy. Platelet count in PRP was adjusted to $150x10^3$/µl. Wells of a 96 well plate were filled with tissue factor (5pM) in buffer pH7.35 (20mM Hepes, 140mM NaCl, 5mg/mL bovine serum albumin). PRP and PPP samples were treated with CXCR7-agonist (100µg/mL) or vehicle control (1% DMSO) for 30 minutes at

room temperature, and then added to the tissue factor containing wells in presence or absence of CRP. By adding the fluorescent thrombin substrate (Z-Gly-Gly-Arg aminomethyl coumarin, 2.5mM), the coagulation reaction was started and continuously monitored. The whole procedure was carried out under constant shaking and at 37°C. Calibration was done using a thrombin calibrator. Finally, peak thrombin generation was measured using the Thrombinoscope software (Stago, Germany), and reported as Thrombin (nM). [14] All samples were run in triplicates, and the data are mean±S.E.M derived from 3 independent experiments.

Thromboelastography: TEG, which is a whole blood haemostasis analysis system involving coagulation factors and platelets was used to complement the observation from plasma-based coagulation tests (PT and APTT) performed after *in vivo* administration of CXCR7-agonist in mice. The TEG6s® system was employed with PlateletMapping® Assay catridges (Haemonetics, Germany) as per manufacturer's instructions in the HKH (Kaolin with Heparinase), ActF (ActivatorF) and ADP (adenosine-5'-diphosphate) assays. The PlateletMapping assay consists of a set of treatments in separate channels that run parallely including platelet activating ADP, which together with ActivatorF, when used in heparinized blood can measure the extent of platelet activation. Combined with the HKH which depends on Kaolin induced coagulation processes this provides additional information on the extent of platelet involvement in the hemostatic process in presence of a platelet stimulus i.e. ADP. Time to initiation of the appearance of first clot (R) and clot strength deciphered as maximum amplitude (MA), percent of ADP-induced aggregation and percent of inhibition imposed on ADP induced aggregation in presence of an anti-platelet agent i.e. CXCR7-agonist were determined . Heparinized blood samples were treated with either vehicle control (1% DMSO) or 100µg/mL of CXCR7-agonist for 30 minutes at room temperature before starting the respective TEG6s assays. Data are mean±S.E.M for 5 independent experiments performed with healthy donors.

Collection of control, HIT sera and corresponding IgG fractions: Sera and corresponding IgG fractions were isolated from 3 patients with clinically and serologically confirmed HIT-associated thrombosis (using 4Ts score 4-6, ELISA and HIPA positive). The probability of HIT was evaluated by the treating physician using the 4Ts-scoring system, as previously described [15, 16]. Serum samples from 3 healthy control subjects and 3 HIT patients were used in the study.

The commercially available IgG-EIA (Zymutest HIA, IgG, Hyphen BioMed, Neuville-sur-Oise, France) was used for ELISA estimations according to manufacturers' instructions. A sample was considered HIT positive if the optical density (OD) was higher than 0.5.[17] The HIPA test was performed to investigate the capability of antibodies in the sera to activate platelets as previously described [17]. Each serum was tested with washed platelets from four different healthy donors in the absence (buffer alone) or in the presence of heparin (0.2IU/mL and 100IU/mL). Reactions were performed in microtiter wells containing spherical stir bars and stirred at approximately 500 r.p.m. Wells were investigated optically at five-minute intervals for the loss of turbidity. A serum was interpreted as reactive (positive) if a shift from turbidity to transparency occurred within 30 min in at least two platelet suspensions in the presence of 0.2IU/mL, but not 100IU/mL heparin. Each HIPA test included a set with diluted serum from a known HIT positive patient as a positive control and a set with serum from a healthy donor as a negative control[16].

Patient characteristics Patient ID.	**4T-Score**	**HIPA**	**ELISA**
HP001	5	positive	3.072
P002	6	positive	2.970
P003	4	positive	3.600

The Immunoglobulin G (IgG) fractions were directly isolated from healthy control and HIT patient sera. To exclude non-specific effects like the activation of complement or of other serum proteins, all sera were heat-inactivated at 56°C for 25 min, which was followed by a

centrifugation step at 5000xg. The sera supernatant thus obtained were used for experimental purpose and functional analysis as described in the following sections. IgG fractions were isolated from 3 serum samples per group (from 3 healthy controls and 3 HIT patients) using a commercially available IgG purification kit (MelonTM-Gel IgG Spin Purification Kit, Thermo Fisher Scientific, Waltham, USA) according to the manufacturer's instructions.

Functional analysis with HIT sera/IgG fractions:

HIPA-test: In the experimental HIPA test washed platelets from healthy donors were pre-incubated with CXCR7-agonist (25µg/mL and 100µg/mL) or vehicle control (DMSO) for 30 minutes before performing the HIPA test. Data are mean±S.E.M from 3 independent HIPA tests.

Ex vivo thrombus formation assessed in parallel plate flow chamber assay: Heparinized (0.2IU/mL) blood from healthy human subjects (n=5) was pre-treated with vehicle control (1% DMSO) or CXCR7-agonist (100µg/mL) for 30 minutes, then treated with sera from control healthy individuals or HIT-positive patients at 1:10 (v/v) at room temperature and perfused through a transparent flow chamber (slit depth 50µm) over a collagen (100µg/mL)-coated surface at $1000s^{-1}$ wall shear rate. As described earlier, after blood perfusion, the chamber was rinsed with PBS and images were captured from at least 6 different randomly chosen microscopic areas (Axiovert 200, Carl Zeiss, optical objective 20x). Analysis of thrombus area was done offline with AxioVision software (Carl Zeiss).[1] Data are mean±S.E.M from 5 independent experiments performed with blood from 5 healthy subjects and sera from 3 HIT-positive patients, and 3 healthy control subjects.

Platelet and neutrophil activation: Heparinized (0.2IU/mL) whole blood from healthy donors were treated with vehicle control or CXCR7-agonist (100µg/mL) for 30 minutes then incubated with control sera (n=3) and those from HIT-positive patients (n=3) at 1:10 (v/v) for 1hr at room temperature to assess platelet surface exposure of p-selectin (CD62P), PAC-1 binding and neutrophil active-CD11b by flow cytometry as specified earlier. All experimental samples were

set up and acquired in duplicates. Data are mean±S.E.M from experiments performed with blood from 5 healthy subjects.

Platelet-neutrophil aggregate formation: To ascertain formation of platelet ($CD42b^+$)-neutrophil ($CD11c^+$) aggregates, heparinized (0.2IU/mL) whole blood samples from healthy donors (n=5) were treated with vehicle control or CXCR7-agonist (100µg/mL) for 30 minutes and thereafter with control sera/IgG (n=3) and sera/IgG from HIT-positive patients (n=3) at 1:10 (v/v) for 1hr at room temperature. Samples were labelled with respective fluorochrome conjugated antibodies for platelets (anti human-CD42b-FITC) and neutrophil (anti human-CD11c-APC) and analyzed by flow cytometry for platelet-neutrophil $CD42b^+CD11c^+$ aggregates as described earlier. All experimental samples were set up and acquired in duplicates. Data are mean±S.E.M from independent experiments performed with blood from 5 healthy subjects and sera/IgG from 3 HIT-positive patients and 3 healthy controls.

Generation of COX-1 and 12-LOX derived pro-thrombotic lipids: Heparinized (0.2IU/mL) whole blood from healthy donors were treated with vehicle control (1% DMSO) or CXCR7-agonist (100µg/mL) for 30 minutes, thereafter incubated with control sera (n=3) and those from HIT-positive patients (n=3) at 1:10 (v/v) for 1hr at room temperature. Samples were centrifuged at 2,500xg for 5 minutes at 4ºC to collect the plasma. Plasma samples were immediately shock frozen in liquid nitrogen and stored at -80ºC for targeted lipidomic analysis for COX-1 derived TxA_2 and 12-LOX derived 12-HETE.

Isolation of peripheral blood human platelets: Washed platelets were isolated from peripheral blood of healthy human subjects as previously described[6]. Briefly, blood from healthy donors was collected in acid-citrate-dextrose (ACD) anti-coagulant (12.5g sodium citrate, 6.82g of citric acid, 10g glucose, 500mL distilled water, adjusted to pH 4.69 with NaOH) and centrifuged at 200xg for 20 minutes without break or acceleration. Platelet-rich plasma (PRP) was collected from the upper 2/3 layer. PRP was diluted with Tyrodes-HEPES buffer (2.5mM HEPES, 150mM NaCl, 1mM KCl, 2.5mM $NaHCO_3$, 0.36mM NaH_2PO_4,

5.5mM glucose, 1 mg/mL BSA, pH 6.5) and centrifuged at 800xg for 10 minutes without break or acceleration. The platelet pellet thus obtained was suspended in PBS (pH7.4) [6] supplemented with $CaCl_2$ or Tyrodes-HEPES buffer (pH7.4). Platelet count was estimated with Sysmex® and adjusted according to experimental demand.

Preparation of murine washed platelets: Blood was collected from the retro-orbital plexus of (8-10) weeks old C57BL/6J mice in ACD anticoagulant (1:4) under isofluran anaesthesia. Blood was centrifuged at 264x g for 5 minutes to obtain PRP. Collected PRP was centrifuged twice at 640xg for 5 minutes to pellet the washed platelets[3, 14]. For further experiments the platelets were resuspended in PBS supplemented with 1mM $CaCl_2$. Platelet count was evaluated with Sysmex® and adjusted as required according to experimental sets.

Collection of activated platelet pellets and releasates from human platelets:

Lipidomics analysis:

Washed platelets ($300x10^6$/sample) from n=11 **healthy donors** were pre-treated with CXCR7-agonist (100µg/mL) or vehicle control (1% DMSO) for 30 minutes at room temperature. Then platelets were either kept under resting condition or activated with thrombin (0.1U/mL) for 15 minutes at room temperature. Thereafter the samples were centrifuged in micro-centrifuge tubes at 600xg for 5 minutes at 4°C. The supernatants were separated from the platelet pellets and both were used for lipid extraction and subsequent lipidomics analysis.

Impact of CXCR7-agonist on the basal platelet lipidome in healthy subjects: In another set of experiment washed platelets ($200x10^6$/sample) from n=5 **healthy donors** were treated with CXCR7-agonist (100µg/mL) for 0, 5, 15, 30 and 60 minutes at room temperature. Platelet samples were immediately shock frozen in liquid nitrogen for estimating time dependent changes to the platelet lipidome under the influence of CXCR7 agonist by untargeted lipidomics analysis for general lipid classes.

Generation and release of 12-HETrE from platelets under the influence of CXCR7-agonist: To evaluate the generation of 12-HETrE in platelets and the release of 12-HETrE in the platelet

microenvironment (supernatant), in a separate set of experiment, platelets from **healthy donors** (n=9) were treated with IP receptor antagonist (RO-1138452-10µM) for 15 minutes at room temperature. Thereafter platelets were treated with CXCR7-agonist (100µg/mL) for 30 and 60 minutes in the presence or absence of IP receptor antagonist. At the end of incubation period, samples were centrifuged in micro-centrifuge tubes at 600xg for 5 minutes at 4°C and the platelet pellet and supernatants were separated, snap frozen in liquid nitrogen and stored at -80°C until further targeted lipidomic analysis for 12-HETrE.

Influence of IP-receptor antagonist, melittin, and G-protein coupling antagonist peptide on the platelet lipidome: To access the impact of IP receptor antagonist (RO-1138452-10µM), Gs coupling antagonist melittin (5µM), and G-protein coupling antagonist peptide (10µM) on the platelet lipidome washed platelets were isolated from n=7 **healthy donors** as described. Platelets were either kept under resting condition or treated with IP receptor antagonist, melittin, or G-protein coupling antagonist peptide at room temperature for 30 minutes. Thereafter samples were snap frozen in liquid nitrogen and stored at -80°C until further targeted (oxylipins) and untargeted (general lipids) lipidomic analysis.

Estimation of pro-inflammatory and thrombotic mediators by cytometric bead array: Isolated washed human platelets ($200x10^6$/sample) from n=5 donors were pre-treated with CXCR7-agonist (100µg/mL) or vehicle control for 30 minutes at room temperature. Then platelets were either kept under resting condition or activated with CRP (5µg/mL) for 30 minutes at room temperature; or treated with IgG fractions isolated from either HIT positive sera (collected from 3 different HIT confirmed donors) or IgG fractions from control sera (collected from 3 different healthy donors) at 1:10 v/v for 1hr at room temperature. Thereafter the samples were centrifuged in micro-centrifuge tubes at 600xg for 5 minutes at 4°C and the supernatants were collected for cytometric bead array (BD Biosciences FACSLyric) (Legendplex®) analysis for human inflammatory chemokines, cytokines, and pro-thrombotic mediators.

cAMP levels in platelets: Washed platelets ($200x10^6$/sample) from n=5 healthy donors were treated with CXCR7-agonist (100µg/mL) for 0, 5, 15, and 30 minutes at room temperature. Thereafter platelet pellets were collected by centrifugation and used for detection of cAMP levels.

Collection of releasates from activated murine platelets: Isolated washed murine platelets ($100x10^6$/sample) were pre-treated with CXCR7-agonist (100µg/mL) or vehicle control for 30 minutes at room temperature. Thereafter platelets were either kept under resting condition or activated with thrombin (0.1U/mL) for 15 minutes at room temperature. The samples were then centrifuged in micro-centrifuge tubes at 650xg for 5 minutes at 4°C and the supernatants were collected for cytometric bead array (Legendplex®) analysis (BD Biosciences FACSLyric) for murine chemokines and cytokines. Data are mean±S.E.M derived from n=10 wild-type C57BL/6J mice.

Western blot analysis: Isolated washed human platelets were pre-treated with vehicle control (1% DMSO) or CXCR7-agonist (100µg/mL) for 15 minutes at room temperature. Then platelets were either kept under resting condition or activated with CRP (5µg/mL) for 10 minutes at room temperature. All platelet samples were lysed at 4°C with lysis buffer [155mM NaCl, 15mM Tris, 1mM EDTA, 0.005 % NaN3, 1 % NP-40, and protease inhibitor cocktail]. Platelet lysates were prepared with reducing sample buffer (Laemmli buffer supplemented with 10 % β-mercaptoethanol) and denatured at 95°C for 5 minutes, separated on an SDS-polyacrylamide gel and transferred onto polyvinylidene fluoride (PVDF) membrane (Millipore) using a SemiDry Transfer Cell System (Peqlab). Equal amounts of protein were loaded in each well, and α-tubulin, or β-actin, or GAPDH were used to assess sample loading as applicable. Subsequently, the membrane was blocked using Rotiblock (1:10 from Roth) and incubated with appropriate primary antibodies against phosphorylated pPLCγ (phospho-PLCγ2-Tyr1217 at 1:750), pSrc (phospho-SrcFamily-Tyr416 reacts with Lyn, Fyn, Lck, Yes and Hck at 1:1000), pPKC (phospho-PKC δ-Thr505 at 1:500), pPI3K [phospho-PI3 Kinase p85 (Tyr458)/p55

(Tyr199) at 1:500], pAkt (p-Akt antibody-Ser473, at 1:200), phospho-p38MAPK [phospho-p38MAPK (Thr180/Tyr182) (3D7) at 1:1000], and anti-α-tubulin (1:1000), anti-β-actin (1:500), anti-GAPDH (1:1000), used as loading control, for overnight at 4°C. For detection, corresponding secondary fluorochrome-labelled antibodies and the Odyssey infrared imaging system (LI-COR, Bad Homburg, Germany) were used[6, 18]. Data are derived from 3 independent experiments.

Intraplatelet cAMP levels by LC-MS/MS analysis:

Sample preparation: Sample extraction was done on ice. The platelet pellets were mixed with 360µL of ice-cold methanol and 20µL of the internal standard (IS) solution (20ng/mL in methanol). The mixture was vortexed for 1 minute and centrifuged at 20,238×g for 3 minutes. The supernatant was transferred to a polypropylene tube and the organic solvent was evaporated at 45°C under a slight stream of nitrogen. The residues were reconstituted in 50µL water containing 0.1% acetic acid.

LC-MS/MS system: Samples were analyzed using liquid chromatography electrospray ionization-tandem mass spectrometry (LC-ESI-MS/MS). The HPLC system consisted of an Agilent 1260 Series binary pump, degasser, and column oven (Agilent Technologies, Waldbronn, Germany) connected to a CTC PAL autosampler (CTC Analytics AG, Zwingen, Switzerland). For detection, a hybrid triple quadrupole-ion trap mass spectrometer 5500 QTRAP (Sciex, Darmstadt, Germany) equipped with a Turbo Ion Spray source was used that operated in negative ion mode. The analytes were separated using an Atlantis T3 column (100 mm×2.1 mm I.D., 3µm particle size and 100 Å pore size; Waters, Milford, MA, USA). The temperature of the column oven was 40°C, and the flow rate was 300µL/minute. The injection volume was 15µL. The separation of the analytes was achieved within a run time of 12 minutes under gradient conditions with eluent A, 0.1% acetic acid, and eluent B, methanol with 10mM ammonium acetate. The gradient program started with 100% A for 1 minute; within 3.5 minutes, the fraction of A was linearly decreased to 15% and remained so for 4.5 minutes. For

0.1-minute, solvent A was increased again to 100% and the column was re-equilibrated for 3.9 minutes. The mass spectrometer was operated in negative multiple reaction monitoring mode (MRM) with a dwell time of 25 ms for all precursor-to-product ion transitions. Entrance potential (EP) was -10V for all transitions while declustering potential (DP), collision energy (CE), and collision cell exit potential (CXP) were optimized manually for each substance. The ionspray voltage was set at -4500V with an ionization source temperature of 550°C. Ion source gases 1 and 2 were set at 50 and 60 psi, respectively, while curtain gas was 40 psi and collision gas 12 psi. All quadrupoles were running at unit resolution. Analyst 1.6 (Sciex) software was used for acquisition Multiquant (Sciex) was used for quantitation.

Sample preparation for lipidomics analysis of platelets from CAD patients: Washed platelets were isolated from arterial blood of CAD patients collected during the percutaneous coronary intervention (PCI) procedure, as previously described[19]. Administration of anti-platelet therapy and statin were considered from the record of medications upon admission. These samples from n=107 CAD patients were processed for untargeted lipidomics analysis for general lipid classes to reveal the status of basal platelet lipidome. The impact of CXCR7-agonist was evaluated on the resting and thrombin activated platelets lipidome in CAD patients, in a separate batch of experiments. Washed platelets isolated from CAD patients (n=15 for general lipids in untargeted analysis and n=7 for oxylipins through targeted lipidomics analysis) were pre-treated with CXCR7-agonist (100µg/mL) or vehicle control (1% DMSO) for 30 minutes at room temperature. Then platelets were either kept under resting condition or activated with thrombin (0.1U/mL) for 15 minutes at room temperature, following which the samples were snap frozen in liquid nitrogen and stored at -80°C until targeted (oxylipins) and untargeted (general lipids) lipidomics analysis.

Lipidomics analysis of platelets and activated platelet releasates:

Lipid extraction from platelet supernatant/releasate: To 96µL of platelet supernatant, 4µL of internal standard solution (C10:0-d19, TXB2-d4, PGE2-d4, HTE-d5, AA-d8, 3 µg/mL of each

compound in MeOH) were added to a final concentration of 120ng/mL of each internal standard. Then, 750µL of MeOH and 2.5mL of MTBE were added. Samples were vortexed and left for 1h at room temperature. Next, 625µL of water was added, and the samples were centrifuged (3500 x g, for 10 minutes). The upper phase was collected, and the lower phase was re-extracted with 1mL of the upper phase of the following mixture: MTBE/MeOH/H_2O (10:3:2.5; v/v/v). The samples were centrifuged again. The upper phases were combined and dried with an EZ2 evaporator from GeneVac (Ipswich, UK) under nitrogen protection. The residues were dissolved in 100µL of MeOH and stored at -20°C till analysis [20].

Lipid extraction from platelet pellet: Lipid extraction was performed with monophasic extraction [21]. To $3x10^8$ platelet pellets 5mL of isopropanol/water 9:1 (v/v) and 5µL of SPLASH® Lipidomix® internal standard mixture was added. For clinical samples (CAD patients, n=107), 4% of SPLASH® Lipidomix®, 100ng/mL arachidonic acid-d_8 and 300ng/mL C18:1-d_7/18:0 Cer were added. After 1h of shaking the supernatant was moved to fresh vials and dried. The dry residue was re-constituted with 100µL of methanol.

Oxylipin extraction: Isopropanol was added to the platelet samples to achieve the ratio isopropanol/water 9:1 (v/v). Mixture of internal standards was added (concentration of stock solution was 25ng/mL in methanol, volume added: 10µL). The supernatant was then diluted with 2mL of the solution: 1M CH_3COONa in water/MeOH 95:5 (v/v) adjusted with acetic acid to pH 6. The samples were loaded on Bond Elut Certify II (3mL/200mg) solid phase extraction cartridges (Agilent). The samples were washed with 5mL of water/methanol 4:1 (v/v) mixture and oxylipins were eluted with 2mL of ethyl acetate/n-hexane/acetic acid 75:24:1; (v/v/v)[22, 23]. The samples were dried and re-constituted in 50µL water/methanol 3:2 (v/v).

Untargeted UHPLC-ESI-QTOF-MS/MS method for lipidomics analysis: 1290 Agilent UHPLC instrument (Agilent, Waldbronn, Germany), PAL-HTX xt DLW autosampler (CTC Analytics AG, Switzerland) and SCIEX TripleTOF 5600+ (SCIEX, Ontario, Canada) were

used for untargeted lipid analysis. ACQUITY CSH C18 column (100mm × 2.1mm; 1.7 µm particle size; Waters Corporation, Millford, MA, USA) was utilized for lipid separation.

The method used for analysis of platelet pellet employed water/acetonitrile 2:3 (v/v) with 0.1% formic acid (v/v) and 10mM ammonium formate as component A and isopropanol/acetonitrile/water 90:9:1 (v/v/v) with 0.1% formic acid (v/v) and 10mM ammonium formate as component B. Gradient run started with 15% B, which increased to 30% B in 2 minutes, then to 48% B in 0.5 minute, next to 82% B in 11 minutes and to 99% B in 0.5 minute; the B level stayed at 99% for 0.5 minute and then dropped in 0.1 minute to the starting level of 15% B for re-equilibration (2.9 minutes). Flow rate was 600µL/min and the column temperature was 65°C. MS scanned m/z from 50-1250 in positive (source voltage 5500V) and negative modes (source voltage -4500V), nebulizer gas, heater gas and the curtain gas were set to 60, 60 and 35 psi, respectively; the source temperature was 350°C, the declustering potential was equal to 80V and collision energy was set at 45±15V [24].

For the platelet releasate analysis we used water with 9.5mM ammonium acetate as component A and isopropanol/acetonitrile/water 10:10:1 (v/v/v) with 9.5mM ammonium acetate as component B. The gradient started with 10% B, which was raised to 20% B in 1 minute, then to 40% B in 8 minutes and to 100% B in 7 minutes, the level was held at 100% B for 2 minutes, then dropped in 0.1 minute to 10% B and the column was re-equilibrated for the final 1.9 minute. Flow rate was 600µL/min and the column temperature was 60°C. The samples were analyzed in MS negative mode, source voltage was -4500V, temperature was 500°C, curtain gas, nebulizer gas and heater gas pressures were equal to 30, 50, 40 psi, respectively and the declustering potential was -80V; collision energy was -20±5V[20].

Targeted micro-UHPLC-ESI-QTrap-MS/MS method for analysis of oxylipins: Oxylipin analysis was performed with Eksigent MicroLC 200 Plus System (Sciex, Ontario, Canada) and QTrap 4500 MS instrument (Sciex). The Eksigent HALO C18 (Sciex) column (50 mm × 0.5 mm; 2.7 µm particle size) was used for compound separation. Mobile phase component A was

water with 0.1% acetic acid and component B was acetonitrile with 0.1% acetic acid. The gradient started with 15% of B and increased to 99% of B in 9 minutes, and then stayed at this level for 1 minute, flow rate was 30µL/min and column temperature was 50°C. Each injection was followed by a washing step with isopropanol and column re-equilibration. MS detection was in negative mode with -4000V source voltage, 400°C source temperature and 25, 20 and 25 psi nebulizer gas, heater gas and curtain gas pressures, respectively. Declustering potential, collision energy and cell exit potential were adjusted individually according to each analyte in selected reaction monitoring mode[22, 23].

Lipidomics data analysis: For untargeted lipidomics MS-Dial[24] was used for peak picking, lipid identification supported with confirmation of correct retention time[21], manual curation and peak integration.

For data from resting and thrombin-activated platelet pellet and corresponding resting and activated platelet supernatant in the presence and absence of CXCR7-agonist, peak heights were normalized by LOWESS algorithm (for samples from healthy donors) or scaled per donor by z-score normalization (for samples from CAD patients; $z = (x-\mu_{\text{all treatments for donor i}})/\sigma_{\text{all treatments for donor i}}$). Statistical evaluation of data from resting and thrombin-activated platelet pellet and corresponding resting and activated platelet supernatant in the presence and absence of CXCR7-agonist was done with the non-parametric paired Wilcoxon signed rank test followed by false discovery rate correction (FDR) computed with R (version i386 3.4.2; R-project for statistical computing). Platelets treated with CXCR7-agonist for different time durations (time course observation) were evaluated with linear regression model. The significance level for the corrected (false discovery rate correction) p-values was 0.05. Multivariate statistics was performed with Sciex MarkerView 1.3.1 software and with SIMCA version 15.0.2 from Sartorius AG (Göttingen, Germany).

Due to the large number of samples (n=107), clinical samples were separated in three processing batches. Thus, subsequently during the batch-wise data processing in MS-Dial,

batches were aligned to merge samples using an in-house developed tool in VBA (in excel). In clinical samples, relative quantification per one-point calibration based on peak heights was performed using isotopically labelled internal standards (ILIS). The internal standard 18:1 (d7) LPC was used to calculate concentrations of LPCs and LPIs, DGs concentrations were calculated with 15:0-18:1 (d7) DG, and for fatty acid (FA) 20:4 (arachidonic acid) and FA 20:3 (dihomogammalinolenic acid), arachidonic acid-d_8 was used.

Normality testing was performed with the Shapiro-Wilk test and variance homogeneity testing with the Bartlett test. Data showing normal distribution were analyzed using non-paired Student´s t-test and for data showing non-normal distribution data the non-parametric Mann-Whitney-U-test was used. Finally, p-values were corrected using Sequential Goodness of Fit (SGoF). All tests were performed in R-Studio 3.5.2 (R Foundation for Statistical Computing, Vienna, Austria, ref. citation: R Core Team (2018). R: A language and environment for statistical computing. R Foundation for Statistical Computing, Vienna, Austria).

References:

1. Chatterjee M, Rath D, Schlotterbeck J, Rheinlaender J, Walker-Allgaier B, Alnaggar N, Zdanyte M, Muller I, Borst O, Geisler T, Schaffer TE, Lammerhofer M, Gawaz M. Regulation of oxidized platelet lipidome: implications for coronary artery disease. Eur Heart J 2017;**38**(25):1993-2005.
2. Rath D, Chatterjee M, Borst O, Muller K, Stellos K, Mack AF, Bongartz A, Bigalke B, Langer H, Schwab M, Gawaz M, Geisler T. Expression of stromal cell-derived factor-1 receptors CXCR4 and CXCR7 on circulating platelets of patients with acute coronary syndrome and association with left ventricular functional recovery. Eur Heart J 2014;**35**(6):386-94.
3. Peng B, Geue S, Coman C, Munzer P, Kopczynski D, Has C, Hoffmann N, Manke MC, Lang F, Sickmann A, Gawaz M, Borst O, Ahrends R. Identification of key lipids critical for platelet activation by comprehensive analysis of the platelet lipidome. Blood 2018;**132**(5):e1-e12.
4. Borst O, Munzer P, Alnaggar N, Geue S, Tegtmeyer R, Rath D, Droppa M, Seizer P, Heitmeier S, Heemskerk JWM, Jennings LK, Storey RF, Angiolillo DJ, Rocca B, Spronk H, Ten Cate H, Gawaz M, Geisler T. Inhibitory mechanisms of very low-dose rivaroxaban in non-ST-elevation myocardial infarction. Blood Adv 2018;**2**(6):715-730.
5. Rheinlaender J, Vogel S, Seifert J, Schachtele M, Borst O, Lang F, Gawaz M, Schaffer TE. Imaging the elastic modulus of human platelets during thrombin-induced activation using scanning ion conductance microscopy. Thromb Haemost 2015;**113**(2):305-11.
6. Chatterjee M, Borst O, Walker B, Fotinos A, Vogel S, Seizer P, Mack A, Alampour-Rajabi S, Rath D, Geisler T, Lang F, Langer HF, Bernhagen J, Gawaz M. Macrophage

migration inhibitory factor limits activation-induced apoptosis of platelets via CXCR7-dependent Akt signaling. Circ Res 2014;**115**(11):939-49.
7. Monteiro MD, Goncalves MJ, Sansonetty F, O'Connor JE. Flow cytometric analysis of calcium mobilization in whole-blood platelets. Curr Protoc Cytom 2003;**Chapter 9**:Unit 9 20.
8. Kawaguchi A, Orba Y, Kimura T, Iha H, Ogata M, Tsuji T, Ainai A, Sata T, Okamoto T, Hall WW, Sawa H, Hasegawa H. Inhibition of the SDF-1alpha-CXCR4 axis by the CXCR4 antagonist AMD3100 suppresses the migration of cultured cells from ATL patients and murine lymphoblastoid cells from HTLV-I Tax transgenic mice. Blood 2009;**114**(14):2961-8.
9. Hu X, Dai S, Wu WJ, Tan W, Zhu X, Mu J, Guo Y, Bolli R, Rokosh G. Stromal cell derived factor-1 alpha confers protection against myocardial ischemia/reperfusion injury: role of the cardiac stromal cell derived factor-1 alpha CXCR4 axis. Circulation 2007;**116**(6):654-63.
10. Hao H, Hu S, Chen H, Bu D, Zhu L, Xu C, Chu F, Huo X, Tang Y, Sun X, Ding BS, Liu DP, Hu S, Wang M. Loss of Endothelial CXCR7 Impairs Vascular Homeostasis and Cardiac Remodeling After Myocardial Infarction: Implications for Cardiovascular Drug Discovery. Circulation 2017;**135**(13):1253-1264.
11. Zhang S, Yue J, Ge Z, Xie Y, Zhang M, Jiang L. Activation of CXCR7 alleviates cardiac insufficiency after myocardial infarction by promoting angiogenesis and reducing apoptosis. Biomed Pharmacother 2020;**127**:110168.
12. Ziegler M, Elvers M, Baumer Y, Leder C, Ochmann C, Schonberger T, Jurgens T, Geisler T, Schlosshauer B, Lunov O, Engelhardt S, Simmet T, Gawaz M. The bispecific SDF1-GPVI fusion protein preserves myocardial function after transient ischemia in mice. Circulation 2012;**125**(5):685-96.
13. Wurster T, Stellos K, Haap M, Seizer P, Geisler T, Otton J, Indermuehle A, Ishida M, Schuster A, Nagel E, Gawaz M, Bigalke B. Platelet expression of stromal-cell-derived factor-1 (SDF-1): an indicator for ACS? Int J Cardiol 2013;**164**(1):111-5.
14. Munzer P, Borst O, Walker B, Schmid E, Feijge MA, Cosemans JM, Chatterjee M, Schmidt EM, Schmidt S, Towhid ST, Leibrock C, Elvers M, Schaller M, Seizer P, Ferlinz K, May AE, Gulbins E, Heemskerk JW, Gawaz M, Lang F. Acid sphingomyelinase regulates platelet cell membrane scrambling, secretion, and thrombus formation. Arterioscler Thromb Vasc Biol 2014;**34**(1):61-71.
15. Lo GK, Juhl D, Warkentin TE, Sigouin CS, Eichler P, Greinacher A. Evaluation of pretest clinical score (4 T's) for the diagnosis of heparin-induced thrombocytopenia in two clinical settings. J Thromb Haemost 2006;**4**(4):759-65.
16. Althaus K, Straub A, Haberle H, Rosenberger P, Hidiatov O, Hammer S, Nowak-Harnau S, Enkel S, Riessen R, Bakchoul T. Heparin-induced thrombocytopenia: Diagnostic challenges in intensive care patients especially with extracorporeal circulation. Thromb Res 2020;**188**:52-60.
17. Althaus K, Pelzl L, Hidiatov O, Amiral J, Marini I, Bakchoul T. Evaluation of a flow cytometer-based functional assay using platelet-rich plasma in the diagnosis of heparin-induced thrombocytopenia. Thromb Res 2019;**180**:55-61.
18. Chatterjee M, Seizer P, Borst O, Schonberger T, Mack A, Geisler T, Langer HF, May AE, Vogel S, Lang F, Gawaz M. SDF-1alpha induces differential trafficking of CXCR4-CXCR7 involving cyclophilin A, CXCR7 ubiquitination and promotes platelet survival. FASEB J 2014;**28**(7):2864-78.
19. Burkhart JM, Vaudel M, Gambaryan S, Radau S, Walter U, Martens L, Geiger J, Sickmann A, Zahedi RP. The first comprehensive and quantitative analysis of human platelet protein composition allows the comparative analysis of structural and functional pathways. Blood 2012;**120**(15):e73-82.
20. Cebo M, Schlotterbeck J, Gawaz M, Chatterjee M, Lämmerhofer M. Simultaneous targeted and untargeted UHPLC-ESI-MS/MS method with data-independent acquisition for

quantification and profiling of (oxidized) fatty acids released upon platelet activation by thrombin. Analytica Chimica Acta 2019.
21. Calderon C, Rubarth L, Cebo M, Merfort I, Lammerhofer M. Lipid Atlas of Keratinocytes and Betulin Effects on its Lipidome Profiled by Comprehensive UHPLC-MS/MS with Data Independent Acquisition Using Targeted Data Processing. Proteomics 2019:e1900113.
22. Cebo M, Fu X, Gawaz M, Chatterjee M, Lammerhofer M. Micro-UHPLC-MS/MS method for analysis of oxylipins in plasma and platelets. J Pharm Biomed Anal 2020;**189**:113426.
23. Cebo M, Fu X, Gawaz M, Chatterjee M, Lammerhofer M. Enantioselective ultra-high performance liquid chromatography-tandem mass spectrometry method based on sub-2microm particle polysaccharide column for chiral separation of oxylipins and its application for the analysis of autoxidized fatty acids and platelet releasates. J Chromatogr A 2020;**1624**:461206.
24. Tsugawa H, Cajka T, Kind T, Ma Y, Higgins B, Ikeda K, Kanazawa M, VanderGheynst J, Fiehn O, Arita M. MS-DIAL: data-independent MS/MS deconvolution for comprehensive metabolome analysis. Nat Methods 2015;**12**(6):523-6.

Supplemental figures, figure legends and legends for video files

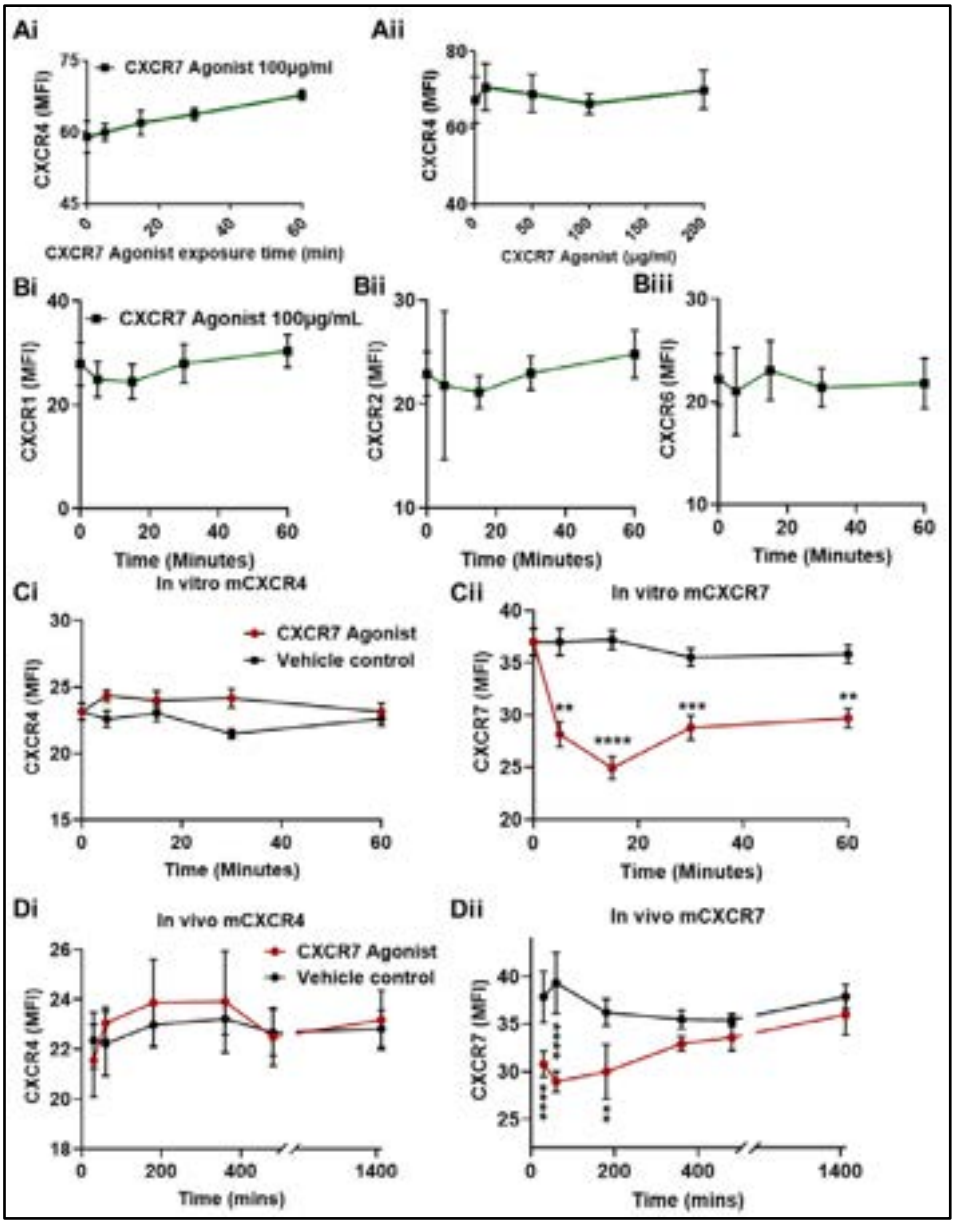

Supplemental Figure S1: Effect of CXCR7-agonist on surface expression of CXCR4, ACKR3/CXCR7 and other CXCR receptors on platelets

Surface expression of CXCR4 on platelets, unlike ACKR3/CXCR7, is not affected under the influence of pharmacological CXCR7-agonist in either a **Ai.** time or **Aii.** dose dependent manner. Data are mean±S.E.M from 4 independent experiments with blood from **4 healthy donors**. CXCR7-agonist (100µg/mL) used in *ex vivo* experiments did not affect the surface expression of other GPCR chemokine receptors (CXCR) **Bi**. CXCR1, **Bii**. CXCR2 or **Biii.** CXCR6 on human platelets. Data are mean±S.D. from 5 independent experiments with blood from **5 healthy donors**. CXCR7 agonist (100µg/mL) given *in vitro* did not affect the surface

expression of **Ci.** CXCR4 on **murine platelets** but **Cii.** internalized ACKR3/CXCR7. Data are mean±S.E.M from experiments done with **5 mice**. CXCR7-agonist (300µg/mouse) administered i.v. did not affect the surface expression of **Di.** CXCR4 on **murine platelets** (at 30 minutes, 1, 3, 6, 8 and 24hrs) but internalized **Dii.** ACKR3/CXCR7 from the platelet surface till 3hrs post administration as compared to vehicle control (1% DMSO). Data are mean±S.D. from experiments done with **5 mice/group** (CXCR7- agonist and vehicle control).

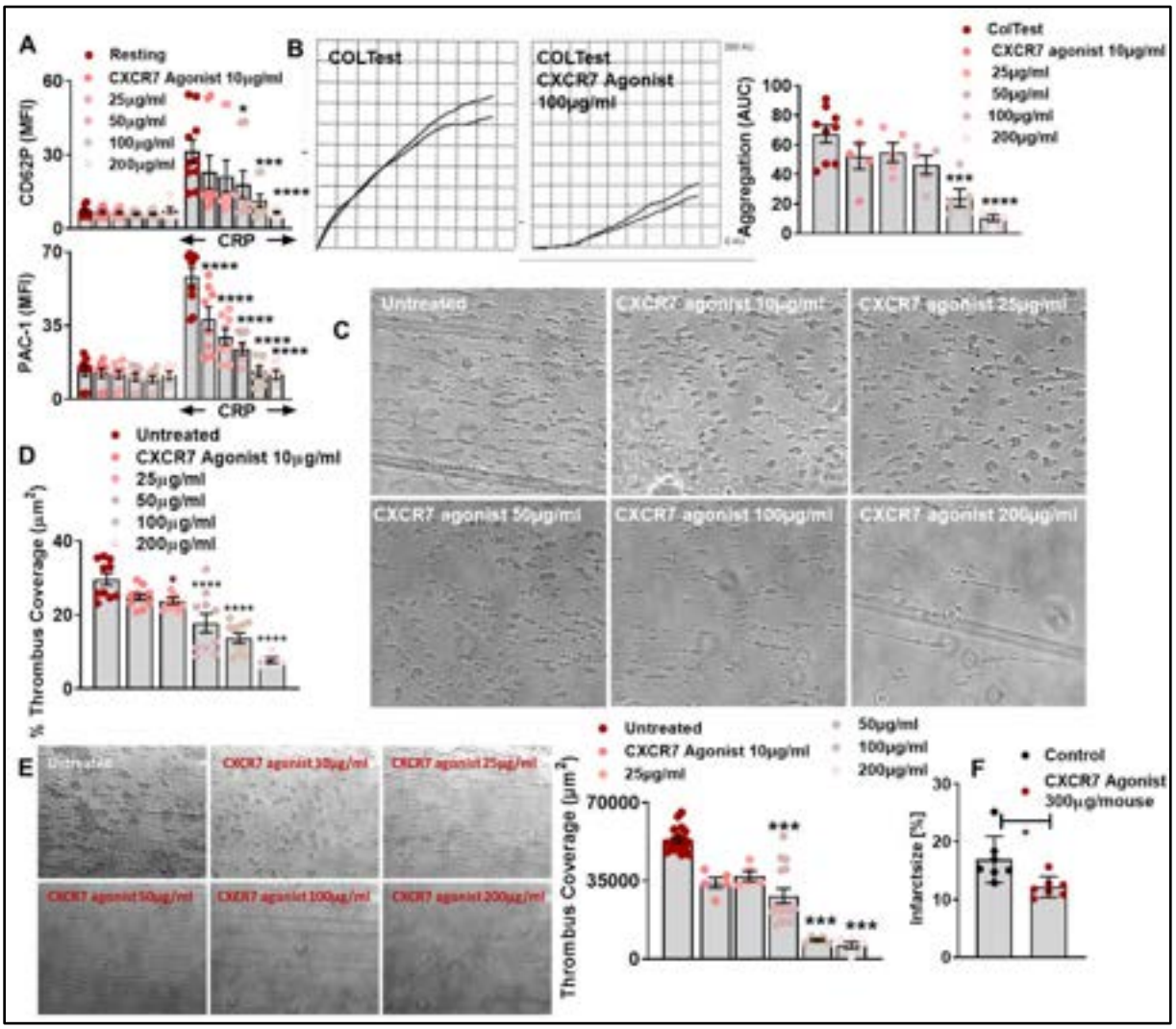

Supplemental Figure S2: Dose dependent effect of CXCR7-agonist on platelet response in human and murine systems

Ex vivo whole blood platelet function assays performed with blood collected from healthy donors showing dose dependent effect of CXCR7-agonist on **A**, platelet surface expression of

CD62P and PAC-1 binding denoting $\alpha_{IIb}\beta_3$-integrin activation **B**, aggregation response to collagen and **C-D**, thrombus formation over collagen coated surface as compared to vehicle control. *p<0.05, ***p<0.001, ****p<0.0001 followed by Sidak's multiple comparisons test. Data are mean±S.E.M from 4-5 independent experiments with blood from 4-5 healthy donors. **E.** Anti-thrombotic effect of CXCR7-agonist deciphered in **murine blood** in the flow chamber assay *in vitro* showing a dose dependent inhibition. Data are mean±S.E.M from 5 independent experiments. ***p<0.001 using Kruskal-Wallis test. **F.** Infarct size in CXCR7-agonist (300µg/mL) and vehicle control (2% DMSO) administered mice 24hrs post-MI. Data are mean±S.D.*<0.01 using unpaired T-test.

Supplemental online Video S3A-F: Anti-thrombotic effects of CXCR7-agonist over collagen observed in T-TAS *ex vivo*

Video files demonstrating the anti-thrombotic effects of CXCR7-agonist (100µg/mL) with respect to vehicle control (1% DMSO) as blood is perfused over collagen coated surface through PL-chips in T-TAS at low (1000/sec), medium (1700/sec) and high (2000/sec) shear rates specified by the manufacturer. These videos are representative of 5 independent experiments performed with blood from 5 healthy donors.

Supplemental online Video S4A-B: Anti-thrombotic effects of CXCR7-agonist over collagen + tissue factor-coated surface seen in T-TAS *ex vivo*

Video files demonstrating the anti-thrombotic effects of **A,** CXCR7-agonist (100µg/mL) with respect to **B,** vehicle control (1% DMSO) as blood is perfused over collagen + tissue factor coated AR-chips in T-TAS at arterial shear rate (800/sec) as specified by the manufacturer. These videos are representative of 5 independent experiments performed with blood from 5 healthy donors.

Supplemental online Video S5A-B: Anti-thrombotic effects of CXCR7-agonist administration in occlusive thrombus formation model in mice.

Video files demonstrating the anti-thrombotic effects of **A,** CXCR7-agonist (100µg/mouse) with respect to **B,** vehicle control (1% DMSO), in counteracting thrombus formation following $FeCl_3$-induced carotid artery injury *in vivo*. These videos are representative of experiments performed with n=14 mice/group.

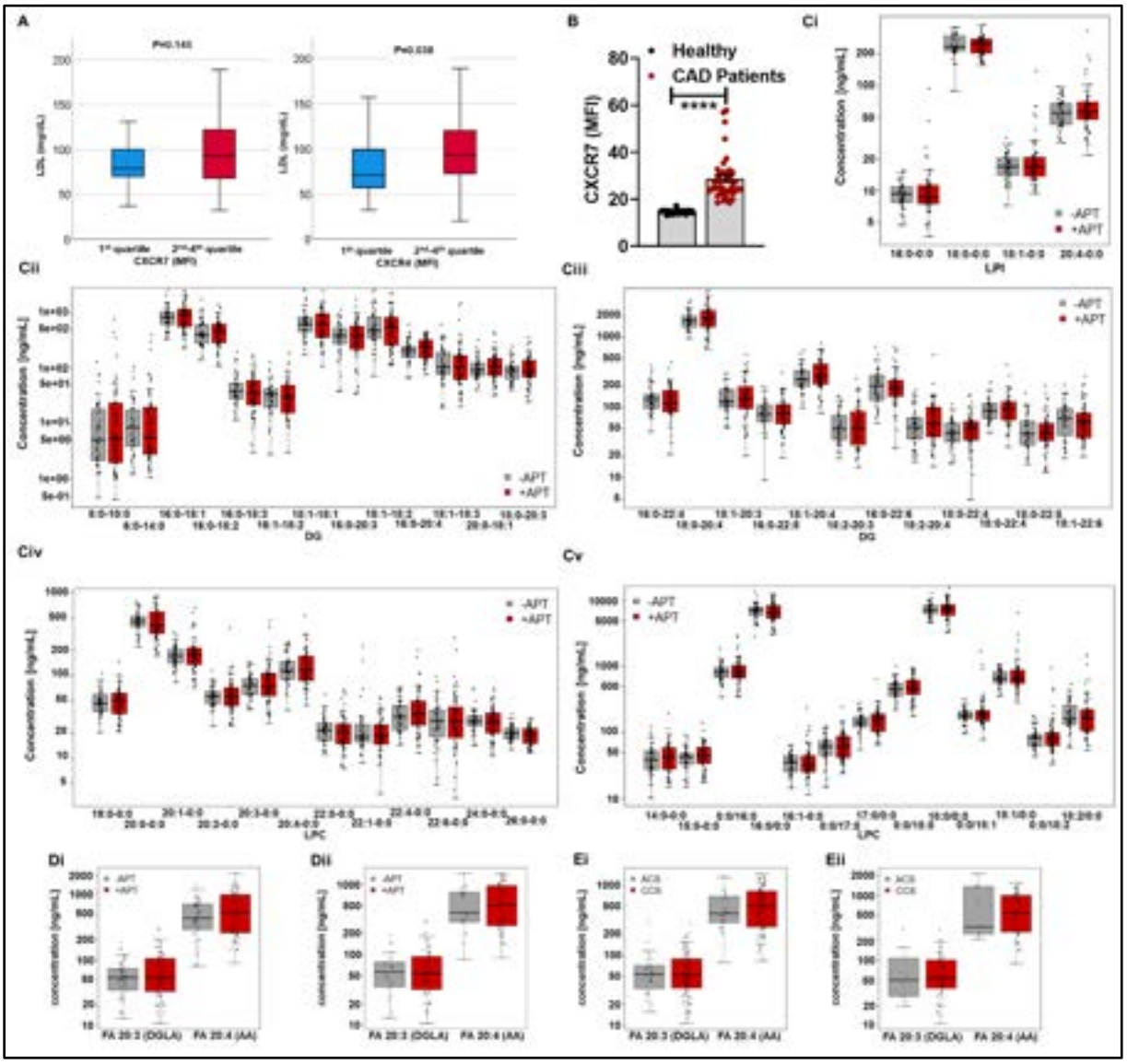

Supplemental Figure S6: Platelet CXCR4 and ACKR3/CXCR7 surface expression in hyperlipidemia and platelet lipidome under the influence of anti-platelet therapy in CAD patients

A. Box-plots (line denotes median) showing stratified ACKR3/CXCR7 and CXCR4 platelet surface expression corresponding to plasma LDL levels in n=106 **CAD patients**. Statistical analysis performed was Mann-Whitney U-test. **B.** Relative surface expression of CXCR7 on

platelets from healthy subjects and CAD patients included for lipidomics and functional analysis following *ex vivo* treatment with CXCR7-agonist (100µg/mL) in this investigation. Data are mean±S.E.M from **n=11 healthy and n=20 CAD patients**. ****p<0.0001 with Mann Whitney U Test. Data from untargeted lipidomics analysis presented as boxplots (line in middle denotes median) showing basal level concentrations of **Ci.** LPIs, **Cii-Biii.** DGs, **Biv-Bv.** LPCs, in platelets from **CAD patients** with or without anti-platelet therapy (APT). (n=107; w/o APT at admission n=46, w/ APT at admission n=61). Concentrations were determined by relative quantification using class-specific ILIS (except LPI, done with surrogate calibrant LPC), and are related to 100µL lipid extract from $3x10^8$ platelets. Boxplots (line in middle denotes median) showing concentrations of AA and DGLA in **Di, all CAD patients** (n=107; w/o-APT: n=46; w/APT: n=61), **Dii, in CAD patients with statin therapy** (n=72; w/o-APT: n=21; w/APT: n=51) and its variance with APT administration in **all CAD patients** depending on **Ei,** disease severity (n=107; ACS: n=26, CCS: n=81) and **Eii, in APT-administered CAD patients** with respect to disease severity (n=61 with APT; ACS: n=10, CCS: n=51). Concentrations were determined by relative quantification using **i**sotope **l**abelled **i**nternal **s**tandard (ILIS) of AA and are related to 100µL lipid extract obtained from $3x10^8$ platelets.

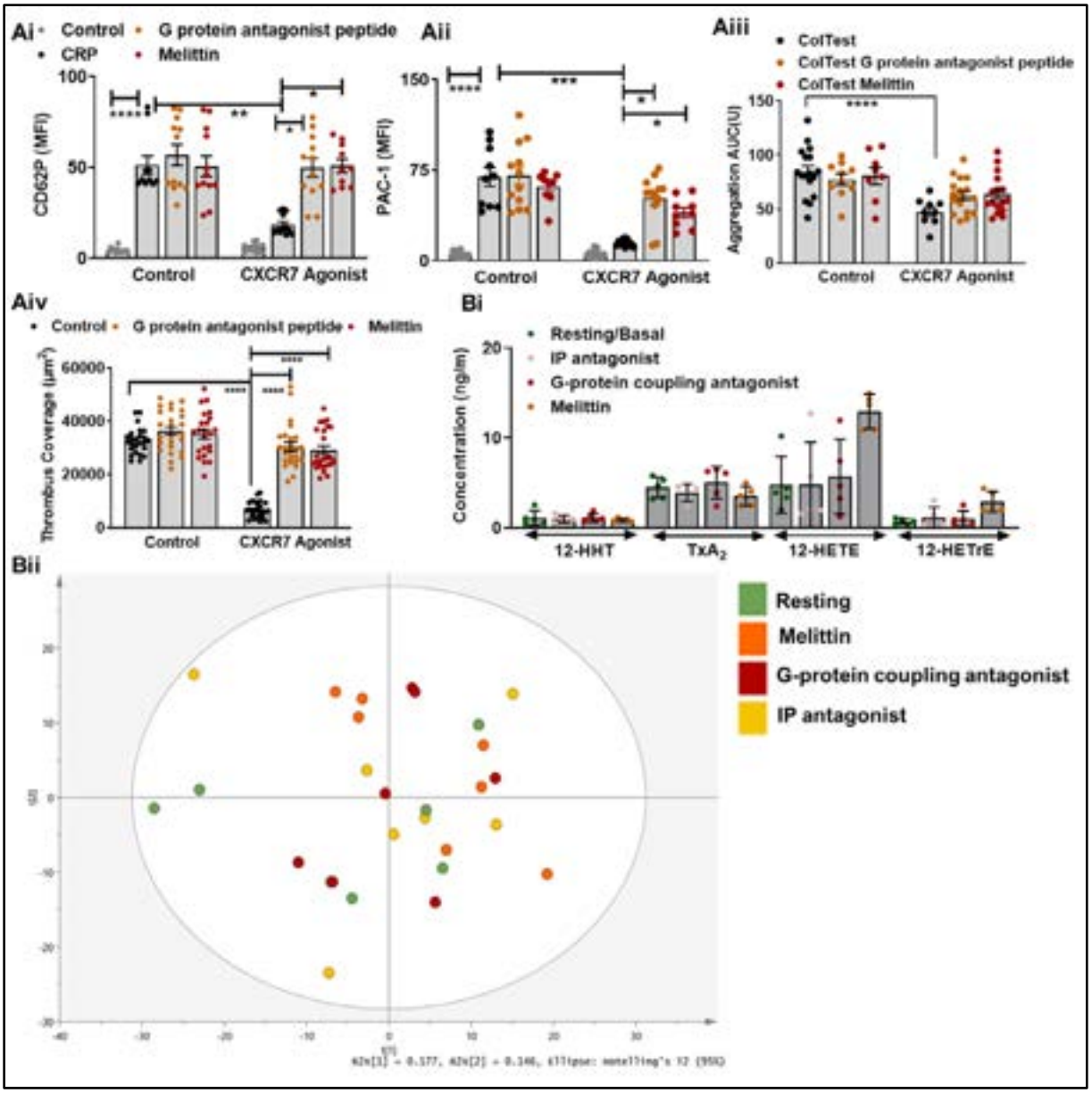

Supplemental Figure S7: Involvement of Gαs-coupled IP receptor in anti-thrombotic actions of CXCR7-agonist

Inhibitory effect of CXCR7-agonist (100µg/mL) on **Ai,** CD62P surface expression **Aii.** PAC-1 binding, (flow cytometry), **Aiii,** collagen-induced aggregation (impedance aggregometry) and **Aiv,** thrombus formation was counteracted by G-protein coupling antagonist peptide (10µM), and melittin (5µM) given as a pre-treatment before CXCR7-agonist for 15 minutes at room temperature. *p<0.05, ***p<0.001, ****p<0.0001 using ANOVA followed by Sidak's multiple comparison test. None of the pharmacological inhibitors interfered with or influenced platelet activation/aggregation/thrombus formation induced by CRP, and collagen respectively.

Bi. Targeted (for oxylipins, n=5) and **Bii.** untargeted (for general lipid classes, n=7) lipidomics analysis of the platelet lipidome of **healthy subjects** demonstrate that the pharmacological inhibitors/antagonist do not induce generation of **Bi.** COX-1 pathway derived (12-HHT, TxA_2) or 12-LOX derived pro-thrombotic (12-HETE) or anti-thrombotic (12-HETrE) oxylipins to a significant extent (FDR adjusted P values >0.05 for each treatment using Wilcoxon signed rank test; n=5 healthy donors) **Bii.** PCA representing variation in lipidomics data across several lipid classes phosphatidylcholine (PC), phosphatidylethanolamine (PE), phosphatidylinositol (PI), lysophosphatidylcholine (LPC), lysophosphatidylethanolamine (LPE), lysophosphatidylinositol (LPI), diacylglycerol (DG), triacylglycerol (TG), sphingomyelin (SM), and Ceramide (Cer) detected in positive and negative mode for resting platelets from **healthy donors** (n=7) and platelets after application of melittin (5µM), G protein antagonist peptide (10µM), or IP-antagonist (RO-1138452 10µM). Lipidomics data are given in concentrations (ng/mL) for $3x10^8$ platelets per 100µL solvent calculated by one-point-calibration to lipid-class-specific isotopically labeled internal standard. Prior PCA, a Z-Score-Scaling for different donors and Pareto-Scaling were applied. PCA reveals no separation depending on the sample treatment (untreated, G protein antagonist peptide, melittin and IP-antagonist).

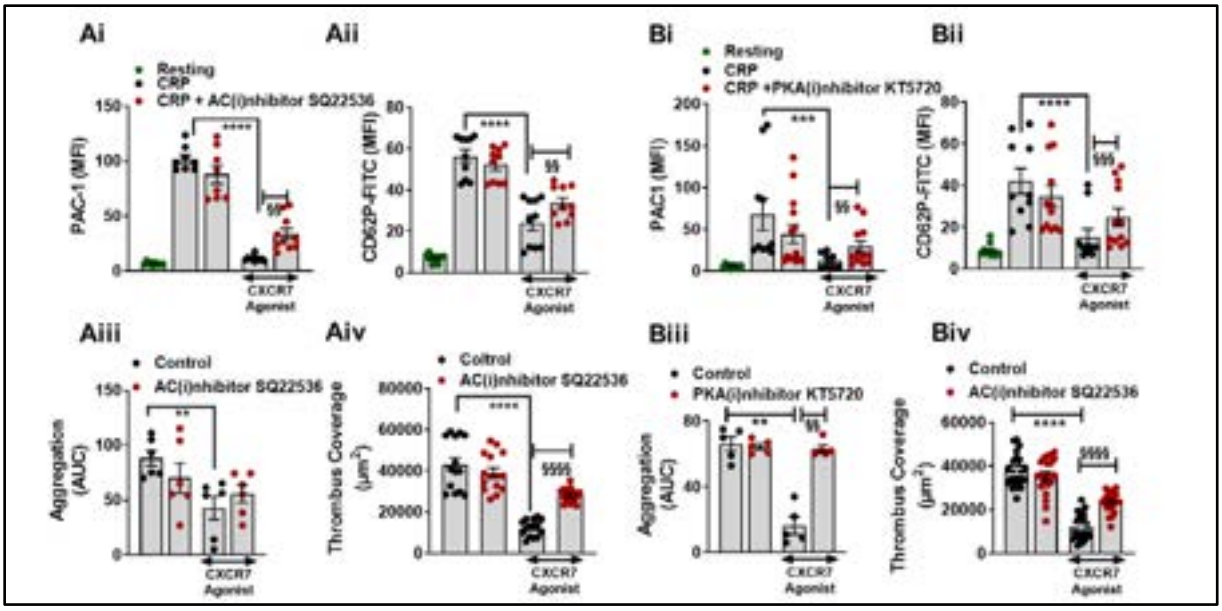

Supplemental Figure S8: Adenylyl cyclase (AC) and cAMP dependent protein kinase (PKA) contribute to the anti-thrombotic effects of CXCR7-agonist.

AC(i)nhibitor SQ22536 (10μM) given as a pre-treatment for 15 minutes at room temperature, counteracted the inhibitory effect of CXCR7-agonist (100μg/mL) on CRP(5μg/mL)-induced platelet **Ai.** PAC-1 binding, **Aii,** CD62P, **Aiii,** collagen-induced platelet aggregation and **Aiv,** thrombus formation. Similarly, the inhibitory effect of CXCR7-agonist (100μg/mL) on CRP (5μg/mL)-induced platelet **Bi,** PAC-1 binding, **Bii,** CD62P surface expression, **Biii,** collagen-induced platelet aggregation and **Biv**, thrombus formation on collagen was counteracted by PKA(i)nhibitor KT5720 (2μM) given as a pre-treatment prior to CXCR7-agonist. Data are mean±S.E.M from 3-5 independent experiments with blood from 3-5 healthy donors with technical replicates. ** or §§ $p<0.01$, *** or §§§ $p<0.001$, **** or §§§§$p<0.0001$. All data analyzed with ANOVA followed by Sidak's multiple comparison test.

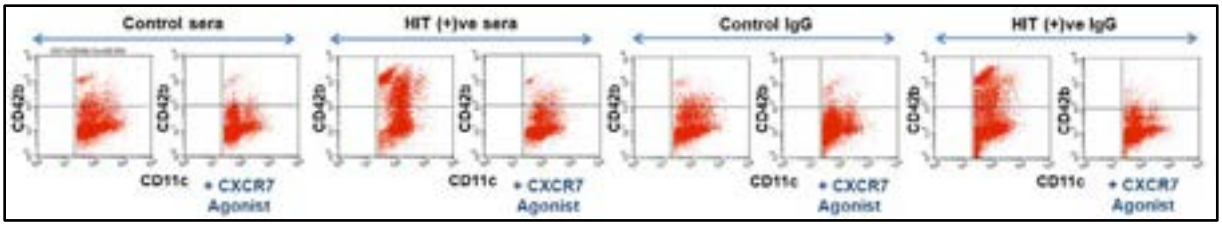

Supplemental Figure S9: CXCR7- agonist reduces thrombo-inflammatory platelet-neutrophil interaction induced by HIT sera and IgG fractions

Flow cytometric quadrant analysis of dot plot showing formation of $CD42b^+$ (anti-human CD42b-FITC)-$CD11c^+$ (anti-human CD11c-APC) platelet-neutrophil aggregates *ex vivo* in blood from healthy donors (n=5 donors) treated with sera or corresponding isolated IgG fractions from control healthy subjects and HIT^+ patients which were incubated at 1:10 v/v dilution for 1hr at room temperature ±CXCR7-agonist (100µg/mL) or vehicle control (1% DMSO) given as a pre-treatment for 30 minutes. CXCR7-agonist reduced the formation of platelet-neutrophil aggregates to a great extent.

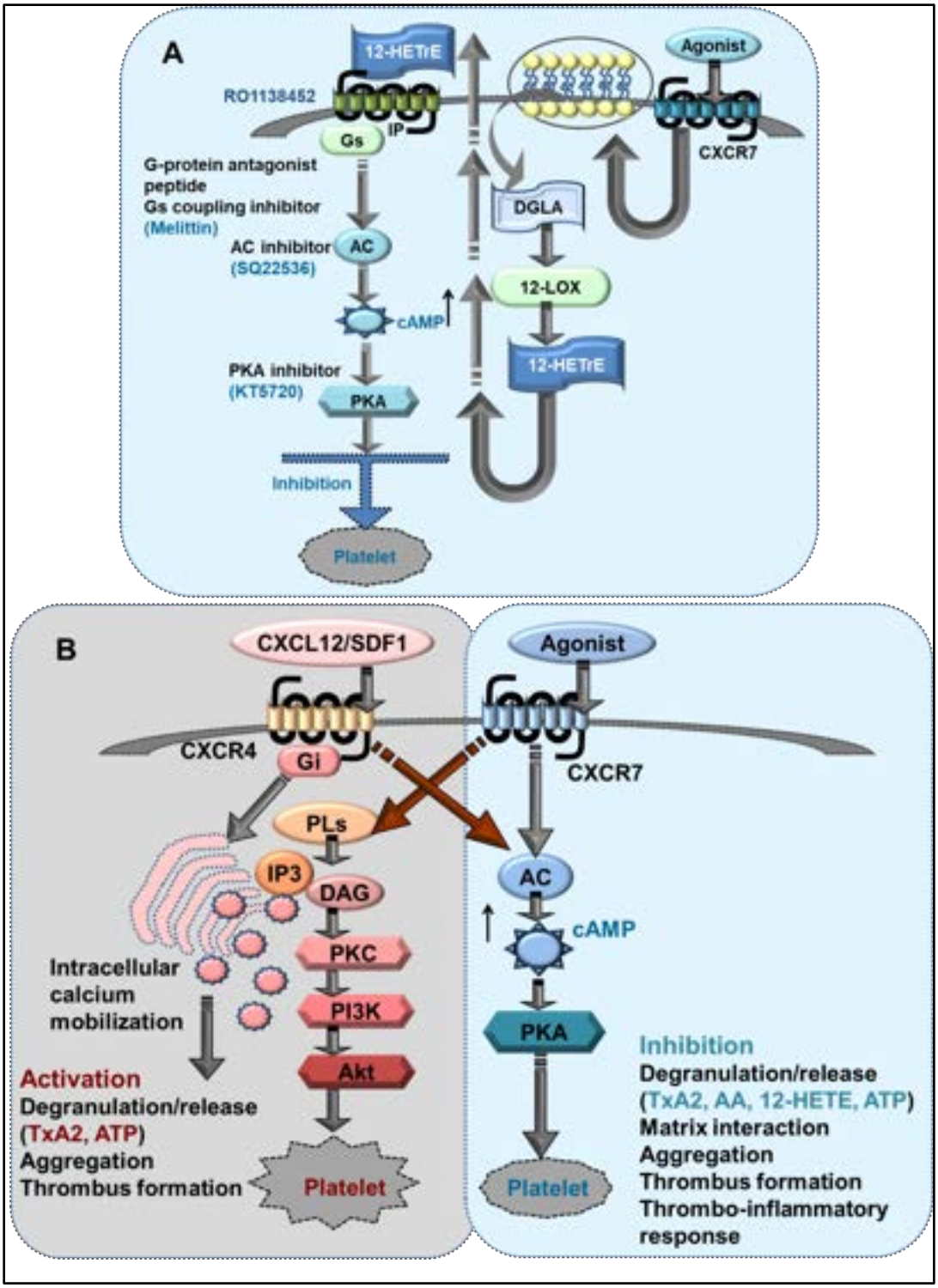

Graphical abstract: Anti-thrombotic mode of action downstream of platelet ACKR3/CXCR7-ligation and its functional dichotomy from CXCR4

A, ACKR3/CXCR7-ligation by a pharmacological agonist alters the intraplatelet lipidome, increases the generation of anti-platelet lipid DGLA and its 12-LOX metabolite 12-HETrE, which engages the Gαs-coupled IP receptor on platelets, elevates cAMP levels and triggers platelet inhibitory AC-cAMP-PKA pathway. Therefore, platelet inhibitory effects of CXCR7-

agonist are reduced in the presence of pharmacological inhibitors of IP, AC, and PKA. **B,** CXCL12/SDF1α engages CXCR4 on platelets to trigger platelet activatory signaling pathway involving PI3K, Akt, intraplatelet-calcium mobilization, TxA_2 production, which promotes platelet aggregation, ATP release, and a pro-thrombotic response. Moreover, CXCR4 being a Gαi-coupled GPCR induces a canonical signaling cascade following ligation by CXCL12/SDF-1α that imposes an inhibitory effect on AC and on the generation of cAMP. On the contrary, ACKR3/CXCR7-ligation on platelets by a pharmacological agonist (VUF11207) triggers the platelet inhibitory signaling cascades involving AC-cAMP-PKA, while counteracting the platelet activatory signaling mediators. This exemplifies the functional dichotomy of CXCR4 and ACKR3/CXCR7 in platelets in mediating pro and anti-thrombotic effects respectively.

2.2 Publication VII

Acute coronary syndrome is associated with a substantial change in the platelet lipidome

Tobias Harm[1], Alexander Bild[1], Kristina Dittrich[2], Andreas Goldschmied[1], Jeremy Nestele[1], Madhumita Chatterjee[1], Xiaoqing Fu[2], Kyra Kolb[1], Tatsiana Castor[1], Oliver Borst[1], Tobias Geisler[1], Dominik Rath[1], Michael Lämmerhofer[2], and Meinrad Gawaz[1*]

[1]Department of Cardiology and Angiology, University Hospital Tu¨bingen, Eberhard Karls University Tübingen, Otfried-Mu¨ller-Straße 10, 72076 Tu¨bingen, Germany; and [2]Institute of Pharmaceutical Sciences, Eberhard Karls University Tübingen, Auf der Morgenstelle 8, 72076 Tübingen, Germany

Reprinted with permission from Cardiovascular Research, Volume 118, Issue 8, May 2022, Pages 1904–1916,

https://doi.org/10.1093/cvr/cvab238

ESC European Society of Cardiology

Cardiovascular Research (2022) **118**, 1904–1916
https://doi.org/10.1093/cvr/cvab238

Acute coronary syndrome is associated with a substantial change in the platelet lipidome

Tobias Harm[1], Alexander Bild[1], Kristina Dittrich[2], Andreas Goldschmied[1], Jeremy Nestele [1], Madhumita Chatterjee [1], Xiaoqing Fu[2], Kyra Kolb[1], Tatsiana Castor[1], Oliver Borst[1], Tobias Geisler[1], Dominik Rath[1], Michael LäMmerhofer [2], and Meinrad Gawaz [1]*

[1]Department of Cardiology and Angiology, University Hospital Tübingen, Eberhard Karls University Tübingen, Otfried-Müller-Straße 10, 72076 Tübingen, Germany; and [2]Institute of Pharmaceutical Sciences, Eberhard Karls University Tübingen, Auf der Morgenstelle 8, 72076 Tübingen, Germany

Received 2 March 2021; revised 21 May 2021; editorial decision 1 July 2021; online publish-ahead-of-print 21 July 2021

Time for primary review: 45 days

Aims Platelets play a key role in the pathophysiology of coronary artery disease (CAD) and patients with enhanced platelet activation are at increased risk to develop adverse cardiovascular events. Beyond reliable cardiovascular risk factors such as dyslipoproteinaemia, significant changes of platelet lipids occur in patients with CAD. In this study, we investigate the platelet lipidome by untargeted liquid chromatography–mass spectrometry, highlighting significant changes between acute coronary syndrome (ACS) and chronic coronary syndrome (CCS) patients. Additionally, we classify the platelet lipidome, spotlighting specific glycerophospholipids as key players in ACS patients. Furthermore, we examine the impact of significantly altered lipids in ACS on platelet-dependent thrombus formation and aggregation.

Methods and results In this consecutive study, we characterized the platelet lipidome in a CAD cohort ($n = 139$) and showed significant changes of lipids between patients with ACS and CCS. We found that among 928 lipids, 7 platelet glycerophospholipids were significantly up-regulated in ACS, whereas 25 lipids were down-regulated compared to CCS. The most prominent up-regulated lipid in ACS, PC18:0 (PC 10:0-8:0), promoted platelet activation and *ex vivo* platelet-dependent thrombus formation.

Conclusions Our results reveal that the platelet lipidome is altered in ACS and up-regulated lipids embody primarily glycerophospholipids. Alterations of the platelet lipidome, especially of medium chain lipids, may play a role in the pathophysiology of ACS.

* Corresponding author. Department of Cardiology and Angiology, University Hospital Tübingen, Eberhard Karls University Tübingen, Otfried-Müller-Str. 10, 72076 Tübingen, Germany. Tel: +49 7071 83688; fax +49 7079 29 5749, E-mail: meinrad.gawaz@med.uni-tuebingen.de

Graphical Abstract

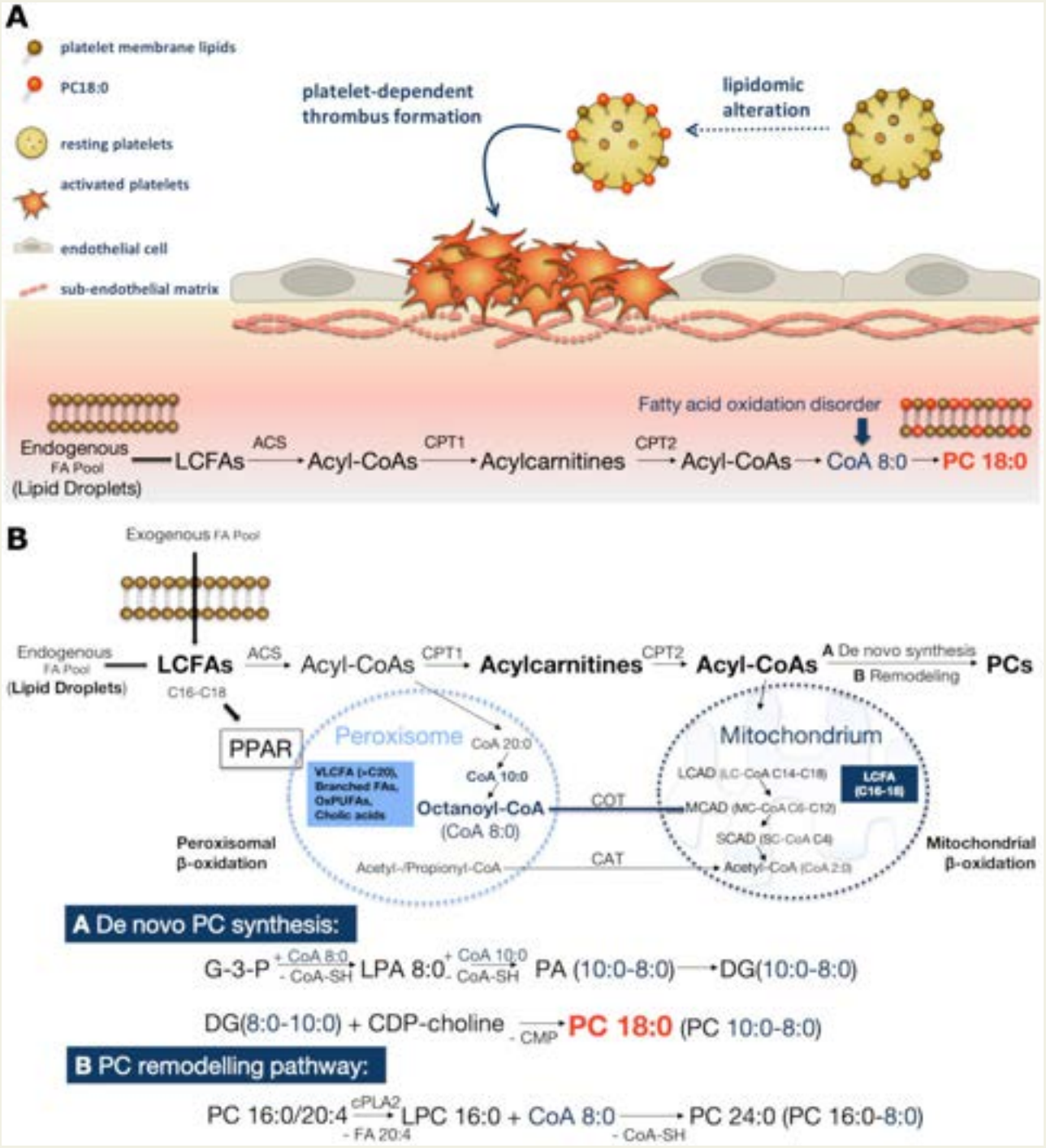

Hypothetical pathways of altered platelet phospholipid synthesis resulting in enhanced PC18:0 expression. Aberrant peroxisomal and/or mitochondrial platelet fatty acid oxidation leads to increased levels of medium chain fatty acyl-CoA (CoA 8:0 and CoA 10:0) which are utilized for *de novo* PC18:0 synthesis. Remodelling of glycerophospholipids results in enhanced PC24:0 synthesis. Their integration into the platelet cell membrane may influence platelet function.
ACS, acyl-CoA synthetase; AT, acyltransferases; CAT, carnitine acetyltransferase; CDP, cytidinediphosphocholine; CoA, coenzyme A; COT, carnitine octanoyltransferase; CPT1/2, carnitine palmitoyltransferase; FA, fatty acid; FFA, free fatty acid; LCAD, long-chain acyl-CoA dehydrogenase; LPCAT, lysophosphatidylacyltransferase; MCAD, medium-chain acyl-CoA dehydrogenase; MI, mitochondrium; PO, peroxisome; SCAD, short-chain acyl-CoA dehydrogenase; VLCFA, very long chain FA.

Keywords Acute coronary syndrome • Platelet lipidome • Biomarker • Thrombo-inflammation

1. Introduction

Platelets are critically involved in the pathophysiology of acute coronary syndrome (ACS).[1–4] At site of rupture of a coronary plaque, platelets adhere to collagen exposed towards the blood stream, accumulate and promote thrombosis that limits coronary perfusion leading to myocardial ischaemia.[5–8] Antiplatelet therapy is the cornerstone in treatment or secondary prevention of ACS.[9] Enhanced platelet hyper-reactivity is a risk factor for thromboischaemic events in patients with coronary artery disease (CAD).[10–13] Patients with enhanced platelet activation are at increased risk to develop adverse cardiovascular events including myocardial infarction, ischaemic stroke, and death.[12] Furthermore, sustained activation of circulating platelets promotes thrombo-inflammation and atheroprogression in CAD which determines the long-term course of the disease.[12] Cardiovascular risk factors such as dyslipoproteinaemia or diabetes promote platelet activation.[14–16] The underlying molecular mechanisms are incompletely understood. Previously we observed that binding of oxidized low-density lipoproteins (oxLDL) on circulating platelets is increased in ACS patients and is associated with enhanced platelet activity.[14] Later on we further documented elevated intraplatelet levels of oxLDL in CAD patients and even more in ACS patients.[17,18] The purpose of the present study was to evaluate and to define changes in the platelet lipidome in a consecutive cohort of patients with CAD ($n = 139$). We found that the platelet lipidome is significantly altered in patients with acute when compared to chronic coronary syndrome (CCS). Changes in the platelet lipidome may contribute to the pathophysiology of ACS and comprehensive analysis of intraplatelet lipids may offer novel diagnostic options to monitor therapeutic efficacy in patients with CAD.

2. Methods

2.1 Study population

One hundred and thirty-nine patients with symptomatic CAD were enrolled in this study (*Table 1*). Patients were consecutively recruited into the study between February and May 2017 at the University Hospital of Tübingen. All patients were treated for symptomatic CAD and the severity of the disease was analysed by coronary angiography within 24 h after hospital admission. Blood samples were obtained from the arterial sheath at time of coronary angiography before administration of unfractionated heparin. The study was approved by the local ethics committee (270/2011B01) and all patients gave written informed consent. The experiments were performed in accordance with the ethical standards as laid down in the Declaration of Helsinki.

2.2 Platelet lipidomics

Platelets were isolated for lipidomic analysis as previously described.[19–21] According to standardized protocols, lipid extraction from isolated platelets was performed with a monophasic extraction protocol (2-propanol/water 90:10, v/v).[22] A set of 16 isotopically labelled internal standards [ILIS, final concentrations of 4% SPLASH™ Lipidomix® (14 ILIS), 100 ng/mL arachidonic acid-d8, and 300 ng/mL C18 Ceramide-d7 (d18:1-18:0)] was added prior extraction. The lipid extracts were analysed in three separate batches by a non-targeted lipidomic assay using liquid chromatography coupled to mass spectrometry (UHPLC-ESI-QTOF-MS/MS) using data-independent acquisition with stepwise window acquisition of MS/MS spectra (SWATH) in positive and negative ion mode.

The open-source software MS-DIAL[23] was used for batch-wise data pre-processing including peak picking, alignment, and identification (structural annotation) by matching MS/MS spectra with LipidBlast database. Based on peak tables of each batch from MS-DIAL a reference peak table was generated by an in-house developed batch alignment tool to combine lipidomic data from three batches to one data set. Using the reference peak table, batches were reanalysed in MultiQuant (Sciex, Concord, Ontario, Canada) to extract peak heights of all reference list features. Pre-processed data were normalized using a combination of quality control-based method systematic error removal using random forest (FiehnLab, Davis, CA, USA)[24] and ILIS-based method removal of unwanted variation random (RUVrandom)[25] in RStudio 3.5.2 with the package NormalizeMets.[26] Further details of the data processing method and lipid identification are given in the Supplementary material online.

Normalized peak intensities were submitted to one-way analysis of variance (ANOVA) using JMP® version 14.2.0 to identify peaks varying significantly ($P < 0.05$) between groups. Interpretation of high-dimensional biological data in lipidomics and parallel testing of hypothesis is accompanied by the potential of type I and type II statistical errors. To account for the problem of multiple hypothesis testing and to eliminate accumulation of false-positive results (type I errors), a false discovery rate (FDR) controlling procedure was further adopted to correct significance levels ($P < 0.05$) for FDR ≤5%. Therefore, we implemented sequential goodness of fit (SGoF) testing of lipid peak intensities using Myriads (Free Software Foundation, Inc., Boston, MA, USA). SGoF was adapted to this study as described in lipidomics.[17,27,28] The algorithm is well-suited because of its increasing test power and lowered FDR when exploring large-number data sets ($n = 928$ tests).[29,30] Lipidomic category tree was created using OmniGraffle 7.12 (The Omni Group, Seattle, WA, USA).

2.3 Chemicals and materials

Lipids including PC 16:0/22:6 (1-palmitoyl-2-docosahexaenoyl-sn-glycero-3-phosphocholine, chloroform); Lyso-PC 18:0 (1-stearoyl-2-hydroxy-sn-glycero-3-phosphocholine, powder); LysoPE 16:0 (1-palmitoyl-2-hydroxy-sn-glycero-3-phosphoethanolamine, powder); PC 9:0/9:0 (1,2-dinonanoyl-*sn*-glycero-3-phosphocholine, powder); PC 18:1/14:0 (1-oleoyl-2-myristoyl-sn-glycero-3-phosphocholine, powder); and PC 18:1/16:0 (1-oleoyl-2-palmitoyl-sn-glycero-3-phosphocholine, powder) were purchased from Sigma-Aldrich (Steinheim, Germany), dissolved and stored according to manufacturer's guidelines (note, PC 9:0/9:0 was purchased as physicochemically closest substitute for PC 10:0-8:0 which was not commercially available; for the same reason, PC 18:1/14:0 and PC 18:1/16:0 were replacing PC16:0e/16:1 and PC18:1e/16:0, respectively, in the *ex vivo* experiments). Dulbecco's Phosphate Buffered Saline with Ca^{2+} and Mg^{2+} (PBS) and Dimethyl sulfoxide (DMSO) were purchased from Sigma-Aldrich, Horm Collagen and SKF solution from Takeda Austria GmbH (Linz, Austria), ADP (ADPtest), arachidonic acid (ASPItest), and collagen (COLtest) from F. Hoffmann-La Roche Ltd. (Basel, Switzerland). The fluorescent PC Fluo-PC16:0-6:0 was from Avanti Polar Lipids. CD62P FITC + CD42b PE antibodies were purchased from Beckman Coulter Life Science (Krefeld, Germany). Collagen-related peptide (CRP 0.5 µg/mL) was purchased from Cambcol Laboratories (Cambrigeshire, UK).

2.4 *Ex vivo* platelet-dependent thrombus formation

Platelet-dependent thrombus formation was analysed using a flow chamber as previously described.[31] CPDA-Citrated and DiOC6

Table 1 Baseline characteristics of the patients' cohort

	All ($n = 139$)	CCS Troponin − ($n = 100$, 71.9%)	ACS Troponin + ($n = 39$, 28.1%)	*P*-value
Male, *n* (%)	101 (72.7%)	71 (71.0%)	30 (76.9%)	0.477
Age, years (mean ± SD)	70.6 (±11.2)	70.4 (±10.4)	71.2 (±13.1)	0.310
Body mass index (mean ± SD)	27.1 (±4.7)	27.3 (±4.7)	26.3 (±4.8)	0.170
Cardiovascular risk factors				
Arterial hypertension, *n* (%)	109 (78.4%)	80 (80.0%)	29 (74.4%)	0.473
Hyperlipidaemia, *n* (%)	64 (46.0%)	52 (52.0%)	12 (30.8%)	0.023
Diabetes mellitus, *n* (%)	41 (29.5%)	27 (27.0%)	14 (35.9%)	0.307
Current smoking, *n* (%)	23 (16.5%)	17 (17.0%)	6 (15.4%)	0.817
Ex smoking >6 months, *n* (%)	23 (16.5%)	17 (17.0%)	6 (15.4%)	0.817
Obesity, *n* (%)	65 (46.8%)	54 (54.0%)	11 (28.2%)	0.006
Atrial fibrillation, *n* (%)	33 (23.7%)	24 (24.0%)	9 (23.1%)	0.908
Previous CABG, *n* (%)	13 (9.4%)	11 (11.0%)	2 (5.1%)	0.260
Previous MI, *n* (%)	29 (20.9%)	25 (25.0%)	4 (10.3%)	0.043
Renal function (GFR) (mean ± SD)	74.9 (± 30.63)	73.0 (± 25.7)	79.6 (± 40.6)	0.577
Medication on admission				
Acetylsalicylic acid, *n* (%)	112 (80.6%)	83 (83.0%)	29 (74.4%)	0.257
Clopidogrel, *n* (%)	36 (25.9%)	34 (34.0%)	2 (5.1%)	0.001
Ticagrelor, *n* (%)	44 (31.7%)	31 (31.0%)	12 (30.8%)	0.505
Prasugrel, *n* (%)	9 (6.5%)	6 (6.0%)	3 (7.7%)	0.720
Cangrelor, *n* (%)	1 (0.7%)	0 (0.0%)	1 (2.6%)	0.110
Oral anticoagulants, *n* (%)	33 (23.7%)	28 (28.0%)	5 (12.8%)	0.048
Angiotensin-converting enzyme inhibitors, *n* (%)	71 (51.1%)	53 (53.0%)	18 (46.2%)	0.468
Angiotensin II receptor antagonists, *n* (%)	32 (23.0%)	25 (25.0%)	7 (17.9%)	0.366
Aldosterone antagonists, *n* (%)	28 (20.1%)	24 (24.0%)	4 (10.3%)	0.056
Ca channel antagonists, *n* (%)	38 (27.3%)	31 (31.0%)	7 (17.9%)	0.111
β-blockers, *n* (%)	89 (64.0%)	67 (67.0%)	22 (56.4%)	0.246
Diuretics	54 (38.8%)	42 (42.0%)	12 (30.8%)	0.218
Statins, *n* (%)	92 (66.2%)	76 (76.0%)	16 (41.0%)	0.001
Lipid profile parameters				
LDL-cholesterol (mg/dL) (mean ± SD)	96.0 (±32.9)	94.1 (±33.7)	101.2 (±30.5)	0.193
HDL-cholesterol (mg/dL) (mean ± SD)	47.6 (±16.1)	48.8 (±16.7)	44.4 (±14.0)	0.225
Triglycerides (mg/dL) (mean ± SD)	150.4 (±90.2)	153.4 (±89.6)	142.3 (±92.5)	0.351
Total cholesterol (mg/mL) (mean ± SD)	161.2 (±43.6)	161.0 (±42.7)	161.7 (±46.7)	0.936
Platelets (10^9/L) (mean ± SD)	225.1 (±84.8)	229.9 (±72.7)	230.8 (±110.5)	0.717
Disease				
Stable angina	75 (54.0%)	75 (75.0%)	–	
Unstable angina	25 (18.0%)	25 (25.0%)	–	
NSTEMI	29 (20.9%)	–	29 (74.4%)	
STEMI	10 (7.2%)	–	10 (25.6%)	
Follow-up events (12 months)				
Death	7 (5.0%)	6 (6.0%)	1 (2.6%)	0.375
Myocardial infarction	0 (0.0%)	0 (0.0%)	0 (0.0%)	
Stroke	0 (0.0%)	0 (0.0%)	0 (0.0%)	

Normally distributed data were analysed using Student's *t*-test. Non-normally distributed data were compared using the Mann–Whitney *U* test. Mean values are presented as mean, lower and upper 95% confidence interval. Discrete data were calculated using Chi-square (Pearson). Odds ratio is presented with lower and upper 95% confidence interval.

fluorochrome labelled whole blood was perfused over collagen-coated (100 µg/mL) cover slips with a shear rate of 500/1700 s^{-1} and photo-documented after the blood perfusion was stopped. The thrombus area was quantified in photo-documented images (Nikon Eclipse Ti2-A, NIS-Elements AR, Nikon, Tokyo, Japan). As indicated blood samples were preincubated with lipids or control vehicle (DMSO) for 30 min before analysis in concentrations as indicated. A detailed description of data acquisition and analysis is given in Supplementary material online, *Methods*.

2.5 Platelet impedance aggregometry

Impedance platelet aggregometry was analysed according to standard procedures (Multiplate Analyzer, F. Hoffmann-La Roche Ltd., Basel,

Switzerland).[32] 20 µL ADP 6.5 µM, arachidonic acid (AA) 484 µM, and collagen 3.2 µg/mL were used as agonists. Hirudin whole blood (300 µL per sample) from healthy volunteers was incubated with glycerophospholipids (100 µM) or control vehicle (DMSO) for 30 min before analysis in concentrations as indicated.

2.6 Platelet flow cytometry

The effect of glycerophospholipid on platelet P-selectin expression was determined by flow cytometry (FACS-Calibur flow cytometer, Becton-Dickinson, NJ, USA). Platelets were activated with CRP in the presence of PC18:0, PC38:6 (100 µM), or control diluent and analysed as described.[31]

2.7 Isolation of platelets, platelet spreading and Ca^{2+} measurement

Platelets were isolated as described previously.[27] Spreading experiments of isolated platelets were performed onto immobilized fibrinogen in the presence or absence of PC18:0 or PC38:6 (100 µM), respectively. Intracellular Ca^{2+} measurements were performed in Fura-4-labelled platelets. Lipid membrane integration of PC Fluo-PC16:0-6:0-NBD into adherent platelets was determined by fluorescence microscopy as described in detail in Supplementary material online, *Methods*.

2.8 Statistical analysis

Patient data were analysed using JMP® version 14.2.0 (SAS Institute, Cary, NC, USA). Non-normally distributed data were compared using the Mann–Whitney *U* test. Normally distributed data were analysed using Student's *t*-test. Mean values are presented as mean, lower and upper 95% confidence interval. Discrete data were compared using Chi-square (Pearson). Odds ratio is presented with lower and upper 95% confidence interval.

Correlations of normally distributed data were assessed by Pearson's correlation coefficient (r). Correlations of non-normally distributed data were analysed using Spearman's rank correlation coefficient (ρ). OPLS-DA and PCA-X were performed using SIMCA® by Umetrics version 16.0 (Sartorius AG, Goettingen, Germany).

Experimental data (mean ± SEM) were analysed using GraphPad Prism8 software (GraphPad Software, Inc., San Diego, CA, USA) at $P < 0.05$ statistical significance with two-way analysis of variance using Dunnett's *post hoc* test.

3. Results

3.1 Characterization of the platelet lipidome in coronary artery disease

Recently, we showed that significant changes of the platelet lipidome occur in patients with ACS compared to healthy matched controls.[17] In the present study, we analysed the platelet lipidome by untargeted UHPLC-ESI-QTOF-MS/MS in a large consecutive cohort of patients presenting with symptomatic CAD ($n = 139$). The demographic details and characteristics are given in *Table 1*. Twenty-eight percent of the enrolled patients were diagnosed with troponin-positive ACS (ST-segment elevation myocardial infarction, non-ST-segment elevation myocardial infarction). After clearance of non-verifiable signals, we could identify 928 lipids extracted from isolated platelets (*Figure 1A*). Among those extractable lipids, the main lipid categories were defined as glycerophospholipids (52.2%), glycerolipids (24.2%), sphingolipids (19.0%), fatty acyls (3.7%), and sterol lipids (0.9%) (*Figure 1B*). The distribution of peak intensities and derived concentrations, respectively, of platelet lipids showed a wide variability within the subcategories of lipids. This indicates that the amount of individual lipids and subtypes are highly heterogeneous in platelets (*Figure 2*).

To evaluate whether the platelet lipidome varies with the acuity of the disease, we compared mean intensities of distinct lipids between patients with ACS and CCS (*Figure 3*). We found that among 928, 7 lipids were significantly up-regulated in ACS ($P < 0.05$, FDR < 5%), whereas 25 were down-regulated compared to CCS ($P < 0.05$, FDR < 5%) (*Figure 4*). Significantly up-regulated lipids comprised of lipids exclusively belonging to the category of glycerophospholipids phosphocholines [PC, $n = 6$; PC 34:1e (PC 18:1e/16:0), PC 32:1e (PC 16:0e/16:1), PC 24:0 (PC16:0-8:0), PC 30:4 (PC 10:0-20:4), PC 20:0 (PC 10:0-10:0), PC 18:0 (PC 10:0-8:0)]; phosphoethanolamine [PE, $n = 1$; PE 34:0 (PE 16:0-18:0)] (*Figure 5*). In healthy controls, platelet levels of these identified phospholipids were significantly lower compared to patients with CAD (*Figure 5*). It is striking that these lipids share at least one of three characteristic features: (i) high degree of saturation, (ii) medium chain saturated fatty acid side chains, and (iii) alkenyl or alkyl ether (e) linkage instead of acyl linkage in glycerophospholipids. Among those lipids that were down-regulated, different lipid groups were comprised of glycerophospholipids ($n = 20$), phosphocholines [PC, $n = 14$; PC 36:6 (PC 14:0-22:6), PC 35:4 (PC 15:0-20:4), PC 38:6 (PC 16:0-22:6), PC 37:4 (PC 17:0-20:4(1), PC 17:0-20:4(2)), PC 39:6 (PC 17:0-22:6), PC 38:4 (PC 18:0-20:4), PC 40:6 (PC 18:0-22:6), PC 42:6 (PC 20:0-22:6), PC 42:10 (PC 20:4-22:6), PC 44:10 (PC 22:5-22:5), PC 36:5e (PC16:1e/20:4), PC 42:6e(1) (PC20:0e/22:6)(1), PC 42:6e(2) (PC20:0e/22:6)(2)]; lyso-phospholipids (LPL, $n = 4$; LPC 0:0/18:0, LPC 18:0/0:0, LPE 16:0, LPE 18:0); phosphoethanolamines [PE, $n = 2$; PE 40:7e (PE 18:1e/22:6), PE 42:10 (PE 20:4-22:6)], glycerolipids ($n = 4$), diglycerides [DG, $n = 1$; DG 40:4 (DG 18:0-22:4)]; triglycerides [TG, $n = 3$; TG 56:6 (TG 16:0-18:0-22:6), TG 58:6 (TG 16:0-20:0-22:6), TG 60:10 (TG 18:0-20:4-22:6)], and sphingolipids ($n = 1$), sphingomyelins (SM, $n = 1$; SM d40:1) (*Figure 5*). Here, it is characteristic that these lipids share either (i) high degree of unsaturation (PUFA-PLs, PUFA-DG, PUFA-TGs), or (ii) deacylation (LPE, LPC). Concentration values of significantly altered lipids in ACS compared to CCS are given in Supplementary material online, *Tables S3–S5*.

3.2 Effect of comedication (statins, P2Y12 inhibitors) and comorbidities (hyperlipidaemia, obesity) on platelet lipidome

Furthermore, we tested the effect of comedication (statins, P2Y12 inhibitors) and comorbidities (hyperlipidaemia, obesity) on platelet lipidome. O2PLS-DA analysis for comedications and PCA for comorbidities was performed using all identified lipids specifying subcohorts for both ACS and CCS each with and without confounding factors (*Figure 6* and Supplementary material online, *Figure S8*).

The O2PLS-DA analysis with respect of disease severity and treatment with P2Y12-inhibitors using the full lipid panel (*Figure 6A*) revealed a separation of samples due to ACS or CCS in component t1 of the score plot while no clear separation is observed for subgroups with comedication of P2Y12-inhibitors (cf. CCS subgroups with and without P2Y12-inhibitor because there is only one case for ACS with this medication). A misclassification table indicated that 68% of ACS-naiv cases could be correctly classified by the model, while all cases of both CCS-naiv and CCS-P2Y12 were classified into CCS-naiv subgroup meaning

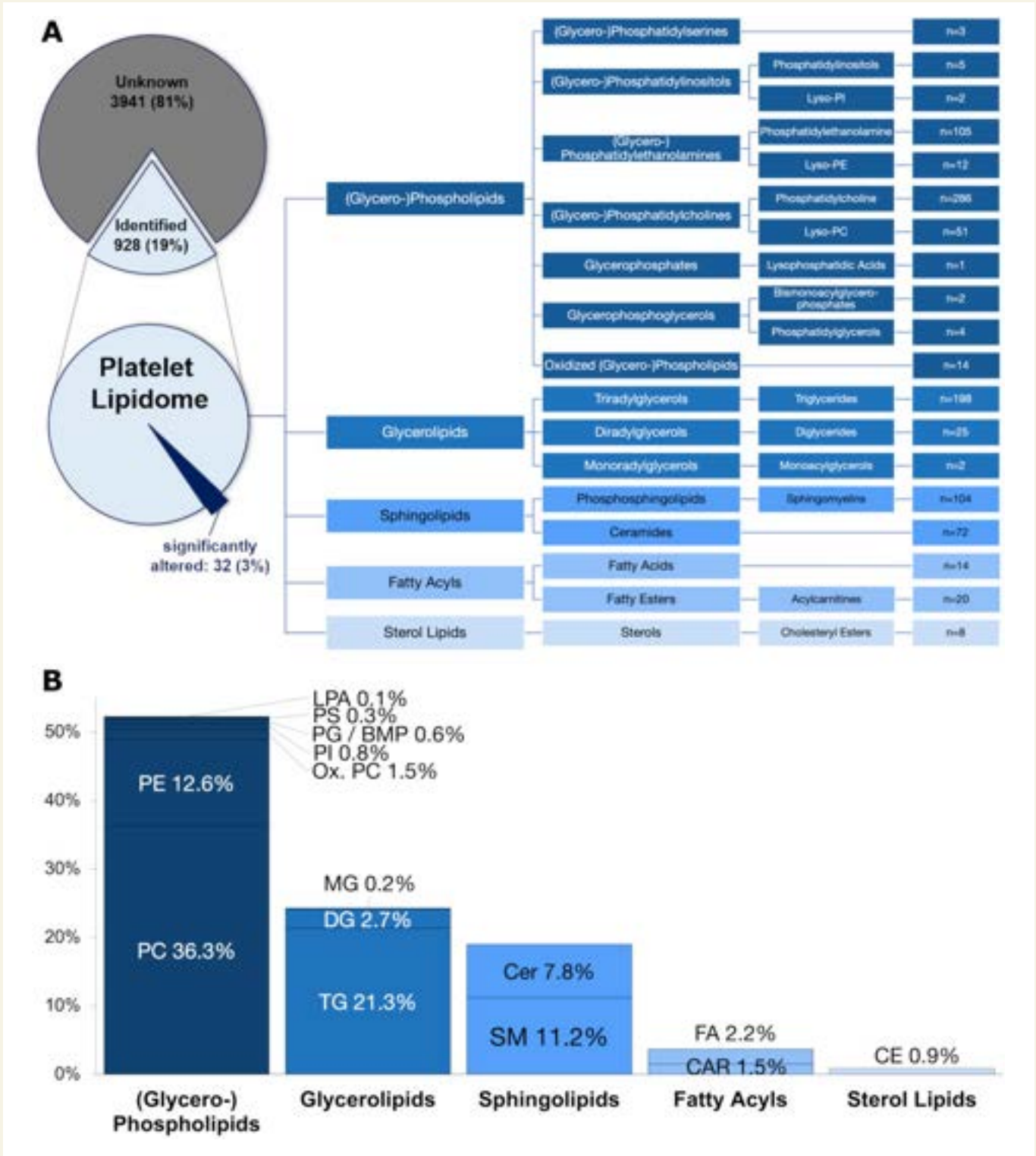

Figure 1 Profiling the human platelet lipidome reveals heterogeneity of detected lipid families. (*A*) Purified platelets were analysed after lipid extraction using UHPLC-ESI-QTOF-MS/MS and data processed using MS-Dial. Identification was performed by MS/MS spectral matching with LipidBlast spectra. Classification was done using Lipid Maps. From left to right untargeted lipidome in this study consists of five categories (glycerophospholipids, sphingolipids, glycerolipids, fatty acyls, and sterol lipids), which can be divided in referring main classes. Small beige boxes on the right indicating single lipids detected and identified in platelets ($n = 928$). (*B*) Bar chart showing the percentage distribution of five lipid categories detected in the platelet lipidome with subdivisions of bars indicating percentages of their referring main lipid classes. With 485 different lipids glycerophospholipids subsume the major category of the platelet lipidome (52.3%), and become the target of further *ex vivo* analysis. Other lipids combine glycerolipids (24.2%), sphingolipids (19.0%), fatty acyls (3.7%), and sterol lipids (0.9%) ($n = 139$, number of patients, $n = 105$ samples were eligible for lipidomics analysis).

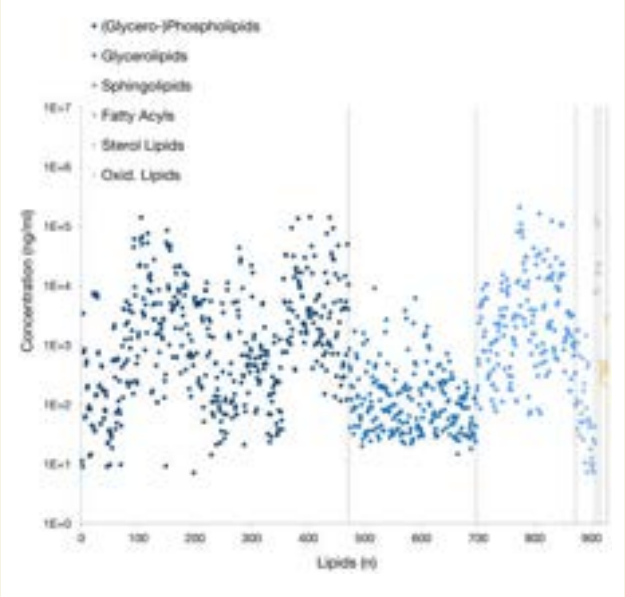

Figure 2 Quantitative analysis displays the platelet lipidome as highly variable. *X*-axis displaying different lipids in the CAD patients cohort ($n = 139$, number of patients, $n = 105$ samples were eligible for lipidomics analysis) and *Y*-axis showing the corresponding log10-scaled mean concentrations of the analysed lipid extract calculated from detected lipid peaks based on class specific internal standards Concentrations are related to 100 µL lipid extract obtained from 3×10^8 platelets. As described earlier glycerophospholipids are the major constituents of the platelet lipidome, therefore also constituting the most dominant lipid category in terms of lipid quantities.

there are no significant differences in the lipidome of the two subgroups. Thus, differences in the lipidome primarily due to disease severity are confirmed by the O2PLS-DA, while the effect of the P2Y12-inhibitors is if at all only of minor extent.

The corresponding O2PLS-DA analysis with statin-treatment as confounding factor reveals primarily a subgroup classification by disease severity (*Figure 6B*, Supplementary material online, *Figures S8* and *S10* and *Table S8*). Moreover, especially in the subgroup of ACS patients, a separation in dependence of statin treatment is obtained indicating an effect of statin medication on the platelet lipidome.

For both comorbidities, hyperlipidaemia and obesity, discriminant analysis did not give successful models with the entire lipid set indicating that comorbidities are not driving factors for the differentiation between ACS and CCS by the lipids of *Figure 4*. Performing principal component analysis also revealed no subclass-specific separation for the comorbidities (*Figure 6C and D* and Supplementary material online, *Table S6*).

As a conclusion, it becomes evident that the investigated confounding factors, i.e. comedication of P2Y12-inhibitors and statins and the cardiovascular risk factors hyperlipidaemia and obesity, do not substantially bias the demonstrated distinction between disease severity (ACS vs. CCS) by the proposed tentative biomarker set of *Figure 5*.

3.3 Effect of significantly regulated platelet lipids on platelet function

Enhanced platelet reactivity is associated with ACS.[3,33] Recently, we found that changes in the platelet lipidome have a significant impact on platelet function.[17,18] To elaborate whether the herein described regulated platelet lipids (ACS vs. CCS) modulate platelet function, we performed *in vitro* function assays in the presence of the identified phospholipids (*Table 2*). Citrated whole blood was pre-incubated with

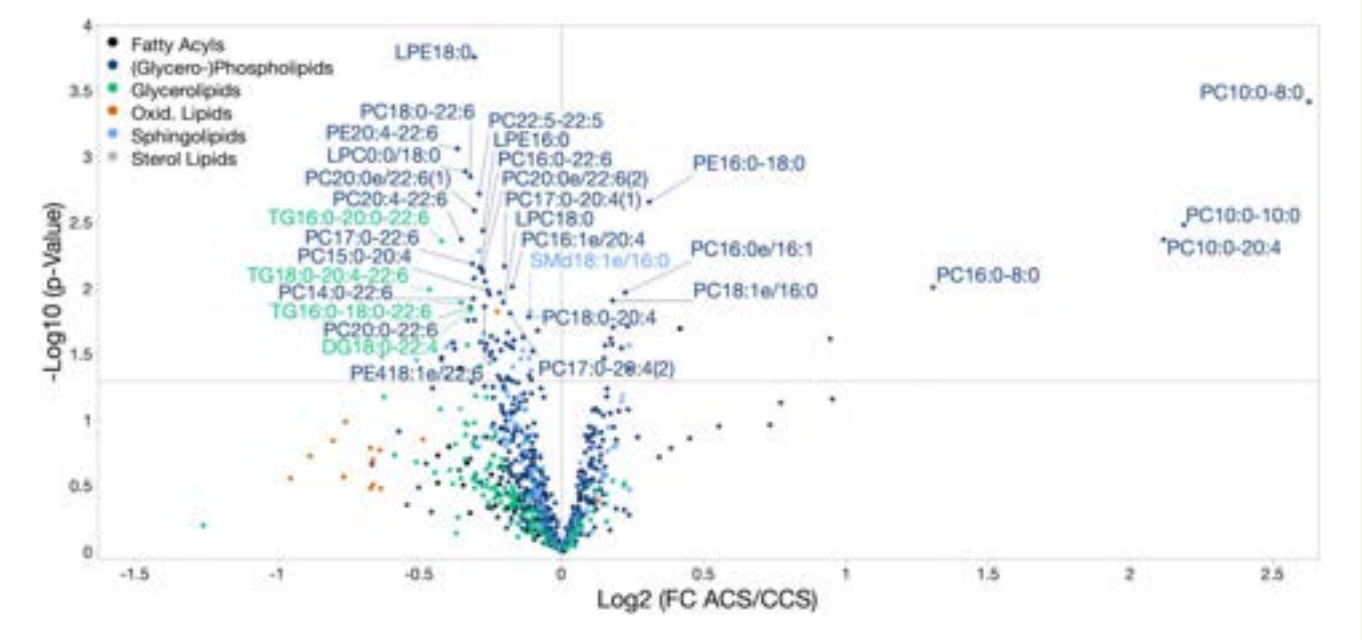

Figure 3 The platelet lipidome is critically altered in acute coronary syndrome. Volcano plot of detected and identified platelet lipids. *X*-axis (fold change, FC) is the base 2 logarithm of the peak intensity ratios (ACS/CCS) (ACS $n = 26$, CCS $n = 79$). Values >1 indicating up-regulation in ACS; <1 down-regulation. *Y*-axis showing negative log10-transformed *P*-values of ANOVA; cut-off for significance is 1.3 ($P < 0.05$). The results after FDR-testing (SGoF $P < 0.05$, FDR < 5%) are labelled and displayed in *Figure 5*.

Figure 4 Lipidomic alteration shows a wide range in acute coronary syndrome. Radar chart displaying semi-quantitatively regulation (log2 FC ACS/CCS) of significantly altered lipids in CAD patients. Seven lipids were significantly up-regulated in ACS (red, SGoF $P < 0.05$, FDR < 5%, one-way ANOVA) exclusively belonging to the category of glycerophospholipids. PC18:0 (PC10:0-8:0) showed highest increase in ACS patients ($n = 26$) (six-fold) compared to CCS ($n = 79$). In contrast 25 lipids were down-regulated in ACS compared to CCS (green, SGoF $P < 0.05$, FDR < 5%, one-way ANOVA). Numbers in brackets indicate either regioisomers (sn-positions unclear while fatty acyl chains are known) or constitutional isomers (lipid species with unknown fatty acyl chains).

various purified phospholipids [PC 18:0 (9:0/9:0) (physicochemically equivalent to PC 10:0-8:0 which was not commercially available); PC 32:1e was tested using its non-alkylether equivalent (i.e. sn1-ester analogue) and sn1/sn2-isomer PC 32:1 (18:1-14:0); PC 18:1e-16:0 was tested using its non-plasmalogen equivalent PC 34:1 (18:1-16:0); down-regulated PC 16:0/22:6, LPC 18:0, LPE 16:0] in concentrations as indicated. Thereafter, platelet-dependent thrombus formation on immobilized collagen was assessed under flow (shear rate, 500 s^{-1} and 1700 s^{-1}). Platelet-dependent thrombus formation was significantly increased in the presence of PC18:0 and PC32:1 under conditions of low (500 s^{-1}) shear rate ($P < 0.01$) when compared to control. Under conditions of high shear rate (1700 s^{-1}) the prothrombotic effect of PC18:0 and PC32:1 was only seen at higher concentrations (*Figure* 7). Similarly, PC18:0 enhanced most prominently both AA- and collagen-induced platelet aggregation ($P < 0.05$) (*Figure* 7).

Furthermore, PC18:0 significantly ($P < 0.05$) increased P-selectin-induced platelet activation in contrast to control (*Figure* 7). To test whether externally added PCs are integrated into the plasma membrane, platelets were incubated with a fluorescent PC, Fluo-PC16:0-6:0, and analysed by fluorescence microscopy and flow cytometry. We found that platelets incorporated PC16:0-6:0 NBD in a concentration-dependent manner substantially in the plasma membrane (*Figure* 7). This experimental data verifies that external phospholipids integrate into the platelet membrane. Furthermore, we analysed the effect of PC18:0 (prothrombotic) in comparison with PC38:6 (no prothrombotic effect) as control on platelet adhesion and spreading. We found that PC18:0 modulated platelet adhesion and spreading onto immobilized fibrinogen compared to PC38:6 control (*Figure* 7). Within the given time frame of 30 min the spreading process of PC18:0-treated platelets was significantly promoted compared to PC38:6 control. Further, PC18:0 significantly enhanced CRP-induced Ca^{2+} signalling in platelets compared to PC38:6 (*Figure* 7). In contrast, the tested glycerophospholipids that were down-regulated in ACS compared to CCS were found to have no significantly enhanced thrombus formation and agonist-induced platelet aggregation compared to control (*Figure* 7). Thus, PC18:0, a lipid that was found to be significantly up-regulated in ACS has a prominent prothrombotic activity which may be relevant in the pathophysiology of ACS.

4. Discussion

The major results of the present study are: (i) significant changes in the platelet lipidome occur in patients with ACS, (ii) up-regulated lipids comprised primarily of lipids belonging to the category of glycerophospholipids, and (iii) among the identified up-regulated glycerophospholipids, PC18:0 was found in *in vitro* studies to exhibit substantial prothrombotic effects. Our findings imply that up-regulation of glycerophospholipids with medium chain fatty acids in platelets may contribute to the pathophysiology of ACS.

Platelet activation is critically involved in the development of ACS. Only recently, the platelet lipidome has been partially studied.[17,18,34] During platelet activation oxidized lipids are, among others, significantly up-regulated which was partially dependent on the aspirin-sensitive cyclooxygenase-1.[34–36] We found that in patients with CAD changes in the platelet lipidome are associated with ACS. In the present study, we characterized the platelet lipidome in a cohort of patients with CAD by untargeted lipidomics technology. We identified 928 lipids extracted from isolated platelets. Main lipid categories were defined as glycerophospholipids, glycerolipids, sphingolipids, fatty acyls, and sterol lipids. Comparison of patients that presented with ACS compared to those with stable CCS revealed that seven lipids were significantly up-regulated in ACS. The up-regulated lipids comprised primarily of glycerophospholipids (phosphocholines and phosphoethanolamine) having high degree of saturation, medium chain saturated fatty acyl side chains and/or ether linkage implying a role in the pathophysiology of ACS. Glycerophospholipids are the main constituents of membrane bilayers and are relevant for assembly of proteins in cell membranes.[37–40] Glycerophospholipids determine the formation of lipid structure of plasma membranes and are involved in the activation of the platelet membrane and thrombin generation.[40,41] Thus, the composition of the platelet plasma membrane regarding glycerophospholipids may affect platelet function, thus platelet-dependent thrombus formation. To test this hypothesis we performed *in vitro* studies with various isolated glycerophospholipids compounds that were found to be up-regulated in ACS. We found that primarily the glycerophospholipid PC18:0 augmented platelet-dependent thrombus formation, platelet aggregation, spreading and Ca^{2+} signalling of platelets. Thus, it is tempting to speculate that some up-regulated PCs such as PC18:0 may contribute to platelet hyper-reactivity in ACS. In our study cohort, we can show by subgroup analysis with subcohorts for the confounding factor in each disease group that the impact of potential comedication (statins, P2Y12 inhibitors) or comorbidities (hyperlipidaemia, obesity) on the described

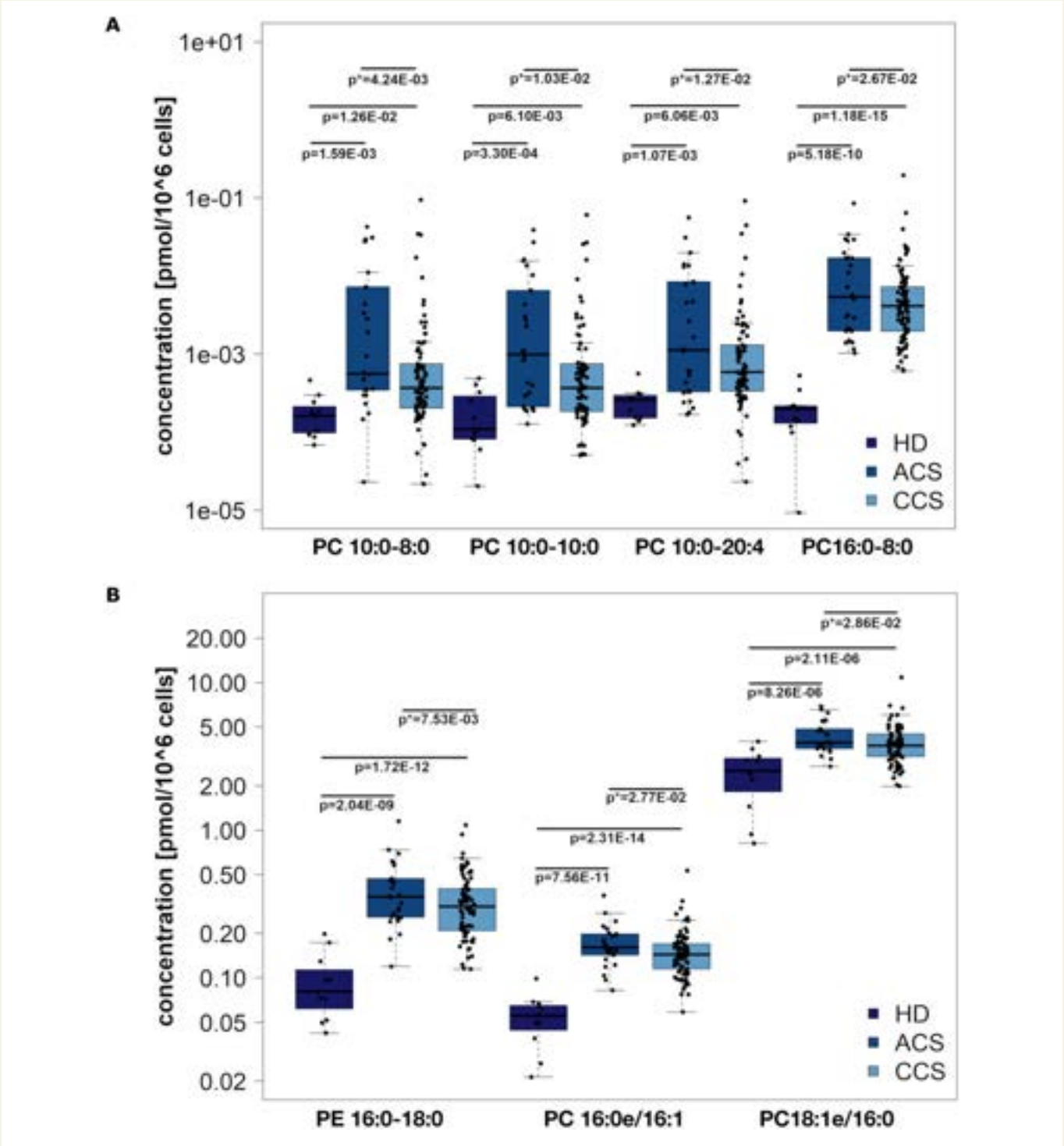

Figure 5 Glycerophospholipids are significantly increased in ACS. Boxplots from normalized peak heights of significantly up-regulated glycerophospholipids in ACS (n = 26) compared to CCS (n = 79). Lipid levels of those lipids were also determined in healthy donors (n = 11). (*A*) The medium chain PCs PC18:0 (PC10:0-8:0; P = 0.004), PC20:0 (PC10:0/10:0; P = 0.010), PC10:0-20:4 (P = 0.0127), and PC24:0 (PC16:0-8:0; P = 0.0267). Levels of those lipids were below limit of detection of this assay (LOD < 3), thus peak heights were imputed by gap filling (extraction of peak maximum for lipid-specific precursor mass in expected retention time window). In (*B*), PC32:1e (PC 16:0e/16:1; P = 0.0075), PE16:0-18:0 (P = 0.0277), and PC18:1e/16:0 (P = 0.0286). Statistical significance was evaluated by one-way ANOVA. P-values were adjusted by SGoF algorithm due to multiple hypotheses testing for ACS-CCS comparisons (indicated by P*), uncorrected P-values are displayed for comparison of ACS and CCS with healthy donors (HD).

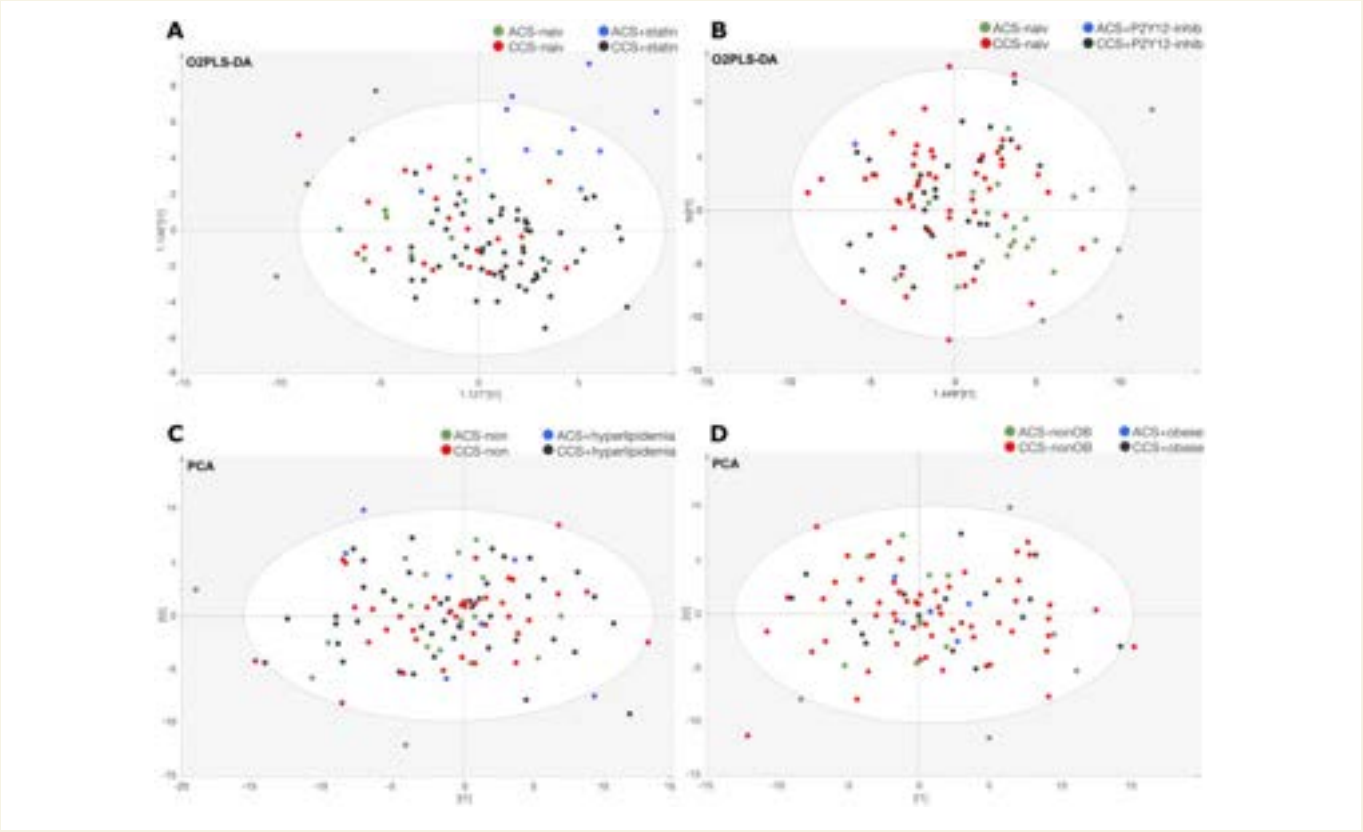

Figure 6 Effect of comedication (statins, P2Y12 inhibitors) and comorbidities (hyperlipidaemia, obesity) on platelet lipidome. OPLS-DA and PCA-X analysis assessing the impact of statin and P2Y12-inhibitor treatment, dyslipidaemia, and obesity on significant regulation of the lipidome in ACS and CCS patients. Data were based on normalized peak intensities of all detected lipids in this study (n = 928). The four subcohorts (ACS±/CCS±) are coloured and labelled. A homogenous spreading of the subgroups (*A*–*D*) implements a minor influence of assessed pharmaceutical treatment and risk factors on the significant findings of altered lipidome in ACS compared to CCS. (*A*) OPLS-DA analysis of statin subcohorts [components: 2 predictive, 14 orthogonal; $R^2X(cum)$ = 0.677, $R^2Y(cum)$ = 0.691, $Q^2(cum)$ = 0.021]. (*B*) OPLS-DA of P2Y12-inibitor subgroups [components: 1 predictive, 14 orthogonal; $R^2X(cum)$ = 0.679, $R^2Y(cum)$ = 0.354, $Q^2(cum)$ = -0.050]. (*C*) PCA-X analysis of hyperlipidaemia in ACS and CCS [components: 15; $R^2X(cum)$ = 0.680, $Q^2(cum)$ = 0.423). (*D*) PCA-X analysis of obesity in this study [components: 13; $R^2X(cum)$ = 0.655, $Q^2(cum)$ = 0.399].

Table 2 Summary of lipids used for platelet-dependent thrombus formation and aggregation *ex vivo* analysis

PC18:0 (9:0/9:0) *1,2-dinonanoyl-sn-glycero-3-phosphocholine*	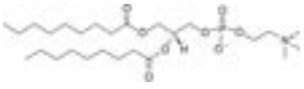	$C_{26}H_{52}NO_8P$ M = 537.667
PC32:1 (14:0/18:1) *1-oleoyl-2-myristoyl-sn-glycero-3-phosphocholine*		$C_{40}H_{78}NO_8P$ M = 732.023
PC34:1 (18:1/16:0) *1-palmitoyl-2-oleoyl-glycero-3-phosphocholine*	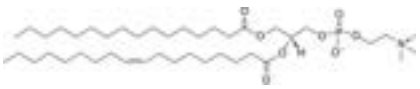	$C_{42}H_{82}NO_8P$ M = 760.076
PC 38:6 (16:0/22:6) *1-palmitoyl-2-docosahexaenoyl-sn-glycero-3-phosphocholine*		$C_{46}H_{80}NO_8P$ M = 806.103
Lyso-PC (18:0) *1-stearoyl-2-hydroxy-sn-glycero-3-phosphocholine*		$C_{26}H_{54}NO_7P$ M = 523.683
Lyso-PE (16:0) *1-palmitoyl-2-hydroxy-sn-glycero-3-phosphoethanolamine*	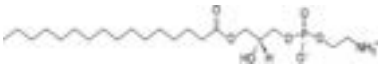	$C_{21}H_{44}NO_7P$ M = 453.550

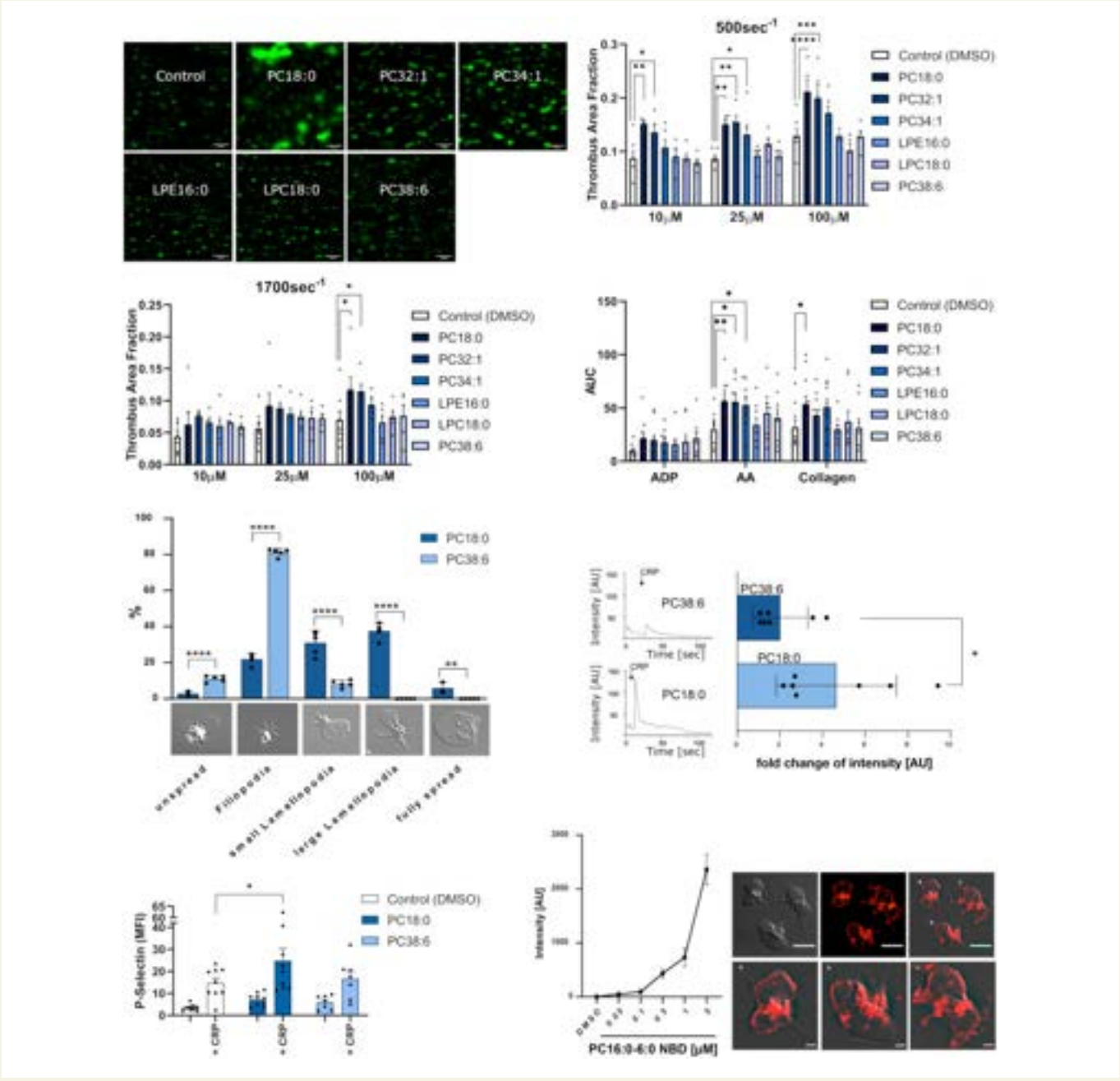

Figure 7 PC18:0 enhances *ex vivo* platelet function and thrombus formation. (*A*) Representative images for $n \geq 5$ independent flow chamber experiments at low shear rate (500 s^{-1}). Scale bar = 50 µm. (*B*) *Ex vivo* platelet-dependent thrombus formation—flow chamber assay with low shear rate (500 s^{-1}) of lipids (10 µM, 25 µM, 100 µM) or DMSO (control) equivalent; quantification of thrombogenicity was done by thrombus area fraction. PC18:0 showed highest thrombus-formatting potential compared to control at all concentrations. PC32:1-dependent thrombus formation was significantly increased at all concentration. PC 34:1-induced thrombus formation was only increased at medium concentration; $n \geq 5$. (*C*) High shear rate (1700 s^{-1}); PC 18:0 and PC32:1 at high concentration significantly enhanced thrombus formation compared to control; $n \geq 5$. (*D*) Impedance platelet aggregometry with hirudinized whole blood in presence of glycerophospholipids (100 µM) or DMSO (incubation 30 min); agonists ADP 6.5 µM, arachidonic acid (AA) 484 µM, collagen 3.2 µg/mL. PC18:0 significantly augmented both AA- and collagen-induced platelet aggregation; PC32:1 and PC34:1 significantly enhanced AA-generated platelet-aggregation compared to control; $n \geq 8$. (*E*) PC18:0 significantly modulated platelet adhesion and spreading onto immobilized fibrinogen compared to PC38:6 control. Formation of filopodia was significantly enhanced in the presence of PC18:0. In contrast formation of lamellopodia was lowered in the presence of PC18:0 compared to PC38:6. The spreading process of PC18:0-treated platelets was significantly promoted compared to PC38:6 control; $n = 5$. (*F*) PC18:0 mediated CD62-P induced platelet activation. Mean intensities of P-Selectin/CD62P were significantly increased in CRP-stimulated platelets in the presence of PC18:0 (100 µM) compared to control (DMSO); $n \geq 6$. (*G*) PC18:0 significantly enhanced CRP-induced Ca^{2+} signalling in platelets compared to PC38:6; $n = 7$. (*H*) Pictures and flow cytometric quantification of integration of lipids in the platelet membrane. Platelets were incubated with fluorescent PC16:0-6:0 NBD, thereafter analysed by fluorescence microscopy and flow cytometry. We found that platelets concentration-dependently incorporated PC16:0-6:0 NBD substantially in the plasma membrane; $n = 4$. Plotted: mean ± SEM; statistics: two-way ANOVA; $^*P < 0.05$; $^{**}P < 0.01$; $^{***}P < 0.001$.

platelet lipidome alterations is minor compared to disease severity, i.e. ACS vs. CCS. However, the significance of our present analysis is constricted by the limited size of the tested study cohort.

Amongst the down-regulated lipids, we found many membrane phospholipids with PUFA (polyunsaturated fatty acid) side chains. PUFA-PLs play a double role for platelet function. Firstly, they regulate membrane fluidity and integrity,[42,43] and secondly, they are involved in signalling of thrombo-inflammatory processes.[44] PUFA-PLs with arachidonic acid (20:4) side chain are substrates for cPLA2 and proinflammatory while PUFA-PLs with docosahexaenoic acid (22:6) side chain are sources for pro-resolving lipid mediators. The down-regulation of PUFA-PLs might thus indicate stronger thrombo-inflammatory processes in ACS.

In the present study, we used a non-targeted lipidomic approach for identifying mostly unbiased and openly potential changes of lipids. Among the identified lipids we selected 19% of the total lipids due to detection threshold and spectral data basis. Thus, we only evaluated a subgroup of lipids for further association analysis. Our results may be also influenced by sample errors due to variations of blood collection and platelet preparation. However, we thoroughly followed a prespecified protocol keeping the experimental random error constant. Unfortunately, we do not have *ex vivo* platelet function data in our patients to correlate with changes in platelet lipidome that may have strengthen our conclusion that alternations in the platelet lipidome affects platelet reactivity. To get some insights in the role of several highly regulated lipids we addressed the effect of selected lipids on platelet function *in vivo*. We chose the lipid concentrations used in our experiments *in vitro* by testing them in a dose–response curve and came up with concentrations as indicated. We agree that we do not know the effective concentrations which might occur *in vivo*. Thus, the *in vitro* data is an approximation towards the *in vivo* situation.

At present, the results of our study and our preliminary experimental approach promotes a hypothesis that an altered lipid composition of the plasma membrane has consequences for platelet function. Both biosynthesis of specific PCs such as PC18:0 within the platelet and incorporation of oxidized phospholipids into the plasma membrane might change the membrane composition with functional relevance. In light of PC18:0, we favour the *de novo* synthesis of PC18:0 in ACS since we could not detect PC18:0 in the plasma compartment (*Graphical abstract*).

Supplementary material

Supplementary material is available at *Cardiovascular Research* online.

Authors' contributions

T.H.: performing data acquisition, experiments, experimental/statistical analysis and interpretation, writing manuscript; A.B.: performing blood sampling, clinical data acquisition; K.D.: performing UHPLC-ESI-QTOF-MS/MS protocols, data acquisition and processing; A.G.: performing blood sampling, clinical data acquisition; J.N.: performing blood sampling, clinical data acquisition; M.C.: revision and critical assessment of the manuscript; X.F.: performing UHPLC-ESI-QTOF-MS/MS protocols, data acquisition and processing; K.K.: performing *in vitro* platelet function analysis; T.C.: assessment of clinical data and manuscript revision; O.B.: assessment of clinical data and manuscript revision; T.G.: assessment of clinical data and manuscript revision; D.R.: performing clinical data acquisition, statistical analysis and manuscript writing; M.L.: performing UHPLC-ESI-QTOF-MS/MS protocols, data acquisition and processing and critical manuscript revision; M.G.: conceptual design, data interpretation, writing and revising manuscript.

Acknowledgements

We thankfully acknowledge the work of Lydia Laptev for assisting us to process the platelet samples for functional analysis.

Conflict of interest: none declared.

Funding

This project was supported by the German Research Foundation (DFG) KFO-274—Project number 190538538, by the German Research Foundation (DFG)—Project number 374031971—TRR 240, funded by the German Research Foundation (DFG)—Project number 335549539—GRK2381, and by the German Foundation for Heart Research (DSHF-F/22/17).

Data availability

The data underlying this article will be shared on reasonable request to the corresponding author.

References

1. Gawaz M, Langer H, May AE. Platelets in inflammation and atherogenesis. *J Clin Invest* 2005;**115**:3378–3384.
2. Ruggeri ZM. Platelets in atherothrombosis. *Nat Med* 2002;**8**:1227–1234.
3. Fuchs I, Frossard M, Spiel A, Riedmuller E, Laggner AN, Jilma B. Platelet function in patients with acute coronary syndrome (ACS) predicts recurrent ACS. *J Thromb Haemost* 2006;**4**:2547–2552.
4. Gawaz M. Role of platelets in coronary thrombosis and reperfusion of ischemic myocardium. *Cardiovasc Res* 2004;**61**:498–511.
5. Arroyo LH, Lee RT. Mechanisms of plaque rupture: mechanical and biologic interactions. *Cardiovasc Res* 1999;**41**:369–375.
6. Bentzon JF, Otsuka F, Virmani R, Falk E. Mechanisms of plaque formation and rupture. *Circ Res* 2014;**114**:1852–1866.
7. Gawaz M. Does uncontrolled platelet activation promote coronary artery disease? *JACC Cardiovasc Imaging* 2016;**9**:855–857.
8. Naghavi M, Libby P, Falk E, Casscells SW, Litovsky S, Rumberger J, Badimon JJ, Stefanadis C, Moreno P, Pasterkamp G, Fayad Z, Stone PH, Waxman S, Raggi P, Madjid M, Zarrabi A, Burke A, Yuan C, Fitzgerald PJ, Siscovick DS, de Korte CL, Aikawa M, Airaksinen KE, Assmann G, Becker CR, Chesebro JH, Farb A, Galis ZS, Jackson C, Jang IK, Koenig W, Lodder RA, March K, Demirovic J, Navab M, Priori SG, Rekhter MD, Bahr R, Grundy SM, Mehran R, Colombo A, Boerwinkle E, Ballantyne C, Insull W Jr, Schwartz RS, Vogel R, Serruys PW, Hansson GK, Faxon DP, Kaul S, Drexler H, Greenland P, Muller JE, Virmani R, Ridker PM, Zipes DP, Shah PK, Willerson JT. From vulnerable plaque to vulnerable patient: a call for new definitions and risk assessment strategies: part II. *Circulation* 2003;**108**:1772–1778.
9. Lewis JP, Backman JD, Reny JL, Bergmeijer TO, Mitchell BD, Ritchie MD, Dery JP, Pakyz RE, Gong L, Ryan K, Kim EY, Aradi D, Fernandez-Cadenas I, Lee MTM, Whaley RM, Montaner J, Gensini GF, Cleator JH, Chang K, Holmvang L, Hochholzer W, Roden DM, Winter S, Altman R, Alexopoulos D, Kim HS, Gawaz M, Bliden K, Valgimigli M, Marcucci R, Campo G, Schaeffeler E, Dridi NP, Wen MS, Shin JG, Fontana P, Giusti B, Geisler T, Kubo M, Trenk D, Siller-Matula JM, Ten Berg JM, Gurbel PA, Schwab M, Klein TE, Shuldiner AR. Pharmacogenomic polygenic response score predicts ischemic events and cardiovascular mortality in clopidogrel-treated patients. *Eur Heart J Cardiovasc Pharmacother* 2020;**6**:203–210.
10. Droppa M, Tschernow D, Müller KAL, Tavlaki E, Karathanos A, Stimpfle F, Schaeffeler E, Schwab M, Tolios A, Siller-Matula JM, Gawaz M, Geisler T. Evaluation of clinical risk factors to predict high on-treatment platelet reactivity and outcome in patients with stable coronary artery disease (PREDICT-STABLE). *PLoS One* 2015;**10**:e0121620.
11. Geisler T, Zürn C, Simonenko R, Rapin M, Kraibooj H, Kilias A, Bigalke B, Stellos K, Schwab M, May AE, Herdeg C, Gawaz M. Early but not late stent thrombosis is influenced by residual platelet aggregation in patients undergoing coronary interventions. *Eur Heart J* 2010;**31**:59–66.
12. Reny JL, Fontana P, Hochholzer W, Neumann FJ, Ten Berg J, Janssen PW, Geisler T, Gawaz M, Marcucci R, Gori AM, Cuisset T, Alessi MC, Berdague P, Gurbel PA, Yong G, Angiolillo DJ, Aradi D, Beigel R, Campo G, Combescure C. Vascular risk levels

affect the predictive value of platelet reactivity for the occurrence of MACE in patients on clopidogrel. Systematic review and meta-analysis of individual patient data. *Thromb Haemost* 2016;**115**:844–855.
13. May AE, Geisler T, Gawaz M. Individualized antithrombotic therapy in high risk patients after coronary stenting. A double-edged sword between thrombosis and bleeding. *Thromb Haemost* 2008;**99**:487–493.
14. Stellos K, Sauter R, Fahrleitner M, Grimm J, Stakos D, Emschermann F, Panagiota V, Gnerlich S, Perk A, Schonberger T, Bigalke B, Langer HF, Gawaz M. Binding of oxidized low-density lipoprotein on circulating platelets is increased in patients with acute coronary syndromes and induces platelet adhesion to vascular wall *in vivo*—brief report. *Arterioscler Thromb Vasc Biol* 2012;**32**:2017–2020.
15. Vinik AI, Erbas T, Park TS, Nolan R, Pittenger GL. Platelet dysfunction in type 2 diabetes. *Diabetes Care* 2001;**24**:1476–1485.
16. Cabeza N, Li Z, Schulz C, Kremmer E, Massberg S, Bultmann A, Gawaz M. Surface expression of collagen receptor Fc receptor-gamma/glycoprotein VI is enhanced on platelets in type 2 diabetes and mediates release of CD40 ligand and activation of endothelial cells. *Diabetes* 2004;**53**:2117–2121.
17. Chatterjee M, Rath D, Schlotterbeck J, Rheinlaender J, Walker-Allgaier B, Alnaggar N, Zdanyte M, Müller I, Borst O, Geisler T, Schäffer TE, Lämmerhofer M, Gawaz M. Regulation of oxidized platelet lipidome: implications for coronary artery disease. *Eur Heart J* 2017;**38**:1993–2005.
18. Peng B, Geue S, Coman C, Münzer P, Kopczynski D, Has C, Hoffmann N, Manke MC, Lang F, Sickmann A, Gawaz M, Borst O, Ahrends R. Identification of key lipids critical for platelet activation by comprehensive analysis of the platelet lipidome. *Blood* 2018;**132**:e1–e12.
19. Burkhart JM, Vaudel M, Gambaryan S, Radau S, Walter U, Martens L, Geiger J, Sickmann A, Zahedi RP. The first comprehensive and quantitative analysis of human platelet protein composition allows the comparative analysis of structural and functional pathways. *Blood* 2012;**120**:e73–e82.
20. Schlotterbeck J, Chatterjee M, Gawaz M, Lammerhofer M. Comprehensive MS/MS profiling by UHPLC-ESI-QTOF-MS/MS using SWATH data-independent acquisition for the study of platelet lipidomes in coronary artery disease. *Anal Chim Acta* 2019;**1046**:1–15.
21. Cebo M, Schlotterbeck J, Gawaz M, Chatterjee M, Lammerhofer M. Simultaneous targeted and untargeted UHPLC-ESI-MS/MS method with data-independent acquisition for quantification and profiling of (oxidized) fatty acids released upon platelet activation by thrombin. *Anal Chim Acta* 2020;**1094**:57–69.
22. Calderón C, Sanwald C, Schlotterbeck J, Drotleff B, Lämmerhofer M. Comparison of simple monophasic versus classical biphasic extraction protocols for comprehensive UHPLC-MS/MS lipidomic analysis of Hela cells. *Anal Chim Acta* 2019;**1048**:66–74.
23. Tsugawa H, Cajka T, Kind T, Ma Y, Higgins B, Ikeda K, Kanazawa M, VanderGheynst J, Fiehn O, Arita M. MS-DIAL: data-independent MS/MS deconvolution for comprehensive metabolome analysis. *Nat Methods* 2015;**12**:523–526.
24. Fan S, Kind T, Cajka T, Hazen SL, Tang WHW, Kaddurah-Daouk R, Irvin MR, Arnett DK, Barupal DK, Fiehn O. Systematic error removal using random forest for normalizing large-scale untargeted lipidomics data. *Anal Chem* 2019;**91**:3590–3596.
25. Livera AMD, Sysi-Aho M, Jacob L, Gagnon-Bartsch JA, Castillo S, Simpson JA, Speed TP. Statistical methods for handling unwanted variation in metabolomics data. *Anal Chem* 2015;**87**:3606–3615.
26. De Livera AM, Olshansky G, Simpson JA, Creek DJ. NormalizeMets: assessing, selecting and implementing statistical methods for normalizing metabolomics data. *Metabolomics* 2018;**14**:54.
27. Meckelmann SW, Hawksworth JI, White D, Andrews R, Rodrigues P, O'Connor A, Alvarez-Jarreta J, Tyrrell VJ, Hinz C, Zhou Y, Williams J, Aldrovandi M, Watkins WJ, Engler AJ, Sardo VL, Slatter DA, Allen SM, Acharya J, Mitchell J, Cooper J, Aoki J, Kano K, Humphries SE, O'Donnell VB. Metabolic dysregulation of the lysophospholipid/autotaxin axis in the chromosome 9p21 gene SNP rs10757274. *Circ Genom Precis Med* 2020;**13**:e002806.
28. Drotleff B, Roth SR, Henkel K, Calderón C, Schlotterbeck J, Neukamm MA, Lämmerhofer M. Lipidomic profiling of non-mineralized dental plaque and biofilm by untargeted UHPLC-QTOF-MS/MS and SWATH acquisition. *Anal Bioanal Chem* 2020;**412**:2303–2314.
29. Carvajal-Rodríguez A, de Uña-Alvarez J, Rolán-Alvarez E. A new multitest correction (SGoF) that increases its statistical power when increasing the number of tests. *BMC Bioinformatics* 2009;**10**:209–209.
30. Castro-Conde I, de Uña-Álvarez J. Adjusted p-values for SGoF multiple test procedure. *Biom J* 2015;**57**:108–122.
31. Witte A, Rohlfing AK, Dannenmann B, Dicenta V, Nasri M, Kolb K, Sudmann J, Castor T, Rath D, Borst O, Skokowa J, Gawaz M. The chemokine CXCL14 mediates platelet function and migration via direct interaction with CXCR4. *Cardiovasc Res* 2021;**117**:903–917.
32. Malehmir M, Pfister D, Gallage S, Szydlowska M, Inverso D, Kotsiliti E, Leone V, Peiseler M, Surewaard BGJ, Rath D, Ali A, Wolf MJ, Drescher H, Healy ME, Dauch D, Kroy D, Krenkel O, Kohlhepp M, Engleitner T, Olkus A, Sijmonsma T, Volz J, Deppermann C, Stegner D, Helbling P, Nombela-Arrieta C, Rafiei A, Hinterleitner M, Rall M, Baku F, Borst O, Wilson CL, Leslie J, O'Connor T, Weston CJ, Adams DH, Sheriff L, Teijeiro A, Prinz M, Bogeska R, Anstee N, Bongers MN, Notohamiprodjo M, Geisler T, Withers DJ, Ware J, Mann DA, Augustin HG, Vegiopoulos A, Milsom MD, Rose AJ, Lalor PF, Llovet JM, Pinyol R, Tacke F, Rad R, Matter M, Djouder N, Kubes P, Knolle PA, Unger K, Zender L, Nieswandt B, Gawaz M, Weber A, Heikenwalder M. Platelet GPIbalpha is a mediator and potential interventional target for NASH and subsequent liver cancer. *Nat Med* 2019;**25**:641–655.
33. Frossard M, Fuchs I, Leitner JM, Hsieh K, Vlcek M, Losert H, Domanovits H, Schreiber W, Laggner AN, Jilma B. Platelet function predicts myocardial damage in patients with acute myocardial infarction. *Circulation* 2004;**110**:1392–1397.
34. O'Donnell VB, Murphy RC, Watson SP. Platelet lipidomics: modern day perspective on lipid discovery and characterization in platelets. *Circ Res* 2014;**114**:1185–1203.
35. Slatter DA, Aldrovandi M, O'Connor A, Allen SM, Brasher CJ, Murphy RC, Mecklemann S, Ravi S, Darley-Usmar V, O'Donnell VB. Mapping the human platelet lipidome reveals cytosolic phospholipase A2 as a regulator of mitochondrial bioenergetics during activation. *Cell Metab* 2016;**23**:930–944.
36. Chatterjee M. Platelet lipidome: dismantling the "Trojan horse" in the bloodstream. *J Thromb Haemost* 2020;**18**:543–557.
37. Koseoglu S, Meyer AF, Kim D, Meyer BM, Wang Y, Dalluge JJ, Haynes CL. Analytical characterization of the role of phospholipids in platelet adhesion and secretion. *Anal Chem* 2015;**87**:413–421.
38. Xiao H, Siddiqui RA, Al-Hassani MH, Sliva D, Kovacs RJ. Phospholipids released from activated platelets improve platelet aggregation and endothelial cell migration. *Platelets* 2001;**12**:163–170.
39. Joist JH, Dolezel G, Cucuianu MP, Nishizawa EE, Mustard JF. Inhibition and potentiation of platelet function by lysolecithin. *Blood* 1977;**49**:101–112.
40. Hu Q, Wang M, Cho MS, Wang C, Nick AM, Thiagarajan P, Aung FM, Han X, Sood AK, Afshar-Kharghan V. Lipid profile of platelets and platelet-derived microparticles in ovarian cancer. *BBA Clin* 2016;**6**:76–81.
41. Hishikawa D, Hashidate T, Shimizu T, Shindou H. Diversity and function of membrane glycerophospholipids generated by the remodeling pathway in mammalian cells. *J Lipid Res* 2014;**55**:799–807.
42. Harayama T, Riezman H. Understanding the diversity of membrane lipid composition. *Nat Rev Mol Cell Biol* 2018;**19**:281–296.
43. Shaikh SR, Kinnun JJ, Leng X, Williams JA, Wassall SR. How polyunsaturated fatty acids modify molecular organization in membranes: insight from NMR studies of model systems. *Biochim Biophys Acta* 2015;**1848**:211–219.
44. Lu Y, Hong S, Tjonahen E, Serhan CN. Mediator-lipidomics: databases and search algorithms for PUFA-derived mediators. *J Lipid Res* 2005;**46**:790–802.

Translational perspective

Metabolomics including platelet lipidomics have recently become a new perspective of ongoing research in various diseases. This study reveals a significant change of platelet lipids in ACS and discloses pro-thrombotic effects primarily of up-regulated glycerophospholipids. Therefore, hitherto unknown alterations of the platelet lipidome, especially of glycerophospholipids, may contribute to the pathophysiology of coronary artery disease.

Supplementary Material

Acute coronary syndrome is associated with a substantial change in the platelet lipidome

Tobias Harm[1], Alexander Bild[1], Kristina Dittrich[2], Andreas Goldschmied[1], Jeremy Nestele[1], Madhumita Chatterjee[1], Xiaoqing Fu[2], Kyra Kolb[1], Tatsiana Castor[1], Oliver Borst[1], Tobias Geisler[1], Dominik Rath[1], Michael Lämmerhofer[2], Meinrad Gawaz[1]

[1]Department of Cardiology and Angiology, University Hospital Tübingen, Eberhard Karls University Tübingen, Otfried-Müller-Straße 10, 72076 Tübingen, Germany
[2]Institute of Pharmaceutical Sciences, Eberhard Karls University Tübingen, Auf der Morgenstelle 8, 72076 Tübingen, Germany

1. Platelet lipidomic methods and data processing

1.1. RP-UHPLC-ESI-QTOF-MS/MS experiment

Platelet lipid extracts were analyzed on an Agilent 1290 series UHPLC instrument (Agilent, Waldbronn, Germany) connected to a Sciex TripleTOF 5600+ mass spectrometer with DuoSpray ion source (Sciex, Concord, Ontario, Canada). A Pal HTC-xt autosampler from CTC (CTC Analytics, Zwingen, Switzerland) was used for sample storage at 4°C during measurement and sample injection (3 µL in positive mode, 5 µL in negative mode).

Chromatograhic conditions and mass spectrometer parameters were adopted from Tsugawa et al.[1] An Acquity UPLC CSH C18 (130Å, 1.7 µm, 2.1 mm X 100 mm) column equipped with an Acquity UPLC CSH C18 VanGuard pre-column (130Å, 1.7 µm, 2.1 mm X 5 mm) (Waters, Eschborn, Germany) was used for reversed-phase chromatography utilized at 65°C. Two mobile phases, (A) 60:40 ACN:H_2O (v/v) and (B) 90:9:1 (v/v) IPA:ACN:H_2O (B) both with 10 mM ammonium formate and 0.1% formic acid were used for a gradient elution with 0.0 min 15% B, 2.0 min 30% B, 2.5 min 48% B, 11.0 min 82% B, 11.5 min 99% B, 12.0 min 99% B, 12.1 min 15% B, and 15.0 min 15% B for re-equilibration at 0.6 mL/min flow.

As general MS parameters, curtain gas was set to 35 psi, nebulizer gas to 60 psi, and drying gas to 60 psi. Ion source temperature was 350°C. In positive mode, ion-spray voltage floating was +5500 V, collision energy was 45V with a spread of 15 V, and declustering potential was 80 V. The mass range was m/z 50-1250. In negative mode, ion-spray voltage floating was -4500 V, collision energy was -45V with a spread of 15 V, declustering potential was -80 V, and the mass range m/z 50-1050.

A data-independent acquisition (DIA) approach was used with sequential window acquisition of all theoretical fragment ion spectra (SWATH), Thus, after a TOF

precursor scan 20 SWATH MS/MS experiments with variable Q1 width covering the entire mass range were performed (Table S).

Table S 1. List of MS and MS/MS experiments within a cycle

Experiment	Positive mode			Negative mode		
	Low border [m/z]	Upper border [m/z]	CE [V]	Low border [m/z]	Upper border [m/z]	CE [V]
TOF	50	1250	10	50	1050	-10
1	50	217.6	45	50	213.5	-45
2	216.6	340.3	45	212.5	271.4	-45
3	339.3	441.4	45	270.4	314.6	-45
4	440.4	524.9	45	313.6	382.6	-45
5	523.9	571.6	45	381.6	427.5	-45
6	570.6	643.4	45	426.5	464.3	-45
7	642.4	687.3	45	463.3	501	-45
8	686.3	720.1	45	500	540.8	-45
9	719.1	740.1	45	539.8	617.5	-45
10	739.1	755	45	616.5	680.3	-45
11	754	764.1	45	679.3	697.1	-45
12	763.1	775.1	45	696.1	724	-45
13	774.1	786.1	45	723	749	-45
14	785.1	793.1	45	748	775.6	-45
15	792.1	806.1	45	774.6	793.1	-45
16	805.1	814.2	45	792.1	811	-45
17	813.2	829.6	45	810	832.6	-45
18	828.6	842.7	45	831.6	854.1	-45
19	841.7	903.3	45	853.1	861.2	-45
20	902.3	1250	45	860.2	1050	-45

1.2. Data processing

As described in the main document, data processing of LC-MS data was performed by using the open-source software MS-DIAL that enables data processing of data-independent data acquisition (DIA) approaches.[1] MS-DIAL performs several processing steps like peak finding, deisotoping, adduct assignment, data deconvolution, and peak alignment between samples within a batch. Moreover, lipid identification is performed in MS-DIAL by matching experimental MS/MS-spectra with the *in-silico* reference spectra database LipidBlast. Identification results were manually curated to avoid missannotations which occur to low extent in automated identification procedures. Normalization and statistical analysis was performed as described in the main document.

Special attention was directed to the identification of those lipids found to be significantly altered in ACS compared to CCS. Based on lipid notation recommendations from Liebisch et al.,[2] the notation of lipids provides different levels of structural information. In case of sufficient spectral information obtained in the untargeted approach, information about lipid class and side chain composition was available for an identified lipid, e.g. PC 10:0-20:4. However, in some cases spectral data in the untargeted assay only provided information about the lipid class and the precursor mass, thus the sum of carbons and double bounds, e.g. PC 18:0. For those lipids a targeted high-resolution multiple-reaction-monitoring (HR-MRM) method was applied to clarify the side chain composition.

1.3. HR-MRM targeted method to further clarify lipid structure

HR-MRM experiments were performed for the upregulated lipids with unknown side chain composition, thus for PC 18:0, PC 20:0, PC 24:0, and PC 32:1e. The identical instrumental setting, RP-LC method, and general MS parameters were used for the

targeted HR-MRM method as for the untargeted approach. In difference, after the TOF precursor scan, MRM MS/MS experiments for the MCFA-PC precursor masses (positive mode: PC 18:0: m/z 538.4, PC 20:0: m/z 566.4, PC 24:0: m/z 622.4; PC 32:1e: m/z 718.6; negative mode: PC 18:0: m/z 582.3, PC 20:0: m/z 610.4, PC 24:0: m/z 666.4, PC 32:1e: m/z 762.6) were conducted. Declustering potential was 80 V / -80 V, collision energy 35 V / -35 V and collision energy spread 25 V for positive mode. The accumulation time for each MRM experiment was 150 ms. Measurements were performed for lipid extracts from platelet pellets as well as for a matrix-matched standard of PC 10:0/10:0 which was the only commercially available authentic standard of the four detected MC-PCs. Data were analyzed with Sciex vendor-software PeakView. Information about fragmentation pattern of assumed lipid species in negative mode were obtained from Lipid Maps® tool "*Predict MS/MS spectrum and generate a list of commonly occurring product ions for glycerophospholipids (negative ion mode)"* [https://www.lipidmaps.org/resources/tools/ index.php]. In positive mode, precursor m/z of each lipid of interest and the corresponding class-specic head group fragment (PC: m/z 184.073) was used.

2. LC-MS/MS data of significantly upregulated lipids in ACS compared to CCS

2.1. Fragmentation pattern of PC, ePC, and PE lipid classes

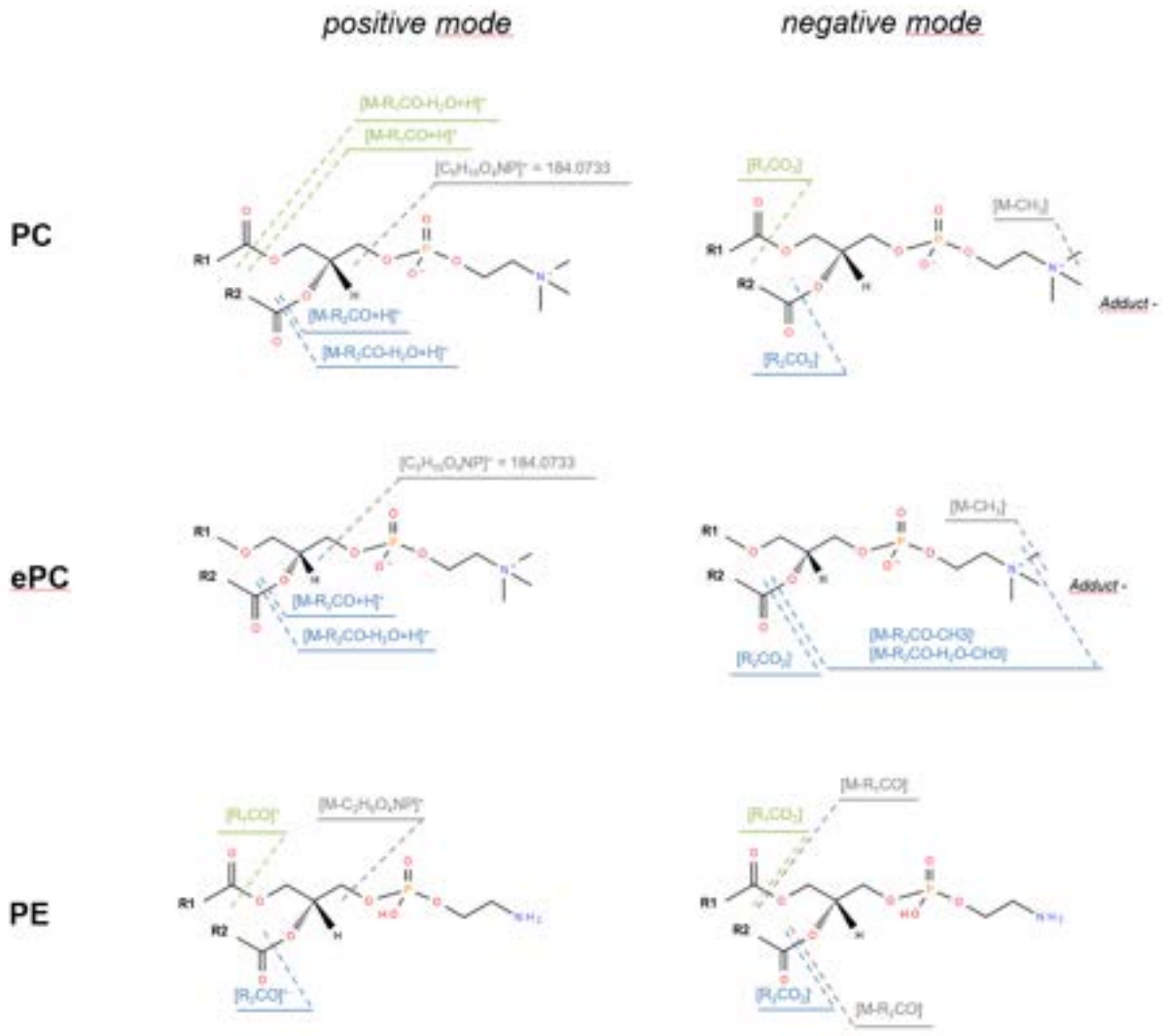

Figure S 1. Fragmentation pattern for positive and negative mode of lipids belonging to PC, etherPC (ePC), or PE lipid classes. Fatty acyl or fatty alkyl side chains are abbreviated with R, indices refer to sn-position on glycerol backbone.

2.2. MS/MS-spectra acquired in targeted and untargeted MS approach

A

PC 18:0 → PC 10:0-8:0 in sample

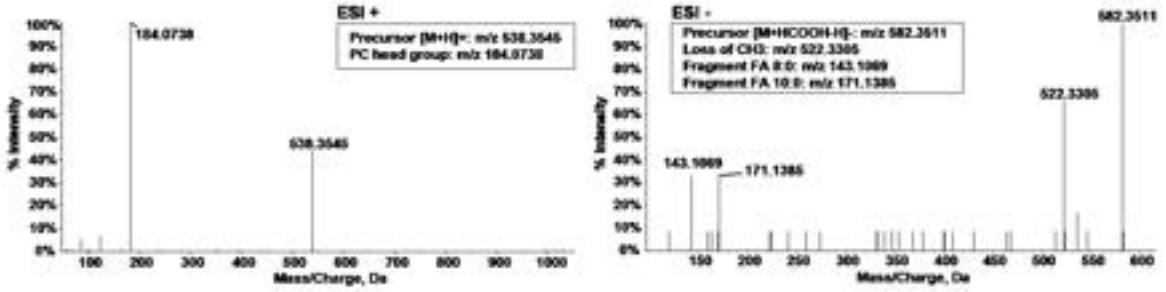

B

PC 20:0 → PC 10:0/10:0 in sample

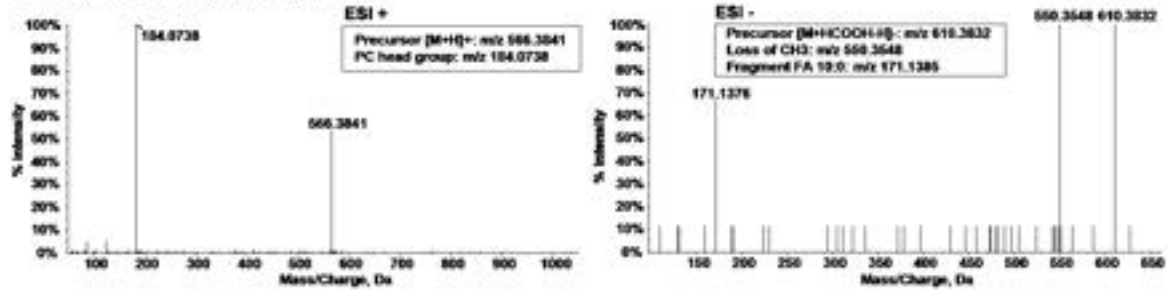

C

PC 20:0 → PC 10:0/10:0 in sample compared to authentic standard

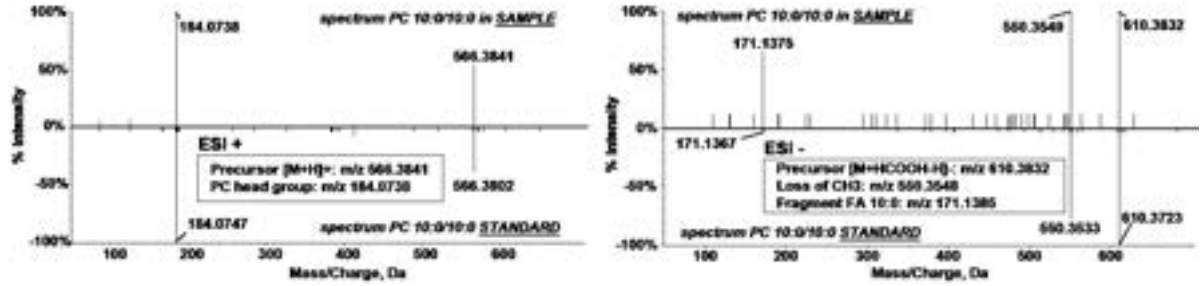

D

PC 24:0 → PC 16:0-8:0 in sample

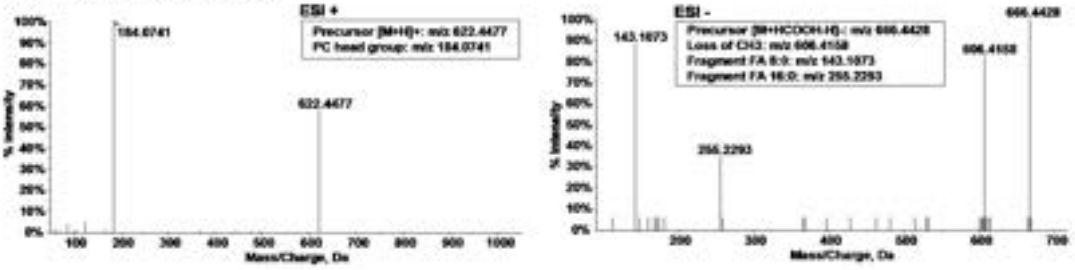

E

PC 32:1e → PC 16:0e/16:1 in sample

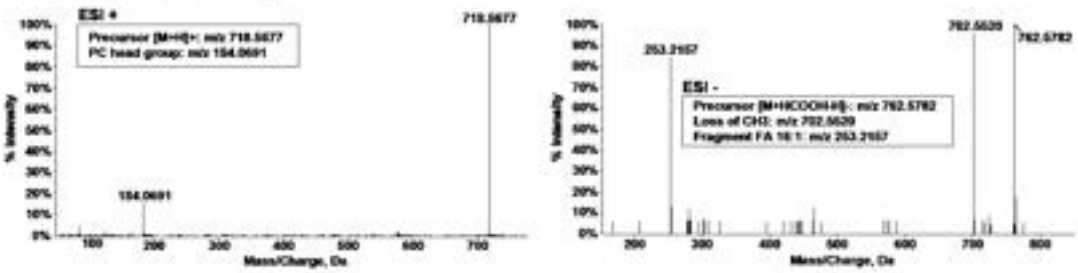

Figure S 2. MS/MS-spectra obtained in HR-MRM-method (see section 1.3) for side chain clarification of (A) PC 18:0, (B) PC 20:0, (D) PC 24:0, (E) PC 32:1e in lipid extracts from platelet pellets. Spectra in positive mode (left column) always include peaks for precursor ion and class-specific fragment ion of phosphatidylcholine-head group (m/z 184.0733). Spectra in negative mode (right column) show peaks for precursor ions, loss of methyl-group, and side-chain-specific fatty acid fragment ions. In panel (C), the MS/MS-spectrum of PC 10:0/10:0 detected in sample is plotted against the spectrum of an authentic standard of PC 10:0/10:0 for both ion modes.

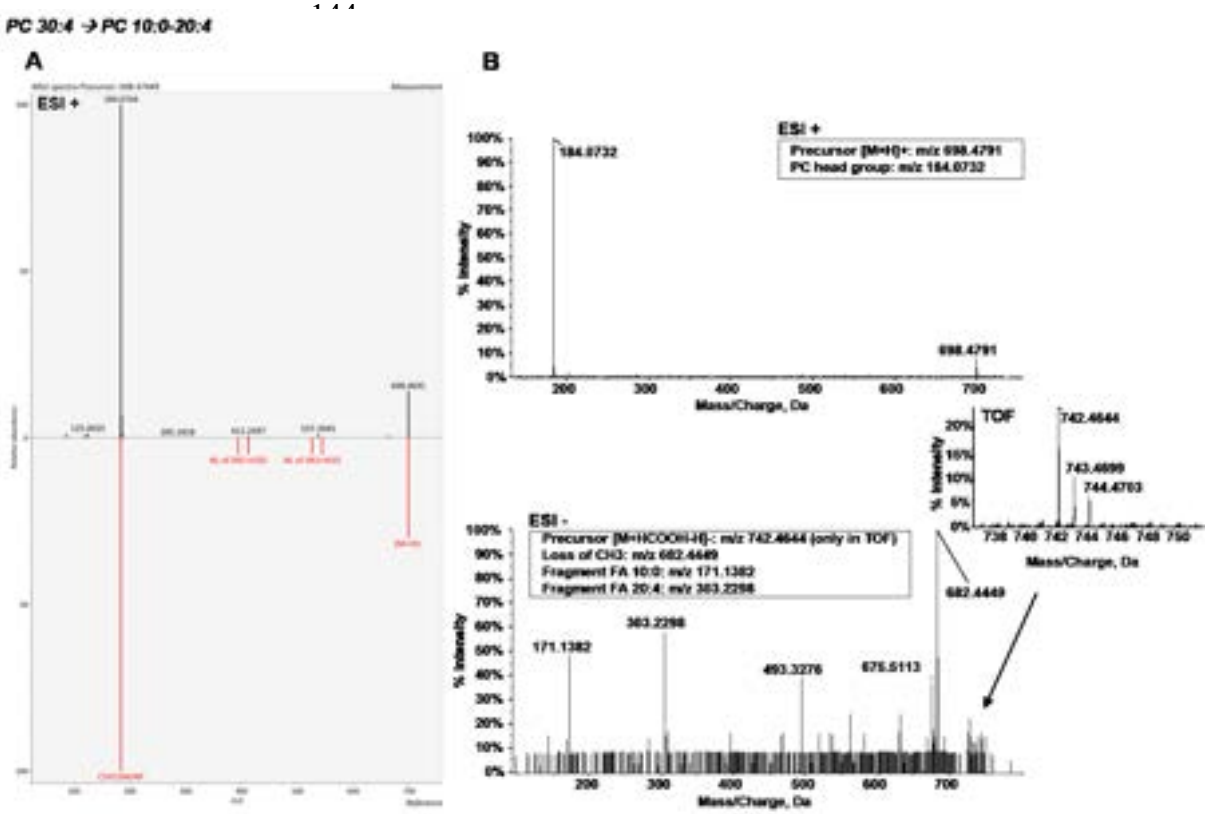

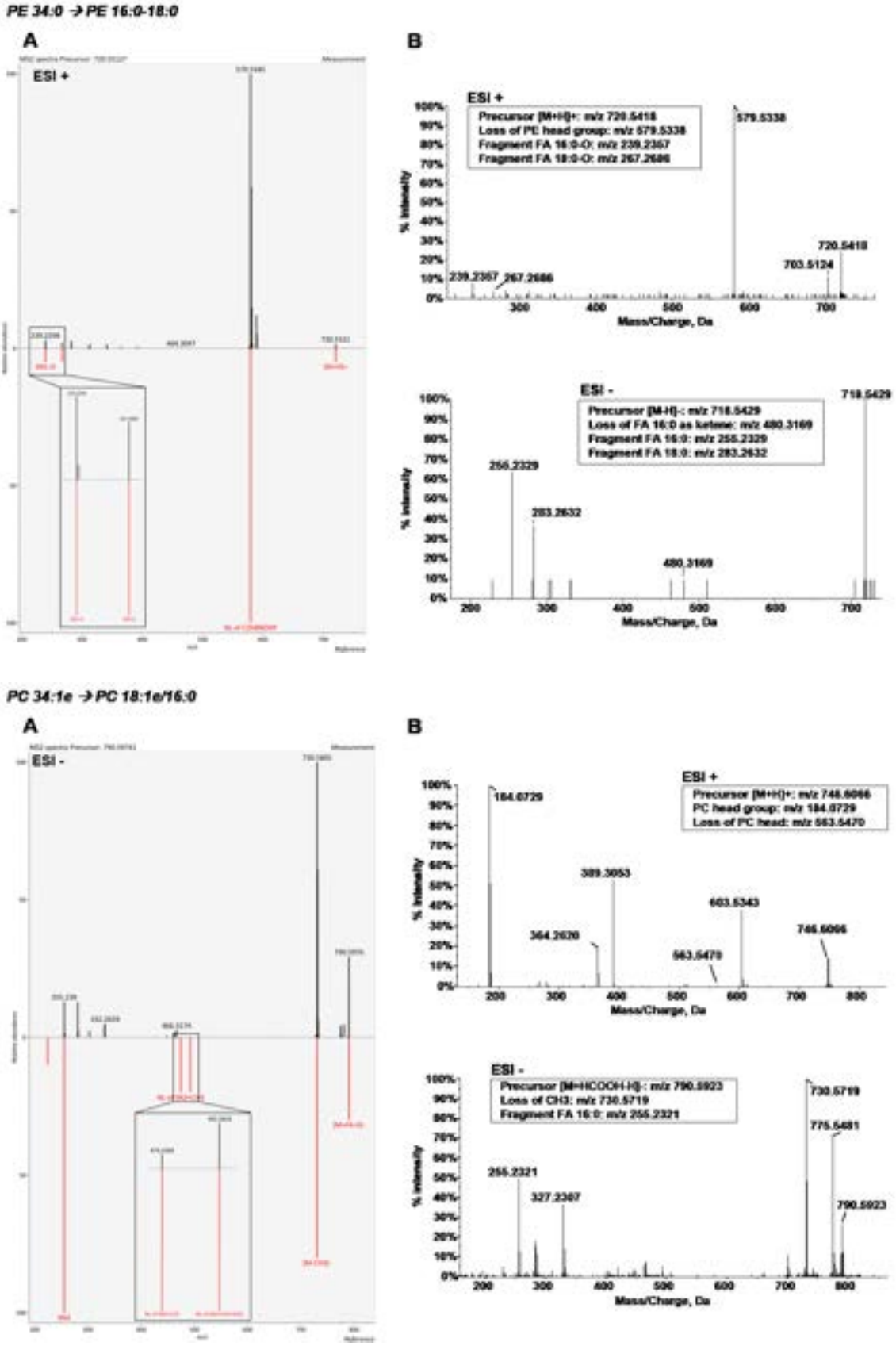

Figure S 3. MS/MS-spectra obtained in untargeted SWATH measurements for PC 30:4, PC 34:0, and PC 34:1e. (A) always shows the deconvoluted measured MS/MS-

spectra matched with corresponding reference spectra from LipidBlast in MS-DIAL in the indicated ESI-mode. In (B) the non-deconvoluted MS/MS-spectra in positive (top) and negative (bottom) mode are shown. Positive mode spectra show precursor ion peaks and class-specific fragment ion peaks, peaks in negative mode belong to precursor ions, methyl-loss, and side-chain-specific fatty acid fragment ions. Due to the acquisition mode, non-deconvoluted SWATH MS/MS-spectra have more peaks than the deconvoluted SWATH MS/MS-spectra and the HR-MRM-MS/MS-spectra. Additional peaks come from coeluting and cofragmented metabolites.

2.3. Exclusion of potential isomeric and isobaric overlap

Following recommendations from Lipid Standards Initiative (LSI, *https://lipidomics-standards-initiative.org/*) potential isomeric and isobaric overlaps for the upregulated lipids, especially for the medium-chain-fatty-acyl-PCs (MCFA-PCs), was checked. The lipids of potential interference are listed in Table S 2.

Table S 2. Lipids for potential isomeric and isobaric overlap based on LSI (https://lipidomics-standards-initiative.org/)

lipid	[M+H]+	t_R [min]	potential isomers*	potential isobars*		
PC 18:0	538.3545	1.67	PE 21:0	PC O-19:0	PS 18:1	
PC 20:0	566.3841	2.48	PE 23:0	PC O-21:0	PS 20:1	
PC 30:4	698.4791	3.46	PE 33:4	PC O-31:4	PS 30:5	PC 30:5 [M+2]
PC 24:0	622.4477	3.77	PE 27:0	PC O-25:0	PS 24:1	
PE 34:0	720.5418	6.47	PC 31:0	PE O-35:0		
PC 32:1e	718.5677	5.47	LPC 32:1	PC 31:1		PC 32:2e [M+2]
PC 34:1e	746.6066	6.13	LPC 34:1	PC 33:1		PC 34:2e [M+2]

*in positive and negative mode

Due to reversed-phase chromatographic separation prior injection into the mass spectrometer all potentially interfering lipids are separated from the lipids of interest as depicted in the Figures S4-S7. In case a potential overlaping lipid was not detected, the expected retention time was estimated by linear correlation within lipid class with same number of double bonds (homology of m/z and RT in RP-LC). Possibility of interference was then checked with estimated retention time for the dedicated lipid (indicated by “estimated”).

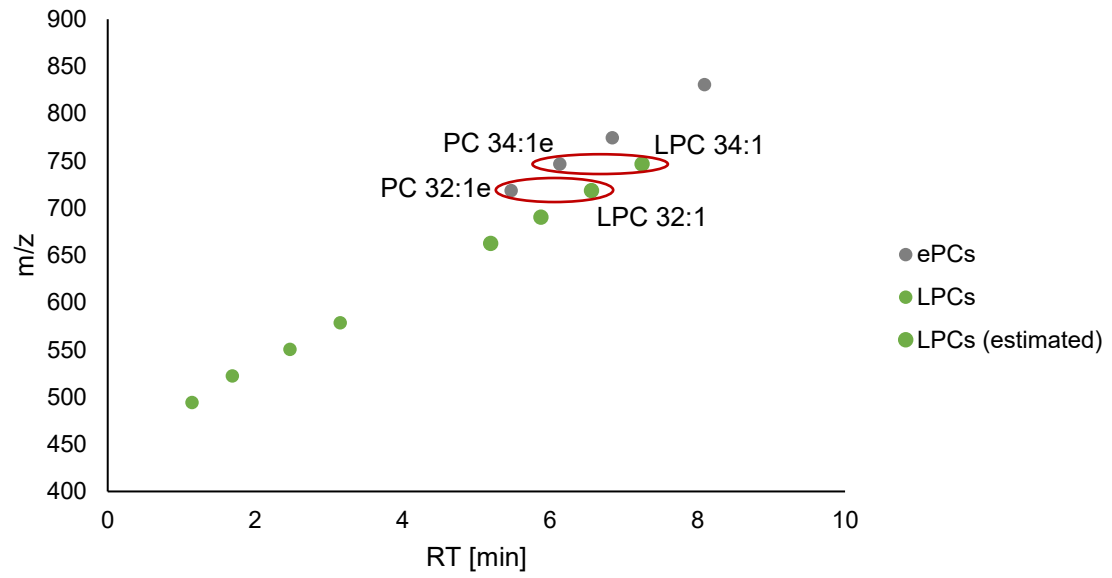

Figure S 4. Exclusion of isomeric overlap of upregulated ePCs with LPCs. Lipid classes are completely separated chromatographically.

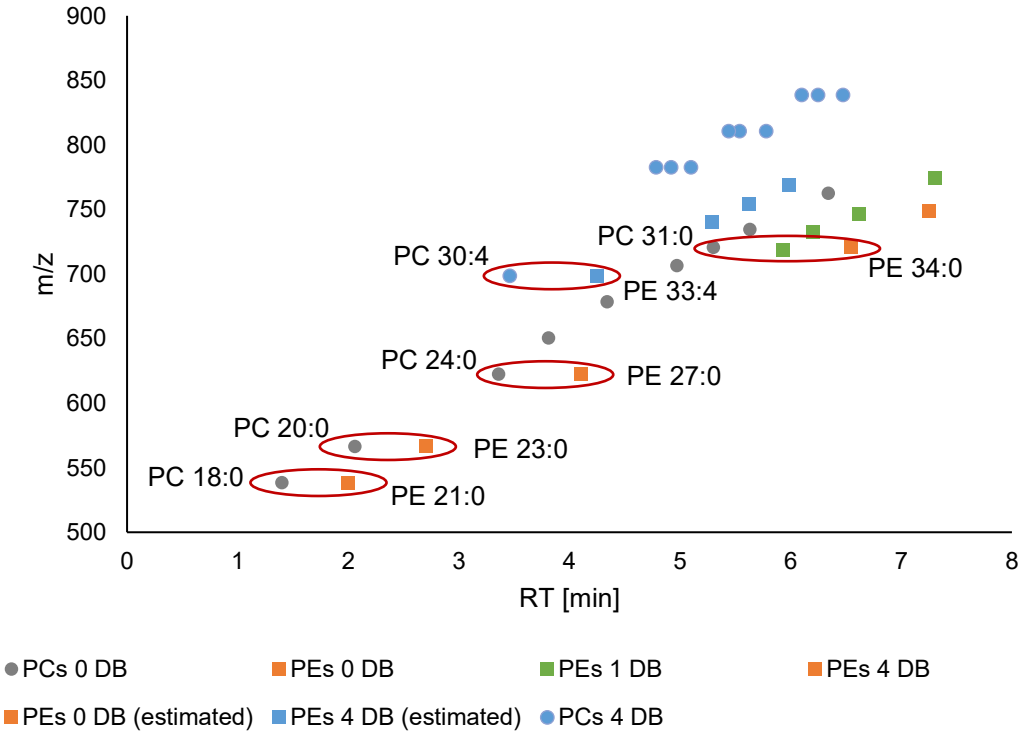

Figure S 5. Exclusion of isomeric overlap of PCs and PEs. Lipid classes are completely separated chromatographically.

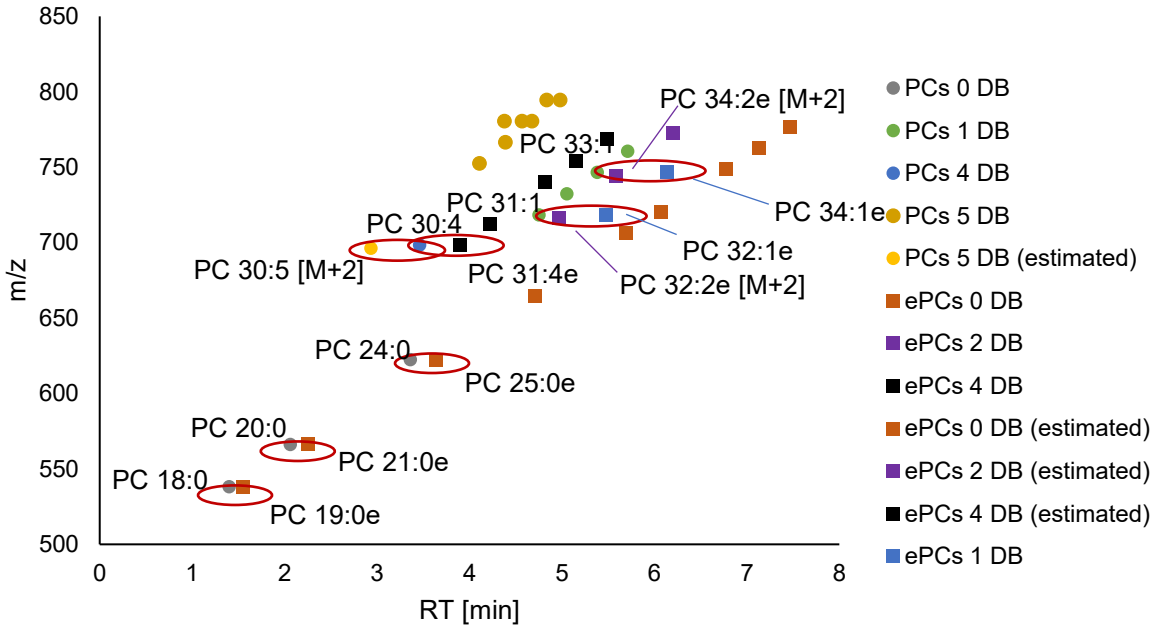

Figure S 6. Exclusion of isobaric overlap of PCs with ePCs as well with PC [M+2]-isotopologues. Lipid classes are completely separated chromatographically.

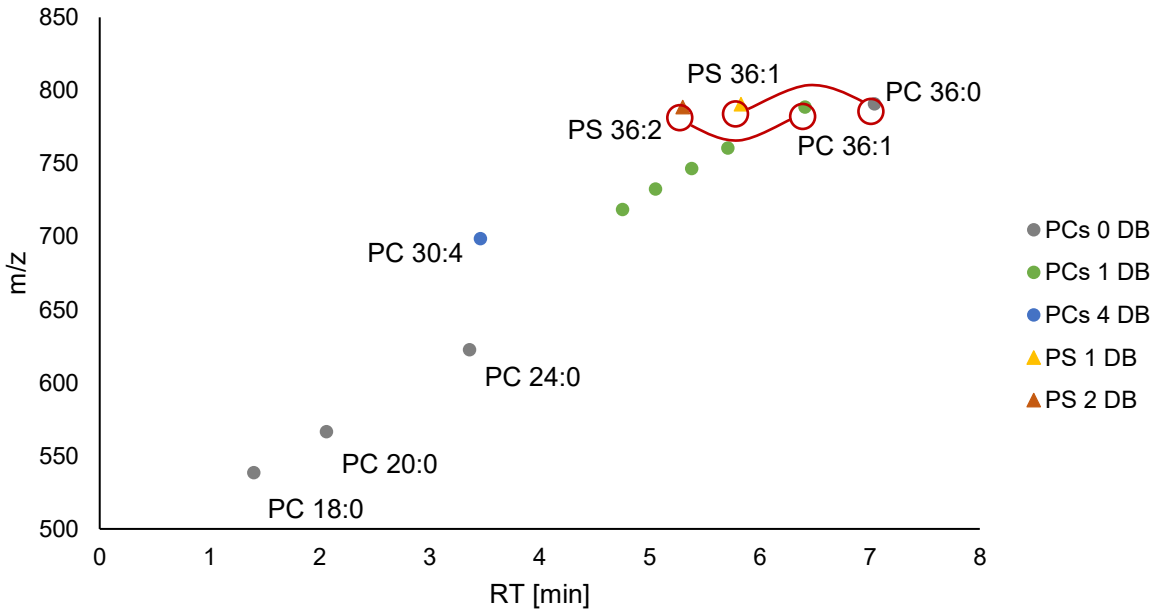

Figure S 7. Exclusion of isobaric overlap of PCs with PSs. PSs with low number of carbons were not detected, thus two other pairs of isobaric PS-PC were used as surrogate to assess the possibility of isobaric overlap between PS and PC lipid classes. For the surrogate pairs it is shown that lipid classes are completely separated chromatographically.

3. Significantly altered lipids in ACS compared to CCS

3.1. Specification of lipid notation and mass accuracy

Table S 3. Specification for significantly altered lipids in ACS compared to CCS in terms of lipid notation, mass accuracy, and structural annotation

regulation	lipid notation		precursor ion	theoretical mass	experimental mass	mass accuracy	spectral matching to*
	lipid species level	fatty acyl/alkyl level		[Da]	[Da]	[ppm]	
upregulation	PC 18:0	PC 10:0-8:0	[M+H]+	538.3503	538.3498	0.98	LipidBlast database
	PC 20:0	PC 10:0/10:0	[M+H]+	566.3816	566.3783	5.91	LipidBlast + authentic standard
	PC 30:4	PC 10:0-20:4	[M+H]+	698.4755	698.4728	3.94	LipidBlast database
	PC 24:0	PC 16:0-8:0	[M+H]+	622.4442	622.4419	3.78	LipidBlast database
	PE 34:0	PE 16:0-18:0	[M+H]+	720.5538	720.5508	4.20	LipidBlast database
	PC 32:1e	PC 16:0e/16:1	[M+H]+	718.5745	718.5734	1.57	LipidBlast database
	PC 34:1e	PC 18:1e/16:0	[M+FA-H]-	790.5960	790.5944	2.09	LipidBlast database
downregulation	SM d40:1	SM d18:1/22:0	[M+H]+	787.6687	787.6675	1.49	LipidBlast database
	PC 38:4	PC 18:0-20:4	[M+H]+	810.6007	810.5991	2.00	LipidBlast database
	PC 36:5e	PC 16:1e/20:4	[M+H]+	766.5745	766.5698	6.20	LipidBlast database
	PC 37:4	PC 17:0-20:4	[M+H]+	796.5851	796.5827	3.01	LipidBlast database
	PC 35:4	PC 15:0-20:4	[M+H]+	768.5538	768.5517	2.80	LipidBlast database
	PC 40:6	PC 18:0-22:6	[M+H]+	834.6007	834.5986	2.58	LipidBlast database
	PE 40:7e	PE 18:1e/22:6	[M-H]-	774.5443	774.5419	3.07	LipidBlast database
	LPE 16:0	LPE 16:0	[M+H]+	454.2928	454.2909	4.24	LipidBlast database
	PC 38:6	PC 16:0-22:6	[M+H]+	806.5694	806.5680	1.77	LipidBlast database
	PC 44:10	PC 22:5-22:5	[M+H]+	882.6007	882.5983	2.69	LipidBlast database
	PC 42:6e	PC 20:0e/22:6	[M+H]+	848.6528	848.6502	3.03	LipidBlast database
	LPE 18:0	LPE 18:0	[M+H]+	482.3241	482.3220	4.35	LipidBlast database
	PC 39:6	PC 17:0-22:6	[M+H]+	820.5851	820.5825	3.14	LipidBlast database
	DG 40:4	DG 18:0-22:4	$[M+NH_4]+$	690.6031	690.6016	2.24	LipidBlast database
	PC 42:6	PC 20:0-22:6	[M+H]+	862.632	862.6282	4.46	LipidBlast database
	LPC 18:0	LPC 18:0	[M+H]+	524.3711	524.3693	3.53	LipidBlast database
	PC 42:10	PC 20:4-22:6	[M+H]+	854.5694	854.5674	2.40	LipidBlast database
	TG 56:6	TG 16:0-18:0-22:6	[M+NH4]+	924.8015	924.7977	4.11	LipidBlast database
	PE 42:10	PE 20:4-22:6	[M-H]-	810.5079	810.5053	3.27	LipidBlast database
	TG 58:6	TG 16:0-20:0-22:6	[M+NH4]+	952.8328	952.8289	4.07	LipidBlast database
	TG 60:10	TG 18:0-20:4-22:6	[M+NH4]+	972.8015	972.7995	2.03	LipidBlast database

* LipidBlast is an *in-silico* database; PC 10:0/10:0 is the only commercially available authentic standard for medium chain PCs

3.2. Concentrations of altered lipids

Table S 4. Concentrations of significantly altered lipids between ACS and CCS patients from one-way ANOVA with SGoF-p-value correction performed with normalized peak intensities (significance level: p-value (SGoF)<0.05). Relative quantification was performed using lipid-class-specific isotopically labelled internal standard and normalized to cell count (pmol/10^6 cells)

regulation	lipid	ACS [pmol/10^6 cells] median [IQR]	CCS [pmol/10^6 cells] median [IQR]	p-value*	p-value (SGoF)*
upregulation	PC 10:0-8:0	5.61E-04 [3.49E-04 - 6.55E-03]	3.61E-04 [1.97E-04 - 7.33E-04]	0.0004	0.0042
	PC 10:0/10:0	9.91E-04 [2.32E-04 - 6.00E-03]	3.63E-04 [1.80E-04 - 7.62E-04]	0.0033	0.0103
	PC 10:0-20:4	1.12E-03 [3.30E-04 - 8.30E-03]	5.90E-04 [3.43E-04 - 1.43E-03]	0.0042	0.0127
	PC 16:0-8:0	5.40E-03 [2.01E-03 - 1.71E-02]	4.14E-03 [1.93E-03 - 7.50E-03]	0.0097	0.0267
	PE 16:0-18:0	0.35 [0.26 - 0.47]	0.30 [0.21 - 0.41]	0.0022	0.0075
	PC 16:0e/16:1	0.16 [0.14 - 0.20]	0.14 [0.11 - 0.17]	0.0107	0.0277
	PC 18:1e/16:0	3.93 [3.60 - 4.82]	3.72 [3.16 - 4.42]	0.0123	0.0286
downregulation	SM d18:1/22:0	47.40 [42.50 - 55.84]	48.70 [41.89 - 55.35]	0.0150	0.0341
	PC 18:0-20:4	19.35 [16.76 - 21.57]	21.95 [17.88 - 24.33]	0.0164	0.0405
	PC 16:1e/20:4	3.60 [2.69 - 4.00]	3.72 [3.23 - 4.48]	0.0097	0.0262
	PC 17:0-20:4	1.05 [0.87 - 1.18]	1.22 [1.00 - 1.52]	0.0068	0.0174
	PC 15:0-20:4	1.32 [1.02 - 1.72]	1.54 [1.22 - 1.90]	0.0103	0.0270
	PC 18:0-22:6	1.67 [1.20 - 2.22]	1.91 [1.50 - 2.56]	0.0088	0.0260
	PE 18:1e/22:6	6.65 [5.08 - 7.61]	6.75 [5.67 - 8.80]	0.0137	0.0302
	LPE 16:0	0.31 [0.27 - 0.36]	0.39 [0.34 - 0.46]	0.0036	0.0107
	PC 16:0-22:6	4.61 [3.31 - 6.27]	5.28 [4.20 - 6.49]	0.0069	0.0218
	PC 22:5-22:5	6.04E-02 [4.32E-02 - 8.97E-02]	7.20E-02 [5.37E-02 - 1.03E-01]	0.0019	0.0073
	PC 20:0e/22:6	0.10 [0.06 - 0.12]	0.11 [0.08 - 0.14]	0.0025	0.0088
	LPE 18:0	1.24 [1.14 - 1.46]	1.52 [1.32 - 1.76]	0.0002	0.0036
	PC 17:0-22:6	5.03E-02 [3.72E-02 - 5.43E-02]	5.74E-02 [4.16E-02 - 7.70E-02]	0.0065	0.0155
	DG 18:0-22:4	1.94E-02 [1.33E-02 - 2.58E-02]	2.44E-02 [1.73E-02 - 3.10E-02]	0.0145	0.0328
	PC 20:0-22:6	9.14E-02 [6.28E-02 - 1.30E-01]	0.12 [0.08 - 0.16]	0.0138	0.0309
	LPC 18:0	3.95 [3.35 - 4.71]	4.65 [3.95 - 5.31]	0.0013	0.0068
	PC 20:4-22:6	1.88 [1.41 - 2.59]	2.39 [1.86 - 3.13]	0.0042	0.0111
	TG 16:0-18:0-22:6	6.64E-02 [4.72E-02 - 8.27E-02]	7.94E-02 [5.81E-02 - 1.11E-01]	0.0128	0.0294
	PE 20:4-22:6	0.52 [0.41 - 0.71]	0.70 [0.53 - 0.85]	0.0009	0.0054
	TG 16:0-20:0-22:6	2.17E-02 [1.63E-02 - 2.96E-02]	3.11E-02 [2.19E-02 - 4.78E-02]	0.0044	0.0132
	TG 18:0-20:4-22:6	3.87E-02 [3.32E-02 - 5.85E-02]	5.63E-02 [3.72E-02 - 8.17E-02]	0.0101	0.0270

*!statistical analysis based on normalized peak intensities

3.3. Sensitivity and estimation of detection limits

Sensitivity and detection limits were estimated to further specify the performance of the LC-MS assay. Due to the untargeted approach, lipid-class-specific surrogate calibrants were used being regarded as representative for all lipid species of a lipid

class. To cover the lipid classes of the significantly up- and downregulated lipids in ACS, the following surrogate calibrants and their isotopically labeled counterparts were used: PC 15:0-18:1 (ILIS: PC 15:0-18:1(d7)), LPC 18:1 (ILIS: LPC 18:1(d7)), PE 15:0-18:1 (ILIS: PE 15:0-18:1(d7)), LPE 18:1 (ILIS: LPE 18:1(d7)), SM d18:1/18:1 (ILIS: SM d18:1/18:1(d9)), DG 15:0-18:1 (ILIS: DG 15:0-18:1(d7)), TG 15:0-18:1-15:0 (ILIS: TG 15:0-18:1(d7)-15:0). A six-point calibration in neat solution was acquired and used to assess the sensitivity via the slope of the calibration curve. Peak areas of the surrogate standards were normalized by the area of the corresponding isotopically labeled internal standard. The limit of detection (LOD) of the surrogate calibrants was estimated by a signal-to-noise (S/N) level of 3. In Table S 5, the values for LOD and sensitivity are presented for the significantly altered lipids in ACS compared to CCS referring to the correspondent class-specific surrogate. For all lipids, the estimated LOD is considerably below the mean concentration level determined over all samples. The sensitivity values indicate that even small differences in the concentration levels can be detected. As a validation parameter, the precision for each lipid species, determined as coefficient of variation in quality control samples, is listed in Table S 5. The precision is always below 30% (acceptance limit of FDA for biomarker studies), for the majority of lipid species it is below 20%, thus within validation recommendations.

Table S 5. Precision, estimated detection limits, and sensitivity determined for class-specific surrogate calibrants.

lipid	lipid concentration[1] [pmol/mL]		precision[2] [%]	surrogate calibrants	
	mean [±SD]	max		LOD[3] [pmol/mL]	sensitivity[4] [area ratio/pmol/mL]
PC 10:0-8:0	1.25E+01 [±3.65E+01]	2.85E+02	23*	0.67	1.72E-03
PC 10:0/10:0	9.65E+00 [±2.55E+01]	1.82E+02	29*	0.67	1.72E-03
PC 10:0-20:4	1.32E+01 [±3.65E+01]	2.76E+02	27*	0.67	1.72E-03
PC 16:0-8:0	3.08E+01 [±6.57E+01]	5.86E+02	20*	0.67	1.72E-03
PE 16:0-18:0	1.07E+03 [±5.69E+02]	3.45E+03	24	1.85	1.51E-03
PC 16:0e/16:1	4.74E+02 [±1.93E+02]	1.60E+03	8	0.67	1.72E-03
PC 18:1e/16:0	1.21E+04 [±3.87E+03]	3.25E+04	5	0.67	1.72E-03
SM d18:1/22:0	1.48E+05 [±3.12E+04]	2.26E+05	15	0.41	1.50E-03
PC 18:0-20:4	6.37E+04 [±1.46E+04]	1.04E+05	8	0.67	1.72E-03
PC 16:1e/20:4	1.13E+04 [±2.98E+03]	2.05E+04	7	0.67	1.72E-03
PC 17:0-20:4	3.72E+03 [±1.21E+03]	7.38E+03	6	0.67	1.72E-03
PC 15:0-20:4	4.62E+03 [±1.57E+03]	1.01E+04	6	0.67	1.72E-03
PC 18:0-22:6	6.04E+03 [±2.46E+03]	1.73E+04	8	0.67	1.72E-03
PE 18:1e/22:6	2.15E+04 [±8.06E+03]	5.62E+04	8	1.85	1.51E-03
LPE 16:0	1.17E+03 [±3.81E+02]	2.32E+03	6	1.67	1.02E-03
PC 16:0-22:6	1.61E+04 [±5.95E+03]	3.68E+04	9	0.67	1.72E-03
PC 22:5-22:5	2.40E+02 [±1.25E+02]	1.04E+03	14	0.67	1.72E-03
PC 20:0e/22:6	3.39E+02 [±1.44E+02]	1.11E+03	8	0.67	1.72E-03
LPE 18:0	4.49E+03 [±1.23E+03]	8.52E+03	7	1.67	1.02E-03
PC 17:0-22:6	1.75E+02 [±6.84E+01]	3.75E+02	10	0.67	1.72E-03
DG 18:0-22:4	7.42E+01 [±3.77E+01]	2.26E+02	24*	2.93	1.28E-03
PC 20:0-22:6	3.65E+02 [±1.87E+02]	1.07E+03	21	0.67	1.72E-03
LPC 18:0	1.37E+04 [±3.99E+03]	2.88E+04	5	0.38	1.40E-03
PC 20:4-22:6	7.25E+03 [±2.89E+03]	1.79E+04	9	0.67	1.72E-03
TG 16:0-18:0-22:6	2.57E+02 [±1.34E+02]	8.05E+02	13	2.98	1.98E-03
PE 20:4-22:6	1.98E+03 [±6.99E+02]	3.96E+03	10	1.85	1.51E-03
TG 16:0-20:0-22:6	1.03E+02 [±5.66E+01]	2.63E+02	16	2.98	1.98E-03
TG 18:0-20:4-22:6	1.82E+02 [±1.15E+02]	7.41E+02	17	2.98	1.98E-03

mean and maximum concentration determined over all samples irrespective of disease for each lipid species

precision determined as coefficient of variation on quality control samples for each lipid species

LOD determined as S/N≈3

slope of calibration curve of class-specific surrogate normalized by its corresponding labeled internal standard in neat solution

*!mean intensity of QCs close to LOQ

3.4. Comedication with statins

To further assess the effect of statin medication on the platelet lipidome, an O2PLS-DA analysis was performed on the subcohort of ACS patients in dependence on the statin treatment (statin-naive: n=14; statin-treated: n=12, Figure S 8). As already indicated in the Figure 6 in the main document, a separation due to statin treatment within this subcohort is observed. For the evaluation of the effect of statins on the lipids which were significantly regulated in ACS compared to CCS, VIP (Variable Importance for the Protection) scores of the O2PLS-DA (Figure S 8) are listed in Table S 6. The higher the VIP score is, the more important the lipid is for the separation of the two sample groups. The majority of lipids is not contributing to the separation of the two groups due to statin treatment (VIP score < 1.1). Most importantly, as highlighted in Table S 6, the medium-chain-fatty-acyl PCs all have scores below 0.5, thus are not

contributing to the grouping and thus seem to be not affected by statin medication. Only 5 lipids of the significantly regulated lipids of Figure 4 show a VIP score > 1.1 indicating that they contribute to the group separation based on statin treatments. However, 118 lipids have a score higher than 1.5 (up to 2.64), thus are responsible for the separation into statin treated and statin-naïve groups in the O2PLS-DA. The corresponding O2PLS-DA analysis for the CCS subgroup did not show a distinction between statin treated and statin-naïve samples. The analysis indicates no significant interference of the impact of statin treatment with the changes in the platelet lipidome between the ACS and CCS subcohorts, meaning the distinction is due to disease severity and not due to statin treatment.

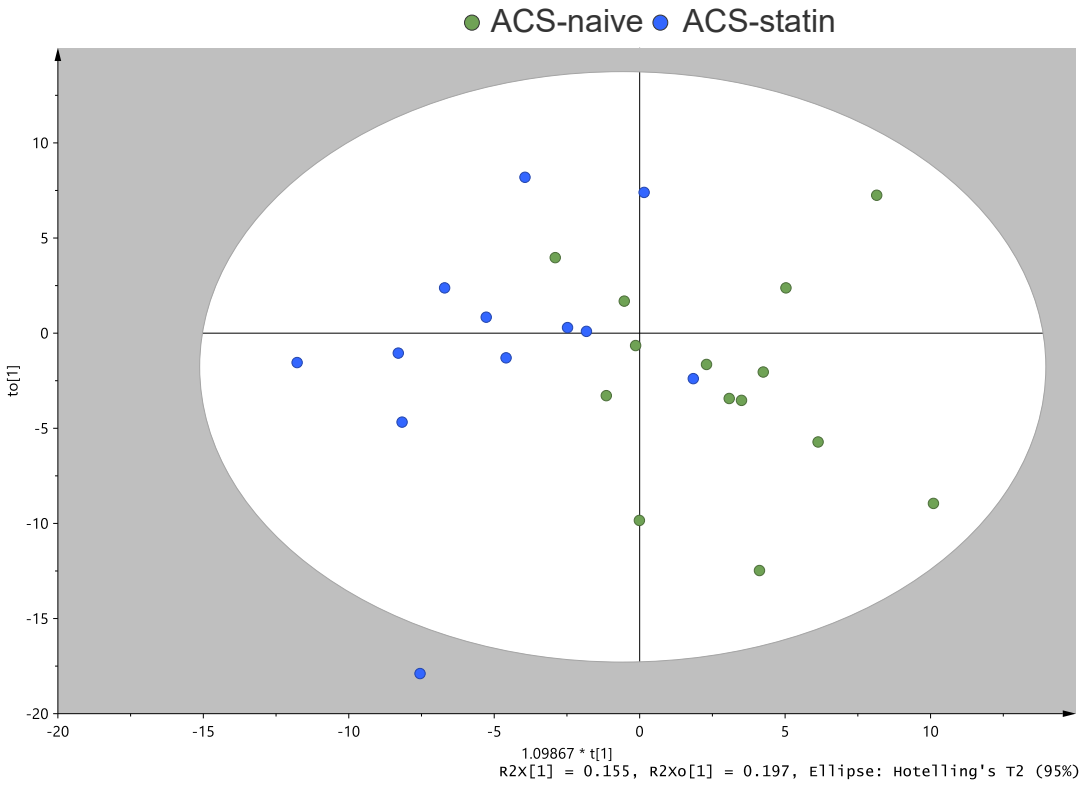

Figure S 8. O2PLS-DA analysis to further assess the impact of statin treatment on the lipidome within the subcohort of ACS patients. Analysis is based on normalized peak intensities of all identified lipids (n=928). (A) O2PLS-DA plot (components: 1 predictive,

5 orthogonal; $R^2X(cum)=0.617$, $R^2Y(cum)=0.531$, $Q^2(cum)=0.2$). Slight separation of statin-naive (n=14) and statin-treated ACS-patients (n=12).

Table S 6. Table showing the VIP scores for lipids being significantly altered in ACS compared to CCS within the O2PLS-DA. Medium-chain-fatty-acyl PCs are highlighted in red but do not contribute to the differentiation of statin-treated and statin-naive samples.

Lipid	VIP scores O2PLS-DA
PC 20:0-22:6	1.5401
PC 20:4-22:6	1.3403
PC 16:1e/20:4	1.2742
PC 17:0-22:6	1.2515
TG 16:0-18:0-22:6	1.1157
PC 22:5-22:5	1.0877
PC 20:0e/22:6	1.0716
TG 16:0-20:0-22:6	1.0634
PE 20:4-22:6	1.0607
TG 18:0-20:4-22:6	1.0417
PC 18:0-22:6	1.0082
PE 18:1e/22:6	0.9107
LPE 18:0	0.8856
SM d18:1/22:0	0.8612
PC 16:0e/16:1	0.8131
PC 16:0-22:6	0.7943
PC 17:0-20:4	0.7705
PC 15:0-20:4	0.7282
PC 18:0-20:4	0.7128
LPE 16:0	0.6337
LPC 18:0	0.6100
PC 18:1e/16:0	0.4719
PC 10:0-8:0	0.3896
DG 18:0-22:4	0.2227
PC 10:0-20:4	0.2147
PC 16:0-8:0	0.2138
PE 16:0-18:0	0.1556
PC 10:0/10:0	0.0378

4. Assessment of alterations in platelet lipids during a twelve-month follow-up

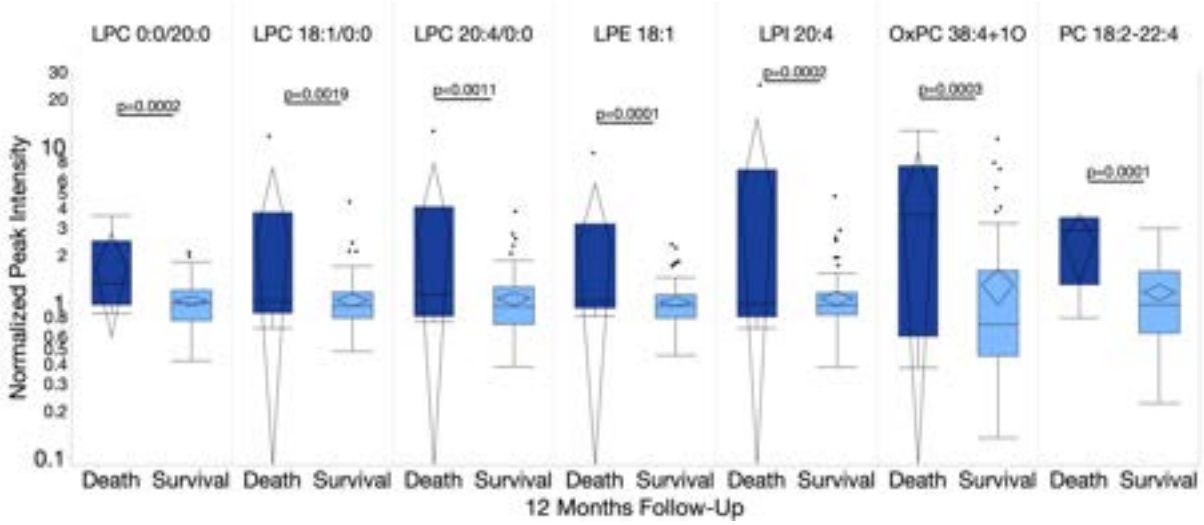

Figure S 9. Significantly enhanced platelet glycerophospholipid expression in patients who died during the twelve-month follow-up.

Only few clinical events during the twelve-months follow-up including 7 deaths occurred in this study cohort. Interestingly, LPC 0:0/20:0 (p=0.0002), LPC 18:1/0:0 (p=0.0019), LPC 20:4/0:0 (p=0.0011), LPE 18:1 (p=0.0001), LPI 20:4 (p=0.0002), OxPC 38:4+1O (p=0.0003) and PC 18:2-22:4 (p=0.0001) were significantly (SGoF $p<0.05$, FDR<0.05, one-way ANOVA) upregulated in patients who died during the twelve months follow-up in contrast to survivors. Here it is striking that these lipids exclusively belong to the category of glycerophospholipids and widely share at least one of the following characteristics: deacetylation (LPC/LPE), medium chain fatty acid side chain, oxidation of phospholipid.

5. Correlation of ACS associated lipids and CAD baseline characteristics

Table S 7. Pearson correlation of continuous clinical parameters and significantly regulated lipids in ACS patients compared to CCS

		Age	BMI	GFR-MDRD	Cholesterol	LDL	HDL	TG	Platelets
upregulation	PC 10:0-8:0	-0.067	0.012	0.138	0.034	0.076	-0.069	0.052	-0.037
	PC 10:0-10:0	-0.077	0.004	0.150	0.016	0.073	-0.065	0.045	-0.018
	PC 10:0-20:4	-0.096	-0.004	0.116	-0.023	0.045	-0.089	0.065	-0.032
	PC 16:0-8:0	-0.070	-0.016	0.112	0.024	0.072	-0.084	0.047	-0.031
	PE 16:0-18:0	0.013	0.019	0.034	-0.063	0.004	-0.260*	-0.043	-0.047
	PC 16:0e/16:1	0.110	-0.114	-0.034	-0.017	-0.028	-0.078	-0.116	0.122
	PC 18:1e/16:0	0.007	-0.048	0.013	-0.076	-0.018	-0.219*	-0.037	0.109
downregulation	SM d40:1(2)	-0.078	0.146	0.113	-0.031	0.036	-0.168	0.060	-0.274**
	PC 18:0-20:4	-0.250*	0.095	0.238*	-0.005	0.041	-0.212	0.297**	-0.204*
	PC 16:1e/20:4	-0.140	-0.058	0.154	0.069	0.060	-0.044	0.003	-0.004
	PC 17:0-20:4(1)	0.092	-0.172	0.045	0.023	0.029	-0.033	0.040	-0.089
	PC 17:0-20:4(2)	-0.135	-0.012	0.100	-0.034	-0.007	-0.149	0.107	-0.097
	PC 15:0-20:4	-0.106	0.055	-0.056	0.082	0.070	-0.079	0.028	0.005
	PC 18:0-22:6	-0.180	0.105	0.119	0.111	0.129	-0.226*	0.269*	-0.235*
	PE 18:1e/22:6	-0.173	0.057	0.089	0.081	0.127	-0.258*	0.183	-0.135
	LPE 16:0	-0.013	-0.045	-0.042	0.073	0.051	-0.068	0.088	-0.127
	PC 16:0-22:6	-0.152	0.120	0.032	0.186	0.156	-0.136	0.242*	-0.140
	PC 22:5-22:5	-0.167	0.160	0.103	0.119	0.103	-0.134	0.134	-0.211*
	PC 20:0e/22:6(1)	-0.103	0.048	0.261**	-0.093	-0.061	-0.203	-0.018	-0.097
	PC 20:0e/22:6(2)	-0.065	-0.008	0.094	-0.026	-0.059	-0.103	0.057	-0.098
	LPE 18:0	-0.012	-0.066	-0.114	0.059	0.021	-0.001	0.070	-0.227
	PC 17:0-22:6	-0.072	0.012	-0.005	0.133	0.081	-0.141	0.213*	-0.145
	DG 18:0-22:4	-0.083	0.102	0.113	-0.091	-0.040	-0.251*	0.245*	-0.159
	PC 20:0-22:6	-0.210*	0.083	0.186	0.238*	0.190	-0.081	0.172	-0.161
	LPC 0:0/18:0	-0.091	-0.105	0.137	0.078	0.059	-0.022	0.160	-0.216
	LPC 18:0/0:0	-0.207*	-0.005	0.225	0.152	0.135	-0.033	0.230*	-0.178
	PC 20:4-22:6	-0.293**	0.137	0.081	0.177	0.179	-0.160	0.260**	-0.141
	TG 16:0-18:0-22:6	-0.034	0.161	0.008	0.187	0.151	-0.033	0.184	-0.277**
	PE 20:4-22:6	-0.161	0.093	0.030	0.081	0.072	-0.131	0.097	-0.157
	TG 16:0-20:0-22:6	-0.134	0.129	0.096	0.182	0.152	-0.054	0.162	-0.260**
	TG 18:0-20:4-22:6	0.006	0.124	0.009	0.074	0.048	-0.093	0.213*	-0.242
	PC 14:0-22:6	-0.100	0.100	0.091	0.301**	0.255*	0.012	0.088	-0.097

Pearson correlation coeffictiants based on lipid concenctrations (pmol/10^6 cells); *p<0.05; **p<0.01

Concentrations of platelet lipids (pmol/10^6 cells) were calculated using lipid-class-specific isotopically labelled internal standard as described in Table S 5.

In this study, critically regulated lipids of the ACS cohort partially showed significant ($p<0.05$) correlations with important clinical parameters, such as age, BMI, GFR, cholesterol, LDL, HDL, triglycerides and platelet levels. It was further noticeable that especially lipids with PUFA-side-chains such as PC 18:0-20:4, PC 18:0-22:6, DG 18:0-22:4 and other showed significant correlations with parameters of the clinical cohort.

6. Subgroup analysis of altered lipids in statin treated versus statin-naïve ACS patients compared to CCS.

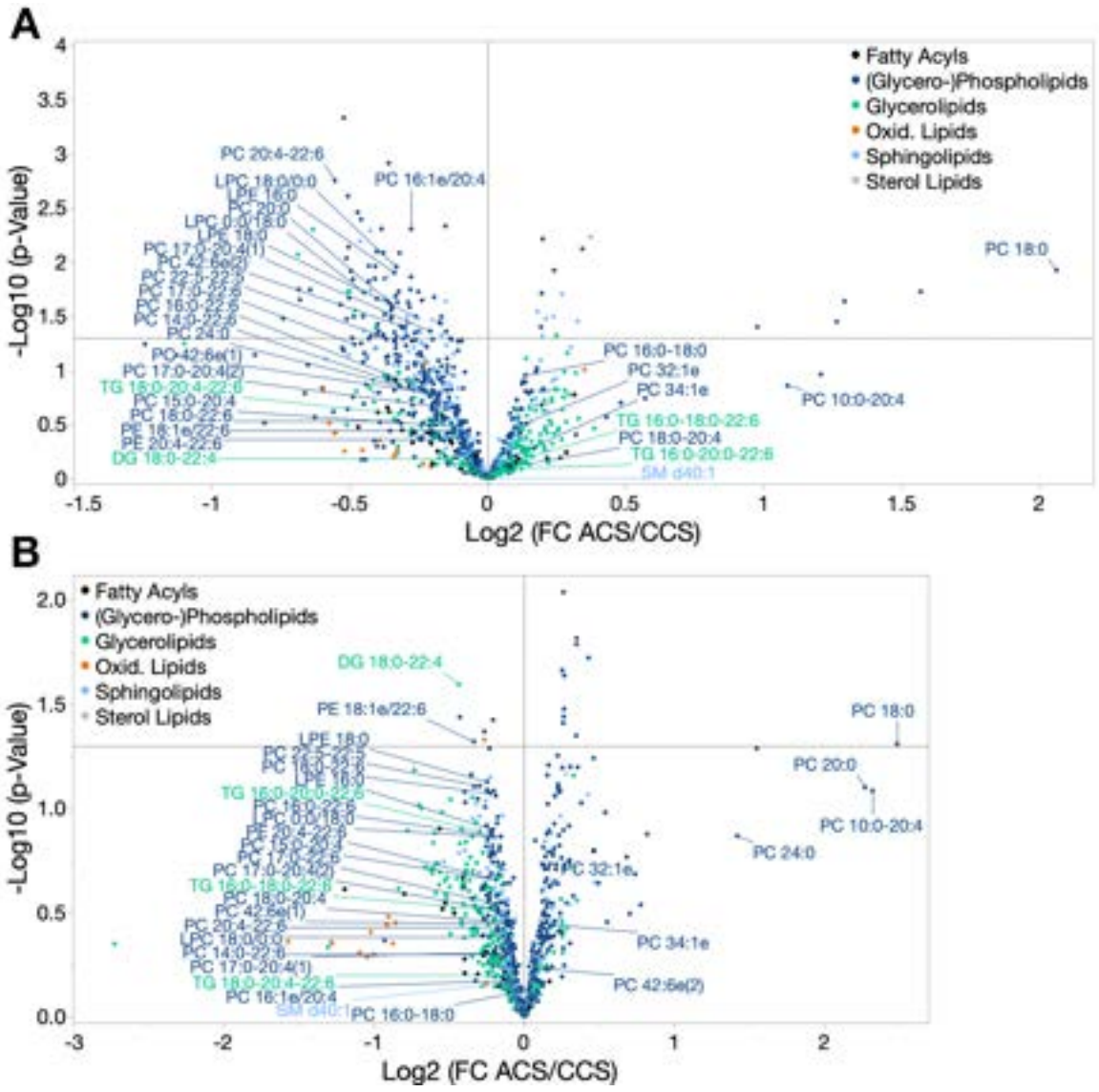

Figure S 10. (A) Volcano plot of detected and identified platelet lipids in statin treated patients X-axis (fold change) is the base 2 logarithm of peak intensity ratios (ACS n=16 / CCS n=76). Values >0 indicate upregulation in ACS; <0 downregulation. Y-axis shows -log10-transformed p-values of ANOVA (cut-off p<0.05). **(B)** As described in Figure S9 A volcano plot of statin-naïve patients was performed for ACS /CCS comparison (ACS n=19, CCS n=28). Thirty-two (32) significantly altered lipids of the overall cohort (ACS/CCS, n=139) were labelled.

Table S 8. In this study statin treated patients showed significant regulations (51 lipids) in ACS patients compared to CCS. Eight lipids were increased in ACS, 43 lipids showed lowered levels compared to CCS. Eleven lipids of the altered lipidome in the overall cohort were also found to be regulated in the statin treated subcohort (corresponds to 28% overlap) (n=7 upregulated in ACS, n=25 downregulated in ACS). Especially PC 18:0 (10:0-8:0), the most significantly upregulated glycerophospholipid was also found to be critically increased in statin treated ACS patients.

Patients (N)	Upregulated*	Downregulated* lipids (*p<0.05/SGoF)		
All (139)	PC 10:0-10:0 PC 10:0-20:4 PC 10:0-8:0 PC 16:0-8:0 PC 16:0e/16:1 PC 18:1e/16:0 PE 16:0-18:0	DG 18:0-22:4 LPC 0:0/18:0 LPC 18:0/0:0 LPE 16:0 LPE 18:0 PC 14:0-22:6 PC 15:0-20:4 PC 16:0-22:6 PC 16:1e/20:4 PC 17:0-20:4(1)	PC 17:0-20:4(2) PC 17:0-22:6 PC 18:0-20:4 PC 18:0-22:6 PC 20:0-22:6 PC 20:0e/22:6(1) PC 20:0e/22:6(2) PC 20:4-22:6 PC 22:5-22:5 PE 18:1e/22:6	PE 20:4-22:6 SM d40:1(2) TG 16:0-18:0-22:6 TG 16:0-20:0-22:6 TG 18:0-20:4-22:6
Statin-treated (92)	Cer-NDS d18:0/18:0 LPE 20:4 PC 10:0-8:0 PE 16:0-22:4 PE 18:0-22:5(1) PE 18:1-22:6 PE 40:5e(2) SM d18:1/22:0	Cer-NP t18:0/22:0 Cer-NP t18:0/24:0 Cer-NS d18:1/22:2 Cer-NS d18:2/20:0 LPC 0:0/18:0 LPC 18:0/0:0 LPC 20:0/0:0 LPC 22:0 LPE 16:0 LPE 18:0 LPE 20:0 PC 15:0-22:6 PC 16:0-20:0 PC 16:1e/20:4 PC 18:0-22:6 PC 18:1-22:6 PC 18:2-20:5(1) PC 19:1-20:4 PC 20:0-20:4 PC 20:1-22:5	PC 20:4-22:6 PC 22:6-22:6(1) PC 35:5 PC 36:5e(2) PC 37:0 PC 38:6e(2) PC 41:2 PC 41:5 PC 42:4e(1) PC 42:5e PC 43:5e PE 16:0-20:5 PE 18:1e/22:4 PE 20:4-22:6 PE 40:9 PI 18:1-20:4 PS 18:1-20:4 SM d30:1 SM d31:1 TG 56:5(1)	TG 60:1 TG 60:5 TG 60:9(1)
Statin-naïve (47)	-	-		

In the statin-naïve subgroup no significant changes between ACS and CCS patients were found. However, PC 18:0 (10:0-8:0) showed a trend of increased levels in ACS patients also in this subcohort without statin treatment.

7. Experimental Methods

7.1. Platelet-dependent thrombus formation *ex vivo* under flow

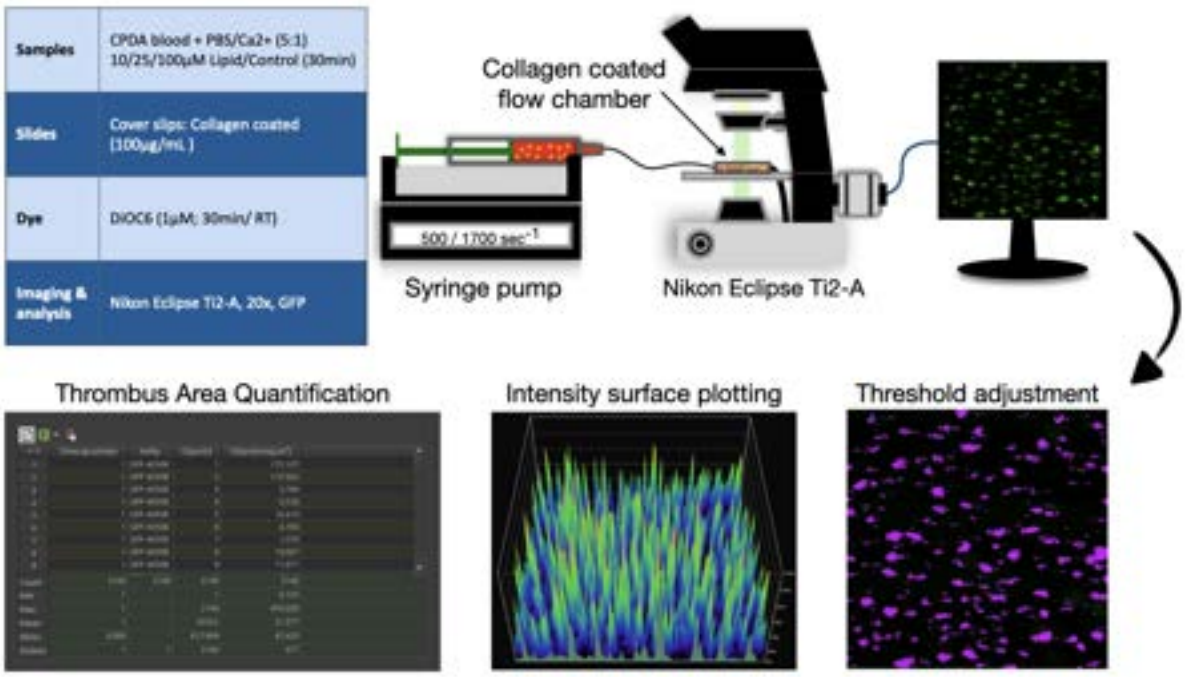

Figure S 11. *Ex vivo* platelet-dependent thrombus formation.

Platelet-dependent thrombus formation was analysed using a flow chamber perfusion assay. As indicated blood samples were preincubated with lipids or control vehicle (DMSO) for 30 minutes before analysis in concentrations as indicated (10 µM, 25 µM, 100 µM). 1000 µl 5:1 PBS-Ca^{2+} (Sigma-Aldrich, Steinheim, Germany) diluted, CPDA-citrated and DiOC6 (1 µM, 30 min incubation; Thermo Fisher Scientific Karlsruhe, Germany) fluorochrome labelled whole blood was perfused over collagen-coated (100 µg/ml, Volume 200 µl) cover slips (24 x 60 mm^2; Horm Kollagen, SKF-Solution, Takeda Austria GmbH (Linz, Austria)) with a shear rate of 500/1700s^{-1} and photo-documented after the blood perfusion was stopped and the transparent chamber was rinsed with

1000 µl PBS-Ca^{2+}. During the perfusion 1 min videos were taken (1s/frame). The thrombus area was quantified in five different photo-documented images (Nikon Eclipse Ti2-A, CFI Super Plan Fluor ADM, 20x Magnification, N.A. 0.45; GFP Filter, 466/40nm Wavelength; NIS-Elements AR, Nikon, Tokyo, Japan). The covered area was analyzed as seen above (threshold scaling, intensity and thrombus area quantification) and the mean percentage of covered area was determined (thrombus area fraction).

7.2. Platelet impedance aggregometry

According to standardized protocols platelet impedance aggregometry was performed using Multiplate Analyzer (F. Hoffmann-La Roche Ltd., Basel, Schweiz). Hirudinized whole blood (300 µl) from healthy donors was incubated with glycerophospholipids (100 µM) or DMSO as control for 30 minutes at room temperature. Thereafter, stimulation of measuring cells was performed with 20 µL adenosine diphosphate (ADP) 6.5 µM, arachidonic acid (AA) 484 µM or collagen 3.2 µg/mL.

Platelet impedance was assessed for 6 minutes and area under the curve (AUC) was integrated into further analysis.

7.3. Platelet spreading

Human platelets were isolated from venous blood, drawn and collected in acid-citrate-dextrose (ACD)-buffer. After centrifugation at 209 x g for 20 min platelet-rich plasma (PRP) was removed. Thereafter, Tyrodes-HEPES buffer (HEPES 2.5 mM; NaCl, 150 mM; KCl, 1 mM; NaHCO3, 2.5 mM; NaH2PO4, 0.36 mM; glucose, 6 mM; BSA, 1 mg/ml; pH 6.5) was added and centrifuged again at 822 x g for 10 min. The platelet

pellet was resuspended in Tyrodes-HEPES buffer (pH 7.4, supplemented with 1 mM CaCl2 and 1 mM MgCl2) after removing the supernatant.

Isolated human platelets in Tyrodes buffer (pH 7.4) were supplemented with 1 mM CaCal2 and PC18:0 or PC38:6 (100 µg/ml), thereafter, platelets were activated with 1 µg/ml CRP (CRP-XL, CambCol, Cambridge, UK) and incubated on fibrinogen-coated (100 µg/ml; Sigma Aldrich Co., St. Louis, Missouri, USA) coverslips for 30 min at room temperature. Afterwards platelets were fixed for 15 min with 4 % paraformaldehyde (Sigma Aldrich Co., St. Louis, Missouri, USA) and washed three times with PBS. The coverslips were mounted onto slides and five images from randomly selected areas were taken (Nikon Eclipse Ti2-A, 100x DIC objective). Subsequently a quarter of each image with at least 20 cells was analyzed.

7.4. Measurement of cytosolic Ca^{2+} concentration on adherent single platelets

Fura-4 fluorescence was used to determine the change in the cytosolic Ca^{2+} concentration during CRP stimulation after PC 18:0 or PC 38:6 treatments.

Washed human platelets were loaded with Fura-4 (5 µM, Life Technologies, California, USA) for 30 min. This was followed by treatment with PC18:0 or PC38:6 for further 20 min on fibrinogen-coated coverslips. The FURA-4 stained platelets were then excited at 494 nm using a fluorescence microscope (Nikon Eclipse Ti2 A; DIC 100x oil objektive). The emitted fluorescence intensity at 506 nm was recorded over 2 minutes using computer software NIS-Elements AR (Nikon, Japan). After 20 seconds of recording, the platelets were activated with 1 µg / ml CRP (CRP-XL CambCol, Cambridge, UK). To estimate the cytosolic Ca^{2+} activity, the fold change in the mean intensity of the fluorescence after CRP stimulation was assessed.

7.5. Platelet flow cytometry

Platelets were selected with CD42b (PE) mAb (Clone SZ2, Beckman Coulter Life Science, Krefeld, Germany) and incubated for 30 min with diluent, PC18:0, or PC38:6 (100 µM) respectively. Thereafter, platelets were stimulated with CRP (0.5 µg/ml) and P-selectin surface expression was analyzed after staining with a fluorochrome-labeled CD62P (FITC) mAb (Clone CLBThromb/6, Beckman Coulter) using a FACSCalibur (Becton-Dickinson NJ, USA).

7.6. Staining of isolated platelets with Fluo-PC16:0-6:0

To test whether externally added PCs are integrated into the plasma membrane, platelets were incubated with a fluorescent PC, Fluo-PC16:0-6:0 NBD (Avanti Polar Lipids, Inc, Alabama, USA), and analyzed by fluorescence microscopy (Nikon Eclipse Ti2-A, 100 x DIC objective) and flow cytometry.

8 STROBE Statement

Table S 9. STROBE checklist

	Item No	Recommendation	Page No
Title and abstract	1	(*a*) Indicate the study's design with a commonly used term in the title or the abstract	2
		(*b*) Provide in the abstract an informative and balanced summary of what was done and what was found	1-2
Introduction			
Background/rationale	2	Explain the scientific background and rationale for the investigation being reported	3
Objectives	3	State specific objectives, including any prespecified hypotheses	3
Methods			
Study design	4	Present key elements of study design early in the paper	4-5
Setting	5	Describe the setting, locations, and relevant dates, including periods of recruitment, exposure, follow-up, and data collection	4
Participants	6	(*a*) *Cohort study*—Give the eligibility criteria, and the sources and methods of selection of participants. Describe methods of follow-up	4

		Case-control study—Give the eligibility criteria, and the sources and methods of case ascertainment and control selection. Give the rationale for the choice of cases and controls *Cross-sectional study*—Give the eligibility criteria, and the sources and methods of selection of participants	
		(*b*) *Cohort study*—For matched studies, give matching criteria and number of exposed and unexposed *Case-control study*—For matched studies, give matching criteria and the number of controls per case	N/A
Variables	7	Clearly define all outcomes, exposures, predictors, potential confounders, and effect modifiers. Give diagnostic criteria, if applicable	4-8
Data sources/ measurement	8*	For each variable of interest, give sources of data and details of methods of assessment (measurement). Describe comparability of assessment methods if there is more than one group	4-8
Bias	9	Describe any efforts to address potential sources of bias	4-8
Study size	10	Explain how the study size was arrived at	4
Quantitative variables	11	Explain how quantitative variables were handled in the analyses. If applicable, describe which groupings were chosen and why	4-8
Statistical methods	12	(*a*) Describe all statistical methods, including those used to control for confounding	8
		(*b*) Describe any methods used to examine subgroups and interactions	8
		(*c*) Explain how missing data were addressed	N/A
		(*d*) *Cohort study*—If applicable, explain how loss to follow-up was addressed *Case-control study*—If applicable, explain how matching of cases and controls was addressed *Cross-sectional study*—If applicable, describe analytical methods taking account of sampling strategy	N/A
		(*e*) Describe any sensitivity analyses	N/A
Results			
Participants	13*	(a) Report numbers of individuals at each stage of study—eg numbers potentially eligible, examined for eligibility, confirmed eligible, included in the study, completing follow-up, and analysed	8-13
		(b) Give reasons for non-participation at each stage	N/A
		(c) Consider use of a flow diagram	N/A
Descriptive data	14*	(a) Give characteristics of study participants (eg demographic, clinical, social) and information on exposures and potential confounders	8-13
		(b) Indicate number of participants with missing data for each variable of interest	N/A
		(c) *Cohort study*—Summarise follow-up time (eg, average and total amount)	N/A
Outcome data	15*	*Cohort study*—Report numbers of outcome events or summary measures over time	N/A
		Case-control study—Report numbers in each exposure category, or summary measures of exposure	
		Cross-sectional study—Report numbers of outcome events or summary measures	
Main results	16	(*a*) Give unadjusted estimates and, if applicable, confounder-adjusted estimates and their precision (eg, 95% confidence interval). Make clear which confounders were adjusted for and why they were included	Table 1

		(*b*) Report category boundaries when continuous variables were categorized	Table 1
		(*c*) If relevant, consider translating estimates of relative risk into absolute risk for a meaningful time period	N/A
Other analyses	17	Report other analyses done—eg analyses of subgroups and interactions, and sensitivity analyses	8-13
Discussion			
Key results	18	Summarise key results with reference to study objectives	13
Limitations	19	Discuss limitations of the study, taking into account sources of potential bias or imprecision. Discuss both direction and magnitude of any potential bias	13-15
Interpretation	20	Give a cautious overall interpretation of results considering objectives, limitations, multiplicity of analyses, results from similar studies, and other relevant evidence	13-15
Generalisability	21	Discuss the generalisability (external validity) of the study results	13-15
Other information			
Funding	22	Give the source of funding and the role of the funders for the present study and, if applicable, for the original study on which the present article is based	15

9 References

1. Tsugawa H, Cajka T, Kind T, Ma Y, Higgins B, Ikeda K, Kanazawa M, VanderGheynst J, Fiehn O, Arita M. MS-DIAL: data-independent MS/MS deconvolution for comprehensive metabolome analysis. *Nat Methods* 2015;**12**:523-526.
2. Liebisch G, Vizcaino JA, Kofeler H, Trotzmuller M, Griffiths WJ, Schmitz G, Spener F, Wakelam MJ. Shorthand notation for lipid structures derived from mass spectrometry. *J Lipid Res* 2013;**54**:1523-1530.

Figure legends

Table S 1. List of MS and MS/MS experiments within a cycle

Table S 2. Lipids for potential isomeric and isobaric overlap based on LSI (https://lipidomics-standards-initiative.org/)

Table S 3. Specification for significantly altered lipids in ACS compared to CCS in terms of lipid notation, mass accuracy, and structural annotation

Table S 4. Concentrations of significantly altered lipids between ACS and CCS patients from one-way ANOVA with SGoF-p-value correction performed with normalized peak intensities (significance level: p-value (SGoF)<0.05). Relative quantification was

performed using lipid-class-specific isotopically labelled internal standard and normalized to cell count (pmol/10^6 cells)

Table S 5. Precision, estimated detection limits, and sensitivity determined for class-specific surrogate calibrants

Table S 6. Table showing the VIP scores for lipids being significantly altered in ACS compared to CCS within the O2PLS-DA. Medium-chain-fatty-acyl PCs are highlighted in red but do not contribute to the differentiation of statin-treated and statin-naive samples

Table S 7. Pearson correlation of continuous clinical parameters and significantly regulated lipids in ACS patients compared to CCS

Table S 8. In this study statin treated patients showed significant regulations (51 lipids) in ACS patients compared to CCS. Eight lipids were increased in ACS, 43 lipids showed lowered levels compared to CCS. Eleven lipids of the altered lipidome in the overall cohort were also found to be regulated in the statin treated subcohort (corresponds to 28% overlap) (n=7 upregulated in ACS, n=25 downregulated in ACS). Especially PC 18:0 (10:0-8:0), the most significantly upregulated glycerophospholipid was also found to be critically increased in statin treated ACS patients

Table S 9. STROBE checklist

Figure S 2. Fragmentation pattern for positive and negative mode of lipids belonging to PC, etherPC (ePC), or PE lipid classes. Fatty acyl or fatty alkyl side chains are abbreviated with R, indices refer to sn-position on glycerol backbone.

Figure S 2. MS/MS-spectra obtained in HR-MRM-method (see section 1.3) for side chain clarification of (A) PC 18:0, (B) PC 20:0, (D) PC 24:0, (E) PC 32:1e in lipid extracts from platelet pellets. Spectra in positive mode (left column) always include

peaks for precursor ion and class-specific fragment ion of phosphatidylcholine-head group (m/z 184.0733). Spectra in negative mode (right column) show peaks for precursor ions, loss of methyl-group, and side-chain-specific fatty acid fragment ions. In panel (C), the MS/MS-spectrum of PC 10:0/10:0 detected in sample is plotted against the spectrum of an authentic standard of PC 10:0/10:0 for both ion modes.

Figure S 3. MS/MS-spectra obtained in untargeted SWATH measurements for PC 30:4, PC 34:0, and PC 34:1e. (A) always shows the deconvoluted measured MS/MS-spectra matched with corresponding reference spectra from LipidBlast in MS-DIAL in the indicated ESI-mode. In (B) the non-deconvoluted MS/MS-spectra in positive (top) and negative (bottom) mode are shown. Positive mode spectra show precursor ion peaks and class-specific fragment ion peaks, peaks in negative mode belong to precursor ions, methyl-loss, and side-chain-specific fatty acid fragment ions. Due to the acquisition mode, non-deconvoluted SWATH MS/MS-spectra have more peaks than the deconvoluted SWATH MS/MS-spectra and the HR-MRM-MS/MS-spectra. Additional peaks come from coeluting and cofragmented metabolites.

Figure S 4. Exclusion of isomeric overlap of upregulated ePCs with LPCs. Lipid classes are completely separated chromatographically.

Figure S 5. Exclusion of isomeric overlap of PCs and PEs. Lipid classes are completely separated chromatographically.

Figure S 6. Exclusion of isobaric overlap of PCs with ePCs as well with PC [M+2]-isotopologues. Lipid classes are completely separated chromatographically.

Figure S 7. Exclusion of isobaric overlap of PCs with PSs. PSs with low number of carbons were not detected, thus two other pairs of isobaric PS-PC were used as surrogate to assess the possibility of isobaric overlap between PS and PC lipid classes. For the surrogate pairs it is shown that lipid classes are completely separated chromatographically.

Figure S 8. O2PLS-DA analysis to further assess the impact of statin treatment on the lipidome within the subcohort of ACS patients. Analysis is based on normalized peak intensities of all identified lipids (n=928). (A) O2PLS-DA plot (components: 1 predictive, 5 orthogonal; $R^2X(cum)=0.617$, $R^2Y(cum)=0.531$, $Q^2(cum)=0.2$). Slight separation of statin-naive (n=14) and statin-treated ACS-patients (n=12).

Figure S 9. Significantly enhanced platelet glycerophospholipid expression in patients who died during the twelve-month follow-up.

Figure S 10. (A) Volcano plot of detected and identified platelet lipids in statin treated patients X-axis (fold change) is the base 2 logarithm of peak intensity ratios (ACS n=16 / CCS n=76). Values >0 indicate upregulation in ACS; <0 downregulation. Y-axis shows -log10-transformed p-values of ANOVA (cut-off $p<0.05$). **(B)** As described in Figure S9 A volcano plot of statin-naïve patients was performed for ACS /CCS comparison (ACS n=19, CCS n=28). Thirty-two (32) significantly altered lipids of the overall cohort (ACS/CCS, n=139) were labelled.

Figure S 11. *Ex vivo* platelet-dependent thrombus formation.

2.3 Publication VIII

Statin Treatment Is Associated with Alterations in the Platelet Lipidome

Tobias Harm[1], Moritz Frey[1], Kristina Dittrich[2], Andreas Goldschmied[1], Anne-Katrin Rohlfing[1], Xiaoqing Fu[2], Adrian Brun[2], Tatsiana Castor[1], Dominik Rath[1], Karin Müller[1], Michael Lämmerhofer[2], Meinrad Gawaz[1*]

[1]Department of Cardiology and Angiology, University Hospital

Tübingen, Eberhard Karls University Tübingen, Tübingen, Germany

[2]Institute of Pharmaceutical Sciences, Pharmaceutical (Bio-)Analysis,

Eberhard Karls University Tübingen, Tübingen, Germany

Reprinted with permission from Thromb Haemost 2023; 123(06): 585-596

https://doi.org/10.1055/s-0043-1764353

Statin Treatment Is Associated with Alterations in the Platelet Lipidome

Tobias Harm[1] Moritz Frey[1] Kristina Dittrich[2] Andreas Goldschmied[1] Anne-Katrin Rohlfing[1] Xiaoqing Fu[2] Adrian Brun[2] Tatsiana Castor[1] Dominik Rath[1] Karin Müller[1] Michael Lammerhofer[2] Meinrad Gawaz[1]

[1] Department of Cardiology and Angiology, University Hospital Tübingen, Eberhard Karls University Tübingen, Tübingen, Germany
[2] Institute of Pharmaceutical Sciences, Pharmaceutical (Bio-)Analysis, Eberhard Karls University Tübingen, Tübingen, Germany

Address for correspondence Meinrad Gawaz, MD, Department of Cardiology and Angiology, University Hospital Tübingen, Eberhard Karls University Tübingen, Otfried-Müller-Str. 10, 72076 Tübingen, Germany (e-mail: meinrad.gawaz@med.uni-tuebingen.de).

Thromb Haemost 2023;123:585–596.

Abstract

Background Platelets are key players in the pathophysiology of coronary artery disease (CAD) and platelet hyperreactivity leads to increased risk of developing adverse cardiovascular events. Further, significant changes in the platelet lipidome occur in patients with acute coronary syndrome (ACS) and critically regulated lipids lead to platelet hyperresponsiveness. Statin treatment is crucial in the treatment and prevention of patients with CAD by remodeling lipid metabolism.

Objective In this study, we investigate the platelet lipidome of CAD patients by untargeted lipidomics, highlighting significant changes between statin-treated and naïve patients.

Methods We characterized the platelet lipidome in a CAD cohort ($n = 105$) by an untargeted lipidomics approach using liquid chromatography coupled to mass spectrometry.

Results Among the annotated lipids, 41 lipids were significantly upregulated in statin-treated patients, whereas 6 lipids were downregulated compared to naïve patients. The most prominent upregulated lipids in statin-treated patients belong to the class of triglycerides, cholesteryl esters, palmitic acid, and oxidized phospholipids, whereas mainly glycerophospholipids were downregulated compared to untreated patients. A more pronounced effect of statin treatment on the platelet lipidome was observed in ACS patients. We further highlight a dose-dependent influence on the platelet lipidome.

Conclusion Our results reveal that the platelet lipidome is altered in CAD patients with statin treatment and upregulated lipids embody mainly characteristic triglycerides, whereas downregulated lipids mostly compromise glycerophospholipids, which may play a role in the pathophysiology of CAD. Results of this study may contribute to the understanding of statin treatment softening the lipid phenotype.

Keywords
- platelets
- lipidome
- statins
- coronary artery disease

received
October 25, 2022
accepted after revision
January 31, 2023
article published online
March 10, 2023

Georg Thieme Verlag KG,
Rüdigerstraße 14,
70469 Stuttgart, Germany

DOI https://doi.org/10.1055/s-0043-1764353.
ISSN 0340-6245.

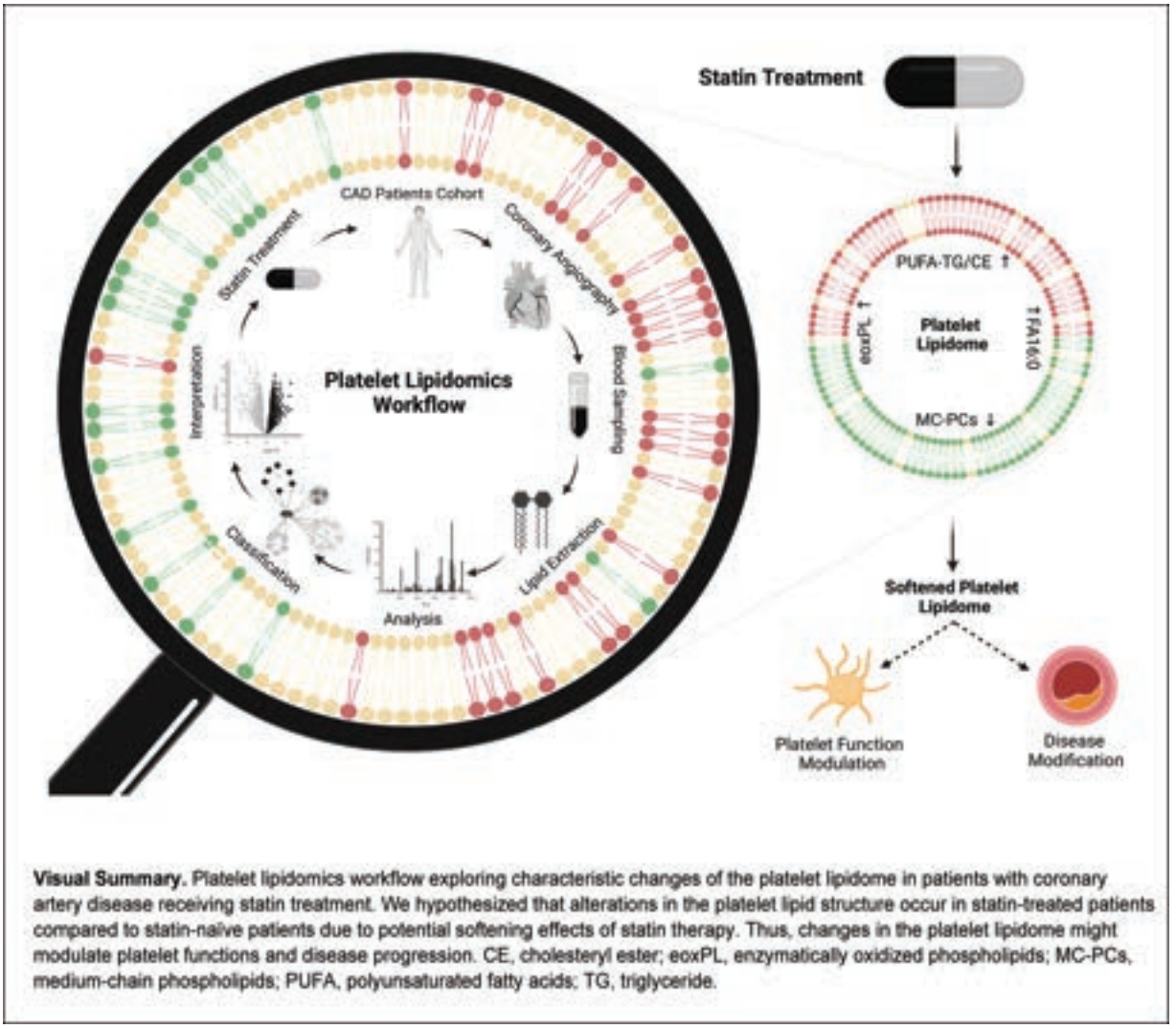

Visual Summary. Platelet lipidomics workflow exploring characteristic changes of the platelet lipidome in patients with coronary artery disease receiving statin treatment. We hypothesized that alterations in the platelet lipid structure occur in statin-treated patients compared to statin-naïve patients due to potential softening effects of statin therapy. Thus, changes in the platelet lipidome might modulate platelet functions and disease progression. CE, cholesteryl ester; eoxPL, enzymatically oxidized phospholipids; MC-PCs, medium-chain phospholipids; PUFA, polyunsaturated fatty acids; TG, triglyceride.

Introduction

Platelets are essentially involved in the pathophysiology of acute coronary syndrome (ACS).[1–4] Platelets adhere to collagen exposed toward the blood stream after decisive occurrence of plaque rupture, and accumulate and promote thrombus formation that limits coronary perfusion leading to acute myocardial ischemia.[4–7] Thus, antiplatelet therapy has become crucial in the treatment and secondary prevention of ACS.[8,9] Further, enhanced platelet hyperreactivity is a major risk factor for thromboischemic events in patients with coronary artery disease (CAD).[10–12] Thus, patients with platelet hyperreactivity are at increased risk to develop adverse cardiovascular events including myocardial infarction, ischemic stroke, and cardiac death.[10] Continuous platelet activation leads to a thrombo-inflammatory state and atheroprogression in CAD patients which, therefore, determines the outcome of the disease.[10] Established cardiovascular risk factors such as dyslipoproteinemia or diabetes promote platelet activation and thus are major targets of treatment and prevention in patients with CAD.[11,13]

Previously, we showed that binding and subsequent internalization of oxidized low-density lipoproteins (oxLDL) on circulating platelets is increased in ACS patients and is further associated with platelet hyperreactivity.[11,14] Further, we found that the platelet lipidome is significantly altered in patients with acute (ACS) when compared to chronic coronary syndrome (CCS). Especially specific glycerophospholipids are upregulated in ACS patients.[15] Here, it was striking that upregulated lipids in patients with ACS primarily composed of medium-chain phosphatidylcholines (MC-PCs) such as PC18:0 (PC 10:0-8:0). Further, MC-PCs were not detectable in healthy donors and were less upregulated in CCS, i.e., disease severity correlated with MC-PC concentrations.[15] Characteristic changes in the platelet lipidome may contribute to the pathophysiology of ACS by promoting enhanced platelet function.[15]

Platelet lipidomics have recently become a new perspective of ongoing research in cardiovascular diseases. In this study, we determine the effect of statin treatment on the platelet lipidome in patients with symptomatic CAD. Hitherto unknown alterations of the platelet lipidome occur in statin-treated patients compared to statin-naïve patients.

Thus, pleiotropic effects of statin may soften the platelet lipidome in patients with CAD.[16]

Methods

Study Population

One-hundred and five patients with symptomatic CAD were enrolled in this study (►**Table 1**). All patients were undergoing coronary angiography within 24 hours after hospital admission and treated for symptomatic CAD. Blood samples were obtained from the arterial sheath at the time of coronary angiography before administration of unfractionated heparin and before coronary stent placement. The study was approved by the local ethics committee (270/2011B01) and all patients gave written informed consent. The experiments were performed in accordance with the ethical standards as laid down in the Declaration of Helsinki. A detailed description of the study design is described in the ►**Supplementary Methods** section (►**Supplementary Material,** available in the online version).

Platelet Lipidomics

Platelets were isolated for lipidomic analysis as recently described[14,15,17] and lipid extraction from isolated platelets was performed with a standardized monophasic extraction protocol (2-propanol/water 90:10, v/v.). As described previously, internal standards (ILIS, final concentrations of 4% SPLASH Lipidomix [14 ILIS], 100 ng/mL arachidonic acid-d8, and 300 ng/mL C18 Ceramide-d7 [d18:1-18:0]) were added to the platelet pellets prior to extraction. Extracted lipids were further processed in three separate batches by a nontargeted, lipidome analysis using reversed-phase liquid chromatography coupled to mass spectrometry (UHPLC-ESI-QTOF-MS/MS). In both positive and negative ion modes, data-independent acquisition with stepwise window acquisition of MS/MS spectra (SWATH) was implemented.

MS-DIAL was used for data preprocessing including peak selecting, alignment, and identification (i.e. structural annotation of detected features) by matching experimental deconvoluted MS/MS spectra with those of the open-source LipidBlast database. Based on referential peak tables of each batch from MS-DIAL, an individual peak table was generated by an in-house developed batch alignment tool to combine lipidomic data from three batches to one data set. Using the reference peak table, batches were further analyzed with MultiQuant software (Sciex, Concord, Ontario, Canada) to extract peak intensities of all reference list features. Lipidomic data were normalized using the quality-control-based method of systematic error removal using random forest (SERRF) (Fiehn Lab, Davis, California, United States) and the ILIS-based method referred to as removal of unwanted variation random (RUVrandom) in RStudio (RStudio Inc., Boston, MA, United States). Further details of the data processing method and lipid identification are given in the **Supplementary Material** (available in the online version).

Normalized peak intensities were analyzed by one-way analysis of variance (ANOVA) using JMP to highlight peaks varying significantly ($p < 0.05$) between treatment groups. To account for the multiple hypothesis testing, a false discovery rate (FDR)-controlling procedure was further adopted to correct significance levels ($p < 0.05$) for FDR $\leq$5%. Therefore, sequential goodness of fit (SGoF) was implemented for testing of lipid peak intensities using Myriads (Free Software Foundation, Inc., Boston, Massachusetts, United States). For statistical comparisons, ratio of means between treatment groups was calculated for each lipid and statistical evaluation and graphic output were performed with different software packages including RStudio and JMP.

Statistical Analysis

Patients' baseline characteristics data were analyzed using JMP (SAS Institute, Cary, North Carolina, United States). Normally distributed data were analyzed using Student's *t*-test, and nonnormally distributed data were compared using the Mann–Whitney U-test. Mean values are presented as mean $\pm$ standard deviation. Discrete data were compared using Chi-square (Pearson). Orthogonal partial least square discriminant analysis (OPLS-DA) and principal component analysis (PCA) analysis were performed using RStudio. Multivariate analyses including OPLS-DA and PCA are suitable for large-scale omics data allowing visualization of group separation due to reduction of plotted dimensions.

Results

Characterization of the Platelet Lipidome in Statin-Treated Patients

Recently, we showed that significant changes of the platelet lipidome occur in patients with ACS compared to CCS and healthy matched controls.[15] In the present study, we analyzed the platelet lipidome in dependence of statin treatment by untargeted UHPLC-ESI-QTOF-MS/MS in a consecutive cohort of patients presenting with symptomatic CAD ($n = 105$). The baseline demographic characteristics of the patient cohort are given in ►**Table 1**.

Sixty eight percent of the enrolled patients were treated with HMG-CoA inhibitors and compared to statin-naïve patients at the time of blood collection. After clearance of nonverifiable signals, we could identify 928 lipids extracted from isolated platelets.

To evaluate the impact of statin treatment on the platelet lipidome, we compared mean concentrations of distinct lipids between patients with statin treatment and statin-naïve patients (►**Fig. 1**). We found that 41 lipids were significantly upregulated in statin-treated patients ($p < 0.05$, FDR < 5%), whereas 6 lipids were downregulated compared to statin-naïve patients ($p < 0.05$, FDR < 5%) (►**Fig. 1**).

Significantly upregulated lipids mostly composed of lipids belonging to the category of glycerolipids (►**Fig. 2**) (triglycerides [TGs]; $n = 35$; TG 14:0-15:0-16:0, TG 14:0-16:0-18:1, TG 15:0-16:0-18:2, TG 15:0-18:1-18:1, TG 16:0-18:0-20:4, TG 16:0-20:4-22:5, TG 16:0-20:4-22:6, TG 18:0-20:4-22:6, TG 45:1, TG 47:0, TG 47:1, TG 47:2, TG 48:1, TG 49:1, TG 50:2, TG 50:5, TG 51:1, TG 51:2, TG 51:3, TG 52:6(4), TG 53:2, TG 53:3(1), TG 53:3(2), TG 53:4(2), TG 54:6(3), TG 55:5, TG 56:4(2), TG 56:4(2), TG 56:5(4), TG 56:7(3), TG 56:8(2), TG 58:5

Table 1 Baseline characteristics of the CAD patients cohort

	All	Statin treatment	Statin naïve	*p*-Value
	(*n* = 105)	(*n* = 71; 67.6%)	(*n* = 34; 32.4%)	
Male, *n* (%)	77 (73)	54 (51.4)	23 (21.9)	0.362
Age, y (mean ± SD)	71.1 (± 10.7)	71.7 (± 10.6)	69.8 (± 11.1)	0.386
Body mass index (mean ± SD)	27 (± 4.4)	27.3 (± 4.3)	26.6 (± 4.7)	0.538
Cardiovascular risk factors				
Arterial hypertension, *n* (%)	85 (81)	59 (83.1)	26 (76.5)	0.418
Hyperlipidemia, *n* (%)	50 (47.6)	39 (54.9)	11 (32.3)	**0.030**
Diabetes mellitus, *n* (%)	29 (27.6)	24 (33.8)	5 (14.7)	**0.041**
Current smoking, *n* (%)	19 (18.1)	13 (18.3)	6 (17.6)	0.934
Ex smoking > 6 mo, *n* (%)	14 (13.3)	9 (12.6)	5 (14.7)	0.775
Obesity, *n* (%)	53 (50.5)	39 (54.9)	14 (41.2)	0.187
Atrial fibrillation, *n* (%)	24 (22.9)	16 (22.5)	8 (23.5)	0.910
Previous CABG, *n* (%)	11 (10.5)	10 (14.1)	1 (2.9)	0.081
Previous MI, *n* (%)	21 (20)	19 (26.8)	2 (5.9)	**0.012**
Renal function (GFR) (mean ± SD)	72.4 (± 29.4)	71.3 (± 23.9)	74.7 (± 38.9)	0.643
Medication on admission				
Statins, *n* (%)	71 (67.6)			
Acetylsalicylic acid, *n* (%)	88 (83.8)	62 (87.3)	26 (76.5)	0.158
Clopidogrel, *n* (%)	30 (28.6)	22 (31)	8 (23.5)	0.429
Ticagrelor, *n* (%)	36 (34.3)	28 (39.4)	8 (23.5)	0.108
Prasugrel, *n* (%)	6 (5.7)	3 (4.2)	3 (8.8)	0.342
Cangrelor, *n* (%)	1 (1)	0	1 (2.9)	0.147
Oral anticoagulants, *n* (%)	27 (25.7)	22 (31)	5 (14.7)	**0.074**
Angiotensin-converting enzyme inhibitors, *n* (%)	55 (52.4)	40 (56.3)	15 (44.1)	0.241
Angiotensin II receptor antagonists, *n* (%)	25 (23.8)	20 (28.2)	5 (14.7)	0.130
Aldosterone antagonists, *n* (%)	21 (20)	16 (22.5)	5 (14.7)	0.348
Ca channel antagonists, *n* (%)	30 (28.6)	23 (32.4)	7 (20.5)	0.210
β-blockers, *n* (%)	72 (68.6)	53 (74.6)	19 (55.9)	0.053
Diuretics, *n* (%)	41 (39)	35 (49.3)	6 (17.6)	**0.002**
Lipid profile parameters				
LDL-cholesterol (mg/dL) (mean ± SD)	96.5 (± 34.7)	89.4 (± 31.4)	111.2 (± 34.6)	**0.001**
HDL-cholesterol (mg/dL) (mean ± SD)	48.6 (± 17.6)	46.6 (± 15.8)	52.3 (± 18.4)	0.235
Triglycerides (mg/dL) (mean ± SD)	145.2 (± 85.1)	148.1 (± 76.3)	142.8 (± 102.7)	0.879
Total cholesterol (mg/mL) (mean ± SD)	161.3 (±45.9)	151.8 (± 43.1)	183.4 (± 38.3)	**0.002**
Platelets (mean ± SD)	235.8 (± 75.8)	213.4 (± 74.1)	254.6 (± 83.1)	0.104
Disease				
Chronic coronary syndrome, *n* (%)	60 (57.1)	43 (60.6)	17 (50)	**0.007**
Unstable angina, *n* (%)	19 (18.1)	16 (22.5)	3 (8.8)	0.088
NSTEMI, *n* (%)	22 (21)	12 (16.9)	10 (29.4)	0.141
STEMI, *n* (%)	4 (3.8)	0 (0)	4 (11.8)	**0.003**

Table 1 (*Continued*)

	All	Statin treatment	Statin naïve	*p*-Value
	(*n* = 105)	(*n* = 71; 67.6%)	(*n* = 34; 32.4%)	
Follow-up events				
Death, *n* (%)	6 (5.7)	4 (5.6)	2 (5.9)	0.959
Myocardial Infarction, *n* (%)	0	0	0	
Stroke, *n* (%)	0	0	0	

Abbreviations: CABG, coronary artery bypass graft; HDL, high-density lipoprotein; LDL, low-density lipoprotein; NSTEMI, non-ST-elevation myocardial infarction; SD, standard deviation; STEMI, ST-elevation myocardial infarction.
Note: Normally distributed data were analyzed using Student's *t*-test, nonnormally distributed data were computed using the Mann–Whitney U-test. Mean values are presented as mean, lower and upper 95% confidence intervals. Discrete data were calculated using Chi-square test (Pearson). All significant *p*-values ($p < 0.05$) of comparison between treatment groups were highlighted bold.

(2), TG 58:6(1), TG 60:11, TG 60:9(1)), sterol lipids (cholesteryl esters [CEs], $n = 4$; CE 20:4, CE 20:5, CE 22:4, CE 22:6), glycerophospholipids (phosphocholines [PCs], $n = 1$; PC 18:0-20:3(1)), and sphingolipids (sphingomyelin [SM], $n = 1$; SM d44:2(2)). It is striking that TGs with fatty acyl (FA) carbon number between 42 and 51 containing low number of double bonds (DB = 1–3) due to mostly monounsaturated fatty acid FA 18:1 (MUFA) or FA 18:2 were significantly upregulated in the statin group (►**Fig. 3A**). Further, CEs with polyunsaturated fatty acids (PUFA), which represents a pool for PUFA-phospholipids (PUFA-PL), were also significantly upregulated in the group of statin-treated patients. Moreover, palmitic acid (FA 16:0) is also amongst the upregulated lipids. In contrast, PUFA-PL levels were significantly decreased in statin-treated patients compared to naïve patients (►**Fig. 2**).

The group of downregulated lipids was primarily composed of PCs ($n = 4$; PC 16:0-18:3(1), 16:0-18:3(2), PC 18:2-18:2, PC 18:2-18:3D); phosphoethanolamines (PEs, $n = 1$; PE 36:4), and sphingolipids (ceramides [Cer], $n = 1$; Cer-NDS d18:0/24:0) (►**Fig. 2**). Interestingly, the MC-PCs (►**Fig. 5**), which were downregulated in patients with ACS, and statin treatment in this study were recently shown to be significantly increased in patients with ACS when compared to CCS or healthy controls. Further, these lipids promote platelet hyperreactivity and therefore might contribute to pathophysiology of ACS.[15] Further correlation analysis of significantly altered lipids in statin-treated patients reveals association with important platelet lipid species and clinical parameters (►**Supplementary Figs. S1**, **S5**, available in the online version).

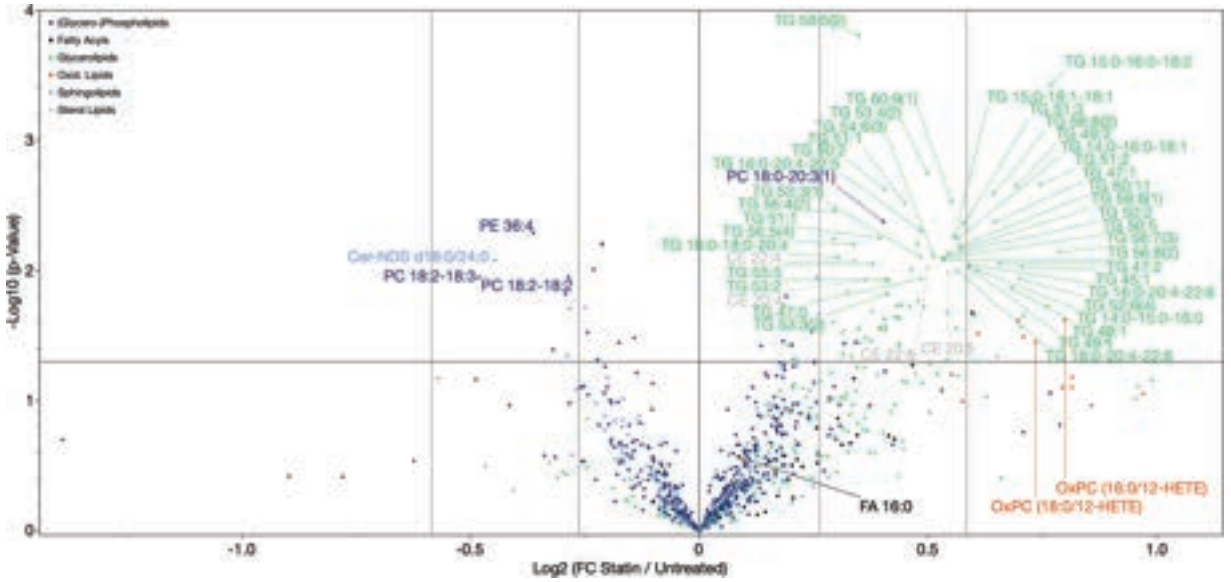

Fig. 1 The platelet lipidome is critically altered in CAD patients with statin treatment compared to statin-naïve patients. Volcano plot of all detected identified platelet lipids in this study (928). *X*-axis (fold change, FC) displays the base 2 logarithm of the concentration ratios (statin/naïve) (statin treatment: $n = 71$, naïve: $n = 34$). Values >1 indicating upregulation in statin treatment; <1 downregulation compared to statin-naïve patients. *Y*-axis showing negative log10-transformed *p*-values of ANOVA. Following multiple comparisons correction, significantly altered lipids (adjusted *p*-value: SGoF $p < 0.05$, FDR < 5%) are labelled and displayed in ►**Fig. 1**. Additionally, we highlighted two characteristic eoxPL (►**Supplementary Table S6**, appearing in the online version) and FA16:0. ANOVA, analysis of variance; CAD, coronary artery disease; eoxPL, enzymatically oxidized phospholipid; FDR, false discovery rate; SGoF, sequential goodness of fit.

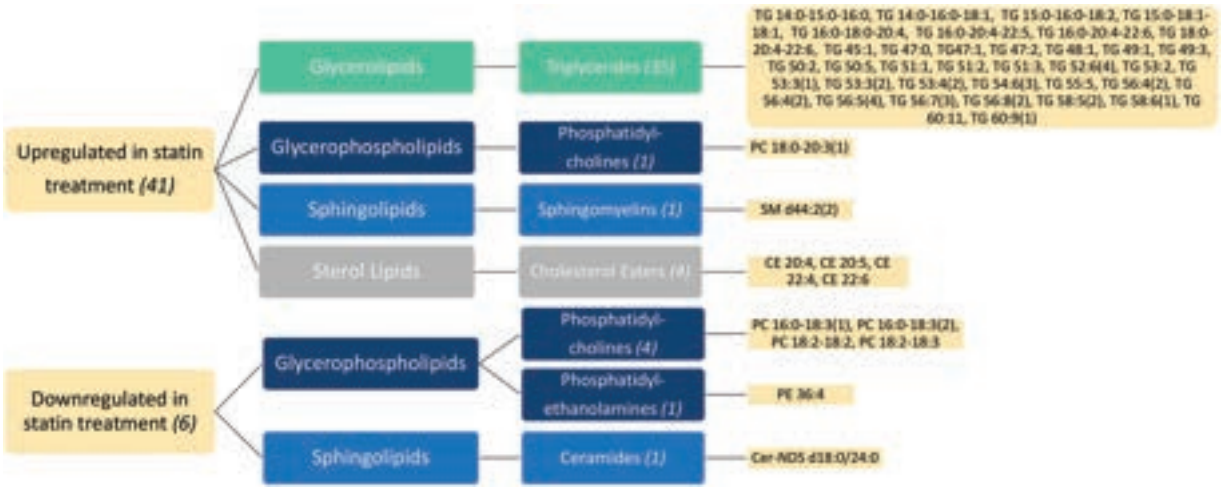

Fig. 2 Profiling the human platelet lipidome in the CAD patient cohort reveals heterogeneity of detected lipid families when comparing patients with statin treatment to those without. The platelet lipidome in this study consists of five lipid categories (fatty acyls, glycerophospholipids, glycerolipids, sphingolipids, and sterol lipids), which can be divided referring to main classes. Small beige brackets on the right summarize single lipids detected and identified in platelets of CAD patients ($n = 928$). Upregulated lipids in patients with statin treatment (upper chart) primarily consist of triglycerides. Downregulated lipids in statin-treated patients compared to statin-naïve patients mostly comprise MC-PCs, which were recently shown to be significantly increased in patients with ACS. ACS, acute coronary syndrome, CAD, coronary artery disease, MC-PC, medium-chain phosphatidylcholine.

Effect of Statin Treatment on the Platelet Lipidome in Patients with Acute Coronary Syndrome

To evaluate whether the influence of statin treatment on the platelet lipidome varies with the acuteness of the disease in CAD patients, we analyzed alterations in the platelet lipidome in the ACS subgroup of this study. Therefore, OPLS-DA analysis in the ACS subgroup was performed using all identified lipids specifying sub-cohorts for both statin-treated and statin-naïve patients.

The OPLS-DA analysis with respect of statin treatment using all identified lipids (►**Supplementary Fig. S2,** available in the online version) revealed a partial separation of samples due to statin treatment compared to statin-naïve patients. Likewise, in the ACS and CCS patient cohorts, a clear separation was observed when comparing statin-treated patients to statin-naïve patients (►**Fig. 4A, B**). Thus, especially in the subgroup of ACS patients, a separation in dependence of statin treatment is obtained, indicating an important effect of statin medication on the platelet lipidome in ACS. Here, especially TGs with carbon chain length between 49 and 55 with mainly MUFA and less PUFA side chain contribute to the separation (see VIP scores in ►**Supplementary Table S2,** available in the online version).

Further, the univariate statistics reveals that 21 lipids were significantly upregulated in patients with statin treatment in the ACS sub-cohort when compared to statin-naïve patients with ACS. Upregulated lipids, besides one PC, exclusively embody TGs (►**Supplementary Fig. S4,** available in the online version).

In contrast, among the downregulated lipids in statin-treated patients with ACS, primarily very long chain lyso-PCs (LPCs; 20:0, 22:0, and 24:0), PCs with very long chain fatty acyls (PC16:0-24:0 (PC40:0), PC 40:1, PC40:2, PC 20:0-20:3 corresponding to PC 40:3), various ether phospholipids, PUFA-PCs as well as two sphingolipids were found to be decreased in contrast to stain-naïve patients (►**Supplementary Fig. S4,** available in the online version). It means that these lipids were upregulated in statin-naïve patients which may alter the membrane fluidity. Further, changes of the above-described lipids may be a consequence of phospholipase PLA2 or peroxisomal activity. Thus, statin modulation of the platelet lipidome may have an impact on platelet integrity or platelet activity (see also ►**Supplementary Table S3,** available in the online version).

As a conclusion, it becomes evident that especially in patients with ACS, alterations in the platelet lipidome occur in patients with statin treatment when compared to statin-naïve patients.

Recently, we found that changes in the platelet lipidome in patients with ACS showed significantly increased levels of MC-PCs. Especially PC 18:0 was significantly upregulated in ACS patients compared to CCS patients and healthy controls.[15] PC 18:0 (10:0-8:0) further promoted enhanced platelet function and thrombus formation ex vivo.[15] To evaluate whether statin treatment may soften the platelet lipidomic phenotype, we determined characteristic changes in the platelet lipidome in ACS patients. Therefore, we had a closer look at the alterations of the lipid concentrations between both statin-treated and naïve patients in the ACS sub-cohort (►**Fig. 5**). Here, it was striking that medium-chain glycerophospholipids (PC 18:0 (10:0-8:0), PC 20:0 (PC 10:0-10:0), PC 24:0 (PC16:0-8:0), PC 30:4 (PC 10:0-20:4)) showed up as the most prominent downregulated lipids in statin-treated patients with ACS compared to statin-naïve patients. In our previous study, these lipids were found to be significantly upregulated in patients with ACS compared to CCS or healthy control, i.e., there was a correlation with disease severity. Thus, their downregulation in the statin

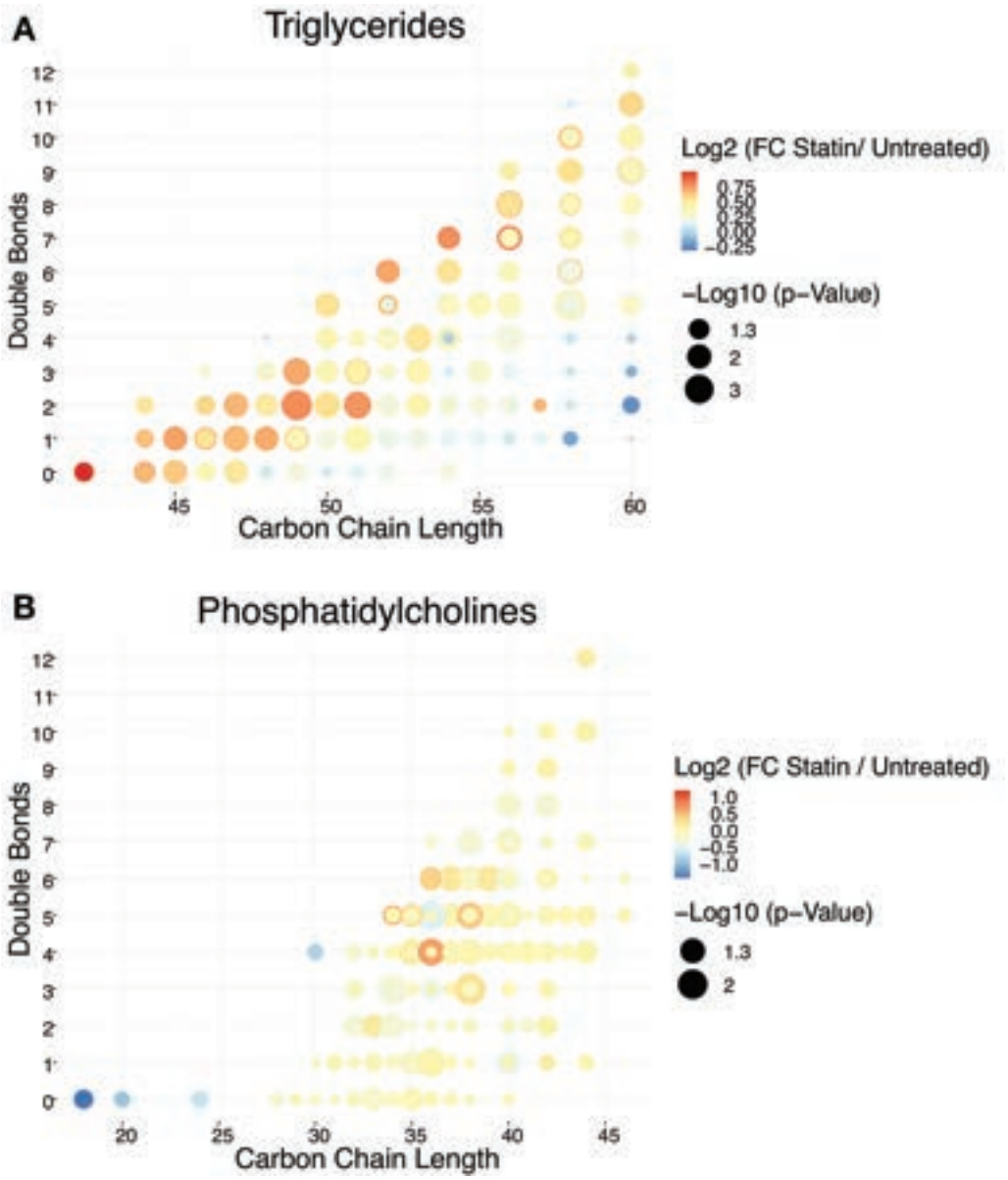

Fig. 3 Upregulation of triglycerides mainly with low fatty acyl carbon number (C < 51) and low double bond number (DB < 3) as well as downregulation of MC-PCs and PUFA-PCs is observed in CAD patients with statin treatment. Dot plot of identified lipids in $n = 105$ patients with symptomatic CAD. Each dot represents a unique lipid species. The *X*-axis represents fatty acyl carbon chain number and *Y*-axis the number of double bonds. Size is scaled by negative Log-transformed *p*-value of comparison between lipid levels in patients with statin treatment compared to naïve patients. Color continuously represents Log2 of fold change between treatment subgroups. (**A**) Triglycerides subsume most prominent lipid class of upregulated lipids in CAD patients with statin treatment compared to naïve patients. (**B**) MC-PCs (chain length between 12 and 24) and PUFA-PCs (more than one double bond) were significantly downregulated in the group of statin-treated patients compared to naïve patients. CAD, coronary artery disease, MC-PC, medium-chain phosphatidylcholine.

group might indicate that statin treatment may soften the platelet lipidome and shift the typically prothrombotic lipidomic phenotype in ACS patients toward a less reactive phenotype.

Effect of Statin Dose-Dependent Alterations on the Platelet Lipidome in Patients with Coronary Artery Disease

Increased levels of statin equivalent doses are linked with a high potency of lowering the plasma lipid profile in patients with CAD and, therefore, decreasing the risk of adverse cardiovascular events.[18–21] To elaborate whether the herein described regulations of the platelet lipidome in statin-treated patients show a dose-dependent effect, we performed correlation analysis of increasing atorvastatin doses (patient subgroups with 10, 20, 40, 80 mg) and platelet lipid concentrations.

Highlighting the lipid concentrations correlating significantly with increasing atorvastatin dose reveals downregulation of eight lipids composed of glycerophospholipids (PCs, $n = 5$; PC 16:0-18:3(1), PC 40:5, PC 38:7, PC 35:5e(3), PC 18:2-18:3); LPCs ($n = 1$; LPC 24:0), and sphingolipids (SM, $n = 2$; SM d30:0, SM d32:1) (►**Fig. 6**). In contrast, 17 lipids

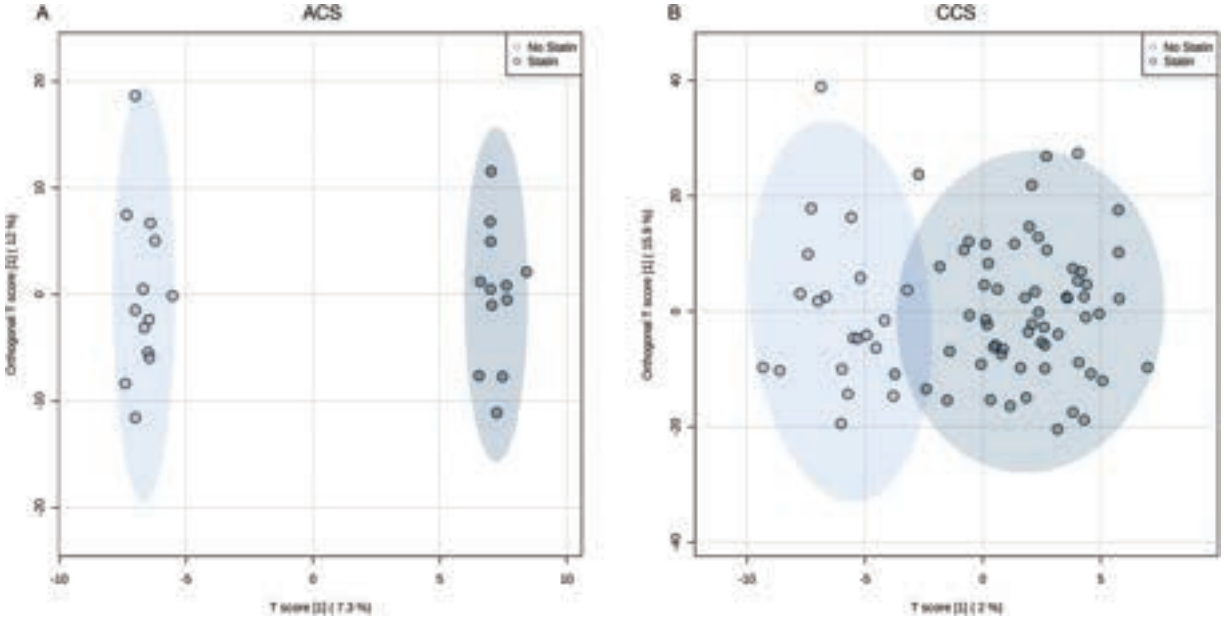

Fig. 4 The platelet lipidome is altered in patients with statin treatment and acute coronary syndrome. Orthogonal partial-least square (OPLS) analysis comprising all identified lipids of patients with statin treatment (dark blue) compared to statin-naïve patients (light blue). Data were based on normalized peak intensities of all identified lipids in this study and VIP scores are given in the ►**Supplementary Tables S4** and **S5** (available in the online version). Dots represent single study subjects and are colored by treatment classes. *X*- and *Y*-axes show the T score and the percentage of explained variance. (**A**) A high degree of between-group variance of patients with statin treatment compared to naïve patients in the ACS sub-cohort points out a major impact of statin treatment on the platelet lipidome in patients with ACS. (**B**) A lower degree of between-group variance of the treatment subgroups implements a minor influence of statin treatment on the platelet lipidome in patients with CCS. However, a clear segregation can be observed, likewise indicating a substantial influence on the lipidome of statin treatment in CCS patients. ACS, acute coronary syndrome; CCS, chronic coronary syndrome.

were significantly upregulated with increasing atorvastatin dose and mainly belonging to the category of glycerolipids (TGs, $n = 17$; TG 14:0-16:0-18:2, TG 14:0-16:0-18:2(1), TG 12:0-18:1-18:2, TG 50:2, TG 16:0-18:0-20:4, TG 53:3(2), TG 52:6(2), TG 50:4, TG 53:3(1), TG 50:3(2), TG 16:0-16:0-20:4, TG 46:2(2), TG 14:0-16:0-18:2, TG 51:3, TG 50:5, TG 49:3, TG 15:0-16:0-18:2) and one fatty acyl derivate (fatty acids [FA], $n = 1$; FA 16:0) (►**Fig. 6**). These findings strengthen the initially described regulations of the platelet lipidome in CAD patients with statin treatment compared to statin-naïve patients. In accordance with plasma levels of LDL, changes in the platelet lipidome seem to correlate with increasing statin equivalent doses.[22] Thus, downregulation primarily of glycerophospholipids with PUFA side chains and upregulation of TGs seem to increase with elevated statin dose (►**Fig. 6**).

Discussion

The major results of the present study are: (1) significant changes in the platelet lipidome occur in CAD patients with statin treatment compared to statin-naïve patients. (2) Upregulated lipids primarily belong to the category of TGs, CEs, and palmitic acid, and the identified downregulated lipids were found to be mostly glycerophospholipids. (3) The most prominent alterations in the platelet lipidome were observed in statin-treated patients with ACS and, furthermore, MC-PCs such as PC 18:0 as well as PUFA-PCs were downregulated in this group compared to statin-naïve patients. (4) A dose-dependent effect of statins highlights upregulation of TGs and downregulation of glycerophospholipids with increasing statin dose.

Our findings imply that statin treatment substantially alters the platelet lipidome in ACS patients. It is tempting to speculate that alteration of platelet lipidome in ACS patients is an important pleiotropic effect of statins which may lead to a better understanding of lowered cardiovascular risk due to statin treatment.

Enhanced platelet reactivity plays an important role in the acute and chronic course of CAD.[1,2,4] Recently, substantial changes of the platelet lipidome have been documented in CAD.[14,15] Changes of platelet lipids occur rapidly upon activation and are associated with enhanced platelet function.[17,23,24] The effect of statins on the platelet lipidome in patients with symptomatic CAD is hitherto unknown.

In our study, we provide evidence that upregulation of TGs, CEs, palmitic acid and downregulation of MC-PC and PUFA-PC levels in platelets of CAD patients with statin treatment may soften the platelet lipidome. Platelet activation is critically involved in the development of ACS and only recently, the platelet lipidome in a large CAD patient cohort has been comprehensively characterised.[14,15]

In the present study, we characterized the platelet lipidome in a cohort of patients with CAD and determined characteristic alterations of platelet lipids between statin-treated and statin-naïve patients by an untargeted lipidomics approach. We found that among 928 lipids, 41 lipids were significantly upregulated in statin-treated patients whereas 6 lipids were downregulated compared to statin-

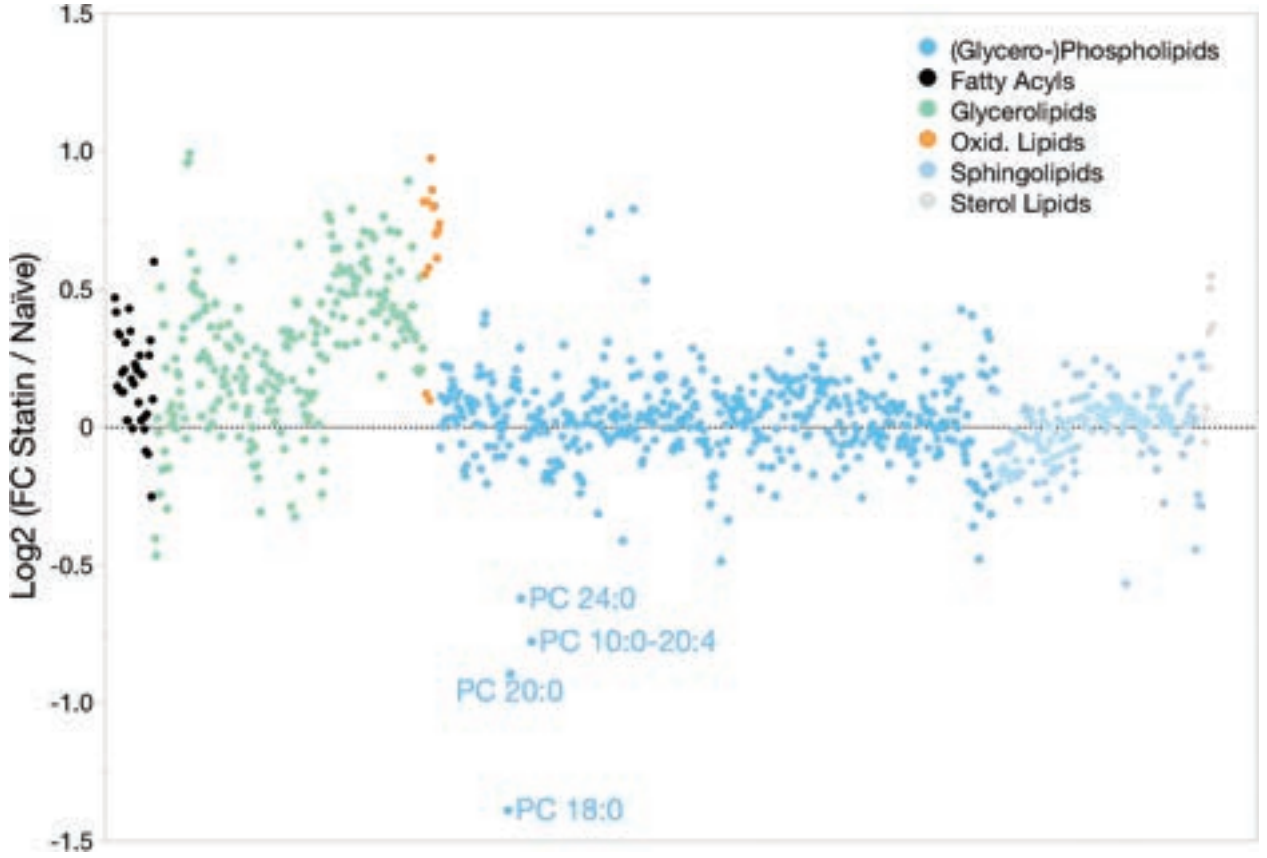

Fig. 5 Medium-chain glycerophospholipids were downregulated in patients with ACS and statin treatment compared to statin-naïve patients. The *Y*-axis displays Log2-transformed fold change of lipids varying between statin-treated ACS patients compared to statin-naïve patients. The *X*-axis lists lipids according to the referring lipid category and lipids are sorted by side-chain length. Among others, PC 18:0 (10:0-8:0) was significantly ($p < 0.05$) decreased in patients with statin medication. This lipid was recently found to be significantly upregulated in patients with ACS when compared to CCS or healthy subjects. Further, PC 18:0 was shown to critically enhance platelet ex vivo function. ACS, acute coronary syndrome; CCS, chronic coronary syndrome.

naïve patients. The upregulated lipids comprised primarily of glycerolipids (TGs). The majority of these TGs upregulated in the statin-treated group have fatty acyl side chains with low degree of unsaturation, due to 18:1 and 18:2 fatty acyl residues. These lipids serve as a pool for MUFA-PCs and 18:2-PCs, of which the former have positive impact on membrane fluidity and of which the latter can be metabolized to 13-HODE with inhibitory effects on thromboxane A_2 synthesis in human platelets.[25–27] Thus, upregulation of these TGs with low degree of unsaturation in the statin-treated patients may indicate effects on platelet function and hemostasis in patients with CAD. Likewise, CEs with PUFA fatty acid side chains and PC 18:0-20:3 concentrations were also significantly increased in statin-treated patients and may serve as a pool for PUFA-PLs. PUFA-PLs play an important role for platelet function.[28,29] They regulate membrane fluidity and integrity and are involved in regulation of thrombo-inflammatory processes.[30–32] PUFA-PLs with eicosatetraenoic acid (20:4) and docosatetraenoic acid (22:4) are proinflammatory and proferroptotic, while PUFA-PLs with eicosapentaenoic acid (20:5) and docosahexaenoic acid (22:6) side chains are sources for pro-resolving lipid mediators. The fact that such PUFAs are stored as PUFA-CEs may lead to the hypothesis that they are less required for remodeling into PUFA-PCs; it might indicate lower thrombo-inflammatory processes. Furthermore, upregulation of TGs and downregulation of glycerophospholipids were linked to a dose-dependent effect of atorvastatin treatment, especially when disease severity is higher. The MC-PCs (PC 18:0, PC 20:0, PC 24:0, PC 10:0-20:4) are a result of increased levels of medium-chain fatty acyl CoAs (resulting from mitochondrial or peroxisomal β-oxidation) which might accumulate due to inhibited mitochondrial MCAD enzyme activity (possibly due to hypoxic conditions; ►**Supplementary Fig. S7** [available in the online version]).[15] The levels of MC-PCs have been shown to correlate with disease severity (higher in ACS than CCS).[15] Statins reduced the MC-PC levels in ACS compared to stain-naïve ACS patients, which could be due to reduced β-oxidation delivering less medium-chain fatty acyl-CoAs. It is striking that TGs and CEs as well as FA 16:0, the product of fatty acid synthesis, are all elevated. The former (TGs and CEs) are usually stored as energy carriers and precursors of membrane lipids in lipid droplets under cellular conditions which require less energy. The increase in fatty acid due to statins has recently been reported for hepatocytes.[33] It seems possible that under the

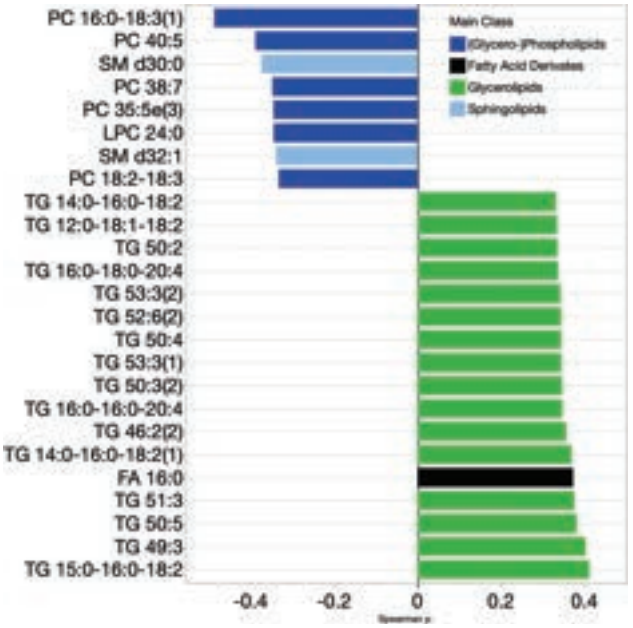

Fig. 6 Atorvastatin dose significantly correlates with alterations in the platelet lipidome of patients with CAD. Patients in this study were grouped according to atorvastatin dose on admission (10, 20, 40, 80mg) and atorvastatin dose was correlated with lipid concentrations of all detected lipids. Top 25 significant correlations ($p < 0.05$) of platelet lipids are displayed with their referring Spearman's ρ. Increasing atorvastatin doses are essentially associated with higher levels of triglycerides (TGs). A complete list of significant correlations is given in ►**Supplementary Fig. S3** (available in the online version).

given phenotype (platelets of statin-treated ACS patients), fatty acid synthesis is elevated (thus increased FA 16:0), consequently fatty acid oxidation reduced (therefore MC-PCs reduced), and synthesized fatty acids stored as TGs and CEs in lipid droplets (due to lower energy requirements).[34]

Thus, regulation of platelet lipidome is significantly altered by increasing statin dose and, thus, softening effects on the platelet lipidome might benefit from higher equivalent doses in CAD patients. Therefore, we hypothesize that in accordance with established cardiovascular risk factor dyslipidemia, adverse effects of critically altered platelet lipids (e.g. MC-PCs and others besides LDL) might be decreased by high-dose statin treatment.[35] Statin treatment is associated with altered platelet function and, thus, statins serve as an antithrombotic drug by inhibiting hemostasis including platelet aggregation in various diseases.[16,36–40] Further, prompt administration of statins is associated with reduction of early adverse cardiovascular events and therefore indicating acute pleiotropic effect of statins.[21,41,42] In our study cohort, we displayed that the impact of co-medication (antiplatelet treatment, oral anticoagulation, β-blockers) and cardiovascular risk factors respectively (diabetes mellitus, arterial hypertension, dyslipidemia, obesity, and smoking status) on the described changes of the platelet lipidome in statin-treated patients is minor (►**Supplementary Fig. S6**, available in the online version).

Only recently, medium-chain glycerophospholipids, such as PC 18:0 (10:0-8:0), were found to be significantly upregulated in ACS patients compared to CCS patients or healthy controls. Moreover, MC-PCs like PC 18:0 promoted platelet hyperreactivity and, thus, might contribute to the pathophysiology of ACS.[15] In the present study, downregulated lipids in patients with statin treatment primarily composed of glycerophospholipids. Especially in the sub-cohort of ACS patients, characteristic medium-chain glycerophospholipids, such as PC 18:0, were downregulated in statin-treated patients. Hence, this indicates that statin treatment in patients with CAD and ACS might partly revert critical upregulation of MC-PC concentrations and thus might decrease platelet hyperreactivity and stop disease progression in ACS patients. Recently, changes in the platelet lipidome have been described to correlate with platelet reactivity in COVID-19.[43] At present, the results of our study imply that statin therapy is associated with an alteration of the platelet lipidome. Although we cannot provide concomitant platelet function data, it is tempting to speculate that statin-dependent changes of the platelet lipidome is a pleiotropic effect of antilipid therapy that has consequences for platelet function in vivo and thus may contribute to the beneficial effect of statins in the course of ACS.

What is known about this topic?

- Acute coronary syndrome is associated with platelet hyperreactivity.
- Substantial changes in the platelet lipidome occur in patients with ACS.
- Changes in the platelet lipidome are linked to enhanced platelet function.
- The effect of statins on the platelet lipidome in patients with CAD is hitherto unknown.

What does this paper add?

- The platelet lipidome is significantly altered in CAD patients with statin treatment compared to statin-naïve patients.
- Significantly increased levels of TGs and downregulation of MC-PCs were shown in patients with symptomatic CAD and statin treatment.
- Most prominent effects of statin treatment on the platelet lipidome, especially on MC-PC such as PC 18:0, were observed in patients with ACS.
- Crucial alterations of the lipid classes TGs and PUFA-PCs correlate positively and negatively with atorvastatin dose, respectively.

Data Availability Statement

The data that support the findings of this study are available on reasonable request from the corresponding author.

Funding

This project was supported in part by the German Research Foundation (DFG) KFO-274 and TRR 240.

Conflict of interest
None declared.

Acknowledgement
We thankfully acknowledge the work of Lydia Laptev for assisting us to process the platelet samples for further analysis.

References

1 Droppa M, Tschernow D, Müller KAL, et al. Evaluation of clinical risk factors to predict high on-treatment platelet reactivity and outcome in patients with stable coronary artery disease (PREDICT-STABLE). PLoS One 2015;10(03):e0121620
2 Geisler T, Zürn C, Simonenko R, et al. Early but not late stent thrombosis is influenced by residual platelet aggregation in patients undergoing coronary interventions. Eur Heart J 2010; 31(01):59–66
3 Geisler T, Langer H, Wydymus M, et al. Low response to clopidogrel is associated with cardiovascular outcome after coronary stent implantation. Eur Heart J 2006;27(20):2420–2425
4 Gawaz M. Does uncontrolled platelet activation promote coronary artery disease? JACC Cardiovasc Imaging 2016;9(07): 855–857
5 Gawaz M, Langer H, May AE. Platelets in inflammation and atherogenesis. J Clin Invest 2005;115(12):3378–3384
6 Bentzon JF, Otsuka F, Virmani R, Falk E. Mechanisms of plaque formation and rupture. Circ Res 2014;114(12):1852–1866
7 Arroyo LH, Lee RT. Mechanisms of plaque rupture: mechanical and biologic interactions. Cardiovasc Res 1999;41(02):369–375
8 Collet J-P, Thiele H, Barbato E, et al; ESC Scientific Document Group. 2020 ESC guidelines for the management of acute coronary syndromes in patients presenting without persistent ST-segment elevation. Eur Heart J 2021;42(14):1289–1367
9 Ibanez B, James S, Agewall S, et al; ESC Scientific Document Group. 2017 ESC Guidelines for the management of acute myocardial infarction in patients presenting with ST-segment elevation: the Task Force for the management of acute myocardial infarction in patients presenting with ST-segment elevation of the European Society of Cardiology (ESC). Eur Heart J 2018;39(02):119–177
10 Reny JL, Fontana P, Hochholzer W, et al. Vascular risk levels affect the predictive value of platelet reactivity for the occurrence of MACE in patients on clopidogrel. Systematic review and meta-analysis of individual patient data. Thromb Haemost 2016;115 (04):844–855
11 Stellos K, Sauter R, Fahrleitner M, et al. Binding of oxidized low-density lipoprotein on circulating platelets is increased in patients with acute coronary syndromes and induces platelet adhesion to vascular wall in vivo–brief report. Arterioscler Thromb Vasc Biol 2012;32(08):2017–2020
12 May AE, Geisler T, Gawaz M. Individualized antithrombotic therapy in high risk patients after coronary stenting. A double-edged sword between thrombosis and bleeding. Thromb Haemost 2008;99(03):487–493
13 Vinik AI, Erbas T, Park TS, Nolan R, Pittenger GL. Platelet dysfunction in type 2 diabetes. Diabetes Care 2001;24(08):1476–1485
14 Chatterjee M, Rath D, Schlotterbeck J, et al. Regulation of oxidized platelet lipidome: implications for coronary artery disease. Eur Heart J 2017;38(25):1993–2005
15 Harm T, Bild A, Dittrich K, et al. Acute coronary syndrome is associated with a substantial change in the platelet lipidome. Cardiovasc Res 2022;118(08):1904–1916
16 Nenna A, Nappi F, Lusini M, et al. Effect of statins on platelet activation and function: from molecular pathways to clinical effects. BioMed Res Int 2021;2021:6661847
17 Peng B, Geue S, Coman C, et al. Identification of key lipids critical for platelet activation by comprehensive analysis of the platelet lipidome. Blood 2018;132(05):e1–e12
18 Sposito AC, Chapman MJ. Statin therapy in acute coronary syndromes: mechanistic insight into clinical benefit. Arterioscler Thromb Vasc Biol 2002;22(10):1524–1534
19 Lopes RD, de Barros E Silva PGM, Damiani LP, et al. Major adverse cardiovascular events after 12 months among patients with acute coronary syndrome receiving loading doses of atorvastatin prior to planned PCI. JAMA 2020;323(08):787–789
20 Øvrehus KA, Diederichsen A, Grove EL, et al. Reduction of myocardial infarction and all-cause mortality associated to statins in patients without obstructive CAD. JACC Cardiovasc Imaging 2021; 14(12):2400–2410
21 Hulten E, Jackson JL, Douglas K, George S, Villines TC. The effect of early, intensive statin therapy on acute coronary syndrome: a meta-analysis of randomized controlled trials. Arch Intern Med 2006;166(17):1814–1821
22 Mihaylova B, Emberson J, Blackwell L, et al; Cholesterol Treatment Trialists' (CTT) Collaborators. The effects of lowering LDL cholesterol with statin therapy in people at low risk of vascular disease: meta-analysis of individual data from 27 randomised trials. Lancet 2012;380(9841):581–590
23 Slatter DA, Aldrovandi M, O'Connor A, et al. Mapping the human platelet lipidome reveals cytosolic phospholipase A2 as a regulator of mitochondrial bioenergetics during activation. Cell Metab 2016;23(05):930–944
24 O'Donnell VB, Murphy RC, Watson SP. Platelet lipidomics: modern day perspective on lipid discovery and characterization in platelets. Circ Res 2014;114(07):1185–1203
25 Magtanong L, Ko PJ, To M, et al. Exogenous monounsaturated fatty acids promote a ferroptosis-resistant cell state. Cell Chem Biol 2019;26(03):420.e9–432.e9
26 Li D, Li Y. The interaction between ferroptosis and lipid metabolism in cancer. Signal Transduct Target Ther 2020;5(01):108
27 Yamaja Setty BN, Berger M, Stuart MJ. 13-Hydroxyoctadeca-9,11-dienoic acid (13-HODE) inhibits thromboxane A2 synthesis, and stimulates 12-HETE production in human platelets. Biochem Biophys Res Commun 1987;148(02):528–533
28 McEwen BJ, Morel-Kopp MC, Chen W, Tofler GH, Ward CM. Effects of omega-3 polyunsaturated fatty acids on platelet function in healthy subjects and subjects with cardiovascular disease. Semin Thromb Hemost 2013;39(01):25–32
29 Lagarde M, Guichardant M, Bernoud-Hubac N, Calzada C, Véricel E. Oxygenation of polyunsaturated fatty acids and oxidative stress within blood platelets. Biochim Biophys Acta Mol Cell Biol Lipids 2018;1863(06):651–656
30 Shaikh SR, Edidin M. Polyunsaturated fatty acids and membrane organization: elucidating mechanisms to balance immunotherapy and susceptibility to infection. Chem Phys Lipids 2008;153 (01):24–33
31 Harayama T, Riezman H. Understanding the diversity of membrane lipid composition. Nat Rev Mol Cell Biol 2018;19(05): 281–296
32 Lu J, Jilling T, Li D, Caplan MS. Polyunsaturated fatty acid supplementation alters proinflammatory gene expression and reduces the incidence of necrotizing enterocolitis in a neonatal rat model. Pediatr Res 2007;61(04):427–432
33 Galicia-Garcia U, Jebari S, Larrea-Sebal A, et al. Statin treatment-induced development of type 2 diabetes: from clinical evidence to mechanistic insights. Int J Mol Sci 2020;21(13):4725
34 Olzmann JA, Carvalho P. Dynamics and functions of lipid droplets. Nat Rev Mol Cell Biol 2019;20(03):137–155
35 Cannon CP, Braunwald E, McCabe CH, et al; Pravastatin or Atorvastatin Evaluation and Infection Therapy-Thrombolysis in Myocardial Infarction 22 Investigators. Intensive versus moderate

lipid lowering with statins after acute coronary syndromes. N Engl J Med 2004;350(15):1495–1504
36 Violi F, Calvieri C, Ferro D, Pignatelli P. Statins as antithrombotic drugs. Circulation 2013;127(02):251–257
37 Sikora J, Kostka B, Marczyk I, Krajewska U, Chałubiński M, Broncel M. Effect of statins on platelet function in patients with hyperlipidemia. Arch Med Sci 2013;9(04):622–628
38 Pignatelli P, Sanguigni V, Lenti L, et al. Oxidative stress-mediated platelet CD40 ligand upregulation in patients with hypercholesterolemia: effect of atorvastatin. J Thromb Haemost 2007;5(06): 1170–1178
39 Blann AD, Gurney D, Hughes E, Buggins P, Silverman SH, Lip GYH. Influence of pravastatin on lipoproteins, and on endothelial, platelet, and inflammatory markers in subjects with peripheral artery disease. Am J Cardiol 2001;88(01):A7–A8, 89–92
40 Serebruany VL, Miller M, Pokov AN, et al. Effect of statins on platelet PAR-1 thrombin receptor in patients with the metabolic syndrome (from the PAR-1 inhibition by statins [PARIS] study). Am J Cardiol 2006;97(09):1332–1336
41 Patti G, Pasceri V, Colonna G, et al. Atorvastatin pretreatment improves outcomes in patients with acute coronary syndromes undergoing early percutaneous coronary intervention: results of the ARMYDA-ACS randomized trial. J Am Coll Cardiol 2007;49 (12):1272–1278
42 Cortellaro M, Cofrancesco E, Arbustini E, et al. Atorvastatin and thrombogenicity of the carotid atherosclerotic plaque: the ATROCAP study. Thromb Haemost 2002;88(01):41–47
43 Schuurman AR, Léopold V, Pereverzeva L, et al. The platelet lipidome is altered in patients with COVID-19 and correlates with platelet reactivity. Thromb Haemost 2022;122(10):1683–1692

Supplementary Methods

Study Design

Patients were consecutively recruited into the study during a 6-month period at the University Hospital of Tübingen and a follow-up period over 12 months was chosen. All patients were treated for symptomatic coronary artery disease (CAD) and the severity of the disease was analyzed by coronary angiography within 24 hours after hospital admission. Thus, we included adult patients with symptomatic CAD, whereas patients without CAD were excluded from this study. In total, 8.6% of patients did not receive percutaneous coronary intervention and were treated conventionally, but all patients were diagnosed with symptomatic CAD during coronary angiography (at least one hemodynamic relevant >50% lumen narrowing coronary artery stenosis.) Patients receiving statin treatment within 4 weeks prior to hospital admission were included in the statin-treatment subgroup, whereas patients with no history of statin medication or paused statin treatment over 4 weeks prior to admission were considered statin-naïve.

Platelet Lipidomic Methods and Data Processing

RP-UHPLC-ESI-QTOF-MS/MS Experiment

As described recently, washed platelets were isolated from peripheral blood.[1] Citrated whole blood was centrifuged at 430 × g for 20 minutes and platelet-rich plasma (PRP) was diluted with Tyrodes-HEPES buffer (HEPES 2.5 mM; NaCl 150 mM; KCl 1 mM; $NaHCO_3$ 2.5 mM; NaH_2PO_4 0.36 mM; glucose 5.5 mM; BSA 1 mg/mL; pH 6.5). PRP/Tyrodes was further centrifuged at 900 × g for 10 minutes to sediment platelets. Platelets were washed and resuspended in Tyrodes-HEPES buffer (pH 7.4; supplemented with $CaCl_2$ 1 mM; $MgCl_2$ 1 mM) used for further lipidomics analysis. Extracted platelet lipid samples were analyzed on an Agilent 1290 series UHPLC instrument (Agilent, Waldbronn, Germany) coupled to a Sciex TripleTOF 5600+ mass spectrometer with DuoSpray ion source (Sciex, Concord, Ontario, Canada) as described recently.[2] Samples were stored at 4°C using HTC-xt autosampler from CTC (CTC Analytics, Zwingen, Switzerland) during measurement and sample injection (3 µL in positive mode, 5 µL in negative mode).

Chromatographic conditions and mass spectrometry (MS) parameters were adopted as described previously.[2,3] Reversed-phase chromatography was performed utilizing Acquity UPLC CSH C18 (130Å, 1.7 µm, 2.1 mm × 100 mm) column equipped with an Acquity UPLC CSH C18 VanGuard pre-column (130Å, 1.7 µm, 2.1 mm × 5 mm) (Waters, Eschborn, Germany) at 65°C. For further processing, two mobile phases, (A) 60:40 ACN:H_2O (v/v) and (B) 90:9:1 (v/v) IPA:ACN:H_2O (B) both with 10 mM ammonium formate and 0.1% formic acid were used for a gradient elution with 0.0 min 15% B, 2.0 min 30% B, 2.5 min 48% B, 11.0 min 82% B, 11.5 min 99% B, 12.0 min 99% B, 12.1 min 15% B, and 15.0 min 15% B for re-equilibration at 0.6 mL/min flow.

MS curtain gas was set to 35 psi, nebulizer gas to 60 psi, and drying gas to 60 psi. Ion source temperature was 350°C in positive mode, ion-spray voltage floating was +5,500 V, collision energy was 45 V (15 V spread), and declustering potential was 80 V. The mass range was m/z 50–1,250. In negative mode, ion-spray voltage floating was −4,500 V, collision energy was −45 V (15 V spread), de-clustering potential was −80 V, and the mass range m/z 50–1,050.

For MS data analysis a data-independent acquisition (DIA) approach was used with sequential window acquisition of all theoretical fragment ion spectra (SWATH). Thus, after a TOF precursor full scan experiment, 20 SWATH MS/MS experiments with variable Q1 width covering the entire mass range were performed (►**Supplementary Table S1**).

Supplementary Table S1 List of MS and MS/MS experiments within a cycle

Experiment	Positive mode			Negative mode		
	Low border [*m*/*z*]	Upper border [*m*/*z*]	CE [V]	Low border [*m*/*z*]	Upper border [*m*/*z*]	CE [V]
TOF	50	1250	10	50	1050	−10
1	50	217.6	45	50	213.5	−45
2	216.6	340.3	45	212.5	271.4	−45
3	339.3	441.4	45	270.4	314.6	−45
4	440.4	524.9	45	313.6	382.6	−45
5	523.9	571.6	45	381.6	427.5	−45
6	570.6	643.4	45	426.5	464.3	−45
7	642.4	687.3	45	463.3	501	−45
8	686.3	720.1	45	500	540.8	−45
9	719.1	740.1	45	539.8	617.5	−45
10	739.1	755	45	616.5	680.3	−45
11	754	764.1	45	679.3	697.1	−45
12	763.1	775.1	45	696.1	724	−45
13	774.1	786.1	45	723	749	−45
14	785.1	793.1	45	748	775.6	−45
15	792.1	806.1	45	774.6	793.1	−45
16	805.1	814.2	45	792.1	811	−45
17	813.2	829.6	45	810	832.6	−45
18	828.6	842.7	45	831.6	854.1	−45
19	841.7	903.3	45	853.1	861.2	−45
20	902.3	1,250	45	860.2	1050	−45

Abbreviations: CE, cholesteryl ester; MS, mass spectrometry.

Data Processing

Due to the large number of samples, lipidomics data were acquired in three separate processing batches. LC-MS data were processed batch-wise using open-source software MS-DIAL.[3] MS-DIAL performs data preprocessing with peak finding, intra-batch alignment, deisotoping, adduct assignment, and lipid annotation by matching experimental deconvoluted MS/MS spectra with in silico reference spectra LipidBlast database. Lipid annotations were curated manually to prevent misannotated lipids in further data analysis. Since the three batches could not be processed all in once, batch-wise processing in MS-DIAL revealed individual feature lists for each batch. Therefore, an in-house inter-batch feature alignment tool was developed in Visual Basic for Applications (VBA) implemented in Excel to merge three feature lists into one. The feature lists from the three respective batches were subjected to the VBA tool including PeakIDs, feature names, accurate mass, adjusted retention time, and peak intensities for quality control (QC) samples. QC samples originated from the same lipid extract and were injected regularly after every fifth sample over the analytical sequence to assess analytical performance intra- and inter-batch. The batch-specific retention time was adjusted to mean retention time over the three batches by linear correlation determined on a subset of features (internal standards and manually aligned features with approximately 2 features per min). Based on accurate mass and retention time similarity, inter-batch alignment was performed, and alignment performance was assessed by mass accuracy between aligned features and peak intensities in QC samples. Consequently, a representative reference feature list was obtained, including all features being detected in at least one batch, but features found in more than one batch were kept as a single entry to avoid redundancies. Based on the reference feature list (one list for positive and negative ionization mode, respectively), data were extracted as peak intensities in a targeted approach using Sciex software MultiQuant (Sciex, Concord, Ontario, Canada).

Data normalization was performed by application of two strategies to remove unwanted technical variation which were selected due to best performance assessed in a prior

evaluation of several normalization methods. First, systematic error removal using random forest (SERRF) was applied which aims to remove unwanted technical errors for each feature based on feature intensities in regularly injected QC-samples using a random forest algorithm.[4] Second, an internal standard based approach was applied on the SERRF-normalized data. Removal of unwanted variation random (RUVrandom)[5] was used. Data normalization was performed in RStudio (R version 3.5.2 with NormalizeMets package7 for RUVrandom, R script from Fan et al[4] for SERRF) and normalized data were further subjected to statistical analysis.

Supplementary Table S2 VIP-scores of OPLS-DA comparison between statin-treated in patients with ACS and CCS, respectively

Lipid	VIP-score	Lipid	VIP-score
	OPLS-DA		OPLS-DA
TG 51:1	2.83	TG 58:1	1.83
TG 15:0-18:1-18:1	2.50	TG 56:5(2)	1.82
TG 49:1	2.43	LPC 22:0	1.82
TG 53:2	2.40	TG 48:1	1.81
TG 56:4(2)	2.35	LPC 24:0	1.81
TG 51:3	2.27	Cer-NDS d18:0/26:1	1.79
TG 16:0-18:0-20:4	2.25	PC 16:0-24:1	1.78
TG 14:0-16:0-18:1	2.14	PC 16:0-24:0	1.77
TG 53:3(2)	2.13	SM d36:2	1.75
PC 17:0-20:4(2)	2.08	TG 49:0	1.74
TG 50:1	2.05	PC 38:4e	1.74
PC 17:0-20:4(1)	2.04	PE 20:0-18:1	1.74
PC 15:0-20:4	2.04	TG 14:0-15:0-16:0	1.73
TG 52:1	2.02	PC 18:1-22:1	1.73
Cer-NDS d18:0/24:1	1.99	FA 16:0	1.71
TG 16:0-16:0-20:2	1.96	LPC 15:0	1.70
TG 16:0-16:0-20:4	1.93	TG 45:1	1.69
TG 56:5(4)	1.90	SM d19:0/20:1	1.69
TG 50:3(2)	1.86	TG 50:5	1.68
TG 14:0-16:0-18:2	1.84	Cer-NDS d18:0/24:0	1.68
PC 18:2-20:5(1)	1.83	PE 18:0-18:2	1.66
PC 37:4e	1.82	PC 16:0-18:3(1)	1.65
PC 18:0-20:4	1.78	SM d35:2	1.65
TG 52:3(2)	1.72	TG 47:2	1.65
PC 18:1-20:1	1.68	TG 46:1(1)	1.65
TG 46:1(2)	1.68	PC 34:2e	1.64
PE 18:1-18:2	1.51	PC 20:4-22:4	1.64
TG 15:0-16:0-18:2	2.65	TG 46:0	1.63
TG 51:2	2.49	SM d36:1	1.63
TG 55:5	2.46	PC 20:0-18:1	1.62
PC 21:1-21:1	2.43	SM d37:2	1.62
PC 40:1	2.30	SM d39:1	1.62
TG 53:4(2)	2.22	TG 56:6(2)	1.61
CE 20:4	2.20	TG 55:2(2)	1.59
TG 50:4	2.19	PC 16:0-20:4(2)	1.59
TG 53:1	2.11	PI 18:1-20:4	1.58

(*Continued*)

Supplementary Table S2 (*Continued*)

Lipid	VIP-score	Lipid	VIP-score
	OPLS-DA		OPLS-DA
TG 49:3	2.08	PE 38:7	1.57
TG 55:2(1)	2.07	LPC 22:1	1.57
PC 18:2-18:3	2.03	PE 18:1e/20:5	1.57
TG 53:3(1)	2.02	TG 52:6(2)	1.55
PE 18:2e/20:5	2.02	PC 18:0e/20:4	1.55
TG 47:1	1.97	Cer-NP t18:0/24:1	1.55
PE 18:1-20:1	1.93	TG 53:4(1)	1.54
TG 16:0-18:0-22:4	1.92	PC 41:2	1.53
PC 38:7	1.92	PC 22:1-22:6	1.53
TG 55:3(1)	1.89	PC 20:5-20:5	1.52
CE 22:4	1.88	SM d38:1	1.52
TG 60:1	1.88	PC 22:1-20:4	1.51
TG 47:0	1.86	PC 34:3e	1.51
PC 40:2	1.84	PE 18:1-22:6	1.51

Abbreviations: ACS, acute coronary syndrome; CCS, chronic coronary syndrome.

Supplementary Table S3 Comparison of altered platelet lipids in patients with statin treatment compared to naïve patients in the overall cohort and the ACS sub-cohort, respectively

Upregulated lipids in statin-treated patients with ACS	Downregulated lipids in statin-treated patients with ACS	Upregulated lipids in statin-treated patients with ACS/CCS	Downregulated lipids in statin-treated patients with ACS/CCS
PC 16:0-22:4	HexCer-NS d18:1/24:0	CE 20:4	Cer-NDS d18:0/24:0
TG 14:0-15:0-16:0	LPC 20:0/0:0	CE 20:5	PC 16:0-18:3(1)
TG 49:1	LPC 22:0	CE 22:4	PC 16:0-18:3(2)
TG 15:0-16:0-18:2	LPC 24:0	CE 22:6	PC 18:2-18:2
TG 50:1	LPE 20:0	PC 18:0-20:3(1)	PC 18:2-18:3
TG 50:2	PC 16:0-20:4(1)	SM d44:2(2)	PE 36:4
TG 51:1	PC 16:0-24:0	TG 14:0-15:0-16:0	
TG 15:0-18:1-18:1	PC 18:2-20:5(2)	TG 14:0-16:0-18:1	
TG 51:2	PC 20:0-20:3	TG 15:0-16:0-18:2	
TG 52:1	PC 34:3e	TG 15:0-18:1-18:1	
TG 16:0-16:0-20:2	PC 35:5e(3)	TG 16:0-18:0-20:4	
TG 53:1	PC 37:0e	TG 16:0-20:4-22:5	
TG 53:2	PC 38:0e	TG 16:0-20:4-22:6	
TG 53:3(1)	PC 38:7	TG 18:0-20:4-22:6	
TG 53:3(2)	PC 40:0e	TG 45:1	
TG 54:2	PC 40:1	TG 47:0	
TG 55:2(1)	PC 40:1e	TG 47:1	
TG 55:2(2)	PC 41:2	TG 47:2	
TG 55:3(2)	PC 42:4	TG 48:1	
TG 16:0-18:0-22:4	PC 44:4e(1)	TG 49:1	
TG 58:5(2)	PE 16:1e/18:2	TG 49:3	

Supplementary Table S3 (*Continued*)

Upregulated lipids in statin-treated patients with ACS	Downregulated lipids in statin-treated patients with ACS	Upregulated lipids in statin-treated patients with ACS/CCS	Downregulated lipids in statin-treated patients with ACS/CCS
	PE 16:1e/20:3	TG 50:2	
	PE 18:2e/20:4	TG 50:5	
	PE 18:2e/20:5	TG 51:1	
	PI 18:0-20:4	TG 51:2	
	PI 39:4	TG 51:3	
	SM d46:2	TG 52:6(4)	
		TG 53:2	
		TG 53:3(1)	
		TG 53:3(2)	
		TG 53:4(2)	
		TG 54:6(3)	
		TG 55:5	
		TG 56:4(2)	
		TG 56:5(4)	
		TG 56:7(3)	
		TG 56:8(2)	
		TG 58:5(2)	
		TG 58:6(1)	
		TG 60:11	
		TG 60:9(1)	

Abbreviations: ACS, acute coronary syndrome; CCS, chronic coronary syndrome.
Note: Eleven lipids were found to be upregulated in statin-treated patients with ACS as well as in the overall cohort and account for 23% overlap.

Supplementary Table S4 VIP-scores of OPLS-DA subgroup analysis between statin-treated and naïve patients with ACS

Lipid	VIP-score	Lipid	VIP-score
	OPLS-DA		OPLS-DA
TG 51:1	2.50	PC 15:0-22:6	1.79
TG 53:2	2.30	PE 34:2e	1.79
TG 15:0-18:1-18:1	2.29	TG 54:5(2)	1.79
TG 50:1	2.29	PC 22:6-22:6(2)	1.78
TG 49:1	2.25	TG 47:1	1.78
TG 52:1	2.23	LPC 20:0/0:0	1.77
TG 16:0-16:0-20:2	2.17	SM d17:0/19:0	1.77
TG 51:3	2.04	LPE 20:0	1.76
TG 46:1(2)	1.85	PC 17:0-22:6	1.76
PC 16:1-18:2	1.83	PE 38:6e(1)	1.75
TG 42:0(2)	1.69	TG 14:0-16:0-18:0	1.74
TG 52:3(2)	1.69	PE 38:7e	1.74
TG 16:0-18:0-20:4	1.62	TG 46:0	1.72
TG 50:3(2)	1.61	TG 46:1(1)	1.71
TG 16:0-17:0-18:0	2.35	TG 53:3(2)	1.69
TG 16:0-18:0-22:4	2.33	TG 44:0	1.69

(*Continued*)

Supplementary Table S4 (*Continued*)

Lipid	VIP-score	Lipid	VIP-score
	OPLS-DA		OPLS-DA
TG 55:2(1)	2.31	TG 46:3	1.69
TG 49:0	2.29	TG 18:0-18:1-18:2	1.69
TG 55:1	2.27	TG 54:1	1.69
TG 53:1	2.25	PC 20:4-20:5	1.68
TG 55:3(1)	2.24	PC 18:2-18:2	1.68
PE 18:2-18:2	2.19	PE 38:3	1.66
TG 52:6(1)	2.17	LPC 20:4/0:0	1.65
TG 51:2	2.16	PC 37:0	1.65
PC 38:3e	2.15	TG 45:1	1.64
TG 58:5(3)	2.12	SM d44:4	1.64
PC 18:2-20:5(1)	2.12	TG 56:4(2)	1.64
TG 54:2	2.11	PC 38:6e(3)	1.64
TG 44:2	2.11	PC 16:0-18:2	1.63
PI 18:1-20:4	2.11	PC 18:3-18:3	1.63
PC 40:2e	2.10	TG 56:5(3)	1.63
TG 53:3(1)	2.06	TG 16:1-18:1-18:2	1.63
TG 14:0-16:0-18:1	2.04	PC 20:2-20:4	1.62
TG 50:2	2.02	PC 20:5-22:6	1.61
SM d18:1/18:1	2.01	SM d36:0	1.61
TG 15:0-16:0-18:2	2.00	PC 19:0-20:4	1.60
TG 52:3(1)	1.98	TG 50:3(1)	1.59
TG 48:1	1.98	PE 18:2e/20:4	1.59
TG 54:0	1.97	PC 36:5e(3)	1.59
TG 56:2(1)	1.94	TG 46:2(2)	1.58
SM d36:3	1.93	SM d35:2	1.57
TG 56:2(2)	1.92	OxPE (16:0/14:0/14-HDPA-n3))	1.57
TG 16:0-18:0-18:0	1.91	PC 42:7e	1.57
TG 55:3(2)	1.91	TG 60:5	1.57
PC 16:0-24:1	1.91	LPC 0:0/18:1	1.57
PC 16:0-22:4	1.91	TG 14:0-16:0-18:2	1.57
PC 20:5e/18:1	1.90	PE 16:0-22:4	1.56
TG 58:6(2)	1.90	TG 52:5	1.56
TG 53:4(1)	1.88	PC 38:7	1.56
LPC 24:0	1.88	TG 56:5(4)	1.55
TG 54:4(2)	1.87	TG 14:0-16:0-20:4	1.54
PC 34:4e	1.87	PC 16:1-20:4	1.54
PC 21:2-21:2	1.87	PC 35:5e(2)	1.53
SM d36:1	1.87	PC 42:2e	1.52
PC 20:5-20:5	1.86	PC 22:1-22:6	1.52
HexCer-NS d18:1/24:0	1.85	TG 16:0-16:0-18:0	1.52
LPC 22:0	1.85	LPC 22:4	1.52
PC 16:0-24:0	1.82	PC 18:1-22:6	1.52
TG 47:0	1.81	PC 20:0-18:1	1.51
TG 14:0-15:0-16:0	1.81	TG 54:6(1)	1.51
TG 55:2(2)	1.80	TG 44:1	1.50

Note: Impact of statin treatment on the platelet lipidome in patients with acute coronary syndrome (ACS) is shown.

Supplementary Table S5 VIP-scores of OPLS-DA subgroup analysis between statin-treated and naïve patients with CCS

Lipid	VIP-score	Lipid	VIP-score
	OPLS-DA		OPLS-DA
TG 16:0-18:0-20:4	3.25	TG 53:2	1.76
TG 56:4(2)	2.94	CAR 20:0	1.76
TG 18:0-20:4-20:4	2.74	PC 42:3e	1.74
TG 16:0-16:0-20:4	2.44	TG 56:6(2)	1.74
PC 16:0-18:3(1)	2.43	TG 49:3	1.74
PE 18:1-22:6	2.35	PE 16:0-18:0	1.74
TG 56:8(2)	2.29	TG 51:3	1.74
TG 56:5(4)	2.28	TG 53:3(2)	1.73
TG 60:9(1)	2.22	TG 56:5(2)	1.73
TG 54:6(2)	2.06	TG 58:4(2)	1.72
Cer-NS d18:2/24:1	1.96	SM d30:0	1.72
TG 16:0-20:4-22:5	1.90	TG 53:3(1)	1.71
TG 51:1	1.84	TG 52:6(3)	1.71
PC 40:6e(1)	1.82	TG 16:0-18:0-22:4	1.71
Cer-NDS d18:0/22:1	1.77	Cer-NS d17:1/23:1	1.71
TG 60:8	2.83	SM d34:3	1.70
PE 18:2e/22:4	2.77	PC 42:5e	1.69
PC 41:4e	2.57	PE 38:3	1.68
PE 18:2e/20:4	2.53	DG 18:0-20:4	1.68
PC 40:3e	2.52	TG 55:3(1)	1.67
TG 58:7(1)	2.48	PC 42:6e(1)	1.66
TG 53:4(2)	2.39	PC 36:7	1.66
PC 42:4e(1)	2.38	Cer-NS d17:1/24:1	1.64
TG 55:5	2.30	Cer-NS d17:1/21:0	1.64
TG 60:9(2)	2.27	Cer-NS d18:1/22:1	1.63
PC 16:1-18:2	2.26	FA 17:0	1.62
PC 36:0e	2.25	TG 58:5(2)	1.62
PC 40:8e(1)	2.24	SM d32:2	1.61
Cer-NS d18:1/24:0	2.22	TG 60:10(2)	1.61
PC 42:4e(2)	2.16	TG 54:5(2)	1.61
PC 16:0-18:3(2)	2.16	HexCer-NS d18:1/22:0	1.61
PC 16:0-16:2	2.16	Cer-NS d18:2/18:0	1.60
Cer-NS d17:1/22:1	2.13	PE 40:5	1.60
TG 58:6(2)	2.12	PE 16:1e/22:6	1.59
PC 38:7	2.07	Cer-NDS d18:0/24:0	1.58
TG 18:0-20:4-22:6	2.03	SM d33:2	1.58
TG 58:9	2.02	PC 40:2e	1.57
PC 43:4e	2.02	TG 51:2	1.57
PC 37:0e	2.02	PC 18:2-20:5(1)	1.57
TG 56:7(2)	1.98	TG 53:4(1)	1.57
PE 18:1e-22:5(2)	1.96	PE 18:0-22:5(1)	1.56
PC 43:5e	1.95	PC 38:0e	1.56

(*Continued*)

Supplementary Table S5 (*Continued*)

Lipid	VIP-score	Lipid	VIP-score
	OPLS-DA		OPLS-DA
Cer-NS d18:1/24:1	1.93	TG 56:6(1)	1.56
TG 50:4	1.88	PE 38:6e(1)	1.55
PE 18:2e/22:6	1.87	Cer-NS d18:1/22:2	1.55
PC 16:0-16:3	1.87	CAR 22:0	1.55
PI 18:1-20:4	1.85	PI 16:0-20:4	1.55
TG 56:3(3)	1.85	PC 16:1-20:5(1)	1.54
TG 60:5	1.84	PC 32:2	1.54
Cer-NS d18:1/22:0	1.83	TG 15:0-16:0-18:2	1.53
PE 18:1e-22:5(1)	1.82	TG 16:0-20:4-22:6	1.53
PE 40:5e(2)	1.82	SM d41:3(1)	1.52
PC 18:2-18:3	1.81	PC 36:1e	1.52
TG 58:5(3)	1.80	TG 56:7(3)	1.52
DG 18:0-20:3	1.80	SM d38:2(2)	1.52
PC 40:0e	1.78	TG 58:7(2)	1.51
PC 44:4e(2)	1.78	PC 14:0-18:2	1.51
PC 40:1e	1.77	PC 18:3-18:3	1.50
PC 16:0e/20:1	1.77	Cer-NP t18:0/24:1	1.50
PE 18:0-22:5(2)	1.76		

Note: Hypothetical impact of statin treatment on platelet lipid metabolism leading to alterations in the platelet lipidome.

Supplementary Table S6 Specification for characteristic enzymatically oxidized phospholipids (eoxPL) in statin-treated patients in terms of lipid notation, mass accuracy, and structural annotation

Lipid Class	oxPL Name	Adduct (+) mode	accurate m/z (+)	Error [ppm]	Adduct (-)	accurate m/z (-)	Error [ppm]	Rt
oxPE	oxPE(P-16:1/14-HAdA)	[M+H]+	768.5538	1.17	[M-H]-	766.5392	-1.63	4.44
oxPE	oxPE(P-16:1/14-HDPA-n3)	[M+H]+	768.5381	4.31	[M-H]-	764.5236	-2.09	4.14
oxPE	oxPE(16:0/14-HDPA-n3)	[M+H]+	782.5330	1.02	[M-H]-	780.5185	-6.41	3.93
oxPE	oxPE(18:0/12-HETE)	[M+H]+	784.5487	-1.78	[M-H]-	782.5341	-3.64	4.50
oxPE	oxPE(16:0/14-HAdA)	[M+H]+	784.5487	2.93	[M-H]-	782.5341	-1.02	4.23
oxPC	oxPC(16:0/12-HETE)	[M+H]+	798.5643	-1.50	[M-H+CHOO]-	842.5553	-2.11	3.87
oxPC	oxPC(16:0/14-HDPA-n3)	[M+H]+	824.5800	-2.30	[M-H+CHOO]-	868.5709	-3.11	3.83
oxPC	oxPC(18:1/12-HETE)	[M+H]+	824.5800	-2.91	[M-H+CHOO]-	868.5709	-1.32	3.93
oxPC	oxPC(16:0/14-HAdA)	[M+H]+	826.5956	0.12	[M-H+CHOO]-	870.5866	-1.49	4.07
oxPC	oxPC(18:0/12-HETE)	[M+H]+	826.5956	-1.57	[M-H+CHOO]-	870.5866	-1.46	4.39
oxPI	oxPI(18:1/12-HETE)	[M+NH4]+	918.5702	-0.87	[M-H]-	899.5291	-2.14	3.55
oxPI	oxPI(18:0/12-HETE)	[M+NH4]+	920.5859	-1.09	[M-H]-	901.5448	-2.91	3.91

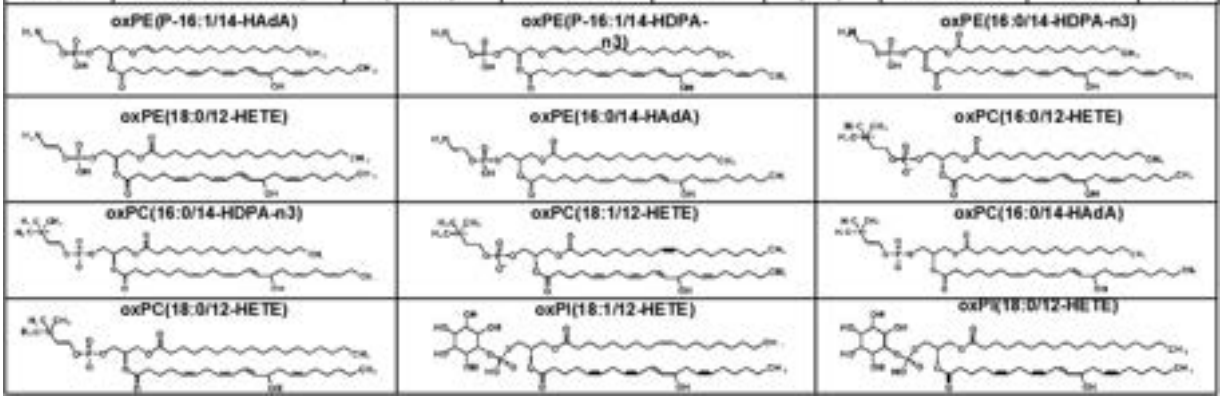

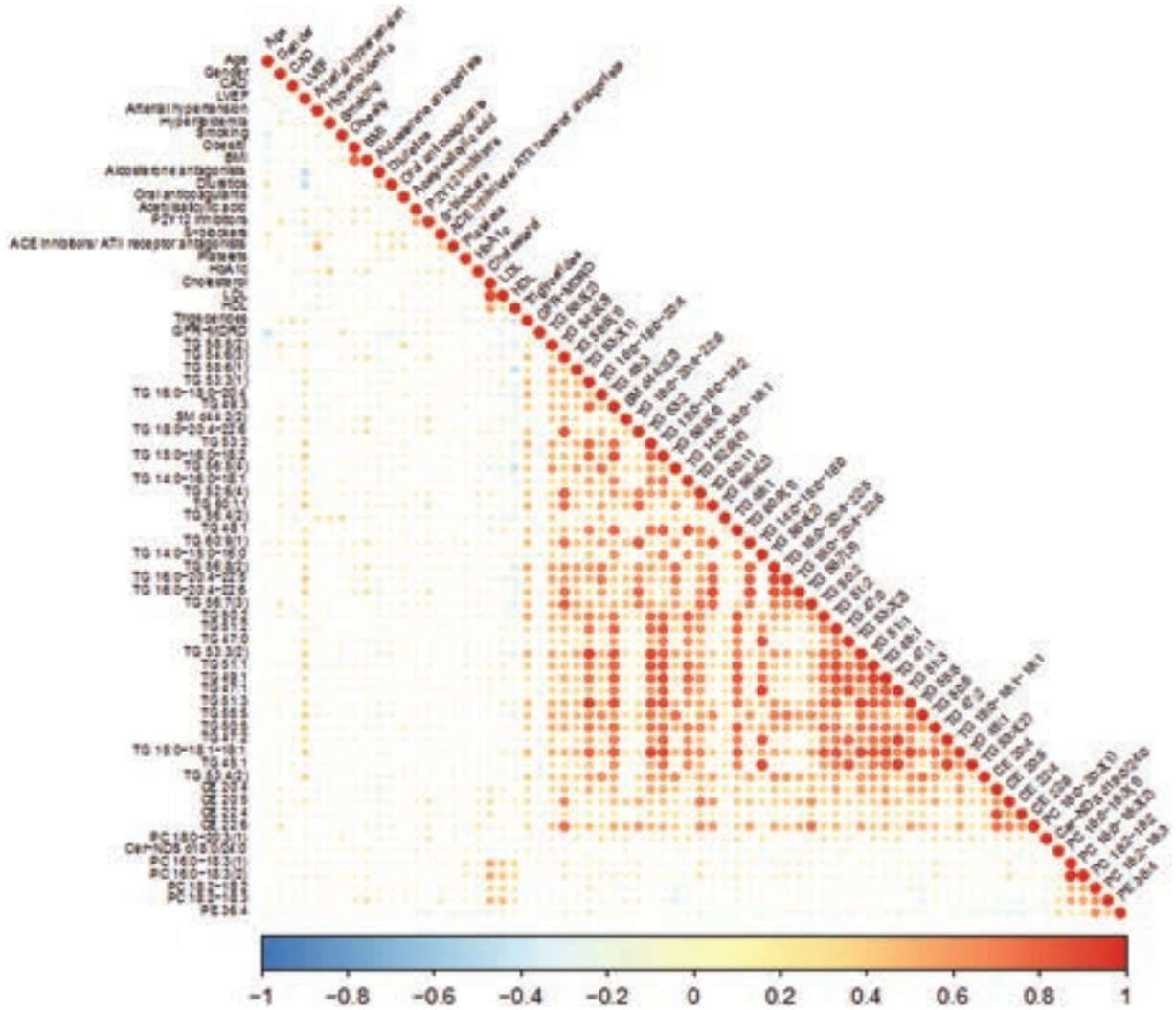

Supplementary Fig. S1 Correlation of altered lipids in statin-treated patients and CAD baseline characteristics. Spearman correlation matrix of important clinical parameters including cardiovascular risk factors, comedication, and levels of significantly regulated lipids in CAD patients with statin treatment compared to naïve patients. Especially upregulated TGs of patients with statin treatment show a strong positive correlation among the species. Further, lipid species partially significantly correlate with important clinical parameters such as age, BMI, left ventricular function, comedication, or cardiovascular risk factors. BMI, body mass index; CAD, coronary artery disease; TG, triglyceride.

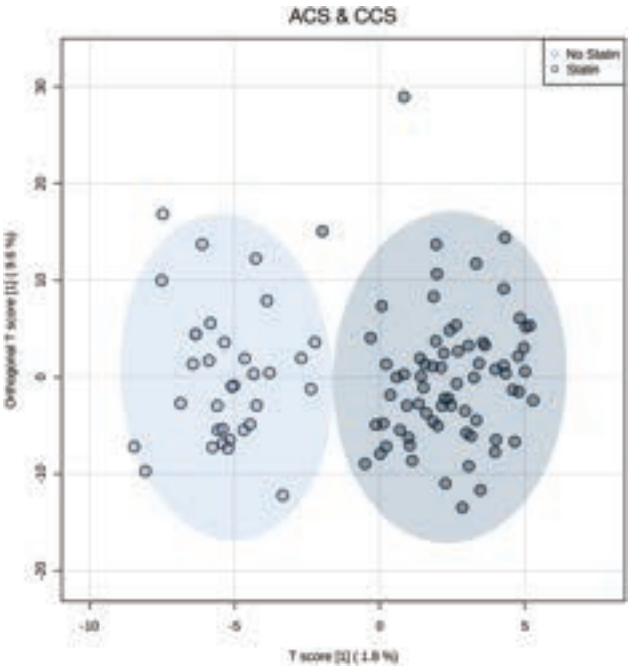

Supplementary Fig. S2 Impact of statin treatment on the platelet lipidome in patients with acute and chronic coronary syndrome. Orthogonal partial-least square discriminant analysis (OPLS-DA) comprising all identified lipids (928) of patients with statin treatment (dark blue) compared to statin-naïve patients (light blue) in the overall cohort ($n = 105$). Data were based on normalized peak intensities of all identified lipids in this study. Statin treatment leads to a distinct separation of subgroups due to alterations of the platelet lipidome. However, a stronger effect of statin treatment on the platelet lipidome is found in the ACS sub-cohort (Fig. 5 A).

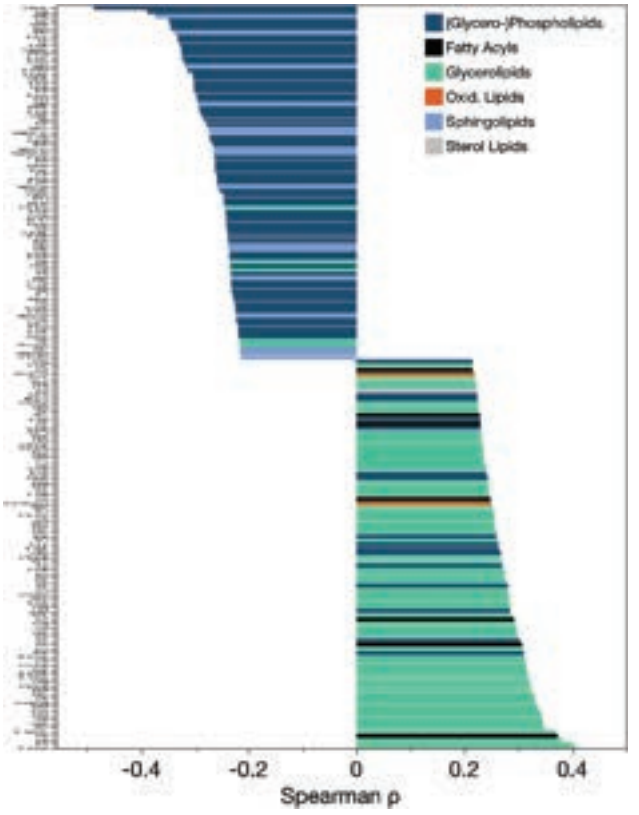

Supplementary Fig. S3 Atorvastatin dose significantly correlates with alterations in the platelet lipidome of patients with CAD. Patients in this study were grouped according to atorvastatin dose on admission (10, 20, 40, and 80 mg, respectively) and atorvastatin dose was correlated with lipid concentrations of all detected lipids. Significant correlations ($p < 0.05$) of platelet lipids are displayed with the referring Spearman's ρ. Increasing atorvastatin doses are essentially associated with higher levels of triglycerides (TGs) and downregulation of glycerophospholipids. CAD, coronary artery disease.

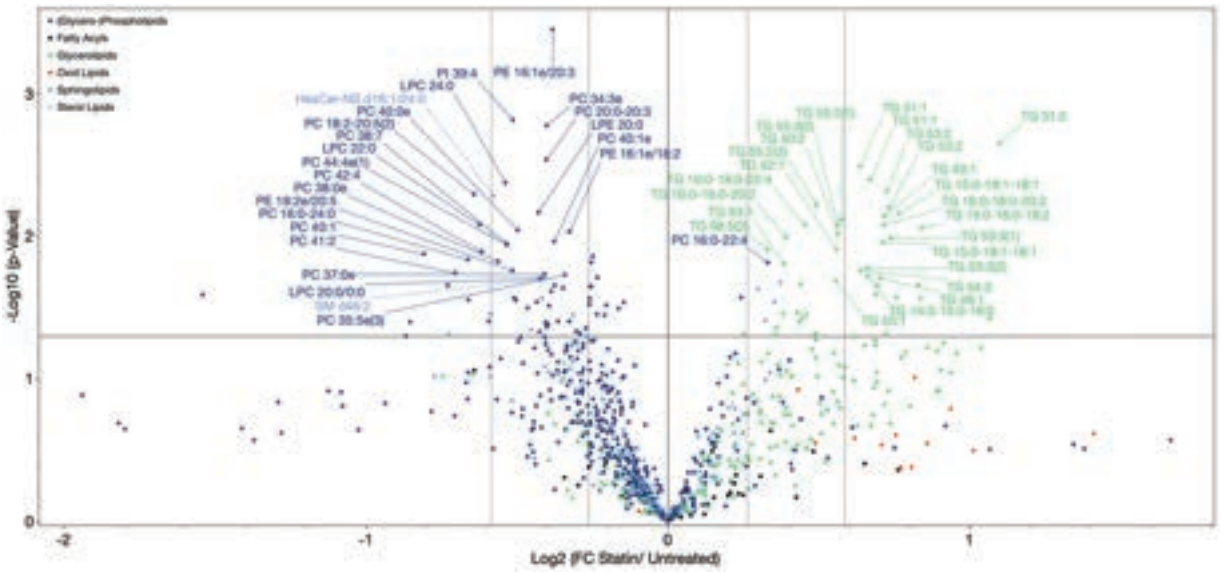

Supplementary Fig. S4 Impact of statin treatment on the platelet lipidome in patients with acute coronary syndrome (ACS). Volcano plot of detected and identified platelet lipids in patient's subgroup with ACS ($n = 45$). *X*-axis (fold change, FC) is the base 2 logarithm of peak intensity ratios (statin/untreated). Values >0 indicate upregulation in statin treatment; <0 downregulation. *Y*-axis showing negative log10-transformed *p*-values of ANOVA; cut-off for significance is SGoF $p < 0.05$. Significantly altered lipids (SGoF $p < 0.05$, FDR < 5%, FC > 1.2) are labelled and colored according to the referring lipid category.

In this study (with the entire cohort), statin-treated patients showed significant regulations of 47 platelet lipids compared to naïve patients. Forty-one lipids were upregulated in statin-treated patients, and 6 lipids were downregulated.

In the ACS sub-cohort ($n = 45$), 48 lipids were significantly altered in patients with statin treatment compared to naïve patients.

Eleven lipids of the altered lipidome in the overall cohort were also found to be regulated in the statin-treated sub-cohort (corresponds to 23% overlap) ($n = 21$ upregulated in statin-treated patients, $n = 27$ downregulated compared to naïve patients). Here, it is striking that, in accordance with the overall cohort, besides one PUFA-PC, upregulated lipids exclusively belong to the class of triglycerides. In contrast, downregulated lipids in statin-treated patients, corresponding to higher levels present in statin-naïve patients, primarily embody PUFA-PCs, ether-phospholipids, lyso-PCs with very long chain fatty acyls, PCs with very long chain fatty acyls, and two sphingolipids (►**Supplementary Table S3**).

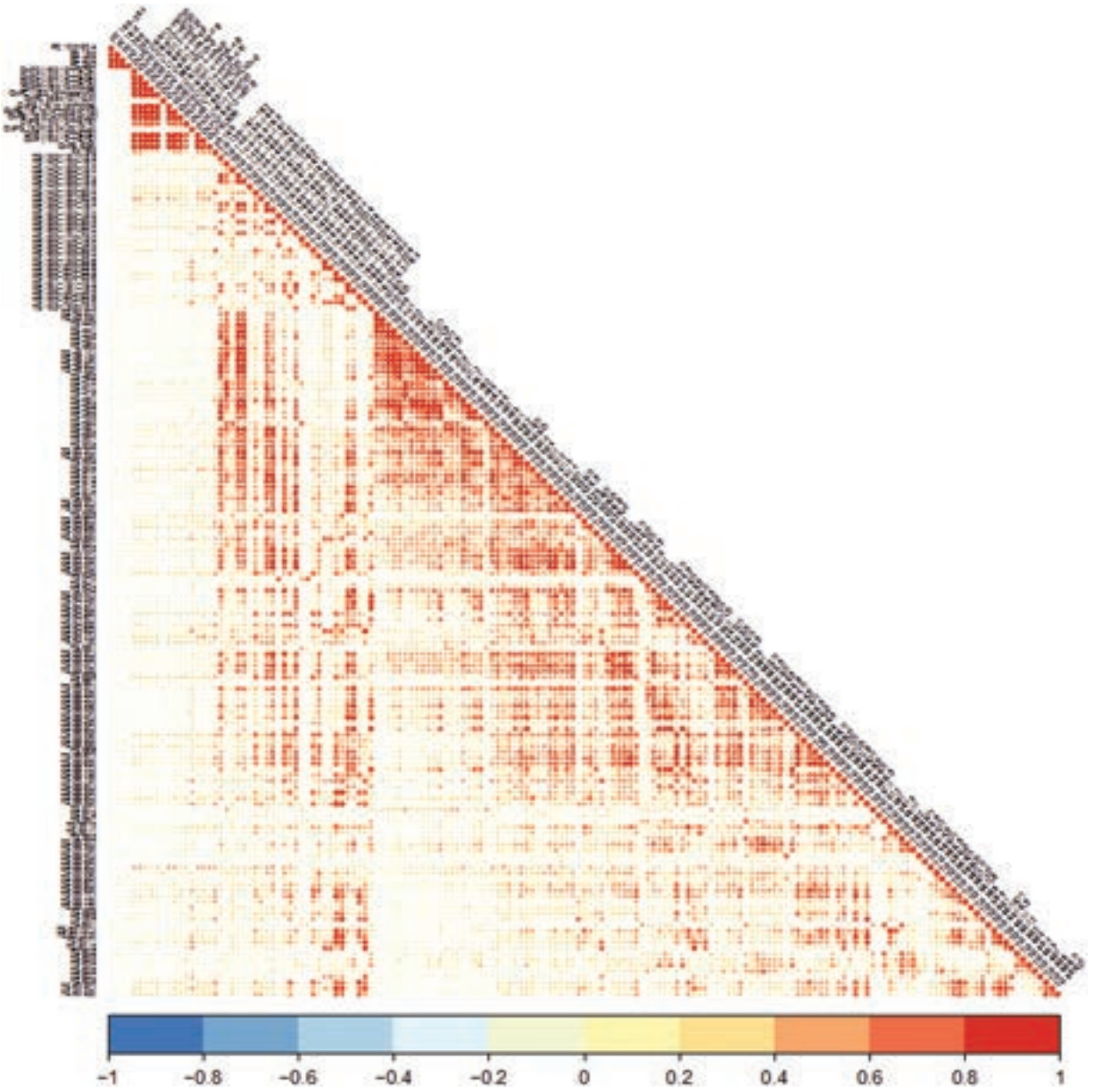

Supplementary Fig. S5. Correlation of characteristically altered lipid classes in patients with statin treatment. Pearson correlation of characteristic lipids of this study including triglycerides (TGs), medium-chain phosphatidylcholines (MC-PCs) such as PC 18:0 as well as oxidized phospholipids (OX-PL) and palmitic acid (FA 16:0). Especially lipid class-specific correlations highlight a significant ($p < 0.05$) strong positive correlation among the species.

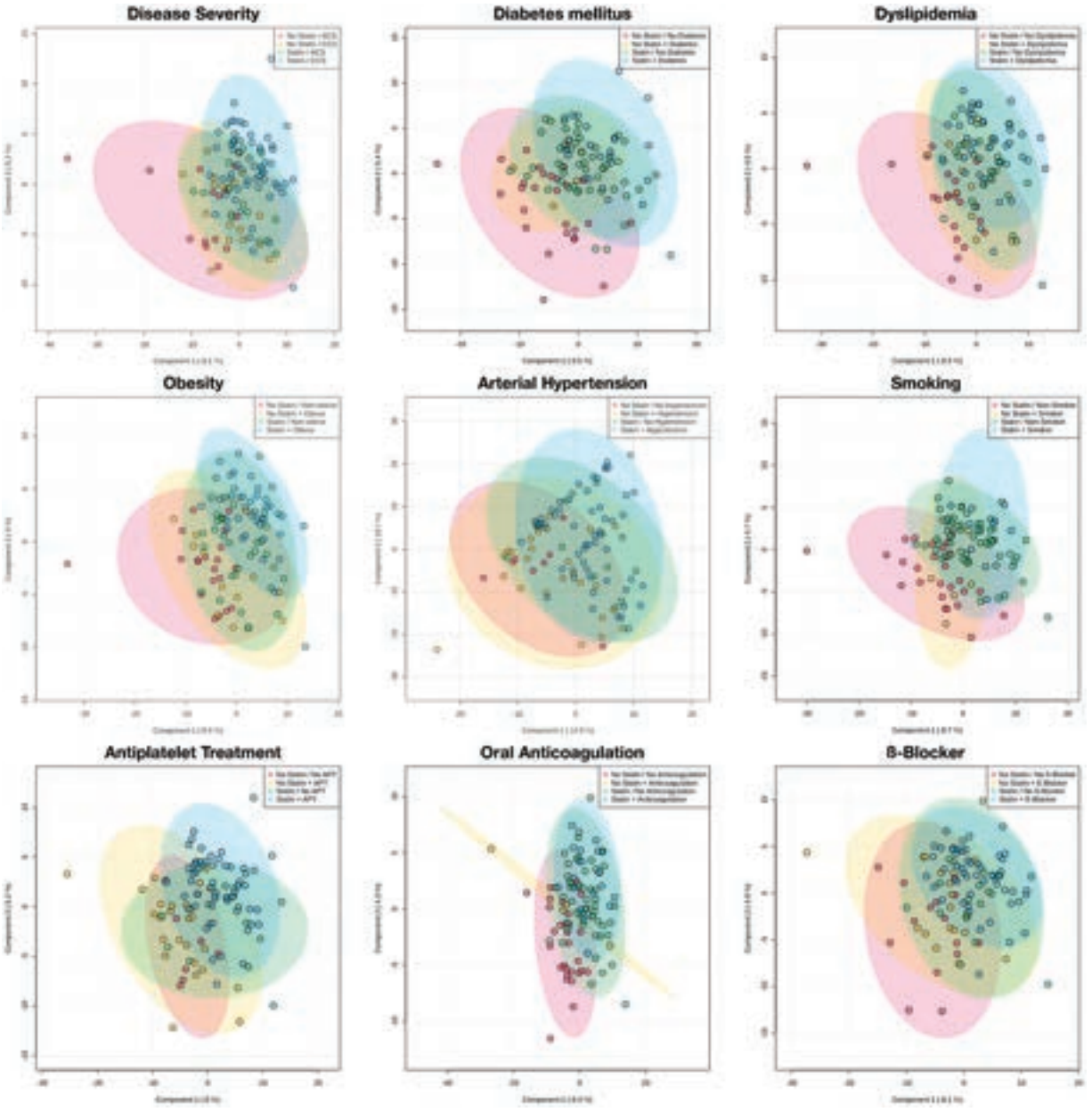

Supplementary Fig. S6. Impact of co-medication and cardiovascular risk factors on the platelet lipidome. Principal component analysis (PCA) of all detected lipids in this study to elucidate the impact of co-medication (anticoagulation, antiplatelet treatment, β-blockers) and cardiovascular risk factors (diabetes mellitus, dyslipidemia, obesity, arterial hypertension, smoking status) on the platelet lipidome. The four sub-cohorts (statin ±/naive ±) are colored and labelled. A distinct separation between statin-treated and naïve patients is observed, but a homogeneous spreading of the subgroups implements a minor influence of assessed risk factors and co-medication on significant findings of an altered lipidome in patients with statin treatment.

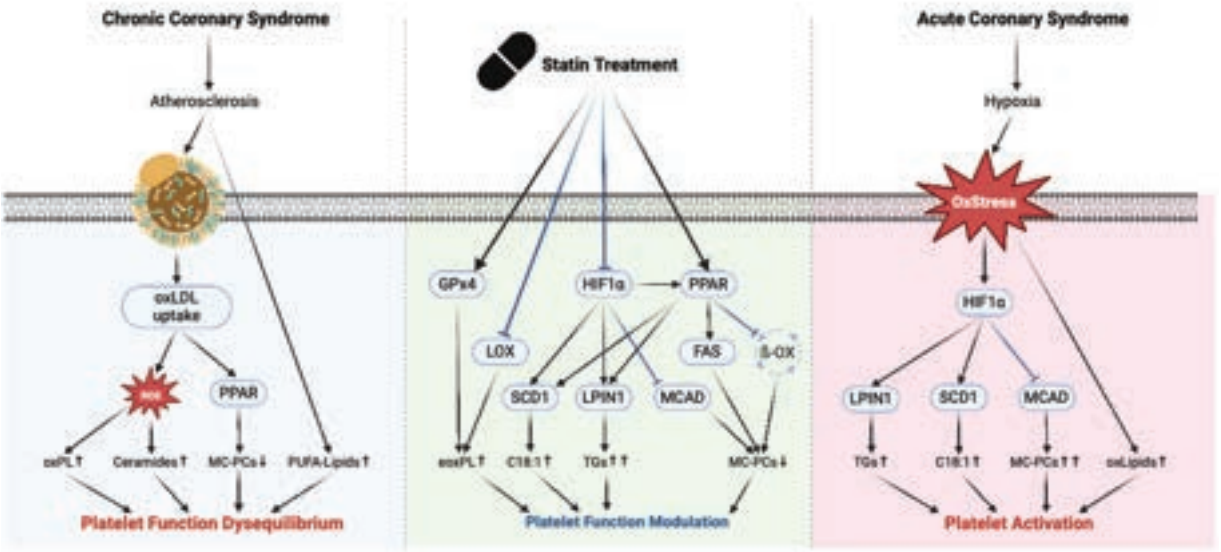

In the pathophysiology of acute coronary syndrome (ACS), myocardial ischemia leads to increased oxidative stress levels and thus upregulation of hypoxia-inducible factor 1 α (HIF1α).[6] Further, reactive oxygen species (ROS) promote lipid peroxidation and therefore, oxidized lipid species enhance platelet function in patients with CAD.[1,7] Increased HIF1α expression induces inhibition of medium-chain acyl-CoA dehydrogenase resulting in a high concentration of medium-chain phospholipids (MC-PCs).[8] MC-PCs such as PC18:0 promote ex vivo platelet function and thus may contribute to the pathophysiology of ACS.[2] In patients with chronic coronary syndrome, incorporation of oxidized low-density lipoprotein (oxLDL) is enhanced and increased oxLDL levels promote ROS generation and induction of peroxisome proliferator-activated receptor (PPAR).[1,9,10] Statin treatment was shown to inhibit expression of HIF1α and modify downstream pathways including lipid metabolism.[11,12] Furthermore, direct activation of PPAR in patients with statin treatment may inhibit beta oxidation and promote fatty acid synthesis by increasing fatty acid synthetase (FAS) levels.[13,14] Thus, disinhibition of MCAD and PPAR-dependent effects due to statin treatment might result in downregulation of MC-PCs as shown in this study. Additionally, statin-induced expression of phosphatidase phosphatase (LPIN1) and stearoyl-CoA desaturase (SCD1), via PPAR activation, may result in increased TG levels.[15,16] Further, upregulation of characteristic enzymatically oxidized phospholipids (eoxPL) in statin-treated patients might result from activation of phospholipid hydroperoxide glutathione peroxidase (GPx4).[17,18] Besides others, eoxPL such as HETE-PLs are essential in regulation of platelet function and hemostasis.[19] In conclusion, we hypothesize that statin treatment in patients with CAD may soften the platelet lipidome and thus modify platelet function.

Funding

This project was supported in part by the German Research Foundation (DFG) KFO-274 and TRR 240.

References

1 Chatterjee M, Rath D, Schlotterbeck J, et al. Regulation of oxidized platelet lipidome: implications for coronary artery disease. Eur Heart J 2017;38(25):1993–2005
2 Harm T, Bild A, Dittrich K, et al. Acute coronary syndrome is associated with a substantial change in the platelet lipidome. Cardiovasc Res 2022;118(08):1904–1916
3 Tsugawa H, Cajka T, Kind T, et al. MS-DIAL: data-independent MS/MS deconvolution for comprehensive metabolome analysis. Nat Methods 2015;12(06):523–526
4 Fan S, Kind T, Cajka T, et al. Systematic error removal using random forest for normalizing large-scale untargeted lipidomics data. Anal Chem 2019;91(05):3590–3596
5 De Livera AM, Sysi-Aho M, Jacob L, et al. Statistical methods for handling unwanted variation in metabolomics data. Anal Chem 2015;87(07):3606–3615
6 Semenza GL. Hypoxia-inducible factor 1 and cardiovascular disease. Annu Rev Physiol 2014;76:39–56
7 Su LJ, Zhang JH, Gomez H, et al. Reactive oxygen species-induced lipid peroxidation in apoptosis, autophagy, and ferroptosis. Oxid Med Cell Longev 2019;2019:5080843
8 Huang D, Li T, Li X, et al. HIF-1-mediated suppression of acyl-CoA dehydrogenases and fatty acid oxidation is critical for cancer progression. Cell Rep 2014;8(06):1930–1942
9 Stellos K, Sauter R, Fahrleitner M, et al. Binding of oxidized low-density lipoprotein on circulating platelets is increased in patients with acute coronary syndromes and induces platelet adhesion to vascular wall in vivo–brief report. Arterioscler Thromb Vasc Biol 2012;32(08): 2017–2020
10 Taketa K, Matsumura T, Yano M, et al. Oxidized low density lipoprotein activates peroxisome proliferator-activated receptor-alpha (PPARalpha) and PPARgamma through MAPK-dependent COX-2 expression in macrophages. J Biol Chem 2008;283 (15):9852–9862

11 Nakashima Y, Miyagi-Shiohira C, Noguchi H, Omasa T. Atorvastatin inhibits the HIF1α-PPAR axis, which is essential for maintaining the function of human induced pluripotent stem cells. Mol Ther 2018;26(07):1715–1734
12 Kim E-H, Ko HY, Yu AR, et al. Inhibition of HIF-1α by atorvastatin during ^{131}I-RTX therapy in Burkitt's lymphoma model. Cancers (Basel) 2020;12(05):1203
13 Balakumar P, Mahadevan N. Interplay between statins and PPARs in improving cardiovascular outcomes: a double-edged sword? Br J Pharmacol 2012;165(02):373–379
14 Pawlak M, Lefebvre P, Staels B. Molecular mechanism of PPARα action and its impact on lipid metabolism, inflammation and fibrosis in non-alcoholic fatty liver disease. J Hepatol 2015;62 (03):720–733
15 Igal RA. Stearoyl-CoA desaturase-1: a novel key player in the mechanisms of cell proliferation, programmed cell death and transformation to cancer. Carcinogenesis 2010;31(09): 1509–1515
16 Zhou F, Fan X, Miao Y. LPIN1 promotes triglycerides synthesis and is transcriptionally regulated by PPARG in buffalo mammary epithelial cells. Sci Rep 2022;12(01):2390
17 Li Q, Liu C, Deng L, et al. Novel function of fluvastatin in attenuating oxidized low-density lipoprotein-induced endothelial cell ferroptosis in a glutathione peroxidase4- and cystine-glutamate antiporter-dependent manner. Exp Ther Med 2021; 22(05):1275
18 Li D, Li Y. The interaction between ferroptosis and lipid metabolism in cancer. Signal Transduct Target Ther 2020;5(01):108
19 Lauder SN, Allen-Redpath K, Slatter DA, et al. Networks of enzymatically oxidized membrane lipids support calcium-dependent coagulation factor binding to maintain hemostasis. Sci Signal 2017;10(507):eaan2787

XI. Curriculum vitae

Note: Curriculum vita is removed in online version.

XII. Acknowledgement

I would like to take this opportunity to express my sincere gratitude and appreciation to all those who have helped me during my PhD period in Tübingen. Without their support, guidance, and encouragement, I cannot experience so much fun throughout my research journey.

First and foremost, I am deeply grateful to my supervisor **Prof. Dr. Michael Lämmerhofer**. I could still remember when I finished my master thesis in his group 4 years ago, he encouraged me to continue with PhD while at that time, I didn't have confidence to myself at all and never planned for a PhD study before. I always thought about the moment when I decided to start my PhD and I never regret to have the decision till today. Prof. Dr. Michael Lämmerhofer always provide kind support and guidance during my research, which helped me overcome lots of challenges. I am truly grateful for his dedication, patience, and the valuable feedback at every stage of my thesis and his hard work and optimism inspired me a lot when I met difficulties during my research.

I am also thankful to **Jun. Prof. Dr. Matthias Gehringer** as my second supervisor and for evaluating this thesis.

I would also like to extend my heartfelt thanks to my colleagues: **Dr. Adrian Sievers-Engler** for sharing his knowledge about MS instrument and helping for the MS instrument maintenance check, **Kristina Dittrich** for the efforts on the clinical lipidomics study. Working together with her is always a pleasure. **Simon Jaag** for the willingness to share the knowledge, experiences and caring for the LC and MS instrument and other regulations in the lab. **Feiyang Li** for the kindness to always provide help in terms of lab work and daily life. **Matthias Olfert** and **Cornelius Knappe** for organizing our server and computer related works. **Kristian Serafimov** for organizing our monthly snacks and coffee. **Mirna Maalouf** for her kindness and warm smile. **Adrian Brun** and **Tamara Janker** for the cooperation on the lipidomics work. **Min Su** for taking care the student practical course. **Franz Fießinger** for taking care of laboratory routine. Special thanks to my former colleagues **Dr. Bernhard Drotleff**, **Dr. Carlos Calderón Castro** and **Dr. Malgorzata Cebo** for transferring me the lipidomics knowledge and willingness to share the ideas and helping me at the beginning of my research. And all the former co-workers for the time spending together. I am also grateful to our secretaries, **Michaela Friedrichs** and **Ingrid Straub** for keeping our group running.

I would also like to express my gratitude to the successful collaboration with **Dr. Madhumita Chatterjee** and **Prof. Dr. Meinrad Gawaz** on the platelets project and **Prof. Dr. Friedrich Götz** on the *staphylococcus* project.

I would like to express my deepest appreciation to my family: my parent **Jingang Fu** and **Yuhong Du**, my grandparents **Zhongyun Fu** and **Yanmei Chu** for unconditional love and support from China, to my friends in Tübingen **Luke Tu**, **Jiayi Du**, **Tong Zhang** and **Bowen Cao** for the accompany in Germany and warm concern during my PhD. Their encouragement, patience, and belief in me have been my constant motivation.

Thanks to the **Chinese Government Scholarship (CSC)** for the funding during my PhD study in Tübingen, thanks to **Ulrike Heitkamp** as my house lord to provide me a nice room for my almost 7 years' stay in Tübingen. Thanks to the nice city Tübingen to let me have lot of beautiful memories here.

To the end, I would also like to thank myself for the persistence and never giving up. I am not a smart student as I always know. That's why I always put more efforts and work as hard as possible to reach the destination where I want to go. Now I am standing here, one step away from my destination and looking back to the way, everything's worth it!